Regulation of plasmodesmal receptor sorting and signalling by membrane scaffolds – the role of tetraspanins and flotillins

Sebastian Samwald

April 2022

University of East Anglia

John Innes Centre

This thesis has been submitted for the degree of Doctor of Philosophy

‘Hope is made anew’

When Hope is broken — all is gone,
and for achievements risks are taken,
nothing gained and nothing won,
yet we are all supposed to be unshaken.

Hope acts to dreams like the forge's fire,
hammered against the anvil strong,
shapes and crafts all true desire,
sometimes seconds, sometimes years long.

The molten glass the light reflects,
though the world just takes this art apart,
always in a different way than Hope expects,
therefore it must be made anew day by day in our heart.

Because no matter at what stage the fight,
Hope dies last and not tonight.

August 2021

i. Abstract

Plants can perceive and respond to the presence of microorganisms such as fungi and bacteria in their environment. One way for plants to perceive the presence of fungi is to detect the fungal cell wall component chitin, via pattern recognition receptors (PRR). During the perception of pathogens, plant cells close the membrane lined channels connecting the cytoplasm of adjacent cells (plasmodesmata) by depositing callose in the cell wall, and thereby restrict the molecular flux between neighbouring cells. Three different PRR are necessary for chitin-triggered plasmodesmal closure in Arabidopsis: LYSM DOMAIN GPI-ANCHORED PROTEIN 2 (LYM2), LYSM-CONTAINING RECEPTOR-LIKE KINASE 4 (LYK4), and LYSM-CONTAINING RECEPTOR-LIKE KINASE 5 (LYK5). Out of those three, only LYM2 is enriched at plasmodesmata, and chitin triggers a further increase of this enrichment. However, the molecular mechanisms underlying this process remain to be elucidated.

In this thesis I explore prerequisites and characteristics necessary to achieve this plasmodesmal localisation. I further show that all three receptors LYM2, LYK4 and LYK5 associate with each other in planta, and investigate how LYK5 could be important for chitin-triggered plasmodesmal closure, even though it is absent at plasmodesmata itself.

I further demonstrate that not only receptors but also proteins of two different scaffolding families — the tetraspanins and flotillins — are necessary for these responses. Both of these families are known for their presence and orchestration of specialised membrane domains such as nanodomains. My data reveal that they are also important for signalling responses at the specialised plasmodesmal PM microdomain. I show how both tetraspanins and flotillins are necessary to achieve chitin-triggered ROS bursts, plasmodesmal regulation, as well as plant resistance against pathogenic fungi comparable to wild-type plants.

Together, the data presented in this work generate new insights on how chitin-triggered signalling processes depend on different receptors, and also on their partner scaffolding proteins, thereby creating new hypotheses and opportunities for future investigations.

ii. contents

iii. List of figures

iv. List of tables

vi. Abbreviations used

General abbreviations

Abbreviation	Full text
Arabidopsis	*Arabidopsis thaliana*
AU	Arbitrary unit
BFA	Brefeldin A
BR	brassinosteroid
Ca	*Capsicum annuum*
CDPK	Calcium-Dependent Protein Kinase
co-IP	Co-Immunoprecipitation
Col-0	Arabidopsis ecotype Columbia 0
CRKs	Cysteine (C)-rich receptor kinases
CSLM	Confocal laser scanning microscopy
DIM	Detergent insoluble membranes
dpi	days past infection
DRM	Detergent-resistant membranes
E	FRET-Efficiency
ER	Endoplasmic reticulum
ETI	Effector-triggered immunity
FRAP	Fluorescence Recovery after Photobleaching
FRET-FLIM	Förster resonance energy transfer–fluorescence lifetime imaging
gg	Golden gate
GIPC	Glycosyl inositol phospho ceramides
Gm	*Glycine max*
GSL	GLUCAN SYNTHASE-LIKE proteins, Callose synthases
gw	Gateway
HR	Hypersensitive response
IP	Immunoprecipitation
LysM	Lysin motif
LRR	Leucine-rich repeat
MAMP	Microbe associated molecular patterns
MLD	Malectin-like domain
Mp	*Mimosa pudica*
Mt	*Medicago truncatula*
MCTPs	Multiple C2 domains and Transmembrane region proteins
Nb	*Nicotiana benthamiana*
NLR	Nucleotide-binding leucine-rich repeat
NLS	Nuclear localisation signal
NMR	Nuclear magnetic resonance
ns	Non significant
Os	*Oryza sativa*
PAMP	Pathogen associated molecular patterns

PCC	Pearson correlation coefficient
PD index	Plasmodesmata index
PHB	Prohibitin
PM	Plasma membrane
PVX	Potato virus X
PRR	Pattern recognition receptor
PTI	Pattern-triggered immunity
PTM	Post translational modification
Pto	*Pseudomonas syringae pv. tomato DC3000*
REM	Remorin
RSV	Rice stripe virus
RLCK	Receptor-like cytoplasmic kinase
RK	Receptor kinase
ROS	Reactive oxygen species
RP	Receptor protein
SE	Standard error
Ser	Serine
SD	Standard deviation
SP	Signal peptide
SPFH	Stomatin/prohibitin/flotillin/HflK/C
TEM	Tetraspanin enriched microdomains
TIRF	Internal Reflection Fluorescence Microscopy
UB	Ubiquitin
VAEM	Variable-Angle Epifluorescence Microscopy
Ws-0	Arabidopsis ecotype Wassilevskija 0
WT	Wild-type
Zm	*Zea mays*

Abbreviations of plant proteins

Abbreviation	Full text	Gene locus
ACR4	ARABIDOPSIS CRINKLY 4	AT3G59420
ATIF3-4	INITIATION FACTOR 3-4	AT4G30690
BAK1	BRI1-ASSOCIATED RECEPTOR KINASE	AT4G33430
BIK1	BOTRYTIS-INDUCED KINASE1	AT2G39660
BRI1	BRASSINOSTEROID INSENSITIVE 1	AT4G39400
CaHIR1	Ca HYPERSENSITIVE INDUCED REACTION 1	AY237117
CaLRR1	Ca LEUCINE-RICH REPEAT 1	AY529867
CALS3	CALLOSE SYNTHASE 3	AT5G13000
CAT3	REPRESSOR OF GSNOR1	AT1G20620
CERK1	CHITIN ELICITOR RECEPTOR KINASE 1	AT3G21630
CESA3/6	CELLULOSE SYNTHASE 3/6	AT5G05170 AT5G64740
CLV1	CLAVATA1	AT1G75820

CLC	CLATHRIN LIGHT CHAIN	AT2G40060
CLE40	CLAVATA3/EMBRYO SURROUNDING REGION 40	AT5G12990
CML41	CALMODULIN-LIKE 41	AT3G50770
CP	CAPPING PROTEIN	subunit A: AT3G05520 and B: AT1G71790
CPK11	CALCIUM-DEPENDENT PROTEIN KINASE 11	AT1G35670
CPK5	CALCIUM DEPENDENT PROTEIN KINASE 5	AT4G35310
CPK6	CALCIUM DEPENDENT PROTEIN KINASE 6	AT4G23650
CRK2	CYSTEINE-RICH RLK2	AT1G70520
EFR	EF-TU RECEPTOR	AT5G20480
ELP	ERLIN-LIKE PROTEIN	AT2G03510
ESM1	EPITHIOSPECIFIER MODIFIER 1	AT3G14210
ESP	EPITHIOSPECIFIER PROTEIN, TASTY	AT1G54040
FER	FERONIA	AT3G51550
FLOT1	FLOTILLIN 1	AT5G25250
FLOT2	FLOTILIN 2	AT5G25260
FLOT3	FLOTILLIN 3	AT5G64870
FLS2	FLAGELLIN-SENSITIVE 2	AT5G46330
GAPA-2	GLYCERALDEHYDE 3-PHOSPHATE DEHYDROGENASE A SUBUNIT 2	AT1G12900
GLDT	T-protein	AT1G11860
GSL8	GLUCAN SYNTHASE-LIKE 8	AT2G36850
GOX2	GLYCOLATE OXIDASE 2	AT3G14415
HIR1	HYPERSENSITIVE INDUCED REACTION 1	AT1G69840
HIR2	HYPERSENSITIVE INDUCED REACTION 2	AT3G01290
HSC70-1	HEAT SHOCK COGNATE PROTEIN 70-1	AT5G02500
ICS1	ISOCHORISMATE SYNTHASE 1	AT1G74710
IMK2	INFLORESCENCE MERISTEM KINASE2	AT3G51740
ITD1	INTERCELLULAR TRAFFICKING DOF 1	AT4G00940
LjNFR5	Lj NOD FACTOR RECEPTOR 5	Lj2g3v1828350
LjSYMRK	Lj SYMBIOSIS RECEPTOR KINASE	Lj2g3v1467920
LOX2	LIPOXYGENASE 2	AT3G45140
LYK4	LYSM-CONTAINING RECEPTOR-LIKE KINASE 4	AT2G23770
LYK5	LYSM-CONTAINING RECEPTOR-LIKE KINASE 5	AT2G33580
LYM2	LYSIN MOTIF DOMAIN-CONTAINING GLYCOSYLPHOSPHATIDYLINOSITOL-ANCHORED PROTEIN 2	AT2G17120
MKK4/5	MITOGEN-ACTIVATED PROTEIN KINASE KINASE 4/5	AT1G51660 AT3G21220
MPK3/6	MITOGEN-ACTIVATED PROTEIN KINASE 3/6	AT3G45640 AT2G43790
MAPKKK5	MITOGEN-ACTIVATED PROTEIN MITOGEN-ACTIVATED PROTEIN KINASE KINASE KINASE 5	AT5G66850
MpPMA2	Mp H^+-ATPASE 2	Fleurat-Lessard et al. (1995)
MtFLOT1	Mt FLOTILLIN 1	MTR_3g106480

MtFLOT2	Mt FLOTILLIN 2	MTR_3g106420
MtFLOT3	Mt FLOTILLIN 3	MTR_3g106485
MtFLOT4	Mt FLOTILLIN 4	MTR_3g106430
MtLYK3	Mt LYSINE MOTIF KINASE 3	MTR_5g086130
MtNFP	Mt NOD FACTOR PERCEPTION	MTR_5g019040
MtSYMREM1	Mt SYMBIOTIC REMORIN 1	MTR_8g097320
NbREM1	Nb REMORIN 1	Fu et al. (2018)
NbREM1.3	Nb REMORIN 1.3	Perraki et al. (2018)
NbREM4	Nb REMORIN 4	Niben101Scf02086g00004
NILR2	NEMATODE-INDUCED LRR-RLK 2	AT1G53430
OSCA1.3	HYPEROSMOLALITY-GATED CA2+ PERMEABLE CHANNEL 1.3	AT1G11960
OsBRI1	Os BRASSINOSTEROID-INSENSITIVE 1	LOC_Os01g52050
OsCEBiP	Os CHITIN ELICITOR-BINDING PROTEIN (CEBiP)	LOC_Os03g0133400
OsRAC1	Os ROP RAC-LIKE GTP-BINDING PROTEIN1	LOC_Os01g12900
OsRBOHB	Os RESPIRATORY BURST OXIDASE HOMOGLOG PROTEIN B	Q6J2K5-1
OsREM4.1	Os REMORIN 4.1	LOC_Os07g38170
OsSERK1	Os SOMATIC EMBRYOGENESIS RECEPTOR KINASE	Loc_Os08g07760
PBL27	PBS1-LIKE 27	AT5G18610
PdBG2	PLASMODESMATA β-GLUCANASE 2	AT2G01630
PDCB1	PLASMODESMATA CALLOSE-BINDING PROTEIN 1	AT5G61130
PDLP1	PLASMODESMATA-LOCATED PROTEIN 1	AT5G43980
PIN3	PIN-FORMED 3	AT1G70940
PIP2	PLASMA MEMBRANE INTRINSIC PROTEIN 2	AT3G53420
PRK	PHOSPHORIBULO-KINASE	AT1G32060
PTAC16	PLASTID TRANSCRIPTIONALLY ACTIVE 16	AT3G46780
PYK10	BETA-GLUCOSIDASE 23	AT3G09260
QSK1	QIĀN SHǑU KINASE 1	AT3G02880
RBOHD	RESPIRATORY BURST OXIDASE HOMOLOGUE D	AT5G47910
REM1.2	REMORIN 1.2	AT3G61260
REM1.3	REMORIN 1.3	AT2G45820
RIR1	REMORIN-INTERACTING RECEPTOR 1	AT1G53440
ROP6	RHO-RELATED PROTEIN FROM PLANTS 6	AT4G35020
RPS2	RESISTANT TO P. SYRINGAE 2	AT4G26090
SLP2	SUBTILISIN-LIKE SERINE PROTEASE 2	AT4G34980
StLecRK-IV.1	St LECTIN RECEPTOR KINASE-IV.1	XP_006341207.2
StREM1.3	St REMORIN group 1 homologue 3	NP_001274989 XP_006353306
SUB	STRUBBELIG	AT1G11130
TET1	TETRASPANIN 1, TORNADO 2, TRN2, EKEKO	AT5G46700
TET10	TETRASPANIN10	AT1G63260
TET11	TETRASPANIN11	AT1G18520

TET12	TETRASPANIN12	AT5G23030
TET13	TETRASPANIN13	AT2G03840
TET14	TETRASPANIN14	AT2G01960
TET15	TETRASPANIN15	AT5G57810
TET16	TETRASPANIN 16	AT1G18510
TET17	TETRASPANIN 17	AT1G74045
TET2	TETRASPANIN2	AT2G19580
TET3	TETRASPANIN3	AT3G45600
TET4	TETRASPANIN4	AT5G60220
TET5	TETRASPANIN5	AT4G23410
TET6	TETRASPANIN6	AT3G12090
TET7	TETRASPANIN7	AT4G28050
TET8	TETRASPANIN8	AT2G23810
TET9	TETRASPANIN9	AT4G30430
TFP1	TETRASPANIN FAMILY PROTEIN1 (TOM2AH2)	AT2G20230
TFP2	TETRASPANIN FAMILY PROTEIN2 (TOM2AH3)	AT2G20740
TFP3	TETRASPANIN FAMILY PROTEIN3 (TOM2AH1)	AT4G28770
TKL1	TRANSKETOLASE 1	AT3G60750
TMK1	TRANSMEMBRANE KINASE 1	AT1G66150
TOM2A	TOBAMOVIRUS MULTIPLICATION 2A	AT1G32400
TUB2	TUBULIN BETA CHAIN 2	AT5G62690
TUB4	TUBULIN BETA CHAIN 4	AT5G44340
TUB5	TUBULIN BETA-5 CHAIN	AT1G20010
TUB6	BETA-6 TUBULIN	AT5G12250
TUB7	TUBULIN BETA-7 CHAIN	AT2G29550
ZW9	TRAF-like family protein	AT1G58270
	Gm FLOTILLIN-LIKE GENE	GmNod53b
	Zm KNOTTED1	ZEAMMB73_Zm00001d033859
	STOMATIN-LIKE PROTEIN1	AT4G27585
	STOMATIN-LIKE PROTEIN2	AT5G54100
	ATPase, F1 complex, alpha subunit protein	AT2G07698

Abbreviations of non-plant proteins

Abbreviation	Full text
BCR	B cell receptor
BLI-3	BLIstered cuticle
CD	‘cluster of differentiation’
CD14	Cluster of differentiation 14
CD19	Cluster of differentiation 19
CD79A	Cluster of differentiation 79A
CD79B	Cluster of differentiation 79B
CD81	Cluster of differentiation 81, Tspan28
CD9	Cluster of differentiation 9, Tspan29
DOXA-1	Dual oxidase maturation factor 1
EWI-2	EWI motif-containing protein 2
FtsH	Fts^{-} class H
GLUT1	Glucose transporter 1
HF-I	Host factor I
HflK/C	Protein host factor I region K/C
HopZ1a	HopPsyH 1A
Ig	immunoglobulins
NOX2	NADPH oxidase 2
NOXs	NADPH oxidases
NfeD	Nodulation formation efficiency D
NPHS2	Podcin
PLS1	Punchless 1
SMAD	SMA "small worm phenotype" and MAD family "Mothers Against Decapentaplegic"
STOM	Stomatin
STOML1	Stomatin-like proteins 1
STOML2	Stomatin-like proteins 2
STOML3	Stomatin-like proteins 3
TGF-β	Transforming growth factor β
TLR4	Toll-like receptor 4
TSP-15	CELE_F53B6.1
Yta10	Yeast tat-binding analogs 10
Yta1224	Yeast tat-binding analogs 1224

vii. Publications arising from this thesis

Tee, E.E., Samwald, S., and Faulkner, C. (2022). Quantification of Cell-to-Cell Connectivity Using Particle Bombardment. In Plasmodesmata: Methods and Protocols, Y. Benitez-Alfonso, and M. Heinlein, eds. (New York, NY: Springer US), pp. 263-272.

Cheval, C.*, Samwald, S.*, Johnston, M.G.*, de Keijzer, J., Breakspear, A., Liu, X., Bellandi, A., Kadota, Y., Zipfel, C., and Faulkner, C. (2020). Chitin perception in plasmodesmata characterizes submembrane immune-signaling specificity in plants. Proceedings of the National Academy of Sciences, 201907799.

*These authors contributed equally to this work.

viii. Acknowledgements

First and foremost, I would like to thank my supervisor, Christine. Without her support, mentoring, and guidance, my PhD would not have been possible. Thank you for helping me understand my many many questions and helping me decipher which of my ideas are worth pursuing. I am exceptionally grateful that Christine has always encouraged me to develop, not just my own research but also as a researcher, scientist, and person.

Thank you to all my 'PhD siblings': Annalisa, Matt, Jo, Sally and Emma. For allowing me to notice the hilarious moments in life and making me smile. For all the food, beach trips and happy memories, we share. Thank you to all the members of the Faulkner lab, past and present: Cécilia, Jeroen, Xiaokun, Mina, Andy, Aoife, Estee, and Catherine. Thank you for always being there for me with a cheering answer and advice. A big thank you also needs to go to Nick, who's support, and trust have never wavered. Thank you, Barrie and Thom, for enabling me to properly climb the very steep learning curves of molecular cloning. I would like to thank the facilities and support services at JIC, particularly Sergio, Grant, Eva, Gerhard, Carlo, Tim, and Lesley. Thank you to the John Innes Foundation for funding my PhD. Thank you, Steph, and Ant, for taking a chance with me and allowing me to grow as a scientist. I have had many different mentors and role models before and during my PhD, but I want to particularly highlight and thank Ingeborg, for believing in me and my potential, even when I couldn't see it yet myself.

Thank you to all the friends I made along the way, our conversations, and our laughter. Thank you, Helen, you are the best long distance lab partner one could wish for. Thank you for sharing a home with me, Isa, Lira, Mimi, and Mathias. Thank you, Marco, Lira, Sam, and Nef — the most growth promoting and encouraging rotation cohort. Thank you, Laura, Mikki, Tom, Katharina, Jack, and Helen, for the times at the allotment, the walks, and dragging me out of the house. Thank you, Callum and Phil, for the kayaking trips and our days out together.

A massive thank you to my family, particularly my Papa Klaus and my Mama Martina. Without your support I would have never gotten so far. Thank you to my siblings, Lukas, Magdalena, Tobias, and Barbara — I couldn't have asked for better cheerleaders. I am grateful for all the encouragement from my family: from my grandparents, my cousins, my aunts, and uncles and many more, particularly Veronika and Martha. Thanks also to my great-uncle Sepp, for showing our family that science is a real career.

1 Introduction

1.1 Plant perception of microbes

Cells can perceive other organisms via cell-surface pattern-recognition receptors (PRRs) capable of recognising conserved molecules. The selective binding of these ligands to genetically encoded PRRs, initiates further downstream signalling processes that trigger cellular responses to the presence of a microbe threat. This extracellular recognition of molecules is referred to as pattern-triggered immunity (PTI), by contrast to intracellular recognition of pathogen effector proteins which is termed effector-triggered immunity (ETI) (Dodds and Rathjen, 2010; Ngou et al., 2021).

PRRs capable of perceiving a ligand and initiating signalling processes, can be classified into two main categories. Receptor kinases (RKs) (Goff and Ramonell, 2007; Shiu and Bleecker, 2003; Shiu and Bleecker, 2001), which span from a receptor domain in the extracellular space via a single transmembrane domain into the intracellular cytosol where a kinase domain is located (Jose et al., 2020). By contrast, receptor proteins (RPs), which also consist of an extracellular receptor domain, do not have extended intracellular domain and instead end their C-terminus with a transmembrane domain and a short cytosolic tail (Jamieson et al., 2018) or are anchored into the plasma membrane (PM) via the attachment of a glycosylphosphatidylinositol (GPI) anchor (Gong et al., 2017). Receptor-like cytoplasmic kinases (RLCK) are activated by ligand activated PRRs during the initiation of PTI (Yamaguchi et al., 2013). PRRs have a diverse variety of different extracellular receptor domain that allow selective recognition, such as Lysin motif (LysM) domains (Gust et al., 2012), Cysteine (C)-rich receptor kinases (CRKs) (Quezada et al., 2019), leucine-rich repeats (LRR) (Xi et al., 2019), Lectin (Sun et al., 2020) and Malectin-like domains (Ortiz-Morea et al., 2022). These domains can recognise varying molecules such as specific peptides and polypeptides (Gómez-Gómez et al., 1999; Rhodes et al., 2021; Zipfel et al., 2006), polysaccharides (Erbs et al., 2008; Felix et al., 1993; Gust et al., 2007), or fatty acids and derivatives (Kutschera et al., 2019) as ligands.

This diversity in extracellular perceptive domains achieves the recognition of different ligands acting as elicitors by different RKs and RPs. These molecules can be pathogen- or microbe associated molecular patterns (PAMPs or MAMPs) and can be recognised from pathogenic organisms as well as mutualistic organisms. For example, the perception of flg22 — a peptide fragment of bacterial flagella — is recognised by the *Arabidopsis thaliana* (from here on referred to as Arabidopsis) RK FLAGELLIN SENSITIVE2 (FLS2) (Chinchilla et al., 2006).

Legumes such as *Medicago truncatula* recognise the presence of mutualistically compatible rhizobial bacteria by detection of bacterial lipochitooligosaccharide nodulation (Nod) factors via RKs including NOD FACTOR PERCEPTION (MtNFP) (Amor et al., 2003).

RKs and RPs often undergo heteromeric complex formations, which enable efficient signalling processes utilising co-receptors and can be specifically induced by the presence of a ligand or constitutively formed. For example, FLS2 undergoes flg22 induced complex formation with BRI1-ASSOCIATED RECEPTOR KINASE (BAK1) in Arabidopsis (Chinchilla et al., 2007), while MtNFP and its co-receptor LYSIN MOTIF RECEPTOR-LIKE KINASE3 (MtLYK3) already form a heteromeric interaction in the absence of Nod factors in *M. truncatula* (Moling et al., 2014). Much effort is spent to identify and characterise co-receptors. However, RKs and RPs also form heteromeric interactions with proteins of other classes and families, but the full range of signalling machinery in complex with PRRs is not well described.

1.2 Signal transduction downstream of PRR

The perception of a ligand by a RK or RP activates multiple different signalling processes and cellular changes. Crucially, the elicitor is perceived extracellularly and signalling is transduced intracellularly, for example by kinase domains of RKs phosphorylating other proteins. One such protein which undergoes RK dependent phosphorylation in the presence of an elicitor is the cytosolic BOTRYTIS-INDUCED KINASE1 (BIK1). Treatment of plant tissues with flg22 or elf18 — another bacterial peptide, consisting of the N-terminal peptide of the bacterial elongation factor Tu (Kunze et al., 2004) — triggers RLCKs such as BIK1 to undergo phosphorylation (Lu et al., 2010). However, not all elicitors result in equal BIK1 phosphorylation, as other RLCK can be functional in different signalling pathways (Rao et al., 2018). For example, the fungal cell wall component chitin, does not induce BIK1 phosphorylation in seedlings (Lu et al., 2010) and the ability of the chitin RK CHITIN ELICITOR RECEPTOR KINASE 1 (CERK1) to phosphorylate BIK1 is weak when compared to its ability to phosphorylate PBS1-LIKE 27 (PBL27) (Shinya et al., 2014).

The perception of elicitors such as flg22 and elf18 trigger the activation of the MITOGEN-ACTIVATED PROTEIN (MAP) kinase cascades (Asai et al., 2002; Zipfel et al., 2006). For example, the signal progression from the chitin RKs CERK1 and LYSM-CONTAINING RECEPTOR-LIKE KINASE 5 (LYK5) is relayed via the RCLK PBL27 to the MAPK cascade. The phosphorylation of one MAPK in turn causes the phosphorylation of another MAPK, followed

by a third round of MAPK phosphorylation, which is why this process is referred to as a cascade. In a chitin perceiving plant cell, PBL27 activates this cascade by phosphorylation of MITOGEN-ACTIVATED PROTEIN KINASE KINASE KINASE 5 (MAPKKK5), which in turn phosphorylates MITOGEN-ACTIVATED PROTEIN KINASE KINASE 4 and 5 (MKK4/5), which then again in turn phosphorylates MITOGEN-ACTIVATED PROTEIN KINASE 3 and 6 (MPK3/6) (Kawasaki et al., 2017; Yamada et al., 2016). The MAPK cascade ultimately leads to the phosphorylation of different transcription factors, such as members of the WRKY family, which in turn affect and change gene expression in the nucleus to adapt for the pathogen presence (Adachi et al., 2015).

The detection of MAMPs also leads to changes in the cytosolic and extracellular Ca^{2+} concentrations. RLCKs such as BIK1 and Calcium-Dependent Protein Kinases (CDPKs) can phosphorylate proteins dependent on the cytosolic calcium concentrations. CDPKs consist of a calmodulin-like calcium-sensor and a protein kinase effector domain, and together those two domains enable the CDPKs to perceive changes in the Ca^{2+} ion concentration triggering the phosphorylation of downstream target proteins (Romeis and Herde, 2014). RLCKs, activated by PRR triggered by various elicitors, are capable of phosphorylating and thereby activating the NADPH oxidase RESPIRATORY BURST OXIDASE HOMOLOGUE D (RBOHD) to produce superoxide which dismutates to H_2O_2 (Li et al., 2014; Miller et al., 2009). This process is calcium dependent for CDPKs, but calcium independent for BIK1, mediating RBOHD phosphorylation. RBOHD has multiple potential phosphorylation sites, and although there is some overlap in the phosphorylation sites targeted by BIK1 and CDPKs, they can target some different sites (Kadota et al., 2014). The phosphorylation of different RBOHD sites is not only dependent on the signalling pathway, but also on the signalling pathway's localisation within the membrane. The presence of MAMPs triggers changes to the connections and exchange between adjacent cells, by regulating plasmodesmal closure. In Cheval et al. (2020) we showed that the chitin-triggered PM localised reactive oxygen species (ROS) burst is dependent on the RBOHD phosphorylation sites Ser39/Ser339/Ser343 and Ser133, while the regulation of plasmodesmal cell-to-cell flux is only dependent on the phosphorylation sites Ser347 and Ser133. Different signalling pathways can therefore converge at RBOHD, by different phosphorylation signatures.

The phosphorylation of RBOHD triggers the production of extracellular ROS (Pogány et al., 2009). In Arabidopsis, RBOHD is the primary member of the RBOH family responsible for producing the ROS burst after MAMP perception (Miller et al., 2009). ROS act as secondary messengers for rapid local and long-distance signalling (Miller et al., 2009; Sharma et al.,

2012). Treatment of leaves with MAMPs trigger the start of the ROS burst within minutes, resulting in a strong readout often used to test for elicitor perception capabilities (Sang and Macho, 2017). The ROS burst is able to further activate Ca^{2+} channels in the PM (Bais et al., 2003; Bowler and Fluhr, 2000; Price et al., 1994) thereby further promoting the activation of CDPKs (Dubiella et al., 2013).

The primary MAMP-triggered ROS burst occurs into the extracellular space; however, ROS can also be produced in other cellular compartments and this may further aid in the defence against pathogens (Torres, 2010). For example the MAMP-triggered ROS production in chloroplasts has been shown to be crucial for the execution of hypersensitive response (HR) cell death in plants triggered by pathogens (Liu et al., 2007).

The plant HR is a localised cell death response which occurs rapidly at the point of pathogen contact with the host plant and is associated with being beneficial for pathogen resistance (Balint-Kurti, 2019). The HR response can be triggered by the perception of pathogen effectors via intracellular nucleotide-binding leucine-rich repeat (NLR) proteins — effector-triggered immunity (Coll et al., 2011; Mur et al., 2008). Few MAMPs can trigger HR-like cell death via PRR perception, and most MAMPs alone cannot trigger HR (Feechan et al., 2015). Nonetheless, the interplay between PTI and ETI can lead to an enhanced HR and thereby increased plant resistance against the pathogen (Ngou et al., 2021). This is a prime example of how perception reactions and processes in different cellular compartments can interplay to achieve an enhanced orchestrated immune response in a localised part of the plant. However, there is still no complete understanding of all the complexities and dynamics of compartmentalisation necessary for such responses.

Taken together the perception of pathogens followed by the launching of defence mechanisms result in either susceptibility or resistance of the plant towards the pathogen (Nishimura and Dangl, 2010). This often depends on specific adaptations of the pathogen, such as plant species specific effectors (Zess et al., 2021), as well as adaptations on the plant host side such as evolution of specific NLR proteins detecting effectors of the pathogen (De la Concepcion et al., 2019), and the evolution of appropriate PRRs (Man Ngou et al., 2022). The initial success of the plant immunity responses is also crucial. For example Arabidopsis is capable to control nascent infections of *P. syringae* at low concentrations thereby preventing an outbreak of symptoms, whilst higher inoculums are capable of overcoming this resistance (Ishiga et al., 2011).

1.3 Different plant-microorganism interaction outcomes

A multitude of different organisms can interact with plants, resulting in beneficial to neutral and harmful pathogenic outcomes. Different organisms within the same kingdoms of life can thereby exhibit drastically different behaviours and outcomes for the plant. For example, rhizobia bacteria can undergo a symbiotic relationship with plants, fixing gaseous nitrogen as a nutrient for the plant in exchange for carbon molecules (Oldroyd et al., 2011), whilst other bacteria such as *Pseudomonas syringae* can be detrimental and destructive towards the plant (Xin et al., 2018). Similarly, specialised species of fungi can associate themselves with plants, forming mycorrhiza to enable the beneficial exchange of molecules. For these interactions to proceed in a favourable way for the plant, the plant must successfully detect and identify these microorganisms, such as via PRRs (Gutjahr et al., 2015; Liang et al., 2018; Zipfel et al., 2006).

Some of these microorganisms can change their behaviour depending on their environment and their life cycle stage. Pathogenic fungi generally can be classified according to their life cycles as necrotrophic or biotrophic. Whilst biotrophic fungi derive their nutrients from living host cells, necrotrophic fungi do so from dead or dying cells (Rajarammohan, 2021). Fungi transitioning from an early biotrophic lifestyle to a later necrotrophic lifestyle can be referred to as hemibiotrophs (Rajarammohan, 2021). However, these definitions are not always as black and white as they may seem. For example, the fungus *Botrytis cinerea* is traditionally referred to as a necrotrophic fungus (Chen et al., 2022), causing severe symptoms upon infection (Williamson et al., 2007). Yet, it can also grow asymptomatically as an endophyte without causing any clear disease symptoms (Sowley et al., 2010; van Kan et al., 2014).

1.4 Compartmentalisation of organelles to achieve specialised functions

Eukaryotic cells are compartmentalised, containing different organelles, that have different functions within the cell, such as the nucleus, peroxisomes, mitochondria, vacuoles, the endoplasmic reticulum (ER), the Golgi apparatus, and specifically in plants chloroplasts. Both mitochondria and chloroplasts likely evolved from prokaryotes which were engulfed and previously lived as independent organisms. Through this endosymbiotic relationship these individual organisms over time became completely dependent on and integral parts of the host eukaryotic cell (Sagan, 1967). In this way further diverse compartments could develop

and specialise to fulfil functions otherwise not efficiently possible within less compartmentalised eukaryotic cells, such as electron transport chains or photosystem reactions in chloroplast and citric acid or Krebs cycle reactions in mitochondria.

Even within organelles, further compartmentalisation is possible, which can thereby further enhance desired specialised reactions. For example, within plant chloroplasts the thylakoid membrane is folded and stacked to form called granal stacks, which allows the incorporation of more protein complexes within the same total volume of the organelle, resulting in higher rates of sugar production (Kirchhoff et al., 2002; Pribil et al., 2014). This increased level of spatial compartmentalisation therefore allows to achieve higher rates of reactions. Starch granules within chloroplasts are an example of a specialised energy storage compartmentalisation, as they store glucose subunits in a limited and condensed way as a biopolymer, which can then specifically be degraded during energy deficit times such as night-time (Mérida and Fettke, 2021). This compartmentalisation thereby allows for a temporally coordinated release of glucose, demonstrating how compartmentalisation can be important to achieve tight temporal control over processes.

The concept of compartmentalisation has long been studied and evolved with the progression of imaging techniques such as microscopy. First it allowed the realisation of individual cells making up eukaryotic organisms, then the discovery of organelles within those cells and further compartmentalisations within those organelles. And now the ever-growing arsenal of scientific research techniques over the last decades such as growing biochemical approaches and super-resolution techniques have driven the concept of compartmentalisation for diversification, specialisation, spatiotemporal control and function even further down to a level of compartmentalisation within membrane structures.

1.5 Membrane compartmentalisation

Membranes of plants consist mainly of lipids, generally structured with a polar hydrophilic head connected to a glycerol backbone and hydrophobic tail made up of two fatty acids (Reszczyńska and Hanaka, 2020). These lipids form a phospholipid bilayer which separates neighbouring cells and organelles from their surroundings (Andersen and Koeppe, 2007; Ohlrogge and Browse, 1995). Plant membranes include three main classes of lipids: glycerolipids, sphingolipids and sterols (Reszczyńska and Hanaka, 2020). The most abundant glycerolipids can be separated into four different groups: phospholipids, galactolipids, triacylglycerols and sulfolipids (Kunst et al., 1989; MacDonald et al., 2019). Depending on the modifications of their head group, phospholipids can be further categorised as

phosphatidylcholine, phosphatidylethanolamine, phosphatidylserine, and phosphatidyl-inositol (Kates, 1970). Proteins can be inserted or associated with membranes in different ways depending on hydrophobic, hydrophilic, transmembrane domains or anchor domains (Alberts et al., 2002)

There are different theories and ways to conceptualise the compartmentalisation of biological membranes. Over time the scientific community's knowledge and understanding of PM compartmentalisation has changed and shifted with the available data and therefore resulted in different theories and concepts. These concepts were progressively refined and optimised and thereby resulted in different terminologies.

The fluid mosaic model was originally proposed by Singer and Nicolson (1972) and holds the original basis for all following models. It describes the structure of the PM as a random uniform mosaic of different components — such as phospholipids, cholesterol, proteins and carbohydrates clustered in higher orders in short range of less than tenths of micrometres.

Updated versions of this model allow for clustering of different components to create specialised domains within the PM (Nicolson, 2013).

1.5.1 Detergent resistant membranes — lipid rafts

Initial models of PM compartmentalisation into different domains relied on the self-organising capacity of sterols in model membranes, as well as on biochemical separations of PM fractions. Detergents solubilise the phospholipid cell membrane (Bush and Gertzman, 2016). However, partial resistance of parts of the PM to solubilisation with different non-ionic detergents has been observed particularly at cold temperatures and gave rise to the idea that there are subsections or domains within the PM which cannot be efficiently solubilised with detergents (Bohuslav et al., 1993; Brown and Rose, 1992; Drevot et al., 2002; Kurzchalia et al., 1992; Madore et al., 1999; Röper et al., 2000). These domains have therefore been termed detergent-resistant membranes (DRMs) or detergent insoluble membranes (DIMs).

The discovery of these DRM fractions led to more refined theories of lipid rafts. This idea allows for subsections of the PM to exhibit float/raft-like characteristics on a metaphorical sea surface. The raft itself has integrity and does not disintegrate, whilst embedded in the more homogeneous water surface and flexibly moving in different directions on it. Like a wooden raft constructed to float, representing an ordered partition in comparison to drift wood floating randomly, molecules with a greater tendency to partition into an ordered

environment and state are enriched in DRMs (Brown and London, 1998). Lipids in DRM therefore can be characterised by a highly ordered liquid state, in which acyl chains are tightly packed (Magee and Parmryd, 2003). For example, sphingolipids are enriched, while phospholipids are relatively depleted in DRMs (Brown and Rose, 1992).

In the lipid raft theory, spatial compartmentalisation of the PM is therefore achieved between the lipid rafts and the rest of the PM. Originally lipid rafts were defined biochemically by their insolubility in non-ionic detergents extracted at 4°C, yielding DRMs (Magee and Parmryd, 2003). Due to a high lipid-to-protein ratio resulting in a low density, DRM were also isolated by flotation on sucrose-density gradients (Magee and Parmryd, 2003). The lipid raft theory allowed to develop the hypotheses that specificity and fidelity of signal transduction are achieved by different localisations of proteins which are part of signalling pathways. This therefore allowed to conceptualise the PM and its components not just as a random mosaic, but with distinctive compartmentalised platforms (Janes et al., 2000) .

The use of different detergents, and in varying concentrations as well as changes to extraction temperature resulted in strongly varying proteins present in DRM (Schuck et al., 2003). This has raised concerns over the validity of using detergent-insolubility to describe *in vivo* PM partitionings. For example, Heerklotz (2002) demonstrated that the addition of the detergent Triton itself may create ordered domains in homogeneous fluid membranes, which in turn are Triton resistant in later Triton based membrane solubilisation. The Triton based observations of DRMs may therefore be to a certain degree artefactual observations (Heerklotz, 2002), and this lead to postulations that DRMs should not be identified to resemble membrane rafts (Lichtenberg et al., 2005; Munro, 2003).

At the “raft meeting” in Tomar, Portugal 2003, research groups of this field therefore stated the following: “A general consensus that emerged at this meeting about the nature of a raft in a cell membrane is summarized as follows. Considering the complexity of the system and the poorly understood nature of DRM formation, it is unlikely that DRMs that are derived from cells reflect some pre-existing structure or organization of the membrane.” (Malinsky et al., 2013; Zurzolo et al., 2003).

The lipid raft theory has therefore moved on from DRM definitions and been further refined over time as follows: “Membrane rafts are small (10–200 nm), heterogeneous, highly dynamic, sterol- and sphingolipid-enriched domains that compartmentalize cellular processes. Small rafts can sometimes be stabilized to form larger platforms through protein-

protein and protein-lipid interactions" (Pike, 2006). Membrane rafts can therefore change over time and within their spatial distribution as well as composition — they are spatiotemporally dynamic.

However flawed the lipid raft theory may be, it allowed the generation of hypotheses which build on the compartmentalisation of the PM to achieve functionality of different proteins in different membrane environment signalling pathways. This concept was utilised in the development of further theories, such as the concepts of micro- and nanodomains.

1.6 Micro- and Nanodomains defined

Based on the compartmentalisation aspects of the lipid raft theory other definitions for the observation of partitioning of the PM were created. For this thesis I am following the definition of Ott (2017) for plant nano- and microdomains. This states that nanodomains are defined as distinguishable submicron protein and/or lipid assemblies (usually in the range of 20 nm to 1 µm) represented by homomeric or heteromeric protein complexes that often appear as punctate or partially network-like structures at the cell surface (Ott, 2017). Such nanodomains could either be maintained by constant protein turnover — via recruitment of new proteins into the nanodomain, or may exhibit different temporal lifetimes (Ott, 2017).

Microdomains are significantly larger than nanodomains — which have a lower size limit of about 1 µm — and can be seen as a higher order of nanodomains. Microdomains can be purpose and location specific, exemplified by the Casparian strip domain, cell polar domains, host-derived membranes or plasmodesmata (Jaillais and Ott, 2020; Ott, 2017).

Similar to membrane domains defined by the lipid raft theory, nanodomains are enriched in lipids (Schmid, 2017). Different types of lipids and sterols are not homogeneously distributed within the PM, but rather there is a strong asymmetry between the outer and the inner leaflets (Cooper, 2000). The outer leaflet is rich in glycosphingolipids, sterols and phosphatidylcholine, while the inner leaflet is enriched in phosphoinositides and phospholipids (Cacas et al., 2016; Gronnier et al., 2018; Tjellström et al., 2010). Further to this outer and inner segregation of lipids, patterned lipid bilayers have been used to study that there is lipid segregation laterally in each leaflet allowing for speculation of further independent compartmentalisation (Kusumi et al., 2012; Wu et al., 2004).

Nanodomains are sites of higher liquid-ordered phases and are enriched in sterols and sphingolipids, such as glycosyl inositol phospho ceramides (GIPC), which can interact with phytosterols and thereby increase the lipid order even further (Cacas et al., 2016). Additional

evidence of liquid-ordered compartmentalisation of the PM comes from the liquid-order sensitive dye di-4-ANEPPDHQ, which shows heterogeneous labelling of the PM (Gronnier et al., 2017; Pan et al., 2020). However, by contrast to lipid raft definitions, nano- and microdomains are not only defined by their specialised lipid content in comparison to the rest of the PM, but also by their specific resident proteins.

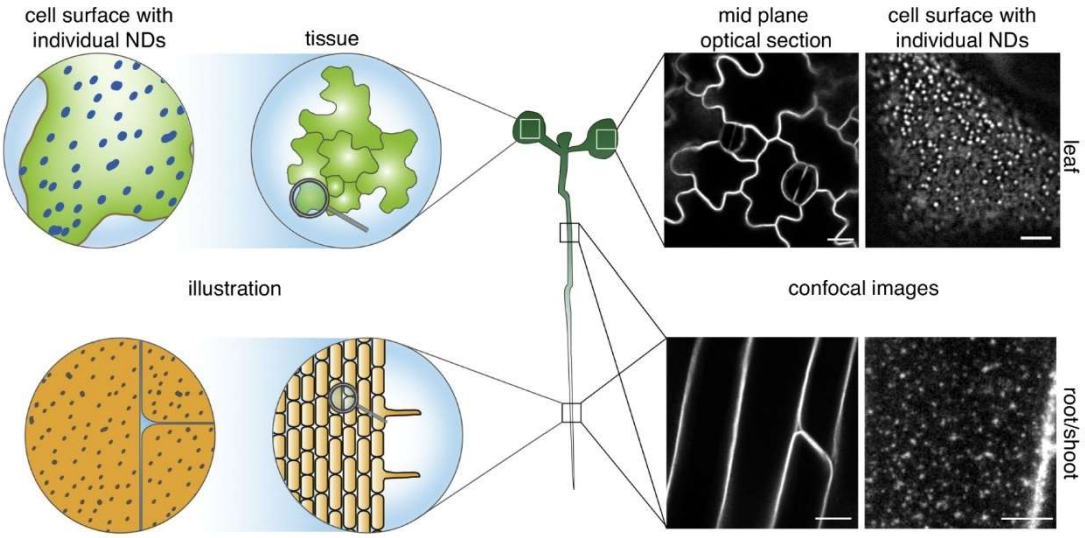

Figure 1-1: Conceptualisation of PM nanodomains. Cell surfaces are compartmentalised by nanodomains, which can be visualised using fluorescent protein translational fusions with fluorophores with advanced confocal laser scanning microscopy (CLSM). The use of conventional CLSM, often results in a lower resolution along the z-axis. However, visual detection of nanodomains is dependent on this, and can therefore not always be observed in mid-plane sections as individual domains, but rather as a falsely homogeneous PM. However, advanced CLSM techniques like Total Internal Reflection Microscopy (TIRFM) or Variable Angle Epifluorescence Microscopy (VAEM) can overcome these limitations. This figure has been reused and adapted with permission from Ott (2017) (https://www.sciencedirect.com/journal/current-opinion-in-plant-biology; Copyright Elsevier). The panels with confocal images had previously been published in Jarsch et al. (2014) and have been reproduced with permission from Oxford University Press (www.plantcell.org; Copyright American Society of Plant Biologists) .

1.7 Nanodomain proteins and their characteristics

Multiple families of proteins are associated with and mark nanodomains, such as remorins (REMs), SPFH (Stomatin, Prohibitin, Flotillin and HflK/C family) proteins, tetraspanins, and GPI-anchored proteins (Jaillais and Ott, 2020; Magal et al., 2009; van Zanten et al., 2009). Although GPI-anchored proteins are often present within DRM and nanodomains (Borner et al., 2005; Demir et al., 2013; Kierszniowska et al., 2009; van Zanten et al., 2009), they themselves do not nucleate and form ordered membrane phase domains (Sevcsik et al., 2015). Individual chapters of this thesis introduce and focus on tetraspanins (chapter 4) and flotillins of the SPFH family (chapter 5). I will therefore only discuss the nanodomain localisations of REMs proteins in this general introduction.

Nanodomain and DRM resident proteins play important roles in elicitor detection and downstream signalling. For example, Lherminier et al. (2009) used transmission electron microscopy of *Nicotiana benthamiana* to demonstrate that cryptogein elicitor-triggered ROS bursts of H_2O_2 at the PM are produced in restricted areas of the PM reminiscent of nanodomains. They further show that antisense constructs of *NtRBOHD* abolished this clustered H_2O_2 production. Later Smokvarska et al. (2020) used Total internal reflection fluorescent microscopy (TIRF) to show *in vivo* localisation of RBOHD of Arabidopsis into nanodomains via photoactivatable fluorophore tagged RBOHD protein localisations, demonstrating that this important signalling component is present and capable of specific complex formations in nanodomains. These studies thereby demonstrated that important signalling proteins can be specifically enriched and functional in nanodomains.

Currently REMs are the best-characterised proteins in plants for their residency in nanodomains (Jaillais and Ott, 2020). The C-terminal anchor (CA) of REMs is a C-terminal lipid binding motif and targets REMs to the cytosolic leaflet of the PM (Gronnier et al., 2017; Konrad et al., 2014; Perraki et al., 2018). Oligomerisation has been proposed to be an important feature of nanodomain localised proteins (Legrand et al., 2019). For example, REMs are capable to oligomerise into trimers (Bariola et al., 2004; Perraki et al., 2012) — a feature important for their recruitment to the PM. Martinez et al. (2019) proposed that trimer-trimer interactions allow for the formation of higher order complexes, thereby allowing REMs a to play role in organising membrane nanodomains.

REMs are involved in a variety of different physiological processes such as in plant-microbe interactions, for example during defence responses against bacteria (Albers et al., 2019). They can also be targeted by pathogens themselves — for example the *N. benthamiana* REMORIN 4 (NbREM4) has been identified as the target of the *Pseudomonas syringae* HopZ1a effector. Different REMs have been shown to interact or be targets of virus encoded proteins. The potato *Solanum tuberosum* StREM1.3 has further been shown to interact with the TRIPLE GENE BLOCK PROTEIN1 of Potato virus X (PVX), and a change in StREM1.3 levels leads to changes in the cell-to-cell movement of this virus (Raffaele et al., 2009). PVX infections further trigger CDPKs to phosphorylate REM proteins, which again results in a restriction of the virus cell-to-cell movement (Perraki et al., 2018). The NSvc4 movement protein of Rice stripe virus (RSV) can bind to the C-terminal domain of *N. benthamiana* REMORIN1 (NbREM1), which abolishes the S-acylation of NbREM1 and thereby allows the virus to overcome host-plant REM-mediated inhibition of cell-to-cell movement (Fu et al., 2018).

Endogenous molecules can also regulate REM function. For example, treatment with Salicylic acid (SA) increases the lipid order as well as the diameter and intensity of nanodomains marked by REMORIN 1.2 (REM1.2), and results in the restriction of the plasmodesmal flux in Arabidopsis (Huang et al., 2019a). The increase in the lipid order triggered by exogeneous SA application is dampened in the double mutant *rem1.2/rem1.3c* which also shows an increased plasmodesmal aperture, while the overexpression of REM1.2 or REM1.3 causes a restriction of the cell-to-cell movement of modified tobacco rattle virus (TRV)-GFP (Huang et al., 2019a). Huang et al. (2019a) thereby demonstrated that the perception of a stimulus such as salicylic acid resulting in changes to plasmodesmata can be dependent on nanodomain localised proteins such as REMs. Many other changes to plasmodesmal flux caused by different stimuli may also be either directly or indirectly dependent on nanodomain defining proteins.

REMs have been found to interact with PRRs, and to be important for their function. Lefebvre et al. (2010) demonstrate that the *M. truncatula* SYMBIOTIC REMORIN 1 (MtSYMREM1) interacts with MtNFP and MtLYK3, which are essential for the perception of signalling molecules of symbiotic bacteria. Liang et al. (2018) later determined that induction of rhizobial infection is dependent on MtSYMREM1, as it is necessary for recruitment of ligand activated MtLYK3 and stabilises the PRR in nanodomains. In the absence of MtSYMREM1, MtLYK3 is destabilised at the PM and undergoes rapid endocytosis upon rhizobial infection, causing premature abortion of the host-cell-infection process (Liang et al., 2018). They

thereby demonstrated how a nanodomain defining protein — a REM — not only interacts with a PRR, but also enables the PRR to initiate signalling pathways after ligand perception. It will be interesting to see if other PRRs and nanodomain defining proteins exhibit similar dynamics to achieve their functions.

Plant hormone signalling can also be dependent on REMs. In rice (*Oryza sativa*) the REM OsREM4.1 can interact with SOMATIC EMBRYOGENESIS RECEPTOR KINASE (OsSERK1), and thereby inhibit the interaction and receptor complex formation between OsSERK1 and the LRR brassinosteroid (BR) receptor BRASSINOSTEROID-INSENSITIVE 1 (OsBRI1) (Gui et al., 2016). In the presence of BRs, OsBRI1 is capable of phosphorylating OsREM4.1, thereby reducing the binding affinity of OsREM4.1 to OsSERK1, which in turn allows for complex formation between OsBRI1 and OsSERK1 to initiate BR signalling (Gui et al., 2016). Gui et al. (2016) thereby demonstrated that a nanodomain defining protein, such as OsREM4.1, not only interacts with a RK, but also is important for the overall modulation of receptor complex dynamics.

REM-receptor interactions in nanodomains are involved in further processes such as key developmental pathways. Abel et al. (2021) demonstrate that the Arabidopsis RK REMORIN-INTERACTING RECEPTOR 1 (RIR1) is present in nanodomains and interacts with REM1.2. Double knockout mutants of *rir1* and its closest homologue *NEMATODE-INDUCED LRR-RLK 2* (*nilr2*), showed a similar dwarfed growth phenotype as rem1.1^{HET}/1.2^{HOM}/1.3^{HOM}/1.4^{HOM} plants, allowing for speculation that these proteins and their interactions might be important for the same signalling processes during plant development and growth (Abel et al., 2021).

Given how more and more evidence is emerging on individual nanodomain defining proteins, such as REMs (Abel et al., 2021; Gui et al., 2016; Lefebvre et al., 2010), interacting with individual PRRs and being important for their signalling functions, it will be interesting to see if this nanodomain dependence of PRR is a general theme or limited to individual proteins.

1.8 Organisation of nanodomains

Martinière and Zelazny (2021) define nanodomain formation and maintenance in plant cells as driven by the interaction of lipids and proteins, as well as by the cell wall/PM/cytoskeleton continuum. However, whether the formation of a nanodomain depends on an initial specific lipid environment which triggers the recruitment and interaction of proteins, or whether some proteins can actively cluster lipids to initiate nanodomain formation remains an open question (Martinière and Zelazny, 2021). Evidence for both the hypotheses of nanodomain formation have been shown in recent years. Platre et al. (2019) demonstrated that nanoclusters of phosphatidylserine (an anionic lipid) stabilise RHO-RELATED PROTEIN FROM PLANTS 6 (ROP6) in nanodomains during auxin perception. In rice the presence of sphingolipids containing 2-hydroxy fatty acids is necessary to enable the interaction of ROP RAC-LIKE GTP-BINDING PROTEIN1 (OsRAC1) with RESPIRATORY BURST OXIDASE HOMOGLOG PROTEIN B (OsRBOHB) in nanodomains enabling chitin-triggered ROS bursts (Nagano et al., 2016).

By contrast to this dependence of proteins on lipids for their presence in nanodomains, the opposite dynamic of lipid presence in nanodomains being dependent on and shaped by nanodomain-residing protein has been shown multiple times as well. For example, REMs have been shown to increase the level of ordered lipid domains (Huang et al., 2019a). Legrand et al. (2019) used solid-state nuclear magnetic resonance (NMR) to determine that the potato REM StREM1.3 not only influences lipid order in membranes, but also has an effect on membrane thickness. Animal SPFH family proteins have been proposed to actively participate in the formation of nanodomains as well, due to their ability to form multimeric complexes and to bind to sterols (Browman et al., 2007; Huber et al., 2006; Langhorst et al., 2005; Ma et al., 2022; Tatsuta et al., 2005). Tetraspanins can form multimeric complexes too, and their crystal structures revealed that they are also capable of binding lipids (Umeda et al., 2020; Zimmerman et al., 2016) making them another candidate protein family which may regulate the presence of lipids in nanodomains.

1.8.1 The cytoskeleton affects nanodomains

These examples show that it is possible that both lipids and proteins influence each other and are important for nanodomain formation and maintenance. However, not only the lipid and protein composition define nanodomains, but also their surroundings affect them. One of the most unified models for membrane organisation is the “picket and fence” model (Kusumi et al., 2005; Martinière and Zelazny, 2021). In this model, the cytoskeleton adjacent to the PM acts as a molecular “fence”, which constrains the diffusion of membrane proteins. In turn the cytoskeleton is anchored to the PM by more fixed transmembrane proteins, the “pickets”, thereby resulting in a reduced lateral diffusion of lipids and proteins, even in the outer PM leaflet (Kusumi et al., 2005; Ritchie et al., 2003).

Numerous studies in both animal and plant model systems have used different cytoskeleton disruptive drugs and showed that nanodomain behaviour and dynamics are dependent on cytoskeletal elements such as cortical actin and microtubules. Different proteins have been used as micro- and nanodomain markers to demonstrate this. Lv et al. (2017) used depolymerisation drugs and Variable-Angle Total Internal Reflection Fluorescence (VA-TIRF) microscopy imaging to demonstrate that HYPERSENSITIVE INDUCED REACTION 1 (HIR1) marked nanodomains are restricted and modulated in their density by the cortical cytoskeleton — with more dependence on microtubules than on actin filaments. By contrast, Liang et al. (2018) observed that treatment with the actin polymerisation inhibitor cytochalasin D caused a reduction in MtSYMREM1 nanodomain density in *M. truncatula* roots, while the destabilisation of microtubules triggered by oryzalin treatment did not affect MtSYMREM1 nanodomain density.

FLS2 is present in nanodomains and flg22 triggers a reduction in displacement of nanodomains which include FLS2 (Bücherl et al., 2017). McKenna et al. (2019) used single-particle tracking to determine changes in the behaviour of FLS2 and determined that both the cortical actin as well as the microtubule cytoskeleton limit the FLS2 marked nanodomain diffusion rates. Curiously, in the same experiment they also demonstrated that the PIN-FORMED 3 (PIN3) marked nanodomain diffusion rate is not limited by the presence of either actin or microtubules. They have thereby determined that different nanodomains might be differently constrained by the same “fence” cytoskeleton, possibly due to presence of different or less “picket” proteins in different nanodomains.

Despite hinderance of lateral mobility of nanodomains by actin or microtubules, the cytoskeleton is not directly affecting the nanodomain structural identity. Daněk et al. (2020)

demonstrated that even after treatment with oryzalin or latrunculin B (preventing actin polymerisation), the overall PM-associated nanodomain patterns of SPFH domain proteins persist. These studies have shown that the cytoskeleton does not initiate the formation nor maintenance of nanodomains. However, microtubules and actin fibres enhance PM compartmentalisation by the creation of “carrels”, which act as a “fence” restricting nanodomains in their lateral mobility. How these spatiotemporal restrictions affect the functional signalling capacity of nanodomain located proteins has yet to be unravelled.

1.8.2 Cell walls affect nanodomains

By contrast to animal cells, plant cells are embedded within comparably rigid cell wall structures — which contain among other components, cellulose, non-cellulosic, and pectic polysaccharides, proteins, phenolic compounds (Houston et al., 2016). These cell walls not only contain the cell, but also constrain lateral movement of proteins reaching from the PM into the extracellular matrix. Therefore, a similar concept as the “picket and fence” model of the cortical cytoskeleton affecting the PM protein lateral diffusion applies to the extracellular side of the PM in plant cells as well.

To study the effects of the plant cell wall on nanodomains, again a variety of different nanodomain resident proteins and approaches have been used. Martiniere et al. (2012) used Fluorescence recovery after photobleaching (FRAP) experiments to demonstrate that the absence of the cell wall in protoplasts or plasmolysed cells increases the lateral mobility of PM proteins. Detachment of the PM from the cell wall by plasmolysis is also capable of increasing the diffusion rates of other nanodomain residing proteins such as FLS2 and PIN3 (McKenna et al., 2019). Pharmacological inhibition of cell wall component synthesis using the cellulose synthase inhibitor 2,6-dichlorobenzonitrile (DeBolt et al., 2007) or with epigallocatechin gallate which inhibits pectin methylesterase (Wolf et al., 2012) also lead to a drastic increase in the diffusion rate and region length occupied by nanodomains of FLS2 and PIN3 (McKenna et al., 2019). Daněk et al. (2020) similarly demonstrated in PM detached from the cell wall by plasmolysis, SPFH family nanodomain proteins have an increased lateral mobility, and that this can even further be increased by enzymatically releasing the PM completely from the cell wall.

These studies demonstrated that not only the cytoskeleton restricts nanodomains in their dynamics in the PM, but that in plants the cell wall also influences those dynamics. The cell wall is capable of influencing the intracellular actin network (Tolmie et al., 2017), making a connection between those two sides of the PM likely. Consistent with the observations of

Sassmann et al. (2018), that there is a cytoskeletal-PM feedback loop, allowing for positional adjustments, McKenna et al. (2019) speculates that the components of the cytoskeleton/PM/cell wall as a continuum can regulate each other through proteins reaching from one side of the PM to the other. Nanodomains and their resident proteins would likely also be influenced by such transmembrane connections. Taken together, not only the cortical cytoskeleton, but also the cell wall affects the dynamic of nanodomains. Nonetheless, many questions regarding if and how this influences nanodomain resident proteins in their signalling capability remain.

1.8.3 Nanodomain residency of proteins can be affected by post-translational modifications

Different post-translational modifications (PTM) can have an impact on the localisation of specific proteins within nanodomains or outside of nanodomains. The attachment of a GPI anchor is a post-translational protein modification, in which a signal peptide (SP) is cleaved off and replaced by a GPI anchor (Beihammer et al., 2020; Strasser et al., 2005). Due to their preference of association with membrane components such as sterols and sphingolipids — which are often enriched in nanodomains — GPI-anchored proteins have been associated strongly with lipid rafts or nanodomains, depending on the nomenclature used (Arumugam et al., 2021; Cordy et al., 2003; Kenworthy et al., 2000; Kierszniowska et al., 2009; Tapken and Murphy, 2015; Trotter et al., 2000; van Zanten et al., 2009).

Protein S-acylation is a PTM, where a cysteine amino acid undergoes a covalent linkage with another molecule via a thioester bond. Commonly S-acylations tends to be an addition of long chain fatty acids. A named subtype of S-acylation is S-palmitoylation, where a hydrophobic 16 carbon lipid chain gets attached to the original protein (Forrester et al., 2011). S-acylation can enhance a proteins membrane affinity (Greaves et al., 2009; Shahinian and Silvius, 1995). Due to a preferred association with other hydrophobic membrane components such as sterols and different fatty acids — which are more likely to be present in ordered PM domains, S-acylation may enhance or be necessary for specific protein nanodomain localisations (Levental et al., 2010a; Levental et al., 2010b). Hemsley et al. (2013) identified 581 putatively S-acylated proteins in Arabidopsis, including some nanodomain resident proteins such as the SPFH family proteins HYPERSENSITIVE INDUCED REACTION (HIR) 1, 2 and 4, and members of the REM family such as REM1.2, REM1.3 as well as 23 RKs and RPs. Borner et al. (2005) further predicted a putative S-acylation site for FLOT1. More recently Kumar et al. (2022) identified 1,094 different Arabidopsis proteins with S-

acylation modified cystines. Taken together this information suggests that S-acylation is a common and potentially important PTM for nanodomain resident proteins.

S-acylation of REMs can contribute to their PM and nanodomain localisation. For example, for *N. benthamiana* NbREM1, S-acylation is necessary for its localisation in nanodomains, and without it, it is targeted to be degraded (Fu et al., 2018). By contrast, S-acylation of *M. truncatula* MtSYMREM1 is contributing to its membrane association but is dispensable for its micro-/nanodomain localisation (Konrad et al., 2014). Chen et al. (2021) demonstrated that the receptorP2K1 undergoes S-acylation, and that its nanodomain localisation is strongly dependent on this PTM. P2K1's phosphorylation status and degradation rates are further affected by this (Chen et al., 2021). Recently Hurst et al. (2021) showed that FLS2 populations undergo a rapid flg22-triggered S-acylation increase in a BAK1-dependent manner. They further showed that this PTM is essential for FLS2-mediated signalling during bacterial infections. These data suggest that PTMs influence nanodomain presence and retention time of proteins, which in turn might be important for a protein's ability to undergo specific complex formations and execute downstream signalling.

1.9 Protein activity in nanodomains

The localisation of a specific protein within or outside of a specific nanodomain may diminish or enhance the protein's activity. For example, a PRR could undergo oligomerisation in a nanodomain dependent way. This can either be due to active inclusion of the PRR with other proteins in the nanodomain, or by active release of important components for oligomerisation from the nanodomain (Fig. 1-2). Such as possibly in the case of the interaction between OsREM4.1 and OsSERK1 in rice as described above. The association of OsSERK1 with OsREM4.1 inhibits the interaction with OsBRI1. Only once OsSERK1 gets released from OsREM4.1, can it interact with OsBRI1 to efficiently initiate signalling (Gui et al., 2016). These interactions could either happen within the same nanodomain — defined by the presence of OsREM4.1 — or the initial interaction between OsSERK1 and OsREM4.1 is present in a nanodomain defined by the REM, and OsSERK1 gets "released" from this nanodomain to interact with OsBRI1. Gui et al. (2016) show data which suggest that the second option is more likely.

Alternatively, a protein could be actively excluded from nanodomains during resting-state conditions, but recruited into nanodomains after elicitor perception, where together with partner proteins it initiates signalling processes (Fig. 1-2B). A third way of how nanodomains may control protein activities could be by actively triggered merging or clustering of different nanodomains, allowing for an overlap of different protein populations only during specific circumstances (Fig. 1-2C). This could either result in domains of bigger sizes or lead to a reorganisation of components followed by subsequent separation. These different association possibilities of a specific protein may lead to different competitive binding or even PTM possibilities, resulting in further different stability, retention or recycling pathway dynamics.

Multiple different nanodomains can be present within the plant PM at the same time. For example, while the Arabidopsis BRI1 and FLS2 are both present in the PM in nanodomain clusters, they do not show a strong nanodomain overlap, suggesting spatiotemporal separation during resting state conditions (Bücherl et al., 2017). Further FLS2 shows a strong overlap with nanodomains defined by REM1.2 (Bücherl et al., 2017), while BRI1 showed an overlap with micro/-nanodomains defined by FLOT1 (Wang et al., 2015c). This multitude of different nanodomains allows for speculation that nanodomain fusion and separation on a dynamic or stable basis, might occur in response to elicitor perception.

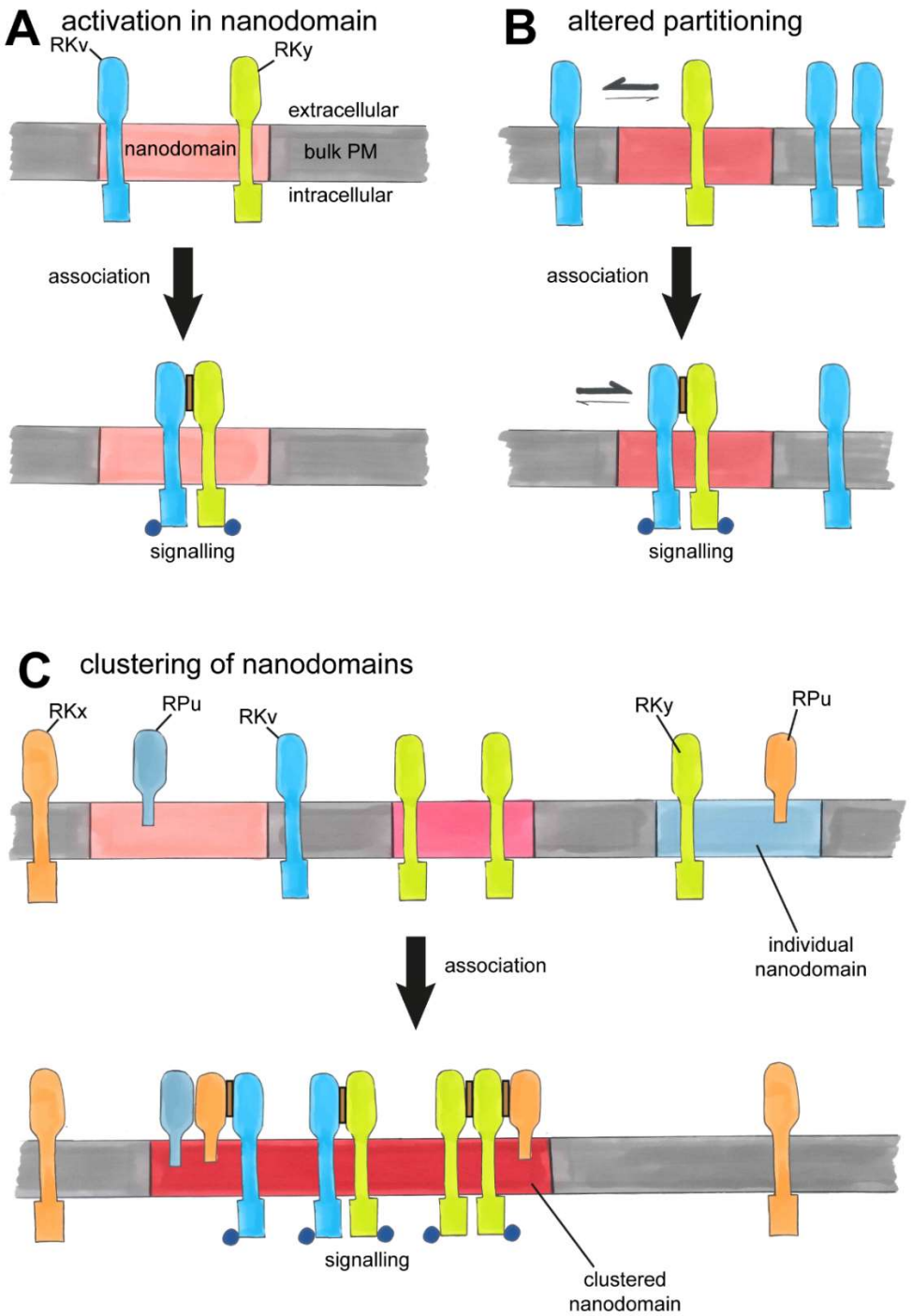

Figure 1-2: Example models of nanodomain partitioning and signal initiation. Different species of RKs and RPs are marked in different colours and labelled with different letters. (A) Both receptor partners are present in the same nanodomain during resting-state conditions, however they do not interact with each other. Upon ligand binding they interact and initiate downstream signalling. (B) The receptor partners are not present within the same nanodomain during resting state conditions. One RK (green) is located within the nanodomain, while other RK (blue) are preferentially excluded from the nanodomain. Upon ligand binding, the previously excluded RK, is now preferentially included in the nanodomain (blue) and can interact with the already nanodomain resident RK (green). (C) Individual nanodomains harbour specific compositions of different proteins. Upon ligand perception these nanodomains undergo dynamic fusion processes, allowing for interactions between the receptors which would otherwise not have been able to physically associate with each other. blue circles: phosphorylation activity symbolic of downstream signalling, RK: receptor kinase, RP: GPI-anchored receptor protein, PM: plasma membrane. Grey: bulk PM. Nanodomains are illustrated in different colours from the surrounding non-nanodomain PM (bulk PM). For illustration purposes nanodomains have been drawn with sharp boarders to the bulk PM, this may not reflect reality. This diagram is redrawn and adapted after Simons and Toomre (2000).

1.10 The plasmodesmal membrane microdomain

The compartmentalisation of multicellular organisms creates a need for efficient communication and exchange of molecules between cells, to coordinate individual and neighbouring cells. By contrast to animal cells, plant cells have an additional hurdle in these transport processes, as they are surrounded by rigid cell walls limiting direct exchange between cells. Plant cells therefore have developed connecting structures between adjacent cells — so called plasmodesmata. Plasmodesmata are membrane-lined bridges, which cross the cell walls of neighbouring cells, thereby connecting the cytoplasms and allowing for a cytoplasmic continuity within the plant (Fig. 1-3).

These plasmodesmata in turn can be seen as compartmentalisations of other cellular structures. For example, the desmotubule which traverses the cell wall inside of plasmodesmata is a continuation of the ER (Nicolas et al., 2017; Robards, 1968, 1971). However, by contrast to the rest of the ER, it is a tightly appressed form of the ER (Overall et al., 1982; Pérez-Sancho et al., 2016) associated with specialised proteins, such as the embedded transmembrane domains of members of the MULTIPLE C2 DOMAINS AND TRANSMEMBRANE REGION PROTEINS (MCTPs) family (Brault et al., 2019). The PM traversing the plasmodesmata is a specialised part of the PM and made up of a specific protein and lipid composition (Brault et al., 2019; Fernandez-Calvino et al., 2011; Grison et al., 2015a).

Plasmodesmata are important and tightly regulated during plant-microbe interactions. The flux between two adjacent cells is tightly regulated by the deposition and degradation of callose in the neck region of plasmodesmata (Benitez-Alfonso et al., 2013; Vatén et al., 2011). The presence of different pathogens, such as bacteria and fungi can be perceived by PRRs, such as flg22 by FLS2 and CALMODULIN-LIKE 41 (CML41) and chitin by LYSM DOMAIN GPI-ANCHORED PROTEIN 2 (LYM2), resulting in the closure of plasmodesmata, which in turn contributes to resistance against pathogens (Faulkner, 2013; Xu et al., 2017). The closure of plasmodesmata occurring simultaneously or triggered by active signalling pathways could have additional additive effects for signalling reactions or might be an independent way of establishing signalling feedback loops (Cheval and Faulkner, 2017). Lipids in the plasmodesmal microdomain.

The PM traversing the cell wall through plasmodesmata is a specialised subsection of the PM, and therefore a further cellular compartmentalisation structure. The plasmodesmal PM

is made up of a special lipid and protein composition — this allows its conceptualisation as a special microdomain (Jaillais and Ott, 2020; Ott, 2017; Tilsner et al., 2011). Analyses of "native" plasmodesmal membrane fractions showed that plasmodesmata are enriched in very-long chain saturated GIPC sphingolipids and sterols in comparison to the bulk of the PM (Grison et al., 2015a; Grison et al., 2015b). This composition is reminiscent of the composition of DRMs or nanodomains within the non-plasmodesmal PM (Cacas et al., 2016), strengthening the hypothesis that plasmodesmal membranes are specialised microdomains.

The GPI-anchored proteins PLASMODESMATA CALLOSE-BINDING PROTEIN 1 (PDCB1) and the ß-1,3-glucanase PdBG2 (AT2G01630) localise to the PM, and are enriched at the plasmodesmal PM in resting-state conditions (Benitez-Alfonso et al., 2013; Grison et al., 2015a; Simpson et al., 2009). Grison et al. (2015a) demonstrate that disruption of the membrane sterol content causes these proteins to lose their plasmodesmata enrichment. These changes of lipid composition by treatment with pharmacological inhibitors acting at different steps in the biosynthesis pathway of sterols — fenpropimorph (Hartmann et al., 2002) and lovastatin (Vögeli and Chappell, 1991) — further altered the callose-mediated plasmodesmal permeability (Grison et al., 2015a). Whether this change of plasmodesmal flux is directly due to changes in the sterol concentration affecting callose deposition, or indirectly by affecting plasmodesmal proteins which in turn modulate callose deposition, remains unclear. However, these experiments demonstrated that the lipid composition of the plasmodesmal PM microdomain may contribute to the specific recruitment of proteins, as well as to the regulation of plasmodesmata.

Recently Grison et al. (2019) showed that QIĀN SHǑU KINASE 1 (QSK1) and INFLORESCENCE MERISTEM KINASE2 (IMK2) are enriched at plasmodesmata and enhance their plasmodesmal localisation in comparison to rest of the PM within minutes when triggered by environmental stimuli (Grison et al., 2019). Hunter et al. (2019) observed a similar behaviour for CYS-RICH RECEPTOR KINASE 2 (CRK2) induced by salt stress, and we observed the same response for LYM2 when induced by chitin (Cheval et al., 2020). Therefore the plasmodesmal protein composition is able to undergo rapid changes and adaptations depending on environmental triggers. However, whether this stimuli-triggered plasmodesmal localisation enhancement is a general mechanism and pattern which other proteins follow too, still needs to be elucidated. Further whether the plasmodesmal PM can undergo changes to its lipid composition in a similar time frame is still not known.

1.11 Proteins in the plasmodesmal microdomain

Plasmodesmata represent a highly specialised interface and are responsible for controlling very specific signalling and communication processes (Otero et al., 2016; Sager and Lee, 2014; Sevilem et al., 2015; Stahl and Faulkner, 2016). The modulation of plasmodesmal flux has been shown to be tightly controlled particularly during stress responses, pathogen infections, growth and development (Faulkner et al., 2013; Liu et al., 2022; Xu et al., 2017; Yadav et al., 2014).

To finely tune and, spatially and temporally regulate plasmodesmal functions, the plasmodesmal PM microdomain contains a variety of specific sets of proteins (Nicolas et al., 2017). If the presence of a protein is enriched at plasmodesmata in comparison to the protein's presence in the PM, this can be assessed by determining a fluorescence intensity ratio between these two localisations and is referred to as a plasmodesmal index (Brault et al., 2019; Grison et al., 2019). Different RKs and RPs have been determined to be enriched at plasmodesmata via translational fusion constructs with fluorophores using CLSM, such as the flg22 receptor FLS2 and CML41 (Cheval et al., 2020; Thor et al., 2020), as well as the chitin receptor protein LYM2 (Faulkner et al., 2013), where both MAMPs triggering localised plasmodesmal responses (Cheval et al., 2020; Xu et al., 2017). Other RK such as STRUBBELIG (SUB), which modulates inter-cell layer signalling during tissue morphogenesis, also localise to plasmodesmata (Vaddepalli et al., 2014). The RKs CLAVATA1 (CLV1) and ARABIDOPSIS CRINKLY4 (ACR4) are enriched at plasmodesmata and show an enhanced interaction with each other in the plasmodesmal PM (Stahl et al., 2013). Activated by the peptide ligand CLAVATA3/EMBRYO SURROUNDING REGION40 (CLE40) they control and restrict root stemness (Stahl et al., 2013).

Multiple members of the REM family, which has been discussed in detail above, are enriched at plasmodesmata and have been shown to be important for plasmodesmal modification and adaptations. For example the potato StREM1.3 is present at plasmodesmata and capable of reducing the virus propagation of PVX through plasmodesmata (Raffaele et al., 2009). Perraki et al. (2018) similarly determined that the *N. benthamiana* NbREM1.3 is present at plasmodesmata, and that NbREM1.3, as well as Arabidopsis REM1.2 and REM1.3 limit the cell-to-cell spread of PVX. Arabidopsis REM1.2 and REM1.3 were further detected at plasmodesmata using transmission electron microscopy, and their presence was shown

to influence plasmodesmal aperture compared to wild type (WT) plants, particularly triggered by SA, and can restrict plasmodesmal TRV spread (Huang et al., 2019a).

The plasmodesmal PM microdomain further contains specific callose-modifying enzymes, which allow for additional callose deposition as well as callose degradation in the plasmodesmal neck region to regulate plasmodesmal flux (Benitez-Alfonso et al., 2013; Vatén et al., 2011). Callose synthases such as GLUCAN SYNTHASE-LIKE 8 (GSL8) and CALLOSE SYNTHASE 3 (CALS3) (also referred to as GLUCAN SYNTHASE-LIKE 12) are required for callose synthesis and deposition, which restricts plasmodesmal flux (Guseman et al., 2010; Vatén et al., 2011). By contrast, plasmodesmal ß-1,3-glucanases degrade and remove callose, thereby allowing for an increase of plasmodesmal flux (Benitez-Alfonso et al., 2013; Levy et al., 2007a). Other plasmodesmal localised proteins such as PLASMODESMATA CALLOSE-BINDING PROTEIN 1 (PDCB 1) are further capable of binding and regulating callose at plasmodesmata, although the mechanism by which this is regulated and how it contributes to plasmodesmal functions is unclear (Simpson et al., 2009).

Another indicator of the special composition of the plasmodesmal PM microdomain is not just that specific proteins are enriched there, but rather that specific other proteins are excluded from this domain. A plasmodesmal exclusion has been observed for the PM proton pump of *Mimosa pudica* H^+-ATPASE 2 (MpPMA2) (Fleurat-Lessard et al., 1995), the aquaporin PLASMA MEMBRANE INTRINSIC PROTEIN 2 (PIP2), as well as the cellulose synthase subunits CELLULOSE SYNTHASE 3 (CESA3) and CESA6 (Grison et al., 2015a).

The plasmodesmal PM microdomain is therefore evidently a special sub-compartmentalisation of the PM. However, even within the plasmodesmal PM microdomain further levels or sub-compartmentalisations are possible, from individual nanodomains to regional domains (Fig. 1-3). These separations might share a bulk of their characteristics, making them all part of the overarching plasmodesmal PM microdomain, but individual evidence suggests that there are differentiations within this microdomain. For example, PDCB1 localises precisely at the neck region of plasmodesmata (Simpson et al., 2009) — which is where the bulk of plasmodesmal callose is present — and thereby modulates the plasmodesmal flux (Hughes and Gunning, 1980; Levy et al., 2007a; Levy et al., 2007b). By contrast to the neck localisation, is the preferential clustering of PLASMODESMATA-LOCATED PROTEIN 1 (PDLP1) inside of the plasmodesmal pore (Maule et al., 2011), which is also capable of reducing the plasmodesmal flux (Thomas et al., 2008).

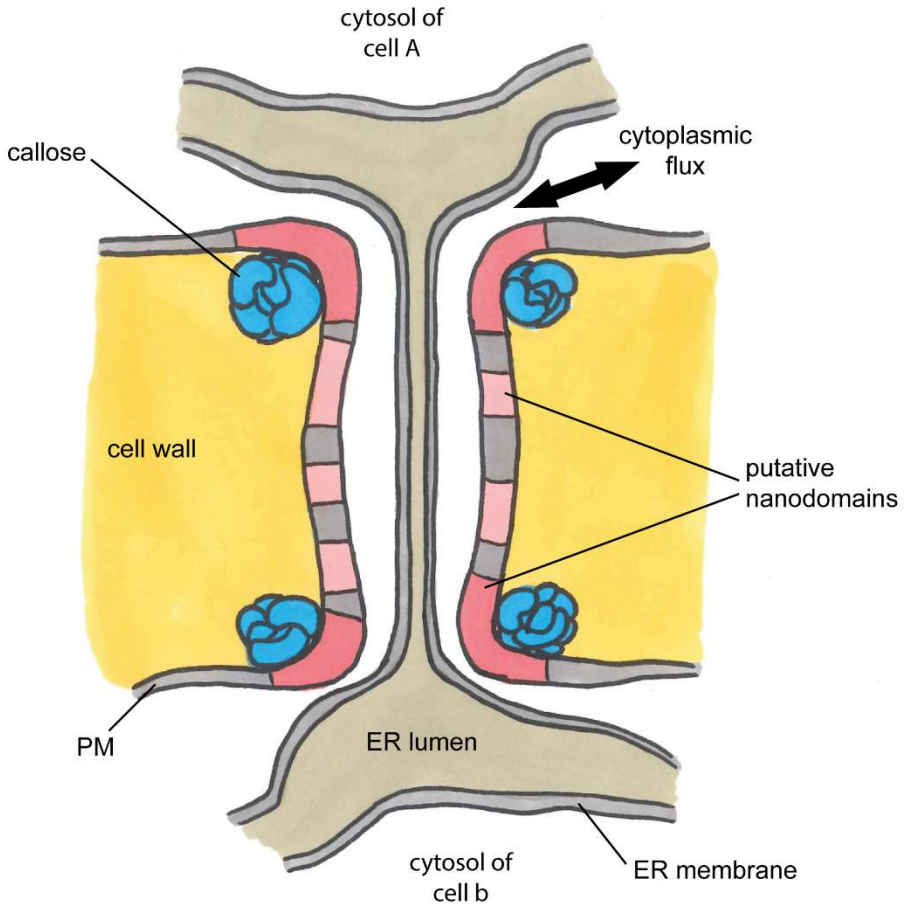

Figure 1-3: Model of plasmodesmal microdomain compartmentalisation within a single plasmodesmata. The possibility for different and multiple nanodomains within the plasmodesmal PM microdomain is drawn in different pink tones. Putatively there should be at least different nanodomains between the callose rich neck regions and the pore lumen regions. PM: plasma membrane, ER: endoplasmic reticulum, This diagram is redrawn and adapted from Maule et al. (2011).

Although some components of the plasmodesmal PM microdomain have already been successfully identified and characterised, there are still a lot of putative components which have not yet been studied in detail (Brault et al., 2019; Kirk et al., 2021), and many questions about plasmodesmata are still unanswered and unclear. How is this specialisation of the plasmodesmal PM microdomain initiated and how is it maintained? Could plasmodesmata membrane identity be keyed to a particular set of “picket and fence” conditions? The composition of biopolymers in the cell wall surrounding plasmodesmata is different from the rest of the bulk of the cell wall — adjacent to plasmodesmata the cell wall is enriched in callose (Fitzgibbon et al., 2010; Turner et al., 1994) and contains a distinct pectin composition (Faulkner et al., 2008; Giannoutsou et al., 2013; Knox and Benitez-Alfonso, 2014; Orfila and Knox, 2000; Roy et al., 1997). The desmotubule is a specialised continuation of the ER (Overall and Blackman, 1996), while the protein and lipid composition of the plasmodesmal PM microdomain differ from the bulk of the PM as well (Brault et al., 2019). Could it be an interplay between a specialised ER compartmentalisation (the desmotubule), a specialised

biopolymer composition surrounding the plasmodesmal cell wall and the specialised protein and lipid composition of the plasmodesmal PM microdomain which all affect and maintain each other?

Many individual threads of evidence point towards the compartmentalisation of the plasmodesmal PM microdomain, in comparison to the rest of the PM, being an important aspect of plasmodesmata. However, many details and facets of its dynamics and characteristics are still unknown. For example, what is the composition of individual nanodomains necessary for enabling efficient signalling processes at plasmodesmata? To understand how protein and lipid composition of the plasmodesmal PM microdomain is established and maintained, it would be of particular interest to understand if and which individual proteins are responsible for these processes, as well as to determine their mechanisms. Given that various RKs and RPs are important for plasmodesmal regulation, the mechanism by which they localise to plasmodesmata could be vital for adjusting the cell-to-cell flux depending on abiotic and biotic stimuli. Could specific nanodomain resident proteins interact with the RKs and RPs, and thereby enable their functions?

1.12 Aims and objectives of this thesis

The RP LYM2 localises to plasmodesmata and is necessary for chitin-triggered plasmodesmal closure. We identified two RKs —LYK4 and LYK5 — which are also required for this process (Cheval et al., 2020). The first main aim of this thesis was to determine if these RKs and LYM2 form signalling complex(es) which are necessary for chitin-triggered regulation at the plasmodesmal PM microdomain, as well as how these proteins' dynamics might be different depending on chitin at the plasmodesmal PM microdomain versus rest of the PM.

Members of the tetraspanin family have been shown to be present at plasmodesmata and to be important during fungal infections. As membrane domain maintaining proteins capable of interacting with other membrane proteins, they are good candidates for domain proteins which recruit specialised machinery to plasmodesmata to execute localised responses. I hypothesise that tetraspanins interact and recruit chitin perceiving receptors in plants and explored their role in plasmodesmal and cellular responses to chitin.

To identify novel membrane domain components of plasmodesmata, I used an unbiased, immunoprecipitation and mass spectrometry approach, using LYK4 as a bait. With this, I aimed to populate our understanding of the membrane domains resident proteins in plasmodesmata that are functionally relevant for chitin-triggered plasmodesmal responses.

Thus, the overarching aim of this thesis was to identify and characterise novel protein components necessary for plasmodesmal modulation during plant-microbe interactions.

2 Materials and Methods

2.1 Plant growth

2.1.1 Arabidopsis seed sterilisation

Arabidopsis seeds were placed in an exicator, together with a glass beaker containing 100 mL Sodium hypochlorite (Purum ~10%, Merck). Chlorine gas was produced by addition of 3 mL HCl (37%) before immediately closing the exicator. The seeds were exposed to the chlorine gas overnight, for a maximum of 14 h.

2.1.2 Selection of Arabidopsis transgenics

After sterilisation, T1 seeds were sown on MS plates (4.41 mg/mL Murashige & Skoog Medium Including Vitamins (Duchefa), 10 mg/mL Sucrose (Fisher), 0.8 mg/mL agar (Formedium)), together with the appropriate selective antibiotic (50 ng/mL Kanamycin, or 10 ng/mL Phosphinothricin (Basta)) and sealed with micropore tape. Plates were stratified in the dark at 4°C for three days, before being placed in a controlled environment room (CER) with 16 h light/8h dark cycles at 20°C.

2.1.3 Arabidopsis growth (soil)

Threshed Arabidopsis seeds were stratified at 4°C in centrifuge tubes without the addition of liquids for two- to four-days in the dark, before sowing individual seeds directly onto soil (90% peat, 10% grit, 4 kg/m^3 dolomitic limestone, 1.2 kg/m^3 osmocote start (ICL)). Arabidopsis plants grown for seed collection purposes were grown in a CER with 'long day' conditions (16 h light at 22°C/8h dark at 20°C). CERs were fitted with Philips 58W fluorescent tubes and two gro-lux tubes per shelf, resulting in a light level at plant hight of roughly 230 µmol m^{-2} s^{-1}, constant relative humidity at 80%. Plants for experiments were grown in Versatile Environmental Test Chambers MLR-352-PE (PHCbi) equipped with six LED T8 colour temperature 4000 K (Newlec) and nine LED T8 colour temperature 6500 K (Newlec) light tubes under 'short day' conditions (10 h light/14 h dark, consistent 22°C).

Table 2-1: Arabidopsis lines used in this work. All Arabidopsis lines used in this work were of the Ecotype Columbia-0 (Col-0). All plant lines with an introduced construct, have their origin in this work. NASC: Nottingham Arabidopsis Stock Centre; nptII: Kanamycin; bar: Basta/PPT; sul: Sulfadiazin.

Line name	Background	NASC number	Line explanation, or introduced construct	Plant resistance cassette
Col-0			Columbia, wild type (WT)	
lyk4	WiscDsLox 297300_01C	N850683	*lyk4* mutant, described in Wan et al. (2012) provided by Gary Stacey	Basta
lyk5-2	SALK_131911C	N631911	*lyk5-2* mutant, described in Cao et al. (2014) provided by Gary Stacey	Kanamycin
	lyk4		*pLYK4::LYK4-mCherry*	Kanamycin (+Basta)
	lyk5-2		*pLYK5::LYK5-turboID-3xFLAG*	Kanamycin
	lyk4		*pLYK4::LYK4-mClover3-3xFLAG_ pAtAct2::TET7-mRuby3-6xHA*	Kanamycin (+Basta)
	lyk4		*pLYK4::LYK4-mClover3-3xFLAG_ pAtAct2::TET8-mRuby3-6xHA*	Kanamycin (+Basta)
tet3	SALK_116766	N616766	*tet3* mutant	Kanamycin
tet7	SALK_205244C	N694330	*tet7* mutant	Kanamycin
tet8	SALK_136039C	N636039	*tet8* mutant, described in Reimann et al. (2017) and Cai et al. (2018)	Kanamycin
	lyk4		*pLYK4::LYK4-mClover3-3xFLAG_ pAtAct2::TET3-mRuby3-6xHA*	Kanamycin (+Basta)
	lyk4		*pLYK4::LYK4-mClover3-3xFLAG_ pAtAct2::FLOT1-mRuby3-6xHA*	Kanamycin (+Basta)
	lyk4		*pLYK4::LYK4-mClover3-3xFLAG_ pAtAct2::FLOT2-mRuby3-6xHA*	Kanamycin (+Basta)
flot1	SALK_203966C	N692506	*flot1* mutant, described in Kroumanova et al. (2019)	Kanamycin
flot2	GK-430C05	N2109061	*flot2* mutant	Sulfadiazin
flot3	SALK_143325C	N669186	*flot3* mutant, described in Kroumanova et al. (2019)	Kanamycin

2.1.4 *Nicotiana benthamiana* growth

Nicotiana benthamiana was grown on soil (100% peat, 4 kg/m^3 dolomitic limestone, 1.2 kg/m^3 osmocote start (ICL)) in a CER at a light intensity of roughly 200-230 µmol/m^2/s, a relative humidity of 85% and a constant temperature at 22°C, at 16h light/8h dark cycles (fitted with Philips 58W fluorescent tubes and two gro-lux tubes per shelf), for four weeks before *Agrobacterium* infiltration.

2.2 Microscopy based techniques

Leaves were cut into roughly 1.5 × 1.5 cm samples and mounted adaxially upwards facing on a slide with double-sided sticky tape. Unless otherwise stated, samples were imaged using a ZEISS LSM800 CLSM equipped with W "N-Achroplan" 20×/0.5 water dipper lens, Plan Apochromat 40×/1.0 water dipper, VIS-IR 63×/1.0 water dipper, C-APOCHROMAT 63×/1.2 water immersion lens objectives. Unless stated otherwise eGFP, mCitrine, and mClover3 constructs were excited at 488 nm with an argon laser and emission was collected at 500 - 546 nm. mCherry, mRFP1, mRuby3 constructs were excited at 561 nm with a DPSS laser, and emission collected at 590 – 617 nm. Aniline blue was excited at 405 nm with an UV light laser and the emission collected at 430 – 485 nm.

2.2.1 Callose staining of *N. benthamiana*

Callose staining was performed using 0.1% aniline blue (Sigma-Aldrich-415049) in 1×PBS (phosphate buffered saline), pH 7.4. Fully expanded *N. benthamiana* leaves of four-week-old plants were syringe-infiltrated with aniline blue two days after *Agrobacterium* infiltration, immediately before imaging for co-localisation experiments.

2.2.2 Callose quantification in Arabidopsis

Mature individual Arabidopsis leaves of four- to six-week-old plants, were cut, and syringe-infiltrated with 0.01% Silwet L-77 (De Sangosse) with 0.5 mg/mL chitin (mixture of chitin oligosaccharides, NaCoSy, Yaizu Suisankagaku) or mock (0.01% Silwet L-77 in water) and placed for 30 min. on MS (4.41 mg/mL Murashige & Skoog Medium Including Vitamins [Duchefa M0222], 1% Sucrose [Fisher S/8600/60], 0.6% agar [Formedium]) plates with their petioles inserted into the agar to reduce the stress on the leaf. After mounting half of the leaf with the adaxial side up, to a slide with double-sided sticky tape, a droplet of 1% aniline blue (in 1×PBS) was deposited onto the leaf surface. After two minutes the droplet was removed, a droplet of water followed by a coverslip was gently placed onto the leaf, and the callose deposits between epidermal cells were imaged as z-stacks. To ensure comparability, the image acquisition settings were tested in multiple different sites before determining the best acquisition settings for laser intensity and gain to ensure capture of the whole bandwidth of fluorescence intensity detection. From then onwards only the exact same settings were used for the rest of the experiment. For each genotype and treatment five leaves, with two sites per fully-extended leaf of four to six week old Arabidopsis plants, were imaged. Aniline blue was excited using a 405 nm UV-light laser, at 3.5% power. Z-stacks were set to 8-12 slices per stack and an interval between slices of 1 µm was kept constant within

the experiment. Images were collected with image size 1024 × 1024 pixels, 16 bit depth and 4 line averaging.

Aniline blue signal at plasmodesmata was quantified in Fiji (Schindelin et al., 2012) using macros developed by Annalisa Bellandi and Matthew Johnston. First the macro converts the image to binary grayscale, using a user-defined experimental-specific threshold, using the 'convert tomask' command. I used 20 000 as a threshold consistently throughout my experiments. The threshold was chosen to ensure the optimal recognition of plasmodesmata at the cell periphery while keeping the noise and background signals to a minimum. The 'analyse particles' command determined the number of particles in the image which fit the criteria of a set minimum and maximum size, which is again experiment-specific and user-defined. I defined my minimum size as 10, and the maximum size as 450, and kept them consistent throughout my experiments. I set those criteria ensuring that spots of signal which were not plasmodesmata, but made it through the previous thresholding process, were not included in the further analysis. The 'analyse particles' command was then used to extract the number of particles, size and integrated density (the sum of all the pixel intensities). These data were then further analysed in R (R Core Team, 2021) using a script developed by Matthew Johnston and adapted by Annalisa Bellandi (https://github.com/faulknerfalcons/PD_detection). The summary of plasmodesmata measurements obtained included the mean number, size, and integrated density of all the detected particles per z-stack. The mean integrated density was used for further statistical analysis. This is the mean total intensity of aniline blue staining signal per plasmodesmata in each z-stack, which as aniline blue stains callose, correlates to the levels of callose at each detected plasmodesma. Statistical analysis for comparisons between treatments of the same genotype were carried out using the Wilcoxon signed-rank test.

2.2.3 Quantification of the plasmodesmal Index

Fully expanded leaves of four-week-old *N. benthamiana* plants were syringe-infiltrated with either 0.5 mg/mL chitin or water (mock), while still attached to the plant, three days after infiltration with *Agrobacterium* carrying constructs to express *pAtAct2::TET3-mRuby3-6×HA*, *pAtAct2::TET8-mRuby3-6×HA*, *pAtAct2::TET8-mRuby3-6×HA*. The petiole was cut 30 min. later, and the same areas were infiltrated with 0.5 mg/mL chitin in 0.1% aniline blue (in 1×PBS) or just 0.1% aniline blue (in 1×PBS, mock). 10 z-stacks per leaf and treatment were acquired, with 10 slices at 1.89 µm distance each, 4×line averaging and 16 bits per pixel. Both the fluorescence of the tetraspanin constructs as well as of aniline blue were acquired. Three experimental repeats with independent transient *N. benthamiana* transformations were carried out.

Using ImageJ (Schindelin et al., 2012) each z-stack was z-projected, and a script was used to define 49 equally sized square boxes in every projection. In every box, the plasmodesmata marked by the aniline blue channel, the closest to the centre was chosen to be measured. A region of interest (ROI) was drawn by hand using the polygon tool around the plasmodesmata and a second region of interest was drawn around the PM close by the plasmodesmata. If a box did not have a clearly distinguishable plasmodesmata by aniline blue staining, no measurement was taken from within that box. Both ROIs were measured for their mean grey value of the mRuby3 signal. The mean grey value of each plasmodesmal ROI was divided by the mean grey value of the PM ROI to result in the plasmodesmal index of an individual plasmodesmata. The mean of all the plasmodesmal indexes from plasmodesmata selected from the same images was calculated and this individual value per z-stack was used for further statistical analysis using a Wilcoxon signed-rank test.

2.2.4 Pearson correlation for protein correlation quantification

The Pearson correlation coefficient analysis to quantify the correlation between two different fluorescently tagged membrane proteins has been carried out in Fiji (Schindelin et al., 2012) using the JACoP plugin (Bolte and Cordeliéres, 2006). Regions which showed additional fluorescence possibly from underlying structures such as chloroplasts were excluded from the image analysis. The Pearson's coefficient was determined for every image individually using Costes' automatic threshold. One value was returned per image and used for further statistical analysis. Statistical analysis to compare between different treatments was carried out using the Mann-Whitney-Wilcoxon test.

2.3 Bacterial strains

Escherichia coli DH5α cells were used for all basic molecular biology, apart from the assembly and propagation of level 2 golden gate constructs where I used DH10B cells. *Agrobacterium tumefaciens* (referred to as *Agrobacterium* in this thesis) strain GV3101 was used for all Arabidopsis transformations as well as *N. benthamiana* transient expressions.

2.4 Cloning

Golden Gate cloning (Engler et al., 2014) was used to generate the plasmids used in this work. I used the following pipeline to generate level 0 constructs. The fragment of interest was amplified from gDNA or cDNA using PCR (utilising Phusion® high fidelity polymerase; New England Biolabs), separated via electrophoresis in a 1% agarose gel (with 0.5 µg/mL ethidium bromide). The gel was visualised using a UV transilluminator and the band corresponding to the expected size was removed from the gel using a fresh razor blade. I extracted the DNA fragment from the gel using the QIAquick® Gel Extraction kit (QIAGEN) and protocol. The purified DNA fragment was inserted into the appropriate plasmid backbone together with the following components: 100-200 ng of acceptor plasmid in a 3:1 molar ratio of insert(s):acceptor, 1 µL T4 Ligase buffer (New England Biolabs), 1 µL Bovine Serum Albumin (10×), 0.25 µL BpiI (New England Biolabs), 0.25 µL T4 Ligase (400U/µL) (New England Biolabs), in a total volume of 10 µL. For the assembly of level 1 and level 2 plasmids, I used the following components: 1 µL of every lower-level plasmid at 100 ng/µL, 2 µL T4 Ligase buffer (New England Biolabs), 2 µL Bovine Serum Albumin (10×), 0.5 µL BpiI (New England Biolabs) or BsaI (Thermo Scientific), 0.5 µL T4 Ligase (400U/µL) (New England Biolabs), in a total volume of 20 µL.

Golden gate expression constructs (Table 2-2) were assembled using the components detailed in Table 2-3, which in turn were generated with the primers listed in Table 2-5. Expression constructs

Table 2-2: Golden gate expression constructs used in this work.

Name	Description	Assembled from
FP09017	*35s::mCherry-LYK4-mCitrine*	pICSL86900OD + pICH41388 + FP09005 + FP09008 + AGGT-LYK4-TTCG + FP09009 + EC15320
FP09018	*35s::mCherry-LYK5-mCitrine*	pICSL86900OD + pICH41388 + FP09010 + FP09008 + FP09011 + FP09009 + EC15320
FP09037	*pLYK4::SP$_{LYK4}$-LYK4-mCherry*	pICSL86900OD + FP09033 + FP09005 + FP09035 + pICSL50004 + EC15320
FP09038	*pLYK5::SP$_{LYK5}$-LYK5-mCherry*	pICSL86900OD + FP09034 + FP09010 + FP09036 + pICSL50004 + EC15320
FP09039	*AtAct2::TET3-mCherry*	pICSL86900OD + pICH87644 + FP09030 + pICSL50004 + EC15320
FP09040	*AtAct2::TET7-mCherry*	pICSL86900OD + pICH87644 + FP09031 + pICSL50004 + EC15320
FP09041	*AtAct2::TET8-mCherry*	pICSL86900OD + pICH87644 + FP09032 + pICSL50004 + EC15320
FP09049	*35s::LTI6b-6×HA*	pICSL86900OD + pICH51277 + FP09047 + pICSL50009 + EC15320
FP09056	*35s::LYK4-6×HA*	pICSL86900OD + pICH41388 + FP09005 + FP09035 + pICSL50009 + EC15320
FP09057	*35s::LYK5-6×HA*	pICSL86900OD + pICH41388 + FP09010 + FP09036 + pICSL50009 + EC15320
FP09063	*pLYK5::LYK5-turboID-3×FLAG*	pICSL86900OD + FP09034 + FP09010 + FP09036 + pICSL50040 + EC15320
FP09084	*35s::TET3-mTurq2*	pICSL86900OD + pICH51277 + FP09030 + FP09004 + EC15320
FP09085	*35s::TET7-mTurq2*	pICSL86900OD + pICH51277 + FP09031 + FP09004 + EC15320
FP09086	*35s::TET8-mTurq2*	pICSL86900OD + pICH51277 + FP09032 + FP09004 + EC15320
FP09088	*35s::LYK4-Clover3-3×FLAG*	pICSL86900OD + pICH41388 + FP09005 + FP09035 + FP09079 + EC15320
FP09089	*pAtAct2::TET7-mRuby3-6×HA*	pICSL86900OD + pICH50581 + FP09031 + FP09080 + pICH44300
FP09091	*Position2F_pLYK4::LYK4-mClover3-3×FLAG*	pICH47742 + FP09033 + FP09005 + FP09035 + FP09079 + EC15320
FP09092	*Position3F_pAtAct2::TET3-mRuby3-6×HA*	pICH47751 + pICH87644 + FP09030 + FP09080 + pICH44300
FP09093	*Position3F_pAtAct2::TET7-mRuby3-6×HA*	pICH47751 + pICH87644 + FP09031 + FP09080 + pICH44300
FP09094	*Position3F_pAtAct2::TET8-mRuby3-6×HA*	pICH47751 + pICH87644 + FP09032 + FP09080 + pICH44300
FP09095	*Position3F_pAtAct2::LTi6b-mRuby3-6×HA*	pICH47751 + pICH87644 + FP09047 + FP09080 + pICH44300
FP09096	*Position3F_pLYK5::LYK5-mRuby3-6×HA*	pICH47751 + pICH50581 + FP0910 + FP09036 + FP09080 + pICH44300
FP09099	*pLYK4::LYK4-mClover3-3xFLAG_and_pAtAct2::TET3-mRuby3-6×HA*	pICSL4723 + pICSL31853 + FP09091 + FP09092 + pICH41766
FP09100	*pLYK4::LYK4-mClover3-3×FLAG_ pAtAct2::TET7-mRuby3-6×HA*	pICSL4723 + pICSL31853 + FP09091 + FP09093 + pICH41766
FP09101	*pLYK4::LYK4-mClover3-3×FLAG_ pAtAct2::TET8-mRuby3-6×HA*	pICSL4723 + pICSL31853 + FP09091 + FP09094 + pICH41766
FP09102	*pLYK4::LYK4-mClover3-3×FLAG_ pAtAct2::LTi6b-mRuby3-6×HA*	pICSL4723 + pICSL31853 + FP09091 + FP09095 + pICH41766
FP09103	*pLYK4::LYK4-mClover3-3×FLAG_ pLYK5::LYK5-mRuby3-6×HA*	pICSL4723 + pICSL31853 + FP09091 + FP09096 + pICH41766
FP09107	*Position2F_pLYK5::LYK5-mClover3-3×FLAG*	pICH47742 + FP09034 + FP09010 + FP09036 + FP09079 + EC15320

FP09108	*Position3F_pAtAct2::FLOT1-mRuby3-6×HA*	pICH47751 + pICH87644 + FP09104 + FP09080 + pICH44300
FP09110	*Position3F_pAtAct2::FLOT2-mRuby3-6×HA*	pICH47751 + pICH87644 + FP09097 + FP09080 + pICH44300
FP09113	*pLYK4::LYK4-mClover3-3×FLAG_and_pAtAct2::FLOT1-mRuby3-6×HA*	pICSL4723 + pICSL31853 + FP09091 + FP09108 + pICH41766
FP09114	*pLYK4::LYK4-mClover3-3×FLAG_and_pAtAct2::FLOT2-mRuby3-6×HA*	pICSL4723 + pICSL31853 + FP09091 + FP09110 + pICH41766
FP09115	*pLYK5::LYK5-mClover3-3×FLAG*	pICSL4723 + pICSL31853 + FP09107 + pICH41744
FP09116	*pLYK5::LYK5-mClover3-3×FLAG_and_pAtAct2::FLOT1-mRuby3-6×HA*	pICSL4723 + pICSL31853 + FP09107 + FP09108 + pICH41766
FP09117	*pLYK5::LYK5-mClover3-3×FLAG_and_pAtAct2::FLOT2-mRuby3-6×HA*	pICSL4723 + pICSL31853 + FP09107 + FP09110 + pICH41766
FP09118	*pLYK4::LYK4-mClover3-3×FLAG*	pICSL4723 + pICSL31853 + FP09091 + pICH41744
FP09123	*p35s::FLOT1-mRuby3-6×HA*	pICSL86900OD + pICH51266 + FP09104 + FP09080 + EC15320
FP09128	*pAtAct2::LTi6b-mRuby3-6×HA-TerAtAct2*	pICSL86900OD + pICH87644 + FP09047 + FP09080 + pICH44300
FP09135	*pAtAct2::TET3-mRuby3-6×HA*	pICSL86900OD + pICH87644 + FP09030 + FP09080 + pICH44300
FP09136	*pAtAct2::TET8-mRuby3-6×HA*	pICSL86900OD + pICH87644 + FP09032 + FP09080 + pICH44300
FP09152	*35s::TET7-mRuby3-6×HA*	pICSL86900OD + pICH51277 + FP09031 + FP09080 + pICH41414
FP09155	*35s::LYK5-mRuby3-6×HA*	pICSL86900OD + pICH41388 + FP09010 + FP09036 + FP09080 + pICH41414
FP09167	*35s::TET3-mCherry*	pICSL86955OD + pICH51277 + FP09030 + pICSL50004 + pICH41414
FP09168	*35s::TET7-mCherry*	pICSL86955OD + pICH51277 + FP09031 + pICSL50004 + pICH41414
FP09169	*35s::TET8-mCherry*	pICSL86955OD + pICH51277 + FP09032 + pICSL50004 + pICH41414
FP09176	*35s::LYK4-eGFP*	pICSL86900OD + pICH41373 + FP09005 + FP09035 + FP09175 + pICH41414
FP09195	*35s::TET3-mRFP1*	pICSL86955OD + pICH51277 + FP09030 + FP09179 + pICH41414
FP09196	*35s::TET7-mRFP1*	pICSL86955OD + pICH51277 + FP09031 + FP09179 + pICH41414
FP09197	*35s::TET8-mRFP1*	pICSL86955OD + pICH51277 + FP09032 + FP09179 + pICH41414
FP09199	*35s::FLOT1-mRFP1*	pICSL86955OD + pICH51277 + FP09104 + FP09179 + pICH41414
FP09200	*35s::FLOT2-mRFP1*	pICSL86955OD + pICH51277 + FP09097 + FP09179 + pICH41414

Table 2-3: Golden Gate parts used in constructing expression constructs in this work. The primers used to domesticate and generate the level 0 constructs as well as the PCR templates are further listed in detail.

Name	Origin	Description	Primers used to create it	Template
pICSL86900 OD	TSL synbio	Binary vector with nos:nptII:ocs selection cassette in backbone. Accepts level 0 modules to assemble one transcriptional unit (GGAG-CGCT)		
pICSL86955 OD	TSL synbio	Binary vector with nos:bar:nos selection cassette in backbone. Accepts level 0 modules to assemble one transcriptional unit (GGAG-CGCT).		
pICH47742	TSL synbio	Position 2-F, AddGene #48001		
pICH47751	TSL synbio	Position 3-F, AddGene #48002		
pICSL4723	TSL synbio	Binary vector no plant selection cassette ORANGE/WHTE cloning selection, AddGene #48015		
pICH41766	TSL synbio	End-linker for level 2 construction, pELE-3 AddGene #48018		
pICH41744	TSL synbio	End-linker for level 2 construction, pELE-2 AddGene #48017		
pICH41388	TSL synbio	*GGAG_P-CaMV35SShort_TACT*, AddGene #50253		
pICH87644	TSL synbio	*GGAG_P-AtuNos_5U-TMV_AATG*, AddGene #50274		
pICH51277	TSL synbio	*GGAG_P-CaMV35SShort_5U-TMV_AATG*, AddGene #50267		
pICH50581	TSL synbio	*GGAG_P-AtACT2_TACT*, AddGene #50256		
pICSL31853	TSL synbio	*TGCC-Nos:ecbeNPTII+Intron:NosT-GCAA*		
pICH51266	TSL synbio	*GGAG_P-CaMV35SLong_5U-TMV_AATG*, AddGene #50267		
pICH41373	TSL synbio	*GGAG_CaMV35SLong_TACT*, AddGene #50252		
FP09033	this work	*pL0M-P-GGAG-pLYK4::-TACT*	ss059+ss060	Arabidopsis gDNA
FP09034	this work	*pL0M-P-GGAG-pLYK5::-TACT*	PartA: ss062+ss063, PartB: ss064+ss065, PartC: ss066+ss067, PartD: ss068+ss069, PartE: ss070+ss071	Arabidopsis gDNA
FP09005	this work	*pL0M-5U-TACT-SP$_{LYK4}$-AATG*	ss014+ss015	Arabidopsis gDNA
FP09010	this work	*pL0M-5U-TACT-SP$_{LYK5}$-AATG*	ss027+ss027	Arabidopsis gDNA
FP09008	this work	*pL0M-NT2-AATG-mCherry-AGGT*	ss022+ss023	pICSL50004
FP09011	this work	*pL0M-CDS2ns-AGGT-LYK5 (noSP)-TTCG*	ss030+ss031	domesticated LYK5 from Cecilia Cheval
FP09030	this work	*pL0M-CDS1ns-AATG-TET3-TTCG*	PartA: ss043+ss044, PartB: ss045+ss046,	Arabidopsis gDNA

			PartC: ss047+ss048	
FP09031	this work	*pL0M-CDS1ns-AATG-TET7-TTCG*	PartA: ss051+ss052, PartB: ss053+ss054	Arabidopsis gDNA
FP09032	this work	*pL0M-CDS1ns-AATG-TET8-TTCG*	PartA: ss055+ss056, PartB: ss057+ss058	Arabidopsis gDNA
FP09035	this work	*pL0M-CDS1ns-AATG-LYK4 (no SP)-TTCG*	ss073+ss074	Arabidopsis gDNA
FP09036	this work	*pL0M-CDS1ns-AATG-LYK5 (no SP)-TTCG*	ss076+ss031	Arabidopsis gDNA
FP09047	this work	*pL0M-CDS1ns-AATG-LTI6b-TTCG*	ss083+ss084	Arabidopsis gDNA
FP09097	this work	*pL0M-CDS1ns-AATG-FLOT2-TTCG*	ss138+ss139	Arabidopsis gDNA
FP09104	this work	*pL0M-CDS1ns-AATG-FLOT1-TTCG*	PartA: ss163+ss164, PartB: ss165+ss166, PartC: ss167+ss168, PartD: ss169+ss170	Arabidopsis gDNA
AGGT-LYK4-TTCG	Cecilia Cheval	*AGGT-LYK4-TTCG*		
pICSL50004	TSL synbio	*TTCG_CT-mCherry_GCTT*, AddGene #50316		
pICSL50007	TSL synbio	*TTCG_CT-3×FLAG_GCTT*, SYNBIO#0026		
pICSL50009	TSL synbio	*TTCG_CT-6×HA_GCTT* (Human influenza hemagglutinin) AddGene #50309		
pICSL50009a	TSL synbio	*6xHA* (Human influenza hemagglutinin). Contains a unique 3' sequence for easier PCR amplification		
pICSL50040	TSL synbio	*TTCG-T7 tag + TurboID + 3' 3×FLAG-GCTT*		
FP09079	this work	*pL0M-CT-TTCG-mClover3-3×FLAG-GCTT*	PartA: ss144+ss145, PartB: ss146+ss147	PartA: pKK-BI16-ORF1-3C-mRuby3_ORF2-TEV-mClover3, Addgene #105802, PartB: pICSL50007
FP09080	this work	*pL0M-CT-TTCG-mRuby3-6×HA-GCTT*	PartA: ss148+ss149, PartB: ss150+ss151	PartA: pKK-BI16-ORF1-3C-mRuby3_ORF2-TEV-mClover3, Addgene #105802, PartB: pICSL50009A
FP09175	this work	*pL0M-CT-TTCG-eGFP-GCTT*	created by Christine Faulkner. Verified in this work.	
FP09179	this work	*pL1M-CT-TTCG-mRFP1-GCTT*	gene block synthesis of domesticated product (base 436 G to A)	
FP09009	this work	*pL0M-CT-TTCG-mCitrine-GCTT*	ss025+ss026	

FP09004	this work	*pL0-CT-TTCG-mTurq2-GCTT*	ss012+ss013	pmVenus(L68V)-mTurquoise2, Addgene #60493
pICH41414	TSL synbio	*GCTT_3U+Ter-CaMV35S_CGCT*, AddGene #50337		
EC15320	Ensa	*GCTT-HSP terminator-CGCT*		
pICH44300	TSL synbio	*GCTT_3U+Ter-AtACT2_CGCT*, AddGene #50340		

Table 2-4: Gateway plasmids used in this work and their origin.

Description	Origin
35s::Citrine-LYM2	described in Faulkner et al. (2013)
35s::LYK4-eGFP	Generated by Cecilia Cheval. Described in Cheval et al. (2020)
35s::LYK5-eGFP	Generated by Cecilia Cheval. Described in Cheval et al. (2020)
35s::LYK4-mRFP1	Generated by Cecilia Cheval. Described in Cheval et al. (2020)
35s::LYK5-mRFP1	Generated by Cecilia Cheval. Described in Cheval et al. (2020)
35s::TET7-mRFP1	TET7 in pB7RWG2.0. Generated by Cecilia Cheval (unpublished)
free eGFP	pB7WG2.0.GFP described in Thomas et al. (2008)
35S::SP-RFP-HDEL	pB7WG2.0.RFP_{ER} described in Thomas et al. (2008)
35s::BRI1-mRFP1	BRI1 in pB7RWG2.0. A gift from Cyril Zipfel's laboratory. Described in Bücherl et al. (2017)
35s::BRI1-6×HA	BRI1 in pGWB14. A gift from Cyril Zipfel's laboratory.

2.5 PCR and Primers

The primers used to generate inserts for golden gate cloning are listed in Table 2-5, and the primers used for genotyping and expression analysis of Arabidopsis plants are listed in Table 2-6. All PCR to generate golden gate Level0 components used Phusion® High-Fidelity DNA Polymerase (NEB) and the bounce PCR protocol according to Sam Mugford (2018). All PCR for genotyping or plasmid confirmation purposes used the GoTaq® Flexi (Promega) system. For this the following temperatures and times were used: An initial denaturation step at 95°C for 2 min. was carried out. 35 amplification cycles of 30 sec. at 95°C denaturation, 30 sec. at 50°C annealing, followed by 72°C for 1 min. per 1 kb expected product length, before a final extension at 72°C for 5 min.

Table 2-5: Cloning primers used in this work.

Name	Sequence
ss012 F_mTurq2n_CT	TTGAAGACATTTCGATGGTGAGCAAGGGCGAGGA
ss013 R_mTurq2n_CT	TTGAAGACATAAGCCCTTACTTGTACAGCTCGTCCA
ss014 F_only-SP-of-LYK4_5U	TTGAAGACATTACTATGATCTCGTTTTCATTTCATC
ss015 R_only-SP-of-LYK4_5U	TTGAAGACATCATTCCTGCTGTTGCGAAGGAAGA
ss022 F_mCherry_NT2	TTGAAGACATAATGGTGAGCAAGGGCGAGGAGGA
ss023 R_mCherry_NT2	TTGAAGACATACCTCCCTTGTACAGCTCGTCCATGC

ss025 F_mCit_CT	TTGAAGACATTTCGAGCAAGGGCGAGGAG
ss026 R_mCit_CT	TTGAAGACATAAGCCTACTTGTACAGCTCGTCCATGC
ss027 F_SP-of-LYK5_5U	TTGAAGACATTACTATGGCTGCGTGTACACTCCACGCGC
ss028 R_SP-of-LYK5_5U	TTGAAGACATCATTCCAGCTTTCGCCGGTGACACGG
ss030 F_LYK5_CDS2ns	TTGAAGACATAGGTCAGCAACCGTACGTCAACAA
ss031 R_LYK5_CDS2ns	TTGAAGACATCGAACCGTTGCCAAGAGAGCCGGAAC
ss043 F_TET3_CDS1ns_A	TTGAAGACATAATGAGAACAAGCAACCATCTCAT
ss044 R_TET3_CDS1ns_A	TTGAAGACATTCCTAAGGAAGAACATATCAGCAG
ss045 F_TET3_CDS1ns_B	TTGAAGACATAGGAGACTTAGCCCTGTTGAG
ss046 R_TET3_CDS1ns_B	TTGAAGACATTTTCATTCACATATGAAAAACCGC
ss047 F_TET3_CDS1ns_C	TTGAAGACATGAAACCGGATGGGACACGAGAGGA
ss048 R_TET3_CDS1ns_C	TTGAAGACATCGAACCAAGATGGAAATGACTAGGAT
ss051 F_TET7_CDS1ns_A	TTGAAGACATAATGGTTCAGTGTAGCAACAATCT
ss052 R_TET7_CDS1ns_A	TTGAAGACATATACAATGTTGACCTTAGCCACCT
ss053 F_TET7_CDS1ns_B	TTGAAGACATGTATTCCTCATATTCCTCATTATC
ss054 R_TET7_CDS1ns_B	TTGAAGACATCGAACCCCAACTGCGTTTCCTGTTGT
ss055 F_TET8_CDS1ns_A	TTGAAGACATAATGGCTCGTTGTAGCAACAATCTCGT
ss056 R_TET8_CDS1ns_A	TTGAAGACATACACAAGGAACACGATGTTAACGA
ss057 F_TET8_CDS1ns_B	TTGAAGACATGTGTTCCTCATCATTGTCTACTCT
ss058 R_TET8_CDS1ns_B	TTGAAGACATCGAACCAGGCTTATATCCGTAGGTA
ss059 F_pLYK4::_P	TTGAAGACATGGAGAAACGAATCACATTTGGTGT
ss060 R_pLYK4::_P	TTGAAGACATAGTACCCGTGATTCTGTAAGATTTGG
ss062 F_pLYK5::_level0(P)_A	TTGAAGACATGGAGATTTTCTGTTAAGTTTGAAC
ss063 R_pLYK5::_level0(P)_A	TTGAAGACATCGACTACATCAAGTCATCAACAAG
ss064 F_pLYK5::_level0(P)_B	TTGAAGACATGTCGTCTAACCGAATTTGTATCCG
ss065 R_pLYK5::_level0(P)_B	TTGAAGACATTGGCCTCTTGGATCTCATGTGAAA
ss066 F_pLYK5::_level0(P)_C	TTGAAGACATGCCAAGACCATCTTTATGTCCAT
ss067 R_pLYK5::_level0(P)_C	GTGAAGACATACATCTTCTAGAAAGTTGACCAGG
ss068 F_pLYK5::_level0(P)_D	AGGAAGACATATGTACCAAAATCTCCTCTAATCC
ss069 R_pLYK5::_level0(P)_D	GGGAAGACATTAGACTTATTTAGTCAATGGAAAC
ss070 F_pLYK5::_level0(P)_E	TTGAAGACATTCTACGCCGTCTCCTTTGGTTCAT
ss071 R_pLYK5::_level0(P)_E	TTGAAGACATAGTACCGTTTTGTGGTGTTCTGATCT
ss073 F_LYK4_CDS1ns	TTGAAGACGGAATGCAACAGCCTTATGTCGGAAT
ss074 R_LYK4_CDS1ns	TTGAAGACATCGAACCGTACGACGATTCTTCCCAGT
ss076 F_LYK5_CDS1ns	GGGAAGACATAATGCAGCAACCGTACGTCAACAA
ss083 F_LTI6b_CDS1ns	TTGAAGACGGAATGAGTACAGCCACTTTCGTAGA
ss084 R_LTI6b_CDS1ns	TTGAAGACATCGAACCCTTGGTGATGATATAAAGAG
ss138 F_TET9_CDS1ns	TTGAAGACGGAATGGTACGTTTTAGTAACAGTCTTGTAGGAATACTCAACTTC TTCGTGT
ss139 R_TET9_CDS1ns	TTGAAGACATCGAACCTCAAGAATTGTTGAAACCAT
ss144 F_mClover3-3xFLAG_CT_PartA	AAGAAGACGGTTCGGATGACGATAAGGTGAGCAAGGGCGAGGAGC
ss145 R_mClover3-3xFLAG_CT_PartA	TTGAAGACATACCAGAACCAGAACCCTTGTACAGCTCGTCCAT
ss146 F_mClover3-3xFLAG_CT_PartB	AAGAAGACGGTGGTTCGGATTATAAGGACCATGACGGA

ss147 R_mClover3-3xFLAG_CT_PartB	TTGAAGACATAAGCCCTCACTTATCGTCATCGTCCTTAT
ss148 F_mRuby3-6xHA_CT_PartA	AAGAAGACGGTTCGGATGACGATAAGGTGTCTAAGGGCGAAGAGCT
ss149 R_mRuby3-6xHA_CT_PartA	TTGAAGACATACCAGAACCAGAACCCTTGTACAGCTCGTCCATGC
ss150 F_mRuby3-6xHA_CT_PartB	AAGAAGACGGTGGTTCTCATTCGTACCCATAC
ss151 R_mRuby3-6xHA_CT_PartB	TTGAAGACGGAAGCCCTCAAGCGTAGTCGGGCACATCGTACGGG
ss163 F_AtFLOT1_CDS1ns_PartA	AAGAAGACGGAATGTTCAAAGTTGCAAGAGC
ss164 R_AtFLOT1_CDS1ns_PartA	TTGAAGACATCTCGATACCAGCACCG
ss165 F_AtFLOT1_CDS1ns_PartB	AAGAAGACGGCGAGGACATCAAGCTTTCCAAGAA
ss166 R_AtFLOT1_CDS1ns_PartB	TTGAAGACGGACACGGTGCAAGATTGCCA
ss167 F_AtFLOT1_CDS1ns_PartC	AAGAAGACGGGTGTTCGACGTTTCTCCG
ss168 R_AtFLOT1_CDS1ns_PartC	TTGAAGACATTTTCTGACCCAAGTAAGAGAAGT
ss169 F_AtFLOT1_CDS1ns_PartD	AAGAAGACGGGAAAACTCAAATGGAAGCAGCAA
ss170 R_AtFLOT1_CDS1ns_PartD	TTGAAGACATCGAACCGCTGCGAGTCACTTGCTTCG

Table 2-6: Genotyping and qPCR primers used in this work.

Name	Sequence
ss186 LP_SALK_116766	TATCGGTTTCATCATCTTCGC
ss187 RP_SALK_116766	ACACTTTTGAACGTTCCATGC
ss188 LP_SALK_205244	TGATGTTGTCAAGCAGACCAG
ss189 RP_SALK_205244	AACGGACAAAGTTCCCAATTC
ss190 LP_SALK_136039	TATCCACCACTCGCGTAAAAG
ss191 RP_SALK_136039	TGATATGCATCGAAGTTCAAAAC
ss193 LBb1.3 _better_for_SALK	ATTTTGCCGATTTCGGAAC
ss200 F_promoter_FLOT2	AATTTGCAAAAAGTCTCCGATCCT
ss201 R_within_FLOT2	ATCGATATGATCTTTGACTCCGCG
ss202 F_NJ_GK-430C05_FLOT2	AATTTGCAAAAAGTCTCCGATCCT
ss203 R_SJ_GK-430C05_FLOT2	ATCGATATGATCTTTGACTCCGCG
ss204 GK_o8474	ATAATAACGCTGCGGACATCTACATTTT
ss205 F_AT2G32870	TGCATGAGAGTATAAGATTTGCGT
ss206 R_AT2G32870	TAAAAGAGAAGCTAAAGGACCGCA
ss207 F_NJ_AT2G32870	TGCATGAGAGTATAAGATTTGCGT
ss208 R_SJ_AT2G32870	TAAAAGAGAAGCTAAAGGACCGCA
ss209 LP_SALK_143325	TCCCTTCTCCTAGCCTTTGAG
ss210 RP_SALK_143325	TGTAAATAACCGCGTTTCAATG
ss229 F_Tet3_qPCR	AGAAGACTTAGCCCTGTTGAGTCC
ss230 R_Tet3_qPCR	TGTCCCATCCGGTCTCATTCAC
ss231 F_Tet7_qPCR	TGGGAACGGATCAGGAGTTGTTTG
ss232 R_Tet7_qPCR	CGGCTTACAACAACCAGACTGAAG
ss233 F_Tet8_qPCR	GGAGTTGTCTTGTGGAGAGCAAAG
ss234 R_Tet8_qPCR	TTGCAGCAACCAGACTGAAGAGC

2.6 Bacterial transformations and growth

1 µL of plasmid DNA (50–4000 ng/µL) was mixed with 10-20µL aliquots of electrocompetent *Escherichia coli* DH5α, DH10B or *Agrobacterium* GV3101, and subjected to electroporation (200 ohms resistance, 25 µF capacitance, 2.5 kV voltage). *E. coli* cells were resuspended in 500 µL LB (Luria Broth: 25 mg/mL LB Broth Miller (Formedium)), and *Agrobacterium* cells in 500 µL S.O.C. (20 mg/mL Tryptone (Peptone from casein) (Merck), 5 mg/mL yeast extract (Merck), 0.58 mg/mL NaCl (Fluka), 0.186 mg/mL KCl (Sigma), 2.03 mg/mL $MgCl_2$ (Fisher), 2.46 mg/mL $MgSO_4$, 3.6 mg/mL Glucose (Fisher)). The bacterial suspension was left to recover for 1 h at 37°C for *E. coli* and 2 h at 28°C for *Agrobacterium*, both with 220 rpm agitation. The bacteria were spread evenly on LB-agar plates containing the plasmid resistance corresponding antibiotics: Kanamycin (50 µg/mL), Rifampicin (50 µg/mL), Spectinomycin (50 µg/mL), Carbenicillin (100 µg/mL), Gentamycin (10 µg/mL). *E. coli* was incubated for 12-24 h at 37°C and *Agrobacterium* at 28°C for 40-72 h, before confirmation by PCR of correct plasmid uptake of individual colonies.

2.7 Isolation of plasmid DNA from bacteria

Plasmid DNA from bacteria was extracted according to the protocol of the QIAprep Spin Miniprep Kit (Qiagen). The buffers used were purchased from Qiagen, and used in combination with Mini Spin Columns from Epoch Life Science (EconoSpin® #1910-050/250).

2.8 Extraction of genomic DNA of plants

For genomic DNA extraction from Arabidopsis, one leaf of a minimum size of 1 cm^2 to a maximum size of 4 cm^2 per three to six week old plant was frozen in liquid nitrogen in a centrifuge tube and ground using a Geno/Grinder®. After addition of 100 µL extraction buffer (0.2 M Tris-HCl pH8, 0.4 M LiCl, 25 mM EDTA, 1% SDS), the sample was mixed thoroughly by vortexing, and the soluble fraction collected by centrifugation at 21130 × g for 10 min. at 4°C. 75 µL of ice cooled isopropanol was added to 75 µL of the supernatant and gently mixed. After centrifugation at 21130 × g for 15 min. at 4°C, the supernatant was discarded and the pellet was washed with 200 µL of 70% ethanol. After drying of the pellet at room temperature (RT) for 10-15 min., the pellet was resuspended in 60 µL of nuclease-free water. Concentration and purity of the extracted DNA were assessed using NanoDrop 800 spectrophotometer (Thermo Scientific), and 5-50 ng DNA was used as a template for genotyping PCR using GoTaq® Flexi (Promega).

2.9 Plant transformation

2.9.1 Microprojectile bombardment assays

Microprojectile bombardment assays were performed as described in Faulkner et al. (2013) and Tee et al. (2022). Mature leaves of four- to six-week-old Arabidopsis plants were bombarded with gold particles (1 nm, BioRad), after coating with pB7WG2.0-eGFP and pB7WG2.0-RFP_{ER} in a PDS-1000/He Biolistic Particle Delivery System (BioRad), whilst being placed on petri dishes with their petioles reaching into the media (4.41 mg/mL Murashige & Skoog Medium Including Vitamins, 10 mg/mL Sucrose, 0.6% Agar). Two hours after bombardment, leaves were syringe-infiltrated with 0.5 mg/mL chitin or water (mock). Bombardment sites were assessed 16-30 h after bombardment using a ZEISS LSM800 CLSM, using the W "N-Achroplan" 20×/0.5 water dipper lens objective. The leaves were screened for individual transformation sites marked by ER localised mRFP1. Z-stacks were acquired of the whole area of eGFP movement and total cell number with eGFP presence per individual transformation site was counted. A maximum of 10 sites per leaf were recorded, before moving ono the next leaf, to avoid individual leaf bias. Statistical analysis was carried out using a bootstrap approach according to Johnston and Faulkner (2021) to compare the medians between mock and chitin treated samples.

2.9.2 Transient expression in *N. benthamiana*

Agrobacterium mediated transient expression in *N. benthamiana* was carried out as described in Cheval et al. (2020). In brief, *Agrobacterium* GV3101 carrying the desired plasmid, was cultured overnight in 10 mL LB, containing the corresponding antibiotics. This bacterial suspension was pelleted and resuspended twice in 0.01 M 2-(N-morpholino)ethanesulfonic acid (MES) pH 5.6, 0.01 M $MgCl_2$, 0.01 M acetosyringone, diluting to a final optical density at 600 nm (OD_{600}), of 0.3-0.5 OD_{600} for each expression constructs and 0.2 for the silencing suppressor P19 (Win and Kamoun, 2004). Each *Agrobacterium* strain carrying the desired plasmid was mixed with the *Agrobacterium* strain carrying P19, and syringe-infiltrated into expanded leaves of 4-week-old *N. benthamiana* plants. Leaf material was harvested and processed for experiments two days post-infiltration.

2.9.3 *Agrobacterium* mediated Arabidopsis transformation

Stable genetic transformation of Arabidopsis has been carried out using the floral dip method (Clough and Bent, 1998) adapted by L. Michael Weaver. In brief: A single colony of *Agrobacterium* (GV3101) transformed with the desired plasmid (Table 2-1, 2-2) was inoculated into 10 mL LB liquid culture and grown overnight with the additional appropriate selective antibiotics. 1-2 mL of this culture was used to inoculate 200 mL LB, including the appropriate antibiotics. After a further day of growth, the cultures were centrifuged for 15 min., at 5422 × g, discarded the supernatant and resuspended the pellet in 200 mL infiltration media (2.165 g/L Murashige and Skoog (MS) medium basal salt mix, 50 g/L Sucrose), by shaking. The flask was left for 1-3 h at room temperature (RT) with gentle agitation. Silwet L-77 (50 µL per 200 mL) of was added to the bacterial suspension mixed manually.

Arabidopsis plants were soil-grown during 'long day' conditions, and the first bolts were cut to promote the development of multiple bolts per plant. Any already formed siliques were removed with scissors, as a preparation before the dipping process. Nine Arabidopsis plants grown in a 9 cm diameter pot, were dipped for 45-60 s in the bacterial solution. For this purpose, the bacterial suspension was transferred into a plastic bag, which could be pressed down and flattened once the plant material was inside, to ensure covering all of the plants. Gentle agitation and movement of the bacterial suspension was applied to the plastic bag during this time. After dipping, the plants were completely covered with a black plastic bag overnight, to maintain high humidity and block the light to promote *Agrobacterium* infection.

2.9.4 Protoplast transfection

To generate and transfect protoplasts at a high transformation rate, I used an adaptation of Yoo et al. (2007), with changes as suggested by Jen Sheen's laboratory website (https://molbio.mgh.harvard.edu/sheenweb/protocols_reg.html). In brief, 10 mL of enzyme solution (0.4 M mannitol [pH 6.7 with NaOH], 20 mM KCl, 20 mM 2-(N-morpholino)ethanesulfonic acid (MES) pH 5.7 was prepared and 1.5% (w/v) cellulose R10 and 0.4% (w/v) macerozyme R10 were stirred in using a sterile plastic loop. The solution was heated to 55°C for 10 min., before adding $CaCl_2$ and bovine serum albumin (BSA) to a final concentration of 10 mM and 1 mg/mL respectively) and to solution was filter sterilised into a 5.5 cm diameter plastic petri dish. One side of this petri dish was stacked onto its lid, to pool the enzyme solution on one side. Well-expanded mature leaves from four- to five-week-old plants grown on soil under 'short day' conditions were used for these experiments.

Leaves were placed on a stack of white office paper, and incisions at a distance of 0.5-1 mm were cut with a fresh razor blade. These strips of leaf material were immediately transferred into the enzyme solution with flat ended tweezers. They were first dipped with their adaxial side into the solution, before immediately turning them over to put them with their abaxial side facing the enzyme solution. Twenty leaves were processed per genotype. The petri dishes were closed and left at gentle shaking rotations of roughly 25 rpm, at RT for 3-4 h. The enzyme solution was further agitated at roughly 80-100 rpm for an additional five minutes to allow for a better release of individual protoplasts.

The digested leaf tissue was filtered to remove bigger debris through a W5 (0.5 mM NaCl, 125 mM $CaCl_2$, 5 mM KCl, 2mM 2-(N-morpholino)ethanesulfonic acid (MES) pH 5.7) buffer-wetted mesh. Protoplasts were pelleted in round bottom tubes at 100 × g at 4°C for 2 min., and washed twice more with cooled W5 buffer. The intact protoplast concentration was assessed using a haemocytometer. The protoplasts were pelleted again and resuspended in cooled MMG (0.4M mannitol pH 6.7, 15 mM $MgCl_2$, 4 mM 2-(N-morpholino)ethanesulfonic acid (MES) pH5.7) buffer, to reach a final concentration of $2*10^5$ pp/mL. Depending on the amount of protoplasts to be transfected, a different tube was chosen for the transfection process to ensure appropriate gentle mixing. For 100 – 200 µL of protoplasts 2 mL centrifugation tubes, and for > 800 µL of protoplasts 50 mL conical tubes, were used. 4 µg of each transfection plasmid per 100 µL protoplasts was added to protoplasts and gently mixed by flicking and swirling the tube. A 1.1× protoplast volume of PEG (0.2 M mannitol pH 6.7, 0.1 M $CaCl_2$, 40% (w/v) PEG4000) solution was added at RT, and the tubes gently completely inverted 13 times. The caps were opened to allow for gas exchange and left to incubate for 15 min. at RT. 4.4 × protoplast volume of W5 was added and gently inverted. The protoplasts were pelleted and washed once in W5 and pelleted and resuspended in 1 × protoplast volume with WI buffer. Protoplasts were left undisturbed in a dark cupboard overnight at a 45° angle in round bottom tubes before assessment of fluorescence and transfection rate.

2.10 BFA treatment

N. benthamiana leaves transiently expressing Cit-LYM2, were syringe-infiltrated two days after *Agrobacterium* infiltration, with either 0.05 mM Brefeldin A (BFA) in combination with 0.5 mg/mL chitin or mock (only water). Before imaging, the leaves were again infiltrated with 0.05 mM BFA, 1 % aniline blue (in 1×PBS), with or without 0.5 mg/mL chitin.

2.11 FRAP analysis

Fluorescence recovery after photobleaching (FRAP) experiments were carried out as described in Cheval et al. (2020). In brief: leaves of *N. benthamiana*, two days after *Agrobacterium* infiltration, transiently expressing Cit-LYM2, LYK4-mRFP1, LYK5-mRFP1, were syringe-infiltrated with 0.5 mg/mL chitin or water (mock for 30 minutes). FRAP experiments were carried out using a Leica TCS SP8X CLSM with a 63x/1.20 water immersion objective (Leica HC PL 135 APO CS2 63×/1.20). Citrine was excited at 514 nm, and its emissions detected at 527-550 nm. mRFP1 was excited at 561 nm, and its emission detected at 567-617 nm. Regions of interest (ROIs) were defined for plasmodesmata-localised Cit-LYM2, as well as for PM-localised Cit-LYM2, LYK4-mRFP1 and LYK5-mRFP1. The photobleaching and recovery were carried out as: 30 iterations were imaged at 0.095 s/frame (pre-bleach); 15 (Cit) or 60 (RFP) iterations at 0.095 s/frame (bleach); and 50 iterations at 0.095 s/frame followed by 120 iterations every 0.5 s (post-bleach). For bleaching iterations, the laser power was set to 100% output and the FRAP booster was activated.

The ROI intensity data were normalised to the mean intensity of the first five frames of pre-bleach and corrected for imaging bleaching induced by pre- and post-bleach iterations. To correct for the latter, non-bleached image acquisition decay curves were collected, which themselves were normalised to the mean intensity of the first five pre-bleach frames and were fitted by a LOESS regression. All FRAP data collected was therefore corrected as follows:

$$I_{corr} = I_{norm} + \left(100 - I_{decay}\right) \ [\%]$$

I_{corr} is the corrected intensity used for further analysis, I_{norm} is the normalised intensity, I_{decay} is the modelled intensity of the acquisition decay curve. In order to establish the bleached intensity as a baseline, the data was further transformed as follows:

$$I_{final} = \frac{I_{corr} - I_{blea}}{I_{pre-bleach}} \times 100 \ [\%]$$

I_{final} is the final intensity used for further analysis, I_{bleach} is the intensity measured at the last bleaching frame, $I_{pre-bleach}$ is the mean of the pre-bleach values.

For each of these datasets an individual LOESS curve was modelled, and the curve fit manually sanity checked (Spira et al., 2012). The intensity value at 60 s post-bleach, representing the recovery within 1 min., was used as an approximation of the relative mobile fraction, adapted from Martiniere et al. (2012). A comparisons of estimated marginal means, was carried out using a Tukey's HSD test to determine statistical significance.

2.12 FRET-FLIM analysis

2.12.1 FRET-FLIM using a Leica TCS SP8X

These experiments and analyses have been carried out as documented in Cheval et al. (2020). In brief: Leaves of *N. benthamiana*, two days after *Agrobacterium* infiltration, expressing constructs of interest, were syringe-infiltrated with 0.5 mg/mL chitin or water (mock), 30 min. before usage. FLIM data was acquired 30 – 60 min. after treatment using a 63x/1.2 water immersion objective lens (Leica C-APOCHROMAT 63×/1.2 water). This Leica TCS SP8X, was further equipped with TCSPC (time correlated single photon counting) electronics (PicoHarp 300), photon sensitive detectors (HyD SMD detector), as well as a pulsed laser (while light laser, WLL), capable of emitting a range of 470-670 nm. The WLL was used to excite eGFP at 488nm, with a low laser power (0.5-3%) to avoid unwanted acquisition bleaching of the samples and a repetition rate of 40 Mhz. Emission of eGFP was collected in the range of 509-530 nm, with additional 488 nm and 561 nm notch filters to reduce interference of reflected light. An erythrosine B based instrument response function (IRF) was measured as described by Weidtkamp-Peters and Stahl (2017). A Leica LASX FLIM wizard was linked to the PicoQutn SymPhoTime64 software to acquire the FLIM data. Each image was scanned until a suitable number of photon counts per pixel (minimum 1000) was reached. For FLIM data acquisition, the image size was reduced to 250 × 50 pixels, to allow for a short pixel dwell time of 19 µs. The laser power was adjusted to reach a maximum of 2000 kcounts/s. ROIs at the PM were selected to exclude any fluorescence of potential chloroplast origin. Calculations of lifetime were carried out following the PicoQuant SymPhoTime 64 software instructions for FRET-FLIM-analyses using multi-exponential donors, using a two-exponential decay for eGFP. The lifetimes were initially fitted using the Monte Carlo method, followed by fitting using the Maximum likelihood Estimation (MLE). The $\boldsymbol{\tau}_{DA}$ (amplitude weighted average donor lifetime) of LYK4-eGFP was calculated and used for further statistical analysis. In the text the amplitude weighted average donor lifetime is referred to as $\boldsymbol{\tau}$. These data were analysed using pairwise Wilcoxon rank sum tests using the Bonferroni p-value adjustments for multiple comparisons. All FRET-Efficiencies are further listed in Table 7-2.

2.12.2 FRET-FLIM using a Leica Stellaris 8

These experiments have been carried out on a Leica STELLARIS 8 equipped with a FAst Lifetime CONtrast (FALCON) for FLIM measurements. The Leica LASX FLIM wizard as used to set up the imaging pipeline. Data was acquired using a Leica HC PL APO CS2 63×/1.20 WATER objective, and high precision coverslips (170 ± 5 µm, Paul Marienfeld GmbH & Co. KG) to ensure higher consistency and reducing the need for objective collar corrections. A pulsed white light laser (WLL) was used at 488 nm at 40 MHz, and emission of LYK4-eGFP was collected at 505-545 nm. The format was set to 512×512, the speed to 100, and the pixel dwell time to 15.39 µs, resulting in a frame rate of 0.194 frames/s. Each image was scanned until a suitable number of photon counts per pixel (minimum 1000) was reached.

Analysis of FLIM was carried out in LASX FLIM/FCS. An ROI was drawn using the inverted brush option to exclude any non-PM signals. An intensity threshold was set at 100 to Maximum, and the Fit Model of Multi-Exponential Donor with two components was chosen for LYK4-eGFP and LYK4-mClover3-3×FLAG, and the fitting range adapted to the intensity counts curve. The donor only samples were first analysed, without the additional presence of acceptor proteins and used a the generated $\boldsymbol{\tau}_D$ to calculate a mean value $\boldsymbol{\tau}_D$ for the unquenched donor lifetime. An initial fit was carried out while allowing the model to optimise the IRF Background and the IRF Shift. Then those values were locked, and a further fit carried out. As in the analysis with PicoQuant SymPhoTime 64 above, the $\boldsymbol{\tau}_{DA}$ (amplitude weighted average donor lifetime) of LYK4-eGFP was used for further statistical analysis. These data were analysed using pairwise Wilcoxon rank sum tests using the Bonferroni p-value adjustments for multiple comparisons. All FRET-Efficiencies are further listed in Table 7-2.

2.13 Biochemical methods

2.13.1 Protein extraction for SDS-PAGE and Western blotting

Six leaf discs (cork borer size 4; 8.9 mm diameter) of *N. benthamiana* leaves two days past *Agrobacterium* infiltration (42-55 h), expressing the desired constructs, were placed in a 2 mL centrifuge tube together with a metal ball and the tissue was frozen in liquid nitrogen. The tissue was then ground and homogenised using a Geno/Grinder® at 1000-1200 rpm for 90 sec. 500 µL of ice cold IP buffer (immunoprecipitation buffer: 50 mM Tris-HCl pH 7.5, 150 mM NaCl, 5mM dithiothreitol (DTT), protease inhibitor cocktail (Sigma 5892953001) 1:100,

phosphatase inhibitor (Sigma 04906845001) 1:200, 1 mM phenylmethanesulfonyl fluoride (PMSF), 0.5% IPEGAL® CA-630 (Sigma I3021), 1 mM EDTA, 1 mM $Na_2MoO_4 \times 2H_2O$, 1 mM NaF, 1.5 mM activated Na_3VO_4) were added to each sample. The samples were allowed to defrost on ice with occasional vortex mixing to ensure equal contact with the buffer, and then gently agitated for 30 min. at 4°C. The samples were centrifuged at max. speed (21 130 × g), for 10 min. at 4°C. The supernatant was transferred into a fresh centrifuge tube, centrifuged again, and transferred again, to avoid any contaminations of cell wall debris. This twice centrifuged supernatant was used as the basis protein extraction for co-immunoprecipitations.

2.13.2 Co-immunoprecipitation

For co-immunoprecipitation (co-IP), 50 µL of the protein extract were kept for Input analysis, and 370 µL were processed further. Magnetic beads of GFP-Trap Magnetic Agarose (Chromotek) or Anti-FLAG® M2 Magnetic Beads (Merck) — 20 µL each — were washed four times with ice cold IP buffer, before addition of the protein extract. The protein-bead solution was gently agitated for 30 min. at 4°C. The beads were magnetically separated, and the supernatant removed, before 500 µL ice cold IP buffer were added and gently agitated for 5 min. at 4°C again. This process was repeated 3 times. Proteins were released from the beads by heating to 95°C in Lämmli buffer (final concentration: 20 mM Tris-HCl pH 6.8, 8.3% (v/v) Glycerol, 1% (w/v) Sodium dodecyl sulfate (SDS), 0.0083% (w/v) Bromophenol Blue, 2% (w/v) 2-Mercaptoethanol).

2.13.3 SDS-PAGE and Westen blotting

Gels of 1 mm thickness, 8 cm wide and 7 cm long, with a roughly 6 cm separating gel and 1 cm stacking gel were cast and run using the Bio-Rad Mini-PROTEAN II apparatus (Bio-Rad Laboratories). Separating gels were made to a final concentration of 10% (w/v) acrylamide:bis-acrylamide (37.5:1), 0.1% (w/v) SDS, 390 mM Tris-HCl pH 8.8. The stacking gel was made to a final concentration of 5% (w/v) acrylamide:bis-acrylamide (37.5:1), 1% 0.1% (w/v) SDS, and 12 mM Tris-HCl pH 6.8. Both gels were polymerised by addition of a final concentration of 0.1% (w/v) ammonium persulfate and 0.1% (w/v) Tetramethylethylenediamine. At least half an hour of time was allowed for polymerisation of the separating gel under a layer of deionised water, before casting the stacking gel on the separating gel, as well as before loading the completed gel.

Gels were run in Running buffer (3.03 g/L Tris, 14.4 g/L Glycine, 1% (v/v) SDS) at a constant 140 V, until the dye front ran either off the bottom of the gel or close to the end. If not otherwise stated the dye front has then been cut off the gel before proceeding with the

transfer. The proteins were transferred using the Mini Trans-Blot® Cell (Bio-Rad Laboratories) in Transfer buffer (3.02 g/L Tris, 14.4 g/L Glycine, 20% (w/v) methanol) either for 75 min. at a constant 100 V or overnight (12-16 h) at a constant 30 V, to Immuno-blot® PVDF 0.2 µm membranes (BioRad).

Proteins were separated by SDS-PAGE (10% acrylamide:bis-acrylamide gels if not specified otherwise), and after the transfer visualised as follows: After blocking in 5% milk (20 mM Tris, 150 mM NaCl, 0.1% Tween20, with 5 mg/mL powdered skimmed milk (Tesco/Marvel)), the membranes were left at gentle agitation at 4°C overnight. Primary antibodies conjugates with horseradish peroxidase (HRP) were four times washed off with TBST and immediately visualised. Membranes requiring secondary antibody treatment, were washed once with TBST (Tris-buffered saline: 20 mM Tris, 150 mM NaCl, 0.1% Tween20) by giving a quick manual shake, and then washed three times for five minutes with 5% milk, before addition of the secondary antibody solution.

Proteins were detected with anti-GFP (1:1000, Roche, 11 814 460 167 001), anti-HA (1:5000, Sigma, H3663), anti-HA-HRP (1:5000, Abcam, ab173826), anti-RFP-biotin (1:2000, Abcam, ab34771), Anti-FLAG-HRP (1:5000, Abcam, ab49763), Anti-Ubiquitin (1:2000, Abcam, ab19169) antibodies. I further used anti-mouse-HRP (1:10 000, Sigma, A0168) and anti-rabbit–HRP (1:20 000, Sigma, A0545) for detection of the primary antibodies. HRP was visualised using an ImageQuant LAS500 (GE Healthcare), with SuperSignal™ West Femto (Thermo Scientific).

2.13.4 IP followed by Mass spectrometry

Mature leaves of four- to six-week-old Arabidopsis plants were syringe infiltrated with 0.5 mg/mL chitin or water (mock), sampled 30 min. post infiltration, and frozen in liquid nitrogen. Three leaves were taken from one plant as one sample, their proteins extracted and immunoprecipitated as described above.

The immunoprecipitated proteins were run approximately 5 mm into a 10% resolving gel. Gel slices were prepared according to standard procedures adapted from Shevchenko et al. (2006). Briefly, the slices were washed with 50 mM TEAB buffer pH8 (Sigma), incubated with 10 mM Dithiothreitol (DTT) for 30 min at 65 °C followed by incubation with 30 mM iodoacetamide (IAA) at RT (both in 50 mM TEAB). The further processing and handling of the analysis machines was carried out by the JIC proteomics facility staff Gerhard Saalbach and Carlo de Oliveira Martins, who also supplied the following procedural details.

After washing and dehydration with acetonitrile, the gels were soaked with 50 mM TEAB containing 10 ng/µl Sequencing Grade Trypsin (Promega) and incubated at 40°C for 8 h. The eluted peptide solution was dried down, and the peptides dissolved in 0.1% TFA (Trifluoroacetic acid) with 3% acetonitrile. Aliquots were analysed by nanoLC-MS/MS on an Orbitrap Eclipse™ Tribrid™ mass spectrometer coupled to an UltiMate® 3000 RSLCnano LC system (Thermo Fisher Scientific, Hemel Hempstead, UK). The samples were loaded and trapped using a pre-column with 0.1% TFA at 20 µl min^{-1} for 3 min. The trap column was then switched in-line with the analytical column (nanoEase M/Z column, HSS C18 T3, 100 Å, 1.8 µm; Waters, Wilmslow, UK) for separation using the following long gradient of solvents A (water, 0.05% formic acid) and B (80% acetonitrile, 0.05% formic acid) at a flow rate of 0.2 µl min^{-1} : 0-4 min 3% B (trap only); 4-10 min linear increase B to 8%; 10-60 min increase B to 25%; 60-80 min increase B to 38%; 80-90 min increased to 60%; followed by a ramp to 99% B and re-equilibration to 3% B, for a total running time of 118 minutes.

Data were acquired with the following mass spectrometer settings in positive ion mode: MS1/OT: resolution 120K, profile mode, mass range *m/z* 300-1800, spray voltage 2300 V, AGC $2e^5$, maximum injection time of 50 ms; MS2/IT: data dependent analysis was performed using HCD and CID fragmentation with the following parameters: top20 in IT turbo, centroid mode, isolation window 1.6 Da, charge states 2-5, threshold $1.0e^4$, CE = 30, AGC target $1.0e^4$, maximum inject time 35 ms, dynamic exclusion 1 count, 15 s exclusion, exclusion mass window ±5 ppm.

Recalibrated peaklists were generated with MaxQuant 1.6.10.43 (MaxQB - The MaxQuant DataBase, 2020) in using the Arabidopsis protein sequence database (The Arabidopsis Information Resource (TAIR), 2020) (35,386 entries) plus the Maxquant contaminants database (250 entries). The results from Maxquant with default parameters were used together with search results from an in-house Mascot Server 2.7 (Matrixscience, London, UK) on the same databases. For this search a precursor tolerance of 6 ppm and a fragment tolerance of 0.6 Da was used. The enzyme was set to trypsin/P with a maximum of 2 allowed missed cleavages; oxidation (M) and acetylation (protein N-term) were set as variable modifications; carbamido-methylation (C) as fixed modification. The Mascot search results were imported into Scaffold version 4.11.0 (2020) using identification probabilities of 99% for proteins and 95% for peptides.

For interaction data analysis, SAINTexpress (Teo et al., 2014) was used to analyse the quantitative results produced by Scaffold and generate a BFDR (Bayesian False Discovery Rate) and AvgP (Aware average Probability score) as the SAINT score.

2.13.5 Detection of protein glycosylation

Enzymatic removal of N-linked oligosaccharides from glycoproteins was carried out as an adapted method from New England Biolabs (2015). In brief 0.5 µL of magnetic bead slurry carrying immunoprecipitated proteins of choice (before protein elution), were added to 1 µL of Glycosylation Denaturation Buffer (New England Biolabs) together with 0.85 µL dH_2O, and heated for 5 min. at 95°C, before being cooled down on ice. After the further addition of 2 µL Glycobuffer 2 (New England Biolabs), 2 µL 10% NP40 (New England Biolabs), and 6 µL dH_2O, either 1 µL PNGaseF (New England Biolabs) or 1 µL dH_2O (mock) were added. The samples were incubated for 14 h at 37°C, before the proteins were eluted off the magnetic beads using Lämmli buffer at 95°C and visualised using SDS-PAGE.

2.14 *Botrytis cinerea* infection assay

Botrytis cinerea isolate B05.10 was drop inoculated in the centre of an MEA plate (Malt extract agar and yeast extract: 30 mg/mL Malt extract OXOID (LP0039), 5 mg/mL Oxoid™ Peptone Mycological, 2 mg/mL yeast extract (Merck), 20 mg/mL Agar (Formedium)). This was incubated at 20°C for three days, before cutting a piece of the expanding hyphal edge as an agar plug to inoculate a fresh MEA plate. This petri dish was sealed with micropore tape and roughly 1 cm of it was not sealed to ensure enough air contact to trigger spore formation. After growth for 10-14 days at 20°C, the spores were harvested by flooding the plate with 15 mL of 0.05% TWEEN® 20 (Merck P9416) and using a glass cell spreader to scrape

the conidia off. The spore solution was filtered once through miracloth (Merck), before centrifuging it for 5 min. at 129 × g. The supernatant was discareded and the spore pellet resuspended in 10 mL of 0.25× PDB (0.25× PDB: 6 mg/mL Potato dextrose broth (Formedium)). A 1:1000 dilution in water was used to assess the spore concentration using a haemocytometer. The spore concentration was adjusted to 2.5×10^5 spores/mL. The spore suspension was incubated at RT for 1.5-2 h while shaking at 300 rpm, to induce synchronised germination. The germination was assessed by determining if hyphae were emerging from spores.

Detached leaves of four- to six-week-old Arabidopsis plants were placed with their petiole in WA (water agar: 15 mg/mL agar (Formedium)). Droplets of 2 µL of the spore suspension were placed on the leaf surface, twice per leaf, between the mid-vein and the leaf edge. The plates were sealed with parafilm, wrapped in a single layer of blue roll, and left for four days (10 h: 14 h, light: dark; 22°C). Four days past infection, the plates were photographed, and the lesion sizes measured in ImageJ (v1.52i) (Schneider et al., 2012). Statistical analysis was carried out by fitting a linear mixed-effects models (package lme4 1.1-27.1) accounting for the fixed effect of genotype and the random effect of experimental repeats, followed by comparison of the estimated marginal means using the emmeans package (1.7.0) using a Tukey's HSD test in R (4.1.2).

2.15 Oxidative burst assay

A 96-well-plate was prepared by filling every well with 200 µL dH_2O. Leaf discs of four- to six-week-old Arabidopsis plants were cut into leaf discs (cork borer size 2; 6.3 mm diameter), briefly placed into a petri dish filled with dH_2O (adaxial epidermis facing up), before being placed individually into the wells of the 96-well plate (adaxial epidermis facing up). This plate was placed in the dark overnight at RT covered with aluminium foil. In the morning the water in each well was replaced by 50 µL WS (working solution: 20 µg/mL horseradish peroxidase (AppliChem), 20 µM L-012 (FUJIFILM Wako Pure Chemical Corporation)). Immediately before the plate imaging process was started, 50 µL WS containing 1 mg/mL chitin, or the equivalent dH_2O (mock) were added to each well. A Varioskan™ LUX (Thermo Scientific) was used to collect luminescence information emitted in each well every 30 s for 90 minutes. Statistical analyses were carried out by a fitting linear mixed-effects model (packages lmtest 0.9-38, lme 4 1.1-27.1), followed by comparison of the estimated marginal means using the emmeans package (1.7.0) applying a Tukey's HSD test.

2.16 Graphical data visualisation and statistical analysis

Data visualisation was carried out using R (4.1.2) (R Core Team, 2021), with the ggplot2 package (3.3.5) (Wickham H., 2016). In the box plot, the line within the box marks the median, the box signifies the upper and lower quartiles, and the whiskers represent the minimum and maximum within 1.5 × interquartile range. An '×' has been used to mark the mean of the data. Violin plots represent the data contribution.

All statistical analyses were carried out in in R (4.1.2) (R Core Team, 2021), and denoted in each materials and methods section as well as in each figure legend. All linear models and linear mixed-effects models were carried out using the packages lmtest 0.9-38, and lme 4 1.1-27.1, followed by comparison of the estimated marginal means using the emmeans package (1.7.0) applying a Tukey's HSD test. The Analyses of Variance table data are listed in Table 7-5.

3 Receptor dynamics

3.1 Chapter 3 – introduction

3.1.1 Receptor complex formation for chitin detection

Chitin binding PRRs in plants are characterised by the presence of LysM domains (Sánchez-Vallet et al., 2015). The LysM domain has been originally identified in bacterial enzymes involved in cell wall degradation (Birkeland, 1994; Jerse et al., 1990; Joris et al., 1992). The first chitin binding PRR in plants was identified in rice as the CHITIN ELICITOR-BINDING PROTEIN (OsCEBiP) (Hayafune et al., 2014; Kaku et al., 2006; Kouzai et al., 2014). According to Fliegmann et al. (2011), LysM receptors are not present in algae or mosses and first appeared in the plant lineage in *Selaginella moellendorfii*, while all vascular plants contain at least two genes coding for LysM domain carrying proteins.

At the PM of Arabidopsis, multiple different RKs such as CERK1, LYK4 and LYK5 are important for the perception of chitin (Cao et al., 2014; Miya et al., 2007) — an insoluble polymer of β-1,4-linked N-acetylglucosamine of fungal cell walls (Numata and Kaplan, 2011). Often such receptors do not function as individual protein units in signalling processes, but rather undergo dynamic or stable complex formations — e.g. as in a flg22 ligand-dependent manner between FLS2 and BAK1 (Chinchilla et al., 2007). Depending on the method used to assess this, these potential changes in complex formation can be observed or resemble artifacts and each such result therefore has the be critically assessed based on the experiment used. For the perception of fungal chitin, multiple receptor interactions and complexes have been reported, such as the chitin-dependent association between a CERK1 homodimer (Liu et al., 2012), and heterodimers between CERK1 and LYK5 and the chitin-independent association between CERK1 and LYK4 (Cao et al., 2014).

As described in chapter 1, these receptor complexes are capable of initiating a plethora of further signalling and immunity response processes at the PM, such as allowing BIK1 to phosphorylate and activate RBOHD, which in turn triggers the production of apoplastic ROS (Kadota et al., 2014; Li et al., 2014; Liu et al., 2018). Further receptor complexes can trigger the activation of MAPK cascades via RLCKs (Yamada et al., 2016). However, before this work and Cheval et al. (2020) no comprehensive understanding of the receptors involved and how these processes might be regulated or active at plasmodesmata in chitin-triggered immunity was available.

3.1.2 Chitin-triggered immune signalling at PD

Treatment with MAMPs such as flg22 triggers a reduction of the molecular exchange between two adjacent cells by reducing the plasmodesmal flux (Faulkner et al., 2013; Xu et al., 2017). This change of plasmodesmal flux is achieved by an increase in callose deposition at the plasmodesmal neck region (Xu et al., 2017).

Some components necessary for these plasmodesmal responses triggered by chitin, were already determined. For example, Faulkner et al. (2013) showed that the RP LYM2 is vital for chitin-triggered plasmodesmal closure. Curiously, they also showed that this chitin-triggered response is independent of the RK CERK1, which is important for chitin-triggered PM localised responses as discussed above.

The perception of MAMPs by receptors can relayed to RBOHD via different proteins. By contrast to the bulk of the PM, the activation of plasmodesmal RBOHD is putatively not dependent on BIK1, as *bik1* mutants are still capable of undergoing chitin-triggered plasmodesmal closure. Instead this response is dependent on cytoplasmic CALMODULIN-DOMAIN PROTEIN KINASE 5 (CPK5), CPK6, and CPK11 (Cheval et al., 2020). Chitin-triggered plasmodesmal closure further depends on RBOHD, and in particular its phosphorylation sites Ser39/Ser339/Ser343 and Ser133 (Cheval et al., 2020). Different signalling pathways can therefore converge in the activation of RBOHD.

Chitin triggered signalling processes are mediated through multiple different receptors. LYM2 is a RP which is anchored into the outer envelope of the PM via a GPI anchor (Fliegmann et al., 2011), and therefore needs other protein partners to inducing a signal transduction through the PM into the cytoplasm. This could be achieved via receptor complex formation with a RK involved in chitin detection such as a LysM-RK. The Arabidopsis LysM-RK family consists of five members: CERK1, LYK2, LYK3, LYK4, and LYK5. As CERK1 is not necessary for chitin-triggered plasmodesmal closure (Faulkner et al., 2013), it can be excluded as a potential candidate to form an important complex with LYM2. LYK2 exhibits a very low expression in mature Arabidopsis leaves (Arabidopsis eFP Browser 2.0, 2022; Winter et al., 2007), and in Cheval et al. (2020) we couldn't detect any transcripts in leaves. LYK2 can therefore be speculated to be excluded from playing important for chitin-triggered plasmodesmal closure in this tissue type. In Cheval et al. (2020) we therefore tested mutants of *lyk3*, *lyk4* and *lyk5-2* for their ability to close their plasmodesmata in a chitin dependent manner in leaves. We determined that LYK4 as well as LYK5 are necessary for this response,

while LYK3 is not. This data now allows for speculation that LYM2, LYK4 and LYK5 are capable of forming receptor complexes important for chitin perception at plasmodesmata.

3.1.3 Plasmodesmal localisation of proteins

Scarcely little is known about how proteins localise to plasmodesmata. Four protein sequences were so far published to be involved in plasmodesmal targeting. They can be conceptualised similarly to nuclear localisation signals (NLS), as they are by themselves necessary and sufficient for targeting to their designated compartment, and by contrast to signal peptides are non-cleavable (Yuan et al., 2017). One such plasmodesmata targeting signal is based on the transcription factor INTERCELLULAR TRAFFICKING DOF 1 (ITD1), which contains a sequence necessary for intercellular trafficking as well as plasmodesmal localisation (Chen et al., 2013). A second one is based on the homeobox domain of the *Zea mays* transcription factor ZmKNOTTED1 (Kim et al., 2002; Lucas et al., 1995). The transmembrane domain of PLASMODESMATA-LOCATED PROTEIN 1 (PDLP1) has been identified as a third motif establishing plasmodesmal localisation (Thomas et al., 2008). Possession of a GPI-anchored modification motif resulting in a GPI anchored protein represents a fourth motif which can lead to plasmodesmata localisation (Zavaliev et al., 2016). Although these four sequences have been identified, no universal way of predicting a protein's plasmodesmal localisation has been identified to date, as well as no universal explanation of how a protein is able to be enriched at plasmodesmata.

Different proteins can exhibit different lateral movement dynamics. Components of biological membranes such as proteins and lipids can generally move laterally in the plane of the membrane (Jacobson et al., 2019). However, this "free" lateral movement behaviour depends on intrinsic protein characteristics such as size (Ramadurai et al., 2009), interaction partners (Sheetz et al., 1980) and concentration (Pink, 1985) and whether or not the protein inhabits a domain in the PM and the domain's characteristics (Li et al., 2011). Compartmentalisation of the PM is achieved by domains of higher order with specific protein or lipid compositions. The plasmodesmal PM can be defined as such a special PM microdomain compartmentalisation, being made up of a specific protein and lipid composition (Brault et al., 2019; Grison et al., 2015a), and therefore expected to exhibit particular characteristics of protein lateral mobility. The lateral mobility of membrane proteins might therefore be an important defining characteristic of plasmodesmata and different for proteins localising predominantly in the rest of the PM.

LYM2 is present within the PM and enriched at plasmodesmata (Faulkner et al., 2013). Curiously we noticed that LYM2 enrichment at plasmodesmata increases in a chitin-dependent manner (Cheval et al., 2020). This allows me to ask if this increase in plasmodesmal localisation could be a hook useful in unravelling general patterns of how a protein localises to plasmodesmata? Could this behaviour be triggered by changes in individual protein dynamics and behaviours within the membrane, or even secretion, or protein cycling processes? And how do other interacting proteins interplay in this response and possibly influence it?

3.1.4 Post translational modifications

While studying the involvement of LYK4 and LYK5 in chitin-triggered plasmodesmal closure, we biochemically determined that LYK4 is present at plasmodesmata while LYK5 itself is not (Cheval et al., 2020). So, if LYK5 is absent at plasmodesmata, how can it still affect plasmodesmal responses?

LYK5 at the PM could be important for another protein at the PM, before these assume their role at plasmodesmata. We determined that LYK4 shows a reduced protein size when expressed in a *lyk5-2* mutant (Cheval et al., 2020). This size shift could be due to a LYK5-dependent PTM of LYK4, which in turn influences LYK4's capability to regulate chitin-triggered plasmodesmal closure. This could be one possible way in which LYK5 could influence plasmodesmata localised signalling responses, even though it itself is absent from this microdomain. However, it is still unknown which PTMs LYK4 undergoes and how they could depend on LYK5.

3.1.4.1 Ectodomain shedding

Could cleavage of LYK4 be caused by the absence of LYK5? A plethora of different membrane proteins undergo proteolytic cleavage within their extracellular domains (Lichtenthaler et al., 2018). This process is referred to as ectodomain shedding (Hayashida et al., 2010). It is highly researched in the animal cell biology field — particularly for its roles in the regulation of signalling processes (Adrain et al., 2011; Laurent et al., 2015), as well as for the cleaved ectodomains fulfilling further active role (Grell et al., 1995). However, relatively little research has been published to-date on plant receptor proteins undergoing ectodomain shedding, and how this affects their signalling capabilities. Ectodomain shedding can regulate protein-protein interactions as well as degradation processes. SYMBIOSIS RECEPTOR KINASE (LjSYMRK) of the plant *Lotus japonicus* is a PM-localized RK, whose extracellular domain is made up of a malectin-like domain (MLD) and LRR domains. The malectin-like domain is cleaved at a conserved GDPC motif, in the absence of symbiotic stimulation (Antolín-Llovera et al., 2014b). 41 out of 50 of the Arabidopsis LRR-I RK family members have an ectodomain comprising of an MLD followed by a GDPC motif and LRRs (Hok et al., 2011). It therefore stands to reason that the GDPC motif dependent ectodomain cleavage could be a common feature of these RKs (Antolín-Llovera et al., 2014a).

RKs such as BAK1 can undergo proteolytic cleavage triggered by stimulation of developmental or immunity cues (Zhou et al., 2019). This can further result in downstream effects in the regulation of other RKs. In the example of BAK1, ectodomain shedding has been demonstrated to play a critical role in the phosphorylation of BIK1 (Zhou et al., 2019).

However, how ectodomain shedding is capable of achieving regulatory effects is not always clear or straight forward to determine. For example, LjSYMRK without its ectodomain is more competitive than its full-length version in protein complex formation with NOD FACTOR RECEPTOR 5 (LjNFR5), even though the truncated protein can be more prone to recycling or degradation processes. Thereby the balance in the abundance of the unshed and the shed pool of proteins can be skewed and detected as such, affecting complex formation dynamics and signalling.

Chitin-triggered signalling can also be regulated by ectodomain shedding. Petutschnig et al. (2014) showed that CERK1 undergoes ectodomain shedding and releases the cleaved soluble CERK1 ectodomain into the extracellular space. Different mutant accessions of *cerk1* have been identified with different causes for phenotypes. While *cerk1-2* (T-DNA insertion, Miya et al. (2007)) abolishes the presence of CERK1 proteins, *cerk1-4* (a single nucleotide mutation in position 370 of the coding region of CERK1), results in full length proteins (Petutschnig et al., 2014). However, by contrast to the WT form of CERK1, they cannot undergo ectodomain shedding and therefore result in no detectable form of the soluble CERK1 ectodomain (Petutschnig et al., 2014). Curiously, plants expressing CERK1-4 are still able to carry out canonical PM localised chitin signalling processes. However, they exhibit phenotypes of deregulated cell death in the presence of pathogens as well as hyper-inducible salicylic acid concentrations. This suggests a receptor can directly or indirectly fine-tune and affect signalling and defence pathways depending on its ability to undergo ectodomain shedding.

CERK1 shares high sequence similarities to other chitin binding proteins such as LYK4 and LYK5 (Zhang et al., 2007). Could these RK therefore also undergo ectodomain shedding processes, and could their function be regulated and fine-tuned by them?

3.1.4.2 Ubiquitination

Additive PTMs, such as ubiquitination can also affect protein abundance and regulate interaction processes. Ubiquitination is a biochemical process in which ubiquitin — a 76 amino acid protein — is biochemically attached to another protein (Guo and Tadi, 2022). Ubiquitin itself can be ubiquinated resulting in a polyubiquitin chain attached to the original protein (Swatek and Komander, 2016). Poly-ubiquinated proteins are often primed for

degradation by the 26S proteasome (Kaiser and Huang, 2005). Monoubiquitination can fine-tune signalling processes but does not necessarily lead to protein degradation (Braten et al., 2016; Zhang et al., 2013). LYK5 is known to undergo ubiquitination and its abundance is regulated by this PTM (Liao et al., 2017), making it a reasonable assumption that other closely related LysM -RK such as LYK4 could also be ubiquitinated.

3.1.4.3 Glycosylation

The addition of a carbohydrate moiety called glycosylation can be a cotranslational and/or posttranslational modification of proteins (Abou-Abbass et al., 2016). The main types of glycosylation are N-linked and O-linked glycosylation, depending on if they are attached to a nitrogen or oxygen molecule respectively (An et al., 2009). Uniprot predicts 6 different N-linked glycosylation sites within the ectodomain of LYK4 (https://www.uniprot.org/uniprot/O64825) (The UniProt Consortium, 2021). Additionally, O-linked glycosylation can occur at any threonine or serine amino acid, and there is no common consensus within the protein sequence to predict those glycosylation sites (An et al., 2009). Therefore, it is not possible to predict where and how much LYK4 might be undergoing O-linked glycosylation.

Other PRR such as FLS2 and EF-TU RECEPTOR (EFR) are highly glycosylated and this PTM is important for their signalling functions in plant immunity (Häweker et al., 2010; Nekrasov et al., 2009; Saijo et al., 2009). Glycosylation is therefore a highly likely PTM candidate of LYK4. Particularly as this PTM might directly influence LYK4's function it might be a good candidate for its functional dependence on LYK5.

3.1.5 Overview and aims of this chapter

The aim of this chapter was to evaluate the dynamics of receptors involved in chitin-triggered plasmodesmal closure. I started by elucidating the increase in plasmodesmal enrichment of LYM2 triggered by chitin, to answer if this process is secretion dependent or caused by changes in lateral membrane mobility. Further I aimed to test if and in which combinations LYM2, LYK4 and LYK5 associate with each other, a characteristic their signalling function might be dependent on. In Cheval et al. (2020) we demonstrated that LYK4 changes its protein size depending on the presence or absence of LYK5. I assessed LYK4 for some of the likely PTMs which could be the cause of this, and therefore the reason why chitin-triggered plasmodesmal closure also depends on LYK5.

3.2 Results

3.2.1 LYM2 maintains plasmodesmal association after protein transport inhibition

In Cheval et al. (2020) we described LYM2's curious localisation behaviour, of its fluorescence ratio between plasmodesmata and PM (PD index) increasing in response to the MAMP chitin. It is currently unknown how specific proteins are sorted and enriched at plasmodesmata and only a few plasmodesmal localisation signals have been identified to date (Yuan et al., 2017). Data on virus movement proteins suggest that these proteins transport their cargo to plasmodesmata using secretion mechanisms and the endocytic recycling pathway (Lewis and Lazarowitz, 2010). Connecting the observations of PD index changes and the virus mediated plasmodesmata targeting via endocytosis, lead me to ask: Does the plasmodesmata localisation of LYM2 depend on a functional protein transport and secretion pathway?

The fungal toxin BFA causes a breakdown of the separation between the ER and Golgi compartments via membrane fusions (Nebenführ et al., 2002). Protein secretion is inhibited in BFA-treated cells at an early step in the secretory pathway due to a block in a pre-Golgi compartment (Brandizzi et al., 2002; Klausner et al., 1992). I therefore used BFA treatment assay to test if the disruption of secretion processes disturbs the plasmodesmal localisation of LYM2.

Cit-LYM2 exhibits a preferential plasmodesmal localisation as previously described in Faulkner et al. (2013) under mock conditions (Fig. 3-1A). This plasmodesmal localisation persists 30 min. after treatment with BFA (Fig. 3-1B). As expected, treatment with BFA resulted in the formation of BFA-compartments as observed in Cheng et al. (2017) and Kubiasová et al. (2020) within 30 min marked with Cit-LYM2 fluorescence (Fig. 3-1, marked with *).

Three hours after BFA treatment one can still observe fluorescent foci of Cit-LYM2 associated around callose deposits marked by aniline blue in some cells. However, this association is no longer located between the two adjacent PMs, but rather visible on the intracellular side of the callose deposit. This suggests that 3 h post BFA treatment, Cit-LYM2 fluorescence is associated with endomembrane accumulations adjacent to plasmodesmata but is not located within the plasmodesmal pore. These Cit-LYM2 fluorescence foci can no longer be clearly assigned to the plasmodesmata, but rather raise the possibility of a PM or the PM adjacent ER localisation. Similar observations were also made 5 h after BFA treatment (Fig.

3-1D). As BFA not only affects protein secretion, but also inhibits membrane protein recycling and turnover, this plasmodesmal adjacent association of Cit-LYM2 is not perturbed in the absence of these processes, while the general PM localisation and the localisation within the plasmodesmal pore is.

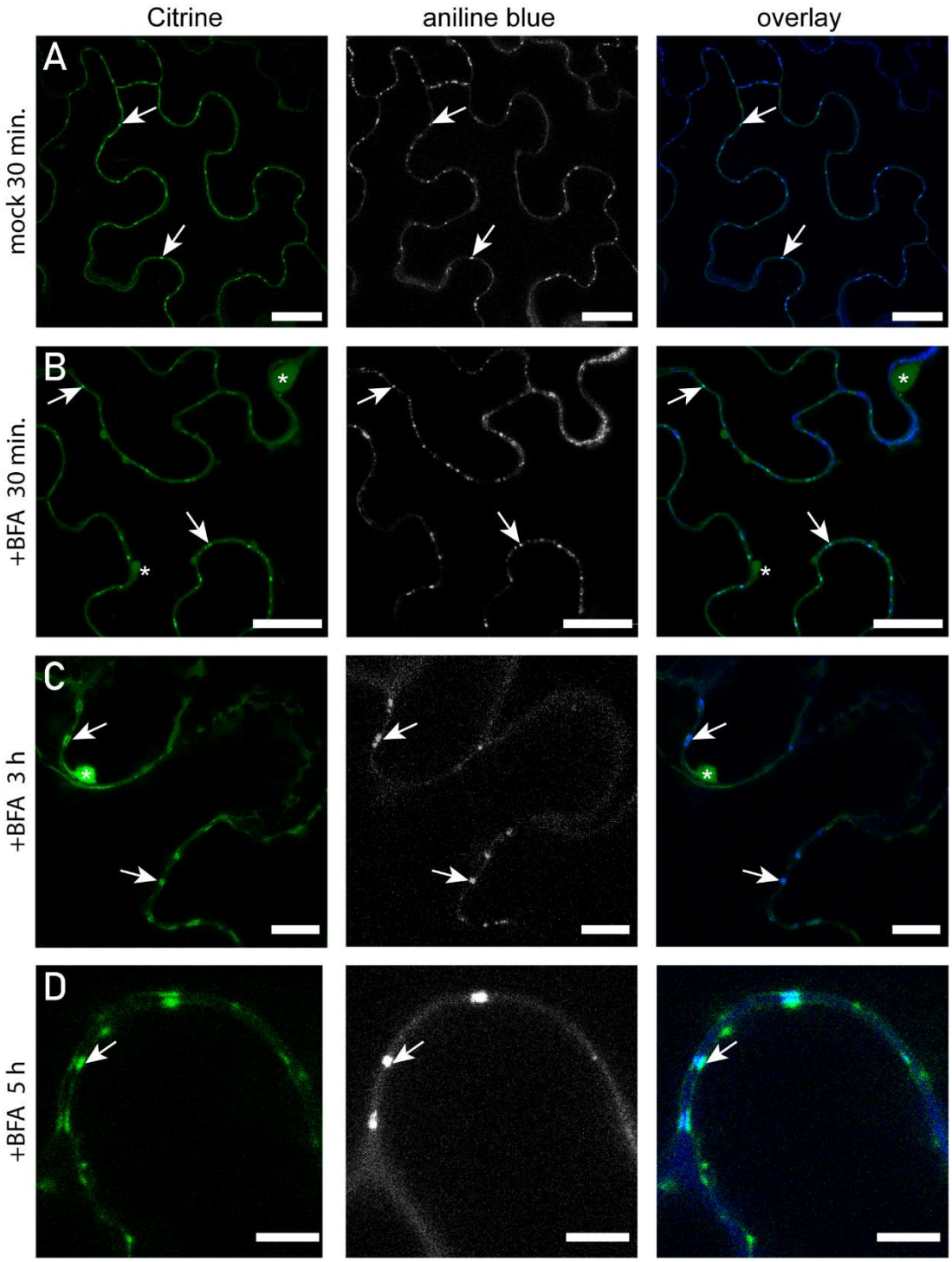

Figure 3-1: BFA induces changes to Cit-LYM2 localisation when transiently expressed in *N. benthamiana*. (A) Mock treated Cit-LYM2 localises at plasmodesmata; co-localising with the plasmodesmal marker aniline blue. (B) Cit-LYM2 fluorescence 30 min after treatment with BFA; resulting in visible BFA compartments marked by Cit-LYM2 as well as continuous co-localisation with aniline blue. (C) Cit-LYM2 fluorescence 3 h after treatment with BFA; resulting in visible BFA compartments marked by Cit-LYM2 as well as continuous co-localisation with aniline blue. (B) Scalebars (A) and (B) 25 µm, (C) 10 µm, (D) 5 µm. Arrows indicate example plasmodesmata and * mark example BFA compartments. This experiment was carried out twice with similar results. In the overlay, blue indicates aniline blue fluorescence and green indicates Cit-LYM2 fluorescence.

3.2.2 Localisation of LYK4 and LYK5

Previously LYK4 and LYK5 were observed to be evenly distributed within the PM, without showing any enhanced localisation at plasmodesmata (Cheval et al., 2020; Erwig et al., 2017; Wan et al., 2012). The PM localisation for LYK4 and LYK5 was confirmed by transiently overexpressing translational fusions with fluorophores in *N. benthamiana* (Fig. 3-2 A and B). Overexpression constructs of LYK4 and LYK5 fused to a fluorophore are capable of increasing chitin-triggered ROS production when transiently expressed in *N. benthamiana* (Cheval et al., 2020). This allows to suggest that LYK4 and LYK5 C-terminal translational fusion proteins are indeed functional. However, as not all RK translational fusions with an epitope tag on the same terminal side exhibit the same functionality (Hurst et al., 2018), no functionality of a RK fusion protein can be guaranteed until proven to be real.

Expression of a gene from its native promoter can enhance the visualisation of preferential plasmodesmal localisation over PM localisation (Thomas et al., 2008). LYK4 and LYK5 fluorophore translational fusion constructs under the control of their native promoter could potentially show a plasmodesmal localisation which is obscured when using a stronger constitutive promoter. I therefore set-out to generate translational fusion constructs for *LYK4-mCherry* and *LYK5-mCherry* under their native promoters complementing their corresponding mutant lines. Erwig et al. (2017) first attempted to create such Arabidopsis lines and chose a native promoter of an arbitrary length of 1 kb which only resulted in clear expression for their *LYK5* construct but not for their *LYK4* construct. To result in levels of expression putatively closer to native expression, longer stretches of DNA before the genes' start codons were chosen as their promoters. They were chosen accordingly to where the previous gene on the chromosome ended, resulting in 1.47 kb for the *LYK4* promoter and 1.56 kb for the *LYK5* promoter. The lines expressing *pLYK4::LYK4-mCherry* constructs in the *lyk4* mutant background produced relatively low fluorescent signals. However, it was still a stable and detectable signal. Using these native promoter driven translational fusion lines of *LYK4* in *lyk4* and *LYK5* in *lyk5* an even PM localisation without any indications of enhanced presence of fluorescence at plasmodesmata was observed (Fig. 3-2 C and D). The same was confirmed in more than eight lines generated by independent genetic transformation of each construct. To allow for stronger conclusions these lines should further be tested for whether or not they indeed are capable of complementing the loss of functions in the *lyk4* and *lyk5-2* mutant backgrounds as well as ensuring their similar to WT expression levels.

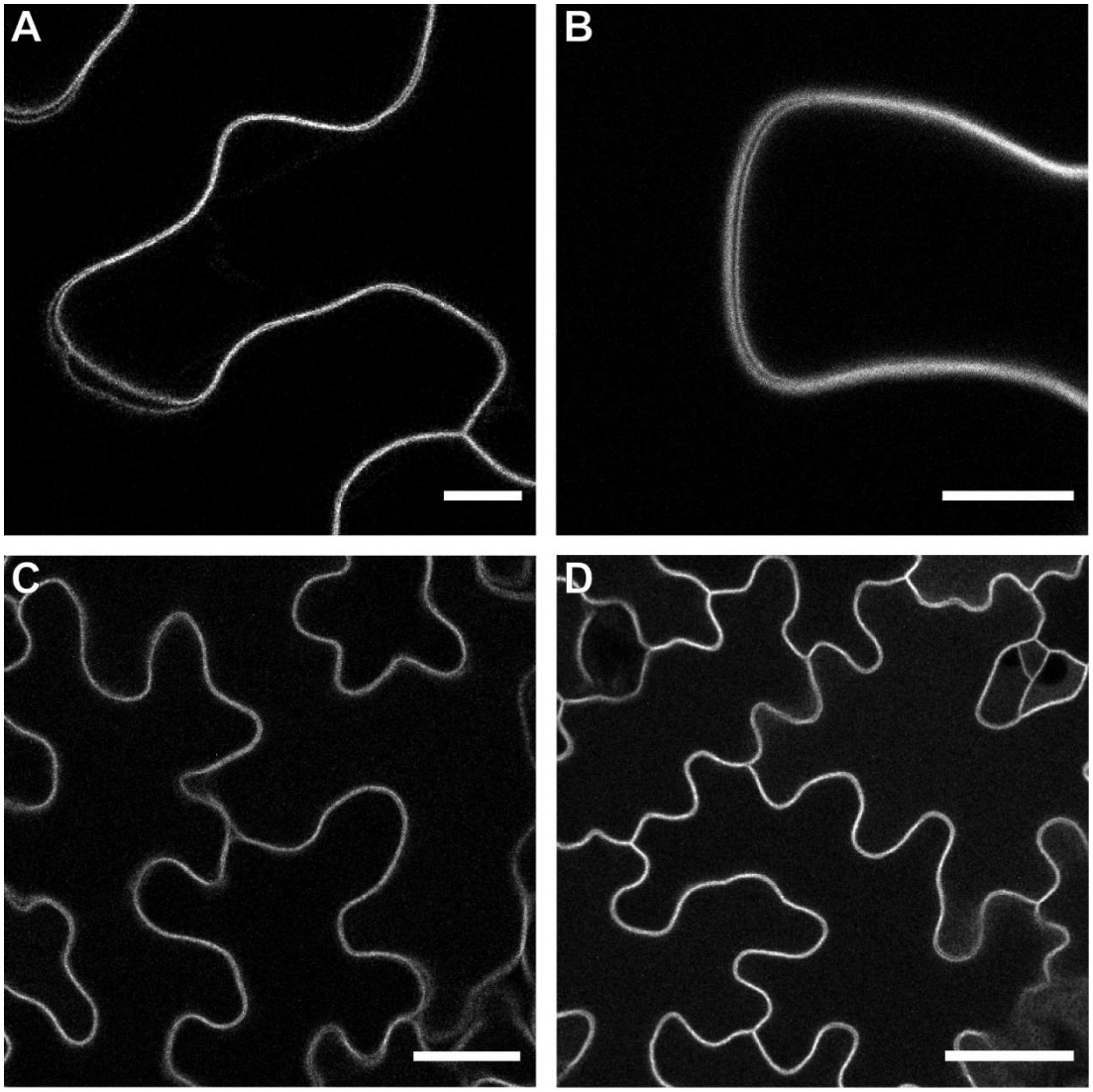

Figure 3-2: Single-plane confocal images in leaves expressing different fluorescent constructs, infiltrated with water before imaging. All *LYK4* and *LYK5* constructs exhibit PM localisation. (A) *35s::LYK4-eGFP*; (B) *35s::LYK5-mRFP1*; (C) *pLYK4::LYK4-mCherry* in *lyk4*; (D) *pLYK5::LYK5-mCherry* in *lyk5-2*. (A) and (B) transiently expressed in *N. benthamiana* with 10 µm scalebars. (C) and (D) stably transformed in Arabidopsis with 25 µm scalebars.

3.2.3 Chitin changes receptor lateral membrane mobility

We demonstrated in Cheval et al. (2020) that Cit-LYM2 undergoes a chitin-triggered change in its PD index. Within half an hour the PD index of LYM2 increases significantly. I wanted to test if this is due to changes in the lateral protein movement of LYM2 within the membrane and therefore carried out Fluorescence Recovery after Photobleaching (FRAP) experiments. For this, the recovery of fluorescence was measured within 60 s for the PD and PM pool of LYM2, as well as the PM pools of LYK4 and LYK5.

A mobile fraction measured in this way indicates the percentage of proteins which undergo an exchange from the non-bleached areas to the bleached areas. For example, 35.94 ± 1.54% (mean ± standard error) of Cit-LYM2 proteins at plasmodesmata exchange from non-

bleached (bulk PM) to bleached (plasmodesmata) areas, indicating that 35.94 ± 1.54% of Cit-LYM2 proteins localised at plasmodesmata get exchanged within 60 s between the PD and the PM. A similar value for Cit-LYM2 exchanges within the PM (37.65 ± 1.60%), and lower values for LYK4-mRFP1 (22.84 ± 0.80%) and LYK5-mRFP1 (27.04 ± 0.76%) exchanging from defined areas of the PM with others were observed.

The lateral mobility of these proteins changes after chitin treatment. Cit-LYM2 (mock 35.94 ± 1.54%) at plasmodesmata showed a significant increase in its mobile fraction when compared to chitin treated samples (38.80 ± 1.67%). No significant changes were observed when comparing mock treated Cit-LYM2 at the PM (37.65 ± 1.60%) with chitin treated samples (39.59 ± 1.88%). This is in contrast to LYK4-mRFP1 and LYK5-mRFP1 which both exhibited a significant increase of their mobile fraction at the PM in the presence of chitin (LYK4-mRFP1 mock 22.84 ± 0.80% to chitin 27.48 ± 0.91%; LYK5-mRFP1 mock 27.04 ± 0.76% to chitin 31.74 ± 0.78%).

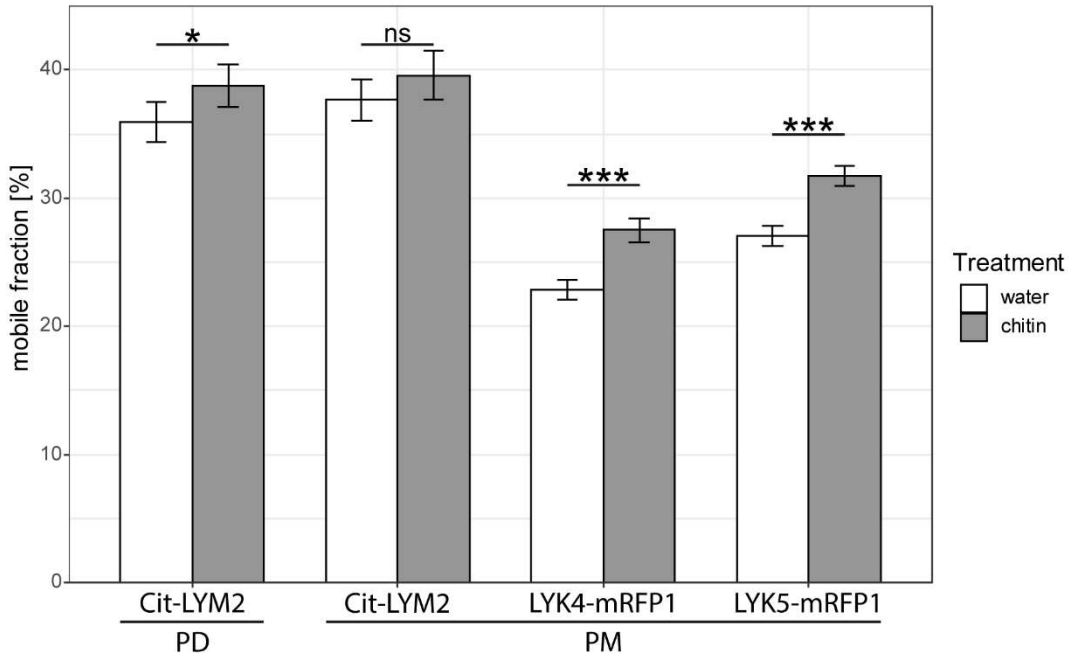

Figure 3-3: Mobile fractions [%] of LYM2, LYK4 and LYK5 as measured by Fluorescence recovery after photobleaching (FRAP) assays within 60 s of post-bleaching. For Cit-LYM2 measurements were taken from plasmodesmata (PD) and PM localised pools of fluorescence. LYK4-mRFP1 and LYK5-mRFP1 pools were measured from the PM. All samples were imaged 30 – 60 min after treatment with either water or chitin. A linear mixed model followed by a Tukey's HSD test was applied to compare the estimated marginal means. Error bars represents the SE. ns: non-significant; * $p<0.05$; *** $p<0.001$. Number of FRAP curves from independent cells analysed is n ≥43 (technical repeats), per construct and treatment. These have been generated from three independent transient expression experiments on different days. This data is replicated from Cheval et al. (2020).

3.2.4 Chitin receptors localise to PM in absence of a cell wall

I wanted to test whetherLYM2, LYK4 and LYK5 associate with each other to achieve their chitin detection and signalling function. To further test if the interactions between two of them would depend on the third one in different combinations, I originally planned to co-transfect protoplasts of mutant Arabidopsis plants with two interaction candidates each.

To test probe for protein-protein interactions, first consistently high rates of successful protoplast transformation had to be achieved, and for this purpose the protocol from Yoo et al. (2007) was adapted and optimised. For the final optimised protocol which consistently resulted in 70-90% transfection rates, please see chapter 2.8.4. In successfully transfected protoplasts all three translational fusions of Cit-LYM2, LYK4-mRFP1 and LYK5-mRFP1 were localised to the PM of the protoplasts (Fig.3-4).

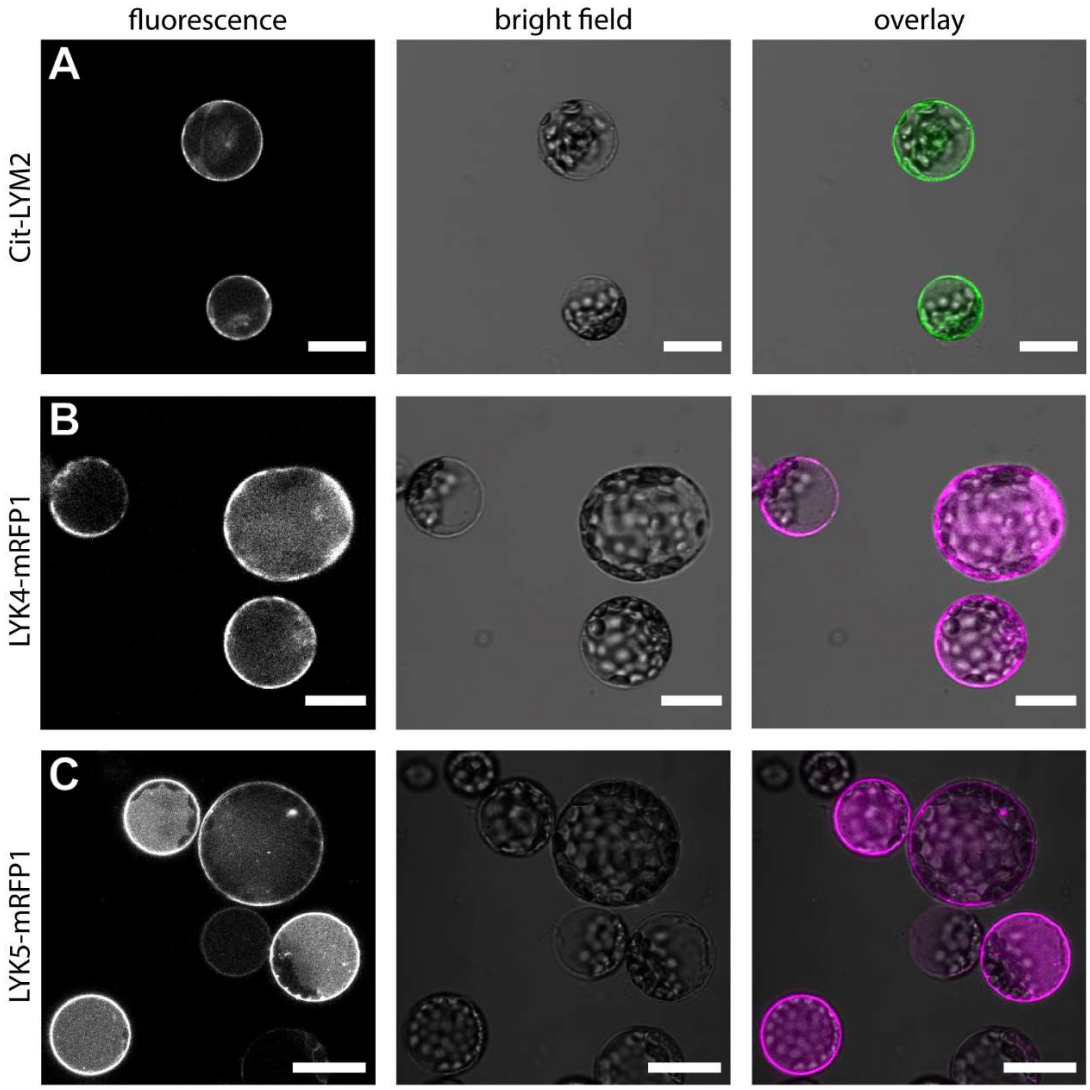

Figure 3-4: Single-plane confocal images of successfully transfected Arabidopsis protoplasts. (A) Cit-LYM2, (B) LYK4-mRFP1, (C) LYK5-mRFP1. All scale bars 25 µm.

3.2.5 Optimisation of co-Immunoprecipitations

Initial co-IP experiments have been carried out with samples generated by co-transfection of protoplasts. These experiments demonstrated the successful detection of the prey LYK5-mRFP1 when immunoprecipitating the bait Cit-LYM2 (Fig. 3-5A). However, these experiments were carried out with a negative association control BRI1-mRFP1 — another PM localised RK, an association not expected as BRI1 is involved in brassinosteroids signalling (Xu et al., 2008). Similarly to LYK5-mRFP1, the negative control BRI1-mRFP1 was detected after anti-GFP immunoprecipitation of Cit-LYM2. Under these experimental conditions I was therefore able to immunoprecipitate a negative control prey with my bait, suggesting that the detection of BRI1-mRFP in Fig. 3-5A is not due to unspecific binding to the magnetic beads.

Proteins can non-specifically bind to antibody-based immunoprecipitation beads (Moser et al., 2009). To test for nonspecific binding of BRI1-mRFP1, I tested whether the negative control BRI1-mRFP1 would also bind to the Anti-GFP beads in the absence of the bait used in this assay as a first trouble shooting step. For this purpose, a co-IP experiment was conducted without the presence of Cit-LYM2 (Fig. 3-5B). In the presence of the bait Cit-LYM2 the negative control BRI1-mRFP1 was detected as a false positive prey. However, in the absence of the bait, BRI1-mRFP1 was not detected in the immunoprecipitation fraction.

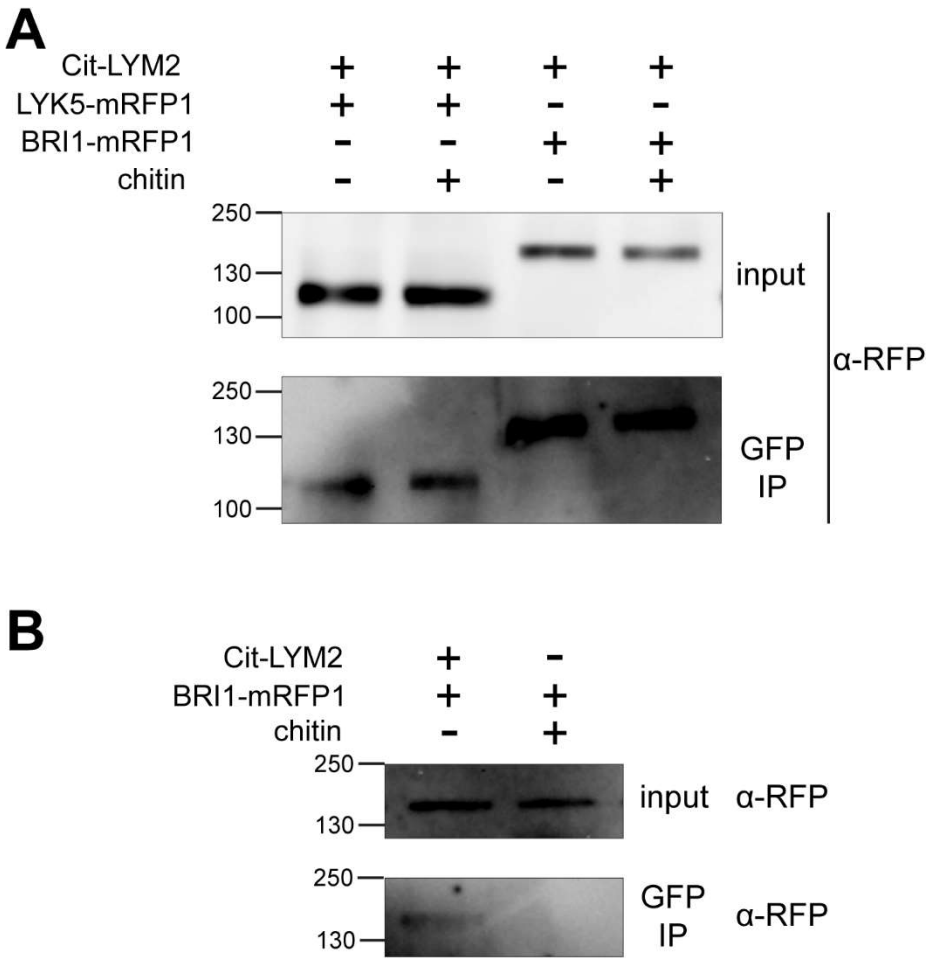

Figure 3-5: Initial co-Immunoprecipitations (co-IPs) from protoplasts experiments to elucidate the association between different receptor proteins. (A) A set of co-IPs precipitating the bait Cit-LYM2 and detecting for the prey LYK5-mRFP1 as well as the negative control BRI1-mRFP1. Both the desired prey as well as the negative control precipitate together with LYM2. (B) A set of co-IPs precipitating onto Anti-GFP beads, in the presence or absence of the bait protein Cit-LYM2 and detected for the presence of the negative control BRI1-mRFP1 in the precipitation. The negative control is not detected in the IP in the absence of the bait Cit-LYM2. These experiments have been carried out using 50 mM Tris-HCl pH7.5, 150 mM NaCl, 1mM EDTA pH8, 1% IGEPAL CA-630, 5mM DTT, 1mM PMSF, protease inhibitor cocktail (Sigma) 1:100, phosphatase inhibitor (Sigma) 1:200 as a buffer.

Extraction, solubilisation and purification of membrane proteins from cells is achieved by detergents (Orwick-Rydmark et al., 2016). The detergent concentration has direct effects on membrane protein aggregation — with a higher detergent concentration generally resulting in a lower protein-protein aggregation and enhanced disruption of lipid rafts (Garner et al., 2008; Li et al., 2021). To test whether an increase or reduction of the detergent (IGEPAL CA-630) leads to an abolishment of false prey signals co-IPs were carried out using a series of different detergent concentrations (Fig. 3-6). Under all different tested detergent concentrations (0.1%, 0.5%, 1%, 1.5%, 2%), the prey BRI1-mRFP1 was detected in the IP of Cit-LYM2.

To maintain proteins under physiological conditions as well as to disrupt ionic and hydrophobic interactions of membrane proteins, the salt NaCl is present in protein extraction buffers (Okamoto et al., 2000). A disruption of these conditions due to non-optimal NaCl concentrations can lead to different membrane protein aggregation states and thereby to nonspecific protein aggregations (Gutmann et al., 2007). To test whether an increase in NaCl concentration leads to a reduced false prey signal when using the bait Cit-LYM2, different salt concentrations were tested (150 mM and 300 mM) in the extraction and IP buffer. In both NaCl concentrations BRI1-mRFP1 was detected in the Cit-LYM2 IP(Fig.3.6).

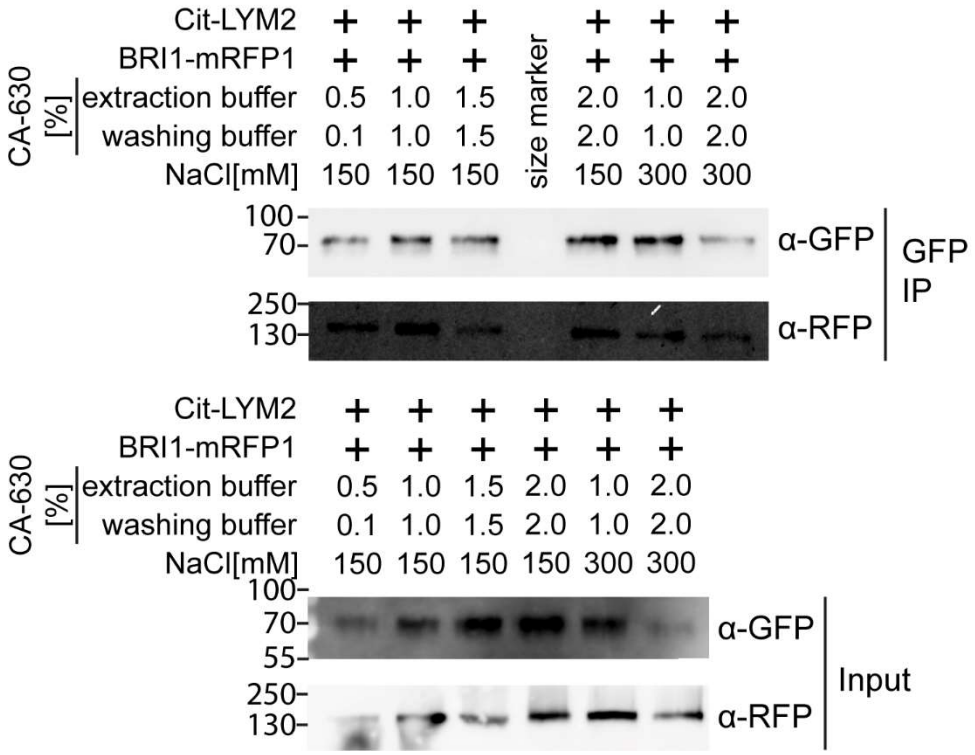

Figure 3-6: Does a variation of the buffer components get rid of the false positive prey signals? A set of co-IPs from protoplasts transiently expressing both Cit-LYM2 as well as BRI1-mRFP1. The bait Cit-LYM2 has been precipitated. The prey BRI1-mRFP1 has been detected in this fraction as well. These experiments have been carried out using 50 mM Tris-HCl pH7.5, 1mM EDTA pH8, 5mM DTT, 1mM PMSF, protease inhibitor cocktail (Sigma) 1:100, phosphatase inhibitor (Sigma) 1:200 as a wash- and extraction-buffer with varying concentrations of IGEPAL CA-630 as well as NaCl.

To avoid the experimental time bottle neck of successfully transfecting protoplasts I changed to using transiently expressing *N. benthamiana* leaves instead. As I struggled with the detection of mRFP1, I further aimed to optimise this. Using monoclonal antibodies to detect for the presence of translational fluorophore fusion proteins does not allow for the same detection sensitivity as with smaller epitope tags which are repeated multiple time, which allow for binding of multiple antibodies per protein. To further increase detection sensitivity, I changed from mRFP1 tagged prey to 6×HA tagged prey proteins. Carrying out the first set of co-IP precipitating Cit-LYM2 and detecting for association with LYK4-6×HA, LYK5-6×HA, or the negative control LTI6b-6×HA, showed a new problem needing optimisation (fig 3-7). In the α-HA blots of the Anti-GFP IP, a signal was detected roughly at the same size as LTI6b-6×HA (~13 kDa), which as a negative control should not be detected in this blot. As this signal overlaps with any potential LTI6b-6×HA signal, it does not allow to clearly determine if this negative control prey results in a signal in the immunoprecipitation or not.

To test if the loading buffer and in particular if the bromophenol blue in the loading buffer could be the cause of this additional signals in a western blot, a gel was run with different concentrations of loading buffer with and without bromophenol blue (Fig. 3-7). When probing a Western blot with α-HA followed by the corresponding α-mouse-HRP antibodies a strong signal at the same height as the running front was detected, where loading buffer including the bromophenol blue was run and in some adjacent lanes. This suggests that bromophenol blue in the loading buffer does cause unspecific antibody binding. For all co-IP experiments using LTI6b-6×HA I therefore used loading buffer without bromophenol blue.

However, even after removal of the artefactual signal seen in Fig. 3-7A, the immunoprecipitated fractions of my co-IPs showed signals for the presence of the negative control LTI6b-6×HA. Further optimisation attempts tested whether the addition of the receptor stabilising compound and phosphatase inhibitor 1 mM Sodium molybdate dihydrate ($Na_2MoO_4 \cdot 2H_2O$) (Mauck et al., 1982; Müller et al., 1982; Ogle, 1983; Rowley et al., 1984), the inhibitor of serine/threonine phosphatases 1 mM NaF (Haier and Nicolson, 2000; Sayeski et al., 2000), and the inhibitor for protein phosphotyrosyl phosphatases 1.5 mM activated Sodium orthovanadate (Na_3VO_4) (Gordon, 1991; Huyer et al., 1997) in the extraction and wash buffer changed the immunoprecipitation success according to Kadota et al. (2016)(Fig. 3-8).

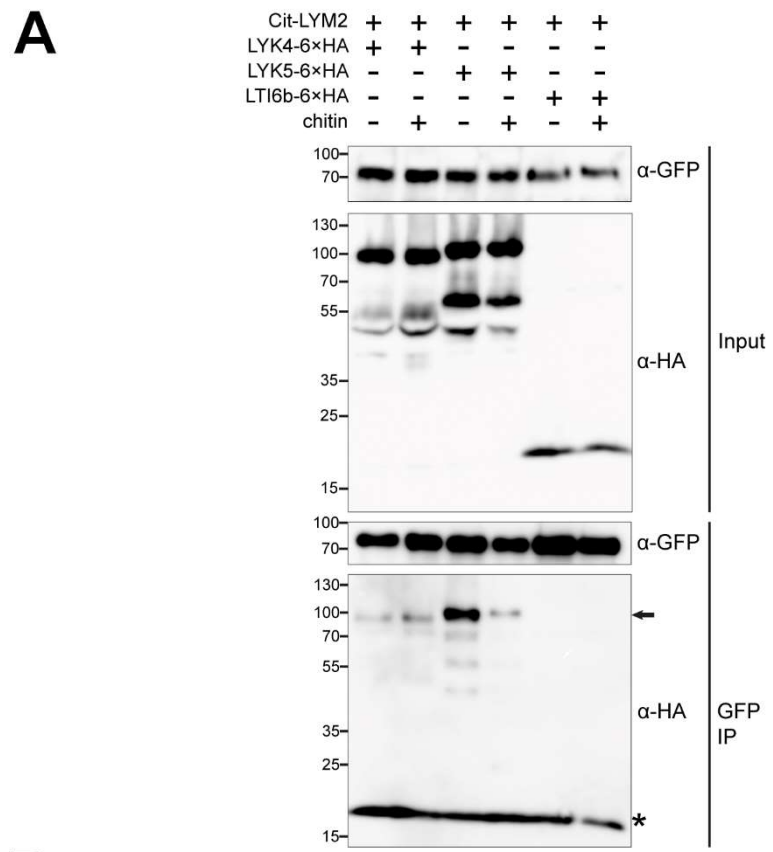
A
Cit-LYM2 + + + + + +
LYK4-6×HA + + - - - -
LYK5-6×HA - - + + - -
LTI6b-6×HA - - - - + +
chitin - + - + - +
100
70
α-GFP
130
100
70
55
35
25
15
α-HA
Input
100
70
α-GFP
130
100
70
55
35
25
15
α-HA
GFP IP
*

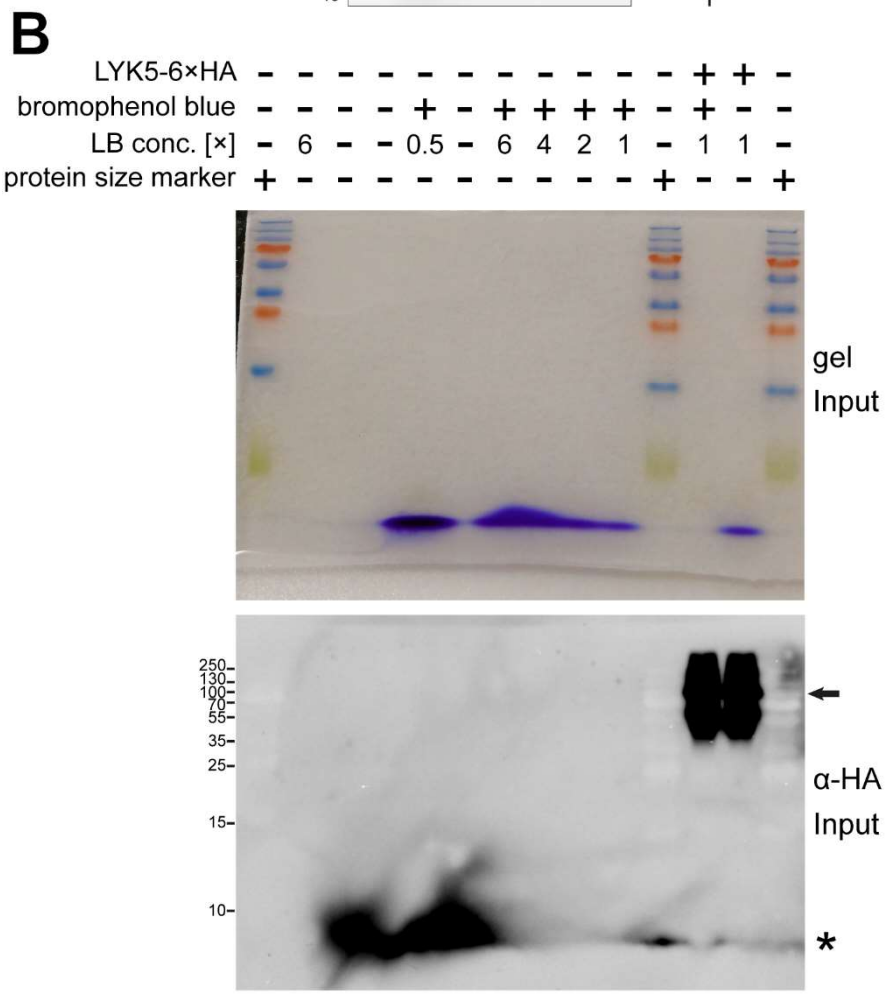
B
LYK5-6×HA - - - - - - - - - - - + + -
bromophenol blue - - - - + - + + + + - + - -
LB conc. [×] - 6 - - 0.5 - 6 4 2 1 - 1 1 -
protein size marker + - - - - - - - - - + - - +
gel
Input
250
130
100
70
55
35
25
15
10
α-HA
Input
*

Figure 3-7: LTI6b-6×HA runs at a similar height as artefacts caused by the bromophenol blue in the loading buffer. (A) Western blot analysis of immunoprecipitated proteins from *N. benthamiana* tissue expressing Cit-LYM2, and LYK4-6×HA, LYK5-6×HA, or LTI6b-6×HA. LYK4-6×HA, LYK5-6×HA (indicated by the arrow) are detected in detergent extracted fractions by IP of Cit-LYM2, as well as a signal throughout the whole blot roughly at the size of LTI6b-6×HA indicated by the *. Input and immunoprecipitated (IP) samples were probed with α-GFP or α-HA antibodies as indicated. The SDS-page gels were 10% Acrylamide/Bis-acrylamide gels. (B) A 15% SDS-page gel with different concentrations of loading buffer as indicated, and two lanes with protein extracts of *N. benthamiana* tissue expressing LYK5-6×HA (indicated by the arrow). The Western blot has been probed with α-HA as indicated. An HRP signal has been detected in most of the blot indicated by the *. The SDS-page gel was a 15% Acrylamide/Bis-acrylamide gel. These experiments have been carried out using 50 mM Tris-HCl pH7.5, 1mM EDTA pH8, 5mM DTT, 1mM PMSF, 0.5% IGEPAL CA-630, protease inhibitor cocktail (Sigma) 1:100, phosphatase inhibitor (Sigma) 1:200 as a wash- and extraction-buffer. PageRuler™ Plus Prestained Protein Ladder (ThermoFisher Scientific) has been used as the protein size marker.

In samples showing a stronger signal of the negative control LTI6b-6×HA in comparison to the other prey proteins in the input, LTI6b-6xHA can be detected after immunoprecipitation of Cit-LYM2, both in the presence as well as the absence of the three phosphatase inhibitor chemicals ($Na_2MoO_4 \cdot 2H_2O$, NaF and activated Na_3VO_4) (Fig. 3-8). However, a clear reduction of this signal in the IP could be observed in samples processed with these inhibitors in their extraction- and wash-buffers. One hypothesis to explain this, is that LTI6b-6×HA had a lot higher concentrations in the input than the other preys, which therefore resulted in a carried over presence in the IP fraction. The same trend of a signal reduction in the IP fraction of samples processed with the three inhibitors was also observed for samples using BRI1-6×HA as prey. Addition of the three inhibitors lead to a stark reduction in the detection of BRI1-6×HA in the IP. This is in contrast to the prey of choice LYK5-6×HA, which is still clearly detectable when processed with the buffers containing these inhibitors. This could be due to the receptor stabilising capabilities of activated Sodium orthovanadate, or due to different phosphorylation preservation, or an entirely different so far unexplored mechanism.

This experiment demonstrates that the addition of the phosphatase inhibitors $Na_2MoO_4 \cdot 2H_2O$, NaF and activated Na_3VO_4 reduces the detection of possibly artefactual negative control prey membrane proteins in co-IPs, although it is not known why this could be the case. All further co-IPs of this work have therefore been carried out using buffers including these additional inhibitors.

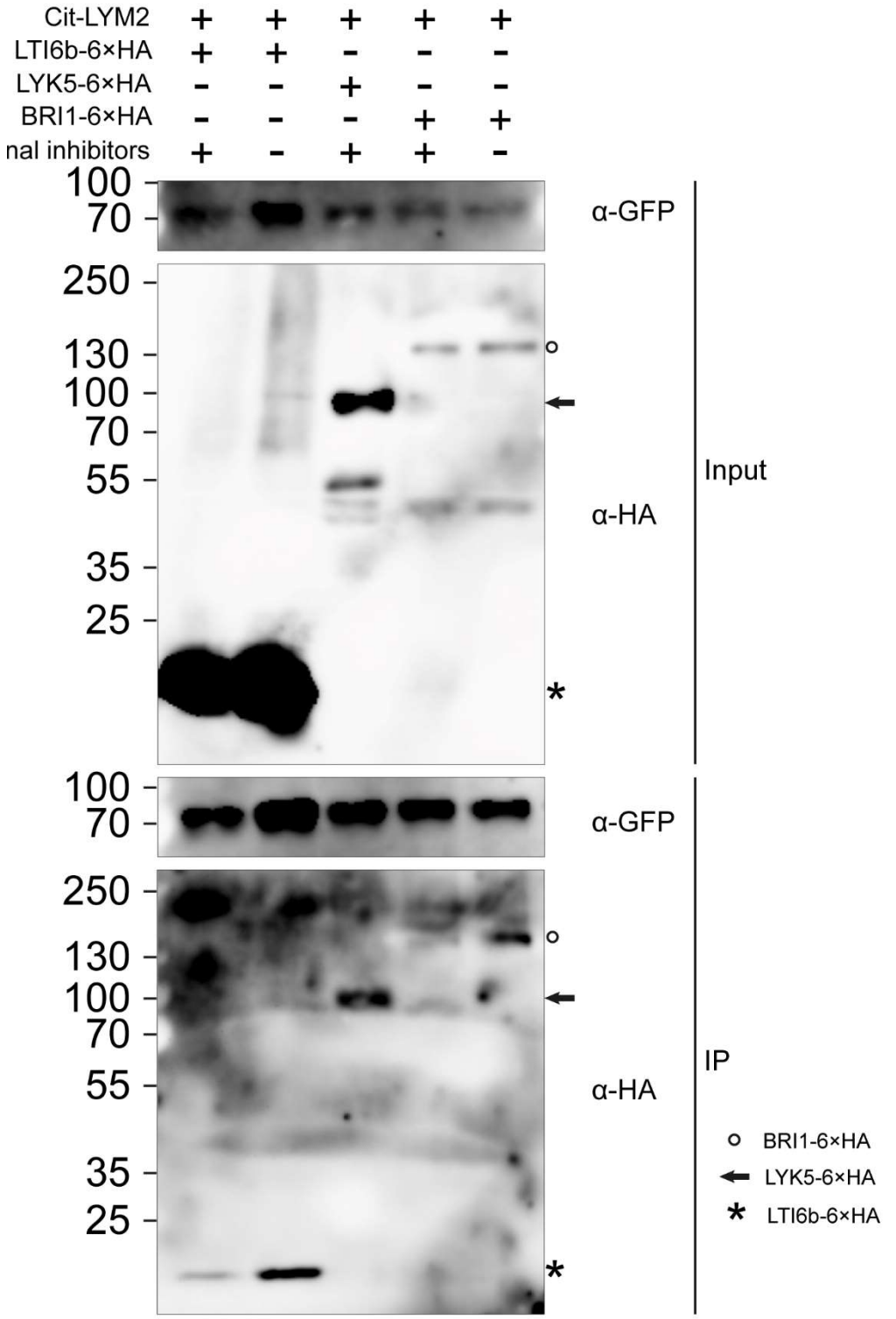

Figure 3-8: Phosphatase inhibitors reduce amount of artefactual negative control detection. Western blot analysis of immunoprecipitated proteins from *N. benthamiana* tissue expressing Cit-LYM2, and LYK5-6×HA, BRI1-6×HA, or LTI6b-6×HA. LYK5-6×HA, BRI1-6×HA and LTI6b-6×HA are detected in detergent extracted fractions by IP of Cit-LYM2. The detection of LTI6b-6×HA in the IP was lowered in the sample which had the additional inhibitors present. BRI1-6×HA is indicated by a circle, LYK5-6×HA by an arrow and LTI6b-6×HA by a *. Input and immunoprecipitated (IP) samples were probed with α-GFP or α-HA antibodies as indicated. The SDS-page gels were 10% Acrylamide/Bis-acrylamide gels. This experiment has been carried out using 50 mM Tris-HCl pH7.5, 1mM EDTA pH8, 5mM DTT, 1mM PMSF, 0.5% IGEPAL CA-630, protease inhibitor cocktail (Sigma) 1:100, phosphatase inhibitor (Sigma) 1:200 as a wash- and extraction-buffer. In lanes indicated to have the additional inhibitor present, the buffer further included 1 mM $Na_2MoO_4 \cdot 2H_2O$, 1 mM NaF and 1.5 mM activated Na_3VO_4.

3.2.6 LYM2, LYK4 and LYK5 associate

Using the optimised conditions of 3.2.5. The three PRR LYM2, LYK5 and LYK5 were tested for their associations between each other (Fig. 3-9 and 3-10). The first experiment showed that the prey LYK5-6×HA immunoprecipitates with the bait LYK4-eGFP, while the negative control LTI6b-6×HA did not (Fig. 3-9). No consistent decrease or increase in the LYK5 prey detection was observed when comparing chitin or water treated samples, suggesting a chitin independent association between LYK4 and LYK5.

The second experimental series showed that the prey LYK4-6×HA and LYK5-6×HA immunoprecipitates with the bait Cit-LYM2, while the negative control LTI6b-6×HA did not (Fig. 3-10). Although similar levels of input were detected of LYK4-6×HA and LYK5-6×HA, a consistently observed a stronger signal for LYK5-6×HA than for LYK4-6×HA in the immunoprecipitation was observed throughout all experiments. This suggests that the association between LYM2 and LYK5 is stronger or more prevalent in the PM than the association between LYM2 and LYK4, or that these two associations have different sensitivities to the extraction buffer and extraction conditions. However, it does not necessarily reveal any information about association prevalence within the plasmodesmata.

In three out of four experimental series, the addition of chitin resulted in a reduction of the prey LYK5-6×HA detection in the Cit-LYM2 IP. Only in one of the four experiments, no significant change in the signal could be detected for LYK5-6×HA between the chitin and the mock treated samples. This suggests, that although the association between LYM2 and LYK5 can be detected, both in the presence and absence of chitin, it is dynamically changing in the presence of chitin. This dynamic change hints at a flexibility and changing protein complex formation upon chitin perception.

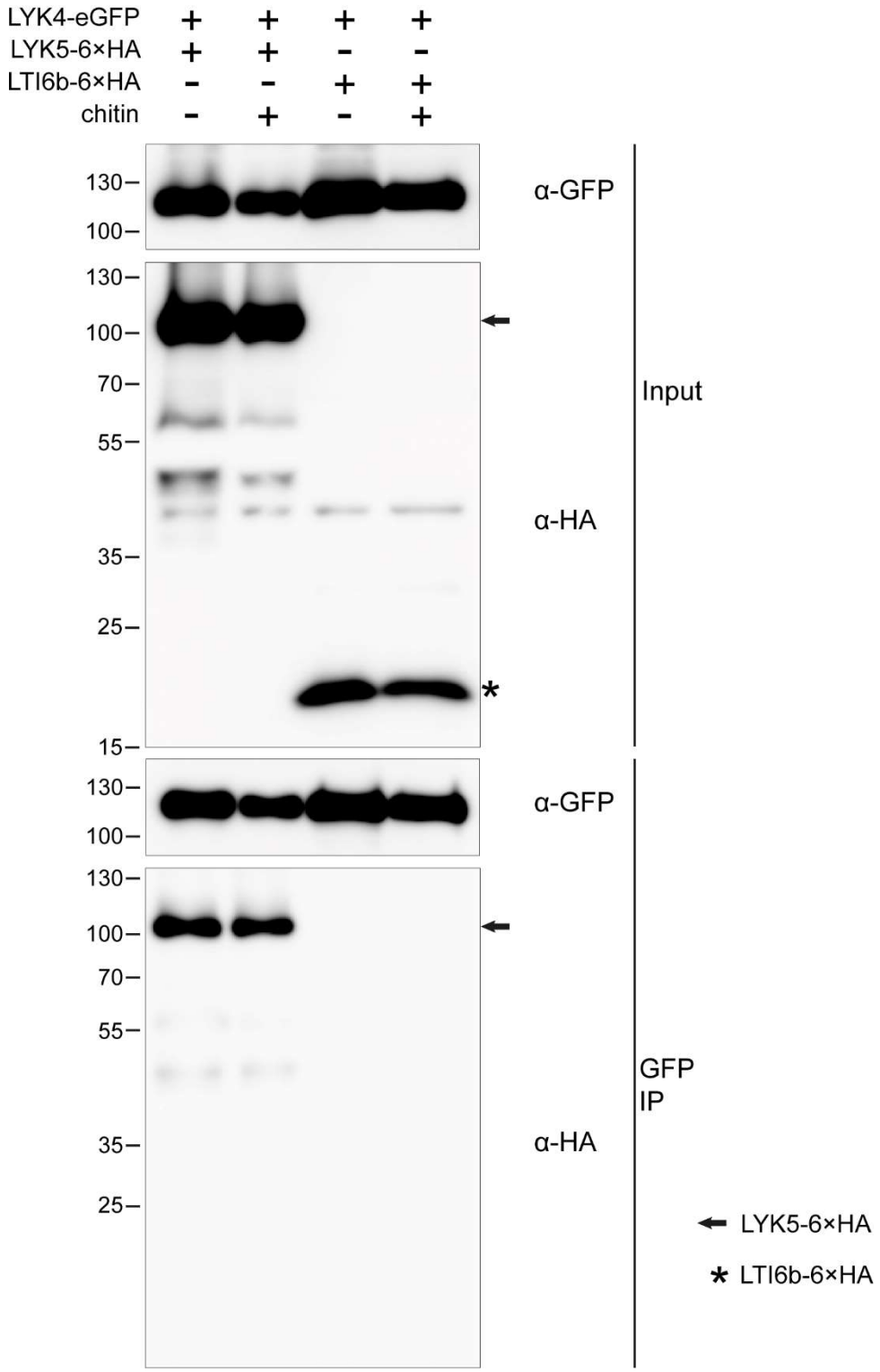

Figure 3-9: LYK4 associates with LYK5 but not with the negative control LTI6b. Western blot analysis of immunoprecipitated proteins from *N. benthamiana* tissue expressing LYK4-eGFP, and LYK5-6×HA, or LTI6b-6×HA. Samples were infiltrated with either 0.5 mg/mL chitin or water (mock) 30 min. before sampling. Only LYK5-6×HA was detected in detergent extracted fractions by IP of LYK4-eGFP. No LTI6b-6×HA was detected in the IP fraction. LYK5-6×HA is indicated by an arrow and LTI6b-6×HA by a *. Input and immunoprecipitated (IP) samples were probed with α-GFP or α-HA antibodies as indicated. The SDS-page gels were 10% Acrylamide/Bis-acrylamide gels. This experiment has been carried out using 50 mM Tris-HCl pH7.5, 1mM EDTA pH8, 5mM DTT, 1mM PMSF, 0.5% IGEPAL CA-630, protease inhibitor cocktail (Sigma) 1:100, phosphatase inhibitor (Sigma) 1:200, 1 mM $Na_2MoO_4 \cdot 2H_2O$, 1 mM NaF and 1.5 mM activated Na_3VO_4 as a wash- and extraction-buffer. This experiment was repeated three times producing similar results. The Western blots shown in this figure are the same as used in Cheval et al. (2020).

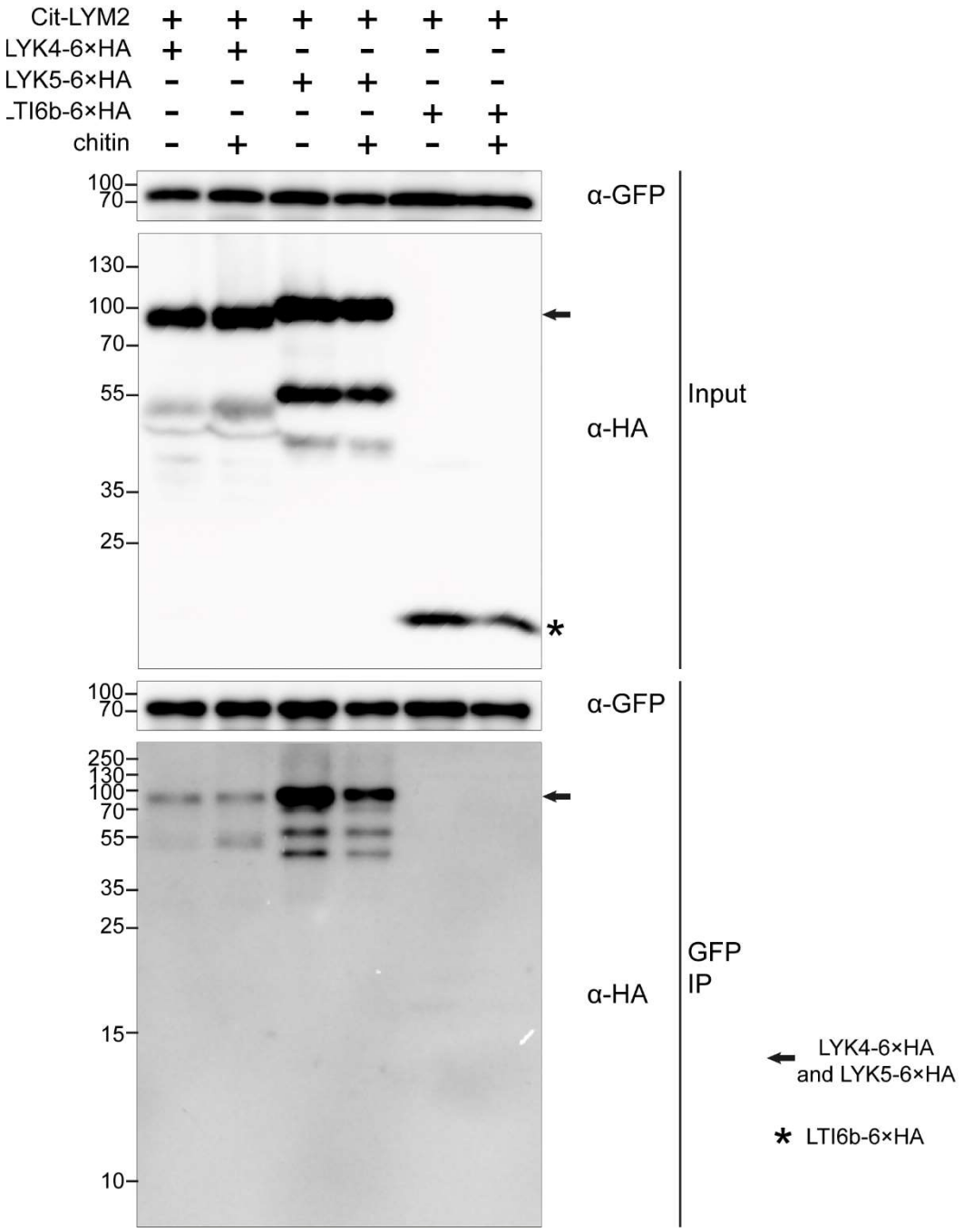

Figure 3-10: LYM2 associates with LYK4 and LYK5, but not with the negative control LTI6b. Western blot analysis of immunoprecipitated proteins from *N. benthamiana* tissue expressing Cit-LYM2, LYK4-6×HA and LYK5-6×HA, or LTI6b-6×HA. Samples were infiltrated with either 0.5 mg/mL chitin or mock 30 min. before sampling. Only LYK4-6×HA and LYK5-6×HA were detected in detergent extracted fractions by IP of Cit-LYM2. No LTI6b-6×HA was detected in the IP fraction. LYK4-6×HA and LYK5-6×HA are indicated by an arrow and LTI6b-6×HA by a *. Input and immunoprecipitated (IP) samples were probed with α-GFP or α-HA antibodies as indicated. The SDS-page gels were 10% Acrylamide/Bis-acrylamide gels, except for the IP gel which was 15%. This experiment has been carried out using 50 mM Tris-HCl pH7.5, 1mM EDTA pH8, 5mM DTT, 1mM PMSF, 0.5% IGEPAL CA-630, protease inhibitor cocktail (Sigma) 1:100, phosphatase inhibitor (Sigma) 1:200, 1 mM $Na_2MoO_4 \cdot 2H_2O$, 1 mM NaF and 1.5 mM activated Na_3VO_4 as a wash- and extraction-buffer. This experiment was repeated four times producing similar results. The Western blots shown in this figure are the same as used in Cheval et al. (2020).

3.2.7 LYK4 and LYK5 undergo ectodomain shedding

While carrying out co-IPs to test for protein associations, LYK4 and LYK5 proteins resulted in multiple bands when detected in Western blots (Fig. 3-9 and 3-10). When stably expressing translational fusion constructs which carry their tag at their cytosolic side, under their native promoters in Arabidopsis and analysing their total protein content via Western blots, both LYK4 and LYK5 constructs also resulted in multiple dominant bands (Fig. 3-11). This is similar to the observations of Antolín-Llovera et al. (2014b) who noticed that *L. japonicus* LjSYMRK shows multiple signals of different sizes — an indicator of ectodomain shedding. LYK4-mCherry resulted in bands the sizes of roughly 116 and 71 kDa (Fig. 3-11A & A'), even though its predicted full-length size including the fluorophore (~26.5kDa) is roughly 92 kDa (excluding the signal peptide). The higher up band therefore migrates ~24 kDa bigger than would be predicted, thereby suggesting the presence of post-translational modifications (PTMs). Further it produces a band which is 45 kDa smaller. This 45 kDa difference could be caused by cleavage or degradation processes during the extraction process or by differences in PTMs, loss of its ectodomain, or a combination of all of these factors.

During the initial phase of this project, I generated further Arabidopsis lines with different experiments in mind. One of these lines (*pLYK5::LYK5-turboID-3xFLAG* in *lyk5-2*) resulted in clear bands the sizes of roughly 130 and 100 kDa (Fig. 3-11B & B') for LYK5-turboID-3×FLAG, while its predicted full-length size would be 112 kDa (excluding the signal peptide). The maximum difference caused by PTMs of LYK5 is therefore ~18 kDa, while the maximum difference purely caused by cleavage of part of its ectodomain is up to 30 kDa. An additive PTM alone can't explain a protein size reduction below the predicted full-length size of a protein. Further, it is therefore not possible to differentiate to which degree the size differences are caused by PTMs or ectodomain shedding in these experiments. However, since the lower dominant bands detected for both proteins are significantly below their predicted size (71 kDa instead of 92 kDa for LYK4-mCherry and 100 kDa instead of 112 kDa for LYK5-turboID-3×FLAG), I aimed to determine if LYK4 and LYK5 undergo a size reductive process such as ectodomain shedding.

To test whether ectodomain shedding can be detected using a confocal microscope and observing the PM and the extracellular space between two adjacent PM, dually tagged constructs of *LYK4* and *LYK5* were created. The N-terminal, and thereby extracellular side was tagged using mCherry (after the signal peptide), and the C-terminal intracellular side of the proteins was tagged using mCitrine (illustrated in Fig. 11-C' & D'). Transiently expressing

these constructs, additional diffuse mCherry fluorescence was observed in the extracellular space instead of just clearly labelling the PM such as the intracellularly located mCitrine does (Fig. 4-11C &D). These diffuse signals between the two PMs suggest the presence of the mCherry fluorophore in the extracellular space. Taken together this suggests that the fluorophore together with a part of the protein's ectodomain was cleaved from the rest of the protein and is now able to diffuse in the extracellular space. This therefore suggests that both LYK4 as well as LYK5 undergo ectodomain cleavage.

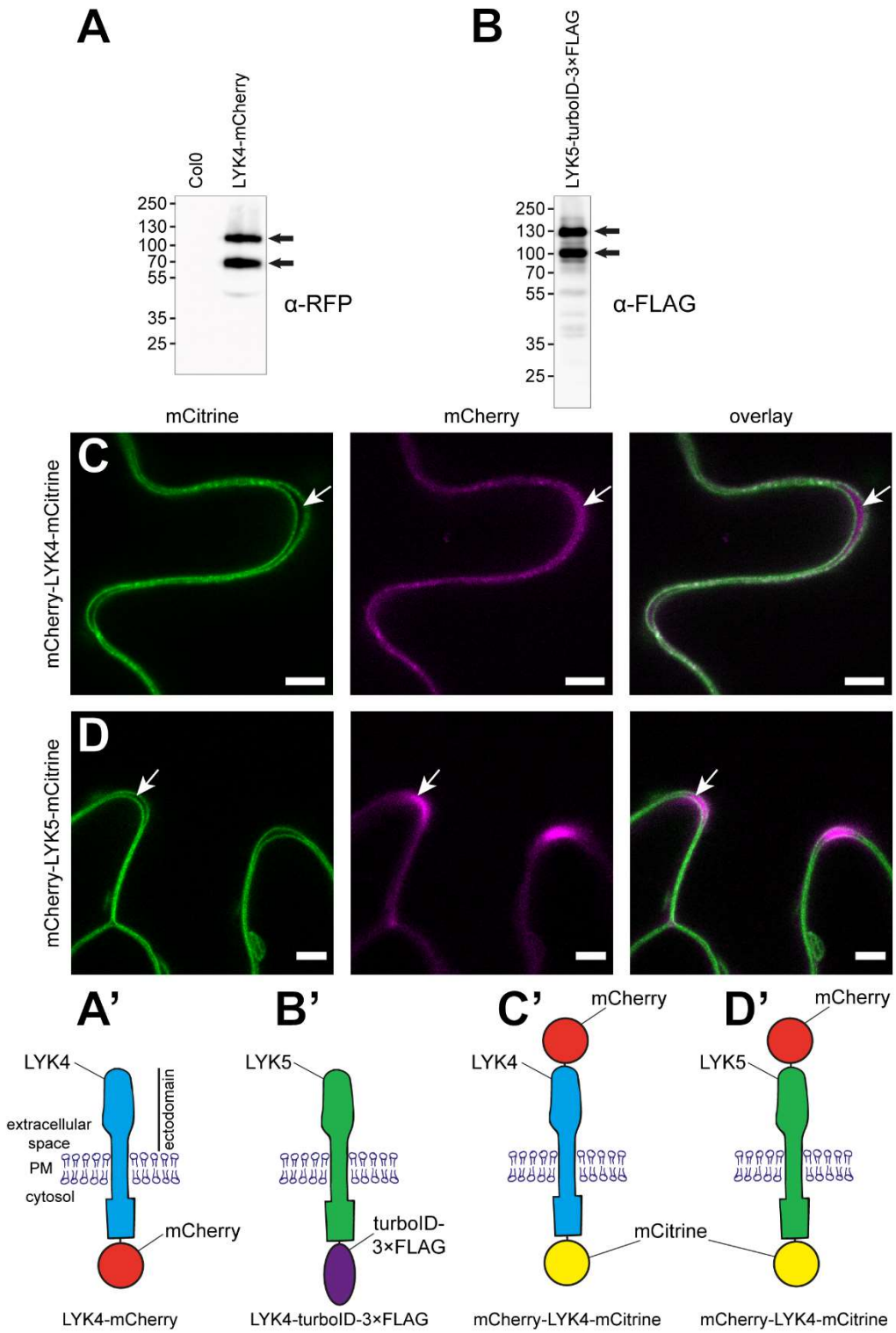

Figure 3-11: LYK4 and LYK5 undergo detectable ectodomain shedding processes. (A) & (B) Western blot analysis of total protein extracts from stable Arabidopsis lines expressing *pLYK4::LYK4-mCherry* in a *lyk4* background or *pLYK5::LYK5-turboID-3×FLAG* in a *lyk5-2* background. The samples were probed with α-RFP or α-FLAG antibodies as indicated. Two bands of different sizes have been detected for both LYK4-mCherry as well as for LYK5-turboID-3×FLAG. (C) & (D) Single-plane confocal images of *N. benthamiana* epidermis cells transiently expressing (C) *35s::mCherry-LYK4-mCitrine* and (D) *35s::mCherry-LYK5-mCitrine*. Arrows indicate the apoplastic space between the PM of two adjacent cells. Fluorescence of mCherry — the N-terminal tag of both constructs — was visualised within the apoplastic space. (C) & (D) Scale bars indicate 5 µm. (A') Cartoon model of fluorophore position of LYK4-mCherry. (B') Cartoon model of biochemical tag position of LYK5-turboID-3×FLAG. (C') Cartoon model of fluorophore positions of mCherry-LYK4-mCitrine. (D') Cartoon model of fluorophore positions of mCherry-LYK5-mCitrine.

3.2.8 Additive PTMs of LYK4

In Cheval et al. (2020) we observed that LYK4-mRFP1 migrates faster on SDS-PAGE gels when extracted from *lyk5-2* protoplasts in two different ways. One change is independent of the presence of chitin, lowering the protein's size by roughly 5 kDa. In the presence of chitin, a second more pronounced shift of roughly 30 kDa is visible. This suggests that LYK4 is stabilised or modified differently depending on the presence of LYK5 and that this might be important for chitin-triggered signalling.

These LYK5 dependent size changes of LYK4 might be the reason for the necessity of LYK5 for a plasmodesmal response, even though it is absent at plasmodesmata. PTM can change the size of a protein and diversify their functions as well as dynamically coordinate signalling processes (Wang et al., 2014). But which PTM(s) does LYK4 undergo, and which one(s) are dependent on the presence of LYK5?

To determine which PTM(s) LYK4 undergoes and result in the full detected size of the protein, the presence of multiple different PTMs was assessed. As LYK5 undergoes ubiquitination and its abundance is regulated by this PTM (Liao et al., 2017), LYK4 was first tested for undergoing ubiquitination to reach its full detected length. α-Ubiquitin (Ub) antibodies were used to detect for immunoprecipitated LYK4-mRFP1 and LYK5-mRFP1. No clear α-Ub signal could be detected for LYK4-mRFP1 at the expected size (Fig. 3-12A). Only LYK5-mRFP1 gave a clear signal at the expected size for the full-length protein. Some smear-like signals are visible in areas indicative of bigger proteins, suggesting the presence of a poly-ubiquitinated version of both LYK4 and LYK5 or interacting proteins, which might be targeted for degradation or alternatively that they associate with polyubiquitinated proteins. This experiment confirmed that LYK5 is ubiquitinated but was not able to detect this PTM for LYK4.

Similarly, to the biochemical attachment of ubiquitin, the protein SMALL UBIQUITIN-RELATED MODIFIER (SUMO) of roughly 10 kDa is attached to another protein during SUMOylation (Geiss-Friedlander and Melchior, 2007). This process is reversible and can alter the localisation of the modified target by altering protein interactions (Bossis and Melchior, 2006; Song et al., 2004), which could explain the LYK5 dependent size shifts of LYK4. However, the α-SUMO antibodies tested by me, to carry out such a determining experiment, did not reveal any signals on Western blots. Although the SUMOplot™ Analysis Program (Abcepta, 2022) predicts three high probability SUMOylation sites in LYK4 (K641, K568, and K375), therefore it could not determined if LYK4 undergoes SUMOylation or not.

There are 6 predicted N-linked glycosylation sites on the ectodomain of LYK4 (https://www.uniprot.org/uniprot/O64825) (The UniProt Consortium, 2021), making this PTM a likely candidate to be present. The enzyme Peptide-N-Glycosidase F (PNGase F) can cleave high mannose, hybrid and complex N-linked glycoproteins between the innermost GlcNAc and asparagine residues (Maley et al., 1989). PNGase F was utilised to test immunoprecipitated LYK4 and the known glycosylated receptor FLS2 as a positive control (Häweker et al., 2010) for N-linked glycosylation. Treatment of both proteins resulted in proteins of lower sizes when compared to mock treated samples (Fig. 3-12B). After removal of N-linked glycosylation LYK4 was detected to be reduced roughly 14 kDa smaller in size. I can therefore conclude that LYK4 glycosylation makes up at least 14 kDa of the full-length detected size of this protein.

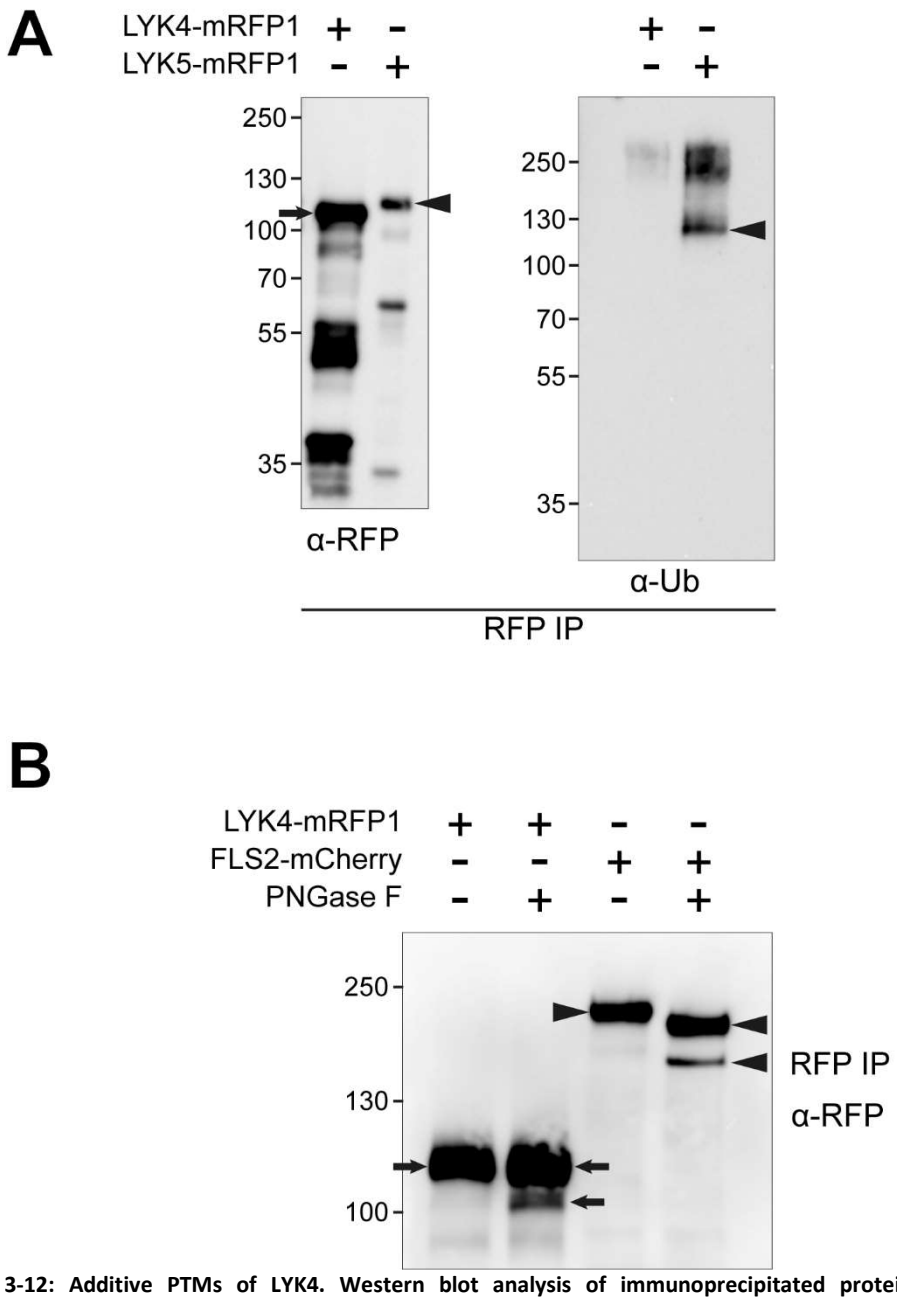

Figure 3-12: Additive PTMs of LYK4. Western blot analysis of immunoprecipitated proteins from *N. benthamiana* tissue expressing LYK4-mRP1, LYK5-mRFP1 or FLS2-mCherry. The IPs have been carried out using a 50 mM Tris-HCl pH7.5, 1mM EDTA pH8, 5mM DTT, 1mM PMSF, 0.5% IGEPAL CA-630, protease inhibitor cocktail (Sigma) 1:100, phosphatase inhibitor (Sigma) 1:200 as a lysis buffer and in the absence of further IGEPAL CA-630 in the wash buffer. (A) 10% Acrylamide/Bis-acrylamide gels were used for SDS-page and probed with α-RFP and α-Ubiquitin (Ub) as indicated. Arrows indicate LYK4-mRFP1, triangles indicate LYK5-mRFP1. Both IPs of LYK4-mRFP1 and LYK5-mRFP1 were detected with α-RFP, but only LYK5-mRFP1 was detected with α-Ub. (B) De-Glycosylation assay with IP samples either mock or treated with PNGase F while still on the magnetic IP beads. 15% Acrylamide/Bis-acrylamide gels were used for SDS-page and probed with α-RFP. Proteins treated with PNGase F migrated faster in gel electrophoresis indicative of a protein size reduction of both LYK4-mRFP1 as well as FLS2-mCherry after de-glycosylation. The De-Glycosylation experiment has been carried out three times with similar results. Arrows indicate LYK4-mRFP1, triangles indicate FLS2-mCherry. In the PNGase F treated sample, a ~ 14 kDa lower band of LYK4-mRFP1 was detected indicating that this protein is glycosylated.

3.3 Discussion

3.3.1 LYM2 plasmodesmal localisation diminishes after BFA treatment

Treatment with BFA lead to a collapse of the Golgi into the ER, followed by the formation of BFA-compartments (figure 3-1, marked with *), as previously described by Dascher and Balch (1994). These compartments exhibited strong fluorescence of Cit-LYM2, demonstrating the presence of this protein within them (Fig. 3-1 B and C). This suggests that LYM2 is present in Golgi mediated secretion processes. After 30 min. of BFA treatment, the plasmodesmal localisation of Cit-LYM2 was still clearly visible in most cells (Fig. 3-1 B), while Cit-LYM2 could only be observed closely associated to plasmodesmata in some cells 3 h after BFA treatment (Fig. 3-1 C). This is similar to the observations made by Thomas et al. (2008) for PDLP1, which retains its plasmodesmal localisation in some cells after BFA treatment. However, even though foci of enhanced fluorescence of Cit-LYM2 around sites marked with aniline blue were observed in some cells, they did not show a perfect overlap anymore. This could be due to a localisation of Cit-LYM2 in ER adjacent to the plasmodesmata but not within the plasmodesmata themselves, or due to Cit-LYM2 localisation in the plasmodesmal neck region, but no longer within the plasmodesmal pore. Five hours after BFA treatment, this plasmodesmal adjacent presence was even more clearly observed in the few cells which still showed Cit-LYM2 associated with plasmodesmata (Fig. 3-1 D). To confirm this plasmodesmal adjacent localisation and to determine if this is truly in the ER or rather within the PM, future experiments co-localising with fluorescent markers for those compartments are needed.

Thomas et al. (2008) concluded that the plasmodesmal localisation of PDLP1 is dependent on an intact secretion pathway, and my experiments confirmed the same for LYM2. However, acquiring images with higher resolution allows me to speculate that even the “left-over” plasmodesmata associated fluorescence is just associated with plasmodesmata instead of localised within them. This could be a very curious line of thought to follow up further, as it opens questions in regard to why and how this the case. Such as; the plasmodesmal localisation of proteins and in particular of LYM2 driven by secretion processes that are physically close by the plasmodesmata and directed via the ER?

The temporal aspect of the change in the Cit-LYM2 localisation pattern allows for further conclusions. In Cheval et al. (2020) we observed a change to the PD index of Cit-LYM2 within 30 min. triggered by chitin. While Cit-LYM2 fluorescence accumulate in BFA bodies within this time frame, a clear plasmodesmal localisations was still observed at this time point,

suggesting that either LYM2 proteins at plasmodesmata do not get recycled and exchanged within 30 min., or alternatively that they do, but that lateral membrane protein dynamics continue to maintain a plasmodesmal localisation independent from membrane protein recycling processes during this time frame.

The changes in plasmodesmal pore localisation after 3 or 5 h, could be due to proteins which previously were present in the plasmodesmal pore having left this localisation to undergo recycling processes, while “new” proteins are not being able to sufficiently occupy this membrane stretch. As it is unknown how LYM2 gets to be localised and enriched at plasmodesmata, it is conceptually possible that it localises there via specifically targeted secretion processes, which are inhibited by BFA. Alternatively, LYM2 could normally laterally move from the bulk of the PM to the plasmodesmal PM, and these two pools could stay in consistent exchange with each other forming a stable equilibrium, which shifts its ratios during the chitin-triggered increase in PD index. In this scenario something is stopping LYM2 to continue these exchange processes in the 3 or 5 h BFA treated samples. This could be a general shift of LYM2’s lateral membrane diffusion behaviour, e.g. another protein which is required for this process could already be completely depleted from the membrane at this point, or the equilibrium’s conditions have shifted in a way that the plasmodesmal pore is no longer a preferential localisation of LYM2. Alternatively, the endomembrane adjacent to plasmodesmata has become an environment which binds and keeps LYM2 fixed in place, not preventing it from diffusing out of the plasmodesmal pore, but from diffusing into the plasmodesmal pore. This observation can therefore be explained by multiple different possible hypotheses, and it will be up to future experiments to truly unravel this dynamic and behaviour further.

The observations in this experiment would allow for greater certainty in their interpretation by the addition of further repeats, and images of greater detail in both mock and chitin treated conditions. This would allow to greatly strengthen and support their conclusions.

3.3.2 LYK4 and LYK5 localise to the PM

Both LYK4-mCherry and LYK5-mCherry expressed from their native promoters in Arabidopsis, resulted in fluorescent signals suggesting an even PM localisation (Fig. 3-2C, D). Expressing them from their native promoters did therefore not reveal a previously obscured plasmodesmal localisation.

Later work in Cheval et al. (2020), used purified plasmodesmata extractions to determine biochemically that LYK5 is not present at plasmodesmata while LYK4 is. This is contrast to the

observations in which LYK4 shows an even PM localisation without discernible foci of enrichment, reminiscent of plasmodesmata. This therefore illustrates that a protein can be present at plasmodesmata while not showing a confocal microscopy determined plasmodesmal enrichment, as conventional confocal microscopy is not sufficient to resolve plasmodesmata. Future experiments using more advanced microscopy techniques such as Airyscan microscopy could possibly overcome this resolution limit and demonstrate a LYK4-mCherry localisation at plasmodesmata.

3.3.3 Dynamic behaviour changes of receptor proteins

FRAP was used to identify changes in the lateral movement behaviour of LYM2, LYK4 and LYK5 triggered by chitin. Changes to protein interactions or complex formations, as well as changes to residency within micro-/nanodomains of the membrane can result in changes of the mobile fraction (Reits and Neefjes, 2001). The chitin-triggered changes in the mobile fractions of LYM2, LYK4 and LYK5, therefore suggest that pools of these proteins can undergo changes in their associations with other proteins or nanodomains in response to chitin.

If two proteins are localised in a complex together or resident within the same nanodomain together, then the overall mobility of the complex or nanodomain respectively, is going to be a defining characteristic of the two proteins' mobility, and similar lateral membrane mobilities for those two proteins would be expected. As there are differences when comparing the PM mobile fractions of LYM2 with LYK4 and LYK5, this suggests that these proteins do not show a complete overlap in their localisations or behaviours and suggests that different pools of these proteins might therefore be present in different complexes or nanodomains.

As LYM2 shows a mobile fraction of 35-40% depending on the conditions and membrane structures, 35-40% of the LYM2 molecules within a plasmodesma pit field get replaced every 60 s. This rapid exchange of proteins indicates a highly balanced equilibrium between pools of proteins at the PM and the plasmodesmal PM as the enrichment at PD is consistently maintained as it otherwise might not be possible to be maintained. This balance might get strongly skewed to one side, even just by slight imbalances in the exchange of proteins towards or away from plasmodesmata. This might be the cause of the increase in PD index observed within 30 min. for Cit-LYM2 in Cheval et al. (2020).

Most transmembrane proteins are rarely included or enriched in ordered domains, based on persistent observations and studies of synthetic membranes (Levental et al., 2011; Levental and Levental, 2015). Recently van Deventer et al. (2020) and Levental et al. (2020) have therefore speculated that lipid rafts do not function by particular inclusion of proteins, but rather by a higher rate of exclusion of most proteins, thereby resulting in different dynamics of retention and equilibriums. Assuming a lipid raft like character of the plasmodesmal PM microdomain, this allows me to form the following hypothesis: The localisation of LYM2 at plasmodesmata is dependent on secretion from the ER to the PM via the Golgi, in the first step and in the second step dependent on LYM2's ability to be present and be retained within the plasmodesmal PM — an ability which not all other proteins share to the same extent. The plasmodesmal localisation of LYM2 is therefore putatively not achieved by a targeted mechanism depositing it directly at plasmodesmata, but rather by the constant exchange and skewed equilibrium between pools of the protein at the plasmodesmata versus pools at the bulk PM driving a preferential retention in the plasmodesmata (Fig. 3-13).

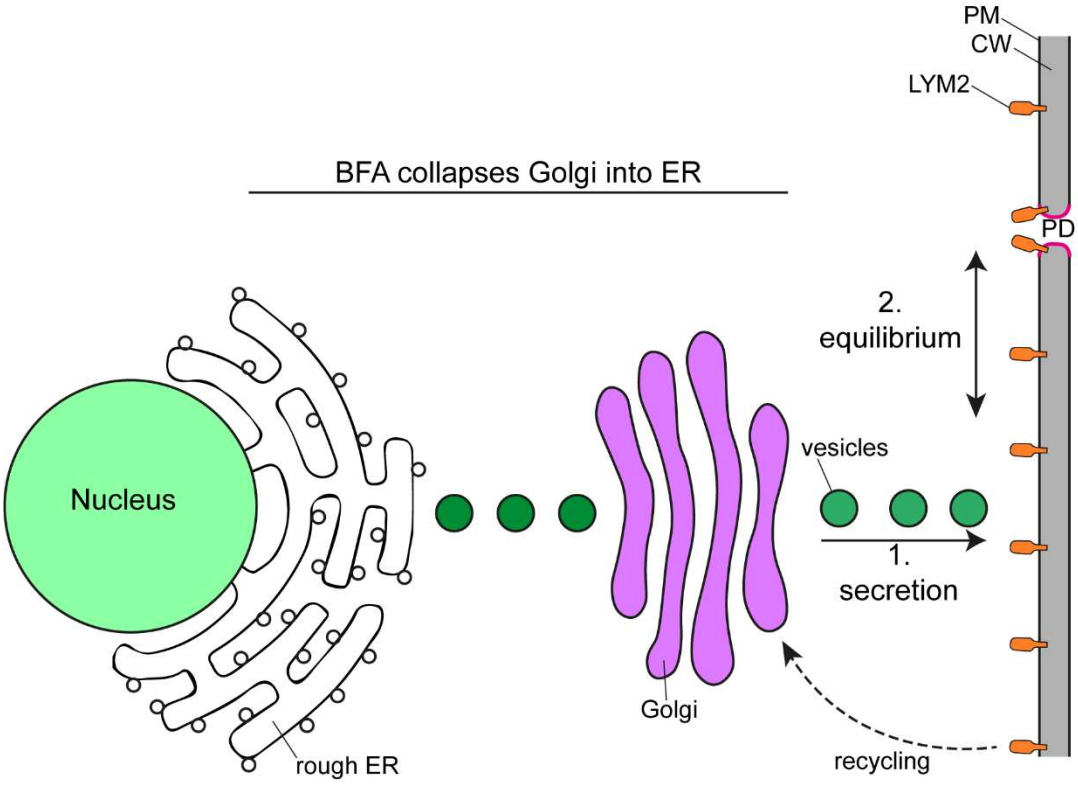

Figure 3-13: A cartoon conceptualisation of how LYM2 localises and enriches at plasmodesmata. Treatment with BFA collapses the Golgi apparatus into the ER, and thereby inhibits the secretion process of new proteins as well as the secretion back to the PM of recycled proteins. In this hypothetical model LYM2 needs to first (1.) reach the PM via Golgi mediated secretion processes. Secondly there is an equilibrium (2.) between the pool of LYM2 proteins in the bulk and the plasmodesmata, with a constant exchange of LYM2 between these two pools. But LYM2 has a higher preference to be present at plasmodesmata or retention at plasmodesmata, thereby resulting in an enrichment. This equilibrium could be skewed during chitin perception, thereby resulting in an increase of the PD index for LYM2. PM: plasma membrane, CW: cell wall, PD: plasmodesmata, ER: endoplasmic reticulum, BFA: Brefeldin A.

3.3.4 LYM2, LYK4 and LYK5 associate with each other

During the co-IP optimisation experiments, the addition of three phosphorylation inhibitors assisted in the reduction of artefactual negative control signals (Fig. 3-7). Theoretically, neither $Na_2MoO_4 \cdot 2H_2O$, NaF nor activated Na_3VO_4 should have an effect on the detection of protein interaction partners in co-IP experiments. I can therefore only speculate how this is achieved. Possibly, dephosphorylated Cit-LYM2 (and other receptors), have a higher affinity to non-specifically interact with other proteins and bind to them during the protein extraction and wash processes. However, this experiment demonstrated that they do have a further effect even if it is unknown why. I have therefore continued to use these three additional phosphatase inhibitors in all further protein extraction and co-IP experiments in this PhD thesis. Further experiments would be needed to also assess if the three inhibitors have any effect in the overall reduction of signal or protein presence to allow for stronger conclusions. Taking the possibility of RKs localising into nanodomains (some with a possible detergent resistant character) in the PM into account, one can further draw hypotheses that possibly during the solubilisation steps of the protein content of plant cells the disruption of nanodomains might only occur partially. Therefore, it is possible to imagine that a co-immunoprecipitation does not always show a protein-protein interaction but possibly also just a presence of both the prey and the bait protein within the same nanodomain. This could be explored further, possibly by utilising other additional chemicals or enzymes to result in disruption of nanodomains to a different degree.

Experiments not relying on confocal microscopy but rather supplying biochemical evidence by detecting proteins from plasmodesmal fractions, showed that not only LYM2 but also LYK4 is present at plasmodesmata (Cheval et al., 2020). However, LYK5 has not been detected at plasmodesmata. On the basis of this evidence, one can infer that there are different receptor protein association possibilities depending on their localisation. In the PM all three receptors can interact with each other, while in the plasmodesmal PM only LYM2 and LYK4 can interact with each other. LYM2 localises to the PM but shows an enhanced localisation at plasmodesmata as well as exhibiting a greater homo-FRET there (Cheval et al., 2020; Faulkner, 2013). An increased homo-FRET indicates an increased protein clustering (Bader et al., 2009), and thereby suggests that LYM2 oligomerises or clusters at plasmodesmata, possibly resulting in the formation of signalling platforms.

Any change of subcellular localisation or membrane domain residency, also changes a protein's availability for protein complex formation. For example, if it moves from its original resident nanodomain into another domain, it is no longer available in the original one, but rather now available in the new localisation. These changes do not have to be absolute, but rather can represent subsets and pools of individual proteins. LYM2 changes its PD index and shows an increased enrichment at plasmodesmata after chitin treatment. As chitin triggers LYM2 to increases its abundance at plasmodesmata, it allows to speculate that this results in more LYM2 to be available for protein complex formation at plasmodesmata.

It further also allows the reverse conclusion that less LYM2 is available for complex formation in the PM. This could be one possible explanation why less LYK5 can be detected in the LYM2 IP (Fig. 3-10) in the presence of chitin. Alternatively, this could also not just be due to the lower availability of LYM2 in the PM, but rather due to an "active dissociation" process between LYM2 and LYK5 or the inhibition of new complex formation upon the detection of chitin. However, the conclusions can only be drawn very cautiously, as all of these experiments have been carried out using a transient overexpression system, and results might not necessarily be representative of the native system.

To independently confirm protein associations, FRET-FLIM analyses were carried out and published in Cheval et al. (2020). Both LYK4 and LYK5 have been observed to undergo ectodomain shedding and could therefore not be tagged with a fluorophore on their extra cellular side (N-terminal). Further, as Cit-LYM2 is a GPI-anchored protein (Faulkner et al., 2013) its fluorophore localises not on the cytosolic side of the PM but rather only on the extracellular side. As FRET can't be measured through a biological membrane, LYM2 is incompatible with LYK4 and LYK5 for FRET experiments, and we could only test and confirm for the association between LYK4 with LYK5. Though no consistent change in the detection LYK5-6×HA when co-immunoprecipitated with LYK4-eGFP when comparing chitin to water treated samples (Fig. 3-9) was observed, such a chitin-triggered difference in association was detected by FRET-FLIM (Cheval et al., 2020). In samples treated with chitin the donor LYK4-eGFP, co-expressing LYK5-mRFP1, exhibited a statistically significant increase in fluorescent lifetime when compared to water treated samples. This hints at a chitin-triggered dissociation or complex relaxation between LYK4 and LYK5 at the PM. My co-IP experiments were not able to detect this change, possibly due to the transient overexpression nature of the system, or due to higher sensitivity for such changes in FRET-FLIM over co-IP protein association determination methods. However, this data indicates that these protein complexes undergo dynamic processes depending on the presence of chitin.

As both LYK4 and LYM2 are present at the PM as well as the plasmodesmal PM (Cheval et al., 2020; Faulkner et al., 2013), it stands to reason that they can undergo complex formation in both compartments. In my co-IP experiments, a consistent change in the levels of prey LYK4 detected when I immunoprecipitated LYM2 as a bait was not identified(Fig. 3-10). This is not unexpected as standard co-IP experiments cannot differentiate between proteins localised to the PM or the plasmodesmal PM. Protein extractions from plasmodesmata require further release from the cell wall matrix to efficiently release plasmodesmata localising proteins (Faulkner and Bayer, 2017). The protein extraction method used in this work does not include such steps and can therefore be assumed to not extract proteins at plasmodesmata with the same efficiency as from the general PM. This probably has resulted in a drastic overrepresentation of PM versus plasmodesmal localised receptor associations. For this reason, it is possible that there is a lot more of the LYM2-LYK4 association present than detected in Fig. 3-10, and these plasmodesmal complexes might further undergo an increase in their formation triggered by chitin at plasmodesmata.

How can LYK5 be crucial for this response if it is not present in the plasmodesmata where the LYM2-LYK4 complex putatively fulfils such a local receptor signalling role? In Cheval et al. (2020) we revealed that there are protein size differences of LYK4 when co-immunoprecipitated off LYM2 in the absence of LYK5 in *lyk5* protoplasts. These contrasting sizes indicate differences in LYK4 post-translational modifications (discussed in chapter 3.3.6) and/or ectodomain shedding (discussed in chapter 3.3.5), protein stability and dynamics depending on the presence or absence of LYK5. LYK4's size differences depending on LYK5, gives further relevance to the LYK4-LYK5 interaction (Fig. 3-9). As LYK5 can not be detected at plasmodesmata, it can be speculated this interaction can only take place within the PM. It therefore stands to reason that LYK4 must be either pre-processed or protected from changes depending on LYK5 within the PM, before it can fulfil its function within the plasmodesmal PM. Taken together these different protein associations highlight the functional importance of the different receptor protein pools within the PM and the plasmodesmal PM, as well as how they interact, exchange or preferentially localise within these pools.

The co-IPs in this thesis have been carried out utilising a biological control in the form of LTI6b with the appropriate tag, such as the other prey of interest. This controls for artefactual binding of membrane proteins during the immunoprecipitation process as well as insufficient membrane disruption. A further technical control in the form of the presence of the prey of interesting but in the absence of the bait could further be carried out to demonstrate that

the prey of interest does not coincidentally also immunoprecipitate to the magnetic beads. As the biological control (LTI6b) already carries the same epitope tag as the prey of interest and does not immunoprecipitate with the bait, the tag can be excluded to artefactually bind to the magnetic beads. However, for completeness it is possible to carry out such technical bait absence controls.

3.3.5 Ectodomain shedding – a possible explanation for differences in detected size

LYK4 and LYK5 fluorophore translational fusion proteins in *N. benthamiana* as well as in Arabidopsis plants result in detection of signals indicative of differently sized proteins. One of these detected sizes is bigger than the predicted full-length version suggesting to be caused by potential additive PTMs, and one is noticeably smaller suggesting to be caused by cleavage processes such as ectodomain shedding.

Evidence of LYK4 and LYK5 undergoing ectodomain shedding was generated by utilising dually tagged constructs with a fluorophore on both the C- as well as the N-terminus of the RKs. This resulted in detection of the C-terminal fluorophore (mCitrine) signals in a clear PM fashion, while the extracellular N-terminal (mCherry) fluorophore was detected in the extracellular space between adjacent cells as well (Fig. 3-11). The mCherry signal is rather diffusely distributed within the extracellular space, indicating that this fluorescent tag possibly together with a part of the RK's ectodomain has been cleaved off from the rest of the ectodomain, and is now no longer bound to the PM. Peptides corresponding to the ectodomains of LYK4 were further found in the soluble fractions of protein extracts by Petutschnig et al. (2014) and ectodomains of LYK5 were found by Meusel (2016) in cell culture supernatants. The different protein sizes together with the removal of the mCherry fluorophore signal from the PM to the extracellular space, suggest that both LYK4 and LYK5 undergo ectodomain shedding. These constructs could be used in future experiments to further demonstrate the ectodomain cleavage via SDS-PAGE and Western blotting, to allow for a visualisation of the cleaved ectodomain as well as the remaining protein from the same samples.

However, how can ectodomain shedding regulate and fine tune signalling processes of receptors? Antolín-Llovera et al. (2014b) found ectodomain shedding in LjSYMRK necessary for functionality. LjSYMRK versions without the MLD of its extracytoplasmic region outcompeted full-length LjSYMRK for interaction with NFR5 thereby interfering with appropriate receptor complex formation. This indicated that the MLD negatively interferes

with complex formation. Presence or absence of ectodomains can therefore down- or up-regulate protein functions in plants. For example, mutants of LjSYMRK without an ectodomain lead to excessive infection thread formation (Antolín-Llovera et al., 2014b). This points towards a role of ectodomain shedding in the fine tuning of the receptor signalling function (Antolín-Llovera et al., 2014a). The different versions of LYK4 and LYK5 (non-shed and shed) could similarly undergo different preferential receptor complex formations and outcompete each other for specific ones. Or alternatively one version is more stable than the other, or is more prone to get recycled, or targeted for degradative processes and ectodomain shedding thereby influences the overall ratios of available proteins. Further, Ectodomain shedding could result in different downstream PTMs of their associated co-receptors, such as in the case of BAK1-BIK1 (Zhou et al., 2019). Ectodomain shedding of LYK4 and LYK5 could therefore be a mechanism to ensure appropriate signalling responses by fine tuning receptor complex formation and protein availability. Full length and putatively ectodomain lacking bands for both LYK4 as well as LYK5 were detected in co-IP experiments. Their abundance ratios in the IP fractions did not obviously shift towards lower sizes suggesting that their ectodomain shed versions do not undergo complex formation more preferentially than their full-length counterparts. Should the co-IP between the receptors in my experiment be due to their shared nanodomain/DRM localisation this would indicate that both the full length as well as the ectodomain lacking version of these proteins maintain their presence in their nanodomains/DRMs.

Possibly the ratio between full length version and the potential ectodomain lacking version of LYK5 in Fig. 3-10 might shift when comparing the input versus the immunoprecipitated samples. This would need further experimental validation in the future to allow for conclusions drawn with certainty.

By contrast to LjSYMRK, both LYK4 and LYK5 do not have a GDPC motive, nor MLD domains. Therefore, the mechanism of shedding might be different and mediated by a different cleaving enzyme — referred to as sheddases in animal cell biology (Clark, 2014; Lichtenthaler et al., 2018). Petutschnig et al. (2014) determined that ectodomain shedding results in a roughly 33 kDa soluble cleavage product of CERK1. LYK4 results in a roughly 45 kDa and LYK5 results in a roughly 30 kDa cleavage product. Given their sequence similarities, it is possible that all three proteins CERK1, LYK4 and LYK5 get cleaved by the same sheddase, possibly recognising the same or a similar motif. Since the ectodomains can also undergo additive PTMs, the size of the cleavage product is not necessarily indicative of the cleavage site within the amino acid sequence. Given the importance of ectodomain shedding in animal cell

biology — particularly signalling processes — and the first detailed accounts of how ectodomain shedding can have influences on plant receptor functions (Antolín-Llovera et al., 2014b; Petutschnig et al., 2014), it will be interesting to see more ectodomain shedding data emerge in plants.

The knowledge that LYK4 and LYK5 undergo possible ectodomain shedding processes enables to see their previous FRAP data (Fig. 3-3) from an additional different angle. FRAP data was acquired from translational fusion proteins which carry their fluorophore tag on the cytosolic side of the PM, and therefore the data represents a sum of the behaviour of shed and non-shed RK. Possibly the two pools of shed and non-shed LYK4 and LYK5, could exhibit different mobile fractions from each other, and therefore different interaction potentials could also be present in different receptor complexes or nanodomains.

It could be further conceivable that the ectodomain shedding processes do not just apply to individual LYK4 or LYK5, but rather to specifically formed complexes. This in turn could affect the whole complexe's dynamics and behaviours, localisations and stability, and therefore fine tune and regulate the receptor complex mediated signalling processes via specific sheddases. Alternatively, an interaction with LYK4 or LYK5 could also regulate the ectodomain shedding processes of secondary proteins, or vice versa, as an interaction partner of LYK4 or LYK5 could be responsible that these proteins undergo ectodomain shedding processes, i.e. by changing their conformation and allowing sheddase recognition motifs to become accessible. It would therefore be interesting to test in future experiments if one can determine LYK4 and LYK5 shed ectodomain interacting proteins, and then test if they are necessary for ectodomain shedding processes of each other.

It could further be logically conceived that the release of chitin binding ectodomains might also be able to regulate the presence of freely available chitin in the apoplast. This could possibly be necessary to "reset" a cell's signalling capacity after the presence of a pathogen has been initially detected. Thereby allowing the cleaved ectodomain itself to further fulfil a function away from the rest of its original full-length protein.

During the co-IP experiments of this thesis often bands of lower sizes have been additionally observed in the Western blots. These could be either specific sizes indicative of protein degradation processes or possibly other processes such as ectodomain shedding. This could be further explored in future work.

3.3.6 LYK4 undergoes additive PTMs

Although LYK4 might possibly undergo phosphorylation processes, typically such a PTM results in an increase of protein size of about 79.99 Da (MacLean et al., 2008).

As no ubiquitin signal of LYK4-mRFP1 was detected (Fig. 3-12A), the inhibition of ubiquitination cannot be concluded to be the reason for the size reduction of LYK4 in *lyk5-2* mutants. By contrast to this, the glycosylation of full length LYK4 was successfully determined.

Häweker et al. (2010) demonstrated that non-glycosylated EFR proteins are rather unstable, while non-glycosylated FLS2 and BAK1 accumulate to significantly higher than native levels, thereby indicating that glycosylation as a PTM can fine tune plant receptor protein abundance and stability. The glycosylation of LYK4 could therefore lead to either an increase or decrease in protein stability, resulting in an increase or decrease in protein abundance, thereby adjusting the availability of this protein.

Glycosylation is necessary for FERONIA (FER) and other PM receptors to fulfil their functions (Lindner et al., 2015; Schoberer and Strasser, 2018). It stands to reason that if indeed the correct glycosylation of LYK4 is dependent on the presence of LYK5, that this is the indirect way in which LYK5 can influence a cell's ability to regulate plasmodesmal flux in a chitin dependent manner. However, how would LYK5 be responsible for a glycosylation PTM of LYK4?

The genome of Arabidopsis encodes for 400 glycosidases (Husaini et al., 2018) — enzymes which are capable of removing specific sugar moieties (Kytidou et al., 2020). At least 15 of these glycosidases are present within the cell wall and the extracellular space (Fry, 2004), allowing them to possibly target the ectodomain of LYK4 in the absence of LYK5. Possibly the presence and interaction with LYK5 could stop these enzymes from successfully targeting LYK4, by making a recognition motif or the glycosylations themselves inaccessible. The association between LYK4 and LYK5 could further possibly already be present before these two proteins undergo secretion processes towards the PM, and the glycosylation could therefore already be affected during the proteins' time in the ER or Golgi.

Although a mechanism of PTM of LYK4 was identified — a ~14 kDa shift does not fully explain either the ~5 nor the ~30 kDa shift observed in *lyk5-2* (Cheval et al., 2020). However, it is possible that the presence of LYK5 is only responsible for a small number of glycosylation reactions and thereby causal of the 5 kDa shift. Further, the ~ 30 kDa shift could be explained

by further non-N-linked glycosylation not being successfully carried out in the absence of LYK5. Alternatively, a so far unexplored PTM could additionally contribute to this, and the size shifts could actually be a result from multiple different modifications and potentially even partial or full ectodomain shedding.

Although I did not manage to determine all the PTM LYK4 potentially undergoes, I determined that it undergoes ectodomain shedding and N-linked glycosylation. Future experiments might reveal multiple more PTM, and how they are necessary or not for LYK4 to fulfil its function in chitin triggered immunity.

3.3.7 Chitin receptor dynamics — a model

The data of this chapter and of Cheval et al. (2020) enable the conceptualisation of a model (Fig. 3-14) of how the different receptors associate with each other. Different associations are possible within the PM and at the plasmodesmal PM microdomain, resulting in chitin-triggered ROS bursts and callose mediated plasmodesmal closure.

Similarly to tetraspanin web concepts described in the next chapter (Fig. 4-2), nanodomains including the proteins discussed in this chapter may not exist in a linear fashion in the PM but rather as accumulations or enrichments of different proteins together in nanodomains. These nanodomains or specific protein enriched areas within the PM, may be present in a "mesh" like fashion, or may be more distinctively separate from each other.

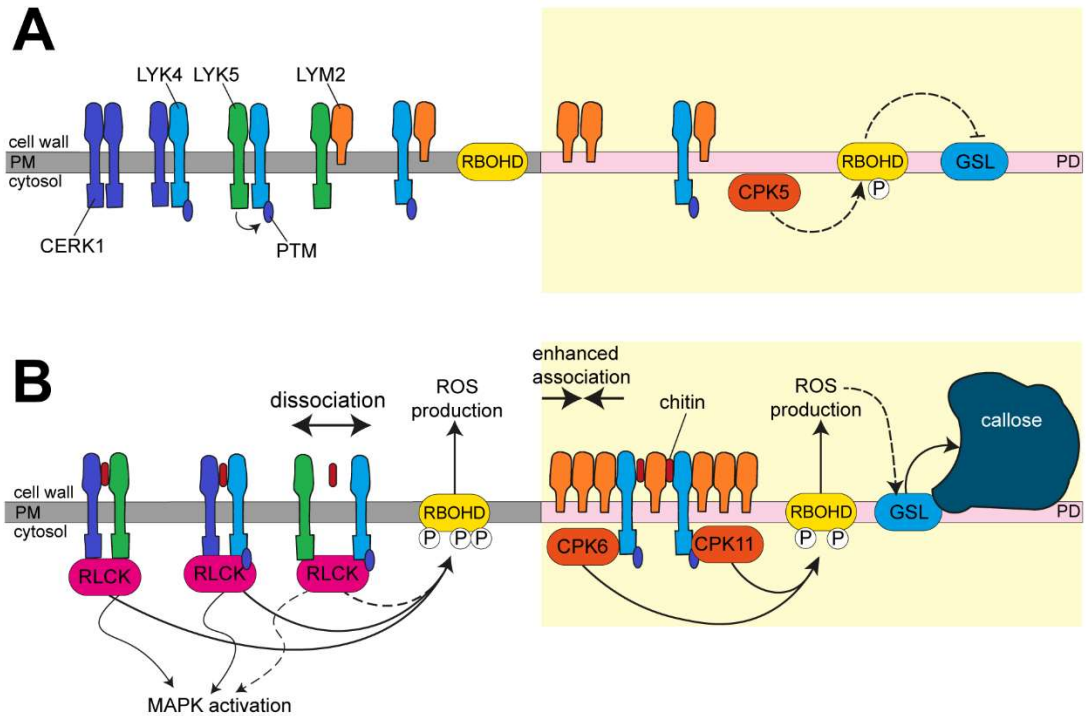

Figure 3-14: A possible model for receptor mediated chitin-triggered immune signalling with a focus on the plasmodesmal response (redrawn and adapted from Cheval et al. 2020). This schematic representation is drawn

as a continuity between the PM (grey) and the plasmodesmal PM microdomain (light pink). Different receptor complex combinations can be present at the PM, such as CERK1-CERK1, CERK1-LYK4, LYK5-LYK4, LYK4-LYM2, LYK5-LYM2. A PTM of LYK4 is dependent on the presence of LYK5. LYK5 is not present at plasmodesmata and therefore only complexes of LYM2 and LYK4 can be formed at plasmodesmata. (A) Resting state conditions in the absence of chitin. CPK5 ensures an inhibition of callose deposition. (B) Chitin-triggered conditions. In the presence of chitin, CERK1-LYK5 can undergo a further complex formation (Cao et al., 2014). Chitin further triggers an increase of LYM2 at plasmodesmata as well as an increase of higher-order-interactions of LYM2 at plasmodesmata (Cheval et al., 2020). The RKs in the PM are capable of activating RLCKs, which in turn activate the MAPK cascades as well as phosphorylate RBOHD. At the plasmodesmal PM, the perception of chitin relies on CPK6 and CPK11 to phosphorylate RBOHD. The activation of RBOHD via phosphorylation leads to ROS production, and in turn to the deposition of callose through callose synthases and thereby to a closure of plasmodesmata. (A) & (B) PM: plasma membrane; PD: plasmodesmata, PTM: post-translational modification; P: phosphorylation, GSL: GLUCAN SYNTHASE-LIKE = callose synthases; RLCKs: receptor-like cytoplasmic kinases.

3.3.8 Conclusion

In this chapter I determined some of the behaviours and characteristics of the PRRs LYM2, LYK4 and LYK5. I generated data which allows to draw hypotheses of how LYM2's preferential plasmodesmal localisation is maintained, and how a chitin-triggered enrichment might be achieved. Next, I showed that all three receptors are capable of associating with each other. To identify how LYK5 can be vital for chitin-triggered plasmodesmal closure without being present at plasmodesmata itself, I investigated which PTMs of LYK4 could be dependent on the presence of LYK5. Taken together, this chapter adds important steps and blocks of knowledge in our understanding of how chitin receptors interplay and chitin-triggered plasmodesmal closure is regulated.

4 Tetraspanins in chitin signalling

4.1 Introduction

4.1.1 What are tetraspanins?

For receptors to successfully function, they not only interact and associate with other receptors, but also with lipids (Tornmalm et al., 2019) and a multitude of proteins from other classes and families (Cao et al., 2021). One such protein family strongly associated with receptors are the tetraspanins (Termini and Gillette, 2017). Tetraspanins are a family of structurally related proteins. They are integrated into the PM of cells by four characteristic transmembrane domains, which give this family its name (Figure 4-1).

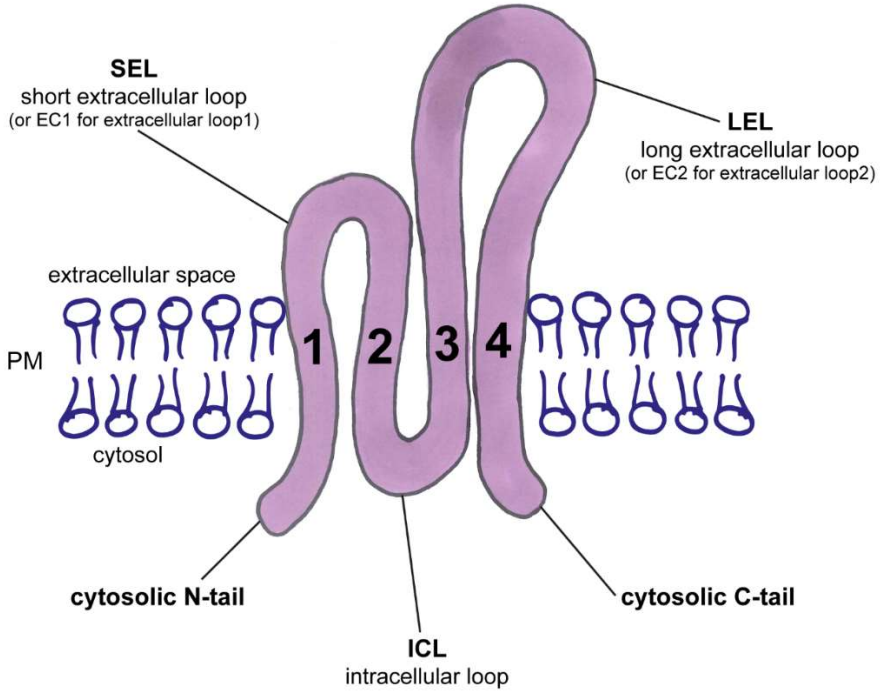

Figure 4-1: A cartoon schematic of the architecture of tetraspanin proteins. The PM is symbolised by a phospholipid bilayer in in blue. The top of the Figure symbolises the extracellular space – i.e., outside of the cell and the lower half of the Figure is in the cytosol – i.e., inside of the cell.

Tetraspanins are inserted in the cell's PM in a conformation that allows both their N-terminal and C-terminal tails to be on the cytoplasmic side of the PM. They have three loops, one in the intracellular space and two (one short and one long) in the extracellular space (Fig. 4-1) (Hemler, 2005). These proteins can form homo- and heterodimers, interacting with tetraspanin proteins of their own kind or other tetraspanins respectively. Further, tetraspanins are able to interact with multiple other tetraspanins and non-tetraspanin proteins simultaneously, enabling the formation of complex oligomers (van Deventer et al., 2017). This allows tetraspanins to act as scaffolds which organise higher order protein

structures in the PM and recruit partner proteins for specific functions. This is fundamental to support both dynamic processes and formation of rigid structures within the PM. Indeed, these oligomerisation processes lead to formation of domains within the PM which have a high concentration of tetraspanins acting as scaffolds (Schmidt et al., 2016). In turn this stabilises and maintains the integrity of these domains (Charrin et al., 2002) which can then act as specialised and organised signalling hubs (Zimmerman et al., 2016). Broadly, tetraspanins act as molecular organisers and facilitators (Hassuna et al., 2009) by establishing a network of tetraspanins called a tetraspanin web (Fig. 4-2) (Hruz et al., 2008).

Tetraspanin webs act as scaffolds which organise the PM, enriching specific areas of the PM with high concentrations of tetraspanins and their interacting proteins. These domains, containing tetraspanins and the additional components they recruit, are classically referred to as tetraspanin enriched microdomains (TEM) (Perez-Hernandez et al., 2013). TEMs can be in dynamic protein exchange with the rest of the PM (Oosterheert et al., 2020), reaching an equilibrium state which can adapt and change in a stimulus dependent manner (Kummer et al., 2020). Due to this creation of specific surrounding environments for the proteins which are present in TEMs, tetraspanins can influence and control the functions of these TEM resident proteins (Lu et al., 2020).

In later years, Zuidscherwoude et al. (2015) have challenged the idea of multiple different species of tetraspanins forming web-like structures. They used dual colour stimulated emission depletion (STED) microscopy to determine that tetraspanins form individual nanoclusters which only display minor overlap and correlation with other tetraspanins. They suggest that rather than a tetraspanin web of multiple tetraspanin species organized into a single domain, tetraspanins form species independent domains which are important for their functionality.

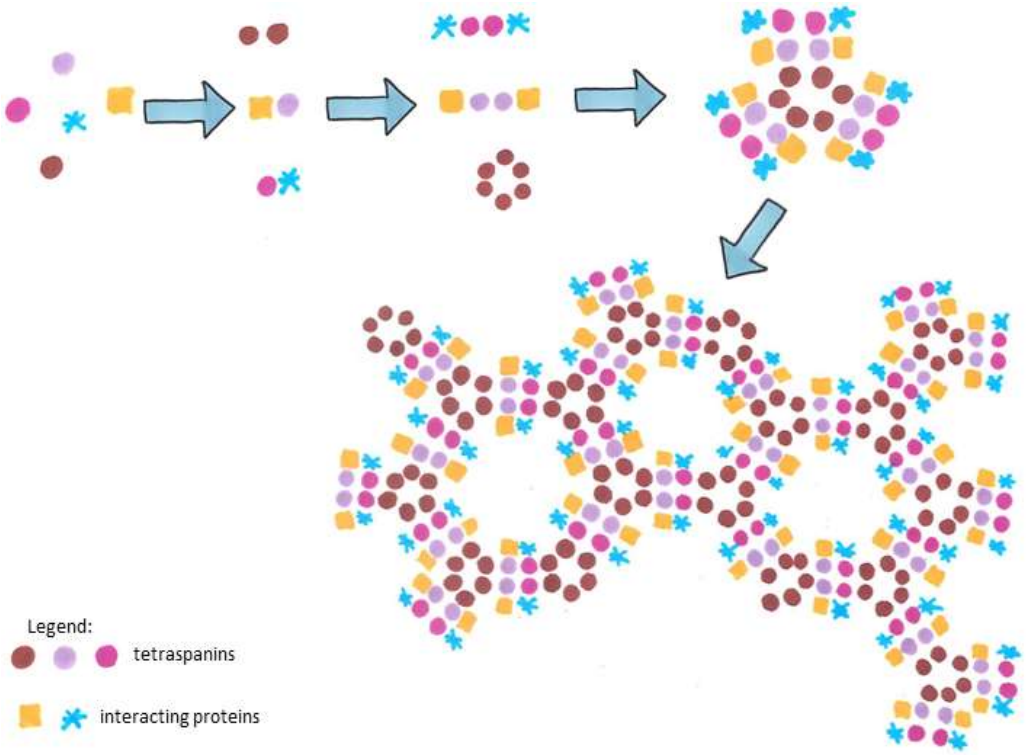

Figure 4-2: Cartoon depiction of a tetraspanin web protein interaction progression. The graphic follows the progression of how interactions between individual tetraspanins followed by interactions with other non-tetraspanin proteins can lead to an organised structure called a tetraspanin web. Tetraspanins are symbolised by coloured circles and other proteins which interact with tetraspanins are symbolised by a yellow square and a blue star sign. Redrawn after Martin et al. (2005).

4.1.2 Tetraspanins immune signalling functions in non-plant kingdoms

Tetraspanin gene families in different organisms have undergone independent duplications and radiation events with the evolutionary history of their organisms' lineages (Huang et al., 2005). Various eukaryotic species have functional tetraspanins, ranging from *Drosophila melanogaster* with 37 tetraspanins (Todres et al., 2000), different groups of nematodes with 9 to 21 tetraspanins (Davis et al., 2022; Harris et al., 2019; WormBase Version WS283, 2022) to humans with 33 tetraspanins (Huang et al., 2005). Huang et al. (2005) suggest that the co-evolution of tetraspanins was an important step in the evolution and transition from unicellular to multicellular organisms. This theory is supported by evidence of the conserved roles of tetraspanins for signalling and inter-cellular communication. For example, tetraspanins are able to regulate the formation and development of cell junctions (Huang et al., 2018), and cross-kingdom immune signalling, exchanges and communication — between organisms belonging to different kingdoms functioning in the generation and secretion of extracellular vesicles (Hurwitz et al., 2016; Jimenez-Jimenez et al., 2019a). Umeda et al. (2020) further suggest two major roles of tetraspanins in microsome (exosome) formation. Firstly, tetraspanin clustering induces membrane curvature, which is then followed by exosome budding. Secondly, association of proteins with the corresponding interacting tetraspanin(s) is part of the vesicular cargo sorting process. In general, tetraspanins can form multiple protein interactions simultaneously and are therefore important in a variety of different biological processes. Their ability to form multiple protein interactions simultaneously results in an 'ordering' of the membrane. This sorting process is necessary for the biosynthetic maturation and regulation of trafficking of some of the tetraspanin partner proteins (Berditchevski and Odintsova, 2007; Saint-Pol et al., 2017) and in receptor mediated immune signalling (Tam et al., 2019; Termini and Gillette, 2017).

The naming system of tetraspanins depends on the organism in which they are described. Many mammalian tetraspanins were originally identified and named after the 'cluster of differentiation' (CD) protocol used to describe antibody binding of surface molecules of leukocytes (Hochheimer et al., 2019; Xiong and Xu, 2014). However, not all CD proteins are tetraspanins nor are all mammalian tetraspanins named after the 'cluster of differentiation' protocol (Hochheimer et al., 2019). In animal cells, tetraspanins are highly important in signalling and particularly immune signalling processes and are therefore involved in cancer (Hemler, 2014; Li et al., 2013; Yang et al., 2008), fertility (Le Naour et al., 2000; Miyado et al., 2000), retinal degeneration (Xu et al., 2004) and infection processes (Hassuna et al., 2009)

ranging from viral (Pileri et al., 1998), protozoan (Silvie et al., 2003), fungal (Artavanis-Tsakonas et al., 2011) and bacterial infections (Mitamura et al., 1992) as well as to prion diseases (Griffiths et al., 2007).

The behaviour of membrane proteins can change in the presence or absence of their corresponding tetraspanin partners. For example, in HEK293 cells (immortalized human embryonic kidney cells) and in human macrophage model cell line U373 the increase in lateral mobility of TOLL-LIKE RECEPTOR 4 (TLR4) upon binding its ligand lipopolysaccharide is dependent on the presence of the tetraspanin CLUSTER OF DIFFERENTIATION 14 (CD14). This process is necessary for successful detection and immune signalling in response to gram-negative bacterial (Klein et al., 2015). The mouse tetraspanin CD82 organises the receptor Dectin-1 to recognise the fungal cell wall component ß-1,3-glucan of *Canadia albicans*, resulting in protein clusters in the phagocytic cup and the regulation of defence signalling (Tam et al., 2019). Broadly, tetraspanins interact with cell surface receptors, suggesting they are important for functions in immune systems.

The functions of some tetraspanins are highly characterised in the human immune system, such as the fusion of multiple micro-/nanodomains to achieve functional signalling processes. For example, in B cells tetraspanins are important in successful detection of antigens and intracellular signalling. The production of antibodies in B cells is mediated by the B CELL RECEPTOR (BCR) complex via antigen-specific activation of B-lymphocytes (Cano and Lopera, 2013). Within the BCR complex two non-tetraspanin proteins CLUSTER OF DIFFERENTIATION 79A (CD79A) and CD79B interact with membrane-bound immunoglobulins (Ig). The non-tetraspanin CD19, is a single transmembrane protein with two Ig-like domains which interacts with the tetraspanin CD81. During resting state conditions — before activation of immune signalling — CD81 and CD19 are forming domains independent of BCR, CD79A and CD79B (Packard and Cambier, 2013). However, upon antigen detection by the BCR, cytoskeletal reorganisation is triggered and the CD19/CD81 and the BCR/CD79A/CD79B domains fuse to form one signalling competent membrane domain activating antibody production, making CD81 an important component of antigen-triggered immunity processes (Kummer et al., 2020; Wang et al., 2012b).

Another way to generate intracellular immune signals is the production of ROS (Tavassolifar et al., 2020). Although tetraspanin proteins themselves are not capable of ROS generation, strong links between them have been observed. In the nematode model system *Caenorhabditis elegans*, tetraspanin TSP-15 is required for the functionality of some ROS

producing enzymes. TSP-15 forms a complex with the dual oxidase BLISTERED CUTICLE (BLI-3) and the DUAL OXIDASE MATURATION FACTOR (DOXA-1). TSP-15 has been demonstrated to be necessary for the activation of these enzymes (Moribe et al., 2012; Moribe and Mekada, 2013). Lambou et al. (2008) showed a genetically linked presence of ROS producing enzyme NADPH oxidase 2 (NOX2) and fungal tetraspanin PSL1, in fungal genomes. The fungal tetraspanins MgPLS1 of *Magnaporthe grisea* and BcPLS1 of *Botrytis cinerea* are required for successful penetration of their plant host's leaves (Clergeot et al., 2001; Gourgues et al., 2004; Lambou et al., 2008). Co-localisation studies of Siegmund et al. (2013) reveal a localisation of BcNOXs (NADPH oxidases) complexes and BcPLS1 in similar membrane structures, as well as similar phenotypes of knock-out strains, such as a defect in appressoria-mediated host cell penetration (Siegmund et al., 2013). Later studies in *Magnaporthe oryzae* revealed that the absence of MoPLS1 also causes similar phenotypes as the absence of MgNOX2, such as the mislocalisation of F-actin, septin, and the septin kinase Chm1, further linking tetraspanins to NADPH oxidases (Ryder et al., 2013).

Tetraspanins can up or down regulate signalling processes depending on their associated receptor proteins and the context of the response. Using cancer as an example for immune signalling processes Wang et al. (2015b) demonstrate how tetraspanin protein complexes can fulfil different regulatory functions depending on the presence or absence of specific associated proteins in mammalian cells. In the presence of the tetraspanin partner EWI MOTIVE CONTAINING PROTEIN 2 (EWI-2), the tetraspanins CLUSTER OF DIFFERENTIATION 9 (CD9 = Tspan29) and CD81 (=Tspan28) interact with EWI-2 and are not available to interact with TRANSFORMING GROWTH FACTOR BETA (TGF-β) receptors, thereby limiting TGF-β signalling. However, this situation changes in late-stage melanoma cells, as EWI-2 is downregulated. The lack of this competitively binding protein allows CD9 and CD81 to interact with TGF-β receptors, producing stable and actively signalling TGF-β receptor complexes. This leads to increased SMAD (SMA "small worm phenotype" and MAD family "Mothers Against Decapentaplegic") protein family transducing signalling from the PM to the nucleus. CD9 and CD81 therefore act in a negatively regulatory manner in a resting state system. This system exemplifies how tetraspanins are crucial for the prevention and progression of cancer, by their interactions with other proteins and thereby their ability to regulate the function of immune signalling components such as receptors.

4.1.3 Tetraspanins in plants

There are 17 canonical tetraspanins in the model species Arabidopsis (Cnops et al., 2006) and therefore it is reasonable to expect that they play many varied roles in plants as well. However, very few have of these roles so far been elucidated.

The first phenotype for a tetraspanin mutant in plants was identified by Olmos et al. (2003) in the *ekeko* mutant (*EKEKO* is *TET1* and is also referred to as *TORNADO2*); this resulted in slow plant development and severely curled-up or drilled leaves which are curled and twisted at the same time resembling a drill- or screw-like pattern. TET1 functions in patterning processes in leaf development (Cnops et al., 2006) and affects cellular decisions in the peripheral zone of the shoot apical meristem (Chiu et al., 2007). Single tetraspanin mutants of *tet5* and *tet6* did not display visible phenotypes. However, double mutants of *tet5*/*tet6* resulted in plants with an enlarged leaf size due to a significantly enhanced total number of cells per leaf and longer primary roots (Wang et al., 2015a). Despite these phenotypes, no evidence of how TET1, TET5 or TET6 act on a molecular basis has been published to date.

Plant tetraspanins are able to interact with themselves and other members of the tetraspanin family. Boavida et al. (2013) demonstrated that Arabidopsis tetraspanins homo- and hetero-dimerise when expressed in yeast utilising a split-ubiquitin system. It therefore stands to reason that plant tetraspanins form similar interactions and associations in the form of TEMs and the tetraspanin web as animal tetraspanins do (Hemler, 2005). However, no studies regarding if, or in which way, plant tetraspanins form domains or webs have been published to date.

Different plant tissues express different subsets of tetraspanin genes. Expression and presence of different tetraspanins at different times of the plant life cycle and in different plant organs, may indicate specificity in their roles as membrane organising proteins. Over the last decade three publications used putative native *TETRASPANIN* promoters to express either GUS-reporter constructs, nuclear localised fluorophores, cytosolic fluorophores or fluorescent protein translational fusions of the corresponding tetraspanins (Boavida et al., 2013; Reimann, 2018; Wang et al., 2015a).

Constructs expressing tetraspanins from their native promoters were used to define the localisations of these tetraspanins. These publications partially contradict themselves regarding organ specific tetraspanin expression. For example Reimann (2018) reports a strong expression of *TET3* in roots tips and particularly in the root meristem, while Wang et

al. (2015a) reports no expression for this gene in these tissues. Meanwhile Boavida et al. (2013) reports expression of *TET7* in the central cell and antipodals of female gametophytes, while Reimann (2018) reports *TET7* not to be expressed in these cells. These and other differences could be due to the different lengths of cloned putative native promoters or different insertion sites within the genome causing different spatiotemporal regulation of expression. However, the actual cloned lengths of these promoters have not all been documented fully within these publications and can therefore not be directly compared, making this explanation remain speculative. In comparison the Arabidopsis eFP Browser 2.0 (2022) shows expression of *TET7* in most tissues including different floral growth stages and leaves of different ages.

Like in animals, functional plant immune responses may depend on tetraspanins and their protein interactions. In a recent study by Cai et al. (2018), the tetraspanins TET8 and TET9 were identified to play a key role in plant immunity against fungi. When *TET9* was silenced in a *tet8* mutant, these plants exhibited enhanced susceptibility to *Botrytis cinerea*, and both tetraspanins localise to the plant-microbe interface as well as to plant extracellular vesicles. Cai et al. (2018) performed the first successful co-immunoprecipitation of tetraspanins in plants, where they used TET8-FLAG as bait to detect TET9-GFP as prey and *vice versa*. This confirmed the first tetraspanin-tetraspanin interaction *in planta*, but no data identifying other non-tetraspanin interacting proteins such as the immune receptor proteins involved in fungal defence processes was shown in this publication.

While compiling this thesis, Guo et al. (2022) published the first interaction and characterisation between a plant tetraspanin and a RK. They demonstrated that *Solanum tuberosum* StTET8 is a positive regulator of *Phytophora infestans* immunity, and associates with StLecRK-IV.1 (LECTIN RECEPTOR KINASE-IV.1). The presence of StLecRK-IV.1 affects and reduces the stability of StTET8, thereby resulting in an antagonistic effect reducing the *P. infestans* resistance. This study showed how a plant tetraspanin protein can be incremental to achieve plant resistance against a pathogen.

Tetraspanin gene expression can be dynamically regulated by environmental and developmental stimuli. For example, the inhibition of root cell elongation by the plant hormone ethylene —applied as its precursor 1-aminocyclopropane-1-carboxlic acid — downregulates the expression of *TET7* significantly (Markakis et al., 2012). The HEAT repeat-containing protein (SWEETIE) mutant has changes in multiple metabolic, hormonal and stress-related pathways (Veyres et al., 2008). One of the most upregulated genes in this

mutant is TET9, allowing for speculations that TET9 is involved in some of those pathways (Veyres et al., 2008). TET8 and TET9 are close homologues to TET7 sharing the closest similarities within the family of tetraspanins. Both TET8 and TET9 have been implicated in plant immune responses (Cai et al., 2018; Guo et al., 2022), allowing to form the hypothesis that their closest homologue TET7 fulfils similar functions. Out of these three, *TET9* shows a 10 to 100 times lower expression than *TET7* and *TET8* (Arabidopsis eFP Browser 2.0, 2022; Toufighi et al., 2005; Winter et al., 2007) in mature leaf tissues, suggesting TET7 and TET8 play a more dominant role than TET9 in plant defence responses against pathogens and therefore are good targets for functional characterisation.

Plant tetraspanins have an additional specialised membrane compartment in comparison to animal tetraspanins where they can localise — the plasmodesmata. Multiple different plasmodesmal proteome approaches identified tetraspanins as integral components of plasmodesmata. TET3 and TET7 have been detected in the first plasmodesmal proteome (Fernandez-Calvino et al., 2011) and Brault et al. (2018) identified TET1, TET3 and TET8 in purified plasmodesmal fractions. Furthermore, TET2 and TET7 were found in the same experiments to be highly enriched at plasmodesmata (Bayer E. pers. communications 2018). A plasmodesmal proteome of poplar root cells identified the presence of TET1, TET3 and TET8 homologues in plasmodesmal fractions (Leijon et al., 2018). A moss plasmodesmal proteome from gametophytes of *Physcomitrella patens* further identified multiple tetraspanins as plasmodesmal components (Johnston M. et al., unpublished).

These proteomic plasmodesmal associations of tetraspanins have been confirmed in one initial study and indicated in others. It has been shown that a fluorescently tagged version of TET3 accumulates preferentially at plasmodesmata in Arabidopsis (Fernandez-Calvino et al., 2011), and other publications (Boavida et al., 2013; Jimenez-Jimenez et al., 2019b) suggest that this may be true for further tetraspanins as well. Although unconfirmed by co-localisation with plasmodesmata markers or high resolution imaging, Boavida et al. (2013) reports that in their Arabidopsis lines expressing TET5-eGFP under its native promoter, they observed localisation of the chimeric proteins in structures that are likely plasmodesmata. Similarly, Jimenez-Jimenez et al. (2019b) find *Phaseolus vulgaris 35s::PvTET3-GFP* and *35s::PvTET6-GFP* constructs localising in punctae at the cell periphery when transiently expressed in *N. benthamiana*. Although it is not possible to unmistakably conclude a plasmodesmata localisation from the images provided in Jimenez-Jimenez et al.'s work, their data still stand as a strong suggestion of plasmodesmata localisation of PvTET3 and PvTET6.

How tetraspanins (or other proteins) get sorted and localise at plasmodesmata, is still unknown. Jimenez-Jimenez et al. (2019a) speculate that an LVL motif in the fourth transmembrane domain of tetraspanins could be a plasmodesmal sorting signal but this has not been experimentally determined and published yet. Nonetheless, more evidence of plant tetraspanins being plasmodesmal components is slowly emerging. Animal tetraspanins are important for and localise to cell-to-cell junctions (Huang et al., 2018) — structures functionally similar to plasmodesmata which allow symplasmic transfer of molecules from cell-to-cell (Gerdes and Carvalho, 2008; Maule et al., 2012). It is a plausible hypothesis that their role in cell-to-cell communication was already present in the last common ancestor of the plant and animal kingdom.

Interactions of tetraspanins with associated proteins might prove to be as highly important in plants as they are in animal cells. However, no interacting proteins of tetraspanins in plants, apart from dimerization between tetraspanins and one example of a potato tetraspanin, have been identified (Boavida et al., 2013; Cai et al., 2018; Guo et al., 2022). Although some tetraspanin proteins have been found in plasmodesmal extraction proteomes (Brault et al., 2019; Fernandez-Calvino et al., 2011; Leijon et al., 2018) and have been implicated to be present at plasmodesmata (Boavida et al., 2013; Jimenez-Jimenez et al., 2019b), not all have been confirmed for such a localisation. This work therefore aimed to test tetraspanin protein candidates for plasmodesmal localisations.

4.1.4 Aims of this chapter

This work set out to answer if plant tetraspanin proteins are involved in further immune responses against pathogens. Receptors are known to interact and associate with tetraspanins. This chapter aimed to determine such associations between candidate tetraspanins and a fungal chitin receptor. Plant tetraspanins are present at the PM and the plasmodesmata. This chapter explored the localisations of my candidate tetraspanin proteins in the presence of interacting receptor kinases in a chitin-signalling context. Taken together the first foundation stones of mechanistic understanding of how tetraspanins are important for chitin-triggered plant immunity were elucidated in this chapter.

4.2 Results

4.2.1 Tetraspanins were identified in plasmodesmal proteomes

Multiple members of the tetraspanin protein family have been identified in plasmodesmal proteomes (Brault et al., 2019; Fernandez-Calvino et al., 2011; Grison et al., 2015a; Leijon et al., 2018) making them an interesting candidate family to investigate for their plasmodesmal functions. To elucidate the relationship of Arabidopsis tetraspanin proteins regarding their potential functions, phylogenetic tree was generated based on their amino acid sequences (Fig. 4-1A). The amino acid sequence was chosen over DNA to avoid problems caused by nucleotide compositional biases in the DNA sequences and to allow for clustering of possibly greater functionality (Foster and Hickey, 1999). One of the most striking features of this phylogenetic tree is that TOBAMOVIRUS MULTIPLICATION 2A (TOM2A) and its homologues, TETRASPANIN FAMILY PROTEIN1 (TFP1 = TOM2A2), TFP2 (=TOM2AH3), TFP3 (=TOM2A1) cluster together in one clade, making them an outgroup to the rest of the tetraspanins. The tetraspanins *sensu stricto* (TET1 to TET17) and the tetraspanins *sensu lato* (TFP1 to 3 and TOM2A) therefore form distinct clades from each other. This contrasts with their DNA sequence similarity grouping, where the tetraspanins *sensu lato* cluster together with TET16 and TET17 (Fig. 7-1, Table 7-1).

To identify if and which tetraspanins might play an important role in plasmodesmata regulated immunity processes, data was collated of all published plasmodesmal proteomes for a direct comparison of the tetraspanin proteins present in these lists (Table 4-1). I reasoned that the presence of tetraspanins at plasmodesmata could be a feature of individual clades within this protein family, and therefore further generated a more detailled phylogenetic tree of TET1 to TET17 (Fi.g 4-1). In this tree the number of how many plasmodesmal proteomes individual proteins have been detected is annotated, to gather information about clade specificity. These tetraspanins *sensu stricto* form one monophyletic clade when comparing their amino acid sequence similarity. Within this clade they tend to form further clades often containing only two closely related homologues. This is for example the case for TET16/17, TET14/15, etc. The only distinctive monophyletic clade including three genes is formed by TET7, TET8 and TET9.

Eight members of the tetraspanins *sensu stricto* were identified in plasmodesmal extracts (TET1/2/3/4/7/8/9/11). Members of four different clades have been found in plasmodesmal extracts: TET1/2, TET3/4, TET7/8/9 as well as TET11/12, where only TET11 has been detected

but not its closes homologue TET12 (Table 4-1, Fig. 4-1). Of the clade including TET7, TET8 and TET9, all three proteins were identified in plasmodesmal extracts. While TET8 has been recorded as one of the most consistent hits — being present in all proteomes, both TET7 and TET9 have been identified in separate proteomes as well. Taking TET3/4 together with TET7/8/9, they form an intriguing clade as all proteins within it, have been found in plasmodesmal proteomes (Fig. 4-1, Table 4-1). In comparison TFP1 and TOM2A of the *sensu lato* clade have been identified by Leijon et al. (2018) and Bayer (pers. comms.) respectively to be present in plasmodesmal extracts.

Further to the published plasmodesmal proteomes two members of the tetraspanin family were identified in a *Physcomitrium patens* plasmodesmal proteome (M. Johnston – pers. communication). PpA9TQE7 (PHYPA_005721) shares close homology to TET10, and PpA9RCL2 (PHYPA_010772) shares close homology to the clade containing TET7, TET8 and TET9. Transient expression in *N. benthamiana* showed fluorescent foci at plasmodesmata for a PpA9RCL2 fluorophore translational fusion protein, further confirming the plasmodesmal localisation of PpA9RCL2 (M. Johnston – pers. communication).

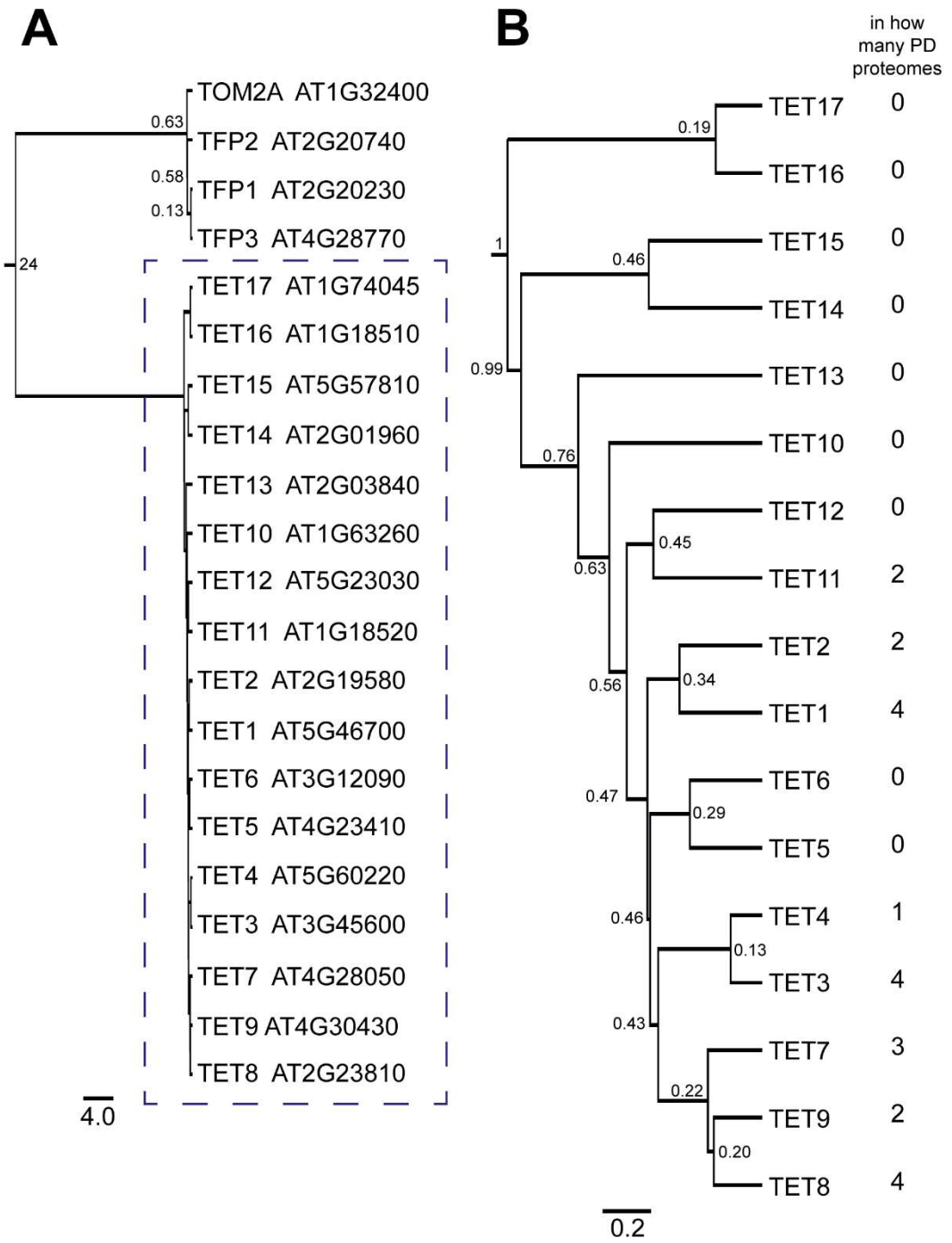

Figure 4-3: Phylogenetic trees of Arabidopsis tetraspanin proteins. A ClustasW 2.1 alignment with a BLOSUM cost matrix was used to generate the original alignment (Fig. 7-1 and Table 7-1) followed by using the Jukes-Cantor Genetic Distance Model and the UPGMA tree building method to generate this tree based on protein amino acid similarity. The node labels are branch confidence values. (A) A phylogenetic tree of all members of the tetraspanin protein family. The blue dashed box shows the tetraspanins *sensu stricto*. (B) A phylogenetic tree of *sensu stricto* tetraspanins. The right column indicates in how many of the four published plasmodesmal proteomes (see Table 4-1) these tetraspanins have been detected.

Table 4-1: Summary table of members of the tetraspanin protein family identified in different plasmodesmal proteomes. Bayer, pers. communications data are an extension of the dataset published as Brault et al. (2019).

		Arabidopsis thaliana (Landsberg erecta) suspension cells	*Arabidopsis thaliana* (Landsberg erecta) suspension cells	*Populus trichocarpa* suspension cells	*Arabidopsis thaliana* (Landsberg erecta) suspension cells
		Fernandez-Calvino et al. (2011)	Grison et al. (2015a)	Leijon et al. (2018)	full data set of Bayer, pers. communication
Protein	**Gene locus**	**total score 0 to 1**	**PD/PM ratio**	**presence of homologue**	**PD/PM ratio**
AtTET1	AT5G46700	0.593	6	hit	92.2
AtTET2	AT2G19580	-	14	-	77
AtTET3	AT3G45600	0.0696-0.629	10	hit	65.3
AtTET4	AT5G60220	-	-	-	
AtTET5	AT4G23410	-	-	-	-
AtTET6	AT3G12090	-	-	-	-
AtTET7	AT4G28050	0.386-0.661	8	-	73
AtTET8	AT2G23810	0.177-0.813	10	hit	98.9
AtTET9	AT4G30430	-	107	-	0.4
AtTET10	AT1G63260	-	-	-	-
AtTET11	AT1G18520	-	29	-	6.3
AtTET12	AT5G23030	-	-	-	-
AtTET13	AT2G03840	-	-	-	-
AtTET14	AT2G01960	-	-	-	-
AtTET15	AT5G57810	-	-	-	-
AtTET16	AT1G18510	-	-	-	-
AtTET17	AT1G74045	-	-	-	-
AtTFP1	AT2G20230	-	NA	hit	-
AtTFP2	AT2G20740	-	NA	-	-
AtTFP3	AT4G28770	-	NA	-	-
AtTOM2A	AT1G32400	-	NA	-	12

4.2.2 Candidate tetraspanin proteins localise to plasmodesmata

To confirm the plasmodesmal proteomic data, the three candidate tetraspanin genes were initially fused with the fluorophore mCherry. Transiently expressed, these constructs exhibited an even PM localisation for TET3-mCherry, TET7-mCherry, TET8-mCherry (Fig.4-4A, B, C). These constructs showed only very rarely individual accumulations of fluorescence at the cell periphery reminiscent of plasmodesmata.

By contrast, when the same TETs were expressed to form a translational fusion protein with an mRuby3-6×HA construct, all three constructs for TET3-mRuby3-6×HA, TET7-mRuby3-6×HA and TET8-mRuby3-6×HA showed a PM localisation with clusters of enriched fluorescence (Fig.4-4D, E, F). Aniline blue staining was used for plasmodesmal callose deposits to demonstrate that these fluorescence signals overlap. These proteins therefore localise to plasmodesmata. The same mRuby3-6×HA based constructs were transformed into Arabidopsis, where they resulted in similar PM localisation with clusters of enriched fluorescence indicative of plasmodesmata (Fig.4-4G, H, I).

Using two different fluorophores has produced different results by confocal microscopy. One fluorophore (mCherry) resulted in a PM localisation of TET3, TET7 and TET8, without clusters of enrichment indicative of plasmodesmata. While constructs with the other (mRuby3-6×HA) showed not only a PM localisation but also a clear presence at plasmodesmata for those three tetraspanins.

4.2.3 Identification of tetraspanin mutants

To assay the function of tetraspanins in Arabidopsis, insertion mutants (*tet3* SALK_116766, *tet7* SALK_205244, *tet8* SALK_136039) were obtained, genotyped and progeny of homozygous plants were used for all further experiments (Fig. 4-5). None of the homozygous plants exhibited any obvious developmental phenotypes but this could be further tested and quantified in the future to ensure it holds true.

All three T-DNA insertion sites were identified by Alonso et al. (2003). The expression of the tetraspanin genes was assessed by qPCR, showing a near zero of relative expression in each mutant (Fig. 4-4). Future work should also include a real-time primer validation of the qPCR primers used.

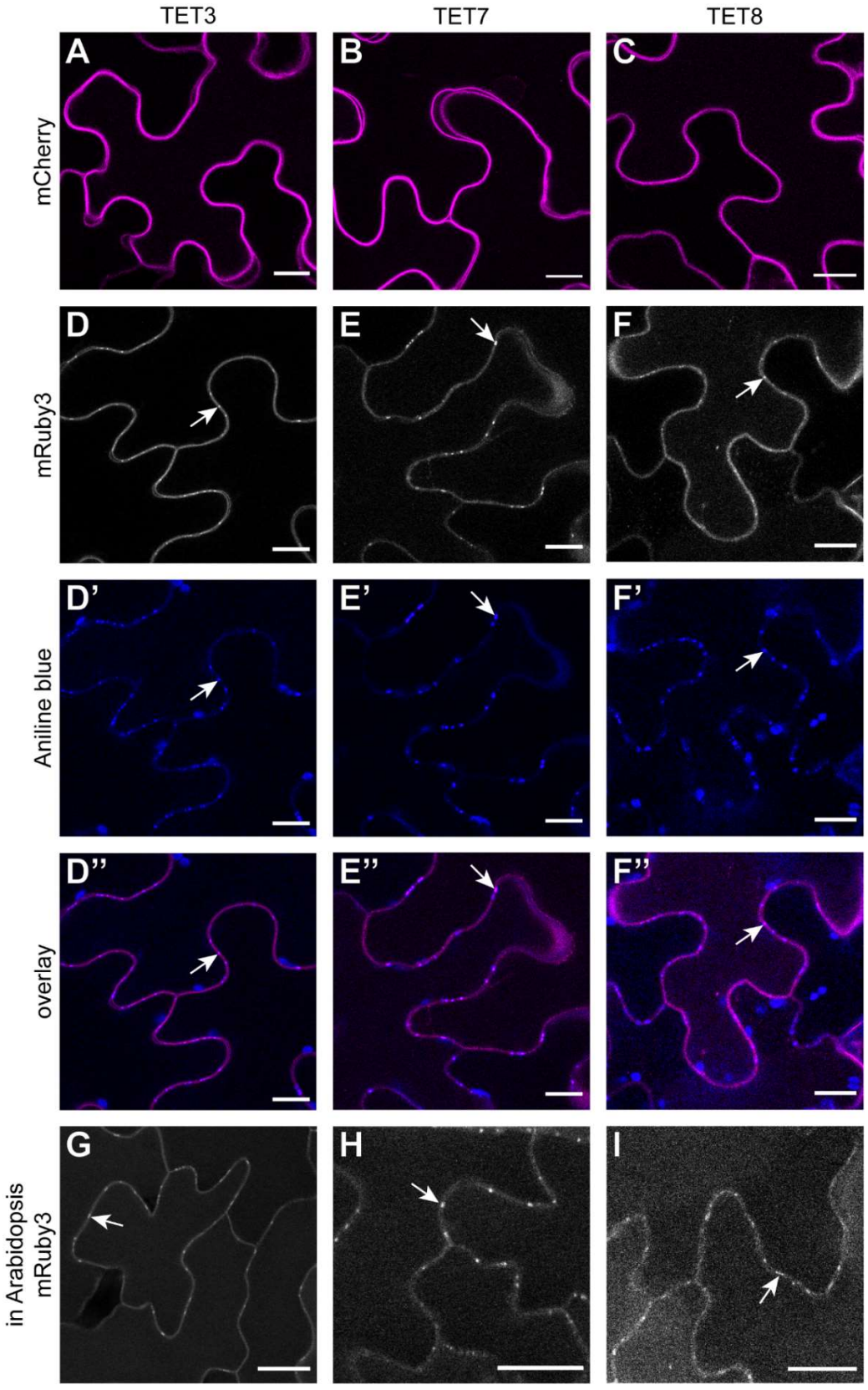

Figure 4-4: Single-plane micrographs comparing tetraspanin localisations. (A) TET3-mCherry; (B) TET7-mCherry; (C) TET8-mCherry; (D)&(G) TET3-mRuby3-6×HA; (E)&(H) TET7-mRuby3-6×HA; (F)&(I) TET3-mRuby3-6×HA. (D), (E) and (F) show mRuby3 fluorescence, aniline blue staining of plasmodesmal callose (') as well as an overlay(''), where the mRuby3 fluorescence is uses the artificial colour magenta. (A) to (F) are leaves of *N. benthamiana* transiently expressing the constructs, which were infiltrated with water or 0.1% aniline blue. (G), (H) and (I) are stable Arabidopsis lines expressing:(G) *AtAct2::TET3-mRuby3-6×HA*, (H) *AtAct2::TET7-mRuby3-6×HA*, (I) *AtAct2::TET8-mRuby3-6×HA*. Arrows indicate example plasmodesmata localisations. All scalebars indicate 15 µm.

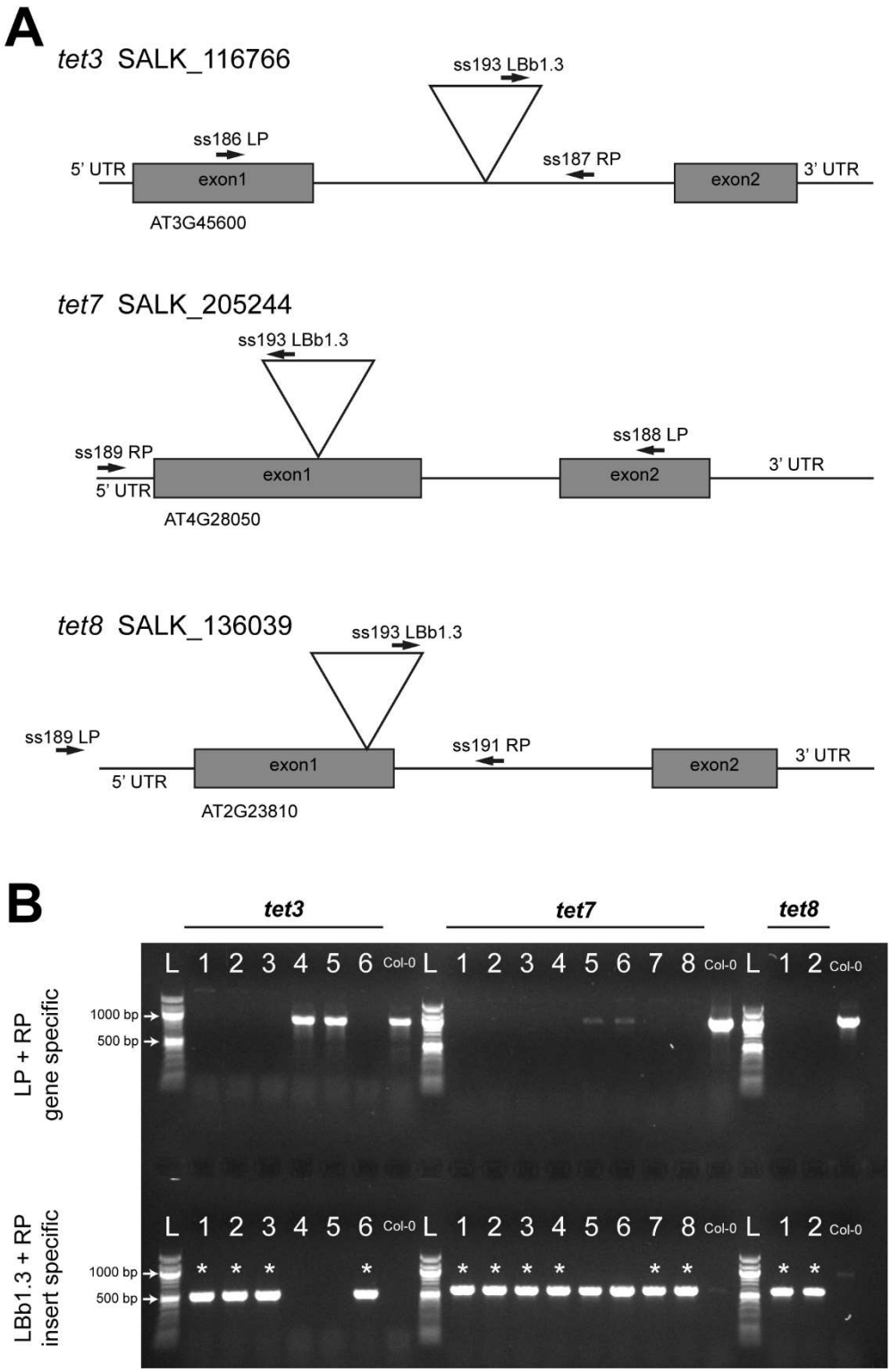

Figure 4-5: Genotyping of tetraspanin mutant plants. (A) Cartoon models of the tetraspanin genes with their T-DNA insertion location (triangle), exons (grey boxes), and primers (black arrows) used to assess individual plants for homozygous presence of the insertion. (B) Electrophoresis gel of genotyping PCR, separated according to individual mutant and plants tested. The gene specific primer combination shows bands in the presence of the WT gene without an insertion. The insert specific primer combination shows bands if an insertion is present. Homozygous plants are indicated by *. For *tet3* the plants #1,2,3 and 6 were homozygous for the insertion. For *tet7* the plants #1-4, 7 and 8 were homozygous, and both *tet8* plants tested were homozygous for their insertions. The primers were designed using T-DNA Primer Design (http://signal.salk.edu/tdnaprimers.2.html). Insertion specific primers result in 300-700 bp products, while WT gene specific primers result in 900-1100 pb products. Col-0 is used as the respective WT control. (A)&(B): LP: left primer, RP: right primer, LBb1.3: SALK insertion specific primer. L: 100 bp DNA Ladder (New England Biolabs).

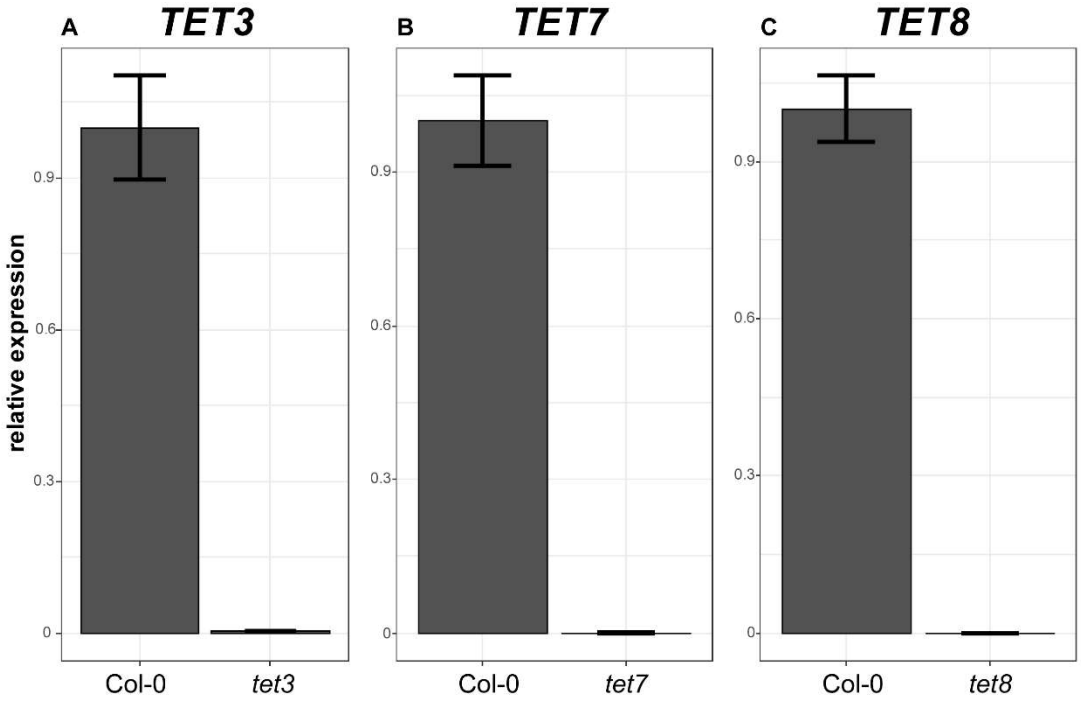

Figure 4-6: Assessment of tetraspanin expression levels by qPCR of homozygous tetraspanin mutant plants. Expression levels were normalised to Actin expression, and then further normalised the expression of the tested gene in Col-0 as 1. (A) The primers ss229 & ss230 were used to determine the expression of *TET3*. (B) The primers ss231 & ss232 were used to determine the expression of *TET7*. (C) The primers ss233 & ss234 were used to determine the expression of *TET8*. (A),(B) & (C)This experiment has been carried out by Andrew Breakspear. I carried out the planning, further data analysis and visualisation. Whiskers indicate the standard error. The data presented consists of three technical repeats.

4.2.4 Arabidopsis tetraspanin mutants have varying susceptibility to *Botrytis cinerea* infections

Absence of vital components of the signalling or immunity response pathways can lead to an enhanced susceptibility to pathogens. Such a change in phenotype can be dependent on if the protein is important for the host response to the particular pathogen. Given that tetraspanins have been associated with the detection of MAMPs (Tam et al., 2019) and frequently associate with receptors, whether tetraspanin mutants show an altered susceptibility to a fungal pathogen was explored.

To explore this question, detached leaf infection assays were carried out, where the necrotic lesions caused by *B. cinerea* four days after spot inoculation were measured and compared. Neither *tet3* nor *tet8* leaf lesions showed a significant difference when compared to the lesions that developed on WT Col-0 leaves (Fig. 4-5). They therefore show no observable changes in susceptibility or resistance to the fungus. However, *tet7* plants exhibited a significantly enhanced lesion size, and therefore susceptibly to *B. cinerea*.

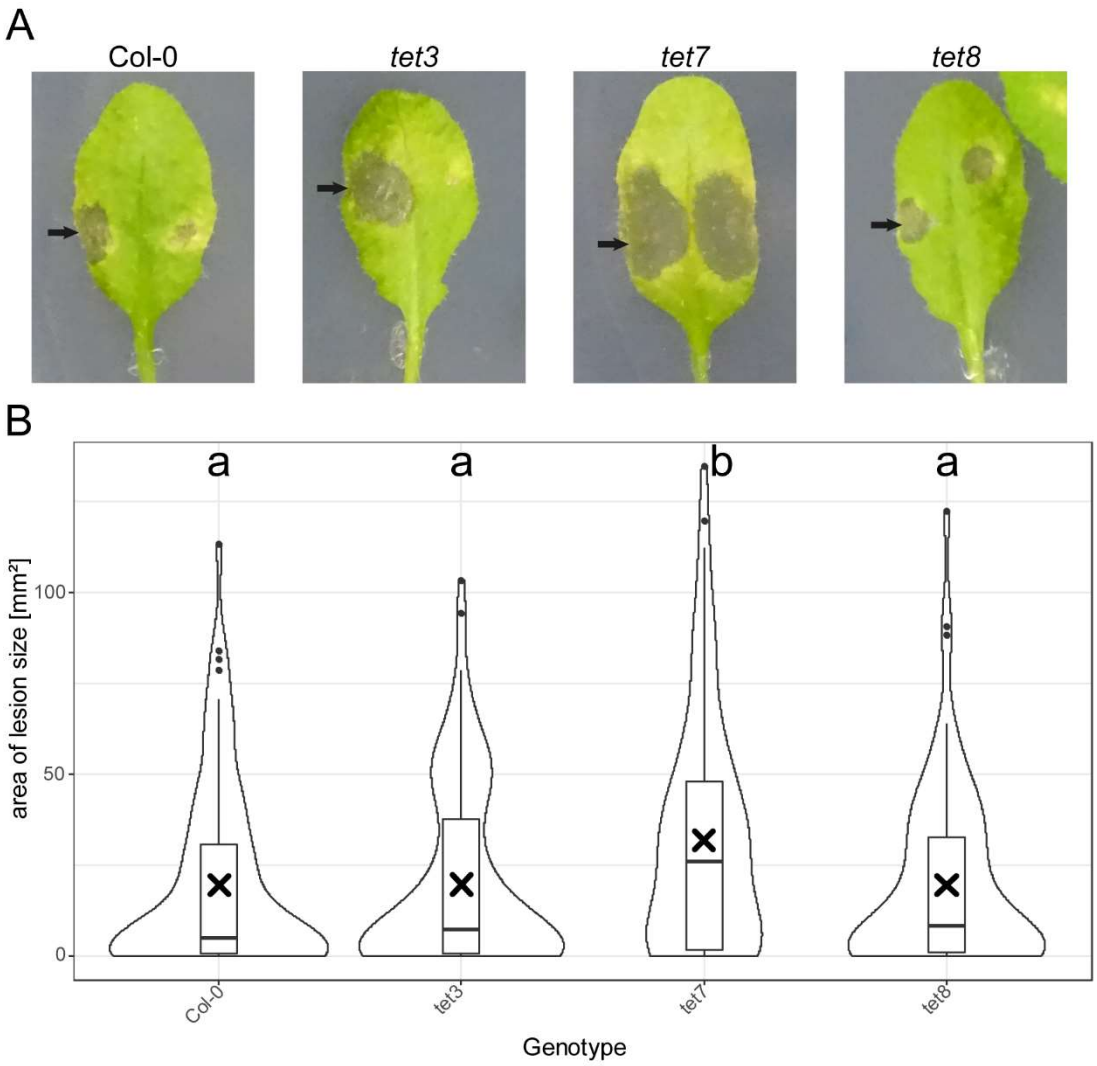

Figure 4-7: Fungal infection assay of tetraspanin mutant plants. Area of necrotic lesions caused by *B. cinerea* infections on detached mature Arabidopsis leaves of four- to six-week-old plants four days after inoculation. (A) Representative photographic images of the progression of *B. cinerea* in detached leaves of Col-0, *tet3*, *tet7*, and *tet8*. Arrows indicate the necrotic lesions. (B) Different letters indicate a significant difference of $p < 0.01$. Statistical analysis was carried out by fitting a linear mixed-effects models accounting for the fixed effect of genotype and the random effect of experimental repeats. Three individual repeats were carried out, resulting in a sample size $n \geq 75$ per genotype. The '×' indicates the position of the mean.

4.2.5 Tetraspanin proteins are involved in ROS production

4.2.5.1 Tetraspanin overexpression alters chitin-triggered ROS production

Plants produce ROS triggered by the presence of MAMPs, such as fungal chitin (Hückelhoven and Seidl, 2016; Miya et al., 2007). Therefore, plant tetraspanins were tested for their influence on ROS production. In the first instance a transient overexpression system in *N. benthamiana* was used, to determine if an increase in tetraspanin proteins can indeed increase the chitin-triggered ROS bursts.

As expected, no statistical differences in the cumulative relative light units produced within 45 min. triggered by control mock (water) treatment was observed between leaves expressing only the *P19* control or tetraspanin constructs (Fig. 4-8A).

The overexpression of *TET3* increases the chitin-triggered ROS production when compared to both the expression of *P19* as well as *LYK4* (Fig. 4-8B). The combination of overexpressing *LYK4* with *TET3* reduces the chitin-induced ROS production in comparison to the overexpression of *TET3* alone (Fig. 4-8B).

There is a possible trend that the expression of *TET7* increases the chitin-triggered ROS burst in comparison to expression of *P19* (p-value 0.0553) (Fig. 4-8C). Further evaluation is needed to validate this behaviour. The overexpression of *TET7* with *LYK4* increases the ROS burst compared to *P19* or *LYK4*, suggesting an additive effect (Fig. 4-8C).

The overexpression of *TET8* causes similar shifts in chitin-triggered ROS production as the overexpression of *TET3*. The overexpression of *TET8* itself increases chitin-triggered ROS production in comparison to *P19* (Fig. 4-8D). However, the co-overexpression of *LYK4* with *TET8* supresses that effect (Fig. 4-8D). This suggests a potential intermediary effect, which needs to be further validated.

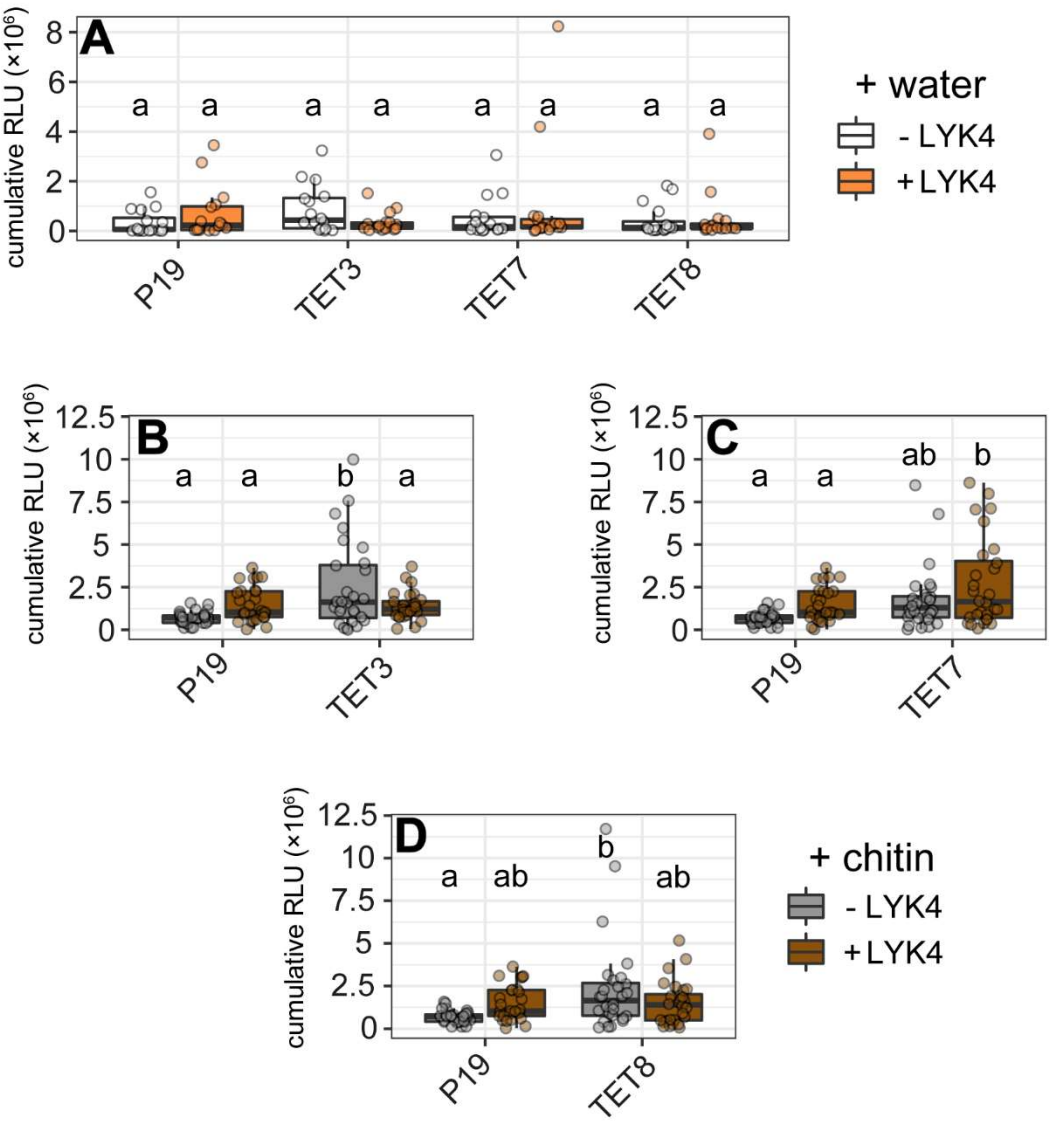

Figure 4-8: Chitin-triggered ROS production during tetraspanin and LYK4 overexpression. Total relative luminescence indicative of ROS produced in leaf discs of *N. benthamiana* overexpressing different combinations of constructs treated with water or chitin within 45 min. Statistical comparison were carried out using a linear mixed model which takes the transient overexpression or non-overexpression of Arabidopsis *35s::LYK4-eGFP* and *35s::TET3-mTurq2*, *35s::TET7-mTurq2* or *35s::TET8-mTurq2* (LYK4 presence + tetraspanin presence + LYK4*tetraspanin presence), further taking a random effect of individual experimental repeats into account. All samples expressed the silencing plasmid *P19* as well as any other overexpressed proteins listed. (A) P19, TET3, TET7, TET8 in absence or presence of overexpressed LYK4 treated with water. No statistically significant differences of $p < 0.05$ were determined. $n \geq 16$ (B) P19 and TET3 in absence or presence of overexpressed LYK4 treated with chitin. (C) P19 and TET7 in absence or presence of overexpressed LYK4 treated with chitin (D) P19 and TET8 in absence or presence of overexpressed LYK4 treated with chitin. (B), (C) and (D) The P19 without tetraspanins, measured data are shown as duplicates in these diagrams, to simplify the graphic explanation of the statistical differences. $n \geq 27$.Different letters (a, b) indicate statistically significant differences in comparisons ($p < 0.05$).

4.2.5.2 Tetraspanin mutants exhibit a decrease in chitin triggered ROS production

In the absence of integral components of perception or signalling pathways, the downstream processes they initiate are perturbed and, in the case of immune signalling, do not result in mounting of the regular defence responses such as ROS production. To test if this is the case for tetraspanin proteins, mutant Arabidopsis plants were used.

When comparing the ROS production of *tet3*, *tet7* and *tet8* with the WT control Col-0 under mock conditions (water treated) no significant differences in the ROS production can be detected (Fig. 4-7). This suggests that the resting-state ROS presence is not perturbed in these mutant plants. When treated with chitin, both *tet7* and *tet8* plants show significantly reduced chitin-triggered ROS production when compared to Col-0 (Fig. 4-7). This shows that chitin-triggered ROS production is perturbed in absence of these tetraspanins, and that both TET7 as well as TET8 positively regulate chitin-triggered ROS production. Even though there is a slight reduction of ROS production observed in *tet3* plants when compared to Col-0, this is not statistically significant suggesting that TET3 is not required for chitin-triggered ROS responses. These results show that TET7 and TET8 positively regulate chitin-triggered ROS production at the PM, while TET3 does not influence PM localised ROS production as such.

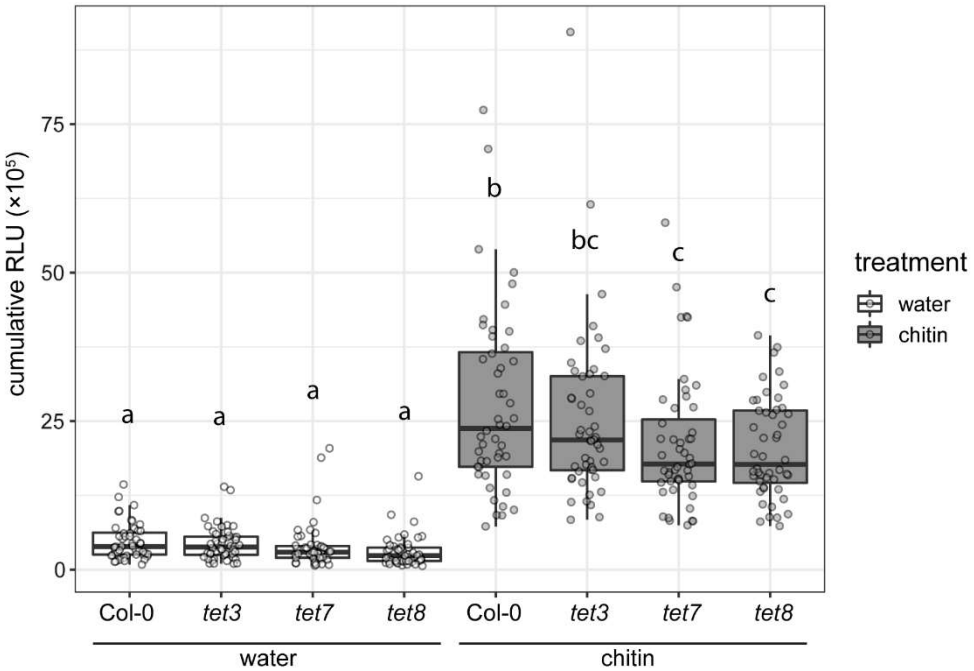

Figure 4-9: Tetraspanin mutants are reduced in chitin-triggered ROS production. Cumulative relative light units (RLU) as acquired within 90 min. of treatment with mock (water) or chitin of leaf discs. Statistical analysis was carried out using a linear mixed-effects model with applied fixed effects terms for genotypes and treatments (genotype + treatment + genotype*treatment) and a random effect term for individual experimental repeats followed by comparison of the estimated marginal means using the emmeans package (1.7.0) (Lenth, 2021) in R (4.1.2) (R Core Team, 2021). Different letters (a, b, and c) indicate statistically significant groups of $p < 0.05$, compared between genotypes and treatments. All individual genotype and treatment combinations have a sample size of n = 48.

4.2.6 Tetraspanin mutants are impaired in chitin-triggered plasmodesmal flux adjustments

I demonstrated that tetraspanins in plants are involved in chitin-triggered ROS production by overexpression resulting in an enhancement of ROS bursts (Fig. 4-6), and mutant plants exhibiting a reduced chitin-triggered ROS burst (Fig. 4-7). Taken together with their plasmodesmal localisation (Fig. 4-2), I wanted to test if they also exhibit chitin dependent plasmodesmal phenotypes. For this purpose, these tetraspanin mutant plants were assessed for chitin-triggered changes to their plasmodesmal flux using a microprojectile bombardment assay that measures the cell-to-cell spread of eGFP through plasmodesmata.

As expected, WT Col-0 plants were able to successfully close their plasmodesmata and restrict the eGFP movement when triggered with chitin (Fig. 4-10). However, similar to *lyk4* and *lyk5-2* knockout plants (Cheval et al., 2020), leaves of *tet3* and *tet7* mutant plants do not restrict the movement of cytosolic eGFP in the presence of chitin (Figure 4-6). This suggests that these plants do not successfully close their plasmodesmata in response to chitin.

Surprisingly, the eGFP movement in the *tet8* mutant plants showed an inverse response profile. In *tet8* plants the eGFP movement was reduced under mock conditions (water infiltrated) relative to that observed in Col-0 and increased in the presence of chitin (Figure 4-10). When using a bootstrapping approach, to compare the mock treated Col-0 data with the chitin treated *tet8* data, no significant difference could be determined ($p = 0.679$), suggesting that these mock treated Col-0 leaves exhibits the same plasmodesmal flux conditions as *tet8* chitin treated leaves. The same also holds true when comparing the chitin treated Col-0 data with the mock treated tet8 data ($p = 1$). The *tet8* mutant plants therefore exhibit exactly the opposite behaviour to Col-0 in a chitin specific manner.

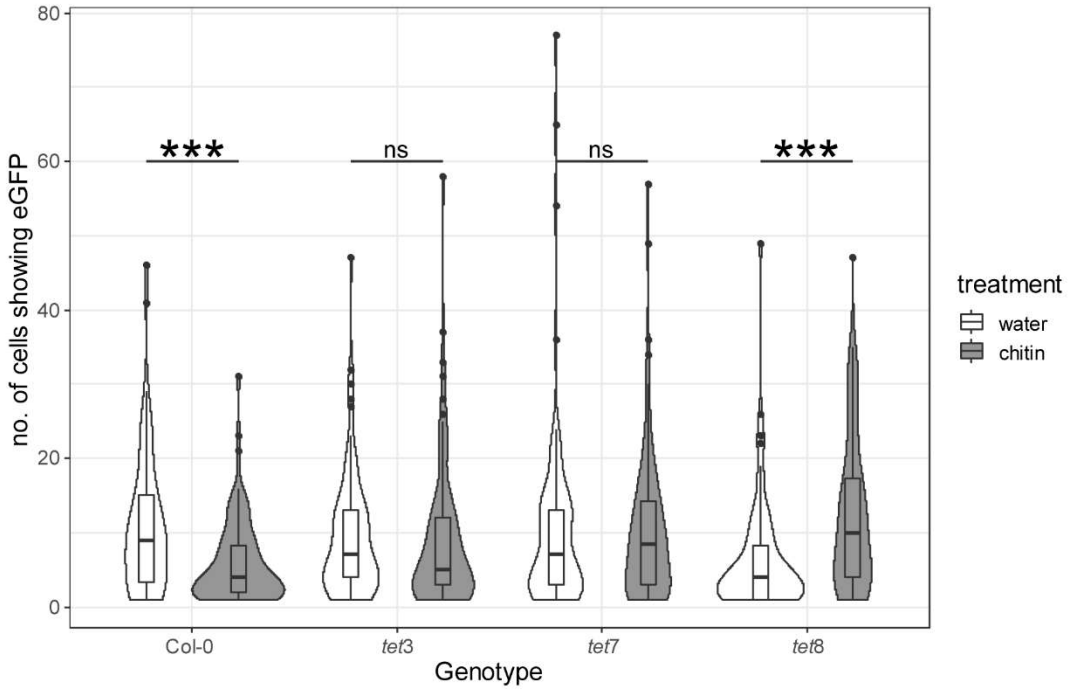

Figure 4-10: Assessment of the cytosolic cell-to-cell flux of tetraspanin mutant plants. Microprojectile bombardment into leaf tissue of 4- to 6-week-old Arabidopsis shows that Col-0, but not *tet3* and *tet7* exhibited reduced movement of eGFP to neighbouring cells in response to chitin, while tet8 exhibited an increase of eGFP movement. Data were collected from more than eight independent biological replicates, 18-26 h after chitin treatment. These data are summarised in a combination of a box plot with a violin plot. The number of bombardment sites (n) counted is ≥86 for each genotype's treatment. Statistical analysis was carried out using a bootstrap approach according to Johnston and Faulkner (2021) to comparing the medians of mock with chitin treated samples. Asterisks indicate statistical significance compared with control conditions. ***P < 0.001.

4.2.7 Tetraspanin mutants differ in their chitin-triggered plasmodesmal callose deposition from Col-0

Plasmodesmal flux is dependent on the amount of callose deposited at plasmodesmata (Zavaliev et al., 2011). As plasmodesmal flux phenotype for tetraspanin mutants (Fig. 4-8) has been observed, I wanted to test if the callose deposition at plasmodesmata correlates with those observations. Callose deposits at plasmodesmata can be visualised by aniline blue staining (Benitez-Alfonso et al., 2013) and their fluorescence intensity quantified by automated image processing (Xu et al., 2017) to measure the amount of callose present at plasmodesmata.

In the WT control Col-0 which reduces plasmodesmal flux of eGFP in response to chitin, the total intensity of aniline blue staining the callose per plasmodesmata is significantly increased by chitin treatment (Fig. 4-11). This was not observed for the *tet3* and *tet7* mutants, where the callose levels did not significantly change between mock and chitin treated plants. In the *tet8* mutant a reduction of aniline blue intensity of plasmodesmal callose deposits in leaves treated with chitin versus mock treated leaves was observed. The

changes in callose levels of all four examined genotypes thereby inversely correspond with their chitin-triggered changes of plasmodesmal flux. Whenever the plasmodesmal flux is reduced in Col-0 (Fig. 4-10), callose is increased in comparison in this genotype and thereby detected as an increase in aniline blue fluorescence (Fig. 4-11). The same also holds true by contrast, as when the plasmodesmal flux is increased in *tet8* (Fig. 4-10), the plasmodesmal aniline blue fluorescence intensity is reduced (Fig. 4-11).

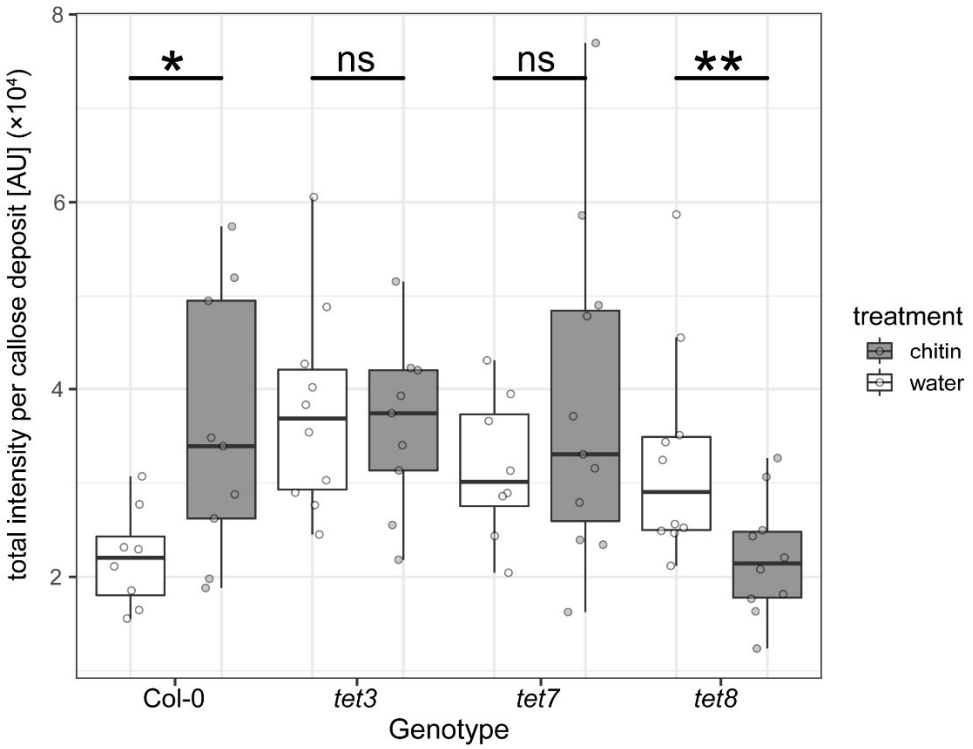

Figure 4-11: Quantification of fluorescence of aniline blue stained plasmodesmal associated callose by automated image analysis in tetraspanin mutants. Col-0 shows an increase in aniline blue stained plasmodesmal callose 30 min after chitin treatment. Neither *tet3* nor *tet7* show a significant change in the fluorescent signal for plasmodesmal callose in the presence of chitin and *tet8* shows a decrease of callose in the presence of chitin. The mean of the fluorescent intensity per z-stack is used for this dataset. Number of z-stacks (n) is ≥ 8 and ** indicates $p < 0.01$ when comparing chitin treated samples with mock treated samples within the same genotype assessed by a Wilcoxon signed-rank test.

4.2.8 Tetraspanins do not increase further at plasmodesmata in response to chitin

Grison et al. (2019) describe the physiological response of QSK1 and IMK2 to osmotic stress, identifying that these RKs accumulate at plasmodesmata in theses stress conditions. Hunter et al. (2019) also show that CRK2 re-localises during salt stress triggered by NaCl treatment and shows an enhanced localisation to plasmodesmata. We demonstrated in Cheval et al. (2020) that LYM2's plasmodesmal index (PD index) — a ratio comparing fluorescence at the PM and the plasmodesmata — increases within 30 min. significantly both in stable transgenic Arabidopsis lines as well as when transiently expressed in *N. benthamiana* leaves. A PM and enriched plasmodesmal localisation for TET3, TET7 and TET8 were determined, and I therefore wanted to test if these proteins undergo a similar dynamically changing plasmodesmal localisation as LYM2.

Comparing the PD index of tetraspanin fluorophore translational fusion proteins either under mock (water infiltrated) or chitin infiltrated conditions, no significant difference was measured (Fig. 4-12). This holds true for all three tested candidate tetraspanins of TET3, TET7 and TET8. Neither of the candidate tetraspanin proteins therefore accumulates or is depleted at plasmodesmata when triggered with chitin. This experiment has been carried out using no further negative or positive controls. Future experiments could consider adding those to the experimental set-up.

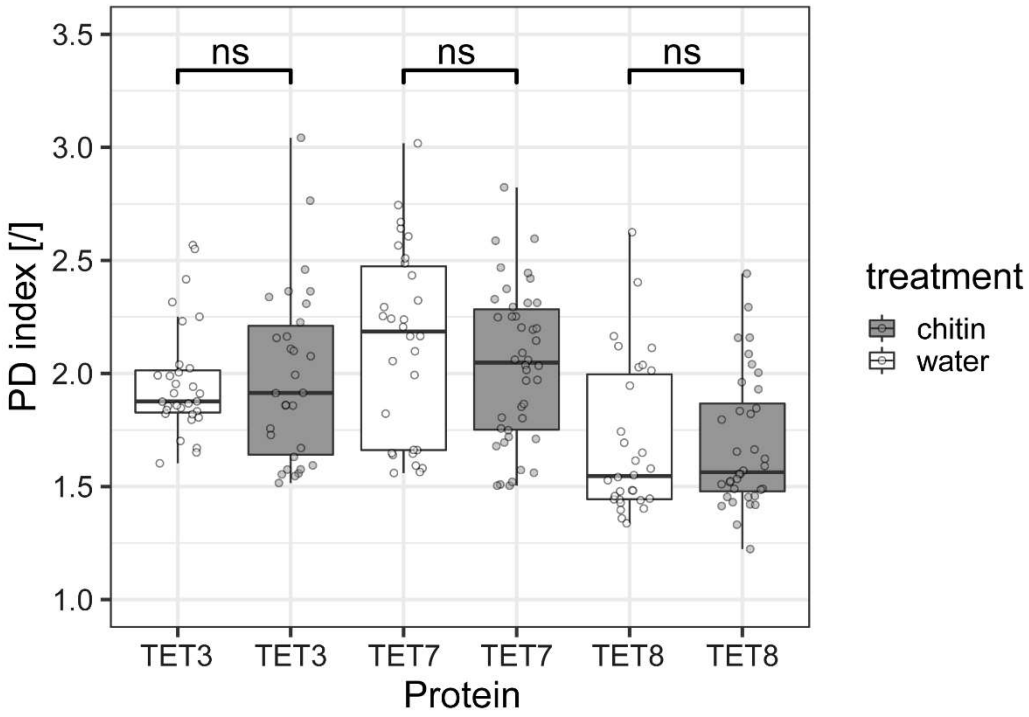

Figure 4-12: The plasmodesmata index of tetraspanins does not change triggered by chitin. Ratio of fluorescence intensity comparing the fluorescence at the plasmodesmata and with adjacent PM fluorescence in leaves of *N. benthamiana* transiently overexpressing TET3-mRuby3-6×HA, TET7-mRuby3-6×HA or TET8-mRuby3-6×HA under the control of the *AtACT2* promoter, three days past *Agrobacterium* infiltration. Statistical analysis was carried out using a Wilcoxon signed-rank test, indicating non significance (p-value: >0.05) across all water versus chitin companions. Sample size for individual z-stacks per overexpressed gene and treatment n ≥ 30, from three different independent repeat experiments.

4.2.9 Tetraspanins associate with the receptor protein LYK4

4.2.9.1 Tetraspanins co-immunoprecipitate with the chitin receptor LYK4

RKs and RPs can be part of protein complexes. This association can be determined via co-immunoprecipitation experiments and identified constitutive such as the associations between LYK4 and LYK5 (Cheval et al., 2020), or CERK1 and LYK4 (Cao et al., 2014), or ligand-dependent associations such as the association of FLS2 with BAK1 (Chinchilla et al., 2007) or CERK1 and LYK5 (Cao et al., 2014).

Like LYM2, the chitin receptor LYK4 is present at plasmodesmata (Cheval et al., 2020). However, by contrast with LYM2— which is a GPI-anchored protein — LYK4's C-terminus extends into the cytosol, which enabled us to it as a C-terminus epitope-tagged variant that associates directly with cytosolic signalling machinery. Therefore, hypothesising that tetraspanins might establish signalling platforms, LYK4 was chosen as the preferential chitin receptor to test for interactions with tetraspanins. As the tetraspanins mutants also showed a vital role for tetraspanin proteins in chitin-triggered plasmodesmal closure, I set out to determine if the plant tetraspanins TET3, TET7 and TET8 associate with LYK4 by co-immunoprecipitation.

The input control Western blots revealed that all translational fusion proteins of interest (TET3-mRuby3-6×HA, TET7-mRuby3-6×HA, TET8-mRuby3-6×HA, LYK4-mClover3-3×FLAG, as well as LTI6b-mRuby3-6×HA) were present in their combinations in the transiently expressing *N. benthamiana* leaves (Fig. 4-13). The bait LYK4-mClover3-3×FLAG was successfully immunoprecipitated, and each of the prey, TET3-mRuby3-6×HA, TET7-mRuby3-6×HA and TET8-mRuby3-6×HA, were detected in the immunoprecipitated fraction as well. Significantly, the negative biological control LTI6b-mRuby3-6×HA was absent. These experiments thereby revealed that all three tetraspanins TET3, TET7 and TET8 co-immunoprecipitated with, and therefore likely associate with LYK4 (Fig. 4-13).

As the interactions between receptor complex resident proteins can change in the presence of an elicitor, I tested if there was a change in association between the tetraspanins and LYK4 in the presence of chitin. For this purpose, samples were infiltrated 30 min. before harvesting and processing with either 0.5 mg/mL chitin or water (mock). In both mock as well as chitin treated samples did the prey proteins TET3-mRuby3-6×HA, TET7-mRuby3-6×HA and TET8-mRuby3-6×HA co-immunoprecipitate with LYK4-mClover3-3×FLAG (Fig. 4-13), and no

consistent chitin-dependent changes the prey abundance of any of the tetraspanins were observed.

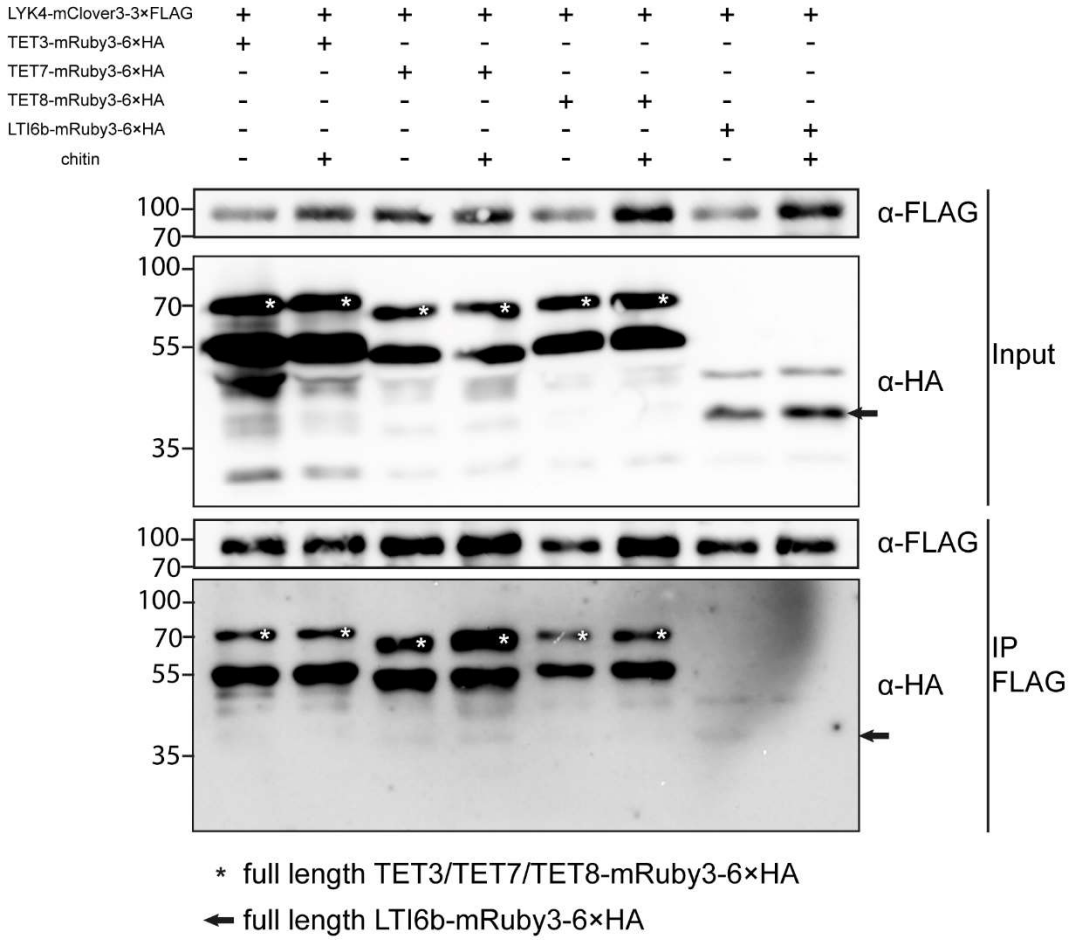

Figure 4-13: LYK4 associates with TET3, TET7 as well as TET8, but not with the negative control LTI6b. Western blot analysis of immunoprecipitated proteins from *N. benthamiana* tissue expressing *pLYK4::LYK4-mClover3-3×FLAG* and *pAtACT2::TET3-mRuby3-6×HA*, *pAtACT2::TET7-mRuby3-6×HA*, *pAtACT2::TET8-mRuby3-6×HA*, and as a negative control the membrane protein *pAtACT2::LTI6b-mRuby3-6×HA*. The leaves were infiltrated with mock (water) or chitin 30 min before sampling. TET3-mRuby3-6×HA, TET7-mRuby3-6×HA, TET8-mRuby3-6×HA are detected in detergent extracted fractions of IP by LYK4-mClover3-3×FLAG. Input and immunoprecipitated (IP) samples were probed with α-FLAG-HRP and α-HA-HRP as indicated. This experiment has been carried out three times with similar results. * indicate the correct sizes corresponding to TET3-mRuby3-6×HA, TET7-mRuby3-6×HA and TET8-mRuby3-6×HA, and the arrow indicates the correct bands for LTI6b-mRuby3-6×HA.

4.2.9.2 LYK4 and TET7 association by FRET-FLIM

Förster resonance energy transfer (FRET) measurements based on Fluorescence lifetime imaging (FLIM) allow for the determination of fluorophore translational fusion proteins by reducing the measured lifetime of a donor fluorophore in the presence of a suitable and physically close acceptor fluorophore (Margineanu et al., 2016). The stronger the shift of the τ_{AvAmp} (amplitude weighted average donor lifetime; from here on out referred to as τ) when comparing the lifetime of the donor in the presence and absence of the corresponding acceptor, the putatively closer are the two fluorophores. FRET has been reported to efficiently occur in distances of ~1-5 nm between the centres of the donor and acceptor (Stryer and Haugland, 1967) and provides a strong support for direct association between two proteins when detected.

In this first set of FRET-FLIM experiments a significant decrease in the observed lifetime of the donor LYK4-eGFP was determined (Fig. 4-14A, gateway construct; from here on gw) (τ = 2.35 ± 0.034 ns) to the lifetime of this donor in the presence of the TET7-mRFP1 acceptor (Fig. 4-14 A; gw) (τ = 1.95 ± 0.12 ns, FRET-Efficiency (E) = 17.02%. All FRET-Efficiencies are listed in Table 7-2) (Fig. 4-14E), giving a strong suggestion that LYK4 associates with TET7 in the PM. In leaves treated with chitin 30 min. before measurements were taken, a significant drop in lifetime was observed (τ = 2.29 ± 0.074 ns to τ = 2.09 ± 0.080, E = 11.06%) when compared to the donor only samples. However, this is a significantly smaller donor lifetime shift when compared to that observed under mock conditions. There is therefore an association between LYK4 and TET7 under mock conditions, which is reduced in the presence of chitin.

By contrast, no such strong shifts in lifetime of the donor LYK4-eGFP were observed in the presence of the negative control BRI1-mRFP1 — both comparing mock treated samples (τ = 2.28 ± 0.063 ns, E = 2.98%) and chitin treated samples (τ = 2.30 ± 0.059 ns, E = 2.13%) (Fig. 4-14E). BRI1-mRFP1 has therefore served as an appropriate negative control, giving more power to the positive results using TET7-mRFP1 as an acceptor.

The first FRET-FLIM series to test for the association between the membrane proteins LYK4 and TET7 was carried out on a Leica SP8X confocal microscope in TCSPC mode using only gateway cloned fluorophore translational fusion constructs and analysed with the software PicoQuant SymPhoTime (Figure 4-14E).

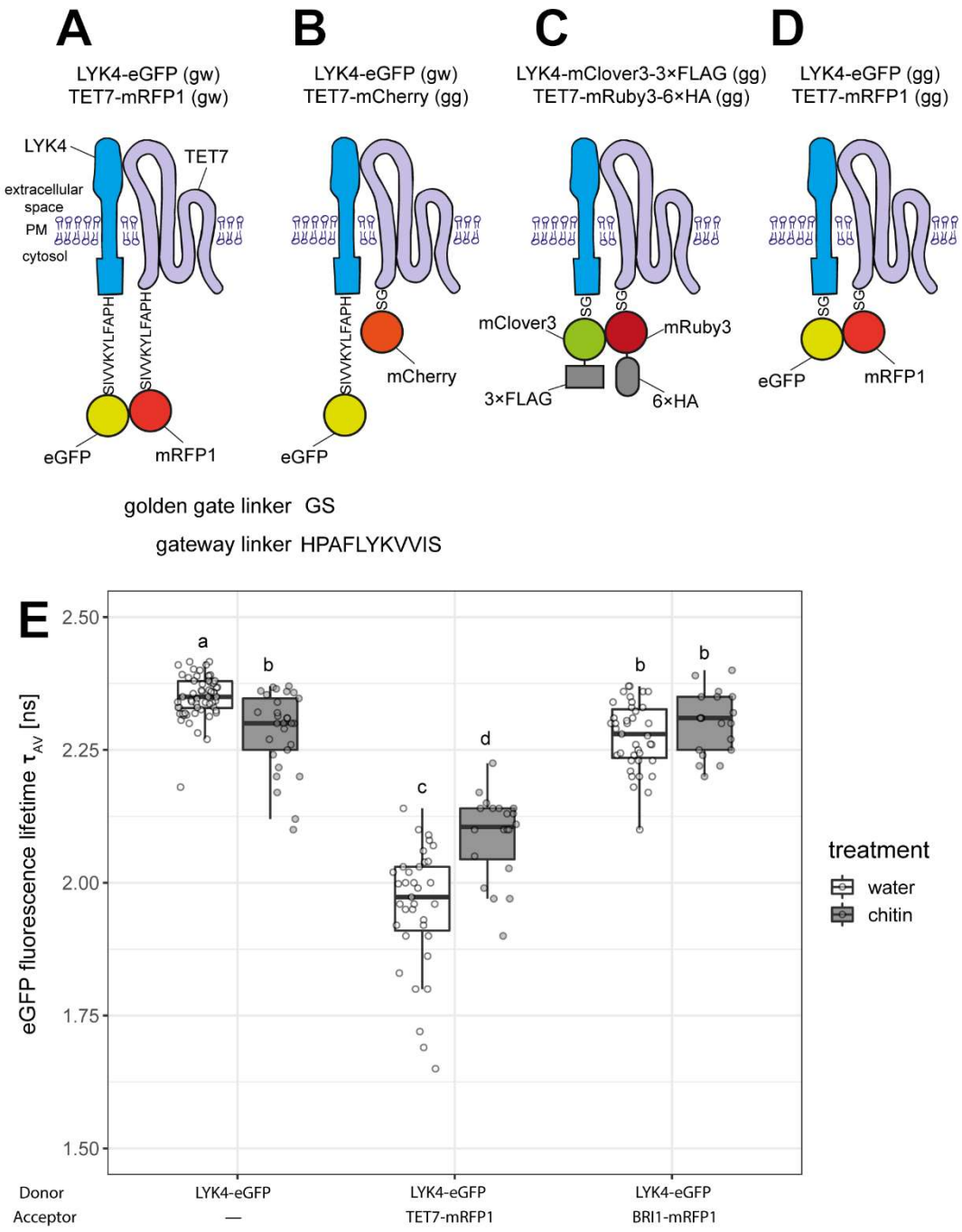

Figure 4-14: FRET-FLIM analysis of the donor LYK4. (A), (B), (C), and (D) Schematic models of fluorophore arrangement using different cloning methods and fluorophores. (A) LYK4-eGFP (gw) and TET7-mRFP1 (gw) used in Fig. 4-14E. (B) LYK4-eGFP (gw), and TET7-mCherry (gg). (C) LYK4-mClover3-3×FLAG (gg) and TET7-mRuby3-6×HA (gg). (B) and (C) were used in Fig. 4-15. (D) LYK4-eGFP (gg) and TET7-mRFP1 (gg) used in Fig. 4-16. (A)to(D) gw: gateway, gg: golden gate. (E) FRET-FLIM analysis of LYK4-eGFP (gw) in the absence and presence of acceptor proteins TET7-mRFP1 (gw) and BRI1-mRFP1 (gw). The constructs were transiently expressed in *N. benthamiana* using the gateway expression plasmids pB7FWG2.0 and pB7RWG2.0 respectively. Leaves were infiltrated with either water (mock) or chitin 30 min before the start of the experiment. Data were collected 30 – 60 min after infiltration. Data were analysed by pairwise Wilcoxon rank sum tests using the Bonferroni p-value adjustments for multiple comparisons. All different letters indicate a statistical significance of $p < 0.01$, samples with the same letter code are not significant. This data is a combination of experiments conducted by me and Cecilia Cheval. Number of images analysed (n) is ≥ 19. Data was acquired using a Leica TCS SP8X.

Further FRET-FLIM experiments (Figure 4-15 and 4-16) were carried out on a Leica Stellaris 8 FALCON in TCSPC mode and analysed with the Leica internal Las X software. Initial experiments using multiple comparable golden gate generated tetraspanin proteins fused to mCherry (golden gate construct, from here on gg) showed a less sizeable shift in the lifetime of the donor LYK4-eGFP (gw) in the presence of TET7 (gg) (Figure 4-15) (donor without an acceptor $\tau = 2.35 \pm 0.030$ ns, to in the presence of, TET7-mCherry gg $\tau = 2.27 \pm 0.026$ ns, E = 3.40%). These low shifts in lifetime were not as expected after the experiments reported in Figure 4-14E.

To elucidate whether this reduction in FRET was due to the acceptor constructs used or due to the different microscope set-up, lifetime shift of the donor in the presence of previously established acceptor fluorophore translational fusion constructs created by gateway cloning were tested. In the presence of LYK5-mRFP1 (gw) the donor lifetime of LYK4-eGFP (gw) dropped significantly to $\tau = 2.13 \pm 0.022$ ns (Figure 4-15) (E = 9.36%), consistent with the shift observed in Cheval et al. (2020). Expressing the acceptor TET7-mRFP1 (gw) construct with LYK4-eGFP (gw) resulted in a reduction of the eGFP lifetime to $\tau = 2.12 \pm 0.044$ ns (E = 7.79%). Even though this is a smaller shift than previously observed (Figure 4-14E), it is nonetheless significantly different from the donor only samples and larger than the shift induced by the mCherry translational fusion of TET7 (gg). This showed the need for further optimisation of the optimal fluorophore and expression levels of the FRET-FLIM constructs used.

As different fluorophores can exhibit different FRET efficiencies for the same donor and acceptor protein (Long et al., 2018), I wanted to test a different fluorophore pair for my proteins of interest. Bajar et al. (2016a) developed mClover3-mRuby3 as a superior green-red fluorophore pair for FRET reactions for their improved photostability, brightness as well as monomeric and mono-exponential properties. To test this pair with my proteins in plants, level0 plasmids of these fluorophores utilising the golden gate cloning system were constructed.

LYK4 and TET7 fused with mClover3 and mRuby3 proved a poor experimental system for FRET-FLIM analysis. LYK4-mClover3 (gg) by itself exhibited a lifetime of $\tau = 2.98 \pm 0.023$ ns and in the presence of TET7-mRuby3 (gg) a small shift to $\tau = 2.92 \pm 0.0394$ (E = 2.01%) (Fig. 4-15) was measured. This is a much smaller shift than observed using LYK4-eGFP (gw) ($\tau = 2.35 \pm 0.0299$) with TET7-mRFP1 (gw) ($\tau = 2.12 \pm 0.044$, E = 9.79%) (Fig. 4-15) and means the pair LYK4-mClover3 (gg) with TET7-mRuby3 (gg) is not as optimal for FRET experiments as LYK4-eGFP (gw) with TET7-mRFP1 (gw). This difference is particularly visible when comparing

the FRET-Efficiencies of 2.01% with 9.79%. While these constructs were useful for biochemical approaches such as co-IPs with multiple antibody binding sites in 3×FLAG and 6×HA, these constructs were not further used in FRET-FLIM.

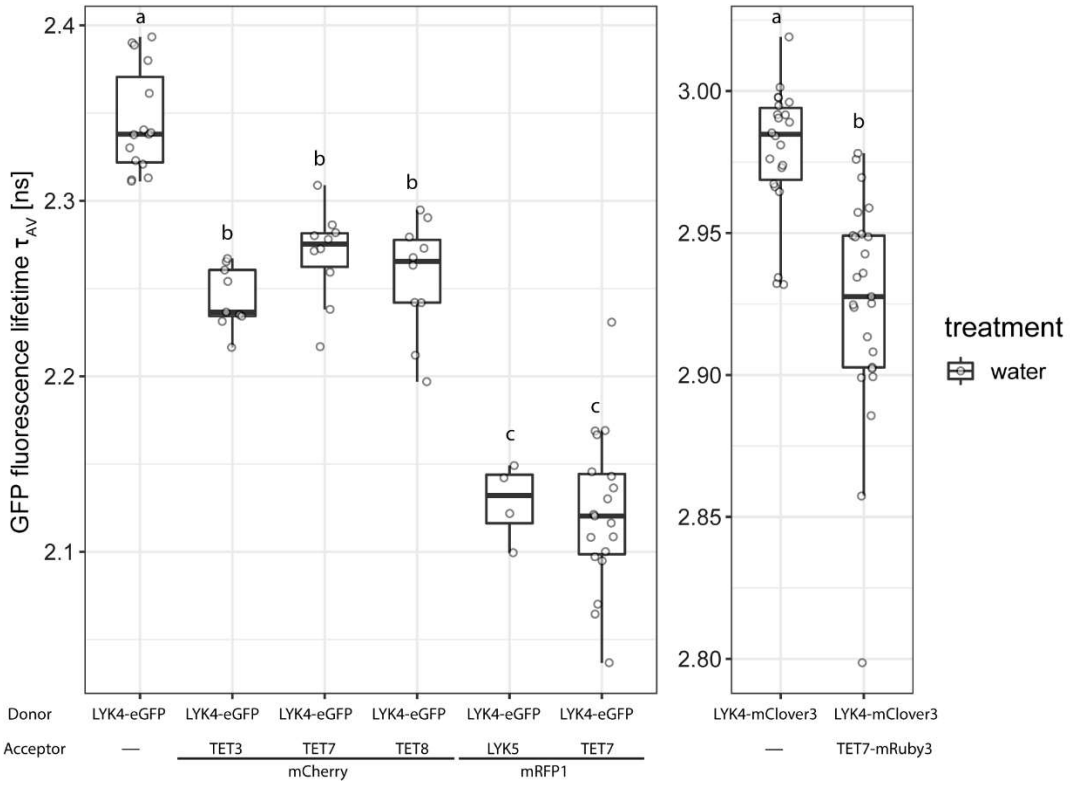

Figure 4-15: First FRET-FLIM experiments using the Leica Stellaris 8 FALCON. FRET-FLIM analysis of LYK4-eGFP (gw) in the absence and presence of acceptor proteins TET3-mCherry (gg), TET7-mCherry (gg), TET8-mCherry (gg), LYK5-mRFP1 (gw) and TET7-mRFP1 (gw). Further FRET-FLIM analysis of LYK4-mClover3-3×FLAG (gg) in the presence and absence of the donor TET7-mRuby3-6×HA (gg). The constructs were transiently expressed in *N. benthamiana*. Leaves were infiltrated with either water (mock) 30 min. before the start of the experiment. Data were collected 30 – 60 min. after infiltration. Data were analysed by pairwise Wilcoxon rank sum tests using the Bonferroni p-value adjustments for multiple comparisons. All different letters indicate a statistical significance of $p < 0.01$, samples with the same letter code are not significant. Number of images analysed n = 4 for LYK5-mRFP1 including samples, $n \geq 9$ for all other samples using LYK4-eGFP as a donor, $n \geq 22$ for all samples using LYK4-mClover as a donor. Data was acquired on a Leica Stellaris 8.

As mRFP1 has proved itself to be a better fluorophore acceptor in LYK4-TET7 (gw) FRET-FLIM protein-protein association experiments, I wanted to compare all three candidate tetraspanins constructed in a standard way with this fluorophore and used the golden gate cloning system for this purpose. Compared to the donor only baseline under mock conditions ($\tau = 2.41 \pm 0.0434$ ns) all three tetraspanin constructs induced a statistically significant drop in the lifetime of LYK4-eGFP (gg) (with TET3-mRFP1 gg $\tau = 2.36 \pm 0.0593$, E = 2.07%; TET7-mRFP1 gg $\tau = 2.37 \pm 0.0467$, E = 1.66%; TET8-mRFP1 gg $\tau = 2.33 \pm 0.0496$, E = 3.32%) (Figure 4-14). Similarly comparing the lifetime of LYK4-eGFP (gw) when treated with chitin ($\tau = 2.38 \pm 0.0376$) suggested that TET3, TET7 and TET8 all induced a drop in the lifetime of LYK4-eGFP (gg) (with TET3-mRFP1 gg $\tau = 2.31 \pm 0.0507$, E = 4.15%; TET7-mRFP1 gg $\tau = 2.30 \pm 0.0353$, E = 4.56%; TET8-mRFP1 gg $\tau = 2.30 \pm 0.0430$, E = 4.56%).

As previously observed for TET7 (Fig. 4-14E and 15), there were significant decreases to the lifetime of LYK4-eGFP between the mock and chitin treated samples for each tetraspanin analysed. However, by contrast to the chitin effect in Figure 4-14E when chitin treatment reduced the drop in LYK4-eGFP (gw) lifetime in the presence of TET7-mRFP1 (gw) (resulting in a lower E), chitin induced a greater drop in LYK4-eGFP (gg) lifetime relative to the control for TET3-mRFP1 (gg), (mock $\tau = 2.36 \pm 0.0593$, E = 2.07%; chitin $\tau = 2.31 \pm 0.0507$, E = 4.15%), TET7-mRFP1 (gg) (mock $\tau = 2.37 \pm 0.0467$, E = 1.66%; chitin $\tau = 2.30 \pm 0.0353$, E = 4.56%) and TET8-mRFP (gg) (mock $\tau = 2.33 \pm 0.0496$, E = 3.32%; chitin $\tau = 2.30 \pm 0.0430$, E = 4.56%).

The shifts in amplitude observed in Fig. 4-16 using golden gate plasmids, are not as strong as observed previously when using the gateway constructed TET7-mRFP1 (gw) ($\tau = 1.95 \pm 0.116$ ns in Fig. 4-14E, E = 17.02%, in Fig. 4-14E; and $\tau = 2.12 \pm 0.0441$ ns, E = 9.79%, in Fig. 4-15). Further, again by contrast with the results of the previous experiment (Fig. 4-14E), the presence of BRI1-mRFP1 (gw) (mock $\tau = 2.31 \pm 0.0893$, E = 4.15%; chitin $\tau = 2.26 \pm 0.0718$, E = 6.22%) resulted in significant reduction in the lifetime of LYK4-eGFP (gg). When comparing the mock and chitin treated samples with BRI1-RFP as the acceptor, no statistically significant difference was detected between the two conditions (Fig. 4-16).

Consistently between the different setups (Fig. 4-14E, 15, 16), a significant decrease in lifetime of the LYK4 donor, in the presence of tetraspanin acceptor constructs, was observed, suggesting an association between these proteins within the PM. As the BRI control in Fig. 4-14E, is consistent with Cheval et al. (2020), and inducing a non-significant change of the donor lifetime, as expected of a negative control, the Fig. 4-14E is likely the more accurate representation of chitin decreasing the association between LYK4 and TET7. While this trend was not observed in Fig. 4-16, the negative control BRI1, also resulted in a significant drop of the donor fluorophore's lifetime. Thus, no directional effect of chitin can be confidently concluded from these experiments and further validation is needed. Regardless, I can conclude that LYK4 is associating with TET3, TET7, and TET8 in the PM, and chitin may influence these associations.

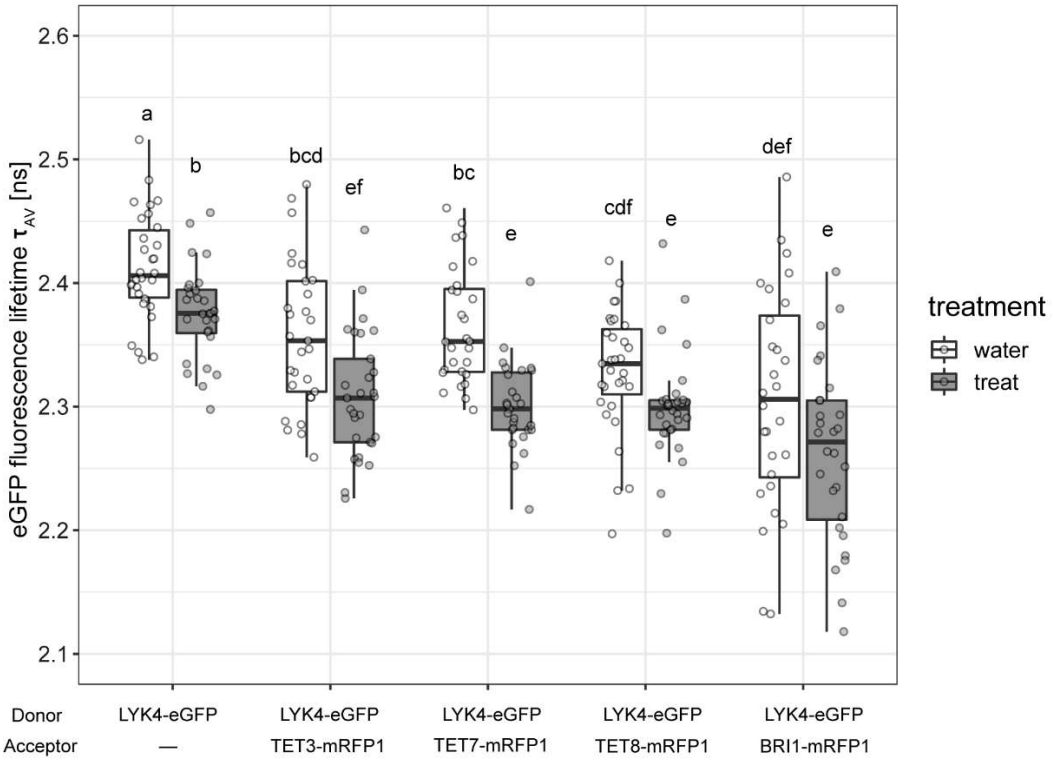

Figure 4-16: FRET-FLIM analysis using a Leica Stellaris 8 and LYK4-eGFP (gg) with mRFP1 (gg) acceptor constructs. FRET-FLIM analysis of LYK4-eGFP (gg) in the absence and presence of acceptor proteins TET3-mRFP1 (gg), TET7-mRFP1 (gg), TET8-mRFP1 (gg), BRI1-mRFP1 (gw). Leaves were infiltrated with either 0.5 mg/mL chitin or water (mock) 30 min before the start of the experiment. Data were collected 30 – 60 min. after infiltration. Data were analysed by pairwise Wilcoxon rank sum tests using the Bonferroni p-value adjustments for multiple comparisons. All different letters indicate a statistical significance of $p < 0.01$, samples with the same letter code are not significant. Number of images analysed (n) is ≥ 27 from three separate experiments. Data was acquired on a Leica Stellaris 8.

4.2.10 Changes in tetraspanin localisations in response to chitin and co-overexpression of LYK4 and LYK5 — observation of aggregating bubbles

Tetraspanins can interact with receptor proteins and form receptor complexes (Susa et al., 2020). An interaction with a tetraspanin can affect the localisation of a receptor, and vice versa a receptor can have an effect on a tetraspanin (Barreiro et al., 2008; Mattila et al., 2013). Depending on the presence of the receptor ligand, receptor proteins can change their presence in receptor complexes, associations in nanodomains, as well as their overall subcellular localisation (Albrecht et al., 2012; Bücherl et al., 2017; Robatzek et al., 2006). The chitin receptor LYK4 associates with TET3, TET7 and TET8 (Fig. 4-13 to 16). I further demonstrated that LYK4 associates with LYK5 (chapter 3-9) in a chitin dependent dynamic manner (Cheval et al., 2020). This makes these receptors ideal first targets to study the effect its presence might have on tetraspanin localisation in a chitin triggered context. Therefore, I investigated how the overexpression of receptors in the presence of their ligands might affect tetraspanin subcellular localisation.

TET3 localises to the PM as well as to PD (Fig. 4-4). Consistent with the PD index data of Fig. 4-12, no differences were observed comparing the TET3-mCherry localisation in the presence or absence of chitin (Fig.4-17B). The co-overexpression of both LYK4-eGFP as well as LYK5-eGFP, both in the presence or absence of chitin, did not induce any changes in the localisation of TET3-mCherry (Fig. 4-17C to F).

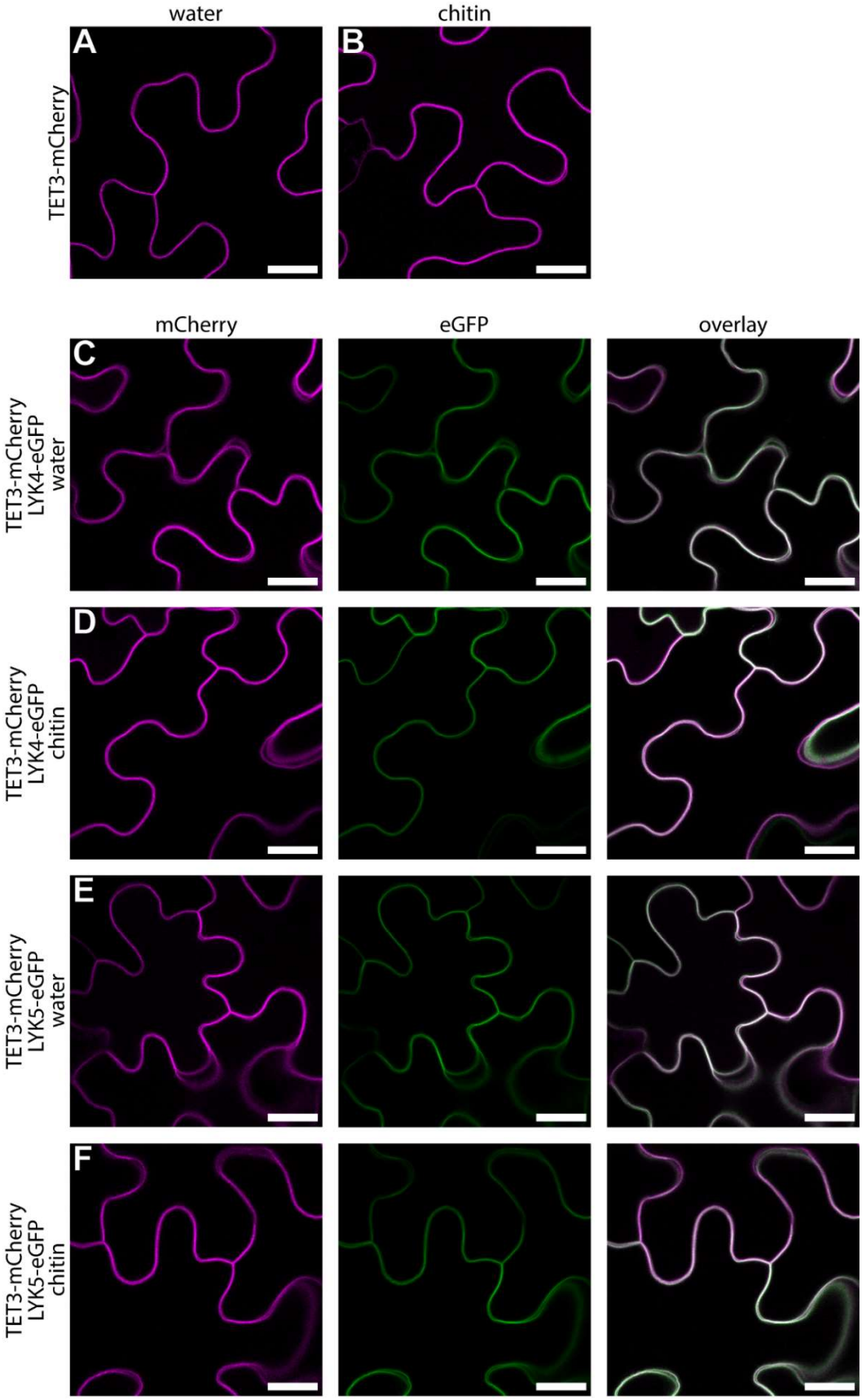

Figure 4-17: TET3-mCherry transiently expressed in *N. benthamiana* leaves, in the absence or presence of LYK4-eGFP or LYK5-eGFP. Micrographs were taken 30-60 min. after infiltration of 0.5 mg/mL chitin or water (mock). Both LYK4-eGFP as well as LYK5-eGFP are expressed using the 35s promoter and TET3-mCherry is under the control of the *AtAct2* promoter. All scalebars indicate 20 µm. Repeated in at least four independent transformation experiments with similar results.

TET7-mCherry is present at the PM, and pools of fluorescence have also been observed in transvacuolar strands as well as at the nuclear envelope, suggesting a possible presence in the ER (Fig.4-18A). Fluorescent signals of TET7-mCherry in aggregations in the extracellular space suggestive of extracellular vesicles (Cai et al., 2018; Guo et al., 2022) (Fig.4-18A to F, indicated by arrows) were detected. This could be a true protein localisation or artefactual due to overexpression. Chitin treatment did not change the localisation of TET7-mCherry (Fig.4-18B).

The same localisations of TET7-mCherry were consistently observed and did not change by co-overexpression of either LYK4-eGFP or LYK5-eGFP in mock treated samples, nor in chitin treated samples (Fig.4-18C to F). The extracellular fluorescence aggregations of TET7-mCherry do not overlay with fluorescence signals for LYK4-eGFP or LYK5-eGFP, but rather are situated between the PM marked by those two proteins. The possibility that this red fluorescent signal could be caused by *Agrobacterium* expressing *the TET7-mCherry* construct in the apoplast cannot be excluded and needs to be further resolved in future experiments.

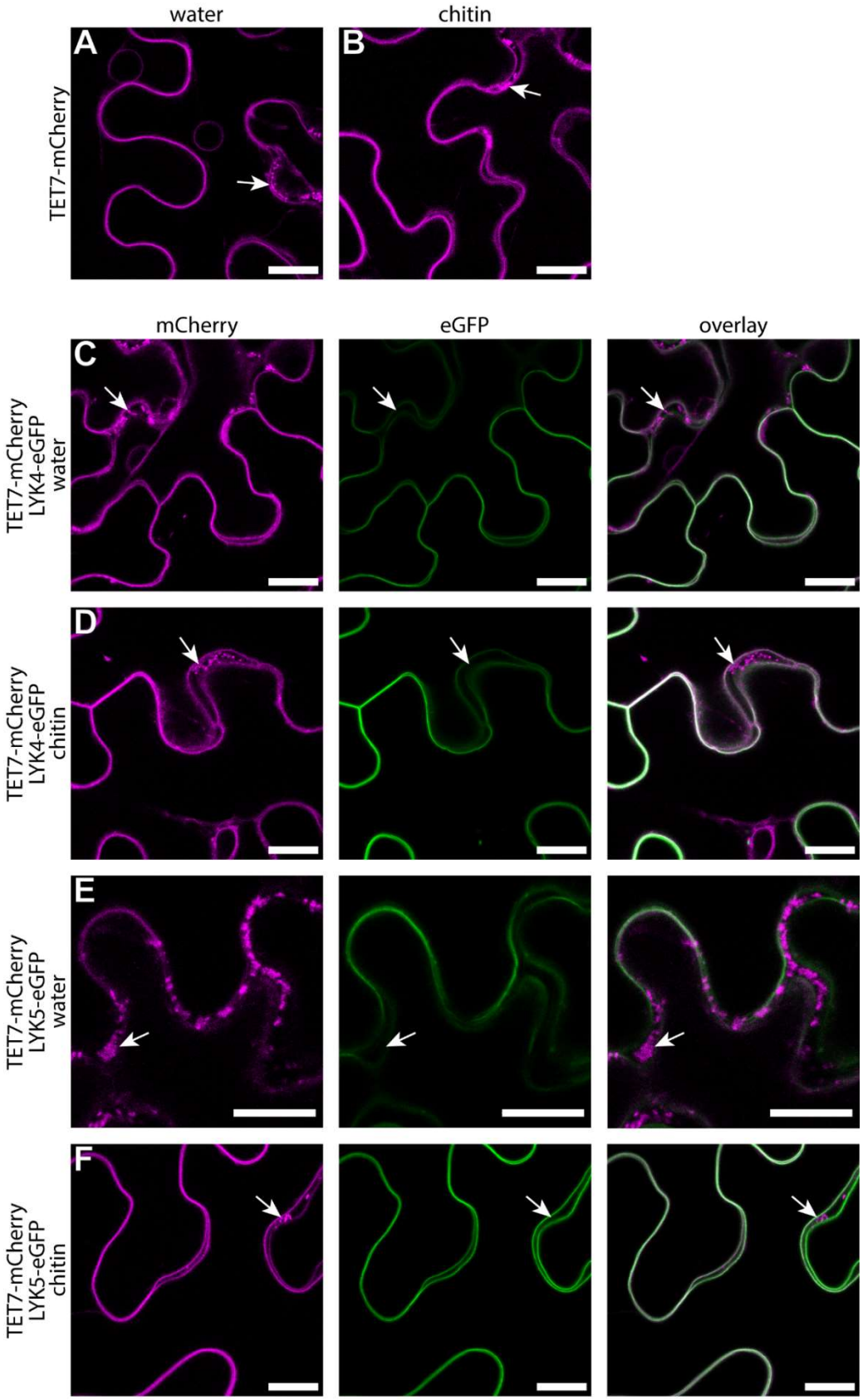

Figure 4-18: TET7-mCherry transiently expressed in *N. benthamiana* leaves, in the absence or presence of LYK4-eGFP or LYK5-eGFP. Micrographs were taken 30-60 min. after infiltration of 0.5 mg/mL chitin or water (mock). Both LYK4-eGFP as well as LYK5-eGFP are expressed using the 35s promoter and TET3-mCherry is under the control of the *AtAct2* promoter. All scalebars indicate 20 µm. Repeated in at least four independent transformation experiments with similar results. Arrows are indicating extracellular fluorescence aggregations of TET7-mCherry.

I observed TET8-mCherry to be present at the PM, with fluorescence pools in the ER as evidence in the nuclear envelope as well as in transvacuolar strands (Fig.4-19). Treatment with chitin did not trigger a change in the localisation of TET8-mCherry (Fig.4-19B). The co-overexpression with LYK4-eGFP did not result in the presence of any TET8-mCherry signals in any further cellular compartments, neither in mock nor in chitin treated samples (Fig.4-19C and D). Similarly, no changes to the cellular localisation of TET8-mCherry proteins when co-overexpressed with LYK5-eGFP in mock treated leaves (Fig. 19-E) were observed. However, in chitin treated samples co-overexpressing TET8-mCherry with LYK5-eGFP, peculiar and consistent phenomenon was noticed. Inside of epidermis cells of these leaves, aggregating bubbles were observed (Fig.4-19F, and Fig.4-20 in detail). These structures exhibit fluorescence signals for both TET8-mCherry as well as LYK5-eGFP. In some cells individual aggregating bubbles were observed (Fig. 4-19F), while in others more aggregating bubbles accumulated in similar positions (Fig. 4-20).

These aggregating bubbles seem to be made up of one to multiple layers of membranous material resulting in thick structures (Fig.4-20B). They can include smaller bubbles within bigger bubble aggregates (Fig.4-20A & B). Due to their size and thick lining they can be observed using brightfield imaging microscopy (Fig. 4-20B). In some cells with multiple aggregating bubbles, a distinctive lack or reduction of fluorescence signals in the PM for both TET8-mCherry as well as LYK5-eGFP was observed (Fig. 4-20B). These comparison experiments of different tetraspanin and receptor constructs showed that the aggregating bubble structures are specific to the combination of the overexpression of TET8-mCherry with LYK5-eGFP in a chitin-triggered manner (Fig.4-17, 18, 19).

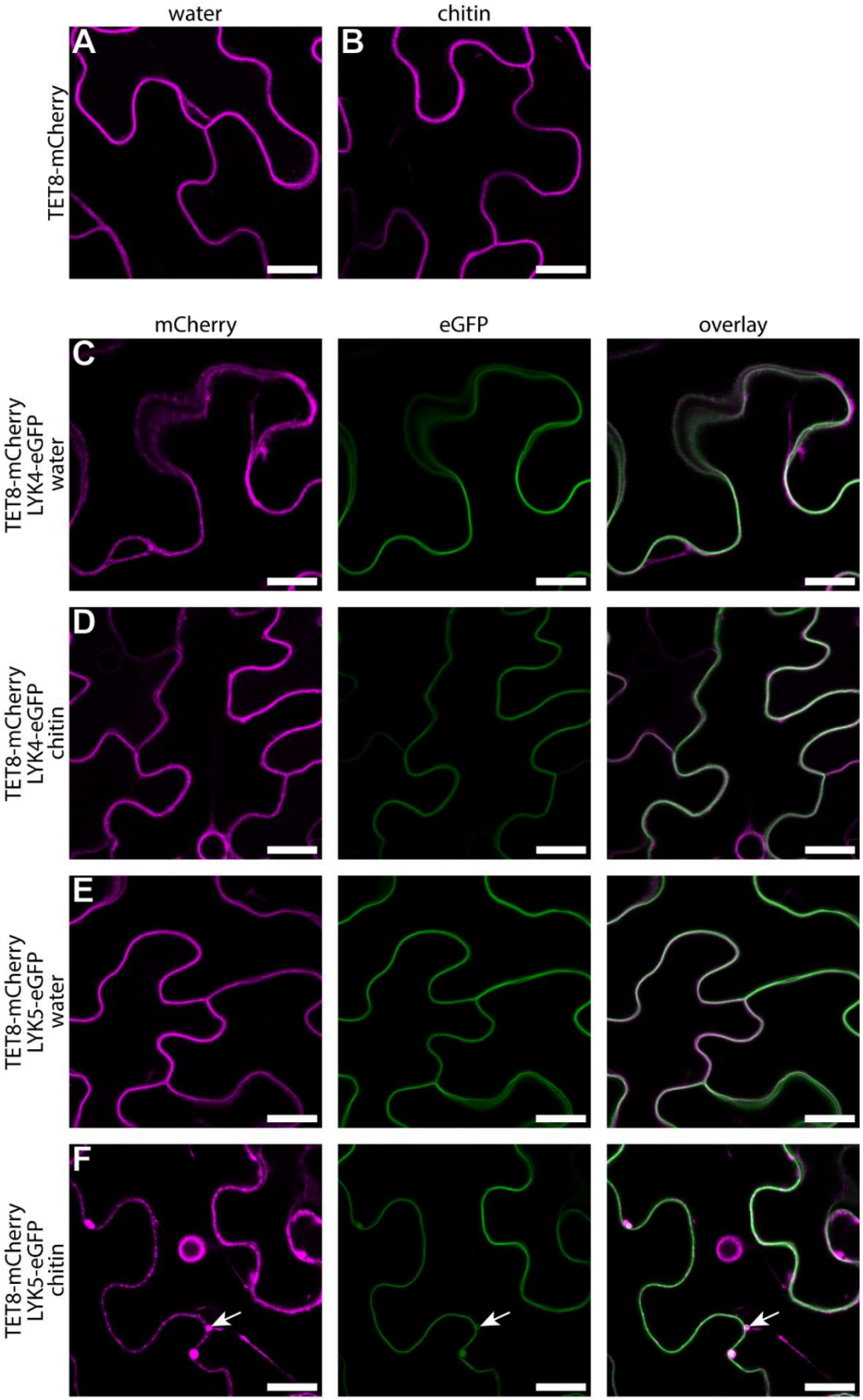

Figure 4-19: TET8-mCherry transiently expressed in *N. benthamiana* leaves, in the absence or presence of LYK4-eGFP or LYK5-eGFP. Micrographs were taken 30-60 min. after infiltration of 0.5 mg/mL chitin or water (mock). Both LYK4-eGFP as well as LYK5-eGFP are expressed using the 35s promoter and TET3-mCherry is under the control of the *AtAct2* promoter. All scalebars indicate 20 µm. Repeated in at least four independent transformation experiments with similar results. Arrows are indicating intracellular aggregating membrane bubbles.

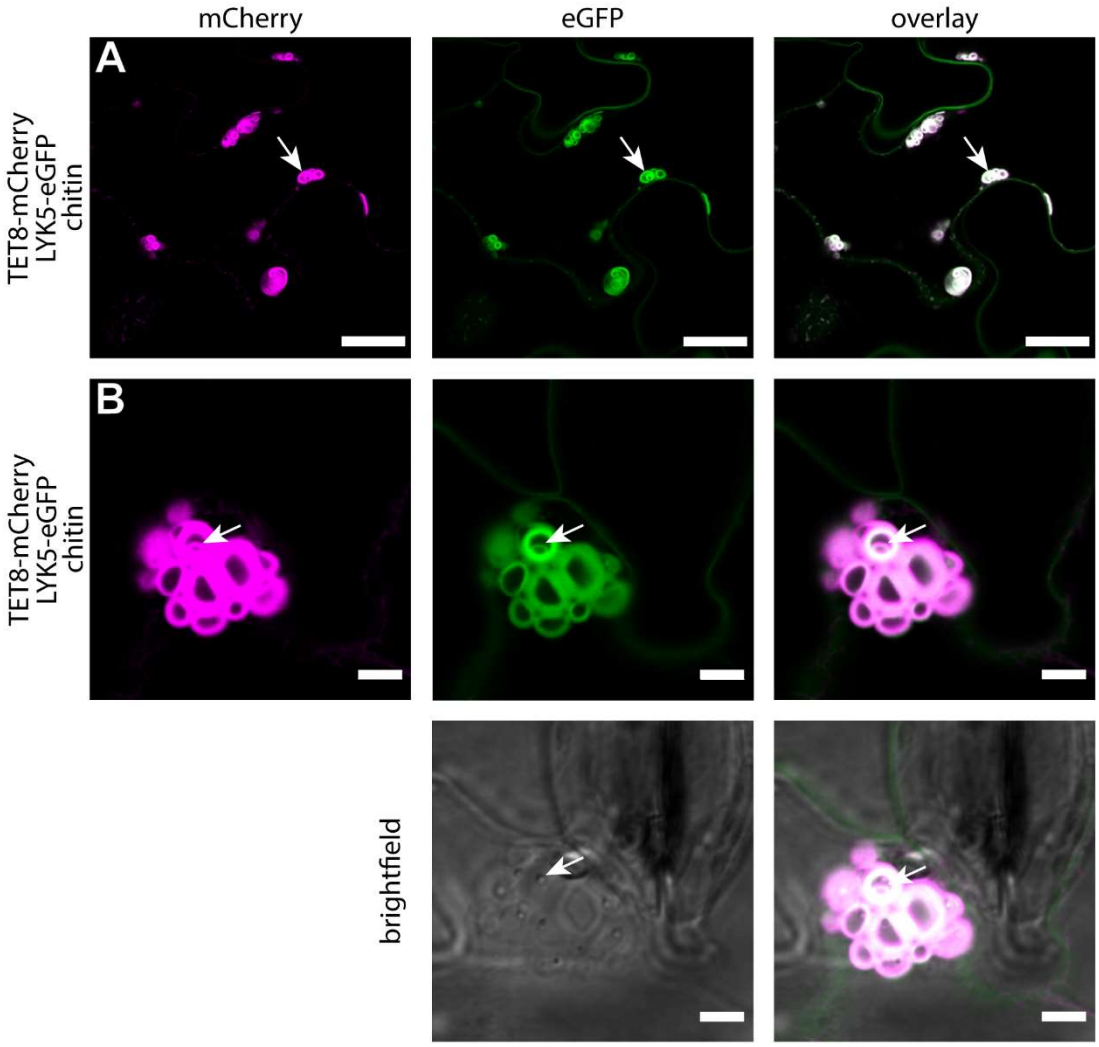

Figure 4-20: Details of aggregating bubble structures *N. benthamiana* leaves transiently expressing *35s::LYK5-eGFP* and *AtAct2::TET8-mCherry* treated with chitin. Micrographs were collected 30 – 60 min. after treatment. Scalebars of the micrographs in (A) 20 µm, and in (B) 5 µm. Repeated in at least four independent transformation experiments with similar results. Arrows are indicating intracellular aggregating membrane bubbles.

4.3 Discussion

4.3.1 Identification of tetraspanins in plasmodesmal proteomes in the context of their phylogenetic relationships

The phylogenetic investigation based on the amino acid sequence of the members of the tetraspanin family concluded that all 17 members of the tetraspanins *sensu strico* (TET1 to TET17) cluster together in one clade and all tetraspanins *sensu lato* (TOM2A, TFP1 to TFP3) cluster together in one clade. Interestingly members of the TOM2A clade have been implicated to be targets of viruses of the genus Tombavirus — particularly *Youcai mosaic virus* and *Tomato mosaic virus* (Fujisaki et al., 2008). They were first identified by Tsujimoto et al. (2003) as interactors of the viral protein TOM1 and are recruited as part of the viral replication complex. Presence of the TOM2A clade proteins leads to high virus multiplication, while knock-out mutant plants show a reduced infection potential, thereby suggesting that these proteins are important for the virus infection (Fujisaki et al., 2008). Although it was assessed that these proteins have enhancing effects on successful infection, little is known to date about their native function. Expressing these genes makes the plants more susceptible to virus infections. Therefore, it is likely that a reason exists, why the plant has not yet lost these susceptibility causing genes over time due to evolutionary pressures. This implicates that they must fulfil an important role for the plant and makes them intriguing future research targets.

Within the tetraspanins *sensu strico* (TET1 to TET17) are seven clades which include two closely related homologues. Arabidopsis has undergone multiple genome duplication events during its evolutionary history (Simillion et al., 2002). These double clades could have potentially arisen from such genome duplication events. Duplicated genes can over time either continue to fulfil the same functions, supress one of the two genes, differentiate and specialise within their niches or free up one of the two to acquire a new function leading to functional divergence (Li et al., 2015a). The suppression of one copy by genomic mutations is one possible explanation why *TET9* shows such low general expression levels in comparison to its sister gene *TET8* (Arabidopsis eFP Browser 2.0, 2022; Winter et al., 2007).

The knowledge of the phylogenetic relationships and closest homologues of the tetraspanin family enables more hypothesis driven research approaches. As one can readily identify the closest related homologues, this enables the formulation of more hypothesis driven research

approaches. As such this approach was used to identify closely related homologues to make educated choices in regard to from which clades and which ones to choose as candidates for my research questions. For example the tetraspanin clade including TET7, TET8 and TET9 (Fig. 4-3) exhibits importance in different plant immunity responses, allowing to conclude that all its members might be involved in these processes. Further this allows speculation that its closest related clade, which includes TET3 and TET4 (Fig. 4-3), could also be involved in those processes.

Multiple tetraspanin proteins have been identified in published plasmodesmal proteomes. Therefore, some members have been implicated as integral plasmodesmal proteins (Fernandez-Calvino et al., 2011). When plasmodesmal protein extractions are carried out, there are limits to the interpretation of the results. Particularly significant is the plant tissue used to extract the proteins as it is not necessarily representative of all plant organs and therefore cannot necessarily capture all the information relevant to all tissues. All published proteomes use cell suspension cultures (Brault et al., 2019; Fernandez-Calvino et al., 2011; Grison et al., 2015a; Leijon et al., 2018). These suspension cultures might have undergone sub-culturing for time frames more than years before the experiments have been carried out, and therefore might not always completely keep their original gene expression behaviour.

Most published plasmodesmal proteomes have been derived from root cell suspension cultures, limiting their applicability for other tissues such as stems, leaves and reproductive organs. For example, the tetraspanins TET12/TET13/TET14/TET15/TET16/TET17 are often specifically expressed in pollen and sperm cells (Reimann, 2018; Reimann et al., 2017). These proteins might still localise to plasmodesmata, but their presence in this cellular compartment might be underexplored as they are very rarely expressed in plant organs such as leaves or roots (Arabidopsis eFP Browser 2.0, 2022; Winter et al., 2007). This expression profile might have obscured a presence at plasmodesmata in published plasmodesmal extract proteomes from root suspension cells. The discovery of two tetraspanin proteins in a *Physcomitrium patens* plasmodesmal proteome (M. Johnston – pers. communication), gives further evidence that tetraspanins might be integral plasmodesmata proteins, as well as that this plasmodesmata association may be ancestral for land plants.

The identification of clades of tetraspanins being present at plasmodesmata (TET1/2, TET3/4, TET7/8/9, and TET11 of the TET11/12 clade) (Fig. 4-1B) allows the speculation that the most recent common ancestor of each of these clades might already have had a plasmodesmal

localisation and all descendants have kept this true. Only TET11 and TET12 have not yet been reported to share this feature as TET11 has been identified to be present at plasmodesmata while TET12 has not. This might be due to several reasons such as sampling bias or methodological constraints. However, if TET12 does indeed prove to not localise to plasmodesmata while TET11 does, it might be a good candidate for future research projects aimed at elucidating to determine how tetraspanins protein are targeted to plasmodesmata.

Both TET1 and TET2 have been identified in plasmodesmal proteomes. They would have been excellent candidates to confirm their plasmodesmal localisation. However, they play a major role in leaf patterning processes and early leaf developmental processes (Chiu et al., 2007; Cnops et al., 2006) — and these were processes not within the scope of this work. They have therefore not been considered as prime candidates in immunity related processes.

TET3 and TET4 are close homologues of each other. They are so closely related that peptides identified by mass spectrometry cannot necessarily be assigned correctly to either of the two specifically. The full data set of Brault et al. (2019) notes this uncertainty. However, even with this mass spectrometry peptide assignment problem, the conclusion can be drawn that at least one member of the TET3/4 clade has been identified to be present in plasmodesmal extracts. *TET4* was shown to be only expressed in dry seeds and senescing siliques while *TET3* is expressed strongly in a multitude of plant organs including leaves (Arabidopsis eFP Browser 2.0, 2022; Winter et al., 2007). The localisation of TET3 has been further confirmed *in planta* by confocal microscopy using a YFP translational fusion construct (Fernandez-Calvino et al., 2011). This combined information led me to pursue the more promising candidate of TET3 over TET4 for future experiments of this thesis.

Only TET11, but not its closest homologue TET12, has been identified in plasmodesmal extracts. In contrast the three-member clade including TET7, TET8 and TET9 have been consistently identified in plasmodesmal proteomes (Brault et al., 2019; Fernandez-Calvino et al., 2011; Grison et al., 2015a; Leijon et al., 2018), giving strong evidence that members of this clade have a plasmodesmal localisation. This makes it another prime candidate clade to elucidate the role of tetraspanins in plasmodesmata. However, *TET9* shows nearly no expression in leaves, by contrast to *TET8* or *TET7* (Arabidopsis eFP Browser 2.0, 2022; Winter et al., 2007). For time and resource reasons the candidate status was therefore limited to TET7 and TET8 in this work.

In summary, the phylogenetic relationships of the tetraspanin family in combination with the published plasmodesmal proteomes allowed the selection of promising candidate proteins for further work. TET3, TET7 and TET8 were identified as candidates and assessed further.

4.3.2 Plasmodesmata localisation of tetraspanins

A TET3-YFP translational fusion was shown to localise to plasmodesmata when stably expressed in sArabidopsis plants (Fernandez-Calvino et al., 2011). Contrary to this, my first localisation data generated of TET3, TET7 and TET8 using an mCherry tag, showed an even localisation to the PM when transiently expressed in *N. benthamiana* leaves (Fig. 4-4A, B, C). My original hypothesis to explain this difference, was that potentially the Arabidopsis tetraspanins would only localise to plasmodesmata in Arabidopsis and not in the heterologous system of *N. benthamiana*. But by using a mRuby3 fluorophore TET3, TET7 and TET8 were successfully detected at plasmodesmata when transiently expressed in N. benthamiana leaves (Fig. 4-D, E, F). Further controls could be carried out in the future with mRuby3-6×HA as a fluorophore and the absence of such a protein to ensure that the detected fluorescent signal is indeed originating from the fluorophore and not a signal detection artefact nor from aniline blue. Another further control could also be an mRuby3 translational fusion of the tetraspanin proteins but without the 6×HA. As different fluorophores can lead to different outcomes of functionality in fusion proteins (Hurst et al., 2018), tests with different fluorophores should be considered too.

mCherry as a fluorescent tag, was previously used for PD localised proteins such as PDLP1 (Gui et al., 2015; Xu et al., 2017). Therefore, this fluorophore shouldn't be the sole reason for why these proteins do not show a PD localisation. Further, a protein can be present at plasmodesmata but not sufficiently enriched in comparison with the PM fractions of the same protein resulting in an even PM distribution when using confocal microscopy. This is due to the small size of plasmodesmata, as conventional confocal microscopy cannot resolve plasmodesmata and if the proteins are not exhibiting a higher rate of fluorescence at plasmodesmata, they will not show a plasmodesmal localisation pattern in micrographs. This has been demonstrated in Cheval et al. (2020) for LYK4. Fluorescently tagged LYK4 exhibits an even PM distribution with no indication of a presence or absence at plasmodesmata when observed by confocal microscopy. Nonetheless biochemical plasmodesmal extraction followed by Western blots, revealed the presence of LYK4 at plasmodesmata. It would therefore have been reasonable to operate under the hypothesis that TET3-mCherry, TET7-

mCherry and TET8-mCherry are present but not enriched at plasmodesmata in *N. benthamiana*.

However, in parallel another fluorophore pair was trialled to optimise FRET-FLIM reactions (see chapter 4.2.9.2 for details) and thus cloned and expressed tetraspanins tagged with an mRuby3 fluorophore construct. In contrast to the mCherry constructs, these TET3-mRuby3-6xHA, TET7-mRuby3-6xHA and TET8-mRuby3-6xHA translational fusions did not only localise to the PM, but also showed enriched fluorescence foci at the cell periphery, which overlap with plasmodesmal callose deposits (Fig.4-2D, E, F). The same localisation pattern could also be observed when these constructs were expressed in Arabidopsis (Fig. 4-2G, H, I). These mRuby3-6xHA tetraspanin constructs could therefore be confirmed to be present at plasmodesmata, as originally suggested for TET3, TET7 and TET8 by the plasmodesmal extract proteomes (Brault et al., 2019; Fernandez-Calvino et al., 2011; Grison et al., 2015a; Leijon et al., 2018).

This curious difference in protein localisation with different fluorophores is beyond the scope of this work but might result in interesting future technical research questions and approaches. It might also lead to more critical evaluation of plasmodesmal localisations or 'non-plasmodesmal localisations' with different fluorophores. However, as TET3, TET7 and TET8 have been identified in plasmodesmal proteomes, which do not have a fluorophore induced bias, the plasmodesmal localisation with mRuby3 as a fluorophore is further indicative of the tetraspanins' presence at plasmodesmata. By contrast, the absence of enrichment of translational fusions of tetraspanins with mCherry at plasmodesmata, does not mean that these proteins are not present at plasmodesmata.

Tetraspanins are enriched at sites of cell-to-cell communication. In mammalian systems, such as keratinocytes, tetraspanins have been observed to accumulate at cell-to-cell contacts forming intercellular junctions (Peñas et al., 2000). These cell-to-cell contact sites are functionally similar to plant plasmodesmata. The localisation of plant tetraspanins to plasmodesmata, therefore allows the formulation of hypotheses in an evolutionary context. For example, that tetraspanins have already been important for cell-to-cell communication and regulation in an early ancestral eukaryote. As well as that their evolutionary conservation points to an importance in their functions.

4.3.3 Absence of individual tetraspanins can lead to enhanced susceptibility to fungal pathogens

Leaves of the *tet7* mutant showed an increase in *B. cinerea* necrotic lesion size four days after spot inoculation (Fig. 4-7). However, inoculating *tet3* and *tet8* plants did not result in any significant changes of susceptibility of detached Arabidopsis leaves to *B. cinerea*. Multiple confounding factors might obscure such an effect, such as specific pathogen effectors. However, this experiment does allow for the strongly supported conclusion that TET7 is important for plant defence responses against fungi in Arabidopsis.

Cai et al. (2018) report an increased lesion size in *tet8* leaves from *B. cinerea* infections. Even though this experiment was repeated three times, no similar results were generated, as *tet8* did not show a significant increase in susceptibility in my experimental set-up. Previously, the increased susceptibility to *B. cinerea* of *tet8* and *tet9* plants was explained by the function of TET8 and TET9 in extracellular vesicles, and the requirement for extra cellular vesicles. From the presence of TET8 and TET9 in extracellular vesicles and enhanced susceptibility it was concluded that TET8- and TET9-associated exosomes contribute to plant immunity against fungal infection by transferring host sRNAs into fungal cells (Cai et al., 2020). However, I offer the alternative hypothesis that the main reason for the reduction of extracellular vesicles in *tet8* is due to TET8's role in the perception of the fungus. The fungus is therefore not efficiently perceived in *tet8* plants followed by mounting of insufficient immunity responses, resulting in an increase in susceptibility. This hypothesis does not deny the connection of extracellular vesicles with tetraspanins in plants. However, Cai et al.'s link between the absence of a tetraspanin resulting in a susceptibility phenotype purely due to changed extracellular vesicle dynamics and behaviour may not explain the full picture.

The different observations of *tet8* susceptibility in my data in comparison to Cai et al. (2018) could be due to multiple different reasons. For example, infection assays may exhibit inherent variability, and a higher sample size might be needed to determine statistically significant differences. This experiment has been carried out with a higher sample size and three independent repeats resulting in the lowest samples size of 75 lesions per genotype. This is in contrast to Cai et al. (2018) who measured a minimum of 10 lesions per genotype in a single experimental assay. Different strains of *B. cinerea* might carry different effector coding genes, resulting in differences in virulence. However, both Cai et al. (2018) and I used the *B. cinerea* isolate B05.10, and the same T-DNA mutant for *tet8*. As there is no difference

between the strains used, this should not be causal for the differences in the experimental results. Further different growth conditions might lead to different experimental outcomes. For example, my susceptibility assays were carried out on detached leaves, while Cai et al. (2018) inoculated attached leaves. These experimental differences might have caused a reduction of the *tet8* leaves enhanced susceptibility in my experiment.

Effects of single knockout mutations on a plant's susceptibility to a pathogen may be masked by a variety of different factors. These include redundancy of the plant gene, as well as the presence of specialised pathogen effector proteins inhibiting the immunity responses of the plant ranging from masking of perceived molecules such as MAMPs, to directly interfering with the signalling pathway or the immunity pathway. Varying growth and experimental conditions may also have influenced the plants susceptibility. Susceptibility results not differing from WT results are therefore not excluding the possibility that the mutated gene is important during infection processes. For example CERK1 is an important chitin receptor (Miya et al., 2007), but *cerk1-2* mutants do not show an increased susceptibility to *Colletotrichum higginsianum* (Faulkner et al., 2013). Using the same logic, both TET3 and TET8 might still be important in plant immunity.

Even though there are many possibly confounding factors, I was able to clearly determine that the *tet7* mutant exhibits an enhanced susceptibility to *B. cinerea*. This allows for the conclusion that TET7 is involved in immune responses to fungi.

Although the absence of expression of the individual tetraspanin transcripts of these mutants has been validated by qPCR (Fig. 4-6), the phenotypes of tetraspanin mutants should further be assessed and validated in at least one more independent secondary mutant each. This should be done to avoid effects of unknown further insertions into the genome in these lines as well as to show that independent insertions indeed result in the same phenotypes.

4.3.4 Tetraspanin overexpression changes chitin-triggered ROS production

To study the mechanism and the importance of tetraspanin proteins of plants in triggering and enabling the ROS production in a MAMP dependent matter, the ROS response to chitin in the presence of tetraspanins was assessed. Overexpression of a limiting component of a signalling pathway can result in a stronger ROS response — such as the overexpression of CRK4, CRK6 and CRK36 which increase flg22 responsiveness thereby resulting in an increase in flg22 triggered ROS production (Yeh et al., 2015).

Experiments measuring the ROS burst of transiently overexpressing leaves (Fig. 4-8) were analysed by using a linear mixed model taking the protein overexpression as well as the treatment and the individual experimental plate affects into account, followed by comparisons of estimated marginal means using the emmeans package (Lenth, 2021). This makes use of the tukey-adjusted p-value for multiple pairwise comparisons, resulting in more conservative p-values than individually carried out direct comparisons. Previously we reported a significant increase of the chitin triggered ROS burst in *N. benthamiana* leaf discs overexpressing a *LYK4* construct (Cheval et al., 2020). I was not able to generate a comparable significant difference value in my dataset with my models which use adjusted p-values for multiple comparisons. However, if carried out as a direct individual comparison using the Mann-Whitney-Wilcoxon test, the data in this thesis when comparing *P19* with *LYK4* overexpressing samples also generates a highly significant result ($p = 0.002079$). The data shown here is therefore still consistent with previously published data. All the significant changes detailed in these experiments pass even more stringent statistical criteria.

The individual overexpression of *TET3* and *TET8* led to an increase in chitin-triggered ROS bursts, and to an intermediate increase of *TET7* (Fig. 4-8C, C, D). These data thereby show that overexpression of all three tetraspanins promotes the chitin-triggered ROS production. Further these experiments have been carried out utilising tetraspanin fluorophore translational fusion constructs. Since these fusion proteins can enhance the chitin triggered signalling processes, the fusions are proteins which can carry out a function. Whether or not this is indeed their native function needs to be determined with further experimental evidence.

The overexpression of *TET3* results in an enhanced chitin-triggered ROS production, and the simultaneous presence of LYK4 has a dampening effect instead of an additive effect (Fig. 4-8B). This could be due to the overexpression of *TET3* enabling a non-LYK4 chitin receptor to more efficiently initiate chitin-triggered ROS production. In samples additionally expressing *LYK4*, TET3 might competitively undergo complex formation with LYK4 and therefore is not as available for the non-LYK4 receptor. Another further possibility could be that in samples individually overexpressing *TET3*, it is able to associate with ROS producing enzymes such as RBOHD and enhance ROS production this way, while TET3 undergoes a different preferential complex formation in samples additionally co-overexpressing *LYK4*. It could also be conceivable that the overexpression of these genes could shift the presence of proteins and their complexes between the PM and the plasmodesmal PM, resulting in different efficiencies in ROS production at these different PM subsections.

Overexpression of *LYK4* or *TET7* individually did not significantly enhance ROS production (Fig. 4-8C). This suggests that in overexpression conditions LYK4 and TET7 are not the limiting components, and other factors and their abundance might define the maximum chitin-triggered ROS production in this system. However, co-overexpression of *LYK4* and *TET7* resulted in a statistically more significant increase in ROS production than when compared to control *P19* samples. This hints at a potential additive effect of LYK4 with TET7, possibly obscured by conservative statistical analysis. Such an additive effect could be due to increases in TET7 allowing for more LYK4 proteins in signalling active complexes or nanodomains. LYK4 and TET7 therefore possibly co-operate or positively regulate each other.

These data whereas the combined overexpression of LYK4 with TET3 or LYK4 with TET7 leads to different results are particularly puzzling. It suggests that there are more complex processes at play rather than a simple “increase if present”. Possibly the overexpression of LYK4 could lead to a depletion of chitin-triggered signalling machinery, for example via endocytosis which has been shown to be important for LYK5 (Erwig et al., 2017). It would be conceivable that the higher abundance of LYK4 either stabilises and prevents signalling components to be endocytosed or alternatively enhances their PM depletion via endocytosis. Further if the used LYK4 translational fusion protein is not fulfilling its exact native function but is still undergoing some complex formations it could result in a dominant negative effect for chitin triggered signalling.

Similarly, to the individual overexpression of TET3, an overexpression of TET8 results in a strong increase of chitin-triggered ROS production (Fig. 4-8B, D). However, this individual TET8 overexpression is not significantly different to the individual LYK4 overexpression or the co-overexpression of LYK4 with TET8 (Fig. 4-8D). These results thereby only allow some limited conclusions, such as that the co-overexpression of LYK4 with TET8 does neither significantly dampen nor enhance chitin-triggered ROS production.

When co-overexpressing the tetraspanin genes together with the chitin receptor LYK4, intriguing effects were identified. Both a dampening as well as an enhancing effect allows speculation of the involvement of tetraspanins for the function of chitin receptors (Fig. 4-8B, C, D). While the co-overexpression of LYK4 with TET3 or TET8 does not result in an additive increase of the chitin induced ROS burst, it possibly does in the simultaneous presence of TET7. The additive effect of LYK4 together with TET7 points towards a further enhancement of the signalling capability of LYK4 in the presence of TET7. The non-additive effects of the co-overexpression of LYK4 with TET3 or TET8 suggest a different relationship for signalling in

a chitin dependent manner. The addition of TET8 does not result in significantly different results, while the addition of TET3 does have a dampening effect. These effects could be explained by different spatiotemporal complex or nanodomain formations and protein presence within them pre-chitin treatment versus post-chitin treatment, as well as different protein associations in the plasmodesmal PM versus the rest of the PM.

I conclude that both the overexpression of tetraspanins, as well as the combined overexpression of tetraspanins together with LYK4, has effects on the ROS production triggered by the presence of fungal chitin. It therefore stands to reason that TET3, TET7 and TET8 are possibly differently but directly involved or associated with proteins which are either in the signalling cascade needed to trigger the chitin-induced ROS burst or in the production of ROS itself.

4.3.5 Tetraspanin proteins are important to achieve the full chitin-triggered ROS burst

I identified that the chitin triggered ROS production is reduced in *tet7* and *tet8* KO plants (Fig. 4-9). This suggests that both TET7 as well as TET8 positively regulate ROS production in response to chitin. Their presence and function in the response pathway could therefore be located somewhere between the perception of chitin and the resulting production of ROS within the signalling cascade or alternatively in receptor or signalling component sorting processes.

The enhanced presence of ROS leads to plasmodesmal closure. This production of ROS — specifically H_2O_2 — followed by changes to plasmodesmal status, is either downstream or independent of the receptors perceiving chitin (Cheval et al., 2020). The production of ROS necessary for plasmodesmal functions happens locally at plasmodesmata. However, the ROS measured in this assay (Fig. 4-9) is mostly produced in the general PM and not the plasmodesmal PM — therefore this assay can only be used to determine general ROS perturbations at the PM. Given that all three tetraspanins TET3, TET7 and TET8 localised to the PM and the PD (Fig. 4-4) it stands to reason that they might fulfil their functions in the PM or the PD. No statistically significant perturbation of ROS production triggered by chitin in the absence of TET3 was detected. This could for example be due to TET3 fulfilling its role of aiding chitin perception followed by ROS production exclusively within the plasmodesmal PM but not the general PM, as observed for LYM2, which exhibits a plasmodesmal localisation and phenotype but no changes to PM chitin-triggered ROS production (Faulkner et al., 2013).

These data show that tetraspanins are important for chitin triggered ROS production. There are 17 canonical tetraspanins in Arabidopsis (Fig. 4-3), many of which are predicted and have been shown to interact with each other (Boavida et al., 2013). Huang et al. (2005) speculate that there are two levels of redundancies for tetraspanin proteins: i. when the functions of tetraspanins are dispensable and not necessary, ii. when the functions of tetraspanins are substitutable for one another due to sequence similarity. It therefore stands to reason that the removal of individual tetraspanin genes from a plant does not completely abolish their functions in chitin triggered ROS production, but rather just reduces its output, as multiple tetraspanins might partially fulfil the same role(s) but not completely. For example, another tetraspanin, such as TET4, might be redundant with TET3, and therefore no phenotypical differences in the ROS burst when comparing the *tet3* mutant to Col-0 might have been

observed. This is particularly reasonable when keeping the closely related particular clades in mind (Fig. 4-3). To overcome this, I propose the generation and use of mutants higher order — in particular targeting full clades such as *tet7/8/9* or *tet3/4*. I expect that this will result in an additive effect for the perturbation and might even result in a total abolishment of the chitin or general elicitor triggered ROS production.

Tetraspanins are putatively not the perceiving components of chitin in the signalling cascade, as they are not receptor or receptor-like proteins, but rather are hypothesised to interact with receptors and receptor complexes as well as being responsible for their dynamics and domain localisations within the PM (Kummer et al., 2020). Given that, it would be interesting to determine in the presence of which other MAMPs the tetraspanin KO plants struggle to elicit a full ROS burst. This could be tested by utilising the same assay I used to test for an array of different elicitors such as flg22, elf18 or other β-glucans, INF1, OPEL or SCOOP12. In this way one could confirm the generality of tetraspanin dependence for the function of different receptor-ligand combinations.

As tetraspanins fulfil a variety of different functions with a plethora of receptors in animal systems (Termini and Gillette, 2017), it is possible that this is a general mechanism in plants as well. With my work I have built the foundation of this hypothesis in plant cells and have found that tetraspanins play a key role in receptor mediated immunity in plants.

4.3.6 Tetraspanin mutants do not close their plasmodesmata in the presence of chitin

No changes in the movement of eGFP was observed in the leaves of *tet3* and *tet7* mutant plants when comparing the absence or the presence of chitin (Fig. 4-10), thereby demonstrating that TET3 and TET7 are necessary for chitin triggered closure of plasmodesmata. The plasmodesmal PM is a specialised microdomain of the PM (Bayer et al., 2014; Faulkner, 2013). In Cheval et al. (2020) we demonstrated how chitin-triggered plasmodesmal closure is induced by plasmodesmal localised machinery and differs from chitin-triggered signalling machinery at the PM. Tetraspanins are master organisers of domains within the PM (Yáñez-Mó et al., 2009), and can thereby affect receptors and their signalling capabilities (Kummer et al., 2020). The absence of individual tetraspanins could therefore disrupt such a function and change the plasmodesmal PM domain environment, and thereby the receptors' ability to signal in a local manner. The absence of TET3 or TET7 therefore could cause a disruption to the plasmodesmal microdomain and its protein composition. Tetraspanins can further interact directly with receptor proteins, resulting in impaired signalling processes in the absence of the tetraspanin partner (Susa et al., 2020). If TET3 or TET7 interact with a chitin receptor such as LYK4 at plasmodesmata to achieve signalling competency, this could be severely impacted in tetraspanin mutants.

In *tet8* a low eGFP movement under mock conditions (water infiltrated) and a significant increase in the presence of chitin were observed (Fig. 4-10). This is exactly the inverse behaviour of the WT control Col-0. A similar phenotype of lowered eGFP movement under mock conditions and an increase after chitin treatment has only been observed once in the published literature in Cheval et al. (2020) for *cpk5* mutant. One hypothesis to partially explain this phenotype is based on a crossbow firing mechanism. In this case TET8 keeps the chitin signalling machinery from firing under mock circumstances. However, in the absence of TET8 holding the machinery back, it fires constantly even during mock conditions. This could be conceptionally possible if TET8 and a chitin receptor such as LYK4 associate together in resting state conditions (i.e., the absence of chitin), where the presence of TET8 stops LYK4 from initiating signalling responses. In this hypothesis, once LYK4 detects chitin it could undergo a conformational shift, change of PTM status, or protein association/dissociation process and thereby either partially or fully loses the signalling blocking function of TET8, allowing a signal initiation. However, in the absence of TET8, LYK4 does not get stopped in its signalling capabilities under resting state conditions, resulting an activation of signalling processes and therefore in a reduction of plasmodesmal flux. Consistently reduced

plasmodesmal flux in resting state conditions has been correlated to reduced plant growth (Thomas et al., 2008). However, the mutation in *tet8* is not lethal nor were any clearly visible growth defects observed.

Curiously the plasmodesmal flux of *tet8* mutants does not stay at a reduced level in the presence of chitin but rather increases to a similar level as Col-0 plants exhibit under mock conditions (Fig. 4-10). Possibly the presence of chitin, still induces a change to a chitin receptor such as LYK4 even in the absence of TET8. However, by contrast to the activation of a signalling function, the lack of TET8 could make this receptor undergo degradative processes, such as endocytosis at a higher rate, or cause it to change nanodomain localisation and actually become signalling incompetent outside of its prime environment. Therefore unintuitively, even though chitin in a WT system triggers the receptor's signalling function by binding to it as a ligand, in a *tet8* mutant, the presence of chitin could lead to an abolishment of constantly firing signalling processes and thereby restore WT like plasmodesmal flux.

In summary, the regulation of plasmodesmal diffusion is severely disturbed in the *tet8* mutant but still sensitive to the presence of chitin, therefore one can conclude that TET8 is involved in the chitin detection and signalling pathway. Further the disrupted eGFP cell-to-cell movement under mock conditions in *tet8* suggests that TET8 is also important for plasmodesmal regulation outside of a chitin-signalling context. In conclusion all the tetraspanins TET3, TET7 and TET8 are involved and important for chitin-triggered plasmodesmal flux regulation.

4.3.7 Plasmodesmal callose deposition in tetraspanin mutant plants corresponds to eGFP movement phenotype

As previously reported the aniline blue mean intensity per plasmodesmal callose deposit — serving as a proxy for callose deposition — increased in Col-0 in the presence of chitin (Fig. 4-11) (Cheval et al., 2020). This is in an inverse correlation to the plasmodesmal flux, which decreases in WT plants in the presence of chitin (Fig. 4-10). Mutant plants of *tet3* and *tet7* showed no significant shift in their mean intensity thereby suggesting that their callose levels stayed the same in the presence of chitin (Fig. 4-11), similarly to their cell-to-cell eGFP flux (Fig. 4-10). The callose levels in *tet8* were reduced after chitin treatment (Fig. 4-11), again inversely correlating with the increase in plasmodesmal flux observed in those plants (Fig. 4-10). The amount of callose deposited at plasmodesmata has thereby been shown to inversely correlate with the plasmodesmal flux when comparing the tetraspanin. Therefore, I can conclude that the plasmodesmal flux phenotypes of *tet3*, *tet7* and *tet8* correlate and might be due to a disruption in the chitin-triggered enhanced callose deposition at plasmodesmata.

4.3.8 Tetraspanin plasmodesmal localisations are not dynamic in response to chitin

In contrast to LYM2 (Cheval et al., 2020), no changes in the PD index of the tetraspanin fluorophore translational fusion constructs of TET3, TET7 or TET8 could be observed triggered by chitin (Fig. 4-12). It therefore stands to reason that the changes of plasmodesmal proteins in the presence of MAMPs is not a general process applicable to all plasmodesmata localised proteins. This gives further functional significance to those instances when this behaviour is observed.

However, the reverse conclusion that tetraspanins are less important in chitin signalling at plasmodesmata — as there is no shift in their localisation pattern — does not apply. Rather that they fulfil their functions in a chitin perception context without changing their relative localisation levels between the plasmodesmal PM and the general PM. This allows for two possibilities of interpretation: i. The tetraspanin proteins stay within their localisation of either plasmodesmal PM or PM no matter if chitin is perceived or not or ii. The tetraspanin proteins have a continuous equal exchange between the plasmodesmal PM and the PM. For every tetraspanin protein, which moves to the plasmodesmal PM from the PM one moves vice versa. This rate of exchange might still differ in the presence of chitin — but if the exchange is equal, this would not appear as a significant shift in this experiment. Given the

theory of tetraspanin webs enabling more stability in the organisation of membranes, it could be more likely that the tetraspanins have more “anchor-like” characteristics and therefore do not undergo drastic changes in their localisation.

Achieving an equal exchange rate between two populations is more complex than proteins remaining where they were before the treatment. Therefore, by applying Occam’s razor principle, it allows to draw the hypothesis that tetraspanins do not move from or towards plasmodesmata triggered by the presence of a MAMP but rather fulfil their functions in the signalling pathway without changing their localisation. Possibly they could also undergo a change in their equilibrium point. Future experiments could use a FRAP based approach, such as used in chapter 3.2.3, to determine if the mobility of tetraspanin proteins changes triggered by chitin. This could be done for both the PM as well as the plasmodesmal PM, and thereby evaluate if indeed they exhibit equal mobile fractions under mock conditions as well as in chitin treated samples.

If tetraspanins and their nanodomains are indeed anchored, receptors could be differentially recruited into these nanodomains, under different conditions. The tetraspanin nanodomains could therefore act as conditional signalling platforms.

4.3.9 Tetraspanins interact with the chitin receptor LYK4

4.3.9.1 Co-immunoprecipitation experiments reveal association of tetraspanins with LYK4

All three tetraspanins tested in this experimental series showed an association with LYK4, while the negative control of LTI6b did not (Fig. 4-13). Not all lipid rafts/DRMs/nanodomains are completely disrupted by detergents (Hibino and Kurachi, 2007), and so a successful membrane protein co-IP experiment does not necessarily allow to conclude for a direct interaction, but rather leaves the possibility that both the bait as well as the prey proteins are present together in a detergent resistant membrane fraction, and therefore are both present together in the immunoprecipitation fraction. These experiments therefore allow for the conclusion that TET3, TET7 and TET8 either directly or indirectly interact with LYK4 or at least reside within the same nanodomain of the PM as LYK4.

Alternatively, the tetraspanins themselves could also be prone to “stick” to the magnetic beads used in the immunoprecipitation. Future experiments could therefore additionally test and control for this.

We have previously reported the association of LYM2 with LYK4 and LYK5 as well as LYK4 with LYK5 (Cheval et al., 2020). As LYK4 associates with TET3, TET7 and TET8, it will therefore be interesting to test in future experiments if LYM2 and LYK5 show a similar association with those tetraspanins.

4.3.9.2 FRET-FLIM reveals dynamic associations between LYK4 and TET3, TET7 and TET8

The first set of experiments were carried out (Fig. 4-14) on a Leica SP8X using the gateway plasmids cloning constructed plasmids pB7FWG2.0, and pB7RWG2.0 to express eGFP and mRFP1 translational fusion proteins respectively. These constructs revealed a strong decrease of the fluorescence lifetime τ of the donor LYK4-eGFP (gw) in the presence of TET7-mRFP1 (gw). This drop in lifetime was reduced in chitin treated samples. These data therefore suggest a strong association between LYK4 and TET7 during resting-state conditions, which loosens in the triggered by chitin, potentially suggesting a dissociation between TET7 and signalling-active LYK4.

To run a comparative experiment using multiple different tetraspanin proteins as FRET-FLIM acceptors, I decided to fuse all three tetraspanin candidates to the fluorophore mCherry at their C-terminus. For this experiment I shifted to using the Leica Stellaris 8 FALCON in TCSPC mode. Using TET3-mCherry (gg), TET7-mCherry (gg) and TET8-mCherry (gg) acceptors resulted in a smaller amplitude shift of the donor lifetime (Fig. 4-15) as when using TET7-mRFP1 (gw) in Fig. 4-14. Particularly puzzling is the result for TET7-mCherry (gg) as I already obtained data with a very strong shift in amplitude in the presence of the TET7-mRFP1 (gw) acceptor (Fig. 4-14).

Given those puzzling results, I confirmed a strong shift in amplitude in the donor lifetime with the previously used LYK5-mRFP1 (gw) and TET7-mRFP1 (gw) gateway constructs to determine if the observed mCherry data was due to the microscope or the analysis technique. Although these values were not as strong as previously observed, they were still significantly stronger than for the translational fusion constructs tagged with mCherry, triggering further troubleshooting experiments to optimise these FRET-FLIM reactions in a comparable way. However, they allow the conclusion that shifts in lifetime > 0.2 ns can be achieved on the Leica Stellaris 8 FALCON in TCSPC mode in my hands.

This difference in lifetime shift based on cloning method and fluorophore choice demonstrated that there is untapped potential to optimise this experimental set-up further. The different cloning methods result in the usage of different expression plasmids, utilising

different versions of the cauliflower mosaic virus promoter (CaMV 35s) and terminators, which can result in different expression levels. In general, a potentially stronger fluorescent signal of the gateway constructs in comparison to the golden gate constructs was observed. Further, both golden gate cloning as well as gateway cloning introduce a 'scar' (or linker sequence) between the coding sequence or the protein and the fluorophore. The golden gate system typically introduces two amino acids, and the gateway system introduces 11 additional amino acids (visualised in Fig. 4-14A, B, C, D). These amino acids could be responsible for changing the orientation of the fluorophore tag in relation to the rest of the protein. Further the different linkers could lead to different effects on steric hindrance of the tested protein pairs.

Different fluorophore pairs further have different potential for FRET and therefore a different potential on the effect of the measured FLIM. When comparing the use of mRFP1 and mCherry for their potential of FRET with the donor eGFP, they result in rather similar values in regard to Quantum yield (a unitless ratio of the number of photons emitted through fluorescence divided by the number of photons absorbed) mRFP1 = 0.25 and mCherry 0.22, as well as similar integral overlap values J(λ) mRFP1 = 1.83 and J(λ) mCherry 1.94 $\times 1e^{15}$ M^{-1} cm^{-1} nm^4(fpbase), as well as their spectral properties (Lambert, 2019). These intrinsic fluorophore properties can therefore cautiously be excluded as being responsible for the different amplitude shift of the donor lifetime in the presence of acceptors with different fluorophore translational fusions. However, similarly to a different scar amino acid sequence, different fluorophores can further result in different orientations in relation to the rest of the protein and therefore and with their own different structures exhibit a different transition dipole moment orientation factor (*k*). mCherry and mRFP1 could differ from each other in this orientation.

To further improve and optimise the FRET-FLIM experiment, a new fluorophore pair was trialled; mClover3 and mRuby3 have not been previously used for studies in plants, but have been developed for their superior properties, in particular for being monomeric and have a mono-exponential lifetime decay (Bajar et al., 2016a; Bajar et al., 2016b). Most fluorophores exhibit a multi-exponential lifetime decay, making it necessary to use the sum of multiple exponents to accurately fit their lifetime models, and thereby making more complex models necessary (Włodarczyk and Kierdaszuk, 2003). Fluorophores with a mono-exponential lifetime decay allow the usage of simpler mathematical models to determine their fluorescence lifetime, as the model only has to estimate one variable for it instead of multiple variables for multi-exponential fluorophores. Denay et al. (2019) speculated that mClover3-

mRuby3 could be a fluorophore pair with high applicability in plant FRET-FLIM experiments. Although the translational fusion proteins LYK4-mClover3-3×FLAG (gg) and TET7-mRuby3-6×HA (gg) produced bright fluorescence signals useful for general confocal microscopy applications (Brightness as a product of Extinction Coefficient and Quantum Yield mClover3 = 85.02 and mRuby3 = 57.6 fpbase) (Lambert, 2019), their donor lifetime shift between the absence and the presence of the acceptor was marginal making them unsuitable for FRET-FLIM assays with these donor and acceptor proteins.

The calculation of the Förster distance in which the energy transfer efficiency is 50% (R_0) (Equation 1) (Schaufele et al., 2005) is dependent on a multitude of different factors such as the refractive index (n), the quantum yield of the donor (Q_D), the overlap integral between the donor and the acceptor spectrum ($J_{(\lambda)}$) and the transition dipole moment orientation factor (*k*), which indicates how the two fluorophores are arranged to each other in the 3D space (Wu and Brand, 1994).

$$R_0 = 0.211 \times \sqrt[6]{k^2 n^{-4} Q_D J_{(\lambda)}} \qquad \text{Equation 1}$$

In simplified approaches with freely rotating orientation planes of fluorescent dyes, k^2 can range between 0 and 4, resulting in a mean k^2 value of 2/3. However, this is inappropriate for fluorescent proteins as the fluorophore cannot freely rotate in all directions (Khrenova et al., 2015). Interacting membrane proteins form two planes of donor and two planes of acceptor molecules(Nazarov et al., 2006). The energy transfer between the two molecules is therefore not just influenced by the distance of the donor and the acceptor, but among other factors also highly influenced by the z-coordinates of the fluorophores and their resulting transition dipole moment planes (Nazarov et al., 2006). The k^2 = 2/3 approach is therefore even further inappropriate for molecules embedded in a membrane, particularly if they are not able to freely rotate (Axelrod, 1979) such as proteins in a complex with each other.

If two fluorophores are oriented to each other in a way that k^2 is close to 0, then the resulting R_0 will be close to 0 as well. Even structurally closely related fluorophores such as proteins of the GFP family do not share a common transition dipole moment (TDM) (Khrenova et al., 2015), resulting in differing orientation factors with the same partner proteins. Even though the fluorophores of LYK4-mClover3-3×FLAG and TET7-mRuby3-6×HA might be just as physically close together, as those of LYK4-eGFP and TET7-mRFP1, they might exhibit a different and lower k^2 value and therefore result in a rather small FRET efficiency.

This does not demonstrate that the fluorophore pair mClover3-mRuby3 is useless for plant FRET-FLIM experiments. As FRET based approaches for protein association can only be used to positively confirm hypotheses of associations, but not be used to prove that there is no association. My data suggests that the orientation factor of membrane protein translational fusions in complexes could be important when they are analysed for their capability to FRET. Future research should take this into account during the experimental design and data interpretation stages. For example, multiple different fluorophore pairs should be tested to determine the most appropriate for the candidate protein pair. Further this could be done using varying lengths of linkers. Additionally, this would allow to test if this effect of linker length and flexibility is consistent between different protein pairs, allowing for future guidelines of minimum linker length to achieve efficient FRET for membrane protein pairs.

mClover3-mRuby3 might still prove very useful in the future for experiments where the two fluorophores are differently oriented to each other than in the case of LYK4-TET7. In such cases the orientation factor k^2 could be close to 0 for GFP-RFP pairs but might be a higher value for the mClover3-mRuby3 pair in the same positions. These experiments have demonstrated the importance of optimisation of FRET-FLIM constructs, and in particular the fluorophores used, to gain the maximum information and value from using this method and confirming a protein association even if initial experiments might give no clear indication of a positive and close association.

Following these optimisation experiments, which determined mRFP1 to be the superior fluorophore to measure the LYK4-TET7 association, mRFP1 translational fusion constructs were generated using golden gate cloning techniques for TET3 (gg), TET7 (gg) and TET8 (gg) and measured the lifetime of the donor in their presence (Fig. 4-16). These data showed a consistent significant shift in lifetime, suggesting an association of all three tetraspanins with LYK4. Disappointingly however, those constructs did not result in the strong amplitude shift previously observed. In particular when comparing the shift of LYK4-eGFP (gw) with TET7-mRFP1 (gw), when the acceptor has been cloned using gateway constructs (Fig. 4-14) (τ = 2.35 ± 0.0399 ns to τ = 1.95 ± 0.116 ns in the presence of the acceptor) in contrast to the golden gate constructed acceptor LYK4-eGFP (gg) with TET7-mRFP1 (gg) (Fig. 4-14) (τ = 2.41 ± 0.0434 ns to τ = 2.37 ± 0.0467 in the presence of the acceptor). This difference could be due to the different linker/scar sequences introduced by the two different methods as well as differences in expression levels as discussed above.

Biologically significant shifts in fluorescence lifetime in the absence versus the presence of the acceptor have been reported as low as 0.09 ns for CLV1-GFP interacting with CLV1-mCherry (Stahl et al., 2013). The shifts reported therefore still align with published literature as sufficiently significant.

Additionally, regarding the reduction in the shift of lifetime the golden gate construct series (Fig.4-16), showed different results in the presence of chitin when compared to gateway construct results (Fig. 4-14E). Previously, the lifetime of chitin treated samples increased significantly in the direction suggesting a reduction of the association between LYK4 and TET7 in the presence of chitin (Fig. 4-14E). However, in the experimental series using the golden gate mRFP1 acceptor construct on the SP8 Stellaris (Fig. 4-16) the opposite effect was observed. Here the presence of chitin induced a significantly lower lifetime suggesting a closer association between LYK4 and TET7 when treated with chitin. These two experimental series have been carried out in different years, with shifts in the growth practices of *N. benthamiana* plants potentially being a reason for the differing results. As our horticultural team strives to improve our plant growth conditions further and the local borehole water used to water the plant changes with the seasons, this might influence the chitin dependent dynamics between LYK4 and the tetraspanins and thereby explain this difference. The cause cannot be determined with certainty at this point. However, no matter in which way the association balance between the receptor and the tetraspanin proteins shifts, it is undeniably that there are shifts depending on chitin, adding a yet unresolved dynamic to this protein interaction.

BRI1-mRFP1 (gw) served as an appropriate negative control when carrying out the gateway construct experiments (Fig. 4-14E). It resulted in only a negligible shift in the donor lifetime, with no statistical difference when compared to the donor only chitin treated samples making it an ideal negative control as it is another PM localised leucine-rich repeat receptor kinase. Yet, this construct induced a significant shift in the donor lifetime in the experimental series of Fig. 4-16. One possible explanation for this is, that this BRI1-mRFP1 plasmid is still the same gateway construct used in Fig. 4-14E instead of a golden gate version as the LYK4-eGFP (gg) donor and the tetraspanin acceptors in this experimental series. This could result in a different fluorophore orientation as well as different expression levels and orientations based on cloning scars as discussed above. For further experiments I therefore recommend keeping not just the fluorophores consistent, but promoter, terminator, linker sequence and expression plasmid as well.

These data (particularly the comparison between Fig. 4-14 and Fig. 4-16) and their differences in lifetime shifts and therefore FRET efficiency and protein association, open the questions of what is different between those constructs and experiments? While the same fluorophore sequences for both the gateway and the golden gate constructs expressing mRFP1 tagged translational fusions was used, differences in the expression vector and different linker sequences between the protein CDS and the fluorophore were still present. The gateway constructs in the pB7RWG2.0 plasmid for mRFP1 translational fusion proteins, result in eleven amino acids (HPAFLYKVVIS) as a linker, while the golden gate scar for these constructs resulted in only two amino acids (GS) linking the translational fusion together. This could allow for the possibility of rotation and orientation changes, which — as discussed above — can create a greatly varying k^2 value resulting in abolishing or enhancing the FRET efficiency.

In the future, two separate approaches should be carried out next to resolve these problems: i. All three tetraspanin genes should be cloned into the same gateway construct originally used (pB7RWG2.0) for acceptor protein expression and ii. a golden gate cassette of the mRFP1 tag including the same linker sequence as the gateway plasmid should be constructed and used to generate translational fusion proteins. These two approaches can then be used to determine if the linker sequence or other intrinsic properties of the gateway expression plasmids are the cause for these differing results.

Despite the differences in results, this experimental series still demonstrates multiple key results. The association between the receptor LYK4 and the tetraspanins TET3, TET7 and TET8 was confirmed with two independent methods: i. co-IPs (Fig. 4-13) and putatively with ii. FRET-FLIM (Fig. 4-14E, 15, 16). This establishes a functional relationship between receptors and tetraspanin proteins and implicates tetraspanin proteins in receptor signalling processes in plant as seen in animals. The ability of tetraspanin proteins to associate with receptors and to regulate their signalling processes is a wide research field so far generally focussing on animal and fungal model systems and of utmost importance for the correct functionality of those signalling processes (for a detailed review see Termini and Gillette (2017)). My experiments have now demonstrated a novel example of this could work in plants. I speculate this to be a more general feature of plant signalling receptors as well, and I expect this to set the foundation of future research unravelling countless questions and allowing us to gain deeper understanding on how plant immunity is regulated and achieved by PM localised proteins and receptors.

Given that tetraspanins localised to not just at the PM, but also to plasmodesmata (Fig. 4-4) and that their absence causes specific chitin-triggered plasmodesmal phenotypes, such as the inability to reduce plasmodesmal flux (Fig. 4-10) or increase plasmodesmal callose deposits (Fig.4-11), it is likely that tetraspanins are also important at plasmodesmata localised signalling processes. Neither my co-IP nor my FRET-FLIM experiments were able to differentiate between protein associations at the PM and the plasmodesmal PM. However, it is possible that TET3, TET7 and TET8 undergo different association dynamics with LYK4 at plasmodesmata. They might for example associate preferentially in the absence of in the presence of chitin, in different ways. For example, LYK4 could associate with TET7 and TET8 in the absence of chitin, and dissociate triggered by chitin, while an association of LYK4 with TET3 could be triggered by chitin. As the presence of chitin in *tet3* and *tet7* mutants does not induce a reduction of plasmodesmal flux, while *tet8* mutants increase their plasmodesmal flux in a chitin triggered manner, this suggests that they might fulfil different functions or interaction needs.

Taken together these results suggest that LYK4 associates with TET3, TET7 and TET8. It is therefore highly likely that if tetraspanins form TEM domains in plants — as they do in animal cells (Saiz et al., 2018) — that this pattern recognition receptor and its further associated partner proteins of the receptor complex reside within the same domains.

This receptor-tetraspanin association might be vital for the signalling capacity of the receptor. As an interaction with tetraspanins could enhance or define the localisation of LYK4 into a tetraspanin-defined-nanodomain, and thereby either enhance its capability for complex formation or interaction with other proteins in this nanodomain or abolish its potential to interact with non-nanodomain resident proteins. This could be an important mechanism in regulating and enhancing chitin-triggered perception and signalling capabilities of a cell.

As tetraspanins can interact with a further plethora of other proteins, the specific tetraspanin might also be important in defining with which proteins LYK4 can interact. This could for example be important in a TET3-defined-nanodomain which has LYK4 present. Possibly this nanodomain does not contribute to the chitin-triggered ROS burst and therefore a mutation in *tet3* does not cause a reduction in this ROS burst (Fig. 4-9), maybe due to a general lack of ROS producing enzymes such as RBOHD. Similarly, the interaction with TET8 in a TET8-defined nanodomain could explain why a *tet8* mutation shows an inverse phenotype to WT plants when observing their plasmodesmal flux in a chitin-triggered context (Fig. 4-10). TET8-

defined-nanodomains might keep LYK4 'locked' up during resting state conditions, either by stopping it from interacting with other proteins or via specific PTMs. But in *tet8* mutants, LYK4 is not scavenged up by TET8-defined-nanodomains and might therefore be available to continuously signal and result in a reduced plasmodesmal flux during resting-state conditions. Correspondingly, the interaction with tetraspanins in a tetraspanin-defined-nanodomain might protect receptors from enhanced degradation processes, thereby influencing the available pools of proteins at the membrane. These and other possible mechanisms show first ideas of how a receptor-tetraspanin interaction might be vital for signalling functions in plants.

4.3.10 Tetraspanin localisations in a chitin and receptor kinase context differ from each other

No changes to the subcellular localisation of TET3 were observed while co-overexpressed with LYK4 or LYK5 constructs, both in the presence or absence of chitin (Fig. 4-17). Similarly, no changes to the localisation of TET7 were observed (Fig. 4-18). This allows me to conclude that neither TET3 nor TET7 change their localisations in the presence of LYK4 or LYK5, or in a chitin-triggered context.

While TET3-mCherry was predominantly present at the PM (Fig. 4-17), TET7-mCherry also exhibited pools of fluorescence in the ER, the nuclear envelope, and the in transvacuolar strands (Fig. 4-18). Further it accumulates in clusters of fluorescence in the apoplastic space. Although there is a possibility for these clusters to be fluorescence originating from *Agrobacterium* microcolonies, these clusters are likely to mark either exocytic vesicles or exocytic processes. Cai et al. (2018) determined that both TET8 and TET9 are present in extracellular vesicles during *B. cinerea* infections, while Guo et al. (2022) observed that *Solanum tuberosum* TET8 is present in extra cellular vesicles during *P. infestans* infections. TET7 is the closest homologue to TET8 and TET9 (Fig. 4-3), giving it a high likelihood to share characteristics with both proteins. TET7-mCherry was observed to be present in putative extracellular vesicles under all tested co-expression as well as in mock and chitin treated conditions. This hints that the presence of TET7 in extracellular vesicles could be constitutive and does not need the presence of a further stimuli. Alternatively, the constitutive transient expression of TET7 could enhance this presence.

I have not observed such putative exocytotic vesicle localisation for either TET3 or TET8. If the presence of TET8 at exocytotic vesicles during *B. cinerea* infections would be due to chitin-triggered processes, this would have resulted in such a localisation in my experiments. Taking this information together I can speculate that the presence or absence of TET3, TET7 and TET8 at exocytotic vesicles is chitin independent. Further I have not observed any clear changes to exocytotic vesicle presence depending on the co-overexpression of LYK4-eGFP and LYK5-eGFP, allowing me to speculate that the overabundance of these proteins does not influence the exocytotic vesicle presence of TET3, TET7 or TET8 either.

Combining the overexpression of TET8 and LYK5 with the presence of chitin, allowed me to observe a cell biology phenomenon for which no similar descriptions in the published literature could be found. This combination resulted in aggregating bubbles of strong

fluorescence intensity (Fig. 4-19F and 4-20) for both the eGFP and the mCherry signals of LYK5 and TET8 respectively. These aggregating bubbles are different from vesicles in their size. As these aggregating bubbles only appear to be visible with the overexpression combination of LYK5 and TET8 in the presence of chitin, but not in any combinations with TET3, or TET7 as well as with LYK4 or under mock conditions, it suggests they are a specific phenomenon. Their thick structures suggest that aggregating bubbles consist of multiple layers of membrane. Visible bubbles within other aggregating bubbles suggest that multiple layers of membrane might be the reason for their thickness. Putatively they originate from the PM, as the aggregating bubbles appear within half an hour after chitin treatment. The depletion of the fluorescence signal from the PM gives further strength to the argument that these structures originate from the PM. Therefore, it is likely these aggregating bubbles arise from endocytic processes.

The function and significance of these aggregating bubbles is unknown. As cells don't normally exhibit structures reminiscent of these aggregating bubbles, their formation is probably an artefact formed by the transient overexpression of two important interacting membrane proteins. However, as it is a phenomenon only observed if the very specific combination of LYK5, TET8 and chitin is present, it might allow us to elucidate their functions in greater detail and resolution in the future, be it an artefactual phenomenon or not.

Future experiments following up on the aggregating bubbles should first investigate if a similar phenomenon is observable in Arabidopsis lines treated with chitin which carry a fluorescent marker for TET8 and LYK5. This could determine if the aggregating bubbles are indeed just an artifact or if there is more physiological functionality underlying. But what could be the reason for the formation of such aggregating bubbles? Sometimes they appear reminiscent of BFA induced bodies in leaf epidermis cells, such as in Erwig et al. (2017). However, BFA leads to the collapse of the Golgi into the ER and the aggregating bubbles but the structures observed consist of multiple membrane layers suggesting they might be different structures.

Operating under the assumption that there are special events when a plant cell would want to push great amounts of its PM within itself, when would that be? And what could trigger this? One hypothesis is that during intracellular arbuscular mycorrhizae symbiosis the host cell has to cover the arbuscules with host membrane structures (Ivanov et al., 2019). This host-symbiont interface membrane needs to reach a high enough surface area to function properly and therefore probably requires a lot of membrane material. LYK5 is a chitin

receptor, and its *M. truncatula* homologue MtLYR4 is important for the detection of chitin oligosaccharides in *M. truncatula* (Feng et al., 2019). The perception of chitin is important for both immunity as well as symbiosis reactions (Zhang et al., 2021). Similarly, to symbiotic processes, a lot of plant membrane material is necessary to cover invasive fungal hyphae growth at the biotrophic interfacial complex (BIC) (Cruz-Mireles et al., 2021; Kankanala et al., 2007; Khang et al., 2010). It therefore stands to reason that the combination of LYK5, TET8 and chitin might mimic conditions where the plant cell needs to invaginate lots of membrane material to cover symbiotic arbuscules or invasive hyphae.

4.3.11 Tetraspanins in a chitin triggered signalling context – a model

The data presented in this chapter enables me to construct a hypothetical model of how tetraspanins are involved in chitin-triggered responses (Fig. 4-21). As I see differences in the ROS responses and plasmodesmal closure in the different tetraspanin mutants, their functions are not completely the same, suggesting a spatiotemporal separation, and thereby their possible presence in different nanodomains.

This model is an extreme over-simplification of a possible model for what the native protein system and localisation might look like. The changes in FRET efficiency between LYK4 and the tetraspanins could for example allow for a change in whether or LYK4 is still as present within the tetraspanin domain, or alternatively LYK4 stays present within said domain, but undergoes changes in conformation. It would be conceivable that chitin triggers a change in LYK4 localisation from one tetraspanin defined nanodomain to another nanodomain — resulting in a “hand-off” situation.

Possibly TET3, TET7 and TET8 are present within the same nanodomain, or they might mark their individual nanodomains and additionally form nanodomains in which all three or only two of them are present. Further experiments using super resolution microscopy approaches as discussed in this chapter should allow to clarify their nanodomain presence and overlap as well as if they indeed also are present in web-like structures in plants.

However, given that Zuidscherwoude et al. (2015) observed a separation between the different tetraspanin marked domains as the most advanced imaging technique publication to date, this model of separated plant tetraspanin membrane domains is currently favoured in the absence of evidence that multiple different tetraspanins are present within the same domain.

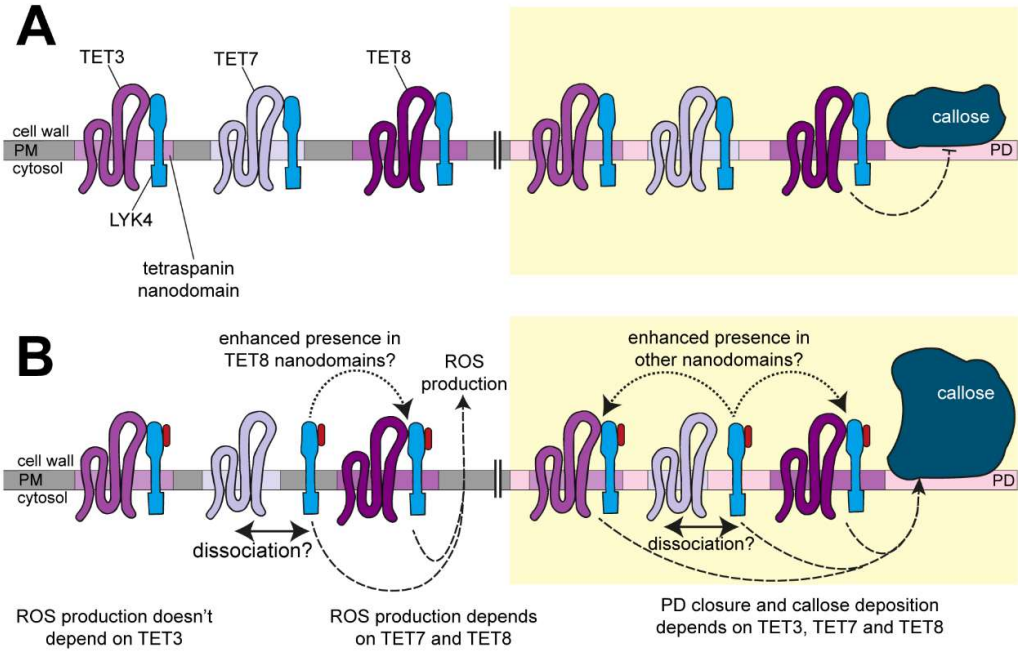

Figure 4-21: A possible model for receptor-tetraspanin mediated chitin-triggered immune signalling with a focus on the plasmodesmal response. This schematic representation is drawn as a continuity between the PM (grey), the plasmodesmal PM microdomain (light pink), and both include tetraspanin defined nanodomains (different shades of purple). Different receptor complex combinations can be present such as associations between LYK4-TET3, LYK4-TET7, LYK4-TET8. Tetraspanin proteins are enriched at plasmodesmata. (A) In the absence of chitin TET8 is necessary to inhibit the deposition of callose (B) Chitin-triggered conditions. The full PM localised ROS production is dependent on TET7 and TET8, but not on TET3. The ability to reduce the plasmodesmal flux in the presence of chitin is dependent on TET3 and TET7. Meanwhile *tet8* shows an inverse regulation and increases the plasmodesmal flux triggered by chitin, indicating that TET8 is also important for WT-like plasmodesmal responses. The association between LYK4 and TET7 is changing triggered by chitin, suggesting a possible dissociation between those two proteins, and therefore a dissociation of LYK4 from a TET7 defined nanodomain. (A) & (B) PD: plasmodesmata; GSL: GLUCAN SYNTHASE-LIKE = callose synthases.

4.3.12 Conclusion

To conclude, I have determined a relationship between tetraspanins, chitin-triggered receptors and signalling, and plant defence against fungi. I have demonstrated the association of TET3, TET7 and TET8 with the chitin receptor LYK4. Thus, I have shed light on the possible mechanism of how tetraspanin presence and function might be directly necessary for chitin receptor functions. Further I have revealed that tetraspanin proteins are essential for the regulation of cell-to-cell flux by determining the inability of mutants to close their plasmodesmata in the presence of chitin. Taken together I have determined previously not reported aspects of the plant immune system and opened the door to ask new questions. Undoubtedly this research has added and will continue to add to the foundations of understanding PM and plasmodesmata localised signalling processes.

5 Flotillins in chitin signalling

5.1 Introduction

The RK LYK4 fulfils not only an important role in PM based chitin detection and signalling (Wan et al., 2012) but also in plasmodesmal-localised chitin detection and flux modulation (Cheval et al., 2020). Proteins associating with LYK4 can therefore potentially function in the chitin perception and signalling pathways of both the general PM as well as the specialised plasmodesmal PM, making LYK4 an ideal anchor point of research into chitin-triggered immune responses. Chapter 3 demonstrated LYK4's capability to interact with the RK LYK5, as well as with the RP LYM2. Chapter 4 used a targeted approach to identify plasmodesmal localised proteins capable of localising in nanodomains which interact with LYK4. I determined that proteins of the tetraspanin family are capable of doing so and are necessary for chitin-triggered immune responses such as the modulation of plasmodesmal flux.

In this chapter I used an unbiased approach to identify proteins associated with LYK4. For this purpose, I generated Arabidopsis lines expressing a LYK4 translational fusion protein under the control of the native *LYK4* promoter. I utilised this plant material via immunoprecipitation assays to identify LYK4 associated proteins via mass spectrometry. A plethora of different proteins which associate with the IP of LYK4 were identified in this experiment, including two stomatin/prohibitin/flotillin/HflK/C (SPFH) proteins of the flotillin family. SPFH proteins mark membrane nanodomains, and therefore these flotillin proteins were chosen as the most interesting candidate proteins and are the focus of this chapter.

5.1.1 What are SPFH proteins?

SPFH proteins are defined by the presence of a characteristic prohibitin homology (PHB) domain and form a large super family of proteins referred to as the SPFH domain family (Browman et al., 2007; Liu et al., 2005). Their core motif is the PHB domain, which is also referred to as band-7 (Pfam entry: Band_7, accession number: PF01145) (Tavernarakis et al., 1999). The presence of the PHB domain allows for membrane association to the inner leaflet of the membrane through acylation sites and putative hydrophobic hairpins (Morrow and Parton, 2005; Otto and Nichols, 2011). Two hydrophobic domains are present within the PHB domain, and are universal to SPFH proteins (Morrow and Parton, 2005). The PHB domain alone can efficiently target a GFP translational fusion protein to the PM but is not enough to facilitate a nanodomain localisation (Morrow et al., 2002), suggesting that other mechanisms or motifs are required to achieve a nanodomain localisation other than just a PHB domain.

5.1.2 Non-flotillin SPFH proteins

5.1.2.1 Stomatins

Five genes code for proteins of the stomatin family in humans: stomatin (STOM), podcin (NPHS2), and stomatin-like proteins 1-3 (STOML1, STOML2, STOML3) (Lapatsina et al., 2012a). Homologues can be found in all higher eukaryotes, archaea and bacteria, thereby suggesting this family is an ancient protein family (Green and Young, 2008; Rivera-Milla et al., 2006). In symbiotic *Rhizobium etli* bacteria, stomatins have been found to be important for bacterial growth as well as for the successful nodule competition on *Phaseolus vulgaris* (common bean) (You et al., 1998). Stomatin proteins can interact with different ion channels, particularly when localised in nanodomains (Chen et al., 2015; Lapatsina et al., 2012b; Poole et al., 2014; Price et al., 2004). They can regulate the activities of those channels, depending on circumstances — e.g. in a cholesterol-dependent manner (Huber et al., 2006). For example human stomatin is involved in sugar transport by interaction with the glucose transporter GLUT1 in erythrocytes (Montel-Hagen et al., 2008). Given how the perception of biotic and abiotic stresses can lead to a rapid influx of calcium ions across the plant cell PM, for example through the Arabidopsis OSCA1.3 channels (Thor et al., 2020), stomatin defined nanodomains could be important in the regulation of these signalling processes in plants as well.

There are two stomatin-like protein in Arabidopsis: STOMATIN-LIKE PROTEIN1 and 2 (AT4G27585; AT5G54100). Although HYPERSENSITIVE INDUCED REACTION 2 (HIR2) also contains a stomatin signature sequence, it is alternatively classed as an HIR protein (Gehl et al., 2014). Gehl et al. (2014) demonstrate that both STOMATIN-LIKE PROTEIN1 and 2 exhibit a clear mitochondrial membrane localisation. Knockout mutants show reduced activity and protein levels of respiratory complex I and supercomplexes, and are therefore implied to affect the stability and/or assembly of these complexes in Arabidopsis (Gehl et al., 2014). Thus, it stands to reason that plant stomatinscan be important for the formation and functionality of membrane protein complexes.

5.1.2.2 Prohibitins

The name giving prohibitin gene (*PHB*) was originally identified by McClung et al. (1989) and characterised as a candidate anti-proliferative gene (also referred to as tumor suppressor genes) in rat liver cells. The two homologous genes in humans *PHB1* and *PHB2* exhibit diverse functions and are widely distributed to different cellular compartments such as the nuclear envelope, the PM and the mitochondria membranes (Knopf et al., 2015; Koushyar et al., 2017; Nijtmans et al., 2000). They are important for a variety of different roles, such as the

regulation of target gene transcription (Gamble et al., 2007), the promotion of cell growth, and centromeric cohesion (Takata et al., 2007). Human prohibitins are further involved in tumorigenesis processes such as cancer cell metastasis and apoptosis, by interactions with other PM localised proteins (Chiu et al., 2013; Fu et al., 2013; Kuramori et al., 2009; Liu et al., 2017). At the PM they can further facilitate entry for viruses in humans, such as during Chikungunya virus infections, where PHB is necessary for virus internalisation from the PM into microglial cells (Wintachai et al., 2012).

There are 7 members of the PHB protein family in Arabidopsis (Gehl et al., 2014). Even though the mammalian PHB1 and PHB2 have been studied extensively, plant prohibitin proteins have not been characterised to a similar extent (Huang et al., 2019b). Some of these plant PHB proteins are close homologues and show at least partial redundancy in mutant complementation experiments — for example the overexpression of *PHB4* is able to restore the root growth speed of *phb3* mutant plants back to WT rates (Van Aken et al., 2007). Van Aken et al. (2007) further demonstrated that PHB1, PHB2, PHB3, PHB4, and PHB6 are present at mitochondria and showed that *phb3* mutants exhibit mitochondrial swelling, as well as slower cell division and decreased cell expansion rates. They speculate that *PHB* genes result in pleotropic effects revealed by growth retardation. Piechota et al. (2015) show that Arabidopsis PHB proteins assist in the assembly of enzymatic complexes at the inner mitochondrial membrane, and therefore speculate that the principal function of PHBs in mitochondria is to support the structural and protein organisation of this membrane.

Seguel et al. (2018) further determined that PHB3 also localises to the envelope membrane of chloroplasts. PHB3/4 and other PHB proteins form a complex with ISOCHORISMATE SYNTHASE 1 (ICS1) at the chloroplast membrane (Seguel et al., 2018), and this is required in pathogen-induced biosynthesis and accumulation of Salicylic acid (SA) (Strawn et al., 2007), thereby linking another non-flotillin SPFH protein family to plant defence responses against pathogens.

5.1.3 HflK/C

The region encoding the gene for the protein host factor I (HF-I) on the *E. coli K-12* chromosome is referred to as hflA region, and all following genes after this region were given names according to this region's name. The genes following the hflA region on the plus strand orientation were therefore designated as hflX, hflK and hflC (Banuett and Herskowitz, 1987; Gautsch and Wulff, 1974; Tsui et al., 1994). HflK/C are proteins localised to the inner membrane of bacteria (Zorick and Echols, 1991). They are comprised of a single N-terminal transmembrane domain as well as a large C-terminal periplasm-exposed domain (Kihara and Ito, 1998; Noble et al., 1993). Individual HflC and HflK proteins are unstable (Banuett and Herskowitz, 1987; Kihara and Ito, 1998), however interaction with each other stabilises them (Banuett and Herskowitz, 1987). This suggests that proteins of this family have to interact with each other to be stable and therefore available for interactions with other proteins.

HflK-HflC complexes are involved in the regulation of membrane protein quality control and homeostasis via interactions and regulations of the membrane-bound proteases Yta10/Yta1224 and FtsH (Kihara et al., 1996). This ability to organise membrane proteins and their homeostasis results in downstream pleotropic effects for the organism (Arnold and Langer, 2002; Bohovych et al., 2015; Glynn, 2017; Patron et al., 2018; Quirós et al., 2015). Although HflK/C proteins are important in bacteria, no close homologues of plants have yet been identified (Gehl et al., 2014) and published.

5.1.3.1 Erlins

Erlins (ER lipid raft proteins) were first discovered in human myelomonocytic cells and define lipid-raft-like domains of the ER membrane (Browman et al., 2006). They are defined as proteins present in detergent-insoluble, low-density fractions of cell lysates, which do not localise to the PM but instead to the ER (Browman et al., 2006). Human Erlin-1 and Erlin-2 undergo oligomerisation in a ratio of 1:2 resulting in a megacomplex of roughly 2 MDa which can mediate the degradation of receptor proteins, such as Inositol 1,4,5-Trisphosphate receptors in mammalian cells (Pearce et al., 2009). Erlin proteins are therefore another example of SPFH domain proteins, which undergo oligomerisation with other proteins of the same family, resulting in complex formation and interaction with other important membrane proteins such as receptors.

Only one erlin homolog, the ERLIN-LIKE PROTEIN (ELP) has been identified in Arabidopsis to date (Gehl et al., 2014). Apart from discussions in review papers, no further characterisation of this protein are published. Daněk et al. (2016) speculate that since ELP contains a putative

transmembrane domain and a coiled-coil motif, it could similarly to mammalian undergo protein complex formation at cellular membranes, and thereby possibly fulfil regulating functions on Arabidopsis receptor proteins as well. *ELP* is expressed throughout all plant organs and developmental stages, and its transcription is upregulated in response to cold and SA treatment as well as during *Phytophthora parasitica* and *Pseudomonas syringae* infections (Daněk et al., 2016), making it an SPFH domain family protein, possibly linked to plant immunity processes.

5.1.3.2 Hypersensitive induced reaction proteins (HIRs)

HIR proteins are a plant specific family of SPFH domain proteins. They have been originally identified by Nadimpalli et al. (2000) in *Zea mays*. Multiple studies have since linked these proteins to plant immune responses. The *Oryza sativa* protein, OsHIR1 has been shown to associate to the PM, and overexpression of this gene in Arabidopsis triggers hypersensitive cell death, as indicated by the spontaneous formation of lesions (Zhou et al., 2010). *Capsicum annuum* LEUCINE-RICH REPEAT 1 (CaLRR1) interacts and functions together with HYPERSENSITIVE INDUCED REACTION 1 (CaHIR1) enhancing cell death induced during *Xanthomonas campestris pv. vesicatoria* infection (Choi et al., 2011). Four HIR genes have been described in Arabidopsis (Gehl et al., 2014). Qi et al. (2011) demonstrated that HIR1, HIR2, HIR3 and HIR4 localise to the PM and associate with each other. Mutant plants of *hir2* and *hir3* are more susceptible than WT plants to *Pseudomonas syringae pv. tomato* (Pto) *DC3000* with the effector AvrRpt2, while the overexpression of *HIR1* and *HIR2* overexpression results in enhanced resistance to Pto DC3000 (Qi et al., 2011), showing the importance of HIR proteins in plant defences against pathogens.

5.1.4 Flotillins in non-plant systems

Independent identification of *Mus musculus* (mouse) and *Drosophila melanogaster* (fruitfly) homologues led to the alternative names of flotillin-1 and -2 as reggie-2 and reggie-1, respectively, and therefore for this protein family (Bickel et al., 1997; Galbiati et al., 1998; Rivera-Milla et al., 2006). Even though flotillin proteins do not possess a transmembrane domain, they localise to the PM via conserved hydrophobic stretches that allow potential interactions with the inner leaflet of the PM in human cells (Morrow et al., 2002; Neumann-Giesen et al., 2004).

Flotillins can undergo the PTM of S-acylation (covalent attachment of fatty acids, such as palmitic acid) close to their N-terminus (Morrow and Parton, 2005). The predominant localisation of flotillins into PM DRMs/nanodomains was first observed in experiments studying the overlap of flotillin-1 and flotillin-2 with GPI-anchored proteins using immunoglobulin labelled electron microscopy as well as CLSM in neurons, astrocytes, and Jurkat cells (Stuermer et al., 2001). The PHB domain of flotillins alone is sufficient to result in targeting to the PM (Morrow et al., 2002). However, S-acylation is necessary for flotillin domain localisation, as the PHB alone is not sufficient for this (Morrow et al., 2002).

Numerous studies have since demonstrated the domain localisation of mammalian flotillins, as well as shown an association of flotillin proteins with surface proteins and intracellular signal transduction proteins such as Src family kinases (e.g. fyn and lck), activated cell adhesion molecules (CAMs), prion protein (PrPc), Thy-1 and cytoskeleton-associated proteins such as ArgBP2, CAP/ponsin, and vinexins (Baumann et al., 2000; Kimura et al., 2001; Kioka et al., 2002; Kokubo et al., 2003; Rivera-Milla et al., 2006; Stuermer et al., 2001; Stuermer et al., 2004). Amaddii et al. (2012) demonstrated that flotillins can directly interact with components of the MAPK cascade, thereby forming complexes with cRAF, MEK1, ERK and KSR. Meister et al. (2013) therefore speculate that flotillins fulfil a MAP kinase cascade scaffolding function. Thereby flotillins can be important for different defence signalling responses.

Most bacterial genomes include flotillin-encoding genes (Green et al., 2009), and translational fusions of bacterial flotillins with a fluorophore also localise to discrete punctate at the PM (Bramkamp and Lopez, 2015). Often the bacterial flotillin gene is part of an operon where the first gene encodes a protease Nodulation formation efficiency D -homolog protein (NfeD) and the second gene encodes the flotillin (Bramkamp and Lopez, 2015). NfeD has

been shown to interact with flotillin to control ion channel opening (Yokoyama and Matsui, 2005).

5.1.5 Flotillins in plants

Three flotillins have been identified in Arabidopsis (Gehl et al., 2014). Previously they have been referred to as FLOT1a (AT5G25250), FLOT1b (AT5G25260) and FLOT2 (AT5G64870) (Jarsch et al., 2014; Yu et al., 2017). To avoid confusion I am using the current nomenclature of TAIR10 (The Arabidopsis Information Resource (TAIR), 2020), which refers to the three flotillins as FLOT1 (AT5G25250), FLOT2 (AT5G25260) and FLOT3 (AT5G64870) consistent with Junková et al. (2018) and Kroumanova et al. (2019).

Plant flotillins are present in nanodomains. Minami et al. (2009) showed that FLOT1 and FLOT2 are present in detergent-resistant PM domains of Arabidopsis like many other Band 7 family proteins. FLOT1 and FLOT2 have gathered attention in plant cell biology for their ability to label nanodomains within the PM when fused to a fluorescent tag (Jarsch et al., 2014). Daněk et al. (2020) further showed that FLOT3 is also able to label such nanodomains. All three plant flotillins can therefore be resident within PM nanodomains.

The ability of flotillins to label nanodomains in the plant PM, has led to them being used as markers to determine if other proteins are present in nanodomains and to study the dynamics as well as behavioural changes of those nanodomains. The sterol-depleting chemical methyl-b-cyclodextrin was used by Li et al. (2012b) to show that the dynamic diffusion of FLOT1-labelled nanodomains within the PM is reduced roughly by a factor of ×100 under sterol-depleted conditions. Furthermore, they identified that in tissues treated with the actin polymerisation inhibitor latrunculin B, the diffusion rates of FLOT1-labelled nanodomains reduced six-fold, as well as resulting in a confinement of the movement to smaller regions. This is in contrast to cells treated with oryzalin — an inhibitor of microtubule polymerisation — which leads to a decrease of FLOT1 nanodomain diffusion rates of up to 120-fold (Li et al., 2012b). They thereby demonstrated that the movement of FLOT1-labelled nanodomains is dependent on the presence of sterols and are more constrained by microtubule-based cytoskeletal elements than by actin polymers. Li et al. (2012b) therefore suggest that microtubule dynamics and reorganisation are more important for changes to flotillin defined nanodomains in plants. Such changes to nanodomains could be stimuli triggered, such as MAMP perception activating plant immune signalling (Bücherl et al., 2017).

These changes could be indicative of the nanodomain's composition changing. Any changes to nanodomain movement and behaviour suggest that the composition of said nanodomain

has changed. This in turn can then allow for different proteins to undergo complex formations or interactions, which were previously not possible or not favoured, or alternatively inhibit or reduce previously favoured interactions. As receptor interaction and complex formation is an important feature in MAMP perception and immune responses (Couto and Zipfel, 2016; Ngou et al., 2022), nanodomain changes could be vital requirements for these processes as well, allowing or inhibiting specific interactions triggered by an elicitor.

Daněk et al. (2020) show data indicating that, not only the cytoskeleton is important for lateral diffusion mobility of FLOT2, but that cell wall elements are even more important. They combined FRAP experiments together with partial enzymatic cell wall removal and pharmacological alteration of cell wall (CW) synthesis and structure to demonstrate that the cell wall constraints are what keeps the immobile fraction of FLOT2-GFP above 90%. FLOT2-labelled nanodomain dynamics within the PM therefore do not only depend on the cytoskeleton but also on the cell wall outside of the cell. As flotillin proteins do not include a transmembrane domain and are localised only to the inner leaflet of the PM (Morrow and Parton, 2005; Otto and Nichols, 2011), this association with the cell wall, has to be due to interactions and associations with proteins which reach through the PM to the cell wall.

Mammalian flotillins have been demonstrated to interact with each other and this is required for their functionality (Affentranger et al., 2011; Baumann et al., 2012). In Arabidopsis plants, Yu et al. (2017) used a FRET-FLIM approach to demonstrate that FLOT1-GFP interacts with FLOT1-mCherry. Thereby they demonstrated that plant flotillin proteins can interact with themselves in a homomeric fashion. They further used yeast two-hybrid assays to show interactions of FLOT1 with FLOT1 as well as FLOT1 with FLOT3, thereby demonstrating that plant flotillins can interact with each other in a heteromeric way. In addition Yu et al. (2017) demonstrated that the amino acids 201-470 of FLOT1 are sufficient to mediate the interactions between FLOT1.

5.1.5.1 Flotillins in plant development

The use of artificial microRNA (amiRNA) knockdown transgenic lines, which affect both *FLOT1* as well as *FLOT2*, lead to the observation that seedling development in these Arabidopsis lines is retarded, as these seedlings exhibit shorter root and hypocotyl lengths (Li et al., 2012b). Li et al. (2012b) further report some indications, that FLOT1 might be involved in clathrin-independent endocytosis, as FLOT1-labelled vesicles exhibit a bigger size than clathrin-dependent endocytotic vesicles, as well as a lack of overlapping fluorescence of FLOT1-GFP with CLATHRIN LIGHT CHAIN (CLC)-mOrange. They speculate that the growth defects in *flot1/2* knockdown lines are due to a reduction of recycling of PM proteins, thereby leading to a slowed cell cycle.

A *flot1* T-DNA insertion mutant (CS444812GK) shows an increased expression of *FLOT1*, which is more noticeable in salt stressed plants (Khalilova et al., 2020). This mutant generates more biomass than WT plants under control conditions, as well as during salt stress. Khalilova et al. (2020) speculate that this could be due to the more intense formation of post-Golgi vesicles and multivesicular bodies in root cells of mutant plants. This could be affecting the biogenesis of vacuoles and vesicular trafficking, and thereby result in differences in maintaining K^+ and Na^+ ion homeostasis in those cells. FLOT1 can thereby at least indirectly be linked to the ion homeostasis and maintenance in plant cells.

Plant flotillins can co-localise with receptors, such as the cell surface TRANSMEMBRANE KINASE 1 (TMK1) with FLOT1 (Pan et al., 2020). TMK1 is capable of stabilising FLOT1-associated nanodomains in an auxin-dependent way. This nanodomain stabilisation in turn is capable of promoting the nanodomain clustering of ROP6 GTPase, which enables the stabilisation of cortical microtubule organisation. Consequently, this has a further positive stabilisation effect on TMK1 and FLOT1 nanodomains. Pan et al. (2020) thereby suggest a new paradigm of receptor-triggered polarity formation: The TMK1 receptor perceives a signal, mediates nanoclustering to a flotillin defined nanodomain, and through this induces the stabilisation of cytoskeleton elements which in turn enhance these responses as a positive feedback loop reinforcing the formation into polarised domains. Flotillins may therefore not only have a role in receptor-based signalling in plants but also in PM protein polarisation processes.

5.1.5.2 Flotillins in plant symbiosis

The animal pathogen genus *Brucella* is closely related to the nitrogen-fixing symbiont *Sinorhizobium meliloti*, and both bacteria have common genes required for infection and invasion processes of their hosts (Batut et al., 2004). The first indication that flotillin proteins might be involved in the infection processes of this group of bacteria came from a proteomic study identifying mouse flotillin-1 to be present in the phagosome — the membrane organelle engulfing intracellular pathogens (Garin et al., 2001). Dermine et al. (2001) further showed that the intracellular parasite *Leshmania donovani* is capable of inhibiting the accumulation of flotillin-1 enriched domains on phagosomes, demonstrating an even clearer link between host flotillins and intracellular bacteria (Watarai et al., 2002).

Early gene annotation models further named some plant flotillins and flotillin-like genes 'nodulins', as a generic name for genes which are expressed uniquely in nodules, as the soybean flotillin-like gene GmNod53b was originally identified as such a nodulin gene (Haney and Long, 2010; Winzer et al., 1999). In soybean root nodules, GmNod53b was further identified at the peribacteriod membrane (Panter et al., 2000) — also referred to as the symbiosis membrane (Whitehead and Day, 2006). Similarly this protein has also been identified in *Pisum sativum* peribacteroid space and peribacteroid membrane preparations (Saalbach et al., 2002).

Given all these indications that plant flotillins are involved in plant symbiosis interactions, Haney and Long (2010) assessed the roles of the *M. truncatula* flotillins MtFLOT1 to MtFLOT4. They determined that early symbiotic events cause strong up-regulation of *MtFLOT2* and *MtFLOT4*, depending on the presence of the bacterial Nod factor as well as the plant host's ability to perceive the Nod factor. Further they demonstrate that MtFLOT2 and MtFLOT4 fluorophore translational fusion constructs localise visually to punctae in the PM of uninoculated root hair cells, as well as MtFLOT2, localising weakly in a polar orientation in those cells. During the infection process MtFLOT4 relocalises preferentially to root hair tips. Using silencing constructs they determined that both MtFLOT2 as well as MtFLOT4 are necessary for successful early nodulation events (Haney and Long, 2010).

Following these initial results Haney et al. (2011) determined a connection between the *M. truncatula* MtLYK3 — which is capable of mediating bacterial infection — and MtFLOT4. In the absence of symbiotic bacteria both MtLYK3-GFP and MtFLOT4-mCherry are present in domains at the PM, which show little co-localisation. However, in the presence of *Sinorhizobium meliloti* these domains exhibit greater overlap, thereby showing that upon

stimulus MtLYK3 moves into MtFLOT4-defined domains (Haney et al., 2011). They further demonstrated that MtFLOT4 mislocalises and exhibits a lower domain density in the kinase-inactive mutant of *MtLYK3*, called *hcl-1*, thereby demonstrating a further co-dependence of the localisation of these two proteins.

Liang et al. (2018) further used this MtLYK3 and MtFLOT4 system during symbiosis initation to resolve the presence of these proteins in nanodomains in greater detail by utilising another scaffolding protein necessary for successful nodule formation MtSYMREM1 (Lefebvre et al., 2010). Upon perception of the symbiotic bacteria, not only MtLYK3 but also MtSYMREM1 co-localises in nanodomains labelled by MtFLOT4 and depending on MtFLOT4 (Liang et al., 2018). Preliminary experiments further demonstrated that this relocation of MtSYMREM1 to nanodomains of MtFLOT4 is dependent on the presence of the actin cytoskeleton, but not on microtubules. Conversely, in the absence of MtSYMREM1 such as in the *symrem1* mutant, the MtLYK3 receptor does not undergo relocalisation to MtFLOT4-labelled nanodomains in inoculated samples, but rather is destabilised at the PM and undergoes endocytosis. This results in premature abortion of cell infections and thereby abortion of infection thread initiation. Using this MtLYK3, MtFLOT4, MtSYMREM1 system, Liang et al. (2018) therefore revealed that correct receptor recruitment into flotillin nanodomains is crucial for signalling processes.

5.1.5.3 Flotillins in plant defence responses

Most studies elucidating the characteristics and dependence of plant immune responses in a flotillin-dependent way use the bacterial MAMP flg22 to elicit a response and use FLOT1 dynamics as a representative example. Callose is not only deposited at plasmodesmata after MAMP elicitation (Xu et al., 2017) — such as by flg22 — but also macroscopically at cell walls (Clay et al., 2009). This macroscopic deposition of flg22-triggered callose is increased in *FLOT1* overexpressing Arabidopsis mutants, and also less callose is deposited in *FLOT1* knockdown mutants (Yu et al., 2017). This demonstrated a direct involvement of FLOT1 either in the perception of flg22, in the progression of the signalling pathway or in the deposition of callose.

FLOT1 is constitutively recycled at the PM via an endocytic pathway (Yu et al., 2017). Treatment with flg22 induces increased endocytosis of PM proteins (Robatzek et al., 2006). Induction of increased endocytosis by flg22 leads to enhanced targeting of FLOT1 to late endosomes and vacuolar compartments, where FLOT1 gradually undergoes degradation processes (Yu et al., 2017). Cui et al. (2018) further demonstrated that FLOT1 and the flg22

receptor FLS2 co-localise in flg22-triggered endocytosis vesicles in a clathrin-independent manner. These studies thereby suggest that PRR endocytosis processes may be associated with FLOT1-labelled but clathrin-independent endocycling.

Nanodomains can change dynamics such as their density, frequency, as well as the proteins present within them (Bücherl et al., 2017). The velocity and diffusion dynamics of FLOT1-labelled nanodomains in the PM change in a flg22-triggered manner (Yu et al., 2017). This study demonstrates that dynamic FLOT1-marked nanodomains can be changed in a MAMP-triggered manner.

Kroumanova et al. (2019) showed that Arabidopsis flotillin genes undergo different transcriptional changes depending on the stress a plant is exposed to. Cold treatment for example increased the expression of *FLOT3*, while salt stress reduced the expression of *FLOT1* and *FLOT2*. Interestingly, inoculation with *P. syringae* did not lead to a significant change of expression of any of the flotillin genes, while treatment with flg22 triggered strong expression increases of *FLOT1*, *FLOT2* and *FLOT3* within 1 h. Inoculation with *B. cinerea* caused an increase in expression of *FLOT1* as well as *FLOT3*. Different stresses thereby change the expression and as a consequence possibly the protein levels of flotillins in plants. Which might be important for the initiation and to carry out stress responses as well as a cellular mechanism to prime for future responses. Different defence and developmental characteristics of *flot1* (SALK_203966C), *flot2* (FLAG_352D08), and *flot3* (SALK_143325C) mutants were further elucidated in the same study (Kroumanova et al., 2019). However, no significant differences were determined in this study in the susceptibility against *P. syringae* or *B. cinerea*, the ROS production triggered by flg22 or elf22, or in the root length of seedlings.

5.1.6 Overview and aims of this chapter

RKs and RPs can form hetero-oligomeric complexes and these protein-protein interactions are necessary to achieve signalling functions (Buendia et al., 2018). I hypothesise that the chitin RK LYK4 interacts with a multitude of different partner proteins and aimed to determine these proteins in an untargeted approach.

Out of the candidates generated by this search, I have chosen two proteins of the flotillin family — an intriguing nanodomain localised protein family (Jarsch et al., 2014). I tested if I could confirm their interaction with LYK4. Considering that these candidates have been determined in a LYK4 interactor screen, and LYK4 is important for chitin-triggered immunity responses, I hypothesised that these candidate genes are also involved in chitin-triggered cellular responses. I aimed to characterise the potential roles of these flotillin proteins by testing mutant line responses in chitin-triggered signalling processes such as the release of an ROS burst or the modulation of plasmodesmal flux. Finally, I tested the hypothesis that these chitin-triggered signalling and cellular phenotypes of flotillin mutants translate into a change of susceptibility to a fungal pathogen infection.

5.2 Results

5.2.1 Identification of LYK4 interaction candidates

Different receptor proteins are necessary for chitin triggered immune responses (Cao et al., 2014; Faulkner et al., 2013). In Cheval et al. (2020) we identified that the receptor kinase LYK4 is present in both the PM as well as the plasmodesmal PM and is necessary for chitin triggered changes to the plasmodesmal flux. I identified that LYK4 associates with LYK5 and LYM2 (chapter 3.2.6). In chapter 4.2.9 I further identified three proteins of the tetraspanin family which associate with LYK4 in a targeted experimental approach. However, which other proteins associate with LYK4, are present in protein complexes and are necessary for LYK4's chitin triggered plasmodesmal changes?

To probe for LYK4-interacting proteins in an unbiased way, stable Arabidopsis lines were generated expressing *pLYK4::LYK4-mCherry* in the *lyk4* mutant background (chapter 3.2.2). Although these lines successfully generate detectable LYK4-mCherry, they have not been assessed for complementation of the *lyk4* mutant phenotypes, and the results are therefore limited in their interpretation and conclusions as no functionality of this translation fusion can be guaranteed. I immunoprecipitated using LYK4-mCherry as a bait and processed these samples for mass spectrometry to determine further proteins present in this fraction.

After initial filtering of these data, 150 putative proteins were identified (full list in the appendix Table 7-4). LYK4 itself exhibited a perfect Bayesian False Discovery Rate (BFDR) of 0 and the highest possible specificity (AvgP) score of 1, suggesting that the IP was indeed specific in protein binding over the Col-0 control samples. Neither LYM2, nor LYK5 or any tetraspanin hits have been identified. The protein hit showing the highest abundance (Table 5-1, 7-4), and AvgP score while also exhibiting a perfect BFDR of 0, is EPITHIOSPECIFIER MODIFIER 1 (EMF1) (Table 5-1), closely followed by GLYCERALDEHYDE 3-PHOSPHATE DEHYDROGENASE A SUBUNIT 2 (GAPA-2) and SUBTILISIN-LIKE SERINE PROTEASE 2 (SLP2).

Of the proteins detected in the highest abundance, multiple members of different protein families were detected (Table 5-1), such as the protein family of flotillins as well as tubulin proteins. Multiple β-tubulin proteins have been identified in the IP with LYK4 such as TUBULIN BETA CHAIN 2 (TUB2), TUB4, TUB5, TUB7 as well as TUB6. Particularly the values of TUB2 suggest an abundant and specific association with LYK4, resulting in AvgP scores of 1 or close to 1, and BFDRs of 0.

Two of the three Flotillin proteins present in Arabidopsis were identified to IP with LYK4 in this experiment (Table 5-1). FLOTILLIN1 (FLOT1) was detected at a lower abundance in water treated samples versus chitin treated samples, thereby resulting in a lower AvgP score of 0.67 for water treated samples and a higher, near maximal AvgP score of 0.99 in chitin treated samples. This data thereby suggests an association between LYK4 and FLOT1 under mock conditions, which is increased by chitin. FLOT2 has only been detected in one chitin treated and one water treated sample (mock: 10 versus chitin 24 observations), which lowered the AvgP specificity score and increased the BFDR, even though it has not been identified in any WT IP control samples at all.

Table 5-1: Putative protein interactors of LYK4. Mass spectrometry results from plants expressing *pLYK4::LYK4-mCherry* in *lyk4*, immunoprecipitated with Anti-RFP magnetic beads. Col-0 plants were used as control. Mature leaves of four- to six-week-old plants, were treated with water or 0.5 mg/mL chitin and harvested 30 min. after treatment. Three leaves were harvested per sample. Three samples of both sets of treatments and genotypes respectively were analysed. Highest hits after filtering including all hits which are present in the test samples, but absence in the control samples or exhibit at least 5×times more peptide hits in the Test samples versus the control samples. AvgP is the calculated corresponding probability scores (AvgP) as the SAINT score. Each interactor is assigned a SAINT score with a probability ranging from 0 to 1, thereby representing the specificity of the interaction (1 represents the highest possible specificity). A Bayesian False Discovery Rate (BFDR) has been further calculated ranging from 0 to 1, representing the likelihood that this protein has been falsely identified.

				Water treated		Chitin treated		Joint results	
protein	**Name**	**Locus**	**Size kDa**	**AvgP water**	**BFDR water**	**AvgP chitin**	**BFDR chitin**	**AvgP all**	**BFDR all**
ESM1	EPITHIOSPECIFIER MODIFIER 1	AT3G14210	44	1.00	0.00	1.00	0.00	1.00	0.00
LYK4	LYSM-CONTAINING RECEPTOR-LIKE KINASE 4	AT2G23770	67	1.00	0.00	1.00	0.00	1.00	0.00
GAPA-2	GLYCERALDEHYDE 3-PHOSPHATE DEHYDROGENASE A SUBUNIT 2	AT1G12900	43	1.00	0.00	0.74	0.03	0.92	0.02
SLP2	SUBTILISIN-LIKE SERINE PROTEASE 2	AT4G34980	81	1.00	0.00	1.00	0.00	0.78	0.14
FLOT1	FLOTILLIN 1	AT5G25250	52	0.67	0.09	0.99	0.00	0.80	0.14
PRK	PHOSPHORIBULO-KINASE	AT1G32060	44	1.00	0.00	1.00	0.00	1.00	0.00
TUB2	TUBULIN BETA CHAIN 2	AT5G62690	51	1.00	0.00	1.00	0.00	0.94	0.00
TUB4	TUBULIN BETA CHAIN 4	AT5G44340	50	0.67	0.09	0.67	0.09	0.67	0.18
TUB5	TUBULIN BETA-5 CHAIN	AT1G20010	50	0.67	0.09	1.00	0.00	0.83	0.09
TUB7	TUBULIN BETA-7 CHAIN	AT2G29550	51	0.33	0.38	NA	NA	0.17	0.51
FLOT2	FLOTILIN2	AT5G25260	51	0.33	0.38	0.33	0.32	0.33	0.39
TUB6	BETA-6 TUBULIN	AT5G12250	51	0.33	0.38	0.33	0.32	0.33	0.39
CAT3	REPRESSOR OF GSNOR1	AT1G20620	57	0.67	0.09	1.00	0.00	0.83	0.12
TKL1	TRANSKETOLASE 1	AT3G60750	80	0.67	0.09	0.67	0.07	0.67	0.18
	ATPase, F1 complex, alpha subunit protein	AT2G07698	86	0.67	0.09	1.00	0.00	0.83	0.09
PTAC16	PLASTID TRANSCRIPTIONALLY ACTIVE 16	AT3G46780	54	0.67	0.09	1.00	0.00	0.83	0.09
GOX2	GLYCOLATE OXIDASE 2	AT3G14415	40	0.33	0.38	0.33	0.32	0.33	0.39
GLDT	T-protein	AT1G11860	44	0.67	0.09	0.97	0.00	0.83	0.12
ZW9	TRAF-like family protein	AT1G58270	45	0.67	0.09	0.96	0.00	0.75	0.15
HSC70-1	HEAT SHOCK COGNATE PROTEIN 70-1	AT5G02500	71	0.67	0.09	0.85	0.02	0.82	0.13
ATIF3-4	INITIATION FACTOR 3-4	AT4G30690	32	0.67	0.09	1.00	0.00	0.83	0.09
LOX2	LIPOXYGENASE 2	AT3G45140	102	0.67	0.09	0.67	0.08	0.64	0.21

5.2.2 Arabidopsis and *M. truncatula* flotillin nomenclature does not correspond

The *M. truncatula* flotillins MtFLOT2 and MtFLOT4 are necessary for successful nodule formation with *Sinorhizobium meliloti* (Haney and Long, 2010). MtFLOT4 has been further identified to be necessary to stabilise Carboxy-terminal region of MtSYMREM1 together with the receptor kinase MtLYK3 in nanodomains during the infection detection process (Liang et al., 2018).

As a flotillin (MtFLOT4) plays such an important role in the nanodomain localisation of a receptor protein (MtLYK3) and this dynamic has been researched in detail (Liang et al., 2018), I wanted to first determine how the Arabidopsis flotillins group with the *M. truncatula* flotillins to resolve which flotillins could potentially be functionally and phylogenetically equivalent. For this purpose, a phylogenetic tree based on the protein sequences of the flotillins from both species was generated (Fig.5-1A). The protein sequences were chosen over DNA sequences to allow for clustering of possible shared and conserved function as well as to avoid problems caused by nucleotide compositional biases in DNA sequences (Foster and Hickey, 1999). Using this phylogenetic tree, I determined that both the Arabidopsis flotillins as well as the *M. truncatula* flotillins cluster together only within their own species, thereby enabling no direct one-to-one gene comparisons.

5.2.3 Flotillin co-localisation with LYK4 in a chitin dependent manner

FLOT1, 2, and 3 were identified in a refined plasmodesmal proteome (Bayer, pers. comms.). Due to their high amino acid sequence similarity FLOT1 and FLOT2 were grouped together reaching a PD/PM ratio (a ratio of protein abundance between plasmodesmata and the PM) of 2.1 — suggesting that at least one of the two results in this PD/PM ratio — while FLOT3 had a PD/PM ratio of 0.5 (Bayer, pers. comms.). Although this is a relatively low ratio result, it does not exclude a possible plasmodesmal localisation for either of these proteins. To determine if the flotillins localise to plasmodesmata, fluorescent translational fusion constructs were generated and transiently expressed them in *N. benthamiana* as well as stably in Arabidopsis. However, by contrast with *FLOT1* and *FLOT2*, all attempts to clone *FLOT3* in multiple different cloning approaches and systems failed.

Both FLOT1 and FLOT2 constructs showed a PM localisation, both in *N. benthamiana* as well as in Arabidopsis (Fig. 5-1). In mid plane optical sections of epidermal cells, they appear to be localised rather homogeneously to the cell boundary, reminiscent of an even PM localisation rather than a plasmodesmal localisation. When expressed stably in Arabidopsis under the *Actin2* promoter, only a weak fluorescence signal for FLOT1 and a barely visible signal for FLOT2 was observed.

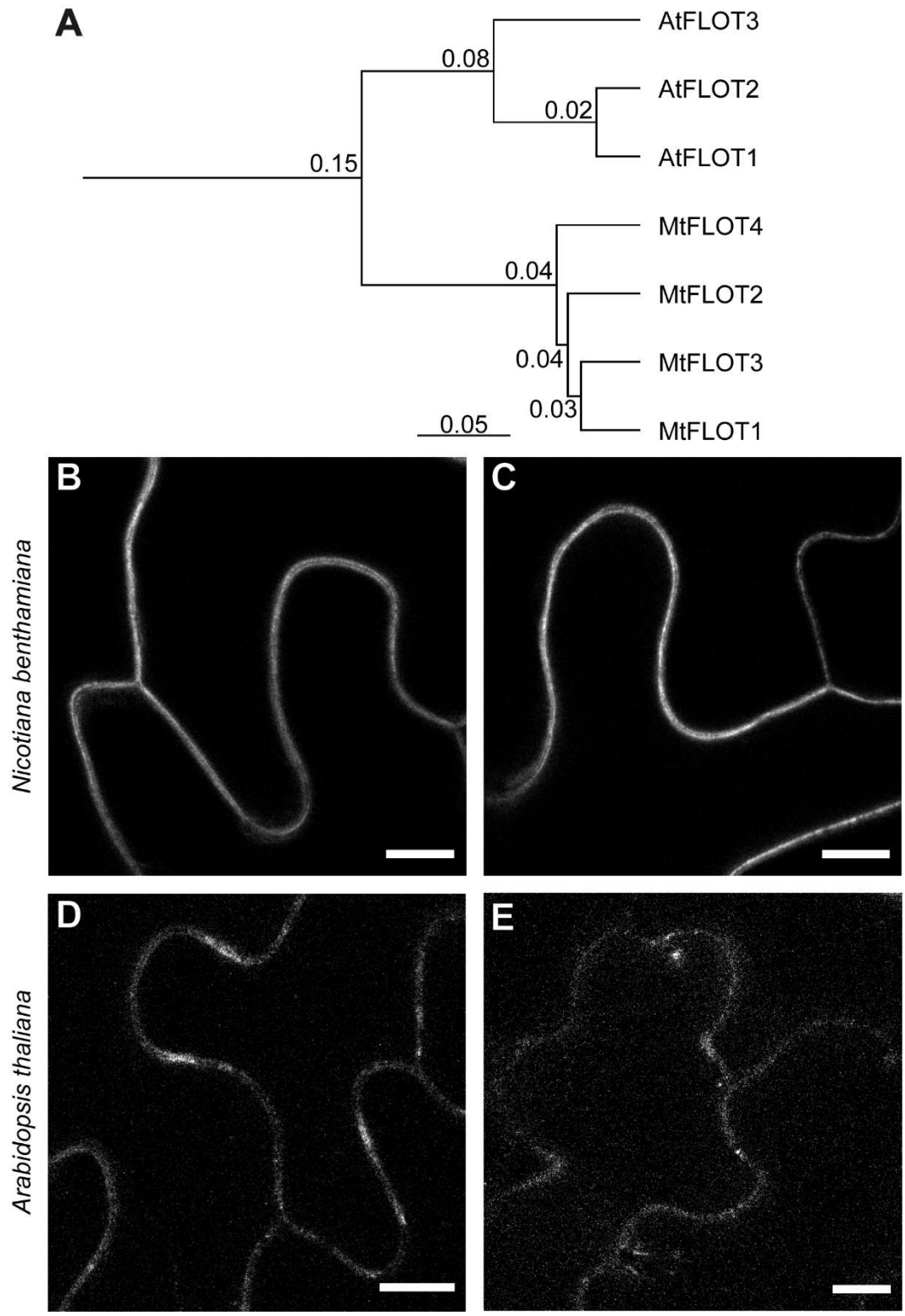

Figure 5-1: Flotillin phylogeny and localisation. (A) Phylogenetic tree of *Arabidopsis* and *Medicago truncatula* flotillin protein families. A ClustalW 2.1 alignment with a BLOSUM cost matrix was used to generate the original alignment followed by using the Jukes-Cantor Genetic Distance Model and the UPGMA tree building method to generate this tree on the basis of protein amino acid similarity (based on the alignment of Fig. 7-2, Table 7-3). The node labels are branch confidence values. (B) to (E) Single-plane confocal images of stable Arabidopsis lines or *N. benthamiana* expressing flotillins, which localise to the PM. The following constructs were used: (B) *p35s::FLOT1-mRFP1*, (C) *p35s::FLOT2-mRFP1*, (D) *pAtAct2::FLOT1-mRuby3-6xHA*, (E) *pAtAct2::FLOT2-mRuby3-6xHA*. All scale bars, 10 µm.

True association between two proteins can only be, if the two are physically close enough to indeed associate with each other. If one of the two proteins (e.g. the flotillin) is predominantly present in a nanodomain, the second protein (e.g. LYK4) would be expected to show a co-localisation to allow for an association between the two. Both FLOT1 and FLOT2, as well as LYK4, were determined to not be present homogeneously within the PM, when observing the PM of epidermis cells facing away from the bulk of the leaf. These inhomogeneities suggest the enriched protein presence within nanodomains. I wanted to test if I could determine a correlation in the fluorescence pattern of the flotillins with LYK4 in the PM, and therefore in the nanodomain localisations of these proteins.

Indeed, a correlation between those protein fluorescent signal domains was determined (Fig. 5-2). All samples analysed resulted in a mean Pearson correlation coefficient (PCC, a comparison value, indicative of if two proteins are co-localised or not, with 0 representing no association between two proteins, and 1 representing full co-localisation (McDonald and Dunn, 2013)) of >0.4. To allow for better control of random chance of correlation one should carry out the same analysis with one of the two channels turned by 90°, which should then result in a great reduction of the correlation coefficient — ideally to 0. In the case of this experiment, I have not used images which are completely filled by a region of interest (ROI). Instead, I used images which in which also areas of no interest are depicted (Fig. 5-2A to D). This is not ideal for such a random chance control to be carried out as this would lead to an artificial exaggeration of how random the correlation is. For future experiments one should therefore either only acquire images in which their whole area is the ROI or limit the analysis ROI to a defined area, in which no “blackness” is present.

As LYK4 is a chitin receptor speculated to undergo endocytosis events depending on chitin (Erwig et al., 2017) and as different amounts of FLOT1 and FLOT2 were present in the IP with LYK4 in my interactor screen (Table 5-1, Table 7-4), I wanted to test if the co-localisation of LYK4 with the flotillins in PM undergoes chitin-triggered changes. A significant reduction in the PCC between LYK4 and FLOT1 was determined in the presence of chitin when compared to mock conditions (Fig. 5-2). A similar shift was not observed when comparing LYK4 with FLOT2 following chitin treatment.

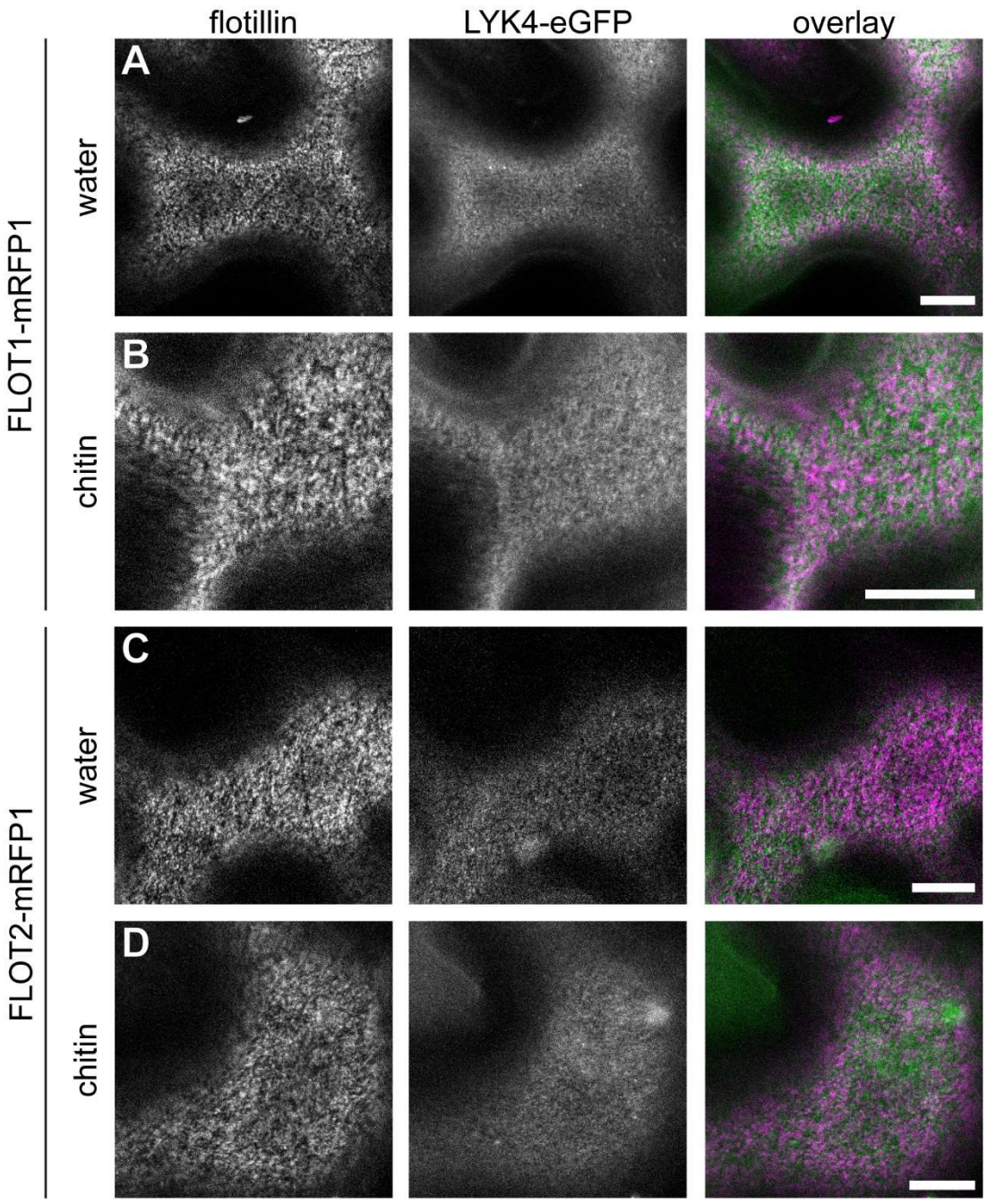
flotillin
LYK4-eGFP
overlay
A
B
C
D
water
chitin
water
chitin
FLOT1-mRFP1
FLOT2-mRFP1

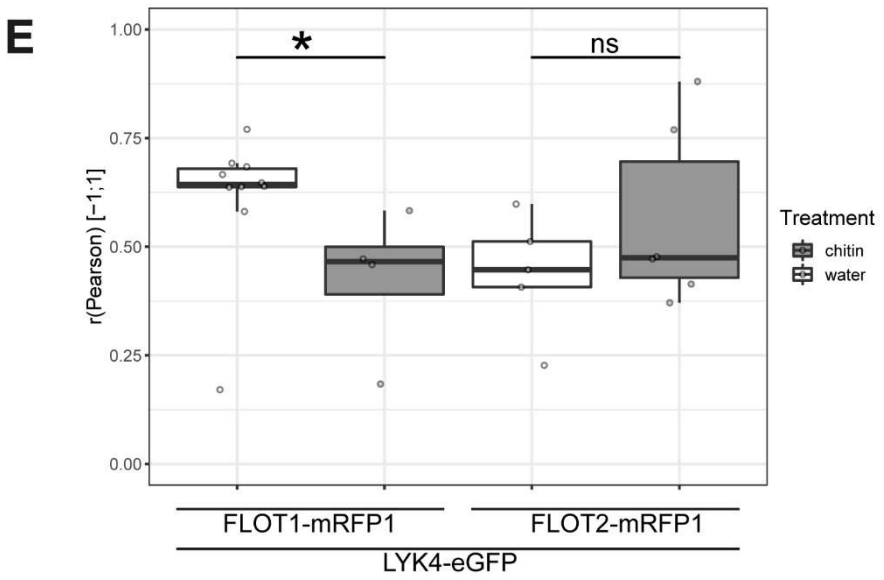
E
*
ns
1.00
0.75
0.50
0.25
0.00
r(Pearson) [−1;1]
Treatment
chitin
water
FLOT1-mRFP1
FLOT2-mRFP1
LYK4-eGFP

Figure 5-2: Domain correlation of LYK4 with FLOT1 and FLOT2.

(A) – (D) Example images of the domain localisation in transient *N. benthamiana* leaf epidermis cells in the PM, co-expressing *35s::LYK4-eGFP* with a flotillin construct. Images were acquired 30-60 min. after treatment with either chitin or mock (water). Additional flotillin construct and treatment of (A) *35s::FLOT1-mRFP1* with water, (B) *35s::FLOT1-mRFP1* with chitin, (C) *35s::FLOT2-mRFP1* with water, (D) *35s::FLOT2-mRFP1* with chitin. (A) to (D) Individual image acquisition channels in greyscale and the overlay with LYK4-eGFP represented in green, and FLOT1-mRFP or FLOT2-mRFP1 represented in magenta. Scalebar is 10 µm in all images. (E) Quantitative co-localisation analysis for LYK4-eGFP with FLOT1-mRFP1 or FLOT2-mRFP1 respectively, after transient co-expression in epidermal leaf cells of *N. benthamiana*. The Pearson correlation coefficient reveals the correlation between the two different fluorescence signals: 0 indicating no correlation, and 1 indicating exact correlation. Statistical comparison was carried out by using Mann-Whitney-Wilcoxon test (sample sizes range from n=4 to n=11, * indicates $p<0.05$).

5.2.4 LYK4 co-IPs with FLOT1 and FLOT2

To validate the association between LYK4 with FLOT1 and FLOT2 a second protein-protein interaction detection experiment was necessary, and the co-IP approach optimised in chapter 3 was therefore used. As part of this experiment, the use of mClover3-3×FLAG as a bait protein tag and the use of mRuby3-6×HA as a prey protein tag was validated by utilising the already described interaction (chapter 3.2.6) between LYK4 with LYK5 (Fig. 5-3). Indeed, these two proteins demonstrate a clear association using these biomolecular tag constructs.

I performed targeted co-IPs with LYK4-mClover3-3×FLAG and FLOT1-mRuby3-6×HA, with LTI6b-mRuby3-6×HA as a control (Fig. 5-3). The co-IPs were carried out as described in chapter 3.2.5. This experiment showed that the prey FLOT1-mRuby3-6×HA immunoprecipitates with the bait LYK4-mClover3-3×FLAG, while the negative control prey LTI6b-mRuby3-6×HA did not. As the mass spectrometry data suggested an enhanced association between LYK4 and FLOT1 in the presence of chitin, the association between LYK4-mClover3-3×FLAG and FLOT1-mRuby3-6×HA was tested for changes in the presence of chitin. However, in this co-IP approach no significant changes could be determined in the association of LYK4 with FLOT1 when comparing chitin or mock treated samples.

I only carried out an interactor identification screen based on the association with LYK4 showing that immunoprecipitates with FLOT1 and FLOT2, but as LYK4 interacts with LYK5, I wanted to test whether LYK5 would also show an association with FLOT1. Thus, targeted co-IPs with LYK5-mClover3-3×FLAG and FLOT1-mRuby3-6×HA, with LTI6b-mRuby3-6×HA as a control were performed. This experiment showed that FLOT1-mRuby3-6×HA immunoprecipitates with LYK5-mClover3-3×FLAG, while the negative control prey LTI6b-mRuby3-6×HA did not (Fig. 5-3A). This association also did not show any significant increases or decreases in FLOT1-mRuby3-6×HA prey signals between mock or chitin treated samples.

To confirm the association between FLOT2, with LYK4 or LYK5 targeted co-IPs were carried out using LYK4-mClover3-3×FLAG or LYK5-mClover3-3×FLAG and FLOT2-mRuby3-6×HA. This experiment showed that the prey FLOT2-mRuby3-6×HA immunoprecipitates with the both the bait LYK4-mClover3-3×FLAG as well as the bait LYK5-mClover3-3×FLAG (Fig. 5-3B).

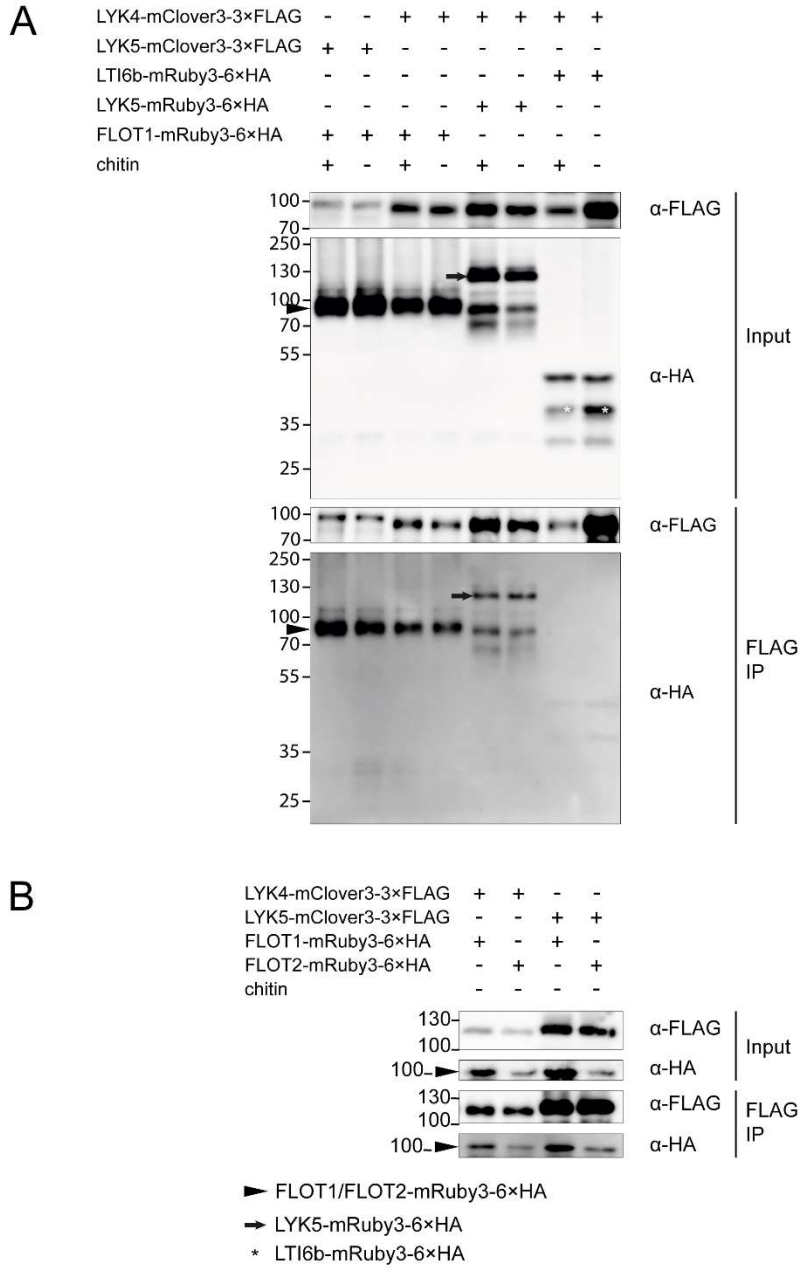

Figure 5-3: LYK4 and LYK5 associate with FLOT1 and FLOT2 respectively, but not with the negative control LTI6b. Western blot analysis of immunoprecipitated proteins from *N. benthamiana* leaf tissue transiently expressing combinations of LYK4-mClover3-3×FLAG, LYK5-mClover3-3×FLAG, FLOT1-mRuby3-6×HA, FLOT2-mRuby3-6×HA, LYK5-mRuby3-6×HA and LTI6b-mRuby3-6×HA. Both FLOT1-mRuby3-6×HA and FLOT2-mRuby3-6×HA are indicated by triangles, while LYK5-mRuby3-6×HA is indicated by an arrow. Input and immunoprecipitated (IP) samples were probed with α-FLAG or α-HA antibodies as indicated. (A) FLOT1-mRuby3-6×HA and LYK5-mRuby3-6×HA were detected in detergent extracted fractions by IP of LYK4-mClover3-3×FLAG. No LTI6b-mRuby3-6×HA was detected in the IP fraction. FLOT2-mRuby3-6×HA was further detected in the detergent extracted fractions by IP of LYK4-mClover3-3×FLAG. This experiment was repeated three times, showing similar results. (B) FLOT1-mRuby3-6×HA and FLOT2-mRuby3-6×HA were detected in the detergent extracted fractions by IP of LYK4-mClover3-3×FLAG and LYK5-mClover3-3×FLAG. This is an initial experiment and has only been carried out once.

5.2.5 Identification of flotillin mutants

To assay for the function of flotillins in Arabidopsis, insertion mutants (*flot1* SALK_203966, *flot2* GK-430C05.1, *flot3* SALK_143325) were obtained, genotyped (Fig. 5-4) and progeny of homozygous plants were used for all further experiments. The mutants *flot1* and *flot3* were previously characterised by Kroumanova et al. (2019). Their T-DNA insertion sites were identified by Alonso et al. (2003) and for *flot2* by Kleinboelting et al. (2012).

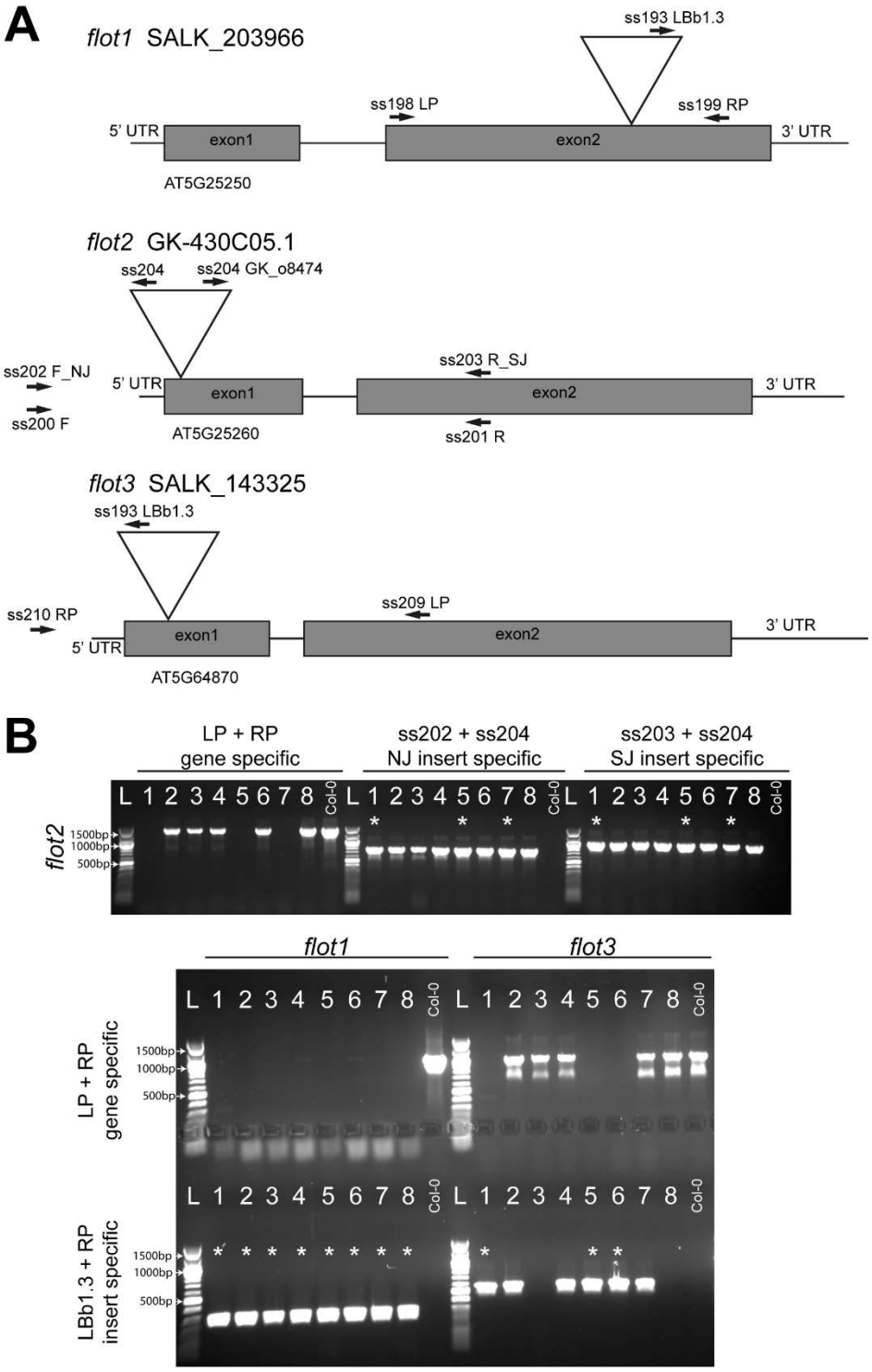

Figure 5-4: Genotyping of flotillin mutant plants. (A) Cartoon models of the flotillin genes with their T-DNA insertion location (triangle), exons (grey boxes), and primers (arrows) used to assess individual plants for homozygous presence of the insertion. (B) Electrophoresis gel of genotyping PCR, separated according to individual mutant and plants tested. The gene specific primer combination shows bands in the presence of the WT gene without an insertion. The insert specific primer combination shows bands if an insertion is present. Homozygous plants are indicated by *. For *flot2* the plants #1, 5, and 7 were homozygous for the insertion. Both the North Junction (NJ) and the South Junction (SJ) of this insertion has been used to verify the insertion. For *flot1* the plants #1-8 were homozygous, and for *flot3* the plants #1, 5, and 6 tested were homozygous for their insertions. The primers were designed using T-DNA Primer Design (http://signal.salk.edu/tdnaprimers.2.html) for *flot1* and *flot3* assessment. The primers for *flot2* assessment were designed using the GABI KAT primer tool from Huep et al. (2014). Insertion specific primers result in 300-700 bp products, while WT gene specific primers result in 900-1100 pb products. Col-0 is used as the respective WT control. (A)&(B): LP: left primer, RP: right primer, LBb1.3: SALK insertion specific primer. L: 100 bp DNA Ladder (New England Biolabs).

5.2.6 Flotillin mutant plants are defective in chitin triggered ROS production

One chitin-triggered plant immune response is the PM-localised production of ROS (Lee et al., 2020). As FLOT1 and FLOT2 additionally partially correlate with the PM domains in which LYK4 is present, I wanted to ask if they are necessary or important in the chitin-triggered ROS production.

As expected, when the leaf disc samples were treated with water, none of the genotypes demonstrated a significant difference to the water-treatment-triggered WT Col-0 control ROS burst (Fig. 5-5). Mutant plants of *flot1*, *flot2* and *flot3* all showed a reduction in the chitin-triggered total ROS production in comparison to the chitin-triggered ROS production of Col-0 leaf discs. None of the mutant plants showed an abolishment of the chitin-triggered ROS burst.

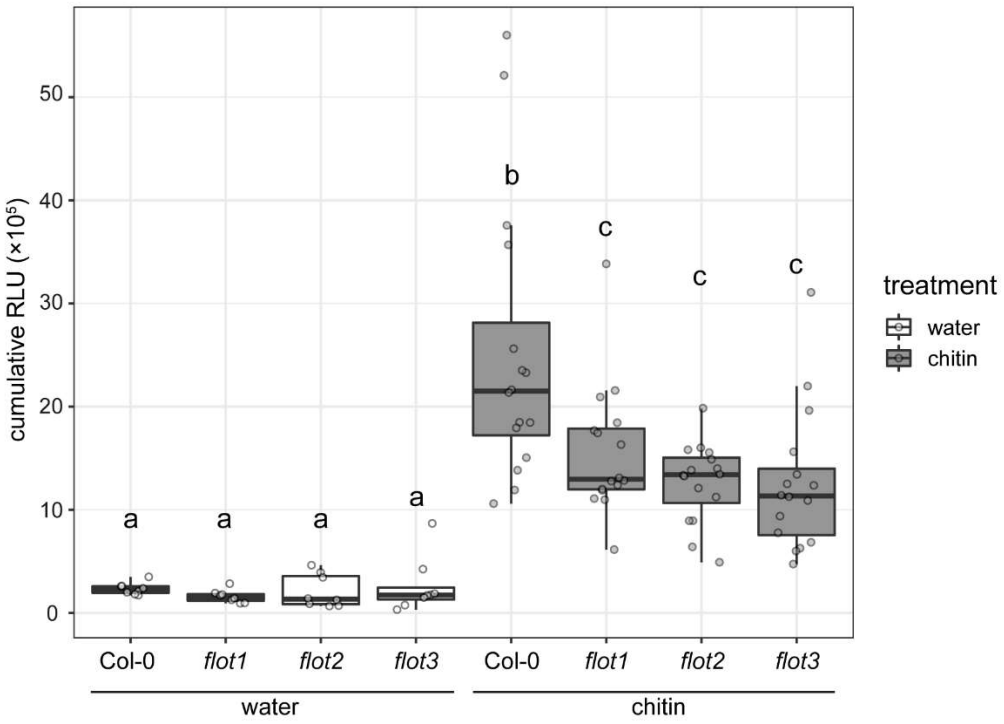

Figure 5-5: Reduction in ROS production triggered by chitin in leaf discs of flotillin mutants. Cumulative relative light units (RLU) as acquired within 90 min. of treatment with mock (water) or chitin. Statistical analysis was carried out by fitting a linear mixed effects model accounting for the fixed additive effects of genotype and treatment. Different letters (a, b, and c) indicate statistically significant groups with $p < 0.05$, compared between genotypes and treatments. All water treated samples have a sample size of n = 8, and all chitin treated samples have a sample size of n = 16.

5.2.7 Flotillin mutants show altered plasmodesmal flux responses

LYK4 is present both at the PM as well as the plasmodesmal PM and is necessary for the chitin-induced reduction of plasmodesmal flux (Cheval et al., 2020). I therefore wanted to test if mutations in the flotillin genes causes a difference to chitin-triggered plasmodesmal flux as well. For this purpose, microprojectile bombardment experiments were carried out, based on the capability of free eGFP to diffuse from a single cell to neighbouring cells. As previously reported (Cheval et al., 2020; Faulkner et al., 2013), control plants of Col-0 exhibit a significant reduction of plasmodesmal flux triggered by chitin. However, no significant changes to the plasmodesmal flux in *flot1* or *flot2* mutant plants could be observed when comparing treatments with mock (water) or chitin (Fig. 5-6). Thereby these mutants demonstrated that they cannot successfully close their plasmodesmata triggered by chitin. By contrast, the *flot3* mutant exhibited similar changes to its plasmodesmal flux as Col-0, showing that this mutant can regulate its plasmodesmal flux in response to chitin.

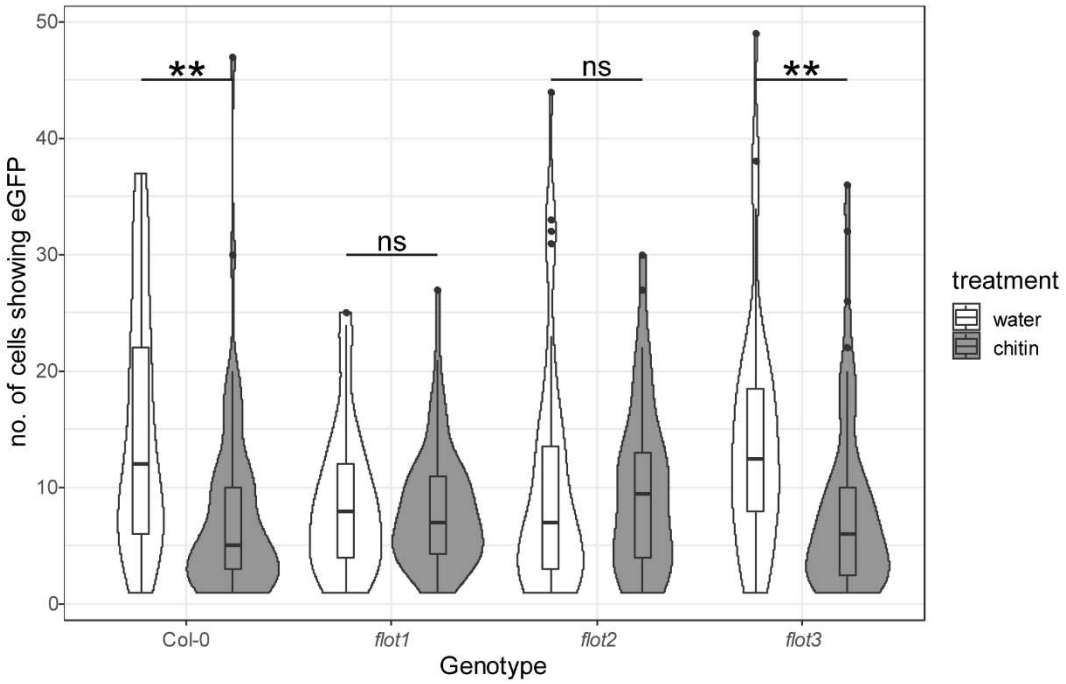

Figure 5-6: Assessment of the cytosolic cell-to-cell flux of flotillin mutant plants. Microprojectile bombardment into leaf tissue of 4- to 6-week-old Arabidopsis shows that Col-0, and *flot3* but not *flot1*, and *flot2* exhibited reduced movement of eGFP to neighbouring cells in response to chitin. These data are summarised in a combination of a box plot with a violin plot. For the box plot, the line within the box marks the median, the box signifies the upper and lower quartiles, and the whiskers represent the minimum and maximum with 1.5 × interquartile range. The violin plot represents the data contribution. The number of bombardment sites (n) counted is ≥46. Asterisks indicate significant difference between the chitin treated samples compared with control conditions. ** indicates $p < 0.01$. Statistical analysis carried out using bootstrapping to compare the medians, according to Johnston and Faulkner (2021).

5.2.8 Flotillin mutants exhibit enhanced susceptibility to *Botrytis cinerea*

I showed that flotillin mutants exhibit different immune response phenotypes such as reduced ROS bursts and the inability to down-regulate plasmodesmal flux triggered by chitin. Based on this evidence, I asked if these proteins have a significant effect not just after treatment with a purified MAMP, but rather during infection with a pathogenic fungus.

For this purpose, detached mature leaves of flotillin mutants were spot inoculated with spore suspensions of *B. cinerea* and measured the resulting progression of fungal growth (Fig. 5-7). Yellowing, chlorotic areas outside of the necrotic lesions are a sign of high virulence of *B. cinerea* (Breen et al., 2022). Leaves of the *flot1* mutant exhibited a bigger size of these chlorotic areas four days past infection (dpi) when compared to the chlorotic areas of Col-0, *flot2*, or *flot3* plants (Fig. 5-7B).

By contrast, an increase in the size of necrotic lesions in the leaves of *flot2* mutants (Fig. 5-7C) was observed, while such an in increase was not observed in the other genotypes. Therefore, the *flot1* and *flot2* mutants show different susceptibility increases against *B. cinerea*, one as an enhanced chlorotic area and one as an enhanced necrotic lesion respectively, while the *flot3* mutant does not show such a phenotype.

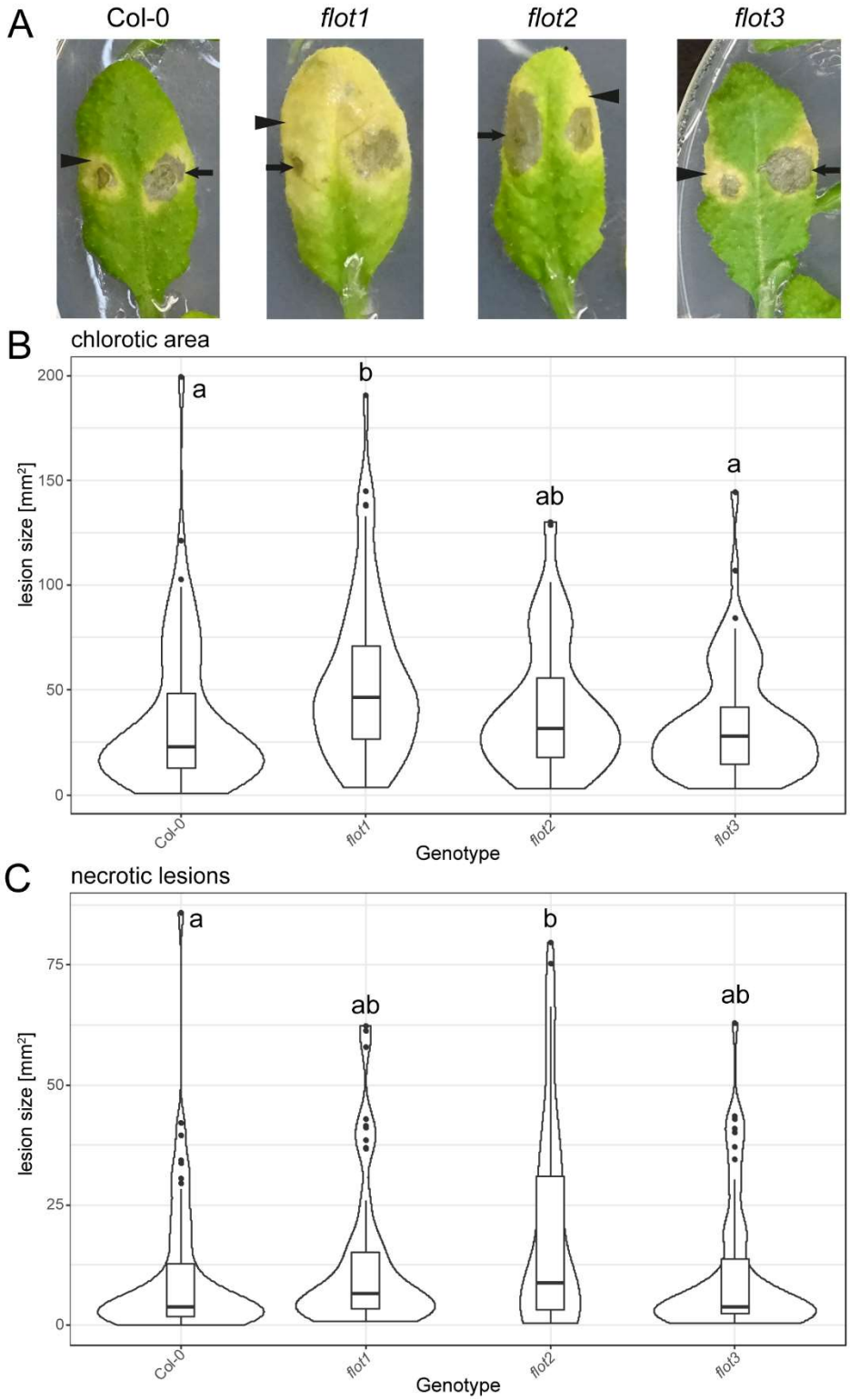

Figure 5-7: Responses of flotillin mutants to a fungal pathogen. The fungal pathogen *B. cinerea* was spot inoculated onto detached leaves. The progression of fungal infection was determined 4 dpi. (A) Representative photographic images of the progression of *B. cinerea* in detached leaves of Col-0, *flot1*, *flot2*, and *flot3*. Arrows indicate necrotic lesions and triangles indicate biotrophic lesions. (B) & (C) A linear mixed-effects model accounting for the fixed effect of genotype and the random effect of experimental repeats. Different letters (a, b, and c) indicate statistically significant differences when comparing the between the genotypes ($p < 0.01$). The number of individual lesion sites (n) counted for each genotype is ≥56, from three different independent experimental repeats. Arrows indicate necrotic lesions; triangles indicate chlorotic areas. (B) Analysis of chlorotic area caused by the fungus. This also includes the necrotic lesion area. The *flot1* mutant exhibits bigger biotrophic lesions than Col-0, *flot2* or *flot3*. (C) Analysis of the necrotic lesion caused by the fungus. The *flot2* mutant exhibits bigger necrotic lesions than Col-0, *flot1* or *flot3*.

5.3 Discussion

5.3.1 Identification of LYK4 candidate interactors

150 different proteins passed the initial screening criteria and were identified by mass spectrometry to associate with LYK4 based on their co-immunoprecipitation (Table 5-1, Table 7-4). Here I will discuss some of the most abundantly identified proteins.

LYK4 localises to the PM and to plasmodesmata, while multiple proteins identified in this screen are known to be present in non PM/plasmodesmata/cell wall cellular compartments. They could therefore be contaminations even if they passed stringent criteria controls. GAPA-2 (Marri et al., 2005), PHOSPHORIBULO-KINASE (PRK) (Marri et al., 2005), PLASTID TRANSCRIPTIONALLY ACTIVE 16 (PTAC16) (Emanuelsson et al., 1999; Pfalz et al., 2006), TRANSKETOLASE 1 (TKL1) (Rocha et al., 2013), INITIATION FACTOR 3-4 (ATIF3-4) (Nesbit et al., 2015; Zheng et al., 2016), and LIPOXYGENASE 2 (LOX2) (Zybailov et al., 2008) localise to chloroplasts. GLYCOLATE OXIDASE 2 (GOX2) further localises to chloroplasts (Armbruster et al., 2009) and peroxisomes (Reumann et al., 2007), while T-protein (GLDT) localises to chloroplasts (Timm et al., 2018) and mitochondria (Engel et al., 2008). REPRESSOR OF GSNOR1 (CAT3) also localises to peroxisomes (Li et al., 2015c) while the HEAT SHOCK COGNATE PROTEIN 70-1 (HSC70-1) has been observed in the cytosol and the nucleus (Zhao et al., 2021). ATPase, F1 complex, alpha subunit protein localises to mitochondria (Heazlewood et al., 2004; Kruft et al., 2001). As LYK4 fulfils its chitin perception and signalling roles at the PM, these candidate proteins are not the most likely to associate with LYK4 at the PM, and therefore not the most likely to be important for its functions.

EPITHIOSPECIFIER MODIFIER 1 (ESM1) was detected at a higher abundance than the bait protein LYK4 itself, and even though individual protein hits were identified in the control samples, data of this protein still resulted in AvgP scores of 1, and BFDR scores of 0, thereby suggesting a high specificity in the association between LYK4 and ESM1 and a low false discovery rate respectively. ESM1 belongs to the GDSL-motif lipase/hydrolase protein family. This subclass of lipolytic enzymes possesses a distinct GDSL amino acid sequence motif (Upton and Buckley, 1995). GDSL-domain proteins have recently been identified to play an important role in auxin-triggered cell wall remodelling and for the synthesis and turnover of suberin (Ursache et al., 2021). A different remodelling of the cell wall is triggered by chitin as callose gets deposited at plasmodesmata to reduce plasmodesmal flux (Cheval et al., 2020). As this is another cell wall modification dependent on the synthesis and turnover of a

biopolymer, one could hypothesise that chitin-triggered callose deposition could also be dependent on or enhanced by a GDSL-domain protein such as ESM1.

ESM1 modifies the EPITHIOSPECIFIER PROTEIN (ESP, also known as TASTY) (Zhang et al., 2006), which in turn promotes the hydrolysis of secondary metabolites of the class of glucosinolates (Lambrix et al., 2001). Some fungi are sensitive to the presence of glucosinolates and exhibit a reduced pathogenicity in their presence (Buxdorf et al., 2013), thereby showing that glucosinolate synthesis is strategy contributing to plant immunity against fungi. Glucosinolates further enhance protection against insect herbivory (Ratzka et al., 2002; Sato et al., 2019). Not only fungi have chitin as a central component of their cell walls (Brown et al., 2020), but insects also use this biopolymer in their cytoskeleton and particularly mouth parts (Elieh-Ali-Komi and Hamblin, 2016; Prince et al., 2014). LYK4 could therefore potentially be linked via ESM1 to the detection of insect chitin in herbivory situations followed by changes to the plant defence system. This potential direct link between glucosinolate production and chitin receptors has so far not been published and opens new routes of research into the activation of herbivory deterrence mechanisms.

ESM1 was also identified to associate with the NLR protein RESISTANT TO P. SYRINGAE 2 (RPS2), which confers resistance to the bacterial pathogen *P. syringae* carrying the avirulence gene avrRpt2 (Mindrinos et al., 1994; Qi and Katagiri, 2009). In the same experiment RPS2 showed an association with the SPFH proteins HIR1 and HIR2 (Qi and Katagiri, 2009). This could suggest a broader role of ESM1 in the interactions in plant defence signalling with SPFH proteins.

Subtilisin-like proteases form a multigene family in Arabidopsis and are predominantly targeted to the extracellular matrix where they can act proteolytically (Golldack et al., 2003; Taylor et al., 1997). SLP2 is part of the SUBTILASE 1 (SBT1) subfamily (Figueiredo et al., 2014). Knockout mutants of *sbt3.3* exhibit an enhanced disease susceptibility to the bacterial pathogen *P. syringae* DC3000 and the fungal pathogen *Hyaloperonospora arabidopsidis*, while overexpression mutants show enhanced disease resistance and enhanced mitogen-activated kinase activation (Ramírez et al., 2013). Ramírez et al. (2013) speculate that this could be due to the proteolytic cleavage of a yet unidentified substrate of SBT3.3. Such a substrate could be a PRR, which by shedding of its ectodomain via SBT3.3. becomes signalling competent and active. Chapter 3.2.7 shows that LYK4 and LYK5 likely undergo ectodomain shedding processes. However, the protease carrying out this proteolytic cleavage is still unknown. As SLP2 associates with LYK4 (Table5-1), it is therefore now a prime candidate to

facilitate the ectodomain shedding of LYK4. This could be determined by assessing LYK4's ectodomain shedding processes in a *slp2* mutant.

SLP2 has been determined to have a PD/PM index of 168.7 (Bayer, pers. comms.) giving a strong suggestion that this protein is enriched at plasmodesmata. Only few of the 56 Arabidopsis subtilisin-like proteases (Figueiredo et al., 2014) have been found in plasmodesmal protein extractions (Kirk et al., 2021), giving the possible association between SLP2 and LYK4 further importance, as this could be the protease responsible for ectodomain shedding of LYK4 at plasmodesmata. However, no subtilisin-like protease family member has been published to date to localise to plasmodesmata by confirmation with other techniques such as confocal microscopy. The confirmation of SLP2's plasmodesmal localisation could therefore be the first step in future lines of research into this protein.

Different members of the protein family of tubulins were identified to associate with LYK4 and have been determined to exhibit varying PD/PM ratios, such as TUB2 0.8, TUB4 0.8, TUB7 0.9, BETA-6 TUBULIN (TUB6) 1.4 (Bayer, pers. comms.). TUB5 has been identified to IP with LYK4 as well but does not have a PD/PM score from the same experiment as the others (Bayer, pers. comms.). Overall, the PD/PM scores of these tubulin proteins are relatively low, suggesting that possibly they are present at plasmodesmata, but either at lower than PM levels or they are semi-equally distributed between the PM and the plasmodesmal PM. Antibody labelling experiments detecting for tubulin, labelled plasmodesmata only slightly more than the cytoplasm in *Chara corallina* (Blackman and Overall, 1998), thereby further suggesting an absence of enrichment of microtubules at plasmodesmata. Treatment with colchicine — a microtubule depolymerizing drug (Bhattacharyya et al., 2008) — has been shown to induce nearly no effect on cell-to-cell conductivity in *Trianea bogotensis* roots (Krasavina et al., 2001), suggesting that microtubules are not or are only minimally important to regulate plasmodesmal flux. Although there is no specific evidence that microtubules are present within plasmodesmata, they can direct cargo towards plasmodesmata (Harries et al., 2009). Microtubules can therefore play a role in plasmodesmal processes even without being present or enriched at plasmodesmata themselves.

The cytoskeletal microtubules consist of different tubulin dimers, and cortical microtubules are closely associated with the PM (Chan and Coen, 2020). Members of the tubulin protein family have been found to be enriched at detergent resistant membranes in Arabidopsis (Minami et al., 2009). These tubulins associating with LYK4, could therefore be a further suggestion that LYK4 resides in a nanodomain within the PM.

The cytoskeleton, and in particular microtubules, can undergo reorganisation processes during fungal infection (Kobayashi et al., 1994; Porter and Day, 2016). The presence of an elicitor itself is able to trigger such a reorganisation of the cytoskeleton (Higaki et al., 2007). For example, treatment with chitin is able to trigger such a cytoskeletal reorganisation (Henty-Ridilla et al., 2013). In *cerk1/lyk4* double mutants the application of chitin does not lead to a reorganisation of actin filaments, thereby suggests that this cytoskeletal reorganisation is dependent on the function of at least one of those two proteins (Li et al., 2015b). From these receptor proteins the signals get translated to the actin filaments by CAPPING PROTEIN (CP), which detects changes in the stress signalling molecule phosphatidic acid, resulting in uncapping of filaments (Huang et al., 2003; Li et al., 2012a). A similar mechanism for chitin-triggered microtubule reorganisation has not yet been published. However, it seems likely that chitin-triggered microtubule reorganisation is dependent on one or more chitin receptor proteins such as LYK4. The association with so many different tubulin proteins allows the formation of the speculative hypothesis that the signal for the chitin-triggered microtubule reorganisation could be processed in a more local way via a protein complex which includes LYK4. This could be evaluated by testing for chitin-triggered microtubule reorganisation in different knock-out mutants such as *lyk4*.

As an alternative hypothesis, the association between LYK4 and tubulins could be important for membrane protein organisation into nanodomains. The actin and microtubule cytoskeleton can regulate PM protein cluster size and dynamics such as of the flg22 receptor FLS2, and thereby have a regulating function on the formation, maintenance and functionality of membrane nanodomains (McKenna et al., 2019). As LYK4 interacts with TET3, 7 and 8 (chapter 4.2.9), and with LYM2 (chapter 3.2.6), and all these proteins are putatively present in nanodomains, it is likely that at least a pool of LYK4 is present in such a nanodomain as well. Therefore, a plausible hypothesis is that LYK4's presence within these nanodomains could be dependent on its association with microtubules. This dependence could be tested by assessing for nanodomain localisation or complex formation in cytoskeleton disrupted conditions, for example via treatments with chemical inhibitors such as oryzalin (Morejohn et al., 1987). Although the abundance of tubulin proteins associating with LYK4 raises intriguing hypotheses and potential future experiments they are not markers for nanodomains themselves — and I therefore chose to prioritise flotillins over the tubulins.

The TRAF-like family protein (ZW9) was identified in the Arabidopsis plasmodesmal proteome by Fernandez-Calvino et al. (2011), but not in any other published plasmodesmal proteomes since then (Kirk et al., 2021). It has been identified as part of the active PYK10 (also referred to as BGLU23) complex, which is a major component of ER-derived organelles called ER bodies (Nagano et al., 2008). The β-glucosidases PYK10 hydrolises scopolin (Ahn et al., 2010), a compound inhibiting growth of the fungal pathogen *Fusarium oxysporum* (Peterson et al., 2003). Nakano et al. (2014) speculate that PYK10 complexed proteins thereby indirectly contribute to plant immune responses through growth inhibition of fungi. Yamada et al. (2020) identified PYK10 to be important in glucosinolate-mediated resistance of Brassicaceae plants against herbivore damage from woodlice. This suggests that ZW9 could also be important in plant defence responses against insects. ZW9 localisation has previously not been experimentally determined and published. However, its indirect association with plant immunity and potential presence at plasmodesmata, as well as association with LYK4, make it an interesting candidate for future studies.

Both FLOT1 and FLOT2 have been identified in the IP of LYK4 (Table 5-1, 7-4), and both were identified with a higher abundance in chitin-treated samples, thereby suggesting that FLOT1 and FLOT2 associate more abundantly with LYK4 in the presence of chitin. As flotillins are the main focus of this chapter, the overall characteristics of this protein family have been discussed in length in the chapter introduction.

5.3.2 Localisation of FLOT1 and FLOT2 in the PM

The flotillin proteins of Arabidopsis and *M. truncatula* form species specific clusters in their phylogenetic tree. This separate grouping between the different flotillin proteins of *M. truncatula* and Arabidopsis does therefore not allow to draw conclusions on which protein of one species is a potential corresponding equivalent protein in the other. Any Arabidopsis flotillin could therefore potentially fulfil the same or similar functions as a flotillin from *M. truncatula*, and their functions have to be experimentally determined.

Although the flotillins are present in a plasmodesmal proteome (Bayer, pers. comms.), fluorophore translational fusion constructs of FLOT1 and FLOT2 did not show an enriched plasmodesmal localisation (Fig. 5-1). However, this result does not prove that FLOT1 or FLOT2 are completely absent at plasmodesmata either. As in the case of LYK4, a protein can be evenly distributed between the PM and the plasmodesmal PM without a particular enrichment at the plasmodesmata, and thereby not be detectable there using conventional CLSM (Cheval et al., 2020). Further, proteins can have predominant localisations in other cellular compartments due to localisation signals which clear obscure plasmodesmal localisations (Kitagawa et al., 2022). Both FLOT1 and FLOT2 localise to domains within the PM (Jarsch et al., 2014; Yu et al., 2017). They do not demonstrate a clear plasmodesmal localisation pattern, but rather exhibit an uneven fluorescence intensity at the PM which may instead be attributable to localisation to specific nanodomains. The unexpectedly low fluorescence signal of FLOT1 and FLOT2 proteins expressed under the *Actin2* promoter in Arabidopsis was an issue for the visualisation and the generation of high-quality images. Future experiments should therefore make use of stronger constitutive promoters or attempt expression using the genes' native promoters.

I determined that LYK4 shows a significant co-localisation with both FLOT1 and FLOT2, each with a mean PCC >0.4 (Fig. 5-2). These results are comparable to the results of Bücherl et al. (2017), who determined similar values for FLS2-eGFP correlation with FLS2-mCherry. This experiment thereby gives the first suggestion, that LYK4 is likely to partially correlate with the same nanodomains as FLOT1 and FLOT2. The sample sizes in this experiment are relatively low and could benefit from further replication. However, these results nonetheless suggest that there is a co-localisation in the fluorescence pattern of LYK4 with both FLOT1 as well as with FLOT2.

The effects of chitin on the correlation between the flotillins and LYK4 were further observed. In this experiment, no difference in the correlation between LYK4 with FLOT2 triggered by

chitin was determined. However, a significant difference in the correlation of LYK4 with FLOT1 when comparing the mock-treated with the chitin-treated samples was observed. The presence of chitin decreases the PCC, suggesting less correlation between those two proteins. This is unexpected, insofar the presence of more FLOT1 associated with LYK4 triggered by chitin was observed in the interactor screen (Table 5-1, 7-4).

Flotillins can be involved in membrane protein transport and turnover (Hülsbusch et al., 2015) and are implicated in endocytosis (Meister and Tikkanen, 2014; Schneider et al., 2008). Erwig et al. (2017) speculate that LYK4 undergoes chitin-induced re-localisation to vesicles. Combined together, a potential hypothesis for the reduction of association between LYK4 and FLOT1 in the PCC compared to the mass spectrometry data could therefore be as follows. LYK4 and FLOT1 associate with each other within the PM under mock conditions. Following chitin treatment, the association between these two proteins is further enhanced, resulting in higher values in the mass spectrometry-based approach (Table 5-1, 7-4). However, at the same time a pool of these proteins re-localises to vesicles, thereby leaving the PM, resulting in a lower correlation as calculated by the PCC (Fig. 5-2), as this experiment is not optimised to pick up on correlating signals outside of the PM and within vesicles. This hypothesis would fit both experimental data, however further experiments such as LYK4/FLOT1 endocytosis evaluations will be necessary to determine if this is indeed correct or not.

5.3.3 Co-IPs confirm interaction of LYK4 with FLOT1 and FLOT2

To confirm the associations of the RK LYK4 with the SPFH proteins FLOT1 and FLOT2 the co-IP methods optimised in chapter 3.2.5 were utilised. An association between LYK4 and LYK5 was demonstrated with FLOT1 or FLOT2 respectively (Fig. 5-3). These experiments did not show a clear indication of more or less association between these proteins triggered by chitin. However, these co-IP approaches might not have the resolution necessary to pick up on more subtle changes. This could be due to them being constitutively overexpressed in a transient system, which in turn could result in the different amounts or ratios of these proteins when compared to the native Arabidopsis system. Quantitative co-IPs in such a transient system might therefore not accurately represent important changes.

For future experiments I would therefore suggest the use of native promoter driven expression lines of Arabidopsis, as this could enable clearer detection of association shifts. Further the additional use of FRET-FLIM might allow for finer observation of changes, as this allows a quantitative analysis of association, and will therefore enable the detection of chitin-

dependent shifts. Taken together, these results confirm that LYK4 associates with FLOT1 and FLOT2.

5.3.4 Flotillin mutants produce less ROS

To test whether chitin-triggered immune responses are influenced by flotillins, multiple phenotyping assays were carried out, starting with an assessment of the chitin-triggered ROS burst in Arabidopsis leaves (Fig. 5-5). A reduction in chitin-triggered ROS production was observed in all three flotillin mutants, *flot1*, *flot2*, as well as *flot3*. This demonstrates that flotillins are indeed necessary for the full chitin-triggered signalling function of a plant. In *rbohd* mutants, the ROS production triggered by the presence of MAMPs is nearly completely abolished (Nühse et al., 2007). Even though the flotillin mutants showed reduced chitin-triggered ROS bursts, by contrast to *rbohd* mutants, their mutations did not lead to a complete abolishment of this MAMP-triggered ROS burst. This could be due to a variety of reasons, such as the continuing presence of other flotillin proteins in these single mutants. These others could potentially rescue the function due to high similarity and potential redundancy. Indeed, FLOT1 and FLOT2 only differ in 21 of their 461 amino acids and their last 11 amino acids at their C-terminal end (95.4% identity) (Fig. 7-2, Table 7-3). Therefore, it seems likely that they can rescue their functions in case of single mutations. In the animal kingdom, new research recently demonstrated that knock-out mutations of individual genes can lead to enhanced expression of related genes within the same family, which are then potentially able to complement the lost function (El-Brolosy et al., 2019). In light of this discovery, it would be interesting to test if these flotillin mutants do indeed show an increase in the gene expression of the other flotillin genes; e.g. if *FLOT2* and *FLOT3* are upregulated in *flot1* mutants. El-Brolosy et al. (2019) suggest the generation of entire gene locus deletions using a CRISPR-CAS9 system, to generate knock-out mutants which do not influence the gene expression of other family members. I have started the generation of such mutants as well as a triple *flot1/2/3* mutant via CRISPR-CAS9 to test this hypothesis as well as to test if the mutations are having an additive effect. These mutants can be used for future experiments

The application of chitin triggers the production of ROS depending on the presence and functionality of chitin receptors (Cao et al., 2014; Petutschnig et al., 2010; Xue et al., 2019). A flotillin interacting with a receptor can have direct impact on the function, localisation and maintenance of the receptor (Amaddii et al., 2012; Hu et al., 2021). Receptors or receptor complexes not localising or being maintained at appropriate levels in flotillin mutants could

therefore be an explanation to why these mutations cause defects in chitin-triggered ROS production.

The result that the *flot3* mutant showed a reduced chitin-triggered ROS production was surprising, insofar as FLOT3 was not identified in the LYK4 mass spectrometry interactor screen. FLOT3 therefore may not associate with LYK4. An association with another chitin receptor or receptor complex, such as CERK1 or LYK5, could be the reason why this mutant exhibits such a phenotype. It will therefore be interesting to test in future experiments if FLOT3 indeed does not associate with LYK4, but does associate with other chitin receptor proteins.

Interestingly, Kroumanova et al. (2019) used the same mutant lines as I did for *flot1* (*SALK_203966*) and *flot3* (SALK_143325) to test for a change to MAMP-triggered ROS bursts by flg22 application and found no significant changes in comparison to WT plants. They further tested a *flot2* allele (FLAG_352D08) in the Arabidopsis ecotype Wassilevskija (Ws-0) for proteinaceous elicitor triggered ROS burst changes, and found no changes to the elf18-triggered ROS bursts in this mutant either. They chose elf18 as Gómez-Gómez et al. (1999) showed that Ws-0 carries a premature stop codon in FLS2, resulting in this ecotype being flg22-insensitive. Taken together with my results of a reduction in the chitin-triggered ROS burst in all three tested flotillin mutants, this could suggest that the flotillins' involvement in MAMP-triggered immunity is specific to at least one, but not all MAMPs. *M. truncatula* can perceive rhizobial lipo-chitooligosaccharides, the so-called "Nod factors" (NFs), which trigger changes in root morphology necessary for successful infection establishment (Murray, 2011). NFs are perceived by RKs, such as the ligand-binding receptor MtNFP and the coreceptor MtLYK3 (Limpens et al., 2003; Smit et al., 2007). The correct signalling processes and localisation of MtLYK3 is dependent on MtFLOT4, thereby further demonstrating the importance of a flotillin to the perception of a microbe-associated molecular pattern.

As a further hypothesis, individual flotillin mutations could be rescued better or more completely by the other members of the protein family in a flg22 signalling context rather than in a chitin signalling context, thereby resulting in drops in chitin-triggered, but not in flg22-triggered ROS production. It will therefore by particularly interesting to test a triple *flot1/2/3* knock-out not just for chitin phenotypes, but also for flg22 and other elicitor-triggered phenotypes. Determining if flotillin mutants are not only disrupting the chitin- or lipo-chitooliogsaccharide-triggered signalling processes but also others signalling processes will yield information regarding to which other receptor proteins might be dependent on

flotillins to function. This will allow future researchers to determine if this is a generalised component of RKs and RPs signalling processes or a specific one for individual specialised ligand perception systems. Future experiments utilising techniques such as elicitor-triggered ROS burst assays or plasmodesmal flux assays of flotillin mutants should therefore also test a variety of different elicitors for their triggered phenotypes.

Although some of the flotillin mutants used in this work have been previously described (Kroumanova et al., 2019), the absence of expression of these genes should still be additionally verified in the future — for example via qPCR approaches. Further have the phenotypes of these mutants only been assessed using single mutant lines per flotillin gene. To validate these phenotypes, the characterisation of a further second independent mutant line per gene will be necessary.

5.3.5 Chitin can't trigger plasmodesmal closure in *flot1* and *flot2*

Using a particle bombardment-based assay, *flot1* nor *flot2* mutants showed that they can reduce their plasmodesmal flux in the presence of chitin in mature leaves (Fig. 5-6). This data demonstrates that both FLOT1 and FLOT2 are necessary for chitin-induced reduction of plasmodesmal flux. The *M. truncatula* MtFLOT4 enables the 'correct' nanodomain localisation of MtLYK3/MtNFP, which in turn in necessary for the establishment of the appropriate signalling processes by MtLYK3/MtNFP (Liang et al., 2018). The interaction of FLOT1 and FLOT2 with LYK4 therefore allows me to speculate that the absence of chitin-triggered changes to plasmodesmal flux in *flot1* and *flot2* mutants could also be due to mislocalisation of LYK4, like the MtFLOT4-MtLYK3-MtNFP system.

Out of the three flotillin mutants assessed, only *flot3* is capable of a chitin-triggered reduction of plasmodesmal flux, similarly to the WT control plants Col-0 (Fig. 5-5). However, similarly to *flot1* and *flot2*, *flot3* shows a reduction in the chitin-triggered ROS burst (Fig. 5-5). This is a divergence in function as flot1 and flot2 show a PM-localised ROS and a plasmodesmal localised phenotype, whereas flot3 shows only a PM ROS phenotype. This suggests that FLOT3 is only involved in the PM chitin detection processes but not in the plasmodesmal responses. This could be a similar divergence to CERK1, which is only necessary for PM, but not for plasmodesmal PM-localised chitin-triggered responses (Faulkner et al., 2013). Whether or not the flotillin-dependent changes to plasmodesmal flux are caused by changes of callose deposition, such as the tetraspanin-dependent changes (Fig. 4-11), remains to be determined in future experiments.

Faulkner (2013) already speculates that SPFH domain proteins play a role in receptor localisation in membrane micro-/nanodomains and thereby possibly in plasmodesmal localisation. If flotillins indeed are responsible for receptor proteins localising to plasmodesmata, this could be tested in future experiments by crossing different plasmodesmal localised translational fusion constructs in a *flot1/2/3* background. To determine if the flotillin plasmodesmal phenotypes are chitin signalling specific or more general immune signalling phenotypes, future experiments should test this by utilising the same mutants and assay but using different MAMPs which trigger plasmodesmal closure in WT plants such as flg22 (Faulkner et al., 2013).

5.3.6 Flotillins are necessary plant defences against fungi

To determine whether the flotillin mutants not only show phenotypes differing from control plants in MAMP-triggered assays but when encountering a pathogen, leaves were inoculated with the fungus *B. cinerea*. These experiments revealed that *flot1* mutants exhibit bigger areas of chlorosis and *flot2* mutants exhibit bigger necrotic lesions 4 dpi compared to WT plants (Fig. 5-7). The enhanced susceptibility observed, allows to draw the conclusion that indeed FLOT1 as well as FLOT2 play an important role in enabling successful plant defence responses.

This is different from the results of Kroumanova et al. (2019), who present data of a similar assay on flotillin mutants where they did not observe a significant difference in lesion size between the mutants and their control plants. Differing experimental conditions could be a reason for this experimental variation, as they can cause different *B. cinerea* virulence (Ciliberti et al., 2015). For example, my experiments were carried out on detached leaves, while Kroumanova et al. (2019) inoculated leaves on plants, with further differences in sample size. A further difference between our experiments is the use of different *B. cinerea* strains. I used B05.10, while Kroumanova et al. (2019) used BMM. Different strains of *B. cinerea* can exhibit differences in virulence (Choquer et al., 2007), and this could be an explanation for these conflicting data.

Curiously *flot1* and *flot2* mutants showed differences in their susceptibility to *B. cinerea* in my experiments. In *flot2* mutants, only the area of the necrotic lesion was bigger compared to Col-0, *flot1* and *flot3*. Conversely, this was not the case in *flot1*, where the fungus caused bigger chlorotic areas, as estimated by the sum of the chlorotic as well as the necrotic lesion size, was significantly enlarged, compared to Col-0, *flot2* and *flot3*. This could hint at varying importance of FLOT1 and FLOT2 within the timeframe of fungal infections, as pathogenic fungi infecting plants undergo different stages of the infection process (Dean et al., 2012). They might be differently important during an initial asymptomatic phase of the infection. FLOT1 might be more important in the early onset detection of the fungus (Choquer et al., 2007; van Kan, 2006), thereby resulting in a larger colonised area in *flot1* mutants while FLOT2 could be more important in the activation of the HR (Govrin and Levine, 2000).

Even though *flot3* mutants showed a reduced chitin-triggered ROS burst (Fig. 5-5), no increase in fungal pathogen susceptibility for this mutant was observed (Fig. 5-7). This is not unsurprising as mutants of important chitin signalling machinery such as *lyk5-2* and *cerk1-2*,

also do not necessarily lead to a *B. cinerea* susceptibility phenotype, as their pathogen recognition machinery might still be sufficient to mount responses consistent with WT plants (Giovannoni et al., 2021). However, it is curious that *flot3* mutants also did not show a plasmodesmal flux phenotype differing from WT plants, whilst both *flot1* and *flot2* showed such a phenotype and these mutations also resulted in an enhanced susceptibility. This could possibly be due to functional diversification between FLOT3 and FLOT1/FLOT2, possibly reflected in the greater differences between FLOT3 when compared with FLOT1 or FLOT2 (Fig. 6-1A). In a simplified hypothesis this would allow to conclude that FLOT1 and FLOT2 are necessary for successful pathogen-triggered plasmodesmal flux reduction (Fig. 5-6), resulting in an increased resistance against the pathogen (Fig. 5-7), while FLOT3 is not necessary for this cellular adaptation. The reduction of the chitin-triggered ROS burst observed in the *flot3* mutant (Fig. 5-5) does not abolish chitin-triggered plasmodesmal closure. *B. cinerea* growth is not inhibited by H_2O_2-induced oxidative stress in planta (Temme and Tudzynski, 2009). Therefore, the reduction of the chitin-triggered ROS burst in *flot3* mutants might not have translated in an observable *B. cinerea* susceptibility effect, while the inability to adjust the plasmodesmal flux of *flot1* and *flot2* did.

Recent work on the protein structure of SPFH domain proteins revealed that they can achieve their nanodomain organisation by the formation of supramolecular complexes of highly homologous proteins of their own family (Ma et al., 2022). Given the high protein homology of FLOT1 with FLOT2 (95.4% sequence identity), plant flotillins could undergo similar multi-protein complex formations to enable the interactions with their partner proteins. Further, experiments in animal systems have observed that the stability of flotillin proteins is interdependent, whereby the absence of one leads to the reduction in protein levels of another (Babuke et al., 2009; Frick et al., 2007; Langhorst et al., 2008; Ludwig et al., 2010). Following this logic, the absence of an individual flotillin could possibly already upset any bigger structures formed by proteins of this family, depending on how much their redundancy might be able to rescue. Future experiments could start with the elucidation of these hypotheses by determining if all three of the plant flotillins indeed do interact with each other, such as by co-IPs or FRET-FLIM approaches.

5.3.7 Model of flotillins in chitin-triggered responses

Taking the data of this chapter together, enables to conceptualise a simplified model of how flotillins are important in chitin-triggered immune responses (Fig. 5-8). All three flotillins (FLOT1, FLOT2 and FLOT3) are necessary to achieve the full WT-like ROS burst. Using IP followed by Mass spectrometric analysis, FLOT1 and FLOT2 showed to enhance their association with LYK4 in the presence of chitin, and their inability to adapt their plasmodesmal flux triggered by chitin showed that they are important for the regulation of plasmodesmal flux, even though there is no conclusive evidence that they themselves are enriched at plasmodesmata. These functional differences suggests that FLOT3 is present in different nanodomains than the other flotillins, and possibly completely absent at plasmodesmata. Following this logic, FLOT1 and FLOT2 could either mark the same or different nanodomains.

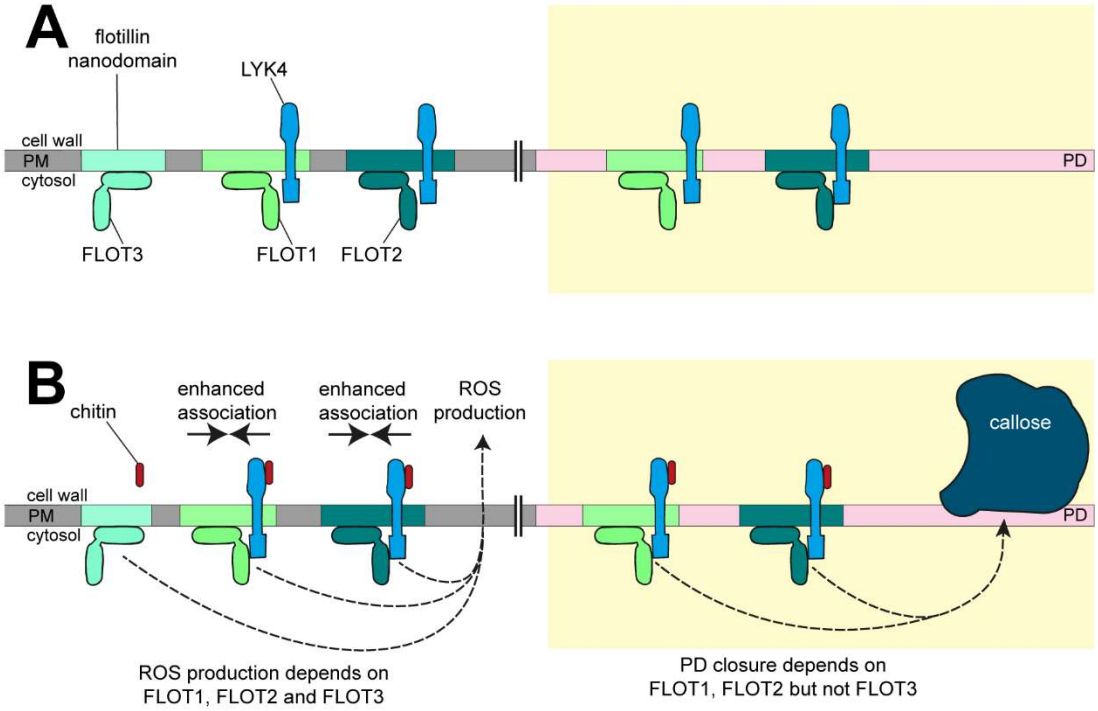

Figure 5-8: A possible model for receptor-flotillin mediated chitin-triggered immune signalling with a focus on the plasmodesmal response. This schematic representation is drawn as a continuity between the PM (grey), the plasmodesmal PM microdomain (light pink), and both include flotillin defined nanodomains (different shades of green). Different receptor complex combinations can be present such as the association between LYK4-FLOT1 and LYK4-FLOT2. The flotillins are not enriched at plasmodesmata but might still be present within them. (A) Resting state conditions in the absence of chitin. (B) Chitin-triggered conditions. In the presence of chitin, the mass spectrometry interactor screen of LYK4 revealed an enhanced association between LYK4-FLOT1 and LYK4-FLOT2. The ability to elicit a full chitin-triggered ROS burst depends on all three flotillins (FLOT1, FLOT2 and FLOT3). By contrast the chitin triggered plasmodesmal closure depends only on FLOT1 and FLOT2, but not on FLOT3. (A) & (B) PM: plasma membrane; PD: plasmodesmata.

5.3.8 Conclusion

The data presented in this chapter provides some key steppingstones in the advancement of our knowledge of plant pathogen recognition and signalling processes. I have determined that a family of nanodomain-localised proteins — the flotillins — not only show associate with a PRR, but themselves are necessary for optimal signalling and defence responses against pathogens, and in particular in the pathogen-triggered regulation of plasmodesmata. Thereby I have added new components to these signalling pathways. This contribution to scientific knowledge will allow further hypotheses to be formulated and research questions to be built upon it, ultimately further enabling our efforts as a scientific community in understanding the plant immune system.

6 Final Discussion

6.1.1.1 Total summary and theories of nanodomains

In this work I demonstrated that proteins of the tetraspanin and flotillin families are important for chitin-triggered plasmodesmal regulation. I observed different dynamics between receptors, receptors with tetraspanins and receptors with flotillins, and have sorted this information into one comprehensive model (Fig. 6-1).

I showed that TET3, TET7 and TET8 can exhibit an enhanced localisation at plasmodesmata over their localisation at the rest of the PM (Fig. 4-4), while there is little evidence that flotillins localise at plasmodesmata too (Fig. 5-1). I demonstrated that LYK4 can associate with TET3, TET7 and TET8 (chapter 4.2.9) as well as with FLOT1 and FLOT2 (Fig. 5-3). This association might be important in ensuring the presence of LYK4 in the appropriate nanodomains together with the appropriate partner proteins. The tetraspanin and flotillin proteins, might act as a scaffold for LYK4 and its associated proteins, and thereby ensure the appropriate protein composition of plasmodesmal PM microdomains.

I revealed contrasting dynamics between the involvement of these nanodomain resident proteins in chitin-triggered responses. For example, the mass spectrometry data suggests that chitin triggers a stronger association between LYK4 and FLOT1 and FLOT2 (Table 7-4). By contrast via FRET-FLIM data I observed a chitin-triggered enhanced dissociation between LYK4 and TET7 (Fig. 4-14) within the PM. This suggests that these processes might be spatially separate from each other, e.g. a TET7 marked nanodomain might release LYK4, while a FLOT1/FLOT2 marked nanodomain might take up more LYK4 triggered by chitin. Different distinct populations of nanodomains do exist within the same PM (Bücherl et al., 2017), allowing for the hypothetical existence of different tetraspanin and flotillin nanodomains in the PM. This could be extended into further differences between the PM and the PD nanodomains. Therefore, different associations and dynamics for LYK4 in its nanodomain associations could be conceivable even when comparing the PM and PD.

The FRET-FLIM observation that chitin triggers an enhanced dissociation between LYK4 and TET7 (Fig. 4-14), combined with the IP mass spectrometry data showing an enhanced detection of FLOT1 and FLOT2 (Table 5-1) allows for further speculations. Possibly LYK4 is primarily associated with a tetraspanin defined nanodomain, from where it dissociates or gets released triggered by chitin. In turn this might then allow either for an active or passive increase of LYK4 in a flotillin defined nanodomain. This ‘handoff’ hypothesis might be too

simplified to accurately represent the reality. However, it may be a good hypothesis as a starting point to design future research activities which will allow for further unravelling.

TET7 and TET8 have the potential to interact with each other using split-ubiquitin assays yeast (Boavida et al., 2013). Whether they also do so *in planta* and at all times is still an open question. Zuidscherwoude et al. (2015) determined that the more historical way of thinking that tetraspanin defined domains would consist of different tetraspanin species is not holding up to closer examination and that it is rather likely that single tetraspanin protein species form such platforms without other tetraspanin species partners. Possibly TET7 and TET8 could therefore associate with each other, but their association might not be important or relevant for their respective domains.

Further FLOT1 and FLOT3 can interact with each other in split-ubiquitin assays (Yu et al., 2017), and SPFH domain proteins have the potential to interact with other members of the same family to achieve their scaffolding functions (Ma et al., 2022). However, the potential to interact or associate with each other does not always have to translate into the simultaneous presence in the same nanodomain *in planta*.

From experiments carried out in a transient *N. benthamiana* expression system, I determined that LYK4 is associating with both tetraspanins as well as flotillins independently of the presence of chitin. This consistent association might not be representative of the full underlying dynamics, as the transient overexpression system might not be as sensitive to important dynamic changes as native levels of proteins in their native system. Particularly as I observed functional differences between the scaffolding proteins, a simple hypothesis would be to cluster them into differently functional nanodomains (Fig. 6-1). These nanodomains might be dynamic in their temporal and spatial distribution and function and might also recruit or exclude different components triggered by chitin.

Further components and interactions might be vital for the functions of tetraspanin or flotillin nanodomains. FLOT1, FLOT2, FLOT3, TET7, and TET8 are necessary to achieve the full chitin-triggered ROS burst caused by RBOHD at the PM. RBOHD is localised to nanodomains (Noirot et al., 2014) and might show a dynamic association with those tetraspanin/flotillin nanodomains and might, always be present within them, be triggered by chitin to become resident in them or be excluded from them once it is activated.

Even though I was able to determine general trends between flotillin and tetraspanin proteins in chitin-triggered immune signalling, I observed some critical differences that

suggest members these protein families to function differently in chitin signalling. Particularly striking are the differences in the phenotypes of *flot3* and *tet3*. While FLOT3 is necessary for WT-like levels of chitin-triggered ROS bursts at the PM (Fig. 5-5), TET3 is not necessary to achieve this (Fig. 4-9). They further show an inverse phenotype of plasmodesmal regulation, as TET3 is vital to achieve a chitin-triggered reduction of plasmodesmal flux (Fig. 4-10), but *flot3* shows WT-like plasmodesmal responses to chitin (Fig.5-6). These inverse phenotypes point towards a differentiation between the tetraspanin-flotillin-marked nanodomains at the PM, and the tetraspanin-flotillin-marked nanodomains within plasmodesmata, possibly due to different inclusion or exclusion of other proteins.

Collectively this work has enabled the formulation of a first understanding and model of protein associations (Fig. 6-1) important for chitin-triggered immunity and how vital nanodomain resident scaffolding proteins can be for these signalling and response processes. However, there are still a lot of dynamics and processes which are very little understood, and I will discuss some of them as well as some suggested experimental approaches to unravel them, in the text below.

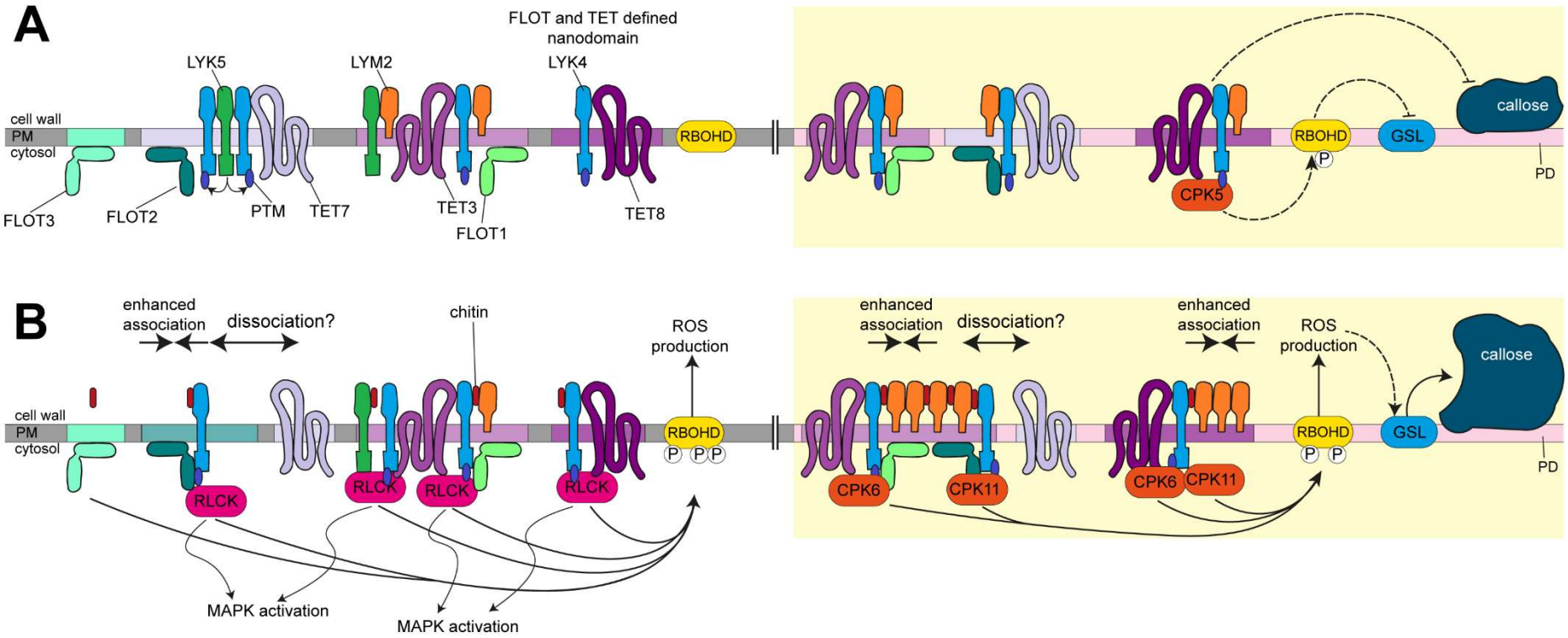

Figure 6-1: A holistic simplified model for receptor mediated chitin-triggered immune signalling in context of associations with flotillins and tetraspanins and a focus on the plasmodesmal response. This schematic representation is drawn as a continuity between the PM (grey), which includes tetraspanin and flotillin defined nanodomains (different shades of green and purple), and the plasmodesmal PM microdomain (light pink). LYM2, LYK4, TET3, TET7 and TET8 can be present at plasmodesmata, while there is no data showing the presence of CERK1, or LYK5 at plasmodesmata. Flotillins have not shown an enrichment at plasmodesmata, but FLOT1 and FLOT2 are functionally important and might be present at plasmodesmata. A multitude of different protein associations has been observed such as LYK4-LYK5, LYK5-LYM2, LYK4-LYM2, LYK4-TET3, LYK4-TET7, LYK4-TET8, LYK4-FLOT1, LYK4-FLOT2. (A) During resting state conditions, in the absence of chitin, CPK5 and TET8 are inhibiting the deposition of callose at plasmodesmata. (B) Chitin triggers an enhanced association between LYK4-FLOT1 and LYK4-FLOT2, whilst changing the dynamics between LYK4 and the tetraspanins. Chitin further triggers an enrichment and higher order of LYM2 at plasmodesmata. Both at the plasmodesmata as well as in the PM, the activation of RBOHD is triggered by phosphorylation, but on different sites and depending on different kinases such as CKP6 and CPK11 within the plasmodesmal PM microdomain. The cytoplasmic kinases also trigger further cellular responses such as the MAPK cascades. This model is a summary of the models shown in Fig. 3-14, 4-21, 5-8. PM: plasma membrane; PD: plasmodesmata, PTM: post-translational modification; P: phosphorylation, GSL: GLUCAN SYNTHASE-LIKE = callose synthases; RLCK: receptor-like cytoplasmic kinases.

6.2 Further considerations, questions, and proposals

6.2.1 Involvement of TETs/FLOTs in other immune responses

I have tested mutants of tetraspanins and flotillins for impairments in a selection of the signalling and response processes triggered by chitin. However, chitin does trigger further cellular processes in WT plants, and future experiments could ask questions focussed on those. For example, the chitin-triggered activation of the MAPK cascade in tetraspanin and flotillin mutants could be assessed using a SDS-PAGE and Western blots approach with antibodies specific to changes to the phosphorylation status of p44/42 MAPK. Or RNA-sequencing experiments on these tetraspanin and flotillin mutants during chitin perception, could be carried out to elucidate differences in gene regulation caused by the absence of these scaffolding proteins.

6.2.2 Roles of TETs/FLOTs in other pathogen contexts

In this work I studied the dynamics and associations of receptors, tetraspanins and flotillins in response to chitin and from a plant-pathogen interaction point of view. However, other MAMPs are also important for the perception of pathogens and during the initiation of symbiosis. For these processes other PRR such as FLS2, EFR, or MtLYK3 are necessary. This opens the question of if, the tetraspanin-LYK4, and flotillin-LYK4 association is specific to LYK4, or also possible with other PRRs and a rather universal mechanism in plant signalling? Does the functionality of other PRRs in plants also depend on flotillins and tetraspanins? And if so, do these PRR also associate with these scaffolding proteins? If this is the case, then the functions and roles of these proteins could allow us to further our understanding of PM localised receptor-mediated signalling processes by vital components. This specificity between scaffolding protein-receptor interaction might be necessary for engineered resistance approaches or for the transfer of functionality of PRR systems from one plant species to another.

These questions could be answered in two different lines of experiments. In an extended chitin-perception context, it would be interesting to see if tetraspanins and flotillins interact with other non-LYK4 chitin PRRs, such as LYM2, LYK5, or CERK1, thereby showing that for scaffolding proteins are important for all PRRs involved in chitin perception. Dynamics of

other PRRs, could be investigated in by using the scaffolding mutants described in this work, and assessing their phenotypes elicited by different MAMPs, such as flg22 or elf18. Similarly, they could also be tested for their susceptibility to different pathogens such as *Pseudomonas syringae*. As flotillins have already shown to be involved in the perception of bacterial symbionts in *M. truncatula (Liang et al., 2018)*, it allows speculation that this protein family might also be important for the perception of bacteria in a pathogenic context — thereby making flg22 an ideal further first candidate MAMP to test. If the tetraspanin or flotillin mutants indeed show differences to WT plants such as ROS bursts or plasmodesmal flux regulation, the RKs and RPs known to be involved in these processes could be screened and assessed for their interactions with the relevant tetraspanins or flotillins.

6.2.3 PTM in a receptor-scaffolding context

6.2.3.1 Assessing the role of PTM of TETs/FLOTs

Both plant tetraspanins and flotillins possess putative S-acylation sites (Borner et al., 2005; Wang et al., 2012a). These sites have been shown to be important for the micro-/nanodomain localisation of tetraspanins (Charrin et al., 2002; Hemler, 2005) as well as the interaction with tetraspanin partner proteins (Mazurov et al., 2007) in animal model systems. S-acylation can be important for enabling a network of secondary interactions between both tetraspanins as well as tetraspanin associated proteins (Berditchevski et al., 2002; Charrin et al., 2002; Clark et al., 2004; Hemler, 2005; Yang et al., 2002), thereby ensuring both the appropriate domain stability as well as its appropriate components.

As plasmodesmata are a specialised PM microdomain and show enrichment of tetraspanins, this localisation could be dependent on S-acylation of tetraspanins as well. Possibly the fatty acid addition could allow for different preferential localisation in more lipophilic environment, such as hypothetically a plasmodesmata or other micro- and nanodomains. Different chain lengths of this PTM might further allow for more fine control in protein localisations. Mutations of cysteine sites necessary for S-acylation, result in proteins unable to undergo this PTM (Hurst et al., 2021). Mutating tetraspanins in such a way, could be used to test if such proteins still localise to plasmodesmata or not, and whether mutated variants functionally complement the tetraspanin mutants.

These mutated proteins could also further be used to ask if the scaffolding protein-receptor interaction depends on S-acylation. As well as if the non- S-acylation proteins can complement knock-out phenotypes or not and if this PTM therefore is essential for the function of these scaffolding proteins. The resources produced to answer these questions

could then further be used to assess if the PM nanodomain localisations and MAMP-triggered dynamics of domains marked by these proteins depend on S-acylation as well.

6.2.3.2 Could scaffolding proteins be important for LYK4 PTMs?

In Cheval et al. (2020) we observed a PTM of LYK4, which is dependent on the presence of LYK5, and possibly important for chitin-triggered LYK4 mediated plasmodesmal closure. However, could this PTM also be dependent on other proteins interacting with LYK4, such as tetraspanins and flotillins? To answer this question a LYK4 fluorophore translational fusion Arabidopsis line, such as the *pLYK4::LYK4-mCherry* generated in this work could be crossed into different scaffolding protein mutant backgrounds, and the presence or absence of the PTM could be assessed by measuring size differences using SDS-PAGE and Western blots. The exact nature of this PTM is still unknown and further approaches could be undertaken in future experiments to determine it — such as using tandem mass spectrometry (MS/MS) as an unbiased approach, and *in vitro* assays for phosphorylation, ubiquitination, and SUMOylation. Once all of the PTMs of LYK4 are determined, a systematic evaluation of which one(s) is dependent on LYK5 could be undertaken, by expressing and comparing *pLYK4::LYK4-mCherry* in *lyk4* with *lyk5-2* mutants.

6.2.4 Differences between nanodomains

In this work I focussed on only three candidates of the tetraspanin family. However, there are in total 17 canonical tetraspanins in Arabidopsis (Cnops et al., 2006) (Fig. 4-3), and it is likely that some of these might also play a role during pathogen perception and signalling processes. Alternatively, they might also play roles in general membrane features which in turn influence such processes. They might therefore be direct or indirect players. Further candidates should therefore be additionally assessed in future work, even if they were out of the scope for this work.

6.2.4.1 Do different scaffolding proteins mark different nanodomains?

For the generation of my models on how scaffolding proteins of the flotillin and tetraspanin families localise within nanodomains depending on LYK4, I assumed the simplest model, which resulted in these proteins being present in different nanodomains (Fig. 6-1). However, this might not be the case. It is conceivable that LYK4 is resident in multiple different nanodomains in the PM marked by different scaffolding proteins, or at different preferences and ratios. So, might LYK4 be resident in multiple different nanodomains? Or are all of these scaffolding proteins capable of being present in the same domains? Could they form a complex mesh-like structure instead of small domains? How do different scaffolding proteins define a separation between each others' nanodomains if there are different nanodomains? And how do the dynamics of those domains change — particularly during MAMP perception such as chitin? The use of advanced imaging techniques such as VAEM will allow to ask and answer these questions.

Even within the same scaffolding protein family, the different proteins could be present in different nanodomains. For example, as TET3 is not required for chitin-triggered ROS bursts it might not be present within the same nanodomain in the PM as TET7 or TET8, which are required for this response. It will therefore be very informative to see if all of these proteins truly are present within the same distinct nanodomains, in how many different types of nanodomains they exist and how these behave. Advanced microscopy techniques such as VAEM or TIRF could allow for such an assessment. These techniques allow for a greater resolution than standard CLSM techniques and thereby allow to resolve areas of greater density and enrichment of translational fusion proteins with fluorescent tags. Thereby enabling to study their domain distribution, sizes, dynamics, and correlation. Particularly the direct comparisons for multiple protein species at the same time with VAEM or TIRF will allow how to determine how their dynamics differ from one to another.

6.2.4.2 Do changes to receptors affect their nanodomain localisation?

In this work I reported evidence that LYK4 and LYK5 undergo cleavage of their ectodomains (Fig. 3-11), resulting in at least two different populations of these proteins being present at the PM. Depending on which of their domains are responsible for their putative nanodomain localisation and association with tetraspanins and flotillins, this cleavage reaction might change their localisations and dynamics as elucidated with FRAP (Fig. 3-3). These differences could be elucidated by either directly determining the cleavage mechanism and site, followed by the generation of non-cleavable mutant proteins, or by generating cleavage-mimic proteins which do not carry the cleavable ectodomain. Translational fusions with fluorophores of these variant proteins would then allow to test hypotheses of different protein mobility behaviour by FRAP, followed by nanodomain localisations and dynamics by utilising techniques such as VAEM.

6.2.4.3 Scaffolding proteins in ROS production

I have demonstrated that TET7, TET8, FLOT1, FLOT2 and FLOT3 are necessary to achieve WT-like levels of chitin-triggered ROS production. Putatively this is due to their ability to interact with a chitin receptor such as LYK4 and thereby to define its interaction possibilities with other proteins. An additional hypothesis could be that these scaffolding proteins are also responsible for the localisation of the ROS producing enzyme RBOHD. RBOHD was reported to be present in PM domains (Hao et al., 2014; Noirot et al., 2014). The simplest unifying hypothesis would therefore be that RBOHD is resident within the same nanodomains as tetraspanins and flotillins, thereby enabling efficient signalling processes. Alternatively, RBOHD could also be present in a different nanodomain and treatment with chitin triggers its release from this domain or the RBOHD hosting nanodomain to fuse with the receptor hosting nanodomain. Such an example could be if the receptors are predominantly present in tetraspanin defined nanodomains and RBOHD in a flotillin-defined nanodomain pre-chitin-treatment. Upon chitin treatment, these two nanodomains could undergo fusion/merging processes, thereby allowing for spatial and temporal separation and control of the signalling responses. Such dynamics between the receptors, the scaffolding proteins and RBOHD could be observed using VAEM (Bücherl et al., 2017), or FRET-FLIM, and further interactions between these proteins could be determined by co-IPs.

6.2.4.4 Other proteins present at TET/FLOT nanodomains

In this work I showed that LYM2, LYK4 and LYK5 can associate with each other, and that LYK4 can associate with TET3, TET7, TET8, FLOT1 and FLOT2. However, I have not yet gone into greater detail and tested whether LYM2 or LYK5 also associate with these scaffolding proteins, or if they might show different behaviours and dynamics. As LYM2 exhibited a higher mobile fraction in FRAP experiments in comparison to LYK4 or LYK5 (Fig. 3-3), it seems likely that at least pools of these proteins localise to different nanodomains or show generally a different nanodomain localisation preference pattern.

Even though I focussed on tetraspanins and flotillins as scaffolding proteins within this work, there are more scaffolding proteins such as other proteins of the SPFH superfamily and REMs, which could also interplay with these nanodomains. Although these are again interesting hypotheses, they were outside of the scope of this work.

Further, not only scaffolding proteins or individual receptors are present at nanodomains, but rather a plethora of other proteins might be present within them too. To elucidate these proteins, I propose that future experiments should be carried out as mass spectrometry based approaches using different scaffolding proteins as bait for immunoprecipitations, to determine an overview of proteins populating these nanodomains. As the presence and association within nanodomains might be short-lived particularly during elicitor-triggered processes, the use of turbo-ID (an optimised variant of BirA) (Arora et al., 2020) could be an excellent additional tool for this purpose.

6.2.5 Do higher order mutants result in stronger phenotypes?

In this work I have used single mutants to show phenotypes in chitin-triggered response processes. Some of these processes were completely disrupted such as the chitin-triggered plasmodesmal closure in *tet3*, *tet7*, *flot1* and *flot2*. Others however only showed a reduction from WT-like levels such as the chitin-triggered ROS burst which did not get abolished in any of the mutants. If scaffolding proteins of a high similarity such as other tetraspanin proteins in single tetraspanin mutants or other flotillins proteins in single flotillin mutants, can to a certain degree rescue the loss of functions caused by single mutations, I would expect mutants higher order to show an increase in phenotypes such as the chitin-triggered ROS burst.

For this purpose, I had started to generate double and triple mutants of the three Arabidopsis flotillin genes. Further tetraspanin mutants of a higher order could be generated by CRISPR or crossing approaches as well. These mutants can then be used in future experiments to assess the importance of these scaffolding proteins even further.

6.2.6 Are scaffolding proteins important for receptor sorting?

Little is known about how proteins are sorted to and localise to plasmodesmata. However, curious phenomena have been observed such as LYM2 showing a chitin-triggered enrichment at plasmodesmata over the PM (PD index), and a chitin-triggered increase in homo-FRET suggestive of the formation of higher order complexes (Cheval et al., 2020). Tetraspanins do not undergo such a chitin-triggered increase in their PD index (Figure 4-10). However, they and other scaffolding proteins might still be vital for this process as well as the general plasmodesmal localisation of other proteins. To assess if this is indeed dependent on scaffolding proteins, lines expressing translational fusions with fluorophores of important plasmodesmal signalling components such as LYM2 (Cheval et al., 2020; Faulkner et al., 2013), NHL3 (M. Johnston, PhD thesis), CML41 (Xu et al., 2017) and PDLP5 (Wang et al., 2013) could be crossed into scaffolding protein mutants — particularly mutants higher order to fast-track overall assessment — and tested whether they maintain their plasmodesmal localisations and MAMP-triggered behaviour in these mutant backgrounds.

6.2.7 The complexity of nanodomains and scaffolding proteins

As I have shown in this work, the roles, interactions, and localisations of scaffolding proteins and in particular the dynamics of putative nanodomains is not trivial nor simple. To further complicate the matter most eukaryotic organisms, have a plethora of different scaffolding proteins which all in theory could be important or relevant for nanodomain maintenance, as well as protein functions and interactions. This is particularly illustrated by proteins of the tetraspanin family. There are 33 tetraspanins in humans (Huang et al., 2005) and 17 canonical tetraspanins encoded in Arabidopsis (Cnops et al., 2006). Most of which have the ability to interact with each other (Boavida et al., 2013), making analysis and interpretation of individual tetraspanin importance convoluted.

Future studies could therefore make use of model systems which have even fewer tetraspanin genes, such as *Marchantia polymorpha*, which only has three tetraspanin genes (EnsemblPlants, Howe et al. (2020)). This could help advance research into plant scaffolding proteins in an even faster and clearer manner. Currently the research into plant scaffolding proteins and nanodomains is profiting of a vast amount of knowledge already determined in animal and fungal model systems. However, my data has laid a foundation to start the generation of further understanding of these processes in plants, to the point that one day the animal research community will profit off new insights generated in plants as well.

7 Appendices

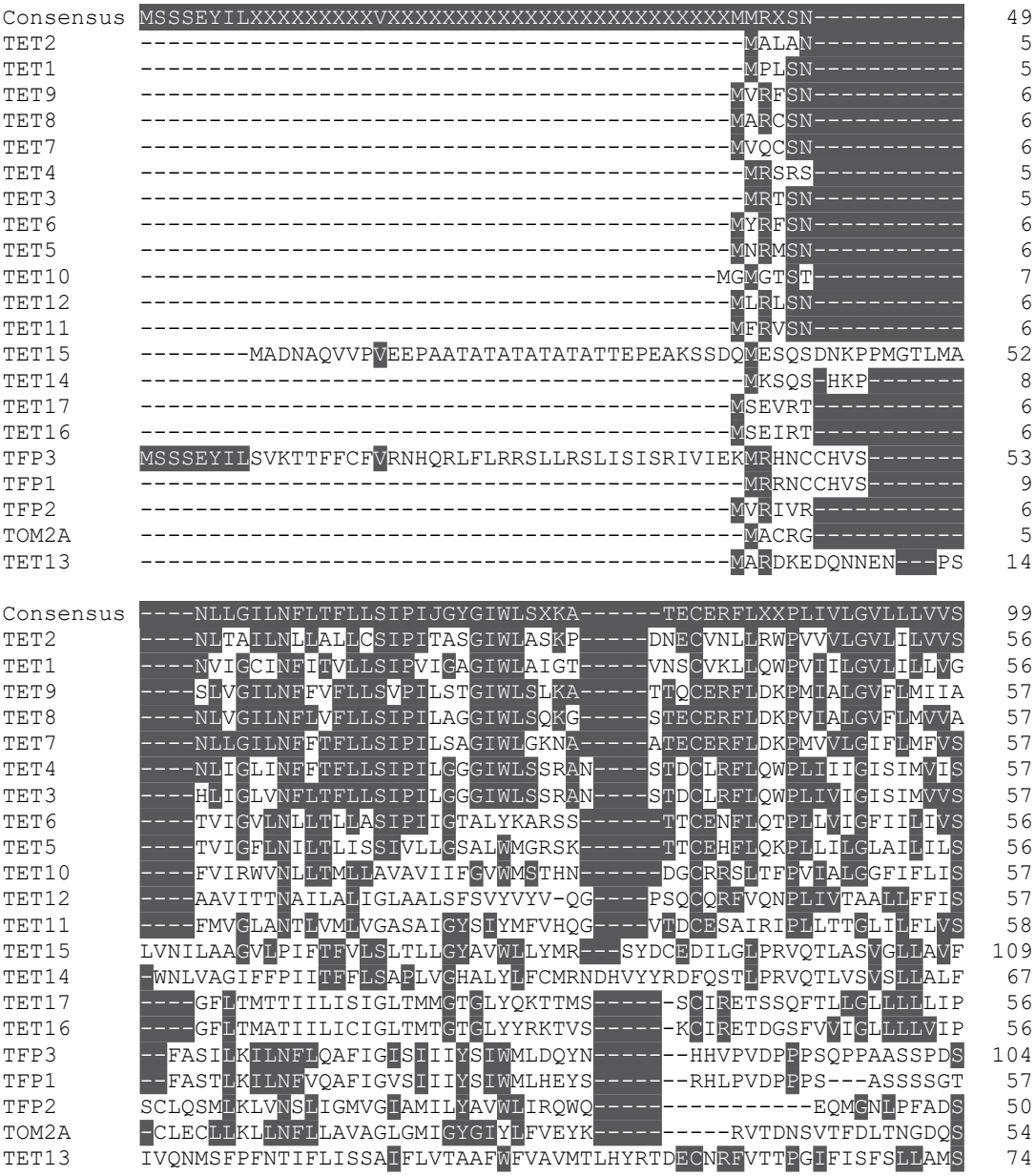

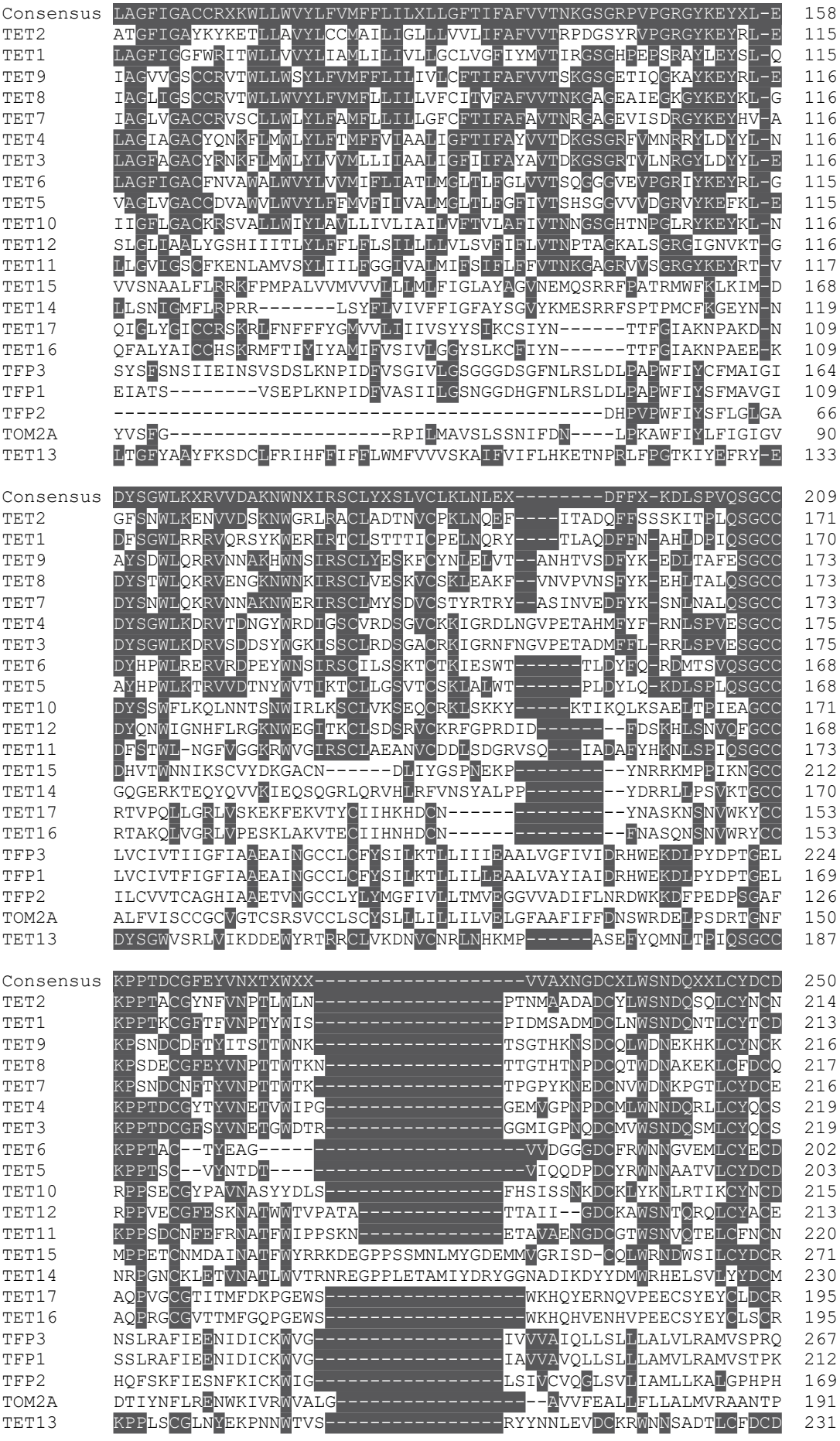
Consensus LAGFIGACCRXKWLLWVYLFVMFFLILXLLGFTIFAFVVTNKGSGRPVPGRGYKEYXL-E 158
TET2 ATGFIGAYKYKETLLAVYLCCMAILIGLLLVVLIFAFVVTRPDGSYRVPGRGYKEYRL-E 115
TET1 LAGFIGGFWRITWLLVVYLIAMLILIVLLGCLVGFIYMVTIRGSGHPEPSRAYLEYSL-Q 115
TET9 IAGVVGSCCRVTWLLWSYLFVMFFLILIVLCFTIFAFVVTSKGSGETIQCKAYKEYRL-E 116
TET8 IAGLIGSCCRVTWLLWVYLFVMFLLILLVFCITVFAFVVTNKGAGEAIECKGYKEYKL-G 116
TET7 IAGLVGACCRVSCLLWLYLFAMFLLILLGFCFTIFAFAVTNRGAGEVISDRGYKEYHV-A 116
TET4 LAGIAGACYQNKFLMWLYLFTMFFVIAALIGFTIFAYVVTDKGSGRFVMNRRYLDYYL-N 116
TET3 LAGFAGACYRNKFLMWLYLVVMLLIIAALIGFIIFAYAVTDKGSGRTVLNRGYLDYYL-E 116
TET6 LAGFIGACFNVAWALWVYLVVMIFLIATLMGLTLFGLVVTSQGGGVEVPGRIYKEYRL-G 115
TET5 VAGLVGACCDVAWVLWVYLFFMVFIIVALMGLTLFGFIVTSHSGGVVVDGRVYKEFKL-E 115
TET10 IIGFLGACKRSVALLWIYLAVLLIVLIAILVFTVLAFIVTNNGSGHTNPGLRYKEYKL-N 116
TET12 SLGLIAALYGSHIIITLYLFFLFLSILLLLVLSVFIFLVTNPTAGKALSGRGIGNVKT-G 116
TET11 LLGVIGSCFKENLAMVSYLIILFGGIVALMIFSIFLFFVTNKGAGRVVSGRGYKEYRT-V 117
TET15 VVSNAALFLRRKFPMPALVVMVVVLLLMLFIGLAYAGVNEMQSRRFPATRMWFKLKIM-D 168
TET14 LLSNIGMFLRPRR-------LSYFLVIVFFIGFAYSGVYKMESRRFSPTPMCFKGEYN-N 119
TET17 QIGLYGICCRSKRLFNFFFYGMVVLIIVSYYSIKCSIYN------TTFGIAKNPAKD-N 109
TET16 QFALYAICCHSKRMFTIYIYAMIFVSIVLGGYSLKCFIYN------TTFGIAKNPAEE-K 109
TFP3 SYSFSNSIIEINSVSDSLKNPIDFVSGIVLGSGGGDSGFNLRSLDLPAPWFIYCFMAIGI 164
TFP1 EIATS--------VSEPLKNPIDFVASIILGSNGGDHGFNLRSLDLPAPWFIYSFMAVGI 109
TFP2 --DHPVPWFIYSFLGLGA 66
TOM2A YVSFG---------------------RPILMAVSLSSNIFDN----LPKAWFIYLFIGIGV 90
TET13 LTGFYAAYFKSDCLFRIHFFIFFLWMFVVVSKAIFVIFLHKETNPRLFPGTKIYEFRY-E 133
Consensus DYSGWLKXRVVDAKNWNXIRSCLYXSLVCLKLNLEX--------DFFX-KDLSPVQSGCC 209
TET2 GFSNWLKENVVDSKNWGRLRACLADTNVCPKLNQEF----ITADQFFSSSKITPLQSGCC 171
TET1 DFSGWLRRRVQRSYKWERIRTCLSTTTICPELNQRY----TLAQDFFN-AHLDPIQSGCC 170
TET9 AYSDWLQRRVNNAKHWNSIRSCLYESKFCYNLELVT--ANHTVSDFYK-EDLTAFESGCC 173
TET8 DYSTWLQKRVENGKNWNKIRSCLVESKVCSKLEAKF--VNVPVNSFYK-EHLTALQSGCC 173
TET7 DYSNWLQKRVNNAKNWERIRSCLMYSDVCSTYRTRY--ASINVEDFYK-SNLNALQSGCC 173
TET4 DYSGWLKDRVTDNGYWRDIGSCVRDSGVCKKIGRDLNGVPETAHMFYF-RNLSPVESGCC 175
TET3 DYSGWLKDRVSDDSYWGKISSCLRDSGACRKIGRNFNGVPETADMFFL-RRLSPVESGCC 175
TET6 DYHPWLRERVRDPEYWNSIRSCILSSKTCTKIESWT------TLDYFQ-RDMTSVQSGCC 168
TET5 AYHPWLKTRVVDTNYWVTIKTCLLGSVTCSKLALWT------PLDYLQ-KDLSPLQSGCC 168
TET10 DYSSWFLKQLNNTSNWIRLKSCLVKSEQCRKLSKKY-----KTIKQLKSAELTPIEAGCC 171
TET12 DYQNWIGNHFLRGKNWEGTTKCLSDSRVCKRFGPRDID-------FDSKHLSNVQFGCC 168
TET11 DFSTWL-NGFVGGKRWVGIRSCLAEANVCDDLSDGRVSQ---IADAFYHKNLSPIQSGCC 173
TET15 DHVTWNNIKSCVYDKGACN------DLIYGSPNEKP---------YNRRKMPPIKNGCC 212
TET14 GQGERKTEQYQVVKIEQSQGRLQRVHLRFVNSYALPP--------YDRRLLPSVKTGCC 170
TET17 RTVPQLLGRLVSKEKFEKVTYCIIHKHDCN------------YNASKNSNVWKYCC 153
TET16 RTAKQLVGRLVPESKLAKVTECIIHNHDCN------------FNASQNSNVWRYCC 153
TFP3 LVCIVTIIGFIAAEAINGCCLCFYSILKTLLIIIEAALVGFIVIDRHWEKDLPYDPTGEL 224
TFP1 LVCIVTFIGFIAAEAINGCCLCFYSILKTLLILLEAALVAYIAIDRHWEKDLPYDPTGEL 169
TFP2 ILCVVTCAGHIAAETVNGCCLYLYMGFIVLLTMVEGGVVADIFLNRDWKKDFPEDPSGAF 126
TOM2A ALFVISCCGCVGTCSRSVCCLSCYSLLLILLILVELGFAAFIFFDNSWRDELPSDRTGNF 150
TET13 DYSGWVSRLVIKDDEWYRTRRCLVKDNVCNRLNHKMP------ASEFYQMNLTPIQSGCC 187
Consensus KPPTDCGFEYVNXTXWXX------------------VVAXNGDCXLWSNDQXXLCYDCD 250
TET2 KPPTACGYNFVNPTLWLN-----------------PTNMAADADCYLWSNDQSQLCYNCN 214
TET1 KPPTKCGFTFVNPTYWIS-----------------PIDMSADMDCLNWSNDQNTLCYTCD 213
TET9 KPSNDCDFTYITSTTWNK-----------------TSGTHKNSDCQLWDNEKHKLCYNCK 216
TET8 KPSDECGFEYVNPTTWTKN----------------TTGTHTNPDCQTWDNAKEKLCFDCQ 217
TET7 KPSNDCNFTYVNPTTWTK-----------------TPGPYKNEDCNVWDNKPGTLCYDCE 216
TET4 KPPTDCGYTYVNETVWIPG----------------GEMVGPNPDCMLWNNDQRLLCYQCS 219
TET3 KPPTDCGFSYVNETGWDTR----------------GGMIGPNQDCMVWSNDQSMLCYQCS 219
TET6 KPPTAC--TYEAG-----------------------VVDGGGDCFRWNNGVEMLCYECD 202
TET5 KPPTSC--VYNTDT----------------------VIQQDPDCYRWNNAATVLCYDCD 203
TET10 RPPSECGYPAVNASYYDLS----------------FHSISSNKDCKLYKNLRTIKCYNCD 215
TET12 RPPVECGFESKNAIWWTVPATA-------------TTAII--GDCKAWSNTQRQLCYACE 213
TET11 KPPSDCNFEFRNATFWIPPSKN-------------ETAVAENGDCGTWSNVQTELCFNCN 220
TET15 MPPETCNMDAINATFWYRRKDEGPPSSMNLMYGDEMMVGRISD-CQLWRNDWSILCYDCR 271
TET14 NRPGNCKLETVNAILWVTRNREGPPLETAMIYDRYGGNADIKDYYDMWRHELSVLYYDCM 230
TET17 AQPVGCGTITMFDKPGEWS-----------------WKHQYERNQVPEECSYEYCLDCR 195
TET16 AQPRGCGVTTMFGQPGEWS-----------------WKHQHVENHVPEECSYEYCLSCR 195
TFP3 NSLRAFIEENIDICKWVG-----------------IVVVAIQLLSLLLALVLRAMVSPRQ 267
TFP1 SSLRAFIEENIDICKWVG-----------------IAVVAVQLLSLLLAMVLRAMVSTPK 212
TFP2 HQFSKFIESNFKICKWIG-----------------LSIVCVQGLSVLIAMLLKALGPHPH 169
TOM2A DTIYNFLRENWKIVRWVALG-----------------AVVFEALLFLLALMVRAANTP 191
TET13 KPPLSCGLNYEKPNNWTVS-----------------RYYNNLEVDCKRWNNSADTLCFDCD 231

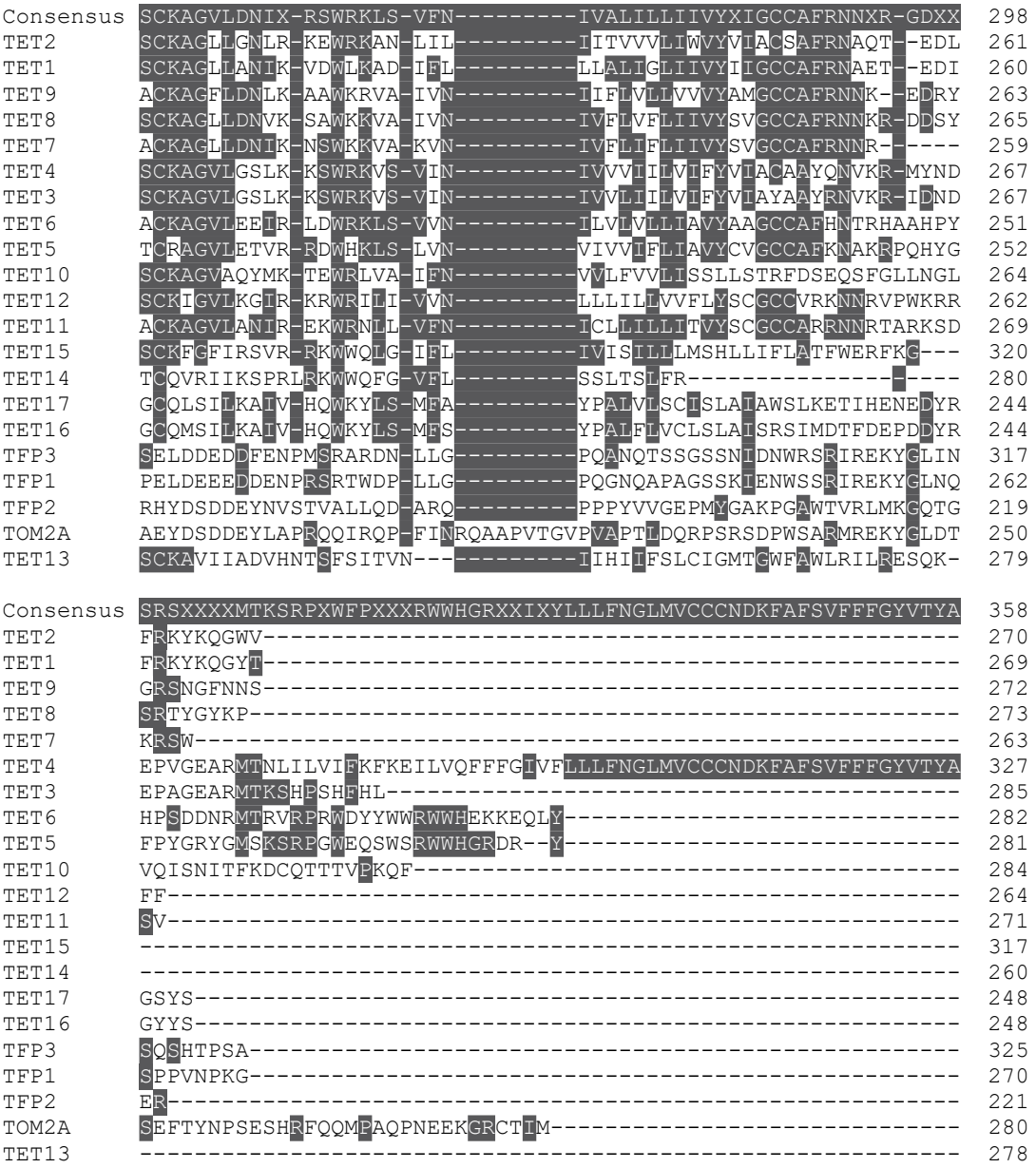

Figure 7-1: Alignment of the tetraspanin protein family. This alignment was created using Geneious Prime® 2019.2.3, with the ClustalW Alignment tool (ClustalW 2.1), applying the cost matrix BLOSUM, with a gap open cost of 10, and a gap extended cost of 0.1.

Table 7-1: Genetic distance of proteins of the tetraspanin family. This table has been created from the protein alignment information of Fig. 7-1.

	TET2	TET1	TET9	TET8	TET7	TET4	TET3	TET6	TET5	TET10	TET12	TET11	TET15	TET14	TET17	TET16	TFP3	TFP1	TFP2	TOM2A	TET13
TET2		51.48%	35.90%	42.49%	40.07%	38.63%	41.52%	36.76%	35.29%	30.40%	27.57%	34.43%	17.01%	12.82%	12.64%	11.90%	9.86%	7.75%	8.70%	8.87%	22.26%
TET1	51.48%		37.13%	42.28%	43.61%	39.13%	41.30%	38.38%	35.79%	31.14%	27.94%	35.90%	18.03%	13.19%	15.24%	13.38%	9.15%	8.10%	9.06%	7.51%	21.55%
TET9	35.90%	37.13%		67.40%	61.42%	41.30%	41.30%	41.24%	37.96%	31.88%	26.91%	35.64%	15.82%	12.00%	17.28%	13.97%	11.93%	10.92%	9.03%	8.19%	20.28%
TET8	42.49%	42.28%	67.40%		65.80%	42.55%	44.73%	39.78%	39.78%	34.55%	33.09%	39.27%	17.51%	12.36%	15.81%	12.50%	9.79%	7.72%	7.55%	6.85%	24.48%
TET7	40.07%	43.61%	61.42%	65.80%		43.17%	44.28%	38.29%	38.66%	30.63%	32.73%	37.82%	16.84%	11.27%	15.07%	13.24%	8.90%	7.86%	7.22%	7.64%	23.08%
TET4	38.63%	39.13%	41.30%	42.55%	43.17%		77.89%	37.12%	35.12%	29.41%	28.47%	34.31%	18.39%	15.94%	13.55%	13.19%	9.47%	9.47%	7.94%	7.96%	21.68%
TET3	41.52%	41.30%	41.30%	44.73%	44.28%	77.89%		40.56%	37.41%	32.06%	29.56%	35.77%	18.06%	15.22%	14.29%	14.29%	8.77%	8.07%	8.30%	7.95%	21.68%
TET6	36.76%	38.38%	41.24%	39.78%	38.29%	37.12%	40.56%		55.48%	25.44%	28.04%	37.87%	15.36%	13.28%	14.72%	16.23%	9.51%	8.13%	10.51%	8.04%	20.92%
TET5	35.29%	35.79%	37.96%	39.78%	38.66%	35.12%	37.41%	55.48%		26.15%	27.68%	33.82%	15.36%	12.18%	16.23%	15.47%	8.10%	7.77%	8.70%	8.04%	22.70%
TET10	30.40%	31.14%	31.88%	34.55%	30.63%	29.41%	32.06%	25.44%	26.15%		25.00%	27.84%	14.24%	9.19%	15.67%	13.06%	8.04%	7.75%	8.66%	7.59%	19.79%
TET12	27.57%	27.94%	26.91%	33.09%	32.73%	28.47%	29.56%	28.04%	27.68%	25.00%		40.81%	12.33%	12.31%	16.10%	16.24%	9.47%	7.94%	6.05%	6.25%	20.79%
TET11	34.43%	35.90%	35.64%	39.27%	37.82%	34.31%	35.77%	37.87%	33.82%	27.84%	40.81%		15.49%	13.19%	13.24%	10.95%	7.77%	9.22%	10.32%	12.15%	21.95%
TET15	17.01%	18.03%	15.82%	17.51%	16.84%	18.39%	18.06%	15.36%	15.36%	14.24%	12.33%	15.49%		36.59%	11.99%	6.82%	6.74%	6.98%	5.30%	6.77%	14.77%
TET14	12.82%	13.19%	12.00%	12.36%	11.27%	15.94%	15.22%	13.28%	12.18%	9.19%	12.31%	13.19%	36.59%		11.99%	6.47%	9.74%	5.76%	2.95%	7.89%	11.19%
TET17	12.64%	15.24%	17.28%	15.81%	15.07%	13.55%	14.29%	14.72%	16.23%	15.67%	16.10%	13.60%	12.07%	11.99%		68.95%	4.64%	3.94%	4.41%	6.43%	13.17%
TET16	11.90%	13.38%	13.97%	12.50%	13.24%	13.19%	14.29%	16.23%	15.47%	13.06%	17.23%	13.24%	9.31%	9.74%	68.95%		5.00%	5.02%	4.04%	7.50%	11.39%
TFP3	9.86%	9.15%	11.93%	9.79%	8.90%	9.47%	8.77%	9.51%	8.10%	8.04%	7.77%	10.95%	6.82%	6.47%	4.64%	5.00%		74.02%	74.02%	26.26%	5.90%
TFP1	7.75%	8.10%	10.92%	7.72%	7.86%	9.47%	8.07%	8.13%	7.77%	7.75%	6.74%	9.22%	6.98%	5.76%	3.94%	5.02%	74.02%		26.39%	25.61%	4.53%
TFP2	8.70%	9.06%	9.03%	7.55%	7.22%	7.94%	8.30%	10.51%	8.70%	8.66%	6.05%	10.32%	5.30%	2.95%	4.41%	4.04%	26.26%	26.39%		24.03%	6.94%
TOM2A	8.87%	7.51%	8.19%	6.85%	7.64%	7.96%	7.95%	8.04%	8.04%	7.59%	6.25%	12.15%	6.77%	7.89%	6.43%	7.50%	26.28%	25.61%	24.03%		3.03%
TET13	22.26%	21.55%	20.28%	24.48%	23.08%	21.68%	21.68%	20.92%	22.70%	19.79%	20.35%	21.95%	14.77%	11.19%	13.17%	11.39%	5.90%	4.53%	6.94%	3.03%	

Table 7-2: FRET Lifetime and Efficiencies using LYK4 as a donor. The mean of the donor fluorescence lifetime as well as its corresponding standard deviation (sd), together with the calculated FRET efficiency.

	Donor	Acceptor	Treatment	Lifetime [ns]	sd	FRET efficiency (E) [%]
data from Fig. 4-14	gw LYK4-eGFP		mock	2.35	0.040	
	gw LYK4-eGFP		chitin	2.29	0.074	
	gw LYK4-eGFP	gw TET7-mRFP1	mock	1.95	0.116	17.02
	gw LYK4-eGFP	gw TET7-mRFP1	chitin	2.09	0.080	11.06
	gw LYK4-eGFP	gw BRI1-mRFP1	mock	2.28	0.063	2.98
	gw LYK4-eGFP	gw BRI1-mRFP1	chitin	2.3	0.059	2.13
data from Fig. 4-15	gw LYK4-eGFP		mock	2.35	0.030	
	gw LYK4-eGFP	gg TET3-mCherry	mock	2.24	0.018	4.68
	gw LYK4-eGFP	gg TET7-mCherry	mock	2.27	0.026	3.40
	gw LYK4-eGFP	gg TET8-mCherry	mock	2.26	0.033	3.83
	gw LYK4-eGFP	gw LYK5-mRFP1	mock	2.13	0.022	9.36
	gw LYK4-eGFP	gw TET7-mRFP1	mock	2.12	0.044	9.79
	gg LYK4-mClover3-3×FLAG		mock	2.98	0.023	
	gg LYK4-mClover3-3×FLAG	TET7-mRuby3-6×HA	mock	2.92	0.039	2.01
data from Fig. 4-16	gg LYK4-eGFP		mock	2.41	0.043	
	gg LYK4-eGFP		chitin	2.38	0.038	
	gg LYK4-eGFP	gg TET3-mRFP1	mock	2.36	0.059	2.07
	gg LYK4-eGFP	gg TET3-mRFP1	chitin	2.31	0.051	4.15
	gg LYK4-eGFP	gg TET7-mRFP1	mock	2.37	0.047	1.66
	gg LYK4-eGFP	gg TET7-mRFP1	chitin	2.3	0.035	4.56
	gg LYK4-eGFP	gg TET8-mRFP1	mock	2.33	0.050	3.32
	gg LYK4-eGFP	gg TET8-mRFP1	chitin	2.3	0.043	4.56
	gg LYK4-eGFP	gg BRI1-mRFP1	mock	2.31	0.089	4.15
	gg LYK4-eGFP	gg BRI1-mRFP1	chitin	2.26	0.072	6.22

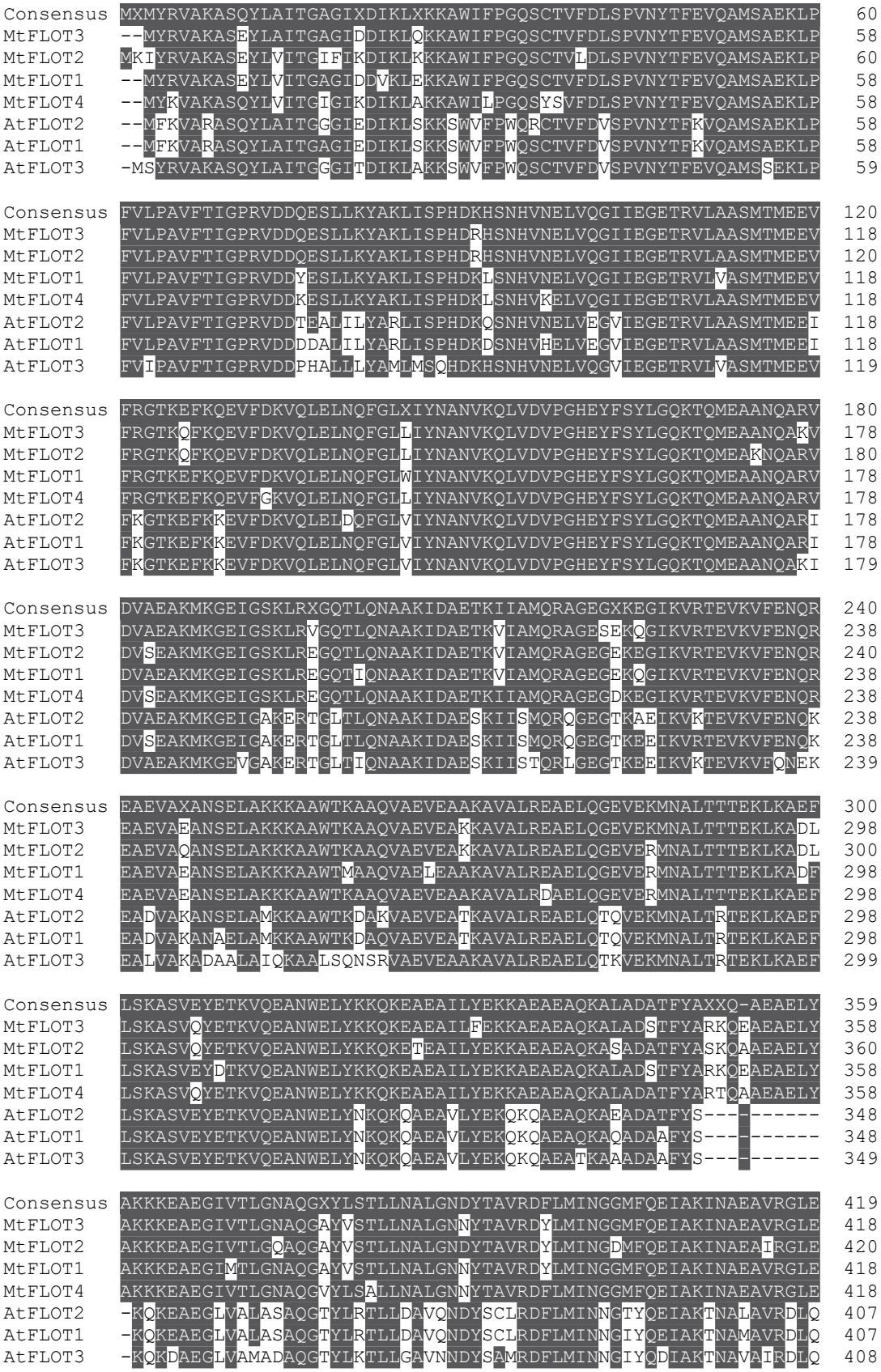
Consensus MXMYRVAKASQYLAITGAGIXDIKLXKKAWIFPGQSCTVFDLSPVNYTFEVQAMSAEKLP 60
MtFLOT3 --MYRVAKASEYLAITGAGIDDIKLQKKAWIFPGQSCTVFDLSPVNYTFEVQAMSAEKLP 58
MtFLOT2 MKIYRVAKASEYLVITGIFIKDIKLKKKAWIFPGQSCTVLDLSPVNYTFEVQAMSAEKLP 60
MtFLOT1 --MYRVAKASEYLVITGAGIDDVKLEKKAWIFPGQSCTVFDLSPVNYTFEVQAMSAEKLP 58
MtFLOT4 --MYKVAKASQYLVITGIGIKDIKLAKKAWILPGQSYSVFDLSPVNYTFEVQAMSAEKLP 58
AtFLOT2 --MFKVARASQYLAITGGGIEDIKLSKKSWVFPWQRCTVFDVSPVNYTFKVQAMSAEKLP 58
AtFLOT1 --MFKVARASQYLAITGAGIEDIKLSKKSWVFPWQSCTVFDVSPVNYTFKVQAMSAEKLP 58
AtFLOT3 -MSYRVAKASQYLAITGGGITDIKLAKKSWVFPWQSCTVFDVSPVNYTFEVQAMSSEKLP 59
Consensus FVLPAVFTIGPRVDDQESLLKYAKLISPHDKHSNHVNELVQGIIEGETRVLAASMTMEEV 120
MtFLOT3 FVLPAVFTIGPRVDDQESLLKYAKLISPHDRHSNHVNELVQGIIEGETRVLAASMTMEEV 118
MtFLOT2 FVLPAVFTIGPRVDDQESLLKYAKLISPHDRHSNHVNELVQGIIEGETRVLAASMTMEEV 120
MtFLOT1 FVLPAVFTIGPRVDDYESLLKYAKLISPHDKLSNHVNELVQGIIEGETRVLVASMTMEEV 118
MtFLOT4 FVLPAVFTIGPRVDDKESLLKYAKLISPHDKLSNHVKELVQGIIEGETRVLAASMTMEEV 118
AtFLOT2 FVLPAVFTIGPRVDDTEALILYARLISPHDKQSNHVNELVEGVIEGETRVLAASMTMEEI 118
AtFLOT1 FVLPAVFTIGPRVDDDDALILYARLISPHDKDSNHVHELVEGVIEGETRVLAASMTMEEI 118
AtFLOT3 FVIPAVFTIGPRVDDPHALLLYAMLMSQHDKHSNHVNELVQGVIEGETRVLVASMTMEEV 119
Consensus FRGTKEFKQEVFDKVQLELNQFGLXIYNANVKQLVDVPGHEYFSYLGQKTQMEAANQARV 180
MtFLOT3 FRGTKQFKQEVFDKVQLELNQFGLLIYNANVKQLVDVPGHEYFSYLGQKTQMEAANQAKV 178
MtFLOT2 FRGTKQFKQEVFDKVQLELNQFGLLIYNANVKQLVDVPGHEYFSYLGQKTQMEAKNQARV 180
MtFLOT1 FRGTKEFKQEVFDKVQLELNQFGLWIYNANVKQLVDVPGHEYFSYLGQKTQMEAANQARV 178
MtFLOT4 FRGTKEFKQEVFGKVQLELNQFGLLIYNANVKQLVDVPGHEYFSYLGQKTQMEAANQARV 178
AtFLOT2 FKGTKEFKKEVFDKVQLELDQFGLVIYNANVKQLVDVPGHEYFSYLGQKTQMEAANQARI 178
AtFLOT1 FKGTKEFKKEVFDKVQLELNQFGLVIYNANVKQLVDVPGHEYFSYLGQKTQMEAANQARI 178
AtFLOT3 FKGTKEFKKEVFDKVQLELNQFGLVIYNANVKQLVDVPGHEYFSYLGQKTQMEAANQAKI 179
Consensus DVAEAKMKGEIGSKLRXGQTLQNAAKIDAETKIIAMQRAGEGXKEGIKVRTEVKVFENQR 240
MtFLOT3 DVAEAKMKGEIGSKLRVGQTLQNAAKIDAETKVIAMQRAGESEKQGIKVRTEVKVFENQR 238
MtFLOT2 DVSEAKMKGEIGSKLREGQTLQNAAKIDAETKVIAMQRAGEGEKEGIKVRTEVKVFENQR 240
MtFLOT1 DVAEAKMKGEIGSKLREGQTIQNAAKIDAETKVIAMQRAGEGEKQGIKVRTEVKVFENQR 238
MtFLOT4 DVSEAKMKGEIGSKLREGQTLQNAAKIDAETKIIAMQRAGEGDKEGIKVRTEVKVFENQR 238
AtFLOT2 DVAEAKMKGEIGAKERTGLTLQNAAKIDAESKIISMQRQGEGTKAEIKVKTEVKVFENQK 238
AtFLOT1 DVSEAKMKGEIGAKERTGLTLQNAAKIDAESKIISMQRQGEGTKEEIKVRTEVKVFENQK 238
AtFLOT3 DVAEAKMKGEVGAKERTGLTIQNAAKIDAESKIISTQRLGEGTKEEIKVKTEVKVFQNEK 239
Consensus EAEVAXANSELAKKKAAWTKAAQVAEVEAAKAVALREAELQGEVEKMNALTTTEKLKAEF 300
MtFLOT3 EAEVAEANSELAKKKAAWTKAAQVAEVEAKKAVALREAELQGEVEKMNALTTTEKLKADL 298
MtFLOT2 EAEVAQANSELAKKKAAWTKAAQVAEVEAKKAVALREAELQGEVERMNALTTTEKLKADL 300
MtFLOT1 EAEVAEANSELAKKKAAWTMAAQVAELEAAKAVALREAELQGEVERMNALTTTEKLKADF 298
MtFLOT4 EAEVAEANSELAKKKAAWTKAAQVAEVEAAKAVALRDAELQGEVERMNALTTTEKLKAEF 298
AtFLOT2 EADVAKANSELAMKKAAWTKDAKVAEVEATKAVALREAELQTQVEKMNALTRTEKLKAEF 298
AtFLOT1 EADVAKANAELAMKKAAWTKDAQVAEVEATKAVALREAELQTQVEKMNALTRTEKLKAEF 298
AtFLOT3 EALVAKADAALAIQKAALSQNSRVAEVEAAKAVALREAELQTKVEKMNALTRTEKLKAEF 299
Consensus LSKASVEYETKVQEANWELYKKQKEAEAILYEKKAEAEAQKALADATFYAXXQ-AEAELY 359
MtFLOT3 LSKASVQYETKVQEANWELYKKQKEAEAILFEKKAEAEAQKALADSTFYARKQEAEAELY 358
MtFLOT2 LSKASVQYETKVQEANWELYKKQKETEAILYEKKAEAEAQKASADATFYASKQAAEAELY 360
MtFLOT1 LSKASVEYDTKVQEANWELYKKQKEAEAILYEKKAEAEAQKALADSTFYARKQEAEAELY 358
MtFLOT4 LSKASVQYETKVQEANWELYKKQKEAEAILYEKKAEAEAQKALADATFYARTQAAEAELY 358
AtFLOT2 LSKASVEYETKVQEANWELYNKQKQAEAVLYEKQKQAEAQKAEADATFYS----I------ 348
AtFLOT1 LSKASVEYETKVQEANWELYNKQKQAEAVLYEKQKQAEAQKAQADAAFYS----I------ 348
AtFLOT3 LSKASVEYETKVQEANWELYNKQKQAEAVLYEKQKQAEATKAAADAAFYS----I------ 349
Consensus AKKKEAEGIVTLGNAQGXYLSTLLNALGNDYTAVRDFLMINGGMFQEIAKINAEAVRGLE 419
MtFLOT3 AKKKEAEGIVTLGNAQGAYVSTLLNALGNNYTAVRDYLMINGGMFQEIAKINAEAVRGLE 418
MtFLOT2 AKKKEAEGIVTLGQAQGAYVSTLLNALGNDYTAVRDYLMINGDMFQEIAKINAEAIRGLE 420
MtFLOT1 AKKKEAEGIMTLGNAQGAYVSTLLNALGNNYTAVRDYLMINGGMFQEIAKINAEAVRGLE 418
MtFLOT4 AKKKEAEGIVTLGNAQGVYLSALLNALGNNYTAVRDFLMINGGMFQEIAKINAEAVRGLE 418
AtFLOT2 -KQKEAEGLVALASAQGTYLRTLLDAVQNDYSCLRDFLMINNGTYQEIAKTNALAVRDLQ 407
AtFLOT1 -KQKEAEGLVALASAQGTYLRTLLDAVQNDYSCLRDFLMINNGIYQEIAKTNAMAVRDLQ 407
AtFLOT3 -KQKDAEGLVAMADAQGTYLKTLLGAVNNDYSAMRDFLMINNGIYQDIAKTNAVAIRDLQ 408

Figure 7-2: Alignment of the Arabidopsis and *M. truncatula* flotillin protein family. This alignment was created using Geneious Prime® 2019.2.3, with the ClustalW Alignment tool (ClustalW 2.1), applying the cost matrix BLOSUM, with a gap open cost of 10, and a gap extended cost of 0.1.

Table 7-3: Genetic distance of proteins of the Arabidopsis and *M. truncatula* family. This table has been created from the protein alignment information of Fig. 7-2.

	MtFLOT3	MtFLOT2	MtFLOT1	MtFLOT4	AtFLOT2	AtFLOT1	AtFLOT3
MtFLOT3		92.89%	93.10%	91.77%	73.47%	72.96%	70.08%
MtFLOT2	92.89%		91.42%	90.17%	72.63%	71.97%	69.31%
MtFLOT1	93.10%	91.42%		90.79%	73.05%	72.18%	70.29%
MtFLOT4	91.77%	90.17%	90.79%		73.89%	74.06%	70.15%
AtFLOT2	73.47%	72.63%	73.05%	73.89%		95.03%	84.91%
AtFLOT1	72.96%	71.97%	72.18%	74.06%	95.03%		85.20%
AtFLOT3	70.08%	69.31%	70.29%	70.15%	84.91%	85.20%	

Table 7-4: Full list of putative protein interactors of LYK4. Mass spectrometry results from plants expressing *pLYK4::LYK4-mCherry* in *lyk4*, immunoprecipitated with Anti-RFP magnetic beads. Col-0 plants were used as control. Mature leaves of four- to six-week-old plants, were treated with water or 0.5 mg/mL chitin and harvested 30 min. after treatment. Three leaves were harvested per sample. Three samples of both sets of treatments and genotypes respectively were analysed. Highest hits after filtering including all hits which are present in the test samples, but absence in the control samples or exhibit at least 5×times more peptide hits in the Test samples versus the control samples. AvgP is the calculated corresponding probability scores (AvgP) as the SAINT score. Each interactor is assigned a SAINT score with a probability ranging from 0 to 1, thereby representing the specificity of the interaction (1 represents the highest possible specificity). A Bayesian False Discovery Rate (BFDR) has been further calculated ranging from 0 to 1, representing the likelihood that this protein has been falsely identified.

			Abundance in Col-0 samples treated with water			Abundance in Col-0 samples treated with chitin			LYK4-mCherry samples treated with water			LYK4-mCherry samples treated with chitin			Comparison: water treated samples		Comparison: chitin treated samples		Comparison: all samples	
Protein name	**locus**	**size [kDa]**	**#1**	**#2**	**#3**	**#1**	**#2**	**#3**	**#1**	**#2**	**#3**	**#1**	**#2**	**#3**	**AvgP**	**BFDR**	**AvgP**	**BFDR**	**AvgP**	**BFDR**
ESM1 | EPITHIOSPECIFIER MODIFIER 1	AT3G14210	44	3	0	0	5	0	2	13	59	44	39	74	113	1.00	0.00	1.00	0.00	1.00	0.00
LYK4 | PROTEIN KINASE FAMILY PROTEIN / PEPTIDOGLYCAN-BINDING LYSM DOMAIN-CONTAINING PROTEIN	AT2G23770	67	0	0	0	0	0	0	11	53	42	50	72	69	1.00	0.00	1.00	0.00	1.00	0.00
GAPA-2 | GLYCERALDEHYDE 3-PHOSPHATE DEHYDROGENASE A SUBUNIT 2	AT1G12900	43	0	0	0	16	5	13	24	32	35	25	30	30	1.00	0.00	0.74	0.03	0.92	0.02
SLP2 | SUBTILISIN-LIKE SERINE PROTEASE 2	AT4G34980	81	1	2	0	10	7	5	5	44	33	29	24	38	1.00	0.00	1.00	0.00	0.78	0.14
FLOT1 | SPFH/BAND 7/PHB DOMAIN-CONTAINING MEMBRANE-ASSOCIATED PROTEIN FAMILY	AT5G25250	52	0	0	3	12	0	0	0	18	14	36	37	24	0.67	0.09	0.99	0.00	0.80	0.14
PRK | PHOSPHORIBULOKINASE	AT1G32060	44	0	0	0	0	0	0	3	25	18	32	14	28	1.00	0.00	1.00	0.00	1.00	0.00
TUB2 | TUBULIN BETA CHAIN 2	AT5G62690	51	0	0	0	3	0	2	3	22	26	11	21	9	1.00	0.00	1.00	0.00	0.94	0.00
TUB4 | TUBULIN BETA CHAIN 4	AT5G44340	50	0	0	0	0	0	0	0	21	23	0	18	8	0.67	0.09	0.67	0.09	0.67	0.18
TUB5 | TUBULIN BETA-5 CHAIN	AT1G20010	50	0	0	0	0	0	0	0	22	21	7	17	9	0.67	0.09	1.00	0.00	0.83	0.09
TUB7 | TUBULIN BETA-7 CHAIN	AT2G29550	51	0	0	0	0	0	0	0	0	20	0	0	0	0.33	0.38			0.17	0.51
FLOT2 | SPFH/BAND 7/PHB DOMAIN-CONTAINING MEMBRANE-ASSOCIATED PROTEIN FAMILY	AT5G25260	51	0	0	0	0	0	0	0	0	10	24	0	0	0.33	0.38	0.33	0.32	0.33	0.39
TUB6 | BETA-6 TUBULIN	AT5G12250	51	0	0	0	0	0	0	0	0	22	0	0	8	0.33	0.38	0.33	0.32	0.33	0.39
CAT3, SEN2, ATCAT3 | CATALASE 3	AT1G20620	57	1	0	0	2	2	2	0	9	16	6	6	6	0.67	0.09	1.00	0.00	0.83	0.12
TRANSKETOLASE	AT3G60750	80	0	0	0	4	0	7	0	16	14	20	13	2	0.67	0.09	0.67	0.07	0.67	0.18
ATPASE, F1 COMPLEX, ALPHA SUBUNIT PROTEIN	AT2G07698	86	0	0	0	1	0	0	0	8	11	6	9	6	0.67	0.09	1.00	0.00	0.83	0.09

PTAC16 | PLASTID TRANSCRIPTIONALLY ACTIVE 16	AT3G46780	54	0	0	0	0	0	3	0	21	16	13	11	17	0.67	0.09	1.00	0.00	0.83	0.09
ALDOLASE-TYPE TIM BARREL FAMILY PROTEIN	AT3G14415	40	0	0	0	0	0	4	0	20	0	17	0	0	0.33	0.38	0.33	0.32	0.33	0.39
GLYCINE CLEAVAGE T-PROTEIN FAMILY	AT1G11860	44	0	0	0	1	0	3	0	12	12	7	10	10	0.67	0.09	0.97	0.00	0.83	0.12
ZW9 | TRAF-LIKE FAMILY PROTEIN	AT1G58270	45	0	0	0	2	0	0	0	10	9	3	5	17	0.67	0.09	0.96	0.00	0.75	0.15
HSC70-1, HSP70-1, AT-HSC70-1, HSC70 | HEAT SHOCK COGNATE PROTEIN 70-1	AT5G02500	71	0	0	0	1	0	2	0	5	13	7	20	2	0.67	0.09	0.85	0.02	0.82	0.13
AT4G36030.1-DECOY	AT4G36030	?	0	0	0	0	0	0	2	3	1	2	1	0						
TRANSLATION INITIATION FACTOR 3 PROTEIN	AT4G30690	32	0	0	0	2	0	2	0	10	6	8	9	14	0.67	0.09	1.00	0.00	0.83	0.09
LOX2, ATLOX2 | LIPOXYGENASE 2	AT3G45140	102	0	0	0	0	0	3	0	12	10	6	11	1	0.67	0.09	0.67	0.08	0.64	0.21
GS2, GLN2, ATGSL1 | GLUTAMINE SYNTHETASE 2	AT5G35630	47	1	0	0	3	0	2	2	10	7	3	1	4	1.00	0.00	0.39	0.23	0.66	0.20
RIBOSOMAL PROTEIN S11 FAMILY PROTEIN	AT2G36160	16	0	2	0	0	0	0	0	9	5	8	0	0	0.67	0.09	0.33	0.32	0.50	0.29
THIOREDOXIN SUPERFAMILY PROTEIN	AT3G11630	29	0	0	0	2	0	0	0	8	9	7	3	18	0.67	0.09	0.98	0.00	0.77	0.14
MTO3, SAMS3, MAT4 | S-ADENOSYLMETHIONINE SYNTHETASE FAMILY PROTEIN	AT3G17390	43	0	0	0	1	0	1	0	3	8	5	6	2	0.67	0.09	1.00	0.00	0.83	0.12
ATGLDP1, GLDP1 | GLYCINE DECARBOXYLASE P-PROTEIN 1	AT4G33010	113	0	0	0	0	0	2	0	3	9	4	3	2	0.67	0.09	0.68	0.06	0.62	0.22
ATCDSP32, CDSP32 | CHLOROPLASTIC DROUGHT-INDUCED STRESS PROTEIN OF 32 KD	AT1G76080	34	0	0	0	0	0	1	0	1	2	2	2	1	0.33	0.37	0.69	0.05	0.51	0.28
2-CYS PRX B, 2CPB | 2-CYSTEINE PEROXIREDOXIN B	AT5G06290	30	0	0	0	0	0	0	0	6	8	3	0	0	0.67	0.09	0.33	0.32	0.50	0.29
SHM1, STM, SHMT1 | SERINE TRANSHYDROXYMETHYLTRANSFERASE 1	AT4G37930	57	0	0	0	2	0	2	0	9	7	4	3	5	0.67	0.09	0.76	0.03	0.73	0.15
MANNOSE-BINDING LECTIN SUPERFAMILY PROTEIN	AT1G52000	74	0	0	0	0	0	0	0	1	7	3	11	11	0.36	0.30	1.00	0.00	0.68	0.17
SUBTILASE FAMILY PROTEIN	AT3G14240	83	0	0	0	4	0	1	0	4	4	5	9	0	0.67	0.09	0.58	0.16	0.62	0.22
CLPC, ATHSP93-V, HSP93-V, DCA1, CLPC1 | CLPC HOMOLOGUE 1	AT5G50920	?	0	0	0	0	0	0	0	8	9	2	2	0	0.67	0.09	0.67	0.13	0.66	0.20
RIBOSOMAL PROTEIN S3AE	AT3G04840	30	0	2	0	0	0	0	2	3	1	1	2	1	0.37	0.29	0.35	0.27	0.16	0.55
GGT1, AOAT1, GGAT1 | GLUTAMATE:GLYOXYLATE AMINOTRANSFERASE	AT1G23310	53	0	0	0	2	0	2	0	8	6	5	3	2	0.67	0.09	0.47	0.20	0.60	0.23

P-LOOP CONTAINING NUCLEOSIDE TRIPHOSPHATE HYDROLASES SUPERFAMILY PROTEIN	AT3G45850	119	0	0	0	0	0	0	0	0	10	0	4	9	0.33	0.38	0.67	0.09	0.50	0.29
ATCIMS, ATMETS, ATMS1 | COBALAMIN-INDEPENDENT SYNTHASE FAMILY PROTEIN	AT5G17920	84	0	0	0	0	0	2	0	7	7	4	4	0	0.67	0.09	0.55	0.17	0.53	0.26
ATP SYNTHASE ALPHA/BETA FAMILY PROTEIN	AT5G08680	60	2	0	0	0	0	0	2	5	5	2	4	5	0.68	0.07	1.00	0.00	0.68	0.17
LHCB3, LHCB3*1 | LIGHT-HARVESTING CHLOROPHYLL B-BINDING PROTEIN 3	AT5G54270	29	0	0	0	0	0	2	0	3	0	1	5	2	0.33	0.38	0.47	0.20	0.32	0.42
CHR9 | SWITCH 2	AT1G03750	98	0	0	0	0	0	0	0	0	0	0	1	1			0.01	0.51	0.02	0.63
APS1 | ATP SULFURYLASE 1	AT3G22890	51	0	0	0	0	0	0	0	0	5	3	4	2	0.33	0.38	1.00	0.00	0.67	0.19
VAR2, FTSH2 | FTSH EXTRACELLULAR PROTEASE FAMILY	AT2G30950	74	0	0	0	0	0	1	0	5	5	4	1	1	0.67	0.09	0.55	0.17	0.59	0.24
AGT, AGT1, SGAT | ALANINE:GLYOXYLATE AMINOTRANSFERASE	AT2G13360	44	0	0	0	0	0	2	0	3	11	1	2	1	0.67	0.09	0.02	0.49	0.32	0.41
ATSCO1, ATSCO1/CPEF-G, SCO1 | TRANSLATION ELONGATION FACTOR EFG/EF2 PROTEIN	AT1G62750	86	0	0	0	0	0	0	0	2	9	2	6	2	0.67	0.09	1.00	0.00	0.81	0.13
ATJ3, ATJ | DNAJ HOMOLOGUE 3	AT3G44110	38	0	0	0	2	0	0	0	3	2	4	1	1	0.67	0.09	0.34	0.31	0.33	0.41
NIT1, ATNIT1, NITI | NITRILASE 1	AT3G44310	38	0	0	0	0	0	0	0	4	4	3	0	2	0.67	0.09	0.67	0.09	0.67	0.19
CAS | CALCIUM SENSING RECEPTOR	AT5G23060	41	0	0	0	0	0	0	0	3	4	3	3	2	0.67	0.09	1.00	0.00	0.83	0.12
HPR, ATHPR1 | HYDROXYPYRUVATE REDUCTASE	AT1G68010	42	0	0	0	0	0	1	0	7	5	2	0	2	0.67	0.09	0.67	0.09	0.66	0.19
MAT3 | METHIONINE ADENOSYLTRANSFERASE 3	AT2G36880	42	0	0	0	0	0	0	0	0	4	0	0	0	0.33	0.38			0.17	0.51
BIP, BIP2 | HEAT SHOCK PROTEIN 70 (HSP 70) FAMILY PROTEIN	AT5G42020	74	0	0	0	0	0	0	0	0	4	0	0	0	0.33	0.38			0.17	0.51
RIBOSOMAL PROTEIN S5 DOMAIN 2-LIKE SUPERFAMILY PROTEIN	AT5G18380	17	0	0	0	0	0	1	0	4	2	1	2	0	0.67	0.09	0.35	0.27	0.51	0.28
NAD(P)-BINDING ROSSMANN-FOLD SUPERFAMILY PROTEIN	AT4G35250	44	0	0	0	0	0	0	0	0	5	3	1	0	0.33	0.38	0.37	0.24	0.36	0.36
PSBB | PHOTOSYSTEM II REACTION CENTER PROTEIN B	ATCG00680	56	0	0	0	0	0	2	0	5	2	3	0	0	0.67	0.09	0.33	0.38	0.31	0.43
BIFUNCTIONAL INHIBITOR/LIPID-TRANSFER PROTEIN/SEED STORAGE 2S ALBUMIN SUPERFAMILY PROTEIN	AT2G10940	30	0	0	0	0	0	2	3	3	2	4	2	0	1.00	0.00	0.35	0.28	0.52	0.27
PTAC17 | PLASTID TRANSCRIPTIONALLY ACTIVE 17	AT1G80480	49	0	0	0	0	0	2	0	2	4	4	2	2	0.67	0.09	0.36	0.25	0.37	0.35

EIF4A1, RH4, TIF4A1 | EUKARYOTIC TRANSLATION INITIATION FACTOR 4A1	AT3G13920	47	0	0	0	0	0	0	0	3	6	2	2	2	0.67	0.09	1.00	0.00	0.83	0.13
LOS2, ENO2 | ENOLASE	AT2G36530	48	0	0	0	0	0	0	0	3	3	3	1	0	0.67	0.09	0.37	0.24	0.52	0.27
CPN60A, CH-CPN60A, SLP | CHAPERONIN-60ALPHA	AT2G28000	62	0	0	0	0	0	1	0	3	6	0	0	0	0.67	0.09			0.33	0.39
PSBR | PHOTOSYSTEM II SUBUNIT R	AT1G79040	15	0	0	0	0	0	0	0	2	1	0	0	0	0.34	0.35			0.16	0.54
PDF1B, DEF2, ATDEF2 | PEPTIDE DEFORMYLASE 1B	AT5G14660	31	0	0	0	0	0	1	0	0	2	1	0	2	0.33	0.38	0.36	0.26	0.34	0.37
RPS15 | CHLOROPLAST RIBOSOMAL PROTEIN S15	ATCG01120	11	0	0	0	0	0	0	0	4	2	0	0	0	0.67	0.09			0.33	0.40
ATGLDP2, GLDP2 | GLYCINE DECARBOXYLASE P-PROTEIN 2	AT2G26080	114	0	0	0	0	0	0	0	0	4	0	0	0	0.33	0.38			0.17	0.51
RIBOSOMAL PROTEIN S7E FAMILY PROTEIN	AT1G48830	22	0	0	0	0	0	1	0	2	1	1	3	1	0.34	0.35	0.49	0.19	0.40	0.33
RIBOSOMAL L38E PROTEIN FAMILY	AT2G43460	8	0	2	0	0	0	0	0	1	3	2	1	1	0.34	0.34	0.34	0.29	0.19	0.48
ATTIC110, TIC110 | TRANSLOCON AT THE INNER ENVELOPE MEMBRANE OF CHLOROPLASTS 110	AT1G06950	112	0	0	0	0	0	0	0	0	3	0	0	0	0.33	0.38			0.17	0.51
VAR1, FTSH5 | FTSH EXTRACELLULAR PROTEASE FAMILY	AT5G42270	75	0	0	0	0	0	0	0	0	1	2	2	0	0.00	0.50	0.67	0.13	0.34	0.38
IMPA-2 | IMPORTIN ALPHA ISOFORM 2	AT4G16143	59	0	0	0	0	0	0	0	0	5	3	3	0	0.33	0.38	0.67	0.09	0.50	0.29
VHA-A | VACUOLAR ATP SYNTHASE SUBUNIT A	AT1G78900	69	0	0	0	0	0	0	0	2	3	2	2	2	0.67	0.09	1.00	0.00	0.81	0.13
RPS1, ARRPS1 | RIBOSOMAL PROTEIN S1	AT5G30510	45	0	0	0	0	0	0	0	1	3	2	0	0	0.35	0.31	0.33	0.32	0.34	0.38
COATOMER EPSILON SUBUNIT	AT1G30630	33	0	0	0	0	0	0	0	2	5	2	0	0	0.67	0.09	0.33	0.32	0.48	0.31
PORB | PROTOCHLOROPHYLLIDE OXIDOREDUCTASE B	AT4G27440	43	0	0	0	0	0	0	0	0	4	0	0	0	0.33	0.38			0.17	0.51
THI1, TZ, THI4 | THIAZOLE BIOSYNTHETIC ENZYME, CHLOROPLAST (ARA6) (THI1) (THI4)	AT5G54770	37	0	0	0	0	0	0	0	2	4	2	1	0	0.67	0.09	0.34	0.30	0.50	0.29
PTAC13 | PLASTID TRANSCRIPTIONALLY ACTIVE 13	AT3G09210	37	0	0	0	0	0	0	0	0	5	1	0	0	0.33	0.38	0.00	0.57	0.19	0.47
BOU | MITOCHONDRIAL SUBSTRATE CARRIER FAMILY PROTEIN	AT5G46800	31	0	0	0	0	0	0	0	0	2	0	1	0	0.33	0.38	0.00	0.55	0.14	0.56
TIP2, SITIP, GAMMA-TIP2, TIP1;2 | TONOPLAST INTRINSIC PROTEIN 2	AT3G26520	26	0	0	0	0	0	0	0	1	1	0	5	5	0.00	0.58	0.67	0.09	0.36	0.35
30S RIBOSOMAL PROTEIN, PUTATIVE	AT5G24490	35	0	0	0	0	0	0	0	0	2	0	2	2	0.33	0.38	0.67	0.09	0.50	0.30

ACETYL CO-ENZYME A CARBOXYLASE CARBOXYLTRANSFERASE ALPHA SUBUNIT	AT2G38040	85	0	0	0	0	0	0	0	0	5	2	0	0	0.33	0.38	0.33	0.32	0.33	0.40
POR C, PORC | PROTOCHLOROPHYLLIDE OXIDOREDUCTASE C	AT1G03630	44	0	0	0	0	0	0	0	0	2	0	0	0	0.33	0.38			0.14	0.57
CLEAVAGE/POLYADENYLATION SPECIFICITY FACTOR, 25KDA SUBUNIT	AT4G25550	23	0	0	0	0	0	0	0	1	1	2	2	0	0.00	0.49	0.67	0.13	0.34	0.37
KETOL-ACID REDUCTOISOMERASE	AT3G58610	64	0	0	0	0	0	0	0	0	2	0	1	0	0.33	0.38	0.00	0.55	0.14	0.56
PYRIDINE NUCLEOTIDE-DISULPHIDE OXIDOREDUCTASE FAMILY PROTEIN	AT1G74470	52	0	0	0	0	0	0	0	0	4	0	0	0	0.33	0.38			0.17	0.51
RIBOSOMAL PROTEIN S19E FAMILY PROTEIN	AT3G02080	16	0	0	0	0	0	0	0	0	5	0	0	0	0.33	0.38			0.17	0.51
RPS15 | CYTOSOLIC RIBOSOMAL PROTEIN S15	AT1G04270	17	1	0	0	0	0	0	0	1	1	0	2	1	0.00	0.57	0.34	0.28	0.19	0.47
MAB1 | TRANSKETOLASE FAMILY PROTEIN	AT5G50850	39	0	0	0	0	0	0	0	1	1	0	1	0	0.00	0.58	0.00	0.55	0.01	0.68
LOS1 | RIBOSOMAL PROTEIN S5/ELONGATION FACTOR G/III/V FAMILY PROTEIN	AT1G56070	94	0	0	0	0	0	0	0	2	4	0	0	0	0.67	0.09			0.32	0.42
CPHSC70-1 | CHLOROPLAST HEAT SHOCK PROTEIN 70-1	AT4G24280	77	0	0	0	0	0	0	0	2	2	0	0	0	0.67	0.09			0.32	0.42
ADG2, APL1 | ADP GLUCOSE PYROPHOSPHORYLASE LARGE SUBUNIT 1	AT5G19220	58	0	0	0	0	0	1	0	1	1	0	2	2	0.00	0.49	0.67	0.09	0.36	0.35
PIN1AT | PEPTIDYLPROLYL CIS/TRANS ISOMERASE, NIMA-INTERACTING 1	AT2G18040	13	0	0	0	0	0	0	0	2	1	0	1	1	0.34	0.35	0.01	0.51	0.18	0.49
RPL4 | RIBOSOMAL PROTEIN L4	AT1G07320	31	0	0	0	0	0	0	0	2	1	0	0	0	0.34	0.35			0.16	0.54
ATPHB3, PHB3 | PROHIBITIN 3	AT5G40770	30	0	0	0	0	0	0	0	2	0	4	2	2	0.33	0.38	1.00	0.00	0.65	0.20
AOC2 | ALLENE OXIDE CYCLASE 2	AT3G25770	28	0	0	0	0	0	0	0	0	2	2	1	0	0.33	0.38	0.34	0.30	0.34	0.39
EMB2761 | THREONYL-TRNA SYNTHETASE, PUTATIVE / THREONINE--TRNA LIGASE, PUTATIVE	AT2G04842	75	0	0	0	0	0	0	0	0	3	0	0	0	0.33	0.38			0.17	0.53
PIP1B, TMP-A, ATHH2, PIP1;2 | PLASMA MEMBRANE INTRINSIC PROTEIN 1B	AT2G45960	31	0	0	0	0	0	0	0	1	1	0	2	0	0.00	0.49	0.33	0.32	0.18	0.50
MDAR6 | MONODEHYDROASCORBATE REDUCTASE 6	AT1G63940	53	0	0	0	0	0	0	0	0	1	0	0	0	0.00	0.50			0.01	0.65
RIBOSOMAL PROTEIN S13/S15	AT3G60770	17	0	0	0	0	0	0	0	2	1	2	0	0	0.34	0.35	0.33	0.32	0.32	0.41

RIBOSOMAL PROTEIN L30/L7 FAMILY PROTEIN	AT2G01250	28	0	0	0	0	0	0	0	1	2	1	0	0	0.33	0.37	0.00	0.57	0.14	0.57
ATPASE, V1 COMPLEX, SUBUNIT B PROTEIN	AT1G20260	54	0	0	0	0	0	0	0	1	2	0	1	0	0.33	0.37	0.00	0.55	0.14	0.56
MALATE DEHYDROGENASE	AT3G47520	42	0	0	0	0	0	0	0	2	2	0	0	0	0.67	0.24			0.29	0.44
ILA | ILITYHIA	AT1G64790	285	0	0	0	0	0	0	0	1	3	0	0	0	0.34	0.32			0.18	0.50
METHYLTRANSFERASES	AT3G28460	35	0	0	0	0	0	0	0	0	2	0	0	0	0.33	0.38			0.17	0.53
TCH3, ATCAL4 | CALCIUM-BINDING EF HAND FAMILY PROTEIN	AT2G41100	37	0	0	0	0	0	0	0	0	2	1	0	0	0.33	0.38	0.00	0.57	0.17	0.50
APG1, VTE3, IEP37, E37 | S-ADENOSYL-L-METHIONINE-DEPENDENT METHYLTRANSFERASES SUPERFAMILY PROTEIN	AT3G63410	38	0	0	0	0	0	0	0	1	3	0	0	0	0.35	0.31			0.18	0.49
RIBOSOMAL PROTEIN L1P/L10E FAMILY	AT3G63490	38	0	0	0	0	0	0	0	1	1	1	0	0	0.00	0.58	0.00	0.57	0.01	0.68
RPS2 | RIBOSOMAL PROTEIN S2	ATCG00160	27	0	0	0	0	0	0	0	1	0	0	0	0	0.00	0.58			0.00	0.70
GLU1, GLS1, GLUS, FD-GOGAT | GLUTAMATE SYNTHASE 1	AT5G04140	177	0	0	0	0	0	0	0	3	1	0	0	0	0.40	0.28			0.19	0.47
RPT6A, ATSUG1 | REGULATORY PARTICLE TRIPLE-A ATPASE 6A	AT5G19990	47	0	0	0	0	0	0	0	2	1	0	0	0	0.34	0.34			0.15	0.55
ATPHB2, PHB2 | PROHIBITIN 2	AT1G03860	32	0	0	0	0	0	0	0	0	0	4	0	0			0.33	0.32	0.17	0.51
ATPME3, PME3 | PECTIN METHYLESTERASE 3	AT3G14310	64	0	0	0	0	0	0	0	2	1	0	2	0	0.34	0.34	0.33	0.32	0.32	0.41
ATP3 | GAMMA SUBUNIT OF MT ATP SYNTHASE	AT2G33040	35	0	0	0	0	0	0	0	0	1	2	2	0	0.00	0.50	0.67	0.13	0.34	0.38
OXIDOREDUCTASES, ACTING ON THE ALDEHYDE OR OXO GROUP OF DONORS, NAD OR NADP AS ACCEPTOR;COPPER ION BINDING	AT2G19940	44	0	0	0	0	0	0	0	1	1	0	0	0	0.00	0.49			0.01	0.64
MTLPD1 | MITOCHONDRIAL LIPOAMIDE DEHYDROGENASE 1	AT1G48030	54	0	0	0	0	0	0	0	0	2	0	0	0	0.33	0.38			0.14	0.57
TUF, EMB2448, TUFF, VHA-E1 | VACUOLAR ATP SYNTHASE SUBUNIT E1	AT4G11150	26	0	0	0	0	0	0	0	0	1	0	0	0	0.00	0.58			0.00	0.71
FSD1, ATFSD1 | FE SUPEROXIDE DISMUTASE 1	AT4G25100	24	0	0	0	0	0	0	0	2	1	0	0	0	0.34	0.35			0.16	0.54
P40, AP40, RP40, RPSAA | 40S RIBOSOMAL PROTEIN SA	AT1G72370	32	0	0	0	0	0	0	0	0	2	0	0	0	0.33	0.38			0.17	0.53
SVR1 | PSEUDOURIDINE SYNTHASE FAMILY PROTEIN	AT2G39140	45	0	0	0	0	0	0	0	0	2	0	0	0	0.33	0.38			0.14	0.57
DXR, PDE129 | 1-DEOXY-D-XYLULOSE 5-PHOSPHATE REDUCTOISOMERASE	AT5G62790	52	0	0	0	0	0	0	0	2	1	0	0	0	0.34	0.35			0.16	0.54

FCF2 PRE-RRNA PROCESSING PROTEIN	AT1G54770	22	0	0	0	0	0	0	0	0	1	2	0	0	0.00	0.50	0.33	0.32	0.17	0.50
RPN1A, ATRPN1A | 26S PROTEASOME REGULATORY SUBUNIT S2 1A	AT2G20580	?	0	0	0	0	0	0	0	0	2	0	0	0	0.33	0.38			0.14	0.57
RPE, EMB2728 | D-RIBULOSE-5-PHOSPHATE-3-EPIMERASE	AT5G61410	30	0	0	0	0	0	0	0	0	1	0	0	0	0.00	0.50			0.01	0.65
ACP4 | ACYL CARRIER PROTEIN 4	AT4G25050	15	0	0	0	0	0	0	0	0	1	1	0	0	0.00	0.50	0.00	0.57	0.01	0.64
TROL | THYLAKOID RHODANESE-LIKE	AT4G01050	49	0	0	0	0	0	0	0	1	1	0	0	0	0.00	0.58			0.00	0.70
HCEF1 | HIGH CYCLIC ELECTRON FLOW 1	AT3G54050	45	0	0	0	0	0	0	0	0	1	0	0	0	0.00	0.50			0.01	0.65
AT5G19690.1-DECOY	AT5G19690	?	0	0	0	0	0	0	0	0	1	0	0	0						
NDHH | NAD(P)H DEHYDROGENASE SUBUNIT H	ATCG01110	46	0	0	0	0	0	0	0	0	1	0	0	0	0.00	0.50			0.01	0.65
MRAW METHYLASE FAMILY PROTEIN	AT5G10910	49	0	0	0	0	0	0	0	0	1	0	0	0	0.00	0.50			0.01	0.65
CARB | CARBAMOYL PHOSPHATE SYNTHETASE B	AT1G29900	130	0	0	0	0	0	0	0	0	1	0	0	0	0.00	0.50			0.01	0.65
ATP-DEPENDENT CASEINOLYTIC (CLP) PROTEASE/CROTONASE FAMILY PROTEIN	AT1G09130	36	0	0	0	0	0	0	0	1	1	0	0	0	0.00	0.49			0.01	0.64
ATGCN2, GCN2 | ABC TRANSPORTER FAMILY PROTEIN	AT5G09930	76	0	0	0	0	0	0	0	0	1	0	0	0	0.00	0.50			0.01	0.65
ATPDIL2-2, ATPDI10, PDI10, PDIL2-2 | PDI-LIKE 2-2	AT1G04980	48	0	0	0	0	0	0	0	0	1	0	0	0	0.00	0.50			0.01	0.65
CORI3, JR2 | TYROSINE TRANSAMINASE FAMILY PROTEIN	AT4G23600	47	0	0	0	0	0	0	0	0	0	1	0	0			0.00	0.57	0.00	0.69
ELF5 | PROLINE-RICH FAMILY PROTEIN	AT5G62640	56	0	0	0	0	0	0	0	0	1	0	0	0	0.00	0.58			0.00	0.71
COATOMER GAMMA-2 SUBUNIT, PUTATIVE / GAMMA-2 COAT PROTEIN, PUTATIVE / GAMMA-2 COP, PUTATIVE	AT4G34450	98	0	0	0	0	0	0	0	0	1	0	0	0	0.00	0.50			0.01	0.65
ALPHA/BETA-HYDROLASES SUPERFAMILY PROTEIN	AT1G52510	42	0	0	0	0	0	0	0	0	1	0	0	0	0.00	0.50			0.01	0.65
PROTEIN OF UNKNOWN FUNCTION (DUF3411)	AT5G12470	41	0	0	0	0	0	0	0	0	1	0	0	0	0.00	0.50			0.01	0.65
AOS, CYP74A, DDE2 | ALLENE OXIDE SYNTHASE	AT5G42650	58	0	0	0	0	0	0	0	0	1	0	0	0	0.00	0.50			0.01	0.65
MITOCHONDRIAL SUBSTRATE CARRIER FAMILY PROTEIN	AT5G19760	32	0	0	0	0	0	0	0	0	1	0	0	0	0.00	0.50			0.01	0.65
PSEUDOURIDINE SYNTHASE FAMILY PROTEIN	AT5G14460	61	0	0	0	0	0	0	0	0	1	0	0	0	0.00	0.50			0.01	0.65

ATIDD5, IDD5 | INDETERMINATE(ID)-DOMAIN 5	AT2G02070	64	0	0	0	0	0	0	0	0	1	0	0	0	0.00	0.50			0.01	0.65
RPS19 | RIBOSOMAL PROTEIN S19	ATCG00820	11	0	0	0	0	0	0	0	0	1	0	0	0	0.00	0.50			0.01	0.65
FTSZ2-2 | TUBULIN/FTSZ FAMILY PROTEIN	AT3G52750	50	0	0	0	0	0	0	0	0	1	0	0	0	0.00	0.50			0.01	0.65
ATSFGH, SFGH | S-FORMYLGLUTATHIONE HYDROLASE	AT2G41530	32	0	0	0	0	0	0	0	0	1	0	0	0	0.00	0.50			0.01	0.65
MAP1C, MAP1B | METHIONINE AMINOPEPTIDASE 1B	AT1G13270	40	0	0	0	0	0	0	0	0	1	0	0	0	0.00	0.50			0.01	0.65
DELTA-TIP, TIP2;1, DELTA-TIP1, AQP1, ATTIP2;1 | DELTA TONOPLAST INTEGRAL PROTEIN	AT3G16240	25	0	0	0	0	0	0	0	0	0	0	2	0			0.33	0.32	0.17	0.54
PROTEIN OF UNKNOWN FUNCTION (DUF1118)	AT1G74730	21	0	0	0	0	0	0	3	0	0	0	0	0	0.33	0.38			0.17	0.51
ALPHA/BETA-HYDROLASES SUPERFAMILY PROTEIN	AT2G42690	46	0	0	0	0	0	0	0	0	1	0	0	0	0.00	0.50			0.01	0.65
PSAB | PHOTOSYSTEM I, PSAA/PSAB PROTEIN	ATCG00340	82	0	0	0	0	0	0	0	0	1	0	0	0	0.00	0.50			0.01	0.65
RIBOSOMAL PROTEIN S3 FAMILY PROTEIN	AT2G31610	28	0	0	0	0	0	0	0	0	1	0	0	0	0.00	0.50			0.01	0.65
AT5G16910.1-DECOY	AT5G16910	?	0	0	0	0	0	0	0	0	0	1	0	0						
EMB2753 | TETRATRICOPEPTIDE REPEAT (TPR)-CONTAINING PROTEIN	AT1G80410	102	0	0	0	0	0	0	0	0	1	0	0	0	0.00	0.58			0.00	0.71

Table 7-5: Analyses of Variance Table (ANOVA) with Satterthwaite's method. df: degrees of freedom. p-value: * = <0.05, ** = <0.01, *** = <0.001.

Figure	Variable	F-statistic	df	p-value
Fig. 4-7	genotype	5.546	3	**
Fig. 4-8A	LYK4	0.2	1	ns
	tetraspanins	0.5	3	ns
	LYK4:tetraspanins	1.4	3	ns
Fig. 4-8B	LYK4	0.6	1	ns
	TET3	11.5	1	***
	LYK4:TET3	13.1	1	***
Fig. 4-8C	LYK4	7.6	1	**
	TET7	15.2	1	***
	LYK4:TET7	0.07	1	ns
Fig. 4-8D	LYK4	0.03	1	ns
	TET8	9	1	**
	LYK4:TET8	8	1	**
Fig. 4-9	genotype	5.8	3	***
	treatment	510.2	1	***
	genotype:treatment	2.7	3	*
Fig. 5-5	genotype	7.725	3	***
	treatment	88.9243	1	***
	genotype:treatment	3.8251	3	*
Fig. 5-7B	genotype	4.823	3	**
Fig. 5-7C	genotype	4.206	3	**

Bibliography

Abcepta (2022). SUMOplot™ Analysis Program, https://www.abcepta.com/sumoplot.

Abel, N.B., Buschle, C.A., Hernandez-Ryes, C., Burkart, S.S., Deroubaix, A.-F., Mergner, J., Gronnier, J., Jarsch, I.K., Folgmann, J., Braun, K.H.*, et al.* (2021). A hetero-oligomeric remorin-receptor complex regulates plant development. bioRxiv, 2021.2001.2028.428596.

Abou-Abbass, H., Abou-El-Hassan, H., Bahmad, H., Zibara, K., Zebian, A., Youssef, R., Ismail, J., Zhu, R., Zhou, S., Dong, X.*, et al.* (2016). Glycosylation and other PTMs alterations in neurodegenerative diseases: Current status and future role in neurotrauma. Electrophoresis *37*, 1549-1561.

Adachi, H., Nakano, T., Miyagawa, N., Ishihama, N., Yoshioka, M., Katou, Y., Yaeno, T., Shirasu, K., and Yoshioka, H. (2015). WRKY Transcription Factors Phosphorylated by MAPK Regulate a Plant Immune NADPH Oxidase in *Nicotiana benthamiana*. The Plant Cell *27*, 2645-2663.

Adrain, C., Strisovsky, K., Zettl, M., Hu, L., Lemberg, M.K., and Freeman, M. (2011). Mammalian EGF receptor activation by the rhomboid protease RHBDL2. EMBO Reports *12*, 421-427.

Affentranger, S., Martinelli, S., Hahn, J., Rossy, J., and Verena, N. (2011). Dynamic reorganization of flotillins in chemokine-stimulated human T-lymphocytes. BMC Cell Biology *12*, 28.

Ahn, Y.O., Shimizu, B.-i., Sakata, K., Gantulga, D., Zhou, Z., Bevan, D.R., and Esen, A. (2010). Scopolin-hydrolyzing β-glucosidases in roots of Arabidopsis. Plant and Cell Physiology *51*, 132-143.

Albers, P., Üstün, S., Witzel, K., Kraner, M., and Börnke, F. (2019). A Remorin from *Nicotiana benthamiana* Interacts with the *Pseudomonas* Type-III Effector Protein HopZ1a and is Phosphorylated by the Immune-Related Kinase PBS1. Molecular Plant-Microbe Interactions *32*, 1229-1242.

Alberts, B., Johnson, A., Lewis, J., Raff, M., Roberts, K., and Walter, P. (2002). Molecular Biology of the Cell (Garland Science).

Albrecht, C., Boutrot, F., Segonzac, C., Schwessinger, B., Gimenez-Ibanez, S., Chinchilla, D., Rathjen, J.P., de Vries, S.C., and Zipfel, C. (2012). Brassinosteroids inhibit pathogen-associated molecular pattern–triggered immune signaling independent of the receptor kinase BAK1. Proceedings of the National Academy of Sciences *109*, 303.

Alonso, J.M., Stepanova, A.N., Leisse, T.J., Kim, C.J., Chen, H., Shinn, P., Stevenson, D.K., Zimmerman, J., Barajas, P., Cheuk, R.*, et al.* (2003). Genome-wide insertional mutagenesis of *Arabidopsis thaliana*. Science *301*, 653-657.

Amaddii, M., Meister, M., Banning, A., Tomasovic, A., Mooz, J., Rajalingam, K., and Tikkanen, R. (2012). Flotillin-1/Reggie-2 Protein Plays Dual Role in Activation of Receptor-tyrosine Kinase/Mitogen-activated Protein Kinase Signaling. Journal of Biological Chemistry *287*, 7265-7278.

Amor, B.B., Shaw, S.L., Oldroyd, G.E.D., Maillet, F., Penmetsa, R.V., Cook, D., Long, S.R., Dénarié, J., and Gough, C. (2003). The NFP locus of *Medicago truncatula* controls an early step of Nod factor signal transduction upstream of a rapid calcium flux and root hair deformation. The Plant Journal *34*, 495-506.

An, H.J., Froehlich, J.W., and Lebrilla, C.B. (2009). Determination of glycosylation sites and site-specific heterogeneity in glycoproteins. Current opinion in chemical biology *13*, 421-426.

Andersen, O.S., and Koeppe, R.E., 2nd (2007). Bilayer thickness and membrane protein function: an energetic perspective. Annual Review of Biophysics and Biomolecular Structure *36*, 107-130.

Antolín-Llovera, M., Petutsching, E.K., Ried, M.K., Lipka, V., Nürnberger, T., Robatzek, S., and Parniske, M. (2014a). Knowing your friends and foes – plant receptor-like kinases as initiators of symbiosis or defence. New Phytologist *204*, 791-802.

Antolín-Llovera, M., Ried, Martina K., and Parniske, M. (2014b). Cleavage of the SYMBIOSIS RECEPTOR-LIKE KINASE Ectodomain Promotes Complex Formation with Nod Factor Receptor 5. Current Biology *24*, 422-427.

Arabidopsis eFP Browser 2.0 (2022). http://bar.utoronto.ca/efp2/Arabidopsis/Arabidopsis_eFPBrowser2.html.

Armbruster, U., Hertle, A., Makarenko, E., Zühlke, J., Pribil, M., Dietzmann, A., Schliebner, I., Aseeva, E., Fenino, E., Scharfenberg, M.*, et al.* (2009). Chloroplast Proteins without Cleavable Transit Peptides: Rare Exceptions or a Major Constituent of the Chloroplast Proteome? Molecular Plant *2*, 1325-1335.

Arnold, I., and Langer, T. (2002). Membrane protein degradation by AAA proteases in mitochondria. Biochimica et Biophysica Acta (BBA) - Molecular Cell Research *1592*, 89-96.

Arora, D., Abel, N.B., Liu, C., Van Damme, P., Yperman, K., Eeckhout, D., Vu, L.D., Wang, J., Tornkvist, A., Impens, F.*, et al.* (2020). Establishment of Proximity-Dependent Biotinylation Approaches in Different Plant Model Systems. The Plant Cell *32*, 3388-3407.

Artavanis-Tsakonas, K., Kasperkovitz Pia, V., Papa, E., Cardenas Michael, L., Khan Nida, S., Van der Veen Annemarthe, G., Ploegh Hidde, L., Vyas Jatin, M., and Deepe, G.S. (2011). The Tetraspanin CD82 Is Specifically Recruited to Fungal and Bacterial Phagosomes prior to Acidification. Infection and Immunity *79*, 1098-1106.

Arumugam, S., Schmieder, S., Pezeshkian, W., Becken, U., Wunder, C., Chinnapen, D., Ipsen, J.H., Kenworthy, A.K., Lencer, W., Mayor, S.*, et al.* (2021). Ceramide structure dictates glycosphingolipid nanodomain assembly and function. Nature Communications *12*, 3675.

Asai, T., Tena, G., Plotnikova, J., Willmann, M.R., Chiu, W.-L., Gomez-Gomez, L., Boller, T., Ausubel, F.M., and Sheen, J. (2002). MAP kinase signalling cascade in Arabidopsis innate immunity. Nature *415*, 977-983.

Axelrod, D. (1979). Carbocyanine dye orientation in red cell membrane studied by microscopic fluorescence polarization. Biophysical Journal *26*, 557-573.

Babuke, T., Ruonala, M., Meister, M., Amaddii, M., Genzler, C., Esposito, A., and Tikkanen, R. (2009). Hetero-oligomerization of reggie-1/flotillin-2 and reggie-2/flotillin-1 is required for their endocytosis. Cell Signalling *21*, 1287-1297.

Bader, A.N., Hofman, E.G., Voortman, J., en Henegouwen, P.M.P.v.B., and Gerritsen, H.C. (2009). Homo-FRET imaging enables quantification of protein cluster sizes with subcellular resolution. Biophysical Journal *97*, 2613-2622.

Bais, H.P., Vepachedu, R., Gilroy, S., Callaway, R.M., and Vivanco, J.M. (2003). Allelopathy and exotic plant invasion: from molecules and genes to species interactions. Science *301*, 1377-1380.

Bajar, B.T., Wang, E.S., Lam, A.J., Kim, B.B., Jacobs, C.L., Howe, E.S., Davidson, M.W., Lin, M.Z., and Chu, J. (2016a). Improving brightness and photostability of green and red fluorescent proteins for live cell imaging and FRET reporting. Scientific Reports *6*, 20889-20889.

Bajar, B.T., Wang, E.S., Zhang, S., Lin, M.Z., and Chu, J. (2016b). A Guide to Fluorescent Protein FRET Pairs. Sensors *16*, 1488.

Balint-Kurti, P. (2019). The plant hypersensitive response: concepts, control and consequences. Molecular Plant Pathology *20*, 1163-1178.

Banuett, F., and Herskowitz, I. (1987). Identification of polypeptides encoded by an *Escherichia coli locus* (*hflA*) that governs the lysis-lysogeny decision of bacteriophage lambda. Journal of Bacteriology *169*, 4076-4085.

Bariola, P.A., Retelska, D., Stasiak, A., Kammerer, R.A., Fleming, A., Hijri, M., Frank, S., and Farmer, E.E. (2004). Remorins form a novel family of coiled coil-forming oligomeric and filamentous proteins associated with apical, vascular and embryonic tissues in plants. Plant Molecular Biology *55*, 579-594.

Barreiro, O., Zamai, M., Yáñez-Mó, M.a., Tejera, E., López-Romero, P., Monk, P.N., Gratton, E., Caiolfa, V.R., and Sánchez-Madrid, F. (2008). Endothelial adhesion receptors are recruited to adherent leukocytes by inclusion in preformed tetraspanin nanoplatforms. Journal of Cell Biology *183*, 527-542.

Batut, J., Andersson, S.G., and O'Callaghan, D. (2004). The evolution of chronic infection strategies in the alpha-proteobacteria. Nature Reviews Microbiology *2*, 933-945.

Baumann, C.A., Ribon, V., Kanzaki, M., Thurmond, D.C., Mora, S., Shigematsu, S., Bickel, P.E., Pessin, J.E., and Saltiel, A.R. (2000). CAP defines a second signalling pathway required for insulin-stimulated glucose transport. Nature *407*, 202-207.

Baumann, T., Affentranger, S., and Niggli, V. (2012). Evidence for chemokine-mediated coalescence of preformed flotillin hetero-oligomers in human T-cells. Journal of Biological Chemistry *287*, 39664-39672.

Bayer, E.M., Mongrand, S., and Tilsner, J. (2014). Specialized membrane domains of plasmodesmata, plant intercellular nanopores. Frontiers in Plant Science *5*, 507-507.

Beihammer, G., Maresch, D., Altmann, F., and Strasser, R. (2020). Glycosylphosphatidylinositol-Anchor Synthesis in Plants: A Glycobiology Perspective. Frontiers in Plant Science *11*.

Benitez-Alfonso, Y., Faulkner, C., Pendle, A., Miyashima, S., Helariutta, Y., and Maule, A. (2013). Symplastic Intercellular Connectivity Regulates Lateral Root Patterning. Developmental Cell *26*, 136-147.

Berditchevski, F., and Odintsova, E. (2007). Tetraspanins as regulators of protein trafficking. Traffic *8*, 89-96.

Berditchevski, F., Odintsova, E., Sawada, S., and Gilbert, E. (2002). Expression of the Palmitoylation-deficient CD151 Weakens the Association of α3β1 Integrin with the Tetraspanin-enriched Microdomains and Affects Integrin-dependent Signaling*. Journal of Biological Chemistry *277*, 36991-37000.

Bhattacharyya, B., Panda, D., Gupta, S., and Banerjee, M. (2008). Anti-mitotic activity of colchicine and the structural basis for its interaction with tubulin. Medicinal Research Reviews *28*, 155-183.

Bickel, P.E., Scherer, P.E., Schnitzer, J.E., Oh, P., Lisanti, M.P., and Lodish, H.F. (1997). Flotillin and epidermal surface antigen define a new family of caveolae-associated integral membrane proteins. Journal of Biological Chemistry *272*, 13793-13802.

Birkeland, N.K. (1994). Cloning, molecular characterization, and expression of the genes encoding the lytic functions of lactococcal bacteriophage phi LC3: a dual lysis system of modular design. Canadian Journal of Microbiology *40*, 658-665.

Blackman, L.M., and Overall, R.L. (1998). Immunolocalisation of the cytoskeleton to plasmodesmata of *Chara corallina*. The Plant Journal *14*, 733-741.

Boavida, L.C., Qin, P., Broz, M., Becker, J.D., and McCormick, S. (2013). Arabidopsis Tetraspanins Are Confined to Discrete Expression Domains and Cell Types in Reproductive Tissues and Form Homo- and Heterodimers When Expressed in Yeast. Plant Physiology *163*, 696.

Bohovych, I., Chan, S.S.L., and Khalimonchuk, O. (2015). Mitochondrial protein quality control: the mechanisms guarding mitochondrial health. Antioxidants & Redox Signaling *22*, 977-994.

Bohuslav, J., Cinek, T., and Hořejší, V. (1993). Large, detergent-resistant complexes containing murine antigens Thy-1 and Ly-6 and protein tyrosine kinase $p56^{lck}$. European Journal of Immunology *23*, 825-831.

Bolte, S., and Cordeliéres, F.P. (2006). A guided tour into subcellular colocalization analysis in light microscopy. Journal of Microscopy *224*, 213-232.

Borner, G.H.H., Sherrier, D.J., Weimar, T., Michaelson, L.V., Hawkins, N.D., MacAskill, A., Napier, J.A., Beale, M.H., Lilley, K.S., and Dupree, P. (2005). Analysis of Detergent-Resistant Membranes in Arabidopsis. Evidence for Plasma Membrane Lipid Rafts. Plant Physiology *137*, 104-116.

Bossis, G., and Melchior, F. (2006). Regulation of SUMOylation by Reversible Oxidation of SUMO Conjugating Enzymes. Molecular Cell *21*, 349-357.

Bowler, C., and Fluhr, R. (2000). The role of calcium and activated oxygens as signals for controlling cross-tolerance. Trends in Plant Science *5*, 241-246.

Bramkamp, M., and Lopez, D. (2015). Exploring the existence of lipid rafts in bacteria. Microbiology and Molecular Biology Reviews *79*, 81-100.

Brandizzi, F., Snapp, E.L., Roberts, A.G., Lippincott-Schwartz, J., and Hawes, C. (2002). Membrane protein transport between the endoplasmic reticulum and the Golgi in tobacco leaves is energy dependent but cytoskeleton independent: evidence from selective photobleaching. The Plant Cell *14*, 1293-1309.

Braten, O., Livneh, I., Ziv, T., Admon, A., Kehat, I., Caspi, L.H., Gonen, H., Bercovich, B., Godzik, A., Jahandideh, S.*, et al.* (2016). Numerous proteins with unique characteristics are degraded by the 26S proteasome following monoubiquitination. Proceedings of the National Academy of Sciences *113*, E4639.

Brault, M.L., Petit, J.D., Immel, F., Nicolas, W.J., Brocard, L., Gaston, A., Fouche, M., Hawkins, T.J., Crowet, J.-M., Grison, M.S.*, et al.* (2018). Multiple C2 domains and Transmembrane region Proteins (MCTPs) tether membranes at plasmodesmata. bioRxiv.

Brault, M.L., Petit, J.D., Immel, F., Nicolas, W.J., Glavier, M., Brocard, L., Gaston, A., Fouché, M., Hawkins, T.J., Crowet, J.M.*, et al.* (2019). Multiple C2 domains and transmembrane region proteins (MCTPs) tether membranes at plasmodesmata. EMBO Reports *20*, e47182.

Breen, J., Mur, L.A., Sivakumaran, A., Akinyemi, A., Wilkinson, M.J., and Rodriguez Lopez, C.M. (2022). *Botrytis cinerea* Loss and Restoration of Virulence during *In Vitro* Culture Follows Flux in Global DNA Methylation. International Journal of Molecular Sciences *23*.

Browman, D.T., Hoegg, M.B., and Robbins, S.M. (2007). The SPFH domain-containing proteins: more than lipid raft markers. Trends in Cell Biology *17*, 394-402.

Browman, D.T., Resek, M.E., Zajchowski, L.D., and Robbins, S.M. (2006). Erlin-1 and erlin-2 are novel members of the prohibitin family of proteins that define lipid-raft-like domains of the ER. Journal of Cell Science *119*, 3149-3160.

Brown, D.A., and London, E. (1998). Functions of lipid rafts in biological membranes. Annual Review of Cell and Developmental Biology *14*, 111-136.

Brown, D.A., and Rose, J.K. (1992). Sorting of GPI-anchored proteins to glycolipid-enriched membrane subdomains during transport to the apical cell surface. Cell *68*, 533-544.

Brown, H.E., Esher, S.K., and Alspaugh, J.A. (2020). Chitin: A “Hidden Figure” in the Fungal Cell Wall. In The Fungal Cell Wall : An Armour and a Weapon for Human Fungal Pathogens, J.-P. Latgé, ed. (Cham: Springer International Publishing), pp. 83-111.

Bücherl, C.A., Jarsch, I.K., Schudoma, C., Segonzac, C., Mbengue, M., Robatzek, S., MacLean, D., Ott, T., and Zipfel, C. (2017). Plant immune and growth receptors share common signalling components but localise to distinct plasma membrane nanodomains. eLife *6*, e25114.

Buendia, L., Girardin, A., Wang, T., Cottret, L., and Lefebvre, B. (2018). LysM Receptor-Like Kinase and LysM Receptor-Like Protein Families: An Update on Phylogeny and Functional Characterization. Frontiers in Plant Science *9*, 1531-1531.

Bush, K., and Gertzman, A.A. (2016). Chapter 5 - Process Development and Manufacturing of Human and Animal Acellular Dermal Matrices. In Skin Tissue Engineering and Regenerative Medicine, M.Z. Albanna, and J.H. Holmes Iv, eds. (Boston: Academic Press), pp. 83-108.

Buxdorf, K., Yaffe, H., Barda, O., and Levy, M. (2013). The Effects of Glucosinolates and Their Breakdown Products on Necrotrophic Fungi. PLOS One *8*, e70771.

Cacas, J.-L., Buré, C., Grosjean, K., Gerbeau-Pissot, P., Lherminier, J., Rombouts, Y., Maes, E., Bossard, C., Gronnier, J., Furt, F.*, et al.* (2016). Revisiting Plant Plasma Membrane Lipids in Tobacco: A Focus on Sphingolipids. Plant Physiology *170*, 367-384.

Cai, Q., He, B., Weiberg, A., Buck, A.H., and Jin, H. (2020). Small RNAs and extracellular vesicles: New mechanisms of cross-species communication and innovative tools for disease control. PLOS Pathogens *15*, e1008090.

Cai, Q., Qiao, L., Wang, M., He, B., Lin, F.-M., Palmquist, J., Huang, S.-D., and Jin, H. (2018). Plants send small RNAs in extracellular vesicles to fungal pathogen to silence virulence genes. Science *360*, 1126.

Cano, R., and Lopera, H. (2013). Introduction to T and B lymphocytes. In Autoimmunity: From Bench to Bedside, R.-V.A. Shoenfeld Y, et al., editors. , ed. (Bogota (Colombia): El Rosario University Press).

Cao, S., Peterson, S.M., Müller, S., Reichelt, M., McRoberts Amador, C., and Martinez-Martin, N. (2021). A membrane protein display platform for receptor interactome discovery. Proceedings of the National Academy of Sciences *118*, e2025451118.

Cao, Y., Liang, Y., Tanaka, K., Nguyen, C.T., Jedrzejczak, R.P., Joachimiak, A., and Stacey, G. (2014). The kinase LYK5 is a major chitin receptor in Arabidopsis and forms a chitin-induced complex with related kinase CERK1. eLife *3*.

Chan, J., and Coen, E. (2020). Interaction between Autonomous and Microtubule Guidance Systems Controls Cellulose Synthase Trajectories. Current Biology *30*, 941-947.e942.

Charrin, S., Manié, S., Oualid, M., Billard, M., Boucheix, C., and Rubinstein, E. (2002). Differential stability of tetraspanin/tetraspanin interactions: role of palmitoylation. FEBS Letters *516*, 139-144.

Chen, D., Ahsan, N., Thelen, J.J., and Stacey, G. (2019). S-Acylation of plant immune receptors mediates immune signaling in plasma membrane nanodomains. bioRxiv, 720482.

Chen, D., Hao, F., Mu, H., Ahsan, N., Thelen, J.J., and Stacey, G. (2021). S-acylation of P2K1 mediates extracellular ATP-induced immune signaling in Arabidopsis. Nature Communications *12*, 2750.

Chen, H., Ahmad, M., Rim, Y., Lucas, W.J., and Kim, J.-Y. (2013). Evolutionary and molecular analysis of Dof transcription factors identified a conserved motif for intercellular protein trafficking. New Phytologist *198*, 1250-1260.

Chen, H., He, S., Zhang, S., A, R., Li, W., and Liu, S. (2022). The Necrotroph Botrytis cinerea BcSpd1 Plays a Key Role in Modulating Both Fungal Pathogenic Factors and Plant Disease Development. Frontiers in Plant Science *13*.

Chen, Y., Bharill, S., Isacoff, E.Y., and Chalfie, M. (2015). Subunit composition of a DEG/ENaC mechanosensory channel of *Caenorhabditis elegans*. Proceedings of the National Academy of Sciences *112*, 11690.

Cheng, G., Dong, M., Xu, Q., Peng, L., Yang, Z., Wei, T., and Xu, J. (2017). Dissecting the Molecular Mechanism of the Subcellular Localization and Cell-to-cell Movement of the Sugarcane mosaic virus P3N-PIPO. Scientific Reports *7*, 9868.

Cheval, C., and Faulkner, C. (2017). Plasmodesmal regulation during plant–pathogen interactions. New Phytologist, n/a-n/a.

Cheval, C., Samwald, S., Johnston, M.G., de Keijzer, J., Breakspear, A., Liu, X., Bellandi, A., Kadota, Y., Zipfel, C., and Faulkner, C. (2020). Chitin perception in plasmodesmata characterizes submembrane immune-signaling specificity in plants. Proceedings of the National Academy of Sciences, 201907799.

Chinchilla, D., Bauer, Z., Regenass, M., Boller, T., and Felix, G. (2006). The Arabidopsis receptor kinase FLS2 binds flg22 and determines the specificity of flagellin perception. The Plant Cell *18*, 465.

Chinchilla, D., Zipfel, C., Robatzek, S., Kemmerling, B., Nürnberger, T., Jones, J.D.G., Felix, G., and Boller, T. (2007). A flagellin-induced complex of the receptor FLS2 and BAK1 initiates plant defence. Nature *448*, 497-500.

Chiu, C.F., Ho, M.Y., Peng, J.M., Hung, S.W., Lee, W.H., Liang, C.M., and Liang, S.M. (2013). Raf activation by Ras and promotion of cellular metastasis require phosphorylation of prohibitin in the raft domain of the plasma membrane. Oncogene *32*, 777-787.

Chiu, W.H., Chandler, J., Cnops, G., Van Lijsebettens, M., and Werr, W. (2007). Mutations in the *TORNADO2* gene affect cellular decisions in the peripheral zone of the shoot apical meristem of *Arabidopsis thaliana*. Plant Molecular Biology *63*, 731-744.

Choi, H.W., Kim, Y.J., and Hwang, B.K. (2011). The hypersensitive induced reaction and leucine-rich repeat proteins regulate plant cell death associated with disease and plant immunity. Molecular Plant-Microbe Interactions *24*, 68-78.

Choquer, M., Fournier, E., Kunz, C., Levis, C., Pradier, J.-M., Simon, A., and Viaud, M. (2007). *Botrytis cinerea* virulence factors: new insights into a necrotrophic and polyphageous pathogen. FEMS Microbiology Letters *277*, 1-10.

Ciliberti, N., Fermaud, M., Roudet, J., and Rossi, V. (2015). Environmental Conditions Affect *Botrytis cinerea* Infection of Mature Grape Berries More Than the Strain or Transposon Genotype. Phytopathology *105*, 1090-1096.

Clark, K.L., Oelke, A., Johnson, M.E., Eilert, K.D., Simpson, P.C., and Todd, S.C. (2004). CD81 Associates with 14-3-3 in a Redox-regulated Palmitoylation-dependent Manner*. Journal of Biological Chemistry *279*, 19401-19406.

Clark, P. (2014). Protease-mediated ectodomain shedding. Thorax *69*, 682-684.

Clay, N.K., Adio, A.M., Denoux, C., Jander, G., and Ausubel, F.M. (2009). Glucosinolate metabolites required for an Arabidopsis innate immune response. Science *323*, 95-101.

Clergeot, P.H., Gourgues, M., Cots, J., Laurans, F., Latorse, M.P., Pepin, R., Tharreau, D., Notteghem, J.L., and Lebrun, M.H. (2001). PLS1, a gene encoding a tetraspanin-like protein, is required for penetration of rice leaf by the fungal pathogen Magnaporthe grisea. Proceedings of the National Academy of Sciences of the United States of America *98*, 6963-6968.

Clough, S.J., and Bent, A.F. (1998). Floral dip: a simplified method for *Agrobacterium*-mediated transformation of *Arabidopsis thaliana*. The Plant Journal *16*, 735-743.

Cnops, G., Neyt, P., Raes, J., Petrarulo, M., Nelissen, H., Malenica, N., Luschnig, C., Tietz, O., Ditengou, F., Palme, K.*, et al.* (2006). The *TORNADO1* and *TORNADO2* genes function in several patterning processes during early leaf development in *Arabidopsis thaliana*. The Plant Cell *18*, 852-866.

Coll, N.S., Epple, P., and Dangl, J.L. (2011). Programmed cell death in the plant immune system. Cell Death and Differentiation *18*, 1247-1256.

Consortium, T.U. (2020). UniProt: the universal protein knowledgebase in 2021. In Nucleic acids research, pp. D480-D489.

Cooper, G. (2000). The Cell: A Molecular Approach (Sunderland (MA): Sinauer Associates).

Cordy, J.M., Hussain, I., Dingwall, C., Hooper Nigel, M., and Turner Anthony, J. (2003). Exclusively targeting β-secretase to lipid rafts by GPI-anchor addition up-regulates β-site processing of the amyloid precursor protein. Proceedings of the National Academy of Sciences *100*, 11735-11740.

Couto, D., and Zipfel, C. (2016). Regulation of pattern recognition receptor signalling in plants. Nature Reviews Immunology *16*, 537-552.

Cruz-Mireles, N., Eseola, A.B., Osés-Ruiz, M., Ryder, L.S., and Talbot, N.J. (2021). From appressorium to transpressorium—Defining the morphogenetic basis of host cell invasion by the rice blast fungus. PLOS Pathogens *17*, e1009779.

Cui, Y., Li, X., Yu, M., Li, R., Fan, L., Zhu, Y., and Lin, J. (2018). Sterols regulate endocytic pathways during flg22-induced defense responses in Arabidopsis. Development *145*.

Daněk, M., Angelini, J., Malínská, K., Andrejch, J., Amlerová, Z., Kocourková, D., Brouzdová, J., Valentová, O., Martinec, J., and Petrášek, J. (2020). Cell wall contributes to the stability of plasma membrane nanodomain organization of *Arabidopsis thaliana* FLOTILLIN2 and HYPERSENSITIVE INDUCED REACTION1 proteins. The Plant Journal *101*, 619-636.

Daněk, M., Valentová, O., and Martinec, J. (2016). Flotillins, Erlins, and HIRs: From Animal Base Camp to Plant New Horizons. Critical Reviews in Plant Sciences *35*, 191-214.

Dascher, C., and Balch, W.E. (1994). Dominant inhibitory mutants of ARF1 block endoplasmic reticulum to Golgi transport and trigger disassembly of the Golgi apparatus. Journal of Biological Chemistry *269*, 1437-1448.

Davis, P., Zarowiecki, M., Arnaboldi, V., Becerra, A., Cain, S., Chan, J., Chen, W.J., Cho, J., da Veiga Beltrame, E., Diamantakis, S.*, et al.* (2022). WormBase in 2022—data, processes, and tools for analyzing *Caenorhabditis elegans*. Genetics, iyac003.

De la Concepcion, J.C., Franceschetti, M., MacLean, D., Terauchi, R., Kamoun, S., and Banfield, M.J. (2019). Protein engineering expands the effector recognition profile of a rice NLR immune receptor. eLife *8*, e47713.

Dean, R., Van Kan, J.A.L., Pretorius, Z.A., Hammond-Kosack, K.E., Di Pietro, A., Spanu, P.D., Rudd, J.J., Dickman, M., Kahmann, R., Ellis, J.*, et al.* (2012). The Top 10 fungal pathogens in molecular plant pathology. Molecular Plant Pathology *13*, 414-430.

DeBolt, S., Gutierrez, R., Ehrhardt, D.W., and Somerville, C. (2007). Nonmotile Cellulose Synthase Subunits Repeatedly Accumulate within Localized Regions at the Plasma Membrane in Arabidopsis Hypocotyl Cells following 2,6-Dichlorobenzonitrile Treatment. Plant Physiology *145*, 334-338.

Demir, F., Horntrich, C., Blachutzik Jörg, O., Scherzer, S., Reinders, Y., Kierszniowska, S., Schulze Waltraud, X., Harms Gregory, S., Hedrich, R., Geiger, D.*, et al.* (2013). Arabidopsis nanodomain-delimited ABA signaling pathway regulates the anion channel SLAH3. Proceedings of the National Academy of Sciences *110*, 8296-8301.

Denay, G., Schultz, P., Hänsch, S., Weidtkamp-Peters, S., and Simon, R. (2019). Over the rainbow: A practical guide for fluorescent protein selection in plant FRET experiments. Plant Direct *3*, e00189.

Dermine, J.F., Duclos, S., Garin, J., St-Louis, F., Rea, S., Parton, R.G., and Desjardins, M. (2001). Flotillin-1-enriched lipid raft domains accumulate on maturing phagosomes. Journal of Biological Chemistry *276*, 18507-18512.

Dodds, P.N., and Rathjen, J.P. (2010). Plant immunity: towards an integrated view of plant–pathogen interactions. Nature Reviews Genetics *11*, 539-548.

Drevot, P., Langlet, C., Guo, X.-J., Bernard, A.-M., Colard, O., Chauvin, J.-P., Lasserre, R., and He, H.-T. (2002). TCR signal initiation machinery is pre-assembled and activated in a subset of membrane rafts. The EMBO Journal *21*, 1899-1908.

Dubiella, U., Seybold, H., Durian, G., Komander, E., Lassig, R., Witte, C.-P., Schulze, W.X., and Romeis, T. (2013). Calcium-dependent protein kinase/NADPH oxidase activation circuit is required for rapid defense signal propagation. Proceedings of the National Academy of Sciences of the United States of America *110*, 8744-8749.

El-Brolosy, M.A., Kontarakis, Z., Rossi, A., Kuenne, C., Günther, S., Fukuda, N., Kikhi, K., Boezio, G.L.M., Takacs, C.M., Lai, S.-L.*, et al.* (2019). Genetic compensation triggered by mutant mRNA degradation. Nature *568*, 193-197.

Elieh-Ali-Komi, D., and Hamblin, M.R. (2016). Chitin and Chitosan: Production and Application of Versatile Biomedical Nanomaterials. International journal of advanced research *4*, 411-427.

Emanuelsson, O., Nielsen, H., and von Heijne, G. (1999). ChloroP, a neural network-based method for predicting chloroplast transit peptides and their cleavage sites. Protein Science *8*, 978-984.

Engel, N., Eisenhut, M., Qu, N., and Bauwe, H. (2008). Arabidopsis Mutants with Strongly Reduced Levels of the T-Protein Subunit of Glycine Decarboxylase. In, pp. 819-822.

Engler, C., Youles, M., Gruetzner, R., Ehnert, T.-M., Werner, S., Jones, J.D.G., Patron, N.J., and Marillonnet, S. (2014). A Golden Gate Modular Cloning Toolbox for Plants. ACS Synthetic Biology *3*, 839-843.

Erbs, G., Silipo, A., Aslam, S., De Castro, C., Liparoti, V., Flagiello, A., Pucci, P., Lanzetta, R., Parrilli, M., Molinaro, A.*, et al.* (2008). Peptidoglycan and muropeptides from pathogens *Agrobacterium* and *Xanthomonas* elicit plant innate immunity: structure and activity. Chem Biol *15*, 438-448.

Erwig, J., Ghareeb, H., Kopischke, M., Hacke, R., Matei, A., Petutschnig, E., and Lipka, V. (2017). Chitin-induced and CHITIN ELICITOR RECEPTOR KINASE1 (CERK1) phosphorylation-dependent endocytosis of *Arabidopsis thaliana* LYSIN MOTIF-CONTAINING RECEPTOR-LIKE KINASE5 (LYK5). New Phytologist *215*, 382-396.

Faulkner, C. (2013). Receptor-mediated signaling at plasmodesmata. Frontiers in Plant Science *4*, 521.

Faulkner, C., Akman, O.E., Bell, K., Jeffree, C., and Oparka, K. (2008). Peeking into Pit Fields: A Multiple Twinning Model of Secondary Plasmodesmata Formation in Tobacco. The Plant Cell *20*, 1504-1518.

Faulkner, C., and Bayer, E.M. (2017). Isolation of Plasmodesmata. Methods in Molecular Biology *1511*, 187-198.

Faulkner, C., Petutschnig, E., Benitez-Alfonso, Y., Beck, M., Robatzek, S., Lipka, V., and Maule, A.J. (2013). LYM2-dependent chitin perception limits molecular flux via plasmodesmata. Proceedings of the National Academy of Sciences *110*, 9166.

Feechan, A., Turnbull, D., Stevens, L.J., Engelhardt, S., Birch, P.R.J., Hein, I., and Gilroy, E.M. (2015). The Hypersensitive Response in PAMP- and Effector-Triggered Immune Responses. In Plant Programmed Cell Death, A.N. Gunawardena, and P.F. McCabe, eds. (Cham: Springer International Publishing), pp. 235-268.

Felix, G., Regenass, M., and Boller, T. (1993). Specific perception of subnanomolar concentrations of chitin fragments by tomato cells: induction of extracellular alkalinization, changes in protein phosphorylation, and establishment of a refractory state. The Plant Journal *4*, 307-316.

Feng, F., Sun, J., Radhakrishnan, G.V., Lee, T., Bozsóki, Z., Fort, S., Gavrin, A., Gysel, K., Thygesen, M.B., Andersen, K.R.*, et al.* (2019). A combination of chitooligosaccharide and lipochitooligosaccharide recognition promotes arbuscular mycorrhizal associations in *Medicago truncatula*. Nature Communications *10*, 5047.

Fernandez-Calvino, L., Faulkner, C., Walshaw, J., Saalbach, G., Bayer, E., Benitez-Alfonso, Y., and Maule, A. (2011). Arabidopsis Plasmodesmal Proteome. PLOS One *6*, e18880.

Figueiredo, A., Monteiro, F., and Sebastiana, M. (2014). Subtilisin-like proteases in plant–pathogen recognition and immune priming: a perspective. Frontiers in Plant Science *5*.

Fitzgibbon, J., Bell, K., King, E., and Oparka, K. (2010). Super-Resolution Imaging of Plasmodesmata Using Three-Dimensional Structured Illumination Microscopy. Plant Physiology *153*, 1453-1463.

Fleurat-Lessard, P., Bouché-Pillon, S., Leloup, C., Lucas, W.J., Serrano, R., and Bonnemain, J.L. (1995). Absence of plasma membrane H^+-ATPase in plasmodesmata located in pit-fields of the young reactive pulvinus of *Mimosa pudica* L. Protoplasma *188*, 180-185.

Fliegmann, J., Uhlenbroich, S., Shinya, T., Martinez, Y., Lefebvre, B., Shibuya, N., and Bono, J.J. (2011). Biochemical and phylogenetic analysis of CEBiP-like LysM domain-containing extracellular proteins in higher plants. Plant Physiology and Biochemistry *49*, 709-720.

Forrester, M.T., Hess, D.T., Thompson, J.W., Hultman, R., Moseley, M.A., Stamler, J.S., and Casey, P.J. (2011). Site-specific analysis of protein S-acylation by resin-assisted capture. Journal of Lipid Research *52*, 393-398.

Foster, P.G., and Hickey, D.A. (1999). Compositional Bias May Affect Both DNA-Based and Protein-Based Phylogenetic Reconstructions. Journal of Molecular Evolution *48*, 284-290.

Frick, M., Bright, N.A., Riento, K., Bray, A., Merrified, C., and Nichols, B.J. (2007). Coassembly of flotillins induces formation of membrane microdomains, membrane curvature, and vesicle budding. Current Biology *17*, 1151-1156.

Fry, S.C. (2004). Primary cell wall metabolism: tracking the careers of wall polymers in living plant cells. New Phytologist *161*, 641-675.

Fu, P., Yang, Z., and Bach, L.A. (2013). Prohibitin-2 Binding Modulates Insulin-like Growth Factor-binding Protein-6 (IGFBP-6)-induced Rhabdomyosarcoma Cell Migration. Journal of Biological Chemistry *288*, 29890-29900.

Fu, S., Xu, Y., Li, C., Li, Y., Wu, J., and Zhou, X. (2018). Rice Stripe Virus Interferes with S-acylation of Remorin and Induces Its Autophagic Degradation to Facilitate Virus Infection. Molecular Plant *11*, 269-287.

Fujisaki, K., Kobayashi, S., Tsujimoto, Y., Naito, S., and Ishikawa, M. (2008). Analysis of tobamovirus multiplication in *Arabidopsis thaliana* mutants defective in TOM2A homologues. Journal of General Virology *89*, 1519-1524.

Galbiati, F., Volonte, D., Goltz, J.S., Steele, Z., Sen, J., Jurcsak, J., Stein, D., Stevens, L., and Lisanti, M.P. (1998). Identification, sequence and developmental expression of invertebrate flotillins from *Drosophila melanogaster*. Gene *210*, 229-237.

Gamble, S.C., Chotai, D., Odontiadis, M., Dart, D.A., Brooke, G.N., Powell, S.M., Reebye, V., Varela-Carver, A., Kawano, Y., Waxman, J., *et al.* (2007). Prohibitin, a protein downregulated by androgens, represses androgen receptor activity. Oncogene *26*, 1757-1768.

Garin, J., Diez, R., Kieffer, S., Dermine, J.F., Duclos, S., Gagnon, E., Sadoul, R., Rondeau, C., and Desjardins, M. (2001). The phagosome proteome: insight into phagosome functions. The Journal of Cell Biology *152*, 165-180.

Garner, A.E., Smith, D.A., and Hooper, N.M. (2008). Visualization of detergent solubilization of membranes: implications for the isolation of rafts. Biophysical Journal *94*, 1326-1340.

Gautsch, J.W., and Wulff, D.L. (1974). Fine structure mapping, complementation, and physiology of *Escherichia coli hfl* mutants. Genetics *77*, 435-448.

Gehl, B., Lee, C.P., Bota, P., Blatt, M.R., and Sweetlove, L.J. (2014). An Arabidopsis Stomatin-Like Protein Affects Mitochondrial Respiratory Supercomplex Organization. Plant Physiology *164*, 1389-1400.

Geiss-Friedlander, R., and Melchior, F. (2007). Concepts in sumoylation: a decade on. Nature Reviews Molecular Cell Biology *8*, 947-956.

Gerdes, H.-H., and Carvalho, R.N. (2008). Intercellular transfer mediated by tunneling nanotubes. Current Opinion in Cell Biology *20*, 470-475.

Giannoutsou, E., Sotiriou, P., Apostolakos, P., and Galatis, B. (2013). Early local differentiation of the cell wall matrix defines the contact sites in lobed mesophyll cells of Zea mays. Annals of Botany *112*, 1067-1081.

Giovannoni, M., Lironi, D., Marti, L., Paparella, C., Vecchi, V., Gust, A.A., De Lorenzo, G., Nürnberger, T., and Ferrari, S. (2021). The *Arabidopsis thaliana* LysM-containing RECEPTOR-LIKE KINASE 2 is required for elicitor-induced resistance to pathogens. Plant, Cell & Environment *44*, 3775-3792.

Glynn, S.E. (2017). Multifunctional Mitochondrial AAA Proteases. Frontiers in Molecular Biosciences *4*.

Goff, K.E., and Ramonell, K.M. (2007). The Role and Regulation of Receptor-Like Kinases in Plant Defense. Gene Regulation and Systems Biology *1*, 117762500700100015.

Golldack, D., Vera, P., and Dietz, K.-J. (2003). Expression of subtilisin-like serine proteases in Arabidopsis thaliana is cell-specific and responds to jasmonic acid and heavy metals with developmental differences. Physiologia Plantarum *118*, 64-73.

Gómez-Gómez, L., Felix, G., and Boller, T. (1999). A single locus determines sensitivity to bacterial flagellin in Arabidopsis thaliana. The Plant Journal *18*, 277-284.

Gong, B.-Q., Xue, J., Zhang, N., Xu, L., Yao, X., Yang, Q.-J., Yu, Y., Wang, H.-B., Zhang, D., and Li, J.-F. (2017). Rice Chitin Receptor OsCEBiP Is Not a Transmembrane Protein but Targets the Plasma Membrane via a GPI Anchor. Molecular Plant *10*, 767-770.

Gordon, J.A. (1991). Use of vanadate as protein-phosphotyrosine phosphatase inhibitor. In Methods in Enzymology (Academic Press), pp. 477-482.

Gourgues, M., Brunet-Simon, A., Lebrun, M.H., and Levis, C. (2004). The tetraspanin BcPls1 is required for appressorium-mediated penetration of Botrytis cinerea into host plant leaves. Molecular Microbiology *51*, 619-629.

Govrin, E.M., and Levine, A. (2000). The hypersensitive response facilitates plant infection by the necrotrophic pathogen *Botrytis cinerea*. Current Biology *10*, 751-757.

Greaves, J., Prescott, G.R., Gorleku, O.A., and Chamberlain, L.H. (2009). The fat controller: roles of palmitoylation in intracellular protein trafficking and targeting to membrane microdomains (Review). Molecular Membrane Biology *26*, 67-79.

Green, J.B., Lower, R.P.J., and Young, J.P.W. (2009). The NfeD Protein Family and Its Conserved Gene Neighbours Throughout Prokaryotes: Functional Implications for Stomatin-Like Proteins. Journal of Molecular Evolution *69*, 657.

Green, J.B., and Young, J.P.W. (2008). Slipins: ancient origin, duplication and diversification of the stomatin protein family. BMC Evolutionary Biology *8*, 44.

Grell, M., Douni, E., Wajant, H., Löhden, M., Clauss, M., Maxeiner, B., Georgopoulos, S., Lesslauer, W., Kollias, G., Pfizenmaier, K.*, et al.* (1995). The transmembrane form of tumor necrosis factor is the prime activating ligand of the 80 kDa tumor necrosis factor receptor. Cell *83*, 793-802.

Griffiths, R.E., Heesom, K.J., and Anstee, D.J. (2007). Normal prion protein trafficking in cultured human erythroblasts. Blood *110*, 4518-4525.

Grison, M.S., Brocard, L., Fouillen, L., Nicolas, W., Wewer, V., Dörmann, P., Nacir, H., Benitez-Alfonso, Y., Claverol, S., Germain, V.*, et al.* (2015a). Specific Membrane Lipid Composition Is Important for Plasmodesmata Function in Arabidopsis. The Plant Cell *27*, 1228.

Grison, M.S., Fernandez-Calvino, L., Mongrand, S., and Bayer, E.M.F. (2015b). Isolation of Plasmodesmata from Arabidopsis Suspension Culture Cells. In Plasmodesmata: Methods and Protocols, M. Heinlein, ed. (New York, NY: Springer New York), pp. 83-93.

Grison, M.S., Kirk, P., Brault, M.L., Wu, X.N., Schulze, W.X., Benitez-Alfonso, Y., Immel, F., and Bayer, E.M. (2019). Plasma Membrane-Associated Receptor-like Kinases Relocalize to Plasmodesmata in Response to Osmotic Stress. Plant Physiology *181*, 142-160.

Gronnier, J., Crowet, J.-M., Habenstein, B., Nasir, M.N., Bayle, V., Hosy, E., Platre, M.P., Gouguet, P., Raffaele, S., Martinez, D.*, et al.* (2017). Structural basis for plant plasma membrane protein dynamics and organization into functional nanodomains. eLife *6*, e26404.

Gronnier, J., Gerbeau-Pissot, P., Germain, V., Mongrand, S., and Simon-Plas, F. (2018). Divide and Rule: Plant Plasma Membrane Organization. Trends in Plant Science *23*, 899-917.

Gui, J., Zheng, S., Liu, C., Shen, J., Li, J., and Li, L. (2016). OsREM4.1 Interacts with OsSERK1 to Coordinate the Interlinking between Abscisic Acid and Brassinosteroid Signaling in Rice. Developmental Cell *38*, 201-213.

Gui, J., Zheng, S., Shen, J., and Li, L. (2015). Grain setting defect1 (GSD1) function in rice depends on S-acylation and interacts with actin 1 (OsACT1) at its C-terminal. Frontiers in Plant Science *6*.

Guo, H.J., and Tadi, P. (2022). Biochemistry, Ubiquitination. In StatPearls (Treasure Island (FL): StatPearls Publishing LLC.).

Guo, L., Qi, Y., Mu, Y., Zhou, J., Lu, W., and Tian, Z. (2022). Potato StLecRK-IV.1 negatively regulates late blight resistance by affecting the stability of a positive regulator StTET8. Horticulture Research.

Guseman, J.M., Lee, J.S., Bogenschutz, N.L., Peterson, K.M., Virata, R.E., Xie, B., Kanaoka, M.M., Hong, Z., and Torii, K.U. (2010). Dysregulation of cell-to-cell connectivity and stomatal patterning by loss-of-function mutation in Arabidopsis chorus (glucan synthase-like 8). Development *137*, 1731-1741.

Gust, A.A., Biswas, R., Lenz, H.D., Rauhut, T., Ranf, S., Kemmerling, B., Götz, F., Glawischnig, E., Lee, J., Felix, G.*, et al.* (2007). Bacteria-derived peptidoglycans constitute pathogen-associated molecular patterns triggering innate immunity in Arabidopsis. Journal of Biological Chemistry *282*, 32338-32348.

Gust, A.A., Willmann, R., Desaki, Y., Grabherr, H.M., and Nürnberger, T. (2012). Plant LysM proteins: modules mediating symbiosis and immunity. Trends in Plant Science *17*, 495-502.

Gutjahr, C., Gobbato, E., Choi, J., Riemann, M., Johnston, M.G., Summers, W., Carbonnel, S., Mansfield, C., Yang, S.-Y., Nadal, M.*, et al.* (2015). Rice perception of symbiotic arbuscular mycorrhizal fungi requires the karrikin receptor complex. Science *350*, 1521-1524.

Gutmann, D.A.P., Mizohata, E., Newstead, S., Ferrandon, S., Postis, V., Xia, X., Henderson, P.J.F., van Veen, H.W., and Byrne, B. (2007). A high-throughput method for membrane protein solubility screening: the ultracentrifugation dispersity sedimentation assay. Protein Science *16*, 1422-1428.

Haier, J., and Nicolson, G.L. (2000). Time-dependent dephosphorylation through serine/threonine phosphatases is required for stable adhesion of highly and poorly metastatic HT-29 colon carcinoma cell lines to collagen. Anticancer Research *20*, 2265-2271.

Haney, C.H., and Long, S.R. (2010). Plant flotillins are required for infection by nitrogen-fixing bacteria. Proceedings of the National Academy of Sciences *107*, 478.

Haney, C.H., Riely, B.K., Tricoli, D.M., Cook, D.R., Ehrhardt, D.W., and Long, S.R. (2011). Symbiotic rhizobia bacteria trigger a change in localization and dynamics of the *Medicago truncatula* receptor kinase LYK3. Plant Cell *23*, 2774-2787.

Hao, H., Fan, L., Chen, T., Li, R., Li, X., He, Q., Botella, M.A., and Lin, J. (2014). Clathrin and Membrane Microdomains Cooperatively Regulate RbohD Dynamics and Activity in Arabidopsis. The Plant Cell *26*, 1729-1745.

Harries, P.A., Palanichelvam, K., Yu, W., Schoelz, J.E., and Nelson, R.S. (2009). The Cauliflower Mosaic Virus Protein P6 Forms Motile Inclusions That Traffic along Actin Microfilaments and Stabilize Microtubules. Plant Physiology *149*, 1005-1016.

Harris, T.W., Arnaboldi, V., Cain, S., Chan, J., Chen, W.J., Cho, J., Davis, P., Gao, S., Grove, C.A., Kishore, R.*, et al.* (2019). WormBase: a modern Model Organism Information Resource. Nucleic Acids Research *48*, D762-D767.

Hartmann, M.A., Perret, A.M., Carde, J.P., Cassagne, C., and Moreau, P. (2002). Inhibition of the sterol pathway in leek seedlings impairs phosphatidylserine and glucosylceramide synthesis but triggers an accumulation of triacylglycerols. Biochimica et Biophysica Acta *1583*, 285-296.

Hassuna, N., Monk, P.N., Moseley, G.W., and Partridge, L.J. (2009). Strategies for targeting tetraspanin proteins: potential therapeutic applications in microbial infections. Biodrugs *23*, 341-359.

Häweker, H., Rips, S., Koiwa, H., Salomon, S., Saijo, Y., Chinchilla, D., Robatzek, S., and von Schaewen, A. (2010). Pattern recognition receptors require N-glycosylation to mediate plant immunity. Journal of Biological Chemistry *285*, 4629-4636.

Hayafune, M., Berisio, R., Marchetti, R., Silipo, A., Kayama, M., Desaki, Y., Arima, S., Squeglia, F., Ruggiero, A., Tokuyasu, K.*, et al.* (2014). Chitin-induced activation of immune signaling by the rice receptor CEBiP relies on a unique sandwich-type dimerization. Proceedings of the National Academy of Sciences *111*, E404.

Hayashida, K., Bartlett, A.H., Chen, Y., and Park, P.W. (2010). Molecular and cellular mechanisms of ectodomain shedding. Anatomical record (Hoboken, NJ : 2007) *293*, 925-937.

Heazlewood, J.L., Tonti-Filippini, J.S., Gout, A.M., Day, D.A., Whelan, J., and Millar, A.H. (2004). Experimental Analysis of the Arabidopsis Mitochondrial Proteome Highlights Signaling and Regulatory Components, Provides Assessment of Targeting Prediction Programs, and Indicates Plant-Specific Mitochondrial Proteins. The Plant Cell *16*, 241-256.

Heerklotz, H. (2002). Triton promotes domain formation in lipid raft mixtures. Biophysical Journal *83*, 2693-2701.

Hemler, M.E. (2005). Tetraspanin functions and associated microdomains. Nature Reviews Molecular Cell Biology *6*, 801-811.

Hemler, M.E. (2014). Tetraspanin proteins promote multiple cancer stages. Nature Reviews Cancer *14*, 49-60.

Hemsley, P.A., Weimar, T., Lilley, K.S., Dupree, P., and Grierson, C.S. (2013). A proteomic approach identifies many novel palmitoylated proteins in Arabidopsis. New Phytologist *197*, 805-814.

Henty-Ridilla, J.L., Shimono, M., Li, J., Chang, J.H., Day, B., and Staiger, C.J. (2013). The Plant Actin Cytoskeleton Responds to Signals from Microbe-Associated Molecular Patterns. PLOS Pathogens *9*, e1003290.

Hibino, H., and Kurachi, Y. (2007). Distinct detergent-resistant membrane microdomains (lipid rafts) respectively harvest K+ and water transport systems in brain astroglia. European Journal of Neuroscience *26*, 2539-2555.

Higaki, T., Goh, T., Hayashi, T., Kutsuna, N., Kadota, Y., Hasezawa, S., Sano, T., and Kuchitsu, K. (2007). Elicitor-induced cytoskeletal rearrangement relates to vacuolar dynamics and execution of cell death: *in vivo* imaging of hypersensitive cell death in tobacco BY-2 cells. Plant and Cell Physiology *48*, 1414-1425.

Hochheimer, N., Sies, R., Aschenbrenner, A.C., Schneider, D., and Lang, T. (2019). Classes of non-conventional tetraspanins defined by alternative splicing. Scientific Reports *9*, 14075.

Hok, S., Danchin, E.G., Allasia, V., Panabières, F., Attard, A., and Keller, H. (2011). An Arabidopsis (malectin-like) leucine-rich repeat receptor-like kinase contributes to downy mildew disease. Plant, Cell and Environment *34*, 1944-1957.

Houston, K., Tucker, M.R., Chowdhury, J., Shirley, N., and Little, A. (2016). The Plant Cell Wall: A Complex and Dynamic Structure As Revealed by the Responses of Genes under Stress Conditions. Frontiers in Plant Science *7*.

Howe, K.L., Contreras-Moreira, B., De Silva, N., Maslen, G., Akanni, W., Allen, J., Alvarez-Jarreta, J., Barba, M., Bolser, D.M., Cambell, L.*, et al.* (2020). Ensembl Genomes 2020—enabling non-vertebrate genomic research. Nucleic Acids Research *48*, D689-D695.

Hruz, T., Laule, O., Szabo, G., Wessendorp, F., Bleuler, S., Oertle, L., Widmayer, P., Gruissem, W., and Zimmermann, P. (2008). Genevestigator V3: A Reference Expression Database for the Meta-Analysis of Transcriptomes. Advances in Bioinformatics *2008*, 5.

Hu, J., Gao, Y., Huang, Q., Wang, Y., Mo, X., Wang, P., Zhang, Y., Xie, C., Li, D., and Yao, J. (2021). Flotillin-1 Interacts With and Sustains the Surface Levels of TRPV2 Channel. Frontiers in Cell and Developmental Biology *9*.

Huang, C., Fu, C., Wren, J.D., Wang, X., Zhang, F., Zhang, Y.H., Connel, S.A., Chen, T., and Zhang, X.A. (2018). Tetraspanin-enriched microdomains regulate digitation junctions. Cellular and Molecular Life Sciences *75*, 3423-3439.

Huang, D., Sun, Y., Ma, Z., Ke, M., Cui, Y., Chen, Z., Chen, C., Ji, C., Tran, T.M., Yang, L.*, et al.* (2019a). Salicylic acid-mediated plasmodesmal closure via Remorin-dependent lipid organization. Proceedings of the National Academy of Sciences, 201911892.

Huang, R., Yang, C., and Zhang, S. (2019b). The Arabidopsis PHB3 is a pleiotropic regulator for plant development. Plant Signal Behav *14*, 1656036.

Huang, S., Blanchoin, L., Kovar, D.R., and Staiger, C.J. (2003). Arabidopsis Capping Protein (AtCP) Is a Heterodimer That Regulates Assembly at the Barbed Ends of Actin Filaments. Journal of Biological Chemistry *278*, 44832-44842.

Huang, S., Yuan, S., Dong, M., Su, J., Yu, C., Shen, Y., Xie, X., Yu, Y., Yu, X., Chen, S.*, et al.* (2005). The phylogenetic analysis of tetraspanins projects the evolution of cell–cell interactions from unicellular to multicellular organisms. Genomics *86*, 674-684.

Huber, T.B., Schermer, B., Müller, R.U., Höhne, M., Bartram, M., Calixto, A., Hagmann, H., Reinhardt, C., Koos, F., Kunzelmann, K.*, et al.* (2006). Podocin and MEC-2 bind cholesterol to regulate the activity of associated ion channels. Proceedings of the National Academy of Sciences *103*, 17079.

Hückelhoven, R., and Seidl, A. (2016). PAMP-triggered immune responses in barley and susceptibility to powdery mildew. Plant Signal Behav *11*, e1197465-e1197465.

Huep, G., Kleinboelting, N., and Weisshaar, B. (2014). An easy-to-use primer design tool to address paralogous loci and T-DNA insertion sites in the genome of *Arabidopsis thaliana*. Plant Methods *10*, 28.

Hughes, J.E., and Gunning, B.E.S. (1980). Glutaraldehyde-induced deposition of callose. Canadian Journal of Botany *58*, 250-258.

Hülsbusch, N., Solis, G.P., Katanaev, V.L., and Stuermer, C.A.O. (2015). Reggie-1/Flotillin-2 regulates integrin trafficking and focal adhesion turnover via Rab11a. European Journal of Cell Biology *94*, 531-545.

Hunter, K., Kimura, S., Rokka, A., Tran, H.C., Toyota, M., Kukkonen, J.P., and Wrzaczek, M. (2019). CRK2 Enhances Salt Tolerance by Regulating Callose Deposition in Connection with PLDα1. Plant Physiology *180*, 2004-2021.

Hurst, C.H., Myles, S.M., Turnbull, D., Leslie, K., Keinath, N.F., and Hemsley, P.A. (2018). Variable effects of C-terminal tags on FLS2 function - not all epitope tags are created equal. Plant Physiology.

Hurst, C.H., Turnbull, D., Gronnier, J., Myles, S., Pflughaupt, R.L., Kopischke, M., Davies, P., Jones, S., Robatzek, S., Zipfel, C.*, et al.* (2021). S-acylation is a positive regulator of FLS2-mediated plant immunity. bioRxiv, 2021.2008.2030.457756.

Hurwitz, S.N., Conlon, M.M., Rider, M.A., Brownstein, N.C., and Meckes, D.G. (2016). Nanoparticle analysis sheds budding insights into genetic drivers of extracellular vesicle biogenesis. Journal of Extracellular Vesicles *5*, 31295.

Husaini, A.M., Morimoto, K., Chandrasekar, B., Kelly, S., Kaschani, F., Palmero, D., Jiang, J., Kaiser, M., Ahrazem, O., Overkleeft, H.S.*, et al.* (2018). Multiplex Fluorescent, Activity-Based Protein Profiling Identifies Active α-Glycosidases and Other Hydrolases in Plants. Plant Physiology *177*, 24-37.

Huyer, G., Liu, S., Kelly, J., Moffat, J., Payette, P., Kennedy, B., Tsaprailis, G., Gresser, M.J., and Ramachandran, C. (1997). Mechanism of Inhibition of Protein-tyrosine Phosphatases by Vanadate and Pervanadate. Journal of Biological Chemistry *272*, 843-851.

Ishiga, Y., Ishiga, T., Uppalapati, S.R., and Mysore, K.S. (2011). Arabidopsis seedling flood-inoculation technique: a rapid and reliable assay for studying plant-bacterial interactions. Plant Methods *7*, 32.

Ivanov, S., Austin, J., Berg, R.H., and Harrison, M.J. (2019). Extensive membrane systems at the host–arbuscular mycorrhizal fungus interface. Nature Plants *5*, 194-203.

Jacobson, K., Liu, P., and Lagerholm, B.C. (2019). The Lateral Organization and Mobility of Plasma Membrane Components. Cell *177*, 806-819.

Jaillais, Y., and Ott, T. (2020). The Nanoscale Organization of the Plasma Membrane and Its Importance in Signaling: A Proteolipid Perspective. Plant Physiology *182*, 1682-1696.

Jamieson, P.A., Shan, L., and He, P. (2018). Plant cell surface molecular cypher: Receptor-like proteins and their roles in immunity and development. Plant Science *274*, 242-251.

Janes, P.W., Ley, S.C., Magee, A.I., and Kabouridis, P.S. (2000). The role of lipid rafts in T cell antigen receptor (TCR) signalling. Seminars in Immunology *12*, 23-34.

Jarsch, I.K., Konrad, S.S.A., Stratil, T.F., Urbanus, S.L., Szymanski, W., Braun, P., Braun, K.-H., and Ott, T. (2014). Plasma Membranes Are Subcompartmentalized into a Plethora of Coexisting and Diverse Microdomains in *Arabidopsis* and *Nicotiana benthamiana*. The Plant Cell.

Jerse, A.E., Yu, J., Tall, B.D., and Kaper, J.B. (1990). A genetic locus of enteropathogenic Escherichia coli necessary for the production of attaching and effacing lesions on tissue culture cells. Proceedings of the National Academy of Sciences *87*, 7839-7843.

Jimenez-Jimenez, S., Hashimoto, K., Santana, O., Aguirre, J., Kuchitsu, K., and Cárdenas, L. (2019a). Emerging roles of tetraspanins in plant inter-cellular and inter-kingdom communication. Plant Signal Behav *14*, e1581559.

Jimenez-Jimenez, S., Santana, O., Lara-Rojas, F., Arthikala, M.K., Armada, E., Hashimoto, K., Kuchitsu, K., Salgado, S., Aguirre, J., Quinto, C.*, et al.* (2019b). Differential tetraspanin genes expression and subcellular localization during mutualistic interactions in Phaseolus vulgaris. PLOS One *14*, e0219765.

Johnston, M.G., and Faulkner, C. (2021). A bootstrap approach is a superior statistical method for the comparison of non-normal data with differing variances. New Phytologist *230*, 23-26.

Joris, B., Englebert, S., Chu, C.P., Kariyama, R., Daneo-Moore, L., Shockman, G.D., and Ghuysen, J.M. (1992). Modular design of the Enterococcus hirae muramidase-2 and Streptococcus faecalis autolysin. FEMS Microbiology Letters *70*, 257-264.

Jose, J., Ghantasala, S., and Roy Choudhury, S. (2020). Arabidopsis Transmembrane Receptor-Like Kinases (RLKs): A Bridge between Extracellular Signal and Intracellular Regulatory Machinery. International Journal of Molecular Sciences *21*, 4000.

Junková, P., Daněk, M., Kocourková, D., Brouzdová, J., Kroumanová, K., Zelazny, E., Janda, M., Hynek, R., Martinec, J., and Valentová, O. (2018). Mapping of Plasma Membrane Proteins Interacting with *Arabidopsis thaliana* FLOTILLIN 2. Frontiers in Plant Science *9*.

Kadota, Y., Macho, A.P., and Zipfel, C. (2016). Immunoprecipitation of Plasma Membrane Receptor-Like Kinases for Identification of Phosphorylation Sites and Associated Proteins. In Plant Signal Transduction: Methods and Protocols, J.R. Botella, and M.A. Botella, eds. (New York, NY: Springer New York), pp. 133-144.

Kadota, Y., Sklenar, J., Derbyshire, P., Stransfeld, L., Asai, S., Ntoukakis, V., Jones, Jonathan D., Shirasu, K., Menke, F., Jones, A.*, et al.* (2014). Direct Regulation of the NADPH Oxidase RBOHD by the PRR-Associated Kinase BIK1 during Plant Immunity. Molecular Cell *54*, 43-55.

Kaiser, P., and Huang, L. (2005). Global approaches to understanding ubiquitination. Genome Biology *6*, 233.

Kaku, H., Nishizawa, Y., Ishii-Minami, N., Akimoto-Tomiyama, C., Dohmae, N., Takio, K., Minami, E., and Shibuya, N. (2006). Plant cells recognize chitin fragments for defense signaling through a plasma membrane receptor. Proceedings of the National Academy of Sciences *103*, 11086-11091.

Kankanala, P., Czymmek, K., and Valent, B. (2007). Roles for Rice Membrane Dynamics and Plasmodesmata during Biotrophic Invasion by the Blast Fungus. The Plant Cell *19*, 706-724.

Kates, M. (1970). Plant Phospholipids and Glycolipids. In Advances in Lipid Research, R. Paoletti, and D. Kritchevsky, eds. (Elsevier), pp. 225-265.

Kawasaki, T., Yamada, K., Yoshimura, S., and Yamaguchi, K. (2017). Chitin receptor-mediated activation of MAP kinases and ROS production in rice and Arabidopsis. Plant Signal Behav *12*, e1361076-e1361076.

Kenworthy, A.K., Petranova, N., and Edidin, M. (2000). High-Resolution FRET Microscopy of Cholera Toxin B-Subunit and GPI-anchored Proteins in Cell Plasma Membranes. Mol Biol Cell *11*, 1645-1655.

Khalilova, L., Sergienko, O., Orlova, Y., Myasoedov, N., Karpichev, I., and Balnokin, Y. (2020). *Arabidopsis thaliana* Mutant with T-DNA Insertion in the *FLOT1* (At5g25250) Gene Promotor Possesses Increased Resistance to NaCl. Russian Journal of Plant Physiology *67*, 275-284.

Khang, C.H., Berruyer, R., Giraldo, M.C., Kankanala, P., Park, S.-Y., Czymmek, K., Kang, S., and Valent, B. (2010). Translocation of *Magnaporthe oryzae* Effectors into Rice Cells and Their Subsequent Cell-to-Cell Movement. The Plant Cell *22*, 1388-1403.

Khrenova, M., Topol, I., Collins, J., and Nemukhin, A. (2015). Estimating orientation factors in the FRET theory of fluorescent proteins: the TagRFP-KFP pair and beyond. Biophysical Journal *108*, 126-132.

Kierszniowska, S., Seiwert, B., and Schulze, W.X. (2009). Definition of Arabidopsis sterol-rich membrane microdomains by differential treatment with methyl-beta-cyclodextrin and quantitative proteomics. Molecular & Cellular Proteomics *8*, 612-623.

Kihara, A., Akiyama, Y., and Ito, K. (1996). A protease complex in the *Escherichia coli* plasma membrane: HflKC (HflA) forms a complex with FtsH (HflB), regulating its proteolytic activity against SecY. The EMBO Journal *15*, 6122-6131.

Kihara, A., and Ito, K. (1998). Translocation, folding, and stability of the HflKC complex with signal anchor topogenic sequences. Journal of Biological Chemistry *273*, 29770-29775.

Kim, J.Y., Yuan, Z., Cilia, M., Khalfan-Jagani, Z., and Jackson, D. (2002). Intercellular trafficking of a KNOTTED1 green fluorescent protein fusion in the leaf and shoot meristem of Arabidopsis. Proceedings of the National Academy of Sciences *99*, 4103.

Kimura, A., Baumann, C.A., Chiang, S.-H., and Saltiel, A.R. (2001). The sorbin homology domain: A motif for the targeting of proteins to lipid rafts. Proceedings of the National Academy of Sciences *98*, 9098.

Kioka, N., Ueda, K., and Amachi, T. (2002). Vinexin, CAP/ponsin, ArgBP2: a novel adaptor protein family regulating cytoskeletal organization and signal transduction. Cell Structure and Function *27*, 1-7.

Kirchhoff, H., Mukherjee, U., and Galla, H.J. (2002). Molecular Architecture of the Thylakoid Membrane: Lipid Diffusion Space for Plastoquinone. Biochemistry *41*, 4872-4882.

Kirk, P., Amsbury, S., German, L., Gaudioso-Pedraza, R., and Benitez-Alfonso, Y. (2021). Comparative meta-proteomic analysis for the identification of novel plasmodesmata proteins and regulatory cues. bioRxiv, 2021.2005.2004.442592.

Kitagawa, M., Wu, P., Balkunde, R., Cunniff, P., and Jackson, D. (2022). An RNA exosome subunit mediates cell-to-cell trafficking of a homeobox mRNA via plasmodesmata. Science *375*, 177-182.

Klausner, R.D., Donaldson, J.G., and Lippincott-Schwartz, J. (1992). Brefeldin A: insights into the control of membrane traffic and organelle structure. Journal of Cell Biology *116*, 1071-1080.

Klein, D.C.G., Skjesol, A., Kers-Rebel, E.D., Sherstova, T., Sporsheim, B., Egeberg, K.W., Stokke, B.T., Espevik, T., and Husebye, H. (2015). CD14, TLR4 and TRAM Show Different Trafficking Dynamics During LPS Stimulation. Traffic *16*, 677-690.

Kleinboelting, N., Huep, G., Kloetgen, A., Viehoever, P., and Weisshaar, B. (2012). GABI-Kat SimpleSearch: new features of the *Arabidopsis thaliana* T-DNA mutant database. Nucleic Acids Res *40*, D1211-1215.

Knopf, J.D., Tholen, S., Koczorowska, M.M., De Wever, O., Biniossek, M.L., and Schilling, O. (2015). The stromal cell-surface protease fibroblast activation protein-α localizes to lipid rafts and is recruited to invadopodia. Biochimica et Biophysica Acta *1853*, 2515-2525.

Knox, J.P., and Benitez-Alfonso, Y. (2014). Roles and regulation of plant cell walls surrounding plasmodesmata. Current Opinion in Plant Biology *22*, 93-100.

Kobayashi, I., Kobayashi, Y., and Hardham, A.R. (1994). Dynamic reorganization of microtubules and microfilaments in flax cells during the resistance response to flax rust infection. Planta *195*, 237-247.

Kokubo, H., Helms, J.B., Ohno-Iwashita, Y., Shimada, Y., Horikoshi, Y., and Yamaguchi, H. (2003). Ultrastructural localization of flotillin-1 to cholesterol-rich membrane microdomains, rafts, in rat brain tissue. Brain Research *965*, 83-90.

Konrad, S.S., Popp, C., Stratil, T.F., Jarsch, I.K., Thallmair, V., Folgmann, J., Marín, M., and Ott, T. (2014). S-acylation anchors remorin proteins to the plasma membrane but does not primarily determine their localization in membrane microdomains. New Phytologist *203*, 758-769.

Koushyar, S., Economides, G., Zaat, S., Jiang, W., Bevan, C.L., and Dart, D.A. (2017). The prohibitin-repressive interaction with E2F1 is rapidly inhibited by androgen signalling in prostate cancer cells. Oncogenesis *6*, e333-e333.

Kouzai, Y., Nakajima, K., Hayafune, M., Ozawa, K., Kaku, H., Shibuya, N., Minami, E., and Nishizawa, Y. (2014). CEBiP is the major chitin oligomer-binding protein in rice and plays a main role in the perception of chitin oligomers. Plant Molecular Biology *84*, 519-528.

Krasavina, M.S., Ktitorova, I.N., and Burmistrova, N.A. (2001). Electrical Conductance of Cell-to-Cell Junctions and the Cytoskeleton of Plant Cells. Russian Journal of Plant Physiology *48*, 741-748.

Kroumanova, K., Kocourkova, D., Danek, M., Lamparova, L., Pospichalova, R., Malinska, K., Krckova, Z., Burketova, L., Valentova, O., Martinec, J.*, et al.* (2019). Characterisation of Arabidopsis flotillins in response to stresses. Biologia Plantarum *63*, 144-152.

Kruft, V., Eubel, H., Jänsch, L., Werhahn, W., and Braun, H.-P. (2001). Proteomic Approach to Identify Novel Mitochondrial Proteins in Arabidopsis. Plant Physiology *127*, 1694-1710.

Kubiasová, K., Montesinos, J.C., Šamajová, O., Nisler, J., Mik, V., Semerádová, H., Plíhalová, L., Novák, O., Marhavý, P., Cavallari, N.*, et al.* (2020). Cytokinin fluoroprobe reveals multiple sites of cytokinin perception at plasma membrane and endoplasmic reticulum. Nature Communications *11*, 4285.

Kumar, M., Carr, P., and Turner, S.R. (2022). An atlas of Arabidopsis protein S-acylation reveals its widespread role in plant cell organization and function. Nature Plants *8*, 670-681.

Kummer, D., Steinbacher, T., Schwietzer, M.F., Tholmann, S., and Ebnet, K. (2020). Tetraspanins: integrating cell surface receptors to functional microdomains in homeostasis and disease. Medical Microbiology and Immunology.

Kunst, L., Browse, J., and Somerville, C. (1989). A Mutant of Arabidopsis Deficient in Desaturation of Palmitic Acid in Leaf Lipids 1. Plant Physiology *90*, 943-947.

Kunze, G., Zipfel, C., Robatzek, S., Niehaus, K., Boller, T., and Felix, G. (2004). The N terminus of bacterial elongation factor Tu elicits innate immunity in Arabidopsis plants. The Plant cell *16*, 3496-3507.

Kuramori, C., Azuma, M., Kume, K., Kaneko, Y., Inoue, A., Yamaguchi, Y., Kabe, Y., Hosoya, T., Kizaki, M., Suematsu, M.*, et al.* (2009). Capsaicin binds to prohibitin 2 and displaces it from the mitochondria to the nucleus. Biochemical and Biophysical Research Communications *379*, 519-525.

Kurzchalia, T.V., Dupree, P., Parton, R.G., Kellner, R., Virta, H., Lehnert, M., and Simons, K. (1992). VIP21, a 21-kD membrane protein is an integral component of trans-Golgi-network-derived transport vesicles. Journal of Cell Biology *118*, 1003-1014.

Kusumi, A., Fujiwara, T.K., Chadda, R., Xie, M., Tsunoyama, T.A., Kalay, Z., Kasai, R.S., and Suzuki, K.G.N. (2012). Dynamic Organizing Principles of the Plasma Membrane that Regulate Signal Transduction: Commemorating the Fortieth Anniversary of Singer and Nicolson's Fluid-Mosaic Model. Annual Review of Cell and Developmental Biology *28*, 215-250.

Kusumi, A., Nakada, C., Ritchie, K., Murase, K., Suzuki, K., Murakoshi, H., Kasai, R.S., Kondo, J., and Fujiwara, T. (2005). Paradigm shift of the plasma membrane concept from the two-dimensional continuum fluid to the partitioned fluid: high-speed single-molecule tracking of membrane molecules. Annual Review of Biophysics and Biomolecular Structure *34*, 351-378.

Kutschera, A., Dawid, C., Gisch, N., Schmid, C., Raasch, L., Gerster, T., Schäffer, M., Smakowska-Luzan, E., Belkhadir, Y., Vlot, A.C.*, et al.* (2019). Bacterial medium-chain 3-hydroxy fatty acid metabolites trigger immunity in Arabidopsis plants. Science *364*, 178-181.

Kytidou, K., Artola, M., Overkleeft, H.S., and Aerts, J.M.F.G. (2020). Plant Glycosides and Glycosidases: A Treasure-Trove for Therapeutics. Frontiers in Plant Science *11*.

Lambert, T.J. (2019). FPbase: a community-editable fluorescent protein database, https://www.fpbase.org/. Nature Methods *16*, 277-278.

Lambou, K., Malagnac, F., Barbisan, C., Tharreau, D., Lebrun, M.H., and Silar, P. (2008). The crucial role of the Pls1 tetraspanin during ascospore germination in *Podospora anserina* provides an example of the convergent evolution of morphogenetic processes in fungal plant pathogens and saprobes. Eukaryotic Cell *7*, 1809-1818.

Lambrix, V., Reichelt, M., Mitchell-Olds, T., Kliebenstein, D.J., and Gershenzon, J. (2001). The Arabidopsis Epithiospecifier Protein Promotes the Hydrolysis of Glucosinolates to Nitriles and Influences Trichoplusia ni Herbivory. The Plant Cell *13*, 2793-2807.

Langhorst, M.F., Reuter, A., Jaeger, F.A., Wippich, F.M., Luxenhofer, G., Plattner, H., and Stuermer, C.A.O. (2008). Trafficking of the microdomain scaffolding protein reggie-1/flotillin-2. European Journal of Cell Biology *87*, 211-226.

Langhorst, M.F., Reuter, A., and Stuermer, C.A.O. (2005). Scaffolding microdomains and beyond: the function of reggie/flotillin proteins. Cellular and Molecular Life Sciences *62*, 2228-2240.

Lapatsina, L., Brand, J., Poole, K., Daumke, O., and Lewin, G.R. (2012a). Stomatin-domain proteins. European Journal of Cell Biology *91*, 240-245.

Lapatsina, L., Jira, J.A., Smith, E.S.J., Poole, K., Kozlenkov, A., Bilbao, D., Lewin, G.R., and Heppenstall, P.A. (2012b). Regulation of ASIC channels by a stomatin/STOML3 complex located in a mobile vesicle pool in sensory neurons. Open Biology *2*, 120096.

Laurent, S.A., Hoffmann, F.S., Kuhn, P.H., Cheng, Q., Chu, Y., Schmidt-Supprian, M., Hauck, S.M., Schuh, E., Krumbholz, M., Rübsamen, H.*, et al.* (2015). γ-Secretase directly sheds the survival receptor BCMA from plasma cells. Nature Communications *6*, 7333.

Le Naour, F., Rubinstein, E., Jasmin, C., Prenant, M., and Boucheix, C. (2000). Severely reduced female fertility in CD9-deficient mice. Science *287*, 319-321.

Lee, D., Lal, N.K., Lin, Z.-J.D., Ma, S., Liu, J., Castro, B., Toruño, T., Dinesh-Kumar, S.P., and Coaker, G. (2020). Regulation of reactive oxygen species during plant immunity through phosphorylation and ubiquitination of RBOHD. Nature Communications *11*, 1838.

Lefebvre, B., Timmers, T., Mbengue, M., Moreau, S., Hervé, C., Tóth, K., Bittencourt-Silvestre, J., Klaus, D., Deslandes, L., Godiard, L.*, et al.* (2010). A remorin protein interacts with symbiotic receptors and regulates bacterial infection. Proceedings of the National Academy of Sciences *107*, 2343.

Legrand, A., Martinez, D., Grélard, A., Berbon, M., Morvan, E., Tawani, A., Loquet, A., Mongrand, S., and Habenstein, B. (2019). Nanodomain Clustering of the Plant Protein Remorin by Solid-State NMR. Frontiers in Molecular Biosciences *6*.

Leijon, F., Melzer, M., Zhou, Q., Srivastava, V., and Bulone, V. (2018). Proteomic Analysis of Plasmodesmata From Populus Cell Suspension Cultures in Relation With Callose Biosynthesis. Frontiers in Plant Science *9*.

Lenth, R.V. (2021). emmeans: Estimated Marginal Means, aka Least-Squares Means. R package version 1.7.0.

Levental, I., Grzybek, M., and Simons, K. (2010a). Greasing their way: lipid modifications determine protein association with membrane rafts. Biochemistry *49*, 6305-6316.

Levental, I., Grzybek, M., and Simons, K. (2011). Raft domains of variable properties and compositions in plasma membrane vesicles. Proceedings of the National Academy of Sciences *108*, 11411.

Levental, I., Levental, K.R., and Heberle, F.A. (2020). Lipid Rafts: Controversies Resolved, Mysteries Remain. Trends in Cell Biology *30*, 341-353.

Levental, I., Lingwood, D., Grzybek, M., Coskun, Ü., and Simons, K. (2010b). Palmitoylation regulates raft affinity for the majority of integral raft proteins. Proceedings of the National Academy of Sciences *107*, 22050-22054.

Levental, K.R., and Levental, I. (2015). Chapter Two - Giant Plasma Membrane Vesicles: Models for Understanding Membrane Organization. In Current Topics in Membranes, A.K. Kenworthy, ed. (Academic Press), pp. 25-57.

Levy, A., Erlanger, M., Rosenthal, M., and Epel, B.L. (2007a). A plasmodesmata-associated beta-1,3-glucanase in Arabidopsis. The Plant Journal *49*, 669-682.

Levy, A., Guenoune-Gelbart, D., and Epel, B.L. (2007b). β-1,3-Glucanases. Plant Signal Behav *2*, 404-407.

Lewis, J.D., and Lazarowitz, S.G. (2010). Arabidopsis synaptotagmin SYTA regulates endocytosis and virus movement protein cell-to-cell transport. Proceedings of the National Academy of Sciences *107*, 2491.

Lherminier, J., Elmayan, T., Fromentin, J., Elaraqui, K.T., Vesa, S., Morel, J., Verrier, J.L., Cailleteau, B., Blein, J.P., and Simon-Plas, F. (2009). NADPH oxidase-mediated reactive oxygen species production: subcellular localization and reassessment of its role in plant defense. Molecular Plant-Microbe Interactions *22*, 868-881.

Li, D., Chu, W., Sheng, X., and Li, W. (2021). Optimization of Membrane Protein TmrA Purification Procedure Guided by Analytical Ultracentrifugation. Membranes *11*.

Li, J.-T., Hou, G.-Y., Kong, X.-F., Li, C.-Y., Zeng, J.-M., Li, H.-D., Xiao, G.-B., Li, X.-M., and Sun, X.-W. (2015a). The fate of recent duplicated genes following a fourth-round whole genome duplication in a tetraploid fish, common carp (Cyprinus carpio). Scientific Reports *5*, 8199.

Li, J., Henty-Ridilla, J.L., Staiger, B.H., Day, B., and Staiger, C.J. (2015b). Capping protein integrates multiple MAMP signalling pathways to modulate actin dynamics during plant innate immunity. Nature Communications *6*, 7206-7206.

Li, J., Liu, J., Wang, G., Cha, J.-Y., Li, G., Chen, S., Li, Z., Guo, J., Zhang, C., Yang, Y.*, et al.* (2015c). A chaperone function of NO CATALASE ACTIVITY1 is required to maintain catalase activity and for multiple stress responses in Arabidopsis. The Plant Cell *27*, 908-925.

Li, J., Pleskot, R., Henty-Ridilla, J.L., Blanchoin, L., Potocký, M., and Staiger, C.J. (2012a). Arabidopsis capping protein senses cellular phosphatidic acid levels and transduces these into changes in actin cytoskeleton dynamics. Plant Signal Behav *7*, 1727-1730.

Li, L., Li, M., Yu, L., Zhou, Z., Liang, X., Liu, Z., Cai, G., Gao, L., Zhang, X., Wang, Y.*, et al.* (2014). The FLS2-Associated Kinase BIK1 Directly Phosphorylates the NADPH Oxidase RbohD to Control Plant Immunity. Cell Host & Microbe *15*, 329-338.

Li, Q., Yang, X.H., Xu, F., Sharma, C., Wang, H.X., Knoblich, K., Rabinovitz, I., Granter, S.R., and Hemler, M.E. (2013). Tetraspanin CD151 plays a key role in skin squamous cell carcinoma. Oncogene *32*, 1772-1783.

Li, R., Liu, P., Wan, Y., Chen, T., Wang, Q., Mettbach, U., Baluška, F., Šamaj, J., Fang, X., Lucas, W.J.*, et al.* (2012b). A Membrane Microdomain-Associated Protein, Arabidopsis FLOT1, Is Involved in a Clathrin-Independent Endocytic Pathway and Is Required for Seedling Development. The Plant Cell *24*, 2105.

Li, X., Wang, X., Yang, Y., Li, R., He, Q., Fang, X., Luu, D.-T., Maurel, C., and Lin, J. (2011). Single-Molecule Analysis of PIP2;1 Dynamics and Partitioning Reveals Multiple Modes of Arabidopsis Plasma Membrane Aquaporin Regulation. The Plant Cell *23*, 3780-3797.

Liang, P., Stratil, T.F., Popp, C., Marín, M., Folgmann, J., Mysore, K.S., Wen, J., and Ott, T. (2018). Symbiotic root infections in *Medicago truncatula* require remorin-mediated receptor stabilization in membrane nanodomains. Proceedings of the National Academy of Sciences *115*, 5289.

Liao, D., Cao, Y., Sun, X., Espinoza, C., Nguyen, C.T., Liang, Y., and Stacey, G. (2017). Arabidopsis E3 ubiquitin ligase PLANT U-BOX13 (PUB13) regulates chitin receptor LYSIN MOTIF RECEPTOR KINASE5 (LYK5) protein abundance. New Phytologist *214*, 1646-1656.

Lichtenberg, D., Goñi, F.M., and Heerklotz, H. (2005). Detergent-resistant membranes should not be identified with membrane rafts. Trends in Biochemical Sciences *30*, 430-436.

Lichtenthaler, S.F., Lemberg, M.K., and Fluhrer, R. (2018). Proteolytic ectodomain shedding of membrane proteins in mammals-hardware, concepts, and recent developments. The EMBO journal *37*, e99456.

Limpens, E., Franken, C., Smit, P., Willemse, J., Bisseling, T., and Geurts, R. (2003). LysM domain receptor kinases regulating rhizobial Nod factor-induced infection. Science *302*, 630-633.

Lindner, H., Kessler, S.A., Müller, L.M., Shimosato-Asano, H., Boisson-Dernier, A., and Grossniklaus, U. (2015). TURAN and EVAN Mediate Pollen Tube Reception in Arabidopsis Synergids through Protein Glycosylation. PLOS Biology *13*, e1002139.

Liu, J., DeYoung, S.M., Zhang, M., Dold, L.H., and Saltiel, A.R. (2005). The Stomatin/Prohibitin/Flotillin/HflK/C Domain of Flotillin-1 Contains Distinct Sequences That Direct Plasma Membrane Localization and Protein Interactions in 3T3-L1 Adipocytes. Journal of Biological Chemistry *280*, 16125-16134.

Liu, J., Liu, B., Chen, S., Gong, B.-Q., Chen, L., Zhou, Q., Xiong, F., Wang, M., Feng, D., Li, J.-F.*, et al.* (2018). A Tyrosine Phosphorylation Cycle Regulates Fungal Activation of a Plant Receptor Ser/Thr Kinase. Cell Host & Microbe *23*, 241-253.e246.

Liu, J., Liu, Y., Wang, S., Cui, Y., and Yan, D. (2022). Heat Stress Reduces Root Meristem Size via Induction of Plasmodesmal Callose Accumulation Inhibiting Phloem Unloading in Arabidopsis. International Journal of Molecular Sciences *23*.

Liu, P., Xu, Y., Zhang, W., Li, Y., Tang, L., Chen, W., Xu, J., Sun, Q., and Guan, X. (2017). Prohibitin promotes androgen receptor activation in ER-positive breast cancer. Cell Cycle *16*, 776-784.

Liu, T., Liu, Z., Song, C., Hu, Y., Han, Z., She, J., Fan, F., Wang, J., Jin, C., Chang, J.*, et al.* (2012). Chitin-Induced Dimerization Activates a Plant Immune Receptor. Science *336*, 1160-1164.

Liu, Y., Ren, D., Pike, S., Pallardy, S., Gassmann, W., and Zhang, S. (2007). Chloroplast-generated reactive oxygen species are involved in hypersensitive response-like cell death mediated by a mitogen-activated protein kinase cascade. The Plant Journal *51*, 941-954.

Long, Y., Stahl, Y., Weidtkamp-Peters, S., Smet, W., Du, Y., W. J. Gadella, T., Goedhart, J., Scheres, B., and Blilou, I. (2018). Optimizing FRET-FLIM Labeling Conditions to Detect Nuclear Protein Interactions at Native Expression Levels in Living Arabidopsis Roots. Frontiers in Plant Science *9*.

Lu, D., Wu, S., Gao, X., Zhang, Y., Shan, L., and He, P. (2010). A receptor-like cytoplasmic kinase, BIK1, associates with a flagellin receptor complex to initiate plant innate immunity. Proceedings of the National Academy of Sciences *107*, 496-501.

Lu, W., Fei, A., Jiang, Y., Chen, L., and Wang, Y. (2020). Tetraspanin CD9 interacts with α-secretase to enhance its oncogenic function in pancreatic cancer. American Journal of Translational Research *12*, 5525-5537.

Lucas, W.J., Bouché-Pillon, S., Jackson, D.P., Nguyen, L., Baker, L., Ding, B., and Hake, S. (1995). Selective trafficking of KNOTTED1 homeodomain protein and its mRNA through plasmodesmata. Science *270*, 1980-1983.

Ludwig, A., Otto, G.P., Riento, K., Hams, E., Fallon, P.G., and Nichols, B.J. (2010). Flotillin microdomains interact with the cortical cytoskeleton to control uropod formation and neutrophil recruitment. Journal of Cell Biology *191*, 771-781.

Lv, X., Jing, Y., Xiao, J., Zhang, Y., Zhu, Y., Julian, R., and Lin, J. (2017). Membrane microdomains and the cytoskeleton constrain AtHIR1 dynamics and facilitate the formation of an AtHIR1-associated immune complex. The Plant Journal *90*, 3-16.

Ma, C., Wang, C., Luo, D., Yan, L., Yang, W., Li, N., and Gao, N. (2022). Structural insights into the membrane microdomain organization by SPFH family proteins. Cell Research *32*, 176-189.

MacDonald, G.E., Lada, R.R., Caldwell, C.D., Udenigwe, C., and MacDonald, M.T. (2019). Potential Roles of Fatty Acids and Lipids in Postharvest Needle Abscission Physiology. American Journal of Plant Sciences *Vol.10No.06*, 21.

MacLean, D., Burrell, M.A., Studholme, D.J., and Jones, A.M. (2008). PhosCalc: a tool for evaluating the sites of peptide phosphorylation from mass spectrometer data. BioMed Central research notes *1*, 30-30.

Madore, N., Smith, K.L., Graham, C.H., Jen, A., Brady, K., Hall, S., and Morris, R. (1999). Functionally different GPI proteins are organized in different domains on the neuronal surface. The EMBO journal *18*, 6917-6926.

Magal, L.G., Yaffe, Y., Shepshelovich, J., Aranda, J.F., de Marco, M.d.C., Gaus, K., Alonso, M.A., and Hirschberg, K. (2009). Clustering and lateral concentration of raft lipids by the MAL protein. Mol Biol Cell *20*, 3751-3762.

Magee, A.I., and Parmryd, I. (2003). Detergent-resistant membranes and the protein composition of lipid rafts. Genome Biology *4*, 234-234.

Maley, F., Trimble, R.B., Tarentino, A.L., and Plummer, T.H. (1989). Characterization of glycoproteins and their associated oligosaccharides through the use of endoglycosidases. Analytical Biochemistry *180*, 195-204.

Malinsky, J., Opekarová, M., Grossmann, G., and Tanner, W. (2013). Membrane microdomains, rafts, and detergent-resistant membranes in plants and fungi. The Annual Review of Plant Biology *64*, 501-529.

Man Ngou, B.P., Heal, R., Wyler, M., Schmid, M.W., and Jones, J.D.G. (2022). Concerted expansion and contraction of immune receptor gene repertoires in plant genomes. bioRxiv, 2022.2001.2001.474684.

Margineanu, A., Chan, J.J., Kelly, D.J., Warren, S.C., Flatters, D., Kumar, S., Katan, M., Dunsby, C.W., and French, P.M.W. (2016). Screening for protein-protein interactions using Förster resonance energy transfer (FRET) and fluorescence lifetime imaging microscopy (FLIM). Scientific Reports *6*, 28186.

Markakis, M.N., De Cnodder, T., Lewandowski, M., Simon, D., Boron, A., Balcerowicz, D., Doubbo, T., Taconnat, L., Renou, J.P., Hofte, H.*, et al.* (2012). Identification of genes involved in the ACC-mediated control of root cell elongation in *Arabidopsis thaliana*. BMC Plant Biology *12*, 208.

Marri, L., Sparla, F., Pupillo, P., and Trost, P. (2005). Co-ordinated gene expression of photosynthetic glyceraldehyde-3-phosphate dehydrogenase, phosphoribulokinase, and CP12 in *Arabidopsis thaliana*. Journal of Experimental Botany *56*, 73-80.

Martin, F., Martino, D.M., Jans, D.A., Pouton, C., Partridge, L., Monk, P., and Moseley, G.W. (2005). Tetraspanins in Viral Infections: a Fundamental Role in Viral Biology? Journal of Virology *79*, 10839-10851.

Martinez, D., Legrand, A., Gronnier, J., Decossas, M., Gouguet, P., Lambert, O., Berbon, M., Verron, L., Grélard, A., Germain, V.*, et al.* (2019). Coiled-coil oligomerization controls localization of the plasma membrane REMORINs. Journal of Structural Biology *206*, 12-19.

Martiniere, A., Lavagi, I., Nageswaran, G., Rolfe, D.J., Maneta-Peyret, L., Luu, D.T., Botchway, S.W., Webb, S.E., Mongrand, S., Maurel, C.*, et al.* (2012). Cell wall constrains lateral diffusion of plant plasma-membrane proteins. Proceedings of the National Academy of Sciences *109*, 12805-12810.

Martinière, A., and Zelazny, E. (2021). Membrane nanodomains and transport functions in plant. Plant Physiology *187*, 1839-1855.

Mattila, P.K., Feest, C., Depoil, D., Treanor, B., Montaner, B., Otipoby, K.L., Carter, R., Justement, L.B., Bruckbauer, A., and Batista, F.D. (2013). The actin and tetraspanin networks organize receptor nanoclusters to regulate B cell receptor-mediated signaling. Immunity *38*, 461-474.

Mauck, L.A., Day, R.N., and Notides, A.C. (1982). Molybdate interaction with the estrogen receptor: effects on estradiol binding and receptor activation. Biochemistry *21*, 1788-1793.

Maule, A., Faulkner, C., and Benitez-Alfonso, Y. (2012). Plasmodesmata "in Communicado". Frontiers in Plant Science *3*, 30.

Maule, A.J., Benitez-Alfonso, Y., and Faulkner, C. (2011). Plasmodesmata – membrane tunnels with attitude. Current Opinion in Plant Biology *14*, 683-690.

MaxQB - The MaxQuant DataBase (2020).

Mazurov, D., Heidecker, G., and Derse, D. (2007). The inner loop of tetraspanins CD82 and CD81 mediates interactions with human T cell lymphotrophic virus type 1 Gag protein. Journal of Biological Chemistry *282*, 3896-3903.

McClung, J.K., Danner, D.B., Stewart, D.A., Smith, J.R., Schneider, E.L., Lumpkin, C.K., Dell'Orco, R.T., and Nuell, M.J. (1989). Isolation of a cDNA that hybrid selects antiproliferative mRNA from rat liver. Biochemical and Biophysical Research Communications *164*, 1316-1322.

McDonald, J.H., and Dunn, K.W. (2013). Statistical tests for measures of colocalization in biological microscopy. Journal of Microscopy *252*, 295-302.

McKenna, J.F., Rolfe, D.J., Webb, S.E.D., Tolmie, A.F., Botchway, S.W., Martin-Fernandez, M.L., Hawes, C., and Runions, J. (2019). The cell wall regulates dynamics and size of plasmamembrane nanodomains in Arabidopsis. Proceedings of the National Academy of Sciences *116*, 12857.

Meister, M., and Tikkanen, R. (2014). Endocytic trafficking of membrane-bound cargo: a flotillin point of view. Membranes *4*, 356-371.

Meister, M., Tomasovic, A., Banning, A., and Tikkanen, R. (2013). MITOGEN-ACTIVATED PROTEIN (MAP) KINASE Scaffolding Proteins: A Recount. International Journal of Molecular Sciences *14*, 4854-4884.

Mérida, A., and Fettke, J. (2021). Starch granule initiation in *Arabidopsis thaliana* chloroplasts. The Plant Journal *107*, 688-697.

Meusel, C. (2016). Analysis of CERK1 ectodomain shedding and the role of XLG2 in *cerk1-4* cell death execution (Göttingen: Georg-August-Universität Göttingen).

Miller, G., Schlauch, K., Tam, R., Cortes, D., Torres Miguel, A., Shulaev, V., Dangl Jeffery, L., and Mittler, R. (2009). The Plant NADPH Oxidase RBOHD Mediates Rapid Systemic Signaling in Response to Diverse Stimuli. Science Signaling *2*.

Minami, A., Fujiwara, M., Furuto, A., Fukao, Y., Yamashita, T., Kamo, M., Kawamura, Y., and Uemura, M. (2009). Alterations in Detergent-Resistant Plasma Membrane Microdomains in Arabidopsis thaliana During Cold Acclimation. Plant and Cell Physiology *50*, 341-359.

Mindrinos, M., Katagiri, F., Yu, G.-L., and Ausubel, F.M. (1994). The *A. thaliana* disease resistance gene RPS2 encodes a protein containing a nucleotide-binding site and leucine-rich repeats. Cell *78*, 1089-1099.

Mitamura, T., Iwamoto, R., Umata, T., Yomo, T., Urabe, I., Tsuneoka, M., and Mekada, E. (1992). The 27-kD diphtheria toxin receptor-associated protein (DRAP27) from vero cells is

the monkey homologue of human CD9 antigen: expression of DRAP27 elevates the number of diphtheria toxin receptors on toxin-sensitive cells. Journal of Cell Biology *118*, 1389-1399.

Miya, A., Albert, P., Shinya, T., Desaki, Y., Ichimura, K., Shirasu, K., Narusaka, Y., Kawakami, N., Kaku, H., and Shibuya, N. (2007). CERK1, a LysM receptor kinase, is essential for chitin elicitor signaling in Arabidopsis. Proceedings of the National Academy of Sciences *104*, 19613.

Miyado, K., Yamada, G., Yamada, S., Hasuwa, H., Nakamura, Y., Ryu, F., Suzuki, K., Kosai, K., Inoue, K., Ogura, A.*, et al.* (2000). Requirement of CD9 on the egg plasma membrane for fertilization. Science *287*, 321-324.

Moling, S., Pietraszewska-Bogiel, A., Postma, M., Fedorova, E., Hink, M.A., Limpens, E., Gadella, T.W.J., and Bisseling, T. (2014). Nod Factor Receptors Form Heteromeric Complexes and Are Essential for Intracellular Infection in Medicago Nodules. The Plant Cell *26*, 4188-4199.

Montel-Hagen, A., Kinet, S., Manel, N., Mongellaz, C., Prohaska, R., Battini, J.-L., Delaunay, J., Sitbon, M., and Taylor, N. (2008). Erythrocyte Glut1 Triggers Dehydroascorbic Acid Uptake in Mammals Unable to Synthesize Vitamin C. Cell *132*, 1039-1048.

Morejohn, L.C., Bureau, T.E., Molè-Bajer, J., Bajer, A.S., and Fosket, D.E. (1987). Oryzalin, a dinitroaniline herbicide, binds to plant tubulin and inhibits microtubule polymerization *in vitro*. Planta *172*, 252-264.

Moribe, H., Konakawa, R., Koga, D., Ushiki, T., Nakamura, K., and Mekada, E. (2012). Tetraspanin Is Required for Generation of Reactive Oxygen Species by the Dual Oxidase System in *Caenorhabditis elegans*. PLOS Genetics *8*, e1002957.

Moribe, H., and Mekada, E. (2013). Co-occurrence of tetraspanin and ROS generators. Worm *2*, e23415.

Morrow, I.C., and Parton, R.G. (2005). Flotillins and the PHB Domain Protein Family: Rafts, Worms and Anaesthetics. Traffic *6*, 725-740.

Morrow, I.C., Rea, S., Martin, S., Prior, I.A., Prohaska, R., Hancock, J.F., James, D.E., and Parton, R.G. (2002). Flotillin-1/reggie-2 traffics to surface raft domains via a novel golgi-independent pathway. Identification of a novel membrane targeting domain and a role for palmitoylation. Journal of Biological Chemistry *277*, 48834-48841.

Moser, J.J., Chan, E.K.L., and Fritzler, M.J. (2009). Optimization of immunoprecipitation-western blot analysis in detecting GW182-associated components of GW/P bodies. Nature Protocols *4*, 674-685.

Müller, R.E., Traish, A.M., Beebe, D.A., and Wotiz, H.H. (1982). Reversible inhibition of estrogen receptor activation by molybdate. Journal of Biological Chemistry *257*, 1295-1300.

Munro, S. (2003). Lipid rafts: elusive or illusive? Cell *115*, 377-388.

Mur, L.A.J., Kenton, P., Lloyd, A.J., Ougham, H., and Prats, E. (2008). The hypersensitive response; the centenary is upon us but how much do we know? Journal of Experimental Botany *59*, 501-520.

Murray, J.D. (2011). Invasion by Invitation: Rhizobial Infection in Legumes. Molecular Plant-Microbe Interactions *24*, 631-639.

Nadimpalli, R., Yalpani, N., Johal, G.S., and Simmons, C.R. (2000). Prohibitins, Stomatins, and Plant Disease Response Genes Compose a Protein Superfamily That Controls Cell Proliferation, Ion Channel Regulation, and Death. Journal of Biological Chemistry *275*, 29579-29586.

Nagano, A.J., Fukao, Y., Fujiwara, M., Nishimura, M., and Hara-Nishimura, I. (2008). Antagonistic jacalin-related lectins regulate the size of ER body-type beta-glucosidase complexes in *Arabidopsis thaliana*. Plant Cell Physiology *49*, 969-980.

Nagano, M., Ishikawa, T., Fujiwara, M., Fukao, Y., Kawano, Y., Kawai-Yamada, M., and Shimamoto, K. (2016). Plasma Membrane Microdomains Are Essential for Rac1-RbohB/H-Mediated Immunity in Rice. The Plant Cell *28*, 1966-1983.

Nakano, R., Yamada, K., Bednarek, P., Nishimura, M., and Hara-Nishimura, I. (2014). ER bodies in plants of the Brassicales order: biogenesis and association with innate immunity. Frontiers in Plant Science *5*.

Nazarov, P.V., Koehorst, R.B.M., Vos, W.L., Apanasovich, V.V., and Hemminga, M.A. (2006). FRET Study of Membrane Proteins: Simulation-Based Fitting for Analysis of Membrane Protein Embedment and Association. Biophysical Journal *91*, 454-466.

Nebenführ, A., Ritzenthaler, C., and Robinson, D.G. (2002). Brefeldin A: Deciphering an Enigmatic Inhibitor of Secretion. Plant Physiology *130*, 1102.

Nekrasov, V., Li, J., Batoux, M., Roux, M., Chu, Z.-H., Lacombe, S., Rougon, A., Bittel, P., Kiss-Papp, M., Chinchilla, D.*, et al.* (2009). Control of the pattern-recognition receptor EFR by an ER protein complex in plant immunity. The EMBO Journal *28*, 3428-3438.

Nesbit, A.D., Whippo, C., Hangarter, R.P., and Kehoe, D.M. (2015). Translation initiation factor 3 families: what are their roles in regulating cyanobacterial and chloroplast gene expression? Photosynthesis Research *126*, 147-159.

Neumann-Giesen, C., Falkenbach, B., Beicht, P., Claasen, S., Lüers, G., Stuermer, C.A., Herzog, V., and Tikkanen, R. (2004). Membrane and raft association of reggie-1/flotillin-2: role of myristoylation, palmitoylation and oligomerization and induction of filopodia by overexpression. Biochemical Journal *378*, 509-518.

New England Biolabs (2015). PNGase F Protocol, Denaturing Conditions. protocolsio.

Ngou, B.P.M., Ahn, H.-K., Ding, P., and Jones, J.D.G. (2021). Mutual potentiation of plant immunity by cell-surface and intracellular receptors. Nature.

Ngou, B.P.M., Jones, J.D.G., and Ding, P. (2022). Plant immune networks. Trends in Plant Science *27*, 255-273.

Nicolas, W.J., Grison, M.S., and Bayer, E.M. (2017). Shaping intercellular channels of plasmodesmata: the structure-to-function missing link. Journal of Experimental Botany *69*, 91-103.

Nicolson, G.L. (2013). Update of the 1972 Singer-Nicolson Fluid-Mosaic Model of Membrane Structure. Discoveries (Craiova, Romania) *1*, e3-e3.

Nijtmans, L.G.J., de Jong, L., Artal Sanz, M., Coates, P.J., Berden, J.A., Back, J.W., Muijsers, A.O., van der Spek, H., and Grivell, L.A. (2000). Prohibitins act as a membrane-bound chaperone for the stabilization of mitochondrial proteins. The EMBO Journal *19*, 2444-2451.

Nishimura, M.T., and Dangl, J.L. (2010). Arabidopsis and the plant immune system. The Plant Journal *61*, 1053-1066.

Noble, J.A., Innis, M.A., Koonin, E.V., Rudd, K.E., Banuett, F., and Herskowitz, I. (1993). The *Escherichia coli hflA* locus encodes a putative GTP-binding protein and two membrane proteins, one of which contains a protease-like domain. Proceedings of the National Academy of Sciences *90*, 10866.

Noirot, E., Der, C., Lherminier, J., Robert, F., Moricova, P., Kiêu, K., Leborgne-Castel, N., Simon-Plas, F., and Bouhidel, K. (2014). Dynamic changes in the subcellular distribution of the tobacco ROS-producing enzyme RBOHD in response to the oomycete elicitor cryptogein. Journal of Experimental Botany *65*, 5011-5022.

Nühse, T.S., Bottrill, A.R., Jones, A.M., and Peck, S.C. (2007). Quantitative phosphoproteomic analysis of plasma membrane proteins reveals regulatory mechanisms of plant innate immune responses. The Plant Journal *51*, 931-940.

Numata, K., and Kaplan, D.L. (2011). Biologically derived scaffolds. In Advanced Wound Repair Therapies, D. Farrar, ed. (Woodhead Publishing), pp. 524-551.

Ogle, T.F. (1983). Action of glycerol and sodium molybdate in stabilization of the progesterone receptor from rat trophoblast. Journal of Biological Chemistry *258*, 4982-4988.

Ohlrogge, J., and Browse, J. (1995). Lipid biosynthesis. The Plant Cell *7*, 957-970.

Okamoto, T., Schwab, R.B., Scherer, P.E., and Lisanti, M.P. (2000). Analysis of the Association of Proteins with Membranes. Current Protocols in Cell Biology *5*, 5.4.1-5.4.17.

Oldroyd, G.E.D., Murray, J.D., Poole, P.S., and Downie, J.A. (2011). The Rules of Engagement in the Legume-Rhizobial Symbiosis. Annual Review of Genetics *45*, 119-144.

Olmos, E., Reiss, B., and Dekker, K. (2003). The *ekeko* mutant demonstrates a role for tetraspanin-like protein in plant development. Biochemical and Biophysical Research Communications *310*, 1054-1061.

Oosterheert, W., Xenaki, K.T., Neviani, V., Pos, W., Doulkeridou, S., Manshande, J., Pearce, N.M., Kroon-Batenburg, L.M.J., Lutz, M., van Bergen en Henegouwen, P.M.P.*, et al.* (2020). Implications for tetraspanin-enriched microdomain assembly based on structures of CD9 with EWI-F. Life Science Alliance *3*, e202000883.

Orfila, C., and Knox, J.P. (2000). Spatial regulation of pectic polysaccharides in relation to pit fields in cell walls of tomato fruit pericarp. Plant Physiology *122*, 775-781.

Ortiz-Morea, F.A., Liu, J., Shan, L., and He, P. (2022). Malectin-like receptor kinases as protector deities in plant immunity. Nature Plants *8*, 27-37.

Orwick-Rydmark, M., Arnold, T., and Linke, D. (2016). The Use of Detergents to Purify Membrane Proteins. Current Protocols in Protein Science *84*, 4.8.1-4.8.35.

Otero, S., Helariutta, Y., and Benitez-Alfonso, Y. (2016). Symplastic communication in organ formation and tissue patterning. Current Opinion in Plant Biology *29*, 21-28.

Ott, T. (2017). Membrane nanodomains and microdomains in plant–microbe interactions. Current Opinion in Plant Biology *40*, 82-88.

Otto, G.P., and Nichols, B.J. (2011). The roles of flotillin microdomains – endocytosis and beyond. Journal of Cell Science *124*, 3933.

Overall, R.L., and Blackman, L.M. (1996). A model of the macromolecular structure of plasmodesmata. Trends in Plant Science *1*, 307-311.

Overall, R.L., Wolfe, J., and Gunning, B.E.S. (1982). Intercellular communication in Azolla roots: I. Ultrastructure of plasmodesmata. Protoplasma *111*, 134-150.

Packard, T.A., and Cambier, J.C. (2013). B lymphocyte antigen receptor signaling: initiation, amplification, and regulation. F1000prime Reports *5*, 40-40.

Pan, X., Fang, L., Liu, J., Senay-Aras, B., Lin, W., Zheng, S., Zhang, T., Guo, J., Manor, U., Van Norman, J.*, et al.* (2020). Auxin-induced signaling protein nanoclustering contributes to cell polarity formation. Nature Communications *11*, 3914.

Panter, S., Thomson, R., de Bruxelles, G., Laver, D., Trevaskis, B., and Udvardi, M. (2000). Identification with proteomics of novel proteins associated with the peribacteroid membrane of soybean root nodules. Molecular Plant-Microbe Interactions *13*, 325-333.

Patron, M., Sprenger, H.-G., and Langer, T. (2018). m-AAA proteases, mitochondrial calcium homeostasis and neurodegeneration. Cell Research *28*, 296-306.

Pearce, M.M., Wormer, D.B., Wilkens, S., and Wojcikiewicz, R.J. (2009). An endoplasmic reticulum (ER) membrane complex composed of SPFH1 and SPFH2 mediates the ER-associated degradation of inositol 1,4,5-trisphosphate receptors. Journal of Biological Chemistry *284*, 10433-10445.

Peñas, P.F., García-Díez, A., Sánchez-Madrid, F., and Yáñez-Mó, M. (2000). Tetraspanins are Localized at Motility-Related Structures and Involved in Normal Human Keratinocyte Wound Healing Migration. Journal of Investigative Dermatology *114*, 1126-1135.

Perez-Hernandez, D., Gutiérrez-Vázquez, C., Jorge, I., López-Martín, S., Ursa, A., Sánchez-Madrid, F., Vázquez, J., and Yáñez-Mó, M. (2013). The intracellular interactome of tetraspanin-enriched microdomains reveals their function as sorting machineries toward exosomes. The Journal of Biological Chemistry *288*, 11649-11661.

Pérez-Sancho, J., Tilsner, J., Samuels, A.L., Botella, M.A., Bayer, E.M., and Rosado, A. (2016). Stitching Organelles: Organization and Function of Specialized Membrane Contact Sites in Plants. Trends in Cell Biology *26*, 705-717.

Perraki, A., Cacas, J.-L., Crowet, J.-M., Lins, L., Castroviejo, M., German-Retana, S., Mongrand, S., and Raffaele, S. (2012). Plasma Membrane Localization of Solanum tuberosum Remorin from Group 1, Homolog 3 Is Mediated by Conformational Changes in a Novel C-Terminal Anchor and Required for the Restriction of Potato Virus X Movement. Plant Physiology *160*, 624-637.

Perraki, A., Gronnier, J., Gouguet, P., Boudsocq, M., Deroubaix, A.-F., Simon, V., German-Retana, S., Zipfel, C., Bayer, E., Mongrand, S.*, et al.* (2018). REM1.3's phospho-status defines its plasma membrane nanodomain organization and activity in restricting PVX cell-to-cell movement. PLOS Pathogens *14*, e1007378.

Peterson, J., Harrison, H., Jackson, D., and Snook, M. (2003). Biological Activities and Contents of Scopolin and Scopoletin in Sweetpotato Clones. HortScience *38*, 1129-1133.

Petutschnig, E.K., Jones, A.M., Serazetdinova, L., Lipka, U., and Lipka, V. (2010). The lysin motif receptor-like kinase (LysM-RLK) CERK1 is a major chitin-binding protein in *Arabidopsis thaliana* and subject to chitin-induced phosphorylation. Journal of Biological Chemistry *285*, 28902-28911.

Petutschnig, E.K., Stolze, M., Lipka, U., Kopischke, M., Horlacher, J., Valerius, O., Rozhon, W., Gust, A.A., Kemmerling, B., Poppenberger, B.*, et al.* (2014). A novel Arabidopsis CHITIN ELICITOR RECEPTOR KINASE 1 (CERK1) mutant with enhanced pathogen-induced cell death and altered receptor processing. New Phytologist *204*, 955-967.

Pfalz, J., Liere, K., Kandlbinder, A., Dietz, K.-J., and Oelmüller, R. (2006). pTAC2, -6, and -12 Are Components of the Transcriptionally Active Plastid Chromosome That Are Required for Plastid Gene Expression. The Plant Cell *18*, 176-197.

Piechota, J., Bereza, M., Sokołowska, A., Suszyński, K., Lech, K., and Jańska, H. (2015). Unraveling the functions of type II-prohibitins in Arabidopsis mitochondria. Plant Molecular Biology *88*, 249-267.

Pike, L.J. (2006). Rafts defined: a report on the Keystone Symposium on Lipid Rafts and Cell Function. Journal of Lipid Research *47*, 1597-1598.

Pileri, P., Uematsu, Y., Campagnoli, S., Galli, G., Falugi, F., Petracca, R., Weiner, A.J., Houghton, M., Rosa, D., Grandi, G.*, et al.* (1998). Binding of hepatitis C virus to CD81. Science *282*, 938-941.

Pink, D.A. (1985). Protein lateral movement in lipid bilayers. Stimulation studies of its dependence upon protein concentration. Biochimica et Biophysica Acta *818*, 200-204.

Platre, M.P., Bayle, V., Armengot, L., Bareille, J., Marquès-Bueno, M.d.M., Creff, A., Maneta-Peyret, L., Fiche, J.-B., Nollmann, M., Miège, C.*, et al.* (2019). Developmental control of plant Rho GTPase nano-organization by the lipid phosphatidylserine. Science *364*, 57.

Pogány, M., von Rad, U., Grün, S., Dongó, A., Pintye, A., Simoneau, P., Bahnweg, G., Kiss, L., Barna, B., and Durner, J. (2009). Dual roles of reactive oxygen species and NADPH oxidase RBOHD in an Arabidopsis-Alternaria pathosystem. Plant Physiology *151*, 1459-1475.

Poole, K., Herget, R., Lapatsina, L., Ngo, H.-D., and Lewin, G.R. (2014). Tuning Piezo ion channels to detect molecular-scale movements relevant for fine touch. Nature Communications *5*, 3520.

Porter, K., and Day, B. (2016). From filaments to function: The role of the plant actin cytoskeleton in pathogen perception, signaling and immunity. Journal of Integrative Plant Biology *58*, 299-311.

Pribil, M., Labs, M., and Leister, D. (2014). Structure and dynamics of thylakoids in land plants. Journal of Experimental Botany *65*, 1955-1972.

Price, A.H., Taylor, A., Ripley, S.J., Griffiths, A., Trewavas, A.J., and Knight, M.R. (1994). Oxidative Signals in Tobacco Increase Cytosolic Calcium. The Plant Cell *6*, 1301-1310.

Price, M.P., Thompson, R.J., Eshcol, J.O., Wemmie, J.A., and Benson, C.J. (2004). Stomatin Modulates Gating of Acid-sensing Ion Channels*. Journal of Biological Chemistry *279*, 53886-53891.

Prince, D.C., Drurey, C., Zipfel, C., and Hogenhout, S.A. (2014). The leucine-rich repeat receptor-like kinase BRASSINOSTEROID INSENSITIVE1-ASSOCIATED KINASE1 and the cytochrome P450 PHYTOALEXIN DEFICIENT3 contribute to innate immunity to aphids in Arabidopsis. Plant Physiology *164*, 2207-2219.

Qi, Y., and Katagiri, F. (2009). Purification of low-abundance Arabidopsis plasma-membrane protein complexes and identification of candidate components. The Plant Journal *57*, 932-944.

Qi, Y., Tsuda, K., Nguyen, L.V., Wang, X., Lin, J., Murphy, A.S., Glazebrook, J., Thordal-Christensen, H., and Katagiri, F. (2011). Physical Association of Arabidopsis HYPERSENSITIVE INDUCED REACTION Proteins (HIRs) with the Immune Receptor RPS2. Journal of Biological Chemistry *286*, 31297-31307.

Quezada, E.-H., García, G.-X., Arthikala, M.-K., Melappa, G., Lara, M., and Nanjareddy, K. (2019). Cysteine-Rich Receptor-Like Kinase Gene Family Identification in the Phaseolus Genome and Comparative Analysis of Their Expression Profiles Specific to Mycorrhizal and Rhizobial Symbiosis. Genes *10*, 59.

Quirós, P.M., Langer, T., and López-Otín, C. (2015). New roles for mitochondrial proteases in health, ageing and disease. Nature Reviews Molecular Cell Biology *16*, 345-359.

R Core Team (2021). R: A language and environment for statistical computing. (Vienna, Austria: R Foundation for Statistical Computing).

Raffaele, S., Bayer, E., Lafarge, D., Cluzet, S., German Retana, S., Boubekeur, T., Leborgne-Castel, N., Carde, J.-P., Lherminier, J., Noirot, E.*, et al.* (2009). Remorin, a Solanaceae Protein Resident in Membrane Rafts and Plasmodesmata, Impairs Potato virus X Movement. The Plant Cell *21*, 1541.

Rajarammohan, S. (2021). Redefining Plant-Necrotroph Interactions: The Thin Line Between Hemibiotrophs and Necrotrophs. Front Microbiol *12*, 673518-673518.

Ramadurai, S., Holt, A., Krasnikov, V., van den Bogaart, G., Killian, J.A., and Poolman, B. (2009). Lateral Diffusion of Membrane Proteins. Journal of the American Chemical Society *131*, 12650-12656.

Ramírez, V., López, A., Mauch-Mani, B., Gil, M.J., and Vera, P. (2013). An Extracellular Subtilase Switch for Immune Priming in Arabidopsis. PLOS Pathogens *9*, e1003445.

Rao, S., Zhou, Z., Miao, P., Bi, G., Hu, M., Wu, Y., Feng, F., Zhang, X., and Zhou, J.-M. (2018). Roles of Receptor-Like Cytoplasmic Kinase VII Members in Pattern-Triggered Immune Signaling. Plant Physiology *177*, 1679-1690.

Ratzka, A., Vogel, H., Kliebenstein, D.J., Mitchell-Olds, T., and Kroymann, J. (2002). Disarming the mustard oil bomb. Proceedings of the National Academy of Sciences *99*, 11223-11228.

Reimann, R. (2018). Die Funktion von Tetraspaninen in der pflanzlichen Entwicklung und Reproduktion und Studien zum Wachstum von Pollenschläuchen in einer 3D-Matrix (Friedrich-Alexander-Universität Erlangen-Nürnberg).

Reimann, R., Kost, B., and Dettmer, J. (2017). TETRASPANINs in Plants. Frontiers in Plant Science *8*, 545.

Reits, E.A.J., and Neefjes, J.J. (2001). From fixed to FRAP: measuring protein mobility and activity in living cells. Nature Cell Biology *3*, E145.

Reszczyńska, E., and Hanaka, A. (2020). Lipids Composition in Plant Membranes. Cell Biochemistry and Biophysics *78*, 401-414.

Reumann, S., Babujee, L., Ma, C., Wienkoop, S., Siemsen, T., Antonicelli, G.E., Rasche, N., Lüder, F., Weckwerth, W., and Jahn, O. (2007). Proteome Analysis of Arabidopsis Leaf Peroxisomes Reveals Novel Targeting Peptides, Metabolic Pathways, and Defense Mechanisms. The Plant Cell *19*, 3170-3193.

Rhodes, J., Yang, H., Moussu, S., Boutrot, F., Santiago, J., and Zipfel, C. (2021). Perception of a divergent family of phytocytokines by the Arabidopsis receptor kinase MIK2. Nature Communications *12*, 705.

Ritchie, K., Iino, R., Fujiwara, T., Murase, K., and Kusumi, A. (2003). The fence and picket structure of the plasma membrane of live cells as revealed by single molecule techniques (Review). Molecular Membrane Biology *20*, 13-18.

Rivera-Milla, E., Stuermer, C.A., and Málaga-Trillo, E. (2006). Ancient origin of reggie (flotillin), reggie-like, and other lipid-raft proteins: convergent evolution of the SPFH domain. Cellular and Molecular Life Sciences *63*, 343-357.

Robards, A.W. (1968). A new interpretation of plasmodesmatal ultrastructure. Planta *82*, 200-210.

Robards, A.W. (1971). The ultrastructure of plasmodesmata. Protoplasma *72*, 315-323.

Robatzek, S., Chinchilla, D., and Boller, T. (2006). Ligand-induced endocytosis of the pattern recognition receptor FLS2 in Arabidopsis. Genes & Development *20*, 537-542.

Rocha, A.G., Mehlmer, N., Stael, S., Mair, A., Parvin, N., Chigri, F., Teige, M., and Vothknecht, U. (2013). Phosphorylation of Arabidopsis transketolase at Ser^{428} provides a

potential paradigm for metabolic control of chloroplast carbon metabolism. The Biochemical Journal *458*.

Romeis, T., and Herde, M. (2014). From local to global: CDPKs in systemic defense signaling upon microbial and herbivore attack. Current Opinion in Plant Biology *20*, 1-10.

Röper, K., Corbeil, D., and Huttner, W.B. (2000). Retention of prominin in microvilli reveals distinct cholesterol-based lipid micro-domains in the apical plasma membrane. Nature Cell Biology *2*, 582-592.

Rowley, D.R., Chang, C.H., and Tindall, D.J. (1984). Effects of Sodium Molybdate on the Androgen Receptor from the R3327 Prostatic Tumor*. Endocrinology *114*, 1776-1783.

Roy, S., Watada, A.E., and Wergin, W.P. (1997). Characterization of the Cell Wall Microdomain Surrounding Plasmodesmata in Apple Fruit. Plant Physiology *114*, 539-547.

Ryder, L.S., Dagdas, Y.F., Mentlak, T.A., Kershaw, M.J., Thornton, C.R., Schuster, M., Chen, J., Wang, Z., and Talbot, N.J. (2013). NADPH oxidases regulate septin-mediated cytoskeletal remodeling during plant infection by the rice blast fungus. Proceedings of the National Academy of Sciences *110*, 3179-3184.

Saalbach, G., Erik, P., and Wienkoop, S. (2002). Characterisation by proteomics of peribacteroid space and peribacteroid membrane preparations from pea (*Pisum sativum*) symbiosomes. Proteomics *2*, 325-337.

Sagan, L. (1967). On the origin of mitosing cells. Journal of Theoretical Biology *14*, 225-IN226.

Sager, R., and Lee, J.-Y. (2014). Plasmodesmata in integrated cell signalling: insights from development and environmental signals and stresses. Journal of Experimental Botany *65*, 6337-6358.

Saijo, Y., Tintor, N., Lu, X., Rauf, P., Pajerowska-Mukhtar, K., Häweker, H., Dong, X., Robatzek, S., and Schulze-Lefert, P. (2009). Receptor quality control in the endoplasmic reticulum for plant innate immunity. The EMBO Journal *28*, 3439-3449.

Saint-Pol, J., Eschenbrenner, E., Dornier, E., Boucheix, C., Charrin, S., and Rubinstein, E. (2017). Regulation of the trafficking and the function of the metalloprotease ADAM10 by tetraspanins. Biochemical Society Transactions *45*, 937-944.

Saiz, M.L., Rocha-Perugini, V., and Sánchez-Madrid, F. (2018). Tetraspanins as Organizers of Antigen-Presenting Cell Function. Frontiers in Immunology *9*, 1074-1074.

Sam Mugford, S.H. (2018). Bounce PCR. protocolsio.

Sánchez-Vallet, A., Mesters, J.R., and Thomma, B.P.H.J. (2015). The battle for chitin recognition in plant-microbe interactions. FEMS Microbiology Reviews *39*, 171-183.

Sang, Y., and Macho, A.P. (2017). Analysis of PAMP-Triggered ROS Burst in Plant Immunity. Methods in Molecular Biology *1578*, 143-153.

Sassmann, S., Rodrigues, C., Milne, S.W., Nenninger, A., Allwood, E., Littlejohn, G.R., Talbot, N.J., Soeller, C., Davies, B., Hussey, P.J.*, et al.* (2018). An Immune-Responsive

Cytoskeletal-Plasma Membrane Feedback Loop in Plants. Current Biology *28*, 2136-2144.e2137.

Sato, Y., Tezuka, A., Kashima, M., Deguchi, A., Shimizu-Inatsugi, R., Yamazaki, M., Shimizu, K.K., and Nagano, A.J. (2019). Transcriptional Variation in Glucosinolate Biosynthetic Genes and Inducible Responses to Aphid Herbivory on Field-Grown *Arabidopsis thaliana*. Frontiers in Genetics *10*.

Sayeski, P.P., Ali, M.S., and Bernstein, K.E. (2000). The role of Ca2+ mobilization and heterotrimeric G protein activation in mediating tyrosine phosphorylation signaling patterns in vascular smooth muscle cells. Molecular and Cellular Biochemistry *212*, 91-98.

Scaffold version 4.11.0 (2020).

Schaufele, F., Demarco, I., and Day, R.N. (2005). 4 - FRET Imaging in the Wide-Field Microscope. In Molecular Imaging, A. Periasamy, and R.N. Day, eds. (San Diego: American Physiological Society), pp. 72-94.

Schindelin, J., Arganda-Carreras, I., Frise, E., Kaynig, V., Longair, M., Pietzsch, T., Preibisch, S., Rueden, C., Saalfeld, S., Schmid, B.*, et al.* (2012). Fiji: an open-source platform for biological-image analysis. Nature Methods *9*, 676.

Schmid, F. (2017). Physical mechanisms of micro- and nanodomain formation in multicomponent lipid membranes. Biochimica et Biophysica Acta (BBA) - Biomembranes *1859*, 509-528.

Schmidt, T.H., Homsi, Y., and Lang, T. (2016). Oligomerization of the Tetraspanin CD81 via the Flexibility of Its δ-Loop. Biophysical Journal *110*, 2463-2474.

Schneider, A., Rajendran, L., Honsho, M., Gralle, M., Donnert, G., Wouters, F., Hell, S.W., and Simons, M. (2008). Flotillin-Dependent Clustering of the Amyloid Precursor Protein Regulates Its Endocytosis and Amyloidogenic Processing in Neurons. The Journal of Neuroscience *28*, 2874.

Schneider, C.A., Rasband, W.S., and Eliceiri, K.W. (2012). NIH Image to ImageJ: 25 years of image analysis. Nature Methods *9*, 671-675.

Schoberer, J., and Strasser, R. (2018). Plant glyco-biotechnology. Seminars in Cell & Developmental Biology *80*, 133-141.

Schuck, S., Honsho, M., Ekroos, K., Shevchenko, A., and Simons, K. (2003). Resistance of cell membranes to different detergents. Proceedings of the National Academy of Sciences *100*, 5795-5800.

Seguel, A., Jelenska, J., Herrera-Vásquez, A., Marr, S.K., Joyce, M.B., Gagesch, K.R., Shakoor, N., Jiang, S.-C., Fonseca, A., Wildermuth, M.C.*, et al.* (2018). PROHIBITIN3 Forms Complexes with ISOCHORISMATE SYNTHASE1 to Regulate Stress-Induced Salicylic Acid Biosynthesis in Arabidopsis Plant Physiology *176*, 2515-2531.

Sevcsik, E., Brameshuber, M., Fölser, M., Weghuber, J., Honigmann, A., and Schütz, G.J. (2015). GPI-anchored proteins do not reside in ordered domains in the live cell plasma membrane. Nature Communications *6*, 6969.

Sevilem, I., Yadav, S.R., and Helariutta, Y. (2015). Plasmodesmata: channels for intercellular signaling during plant growth and development. Methods in Molecular Biolology *1217*, 3-24.

Shahinian, S., and Silvius, J.R. (1995). Doubly-lipid-modified protein sequence motifs exhibit long-lived anchorage to lipid bilayer membranes. Biochemistry *34*, 3813-3822.

Sharma, P., Jha, A., Dubey, R., and Pessarakli, M. (2012). Reactive Oxygen Species, Oxidative Damage, and Antioxidative Defense Mechanism in Plants under Stressful Conditions. Journal of Botany *2012*.

Sheetz, M.P., Schindler, M., and Koppel, D.E. (1980). Lateral mobility of integral membrane proteins is increased in spherocytic erythrocytes. Nature *285*, 510-512.

Shevchenko, A., Tomas, H., Havli, J., Olsen, J.V., and Mann, M. (2006). In-gel digestion for mass spectrometric characterization of proteins and proteomes. Nature Protocols *1*, 2856-2860.

Shinya, T., Yamaguchi, K., Desaki, Y., Yamada, K., Narisawa, T., Kobayashi, Y., Maeda, K., Suzuki, M., Tanimoto, T., Takeda, J.*, et al.* (2014). Selective regulation of the chitin-induced defense response by the Arabidopsis receptor-like cytoplasmic kinase PBL27. The Plant Journal *79*, 56-66.

Shiu, S.-H., and Bleecker, A.B. (2003). Expansion of the Receptor-Like Kinase/Pelle Gene Family and Receptor-Like Proteins in Arabidopsis Plant Physiology *132*, 530-543.

Shiu, S.H., and Bleecker, A.B. (2001). Plant receptor-like kinase gene family: diversity, function, and signaling. Sci STKE *2001*, re22.

Siegmund, U., Heller, J., van Kann, J.A.L., and Tudzynski, P. (2013). The NADPH Oxidase Complexes in *Botrytis cinerea*: Evidence for a Close Association with the ER and the Tetraspanin Pls1. PLOS One *8*, e55879.

Silvie, O., Rubinstein, E., Franetich, J.F., Prenant, M., Belnoue, E., Renia, L., Hannoun, L., Eling, W., Levy, S., Boucheix, C.*, et al.* (2003). Hepatocyte CD81 is required for *Plasmodium falciparum* and *Plasmodium yoelii* sporozoite infectivity. Nature Medicine *9*, 93-96.

Simillion, C., Vandepoele, K., Van Montagu, M.C.E., Zabeau, M., and Van de Peer, Y. (2002). The hidden duplication past of *Arabidopsis thaliana*. Proceedings of the National Academy of Sciences *99*, 13627-13632.

Simons, K., and Toomre, D. (2000). Lipid rafts and signal transduction. Nature Reviews Molecular Cell Biology *1*, 31.

Simpson, C., Thomas, C., Findlay, K., Bayer, E., and Maule, A.J. (2009). An Arabidopsis GPI-anchor plasmodesmal neck protein with callose binding activity and potential to regulate cell-to-cell trafficking. The Plant Cell *21*, 581-594.

Singer, S.J., and Nicolson, G.L. (1972). The Fluid Mosaic Model of the Structure of Cell Membranes. Science *175*, 720-731.

Smit, P., Limpens, E., Geurts, R., Fedorova, E., Dolgikh, E., Gough, C., and Bisseling, T. (2007). Medicago LYK3, an Entry Receptor in Rhizobial Nodulation Factor Signaling. Plant Physiology *145*, 183-191.

Smokvarska, M., Francis, C., Platre, M.P., Fiche, J.-B., Alcon, C., Dumont, X., Nacry, P., Bayle, V., Nollmann, M., Maurel, C.*, et al.* (2020). A Plasma Membrane Nanodomain Ensures Signal Specificity during Osmotic Signaling in Plants. Current Biology *30*, 4654-4664.e4654.

Song, J., Durrin, L.K., Wilkinson, T.A., Krontiris, T.G., and Chen, Y. (2004). Identification of a SUMO-binding motif that recognizes SUMO-modified proteins. Proceedings of the National Academy of Sciences *101*, 14373.

Sowley, E.N.K., Dewey, F.M., and Shaw, M.W. (2010). Persistent, symptomless, systemic, and seed-borne infection of lettuce by Botrytis cinerea. European Journal of Plant Pathology *126*, 61-71.

Spira, F., Mueller, N.S., Beck, G., von Olshausen, P., Beig, J., and Wedlich-Soldner, R. (2012). Patchwork organization of the yeast plasma membrane into numerous coexisting domains. Nature Cell Biology *14*, 640-648.

Stahl, Y., and Faulkner, C. (2016). Receptor Complex Mediated Regulation of Symplastic Traffic. Trends in Plant Science *21*, 450-459.

Stahl, Y., Grabowski, S., Bleckmann, A., Kühnemuth, R., Weidtkamp-Peters, S., Pinto, Karine G., Kirschner, Gwendolyn K., Schmid, Julia B., Wink, René H., Hülsewede, A.*, et al.* (2013). Moderation of Arabidopsis Root Stemness by CLAVATA1 and ARABIDOPSIS CRINKLY4 Receptor Kinase Complexes. Current Biology *23*, 362-371.

Strasser, R., Stadlmann, J., Svoboda, B., Altmann, F., GlÖSsl, J., and Mach, L. (2005). Molecular basis of N-acetylglucosaminyltransferase I deficiency in Arabidopsis thaliana plants lacking complex N-glycans. Biochemical Journal *387*, 385-391.

Strawn, M.A., Marr, S.K., Inoue, K., Inada, N., Zubieta, C., and Wildermuth, M.C. (2007). Arabidopsis ISOCHORISMATE SYNTHASE Functional in Pathogen-induced Salicylate Biosynthesis Exhibits Properties Consistent with a Role in Diverse Stress Responses. Journal of Biological Chemistry *282*, 5919-5933.

Stryer, L., and Haugland, R.P. (1967). Energy transfer: a spectroscopic ruler. Proceedings of the National Academy of Sciences of the United States of America *58*, 719-726.

Stuermer, C.A., Lang, D.M., Kirsch, F., Wiechers, M., Deininger, S.O., and Plattner, H. (2001). Glycosylphosphatidyl inositol-anchored proteins and fyn kinase assemble in noncaveolar plasma membrane microdomains defined by reggie-1 and -2. Mol Biol Cell *12*, 3031-3045.

Stuermer, C.A., Langhorst, M.F., Wiechers, M.F., Legler, D.F., Von Hanwehr, S.H., Guse, A.H., and Plattner, H. (2004). PrPc capping in T cells promotes its association with the lipid raft proteins reggie-1 and reggie-2 and leads to signal transduction. The FASEB Journal *18*, 1731-1733.

Sun, Y., Qiao, Z., Muchero, W., and Chen, J.-G. (2020). Lectin Receptor-Like Kinases: The Sensor and Mediator at the Plant Cell Surface. Frontiers in Plant Science *11*.

Susa, K.J., Seegar, T.C.M., Blacklow, S.C., and Kruse, A.C. (2020). A dynamic interaction between CD19 and the tetraspanin CD81 controls B cell co-receptor trafficking. eLife *9*, e52337.

Swatek, K.N., and Komander, D. (2016). Ubiquitin modifications. Cell Research *26*, 399-422.

Takata, H., Matsunaga, S., Morimoto, A., Ma, N., Kurihara, D., Ono-Maniwa, R., Nakagawa, M., Azuma, T., Uchiyama, S., and Fukui, K. (2007). PHB2 Protects Sister-Chromatid Cohesion in Mitosis. Current Biology *17*, 1356-1361.

Tam, J.M., Reedy, J.L., Lukason, D.P., Kuna, S.G., Acharya, M., Khan, N.S., Negoro, P.E., Xu, S., Ward, R.A., Feldman, M.B.*, et al.* (2019). Tetraspanin CD82 Organizes Dectin-1 into Signaling Domains to Mediate Cellular Responses to *Candida albican*. The Journal of Immunology.

Tapken, W., and Murphy, A.S. (2015). Membrane nanodomains in plants: capturing form, function, and movement. Journal of Experimental Botany *66*, 1573-1586.

Tatsuta, T., Model, K., and Langer, T. (2005). Formation of membrane-bound ring complexes by prohibitins in mitochondria. Mol Biol Cell *16*, 248-259.

Tavassolifar, M.J., Vodjgani, M., Salehi, Z., and Izad, M. (2020). The Influence of Reactive Oxygen Species in the Immune System and Pathogenesis of Multiple Sclerosis. Autoimmune Diseases *2020*, 5793817-5793817.

Tavernarakis, N., Driscoll, M., and Kyrpides, N.C. (1999). The SPFH domain: implicated in regulating targeted protein turnover in stomatins and other membrane-associated proteins. Trends in Biochemical Sciences *24*, 425-427.

Taylor, A.A., Horsch, A., Rzepczyk, A., Hasenkampf, C.A., and Riggs, C.D. (1997). Maturation and secretion of a serine proteinase is associated with events of late microsporogenesis. The Plant Journal *12*, 1261-1271.

Tee, E.E., Samwald, S., and Faulkner, C. (2022). Quantification of Cell-to-Cell Connectivity Using Particle Bombardment. In Plasmodesmata: Methods and Protocols, Second Edition, Y. Benitez-Alfonso, and M. Heinlein, eds. (Springer Protocols).

Temme, N., and Tudzynski, P. (2009). Does *Botrytis cinerea* Ignore H_2O_2-Induced Oxidative Stress During Infection? Characterization of *Botrytis* Activator Protein 1. Mol Plant Microbe Interact *22*, 987-998.

Teo, G., Liu, G., Zhang, J., Nesvizhskii, A.I., Gingras, A.C., and Choi, H. (2014). SAINTexpress: improvements and additional features in Significance Analysis of INTeractome software. J Proteomics *100*, 37-43.

Termini, C.M., and Gillette, J.M. (2017). Tetraspanins Function as Regulators of Cellular Signaling. Frontiers in Cell and Developmental Biology *5*, 34.

The Arabidopsis Information Resource (TAIR) (2020). www.arabidopsis.org.

The UniProt Consortium (2021). UniProt: the universal protein knowledgebase in 2021. Nucleic Acids Research *49*, D480-D489.

Thomas, C.L., Bayer, E.M., Ritzenthaler, C., Fernandez-Calvino, L., and Maule, A.J. (2008). Specific Targeting of a Plasmodesmal Protein Affecting Cell-to-Cell Communication. PLOS Biology *6*, e7.

Thor, K., Jiang, S., Michard, E., George, J., Scherzer, S., Huang, S., Dindas, J., Derbyshire, P., Leitão, N., DeFalco, T.A.*, et al.* (2020). The calcium-permeable channel OSCA1.3 regulates plant stomatal immunity. Nature *585*, 569-573.

Tilsner, J., Amari, K., and Torrance, L. (2011). Plasmodesmata viewed as specialised membrane adhesion sites. Protoplasma *248*, 39-60.

Timm, S., Giese, J., Engel, N., Wittmiß, M., Florian, A., Fernie, A.R., and Bauwe, H. (2018). T-protein is present in large excess over the other proteins of the glycine cleavage system in leaves of Arabidopsis. Planta *247*, 41-51.

Tjellström, H., Hellgren, L.I., Wieslander, Å., and Sandelius, A.S. (2010). Lipid asymmetry in plant plasma membranes: phosphate deficiency-induced phospholipid replacement is restricted to the cytosolic leaflet. The FASEB Journal *24*, 1128-1138.

Todres, E., Nardi, J.B., and Robertson, H.M. (2000). The tetraspanin superfamily in insects. Insect Molecular Biology *9*, 581-590.

Tolmie, F., Poulet, A., McKenna, J., Sassmann, S., Graumann, K., Deeks, M., and Runions, J. (2017). The cell wall of *Arabidopsis thaliana* influences actin network dynamics. Journal of Experimental Botany *68*, 4517-4527.

Tornmalm, J., Piguet, J., Chmyrov, V., and Widengren, J. (2019). Imaging of intermittent lipid-receptor interactions reflects changes in live cell membranes upon agonist-receptor binding. Scientific Reports *9*, 18133.

Torres, M.A. (2010). ROS in biotic interactions. Physiologia Plantarum *138*, 414-429.

Toufighi, K., Brady, S.M., Austin, R., Ly, E., and Provart, N.J. (2005). The Botany Array Resource: e-Northerns, Expression Angling, and promoter analyses. The Plant Journal *43*, 153-163.

Trotter, J., Klein, C., and Krämer, E.-M. (2000). GPI-Anchored Proteins and Glycosphingolipid-Rich Rafts: Platforms for Adhesion and Signaling. The Neuroscientist *6*, 271-284.

Tsui, H.-C.T., Leung, H.-C.E., and Winkler, M.E. (1994). Characterization of broadly pleiotropic phenotypes caused by an hfq insertion mutation in *Escherichia coli* K-12. Molecular Microbiology *13*, 35-49.

Tsujimoto, Y., Numaga, T., Ohshima, K., Yano, M.-A., Ohsawa, R., Goto, D.B., Naito, S., and Ishikawa, M. (2003). Arabidopsis TOBAMOVIRUS MULTIPLICATION (TOM) 2 locus encodes a transmembrane protein that interacts with TOM1. The EMBO Journal *22*, 335-343.

Turner, A., Wells, B., and Roberts, K. (1994). Plasmodesmata of maize root tips: structure and composition. Journal of Cell Science *107*, 3351-3361.

Umeda, R., Satouh, Y., Takemoto, M., Nakada-Nakura, Y., Liu, K., Yokoyama, T., Shirouzu, M., Iwata, S., Nomura, N., Sato, K.*, et al.* (2020). Structural insights into tetraspanin CD9 function. Nature Communications *11*, 1606.

Upton, C., and Buckley, J.T. (1995). A new family of lipolytic enzymes? Trends in Biochemical Sciences *20*, 178-179.

Ursache, R., De Jesus Vieira Teixeira, C., Dénervaud Tendon, V., Gully, K., De Bellis, D., Schmid-Siegert, E., Grube Andersen, T., Shekhar, V., Calderon, S., Pradervand, S.*, et al.* (2021). GDSL-domain proteins have key roles in suberin polymerization and degradation. Nature Plants *7*, 353-364.

Vaddepalli, P., Herrmann, A., Fulton, L., Oelschner, M., Hillmer, S., Stratil, T.F., Fastner, A., Hammes, U.Z., Ott, T., Robinson, D.G.*, et al.* (2014). The C2-domain protein QUIRKY and the receptor-like kinase STRUBBELIG localize to plasmodesmata and mediate tissue morphogenesis in *Arabidopsis thaliana*. Development *141*, 4139-4148.

Van Aken, O., Pecenková, T., van de Cotte, B., De Rycke, R., Eeckhout, D., Fromm, H., De Jaeger, G., Witters, E., Beemster, G.T., Inzé, D.*, et al.* (2007). Mitochondrial type-I prohibitins of *Arabidopsis thaliana* are required for supporting proficient meristem development. Plant J *52*, 850-864.

van Deventer, S., Arp, A.B., and van Spriel, A.B. (2020). Dynamic Plasma Membrane Organization: A Complex Symphony. Trends in Cell Biology.

van Deventer, S.J., Dunlock, V.E., and van Spriel, A.B. (2017). Molecular interactions shaping the tetraspanin web. Biochemical Society Transactions *45*, 741-750.

van Kan, J.A.L. (2006). Licensed to kill: the lifestyle of a necrotrophic plant pathogen. Trends in Plant Science *11*, 247-253.

van Kan, J.A.L., Shaw, M.W., and Grant-Downton, R.T. (2014). Botrytis species: relentless necrotrophic thugs or endophytes gone rogue? Molecular Plant Pathology *15*, 957-961.

van Zanten, T.S., Cambi, A., Koopman, M., Joosten, B., Figdor, C.G., and Garcia-Parajo, M.F. (2009). Hotspots of GPI-anchored proteins and integrin nanoclusters function as nucleation sites for cell adhesion. Proceedings of the National Academy of Sciences *106*, 18557.

Vatén, A., Dettmer, J., Wu, S., Stierhof, Y.-D., Miyashima, S., Yadav, Shri R., Roberts, Christina J., Campilho, A., Bulone, V., Lichtenberger, R.*, et al.* (2011). Callose Biosynthesis Regulates Symplastic Trafficking during Root Development. Developmental Cell *21*, 1144-1155.

Veyres, N., Danon, A., Aono, M., Galliot, S., Karibasappa, Y.B., Diet, A., Grandmottet, F., Tamaoki, M., Lesur, D., Pilard, S.*, et al.* (2008). The Arabidopsis *sweetie* mutant is affected in carbohydrate metabolism and defective in the control of growth, development and senescence. The Plant Journal *55*, 665-686.

Vögeli, U., and Chappell, J. (1991). Inhibition of a plant sesquiterpene cyclase by mevinolin. Archives of Biochemistry and Biophysics *288*, 157-162.

Wan, J., Tanaka, K., Zhang, X.C., Son, G.H., Brechenmacher, L., Nguyen, T.H., and Stacey, G. (2012). LYK4, a lysin motif receptor-like kinase, is important for chitin signaling and plant innate immunity in Arabidopsis. Plant Physiology *160*, 396-406.

Wang, F., Muto, A., Van de Velde, J., Neyt, P., Himanen, K., Vandepoele, K., and Van Lijsebettens, M. (2015a). Functional Analysis of the Arabidopsis TETRASPANIN Gene Family in Plant Growth and Development. Plant Physiology *169*, 2200-2214.

Wang, F., Vandepoele, K., and Van Lijsebettens, M. (2012a). Tetraspanin genes in plants. Plant Science *190*, 9-15.

Wang, H.-X., Sharma, C., Knoblich, K., Granter, S.R., and Hemler, M.E. (2015b). EWI-2 negatively regulates TGF-β signaling leading to altered melanoma growth and metastasis. Cell Research *25*, 370-385.

Wang, K., Wei, G., and Liu, D. (2012b). CD19: a biomarker for B cell development, lymphoma diagnosis and therapy. Experimental Hematology & Oncology *1*, 36.

Wang, L., Li, H., Lv, X., Chen, T., Li, R., Xue, Y., Jiang, J., Jin, B., Baluška, F., Šamaj, J., *et al.* (2015c). Spatiotemporal Dynamics of the BRI1 Receptor and its Regulation by Membrane Microdomains in Living Arabidopsis Cells. Molecular Plant *8*, 1334-1349.

Wang, X., Sager, R., Cui, W., Zhang, C., Lu, H., and Lee, J.-Y. (2013). Salicylic Acid Regulates Plasmodesmata Closure during Innate Immune Responses in Arabidopsis. The Plant Cell *25*, 2315-2329.

Wang, Y.-C., Peterson, S.E., and Loring, J.F. (2014). Protein post-translational modifications and regulation of pluripotency in human stem cells. Cell Research *24*, 143-160.

Watarai, M., Makino, S., Fujii, Y., Okamoto, K., and Shirahata, T. (2002). Modulation of Brucella-induced macropinocytosis by lipid rafts mediates intracellular replication. Cellular Microbiology *4*, 341-355.

Weidtkamp-Peters, S., and Stahl, Y. (2017). The Use of FRET/FLIM to Study Proteins Interacting with Plant Receptor Kinases. Methods in Molecular Biology *1621*, 163-175.

Whitehead, L., and Day, D. (2006). The peribacteroid membrane. Physiologia Plantarum *100*, 30-44.

Wickham H. (2016). ggplot2: Elegant Graphics for Data Analysis. (Springer-Verlag New York).

Williamson, B., Tudzynski, B., Tudzynski, P., and Van Kan, J.A.L. (2007). Botrytis cinerea: the cause of grey mould disease. Molecular Plant Pathology *8*, 561-580.

Win, J., and Kamoun, S. (2004). pCB301-p19: A Binary Plasmid Vector to Enhance Transient Expression of Transgenes by Agroinfiltration (http://www.kamounlab.net/).

Wintachai, P., Wikan, N., Kuadkitkan, A., Jaimipuk, T., Ubol, S., Pulmanausahakul, R., Auewarakul, P., Kasinrerk, W., Weng, W.-Y., Panyasrivanit, M., *et al.* (2012). Identification of prohibitin as a Chikungunya virus receptor protein. Journal of Medical Virology *84*, 1757-1770.

Winter, D., Vinegar, B., Nahal, H., Ammar, R., Wilson, G.V., and Provart, N.J. (2007). An "Electronic Fluorescent Pictograph" Browser for Exploring and Analyzing Large-Scale Biological Data Sets. PLOS One *2*, e718.

Winzer, T., Bairl, A., Linder, M., Linder, D., Werner, D., and Müller, P. (1999). A novel 53-kDa nodulin of the symbiosome membrane of soybean nodules, controlled by *Bradyrhizobium japonicum*. Molecular Plant-Microbe Interactions *12*, 218-226.

Włodarczyk, J., and Kierdaszuk, B. (2003). Interpretation of fluorescence decays using a power-like model. Biophysical Journal *85*, 589-598.

Wolf, S., Mravec, J., Greiner, S., Mouille, G., and Höfte, H. (2012). Plant cell wall homeostasis is mediated by brassinosteroid feedback signaling. Current Biology *22*, 1732-1737.

WormBase Version WS283 (2022). https://wormbase.org/.

Wu, M., Holowka, D., Craighead, H.G., and Baird, B. (2004). Visualization of plasma membrane compartmentalization with patterned lipid bilayers. Proceedings of the National Academy of Sciences *101*, 13798-13803.

Wu, P.G., and Brand, L. (1994). Resonance Energy Transfer: Methods and Applications. Analytical Biochemistry *218*, 1-13.

Xi, L., Wu, X.N., Gilbert, M., and Schulze, W.X. (2019). Classification and Interactions of LRR Receptors and Co-receptors Within the Arabidopsis Plasma Membrane – An Overview. Frontiers in Plant Science *10*.

Xin, X.-F., Kvitko, B., and He, S.Y. (2018). Pseudomonas syringae: what it takes to be a pathogen. Nature Reviews Microbiology *16*, 316-328.

Xiong, S., and Xu, W. (2014). 10.06 - Human Immune System. In Comprehensive Biomedical Physics, A. Brahme, ed. (Oxford: Elsevier), pp. 91-114.

Xu, B., Cheval, C., Laohavisit, A., Hocking, B., Chiasson, D., Olsson, T.S.G., Shirasu, K., Faulkner, C., and Gilliham, M. (2017). A calmodulin-like protein regulates plasmodesmal closure during bacterial immune responses. New Phytologist *215*, 77-84.

Xu, H., Lee, S.-J., Suzuki, E., Dugan, K.D., Stoddard, A., Li, H.-S., Chodosh, L.A., and Montell, C. (2004). A lysosomal tetraspanin associated with retinal degeneration identified via a genome-wide screen. The EMBO Journal *23*, 811-822.

Xu, W., Huang, J., Li, B., Li, J., and Wang, Y. (2008). Is kinase activity essential for biological functions of BRI1? Cell Research *18*, 472-478.

Xue, D.-X., Li, C.-L., Xie, Z.-P., and Staehelin, C. (2019). LYK4 is a component of a tripartite chitin receptor complex in *Arabidopsis thaliana*. Journal of Experimental Botany *70*, 5507-5516.

Yadav, S.R., Yan, D., Sevilem, I., and Helariutta, Y. (2014). Plasmodesmata-mediated intercellular signaling during plant growth and development. Frontiers in Plant Science *5*.

Yamada, K., Goto-Yamada, S., Nakazaki, A., Kunieda, T., Kuwata, K., Nagano, A.J., Nishimura, M., and Hara-Nishimura, I. (2020). Endoplasmic reticulum-derived bodies enable a single-cell chemical defense in Brassicaceae plants. Communications Biology *3*, 21.

Yamada, K., Yamaguchi, K., Shirakawa, T., Nakagami, H., Mine, A., Ishikawa, K., Fujiwara, M., Narusaka, M., Narusaka, Y., Ichimura, K.*, et al.* (2016). The Arabidopsis CERK1-associated kinase PBL27 connects chitin perception to MAPK activation. The EMBO Journal *35*, 2468-2483.

Yamaguchi, K., Yamada, K., and Kawasaki, T. (2013). Receptor-like cytoplasmic kinases are pivotal components in pattern recognition receptor-mediated signaling in plant immunity. Plant Signal Behav *8*, 10.4161/psb.25662-25610.24161/psb.25662.

Yáñez-Mó, M., Barreiro, O., Gordon-Alonso, M., Sala-Valdés, M., and Sánchez-Madrid, F. (2009). Tetraspanin-enriched microdomains: a functional unit in cell plasma membranes. Trends in Cell Biology *19*, 434-446.

Yang, X., Claas, C., Kraeft, S.-K., Chen, L.B., Wang, Z., Kreidberg, J.A., and Hemler, M.E. (2002). Palmitoylation of tetraspanin proteins: modulation of CD151 lateral interactions, subcellular distribution, and integrin-dependent cell morphology. Mol Biol Cell *13*, 767-781.

Yang, X.H., Richardson, A.L., Torres-Arzayus, M.I., Zhou, P., Sharma, C., Kazarov, A.R., Andzelm, M.M., Strominger, J.L., Brown, M., and Hemler, M.E. (2008). CD151 accelerates breast cancer by regulating alpha 6 integrin function, signaling, and molecular organization. Cancer Research *68*, 3204-3213.

Yeh, Y.-H., Chang, Y.-H., Huang, P.-Y., Huang, J.-B., and Zimmerli, L. (2015). Enhanced Arabidopsis pattern-triggered immunity by overexpression of cysteine-rich receptor-like kinases. Frontiers in Plant Science *6*.

Yokoyama, H., and Matsui, I. (2005). A Novel Thermostable Membrane Protease Forming an Operon with a Stomatin Homolog from the Hyperthermophilic Archaebacterium Pyrococcus horikoshii*. Journal of Biological Chemistry *280*, 6588-6594.

Yoo, S.D., Cho, Y.H., and Sheen, J. (2007). Arabidopsis mesophyll protoplasts: a versatile cell system for transient gene expression analysis. Nature Protocols *2*, 1565-1572.

You, Z., Gao, X., Ho, M.M., and Borthakur, D. (1998). A stomatin-like protein encoded by the slp gene of Rhizobium etli is required for nodulation competitiveness on the common bean. Microbiology *144*, 2619-2627.

Yu, M., Liu, H., Dong, Z., Xiao, J., Su, B., Fan, L., Komis, G., Šamaj, J., Lin, J., and Li, R. (2017). The dynamics and endocytosis of Flot1 protein in response to flg22 in Arabidopsis. Journal of Plant Physiology *215*, 73-84.

Yuan, C., Lazarowitz, S.G., and Citovsky, V. (2017). Identification of Plasmodesmal Localization Sequences in Proteins In Planta. Journal of Visualized Experiments, 55301.

Zavaliev, R., Dong, X., and Epel, B.L. (2016). Glycosylphosphatidylinositol (GPI) Modification Serves as a Primary Plasmodesmal Sorting Signal. Plant Physiology *172*, 1061-1073.

Zavaliev, R., Ueki, S., Epel, B.L., and Citovsky, V. (2011). Biology of callose (β-1,3-glucan) turnover at plasmodesmata. Protoplasma *248*, 117-130.

Zess, E.K., Dagdas, Y.F., Peers, E., Maqbool, A., Banfield, M.J., Bozkurt, T.O., and Kamoun, S. (2021). Regressive evolution of an effector following a host jump in the Irish Potato Famine Pathogen Lineage. bioRxiv, 2021.2010.2004.463104.

Zhang, C., He, J., Dai, H., Wang, G., Zhang, X., Wang, C., Shi, J., Chen, X., Wang, D., and Wang, E. (2021). Discriminating symbiosis and immunity signals by receptor competition in rice. Proceedings of the National Academy of Sciences *118*, e2023738118.

Zhang, X., Zhang, J., Bauer, A., Zhang, L., Selinger, D.W., Lu, C.X., and Ten Dijke, P. (2013). Fine-tuning BMP7 signalling in adipogenesis by UBE2O/E2-230K-mediated monoubiquitination of SMAD6. The EMBO Journal *32*, 996-1007.

Zhang, X.C., Wu, X., Findley, S., Wan, J., Libault, M., Nguyen, H.T., Cannon, S.B., and Stacey, G. (2007). Molecular evolution of lysin motif-type receptor-like kinases in plants. Plant Physiology *144*, 623-636.

Zhang, Z., Ober, J.A., and Kliebenstein, D.J. (2006). The Gene Controlling the Quantitative Trait Locus EPITHIOSPECIFIER MODIFIER1 Alters Glucosinolate Hydrolysis and Insect Resistance in Arabidopsis. The Plant Cell *18*, 1524-1536.

Zhao, H., Jan, A., Ohama, N., Kidokoro, S., Soma, F., Koizumi, S., Mogami, J., Todaka, D., Mizoi, J., Shinozaki, K.*, et al.* (2021). Cytosolic HSC70s repress heat stress tolerance and enhance seed germination under salt stress conditions. Plant, Cell & Environment *44*, 1788-1801.

Zheng, M., Liu, X., Liang, S., Fu, S., Qi, Y., Zhao, J., Shao, J., An, L., and Yu, F. (2016). Chloroplast Translation Initiation Factors Regulate Leaf Variegation and Development. Plant Physiology *172*, 1117-1130.

Zhou, J., Wang, P., Claus, L.A.N., Savatin, D.V., Xu, G., Wu, S., Meng, X., Russinova, E., He, P., and Shan, L. (2019). Proteolytic Processing of SERK3/BAK1 Regulates Plant Immunity, Development, and Cell Death. Plant Physiology *180*, 543-558.

Zhou, L., Cheung, M.-Y., Li, M.-W., Fu, Y., Sun, Z., Sun, S.-M., and Lam, H.-M. (2010). Rice HYPERSENSITIVE INDUCED REACTION Protein 1 (OsHIR1) associates with plasma membrane and triggers hypersensitive cell death. BMC Plant Biology *10*, 290.

Zimmerman, B., Kelly, B., McMillan, B.J., Seegar, T.C.M., Dror, R.O., Kruse, A.C., and Blacklow, S.C. (2016). Crystal Structure of a Full-Length Human Tetraspanin Reveals a Cholesterol-Binding Pocket. Cell *167*, 1041-1051.e1011.

Zipfel, C., Kunze, G., Chinchilla, D., Caniard, A., Jones, J.D.G., Boller, T., and Felix, G. (2006). Perception of the Bacterial PAMP EF-Tu by the Receptor EFR Restricts *Agrobacterium*-Mediated Transformation. Cell *125*, 749-760.

Zorick, T.S., and Echols, H. (1991). Membrane localization of the HflA regulatory protease of *Escherichia coli* by immunoelectron microscopy. Journal of Bacteriology *173*, 6307-6310.

Zuidscherwoude, M., Göttfert, F., Dunlock, V.M.E., Figdor, C.G., van den Bogaart, G., and Spriel, A.B.v. (2015). The tetraspanin web revisited by super-resolution microscopy. Scientific Reports *5*, 12201.

Zurzolo, C., van Meer, G., and Mayor, S. (2003). The order of rafts. EMBO Reports *4*, 1117-1121.

Zybailov, B., Rutschow, H., Friso, G., Rudella, A., Emanuelsson, O., Sun, Q., and van Wijk, K.J. (2008). Sorting signals, N-terminal modifications and abundance of the chloroplast proteome. PLOS One *3*, e1994.